frontiers

RESEARCH TOPICS

GABA SIGNALING IN HEALTH AND DISEASE

Hosted by
Yehezkel Ben-Ari

frontiers in
CELLULAR NEUROSCIENCE

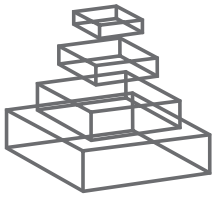

frontiers

Cover image provided by Ibbl sarl, Lausanne CH

ISSN 1664-8714
ISBN 978-2-88919-084-3
DOI 10.3389/978-2-88919-084-3

ABOUT FRONTIERS

Frontiers is more than just an open-access publisher of scholarly articles: it is a pioneering approach to the world of academia, radically improving the way scholarly research is managed. The grand vision of Frontiers is a world where all people have an equal opportunity to seek, share and generate knowledge. Frontiers provides immediate and permanent online open access to all its publications, but this alone is not enough to realize our grand goals.

FRONTIERS JOURNAL SERIES

The Frontiers Journal Series is a multi-tier and interdisciplinary set of open-access, online journals, promising a paradigm shift from the current review, selection and dissemination processes in academic publishing.
All Frontiers journals are driven by researchers for researchers; therefore, they constitute a service to the scholarly community. At the same time, the Frontiers Journal Series operates on a revolutionary invention, the tiered publishing system, initially addressing specific communities of scholars, and gradually climbing up to broader public understanding, thus serving the interests of the lay society, too.

DEDICATION TO QUALITY

Each Frontiers article is a landmark of the highest quality, thanks to genuinely collaborative interactions between authors and review editors, who include some of the world's best academicians. Research must be certified by peers before entering a stream of knowledge that may eventually reach the public - and shape society; therefore, Frontiers only applies the most rigorous and unbiased reviews.
Frontiers revolutionizes research publishing by freely delivering the most outstanding research, evaluated with no bias from both the academic and social point of view.
By applying the most advanced information technologies, Frontiers is catapulting scholarly publishing into a new generation.

WHAT ARE FRONTIERS RESEARCH TOPICS?

Frontiers Research Topics are very popular trademarks of the Frontiers Journals Series: they are collections of at least ten articles, all centered on a particular subject. With their unique mix of varied contributions from Original Research to Review Articles, Frontiers Research Topics unify the most influential researchers, the latest key findings and historical advances in a hot research area!
Find out more on how to host your own Frontiers Research Topic or contribute to one as an author by contacting the Frontiers Editorial Office: researchtopics@frontiersin.org

GABA SIGNALING IN HEALTH AND DISEASE

Hosted By:
Yehezkel Ben-Ari, Institut National de la Santé et de la Recherche Médicale, France

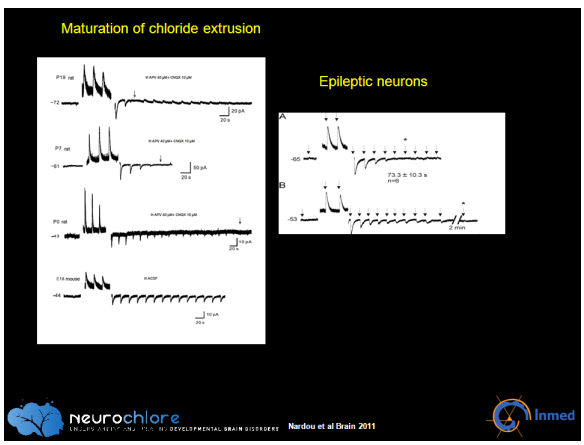

Figure legend: Perforated patch clamp recording of hippocampal neurons to illustrate the wash out of chloride in various conditions. The neurons were clamped at the reversal potential of GABA and therefore focal application of GABA did not generate a current, a large depolarising pulse was then applied and the duration required to return to zero GABA currents was measured to get an insight of chloride removal efficacy. left side: maturation. Note that the return to control values was very long at E 18 (mouse) or P0 (rat) than subsequently with a progressive reduction of the duration until P19. Right figure: long lasting inneficient choride removal in epileptic neurons. A: naive neuron. B: age matched epileptic neuron recorded in a slice after formation in a triple chamber of a chronic epileptic mirror focus. Note the much longer duration of the return to prestimulation values. Reproduced from Nardou, R., Yamamoto, S., Chazal, G., Bhar, A., Ferrand, N., Dulac, O., Ben-Ari, Y., and Khalilov, I. (2011). Neuronal chloride accumulation and excitatory GABA underlie aggravation of neonatal epileptiform activities by phenobarbital. *Brain* 134, 987–1002. doi: 10.1093/brain/awr041; also see Ben-Ari, Y., Gaiarsa, J. L., Tyzio, R., and Khazipov, R. (2007). GABA: a pioneer transmitter that excites immature neurons and generates primitive oscillations. *Physiol. Rev.* 87, 1215–1284. doi: 10.1152/physrev.00017.2006.

GABAergic neurons provide most of the inhibitory drive of adult networks and play major roles in the integrative properties of brain networks. Alterations of GABAergic signals are associated with major neurological disorders and GABA mimetic drugs are widely used as

comfort molecules and to treat several brain disorders. Thus, the inhibitory drive is altered in epilepsies, infantile developmentally related disorders but also Parkinson disease, and anoxo-ischemic insults to just name a few. From the developmental stand point, GABAergic neurons mature before principal neurons and provide an important source of early activities and are thus instrumental in activity dependent modulation of the construction of cortical functional units.

The goal of this Research Topic is to bring together experts studying GABA signals at the molecular, cellular and network levels in physiological and pathological conditions and to examine the fate of GABA signals along transversal ideas linking these diverse domains. A particular emphasis is brain maturation as it is now clear that alteration of developmental sequences -notably of GABA signals- impairs brain development leading to life long deleterious neurological sequels. While this Frontiers Research Topic originated as a repository of work presented at CNCR Amsterdam, papers are invited from researchers continuing to work on this topic as the field expands.

Table of Contents

frontiers in
CELLULAR NEUROSCIENCE

EDITORIAL
published: 09 November 2012
doi: 10.3389/fncel.2012.00045

The yin and yen of GABA in brain development and operation in health and disease

Yehezkel Ben-Ari*

Institut National de la Santé et de la Recherche Médicale, Marseille, France
**Correspondence: ben-ari@inmed.univ-mrs.fr*

Edited by:
Egidio D'Angelo, University of Pavia, Italy

Reviewed by:
Egidio D'Angelo, University of Pavia, Italy

GABA (A) receptor mediated signals have many facets and a plethora of expression mechanisms and consequences on the operation of behaviorally relevant patterns. Starting from the simple view of inhibition/hyperpolarization, the actions of GABA revealed to be far more complex with the identification of interneuronal types, their projections, how they modulate brain patterns, and the crucial roles they serve in health and disease.

As in other fields of neuroscience, recent emphasis has been devoted to gaining a better understanding of the development of GABA signals: developmental neurobiology has invaded all fields of brain research. In this e-book, along the line of a wide range of investigations stressing the roles of GABA in cell proliferation, Young et al. (2010) report their results on GABA actions in the sub ventricular zone. GABAergic interneurons follow a long journey to their assigned targets and we are beginning to know how they are controlled during that journey. Friocourt and Parnavelas (2010) discuss the role of ARX and Livnat et al. (2010) pursue their importance contributions in this domain analyzing the PAF-AH catalytic subunits modulate the Wnt pathway.

Extensive investigations have been devoted to the trophic roles exerted by GABA during maturation. Sernagor et al. (2010) analyze the role of GABAergic signals in development and adult neurogenesis stressing the similarities and differences between different neuronal systems. An interesting twist to these studies is provided by Heistek et al. (2010) showing that maturation of Gaba currents and associated voltage gated currents differ in different strains of rodents leading also to different oscillations generated by networks. This important contribution illustrates how the intrinsic features of GABAergic synaptic currents impact brain operation. This is also analyzed in a different perspective by Baltz et al. (2010) showing that Gaba interneurons play a crucial role in the maturation of brain patterns *in vitro* including the well investigated Giant Depolarizing Potentials (GDPs) that have been identified in developing networks in a wide range of brain preparations and structures during early developmental stages. Somatic projecting interneurons have different brain patterns that are crucial in the generation of behaviorally relevant oscillations. Ellender and Paulsen (2010) analyze these tunes, their generation mechanisms and consequences on the network. Cortical neurons *in vivo* may operate in high-conductance states, due to synaptic activity that are sometimes several-fold larger than the resting conductance. Destexhe (2010) analyze how the contribution of inhibition in such high-conductance states.

The Depolarizing/hyperpolarizing shift during maturation is a fundamental features of brain maturation that along other developmental sequences illustrates how developing currents and signaling in general have a different agenda than adult ones. Excitatory GABA plays a crucial role in the trophic roles that GABA exerts on all developmental mechanisms from proliferation to differentiation, growth, and synapse formation. These features are analyzed here by several groups. Ormond and Woodin (2011) pursue their analysis of the phenomenon of paired pre- and postsynaptic activity in area CA1 of the hippocampus that induces long-term inhibitory synaptic plasticity at GABAergic synapses. These long-term changes in the driving force of GABA is a vivid illustration of how activity impacts brain networks via alterations of intracellular levels of chloride. It is usually assumed that the low levels of Cl in immature neurons is due to the lack of expression of the chloride exporter KCC2, here Khalilov et al. (2011) show that in KCC2 Kos that die at birth, networks generate seizures suggesting that this device is needed in embryos. Valeeva et al. (2010) show how this depolarization that does not reach spike threshold yet can generate action potentials by activating a voltage gated current illustrating the important convergence of synaptic and voltage gated currents. An important conceptual issue receives in the work of Dehorter et al. (2011) an elegant reply. Indeed, if immature patterns generate different patterns they must at some stage shift to adult patterns to enable a smooth passage from patterns devoted to growth and patterns that control behaviors and motricity. Here, the authors show that Medium Spiny neurons that must be quite silent to enable the generation of targeted movement are silenced precisely when the pup start generating these movements; this is mediated by alterations of NMDA receptor mediated currents and voltage gated currents stressing the importance and precision of the timing. Sale et al. (2010) provide two important contributions on the control of plasticity by GABA in the maturation of the visual system and the E/I balance in amblyopia stressing the possible therapeutic perspectives of early corrections of inhibition in visual acuity.

Finally, Nardou et al. (2011) show how Phenobarbital but not diazepam exert a direct action on AMPA/kainate mediated currents illustrating how classical GABA acting drugs used for generations as classical tools to dissect GABA signals can have diverse actions. Cesetti et al. (2012) analyze the roles of GABA in the developmental changes of GABAergic mechanisms in human visual cortex across the lifespan.

Summing up, these studies illustrate vividly the importance of GABAergic signals and how they genuinely control brain operation from the earliest developmental stages sculpting neuronal shapes, controlling their intrinsic features, and determining how they operate in health and disease.

REFERENCES

Baltz, T., de Lima, A. D., and Voigt, T. (2010). Contribution of GABAergic interneurons to the development of spontaneous activity patterns in cultured neocortical networks. *Front. Cell. Neurosci.* 4:15. doi: 10.3389/fncel.2010.00015

Ellender, T. J., and Paulsen, O. (2010). The many tunes of perisomatic targeting interneurons in the hippocampal network. *Front. Cell. Neurosci.* 4:26. doi: 10.3389/fncel.2010.00026

Cesetti, T., Ciccolini, F., and Li, Y. (2012). GABA not only a neurotransmitter: osmotic regulation by $GABA_A$R signaling. *Front. Cell. Neurosci.* 6:3. doi: 10.3389/fncel.2012.00003

Dehorter, N., Michel, F. J., Marissal, T., Rotrou, Y., Matrot, B., Lopez, C., et al. (2011). Onset of pup locomotion coincides with loss of NR2C/D-mediated cortico-striatal EPSCs and dampening of striatal network immature activity. *Front. Cell. Neurosci.* 5:24. doi: 10.3389/fncel.2011.00024

Destexhe, A. (2010). Inhibitory "noise". *Front. Cell. Neurosci.* 4:9. doi: 10.3389/fncel.2010.00009

Friocourt, G., and Parnavelas, J. G. (2010). Mutations in ARX result in several defects involving GABAergic neurons. *Front. Cell. Neurosci.* 4:4. doi: 10.3389/fncel.2010.00004

Heistek, T. S., Timmerman, A. J., Spijker, S., Brussaard, A. B., and Mansvelder, H. D. (2010). GABAergic synapse properties may explain genetic variation in hippocampal network oscillations in mice. *Front. Cell. Neurosci.* 4:18. doi: 10.3389/fncel.2010.00018

Khalilov, I., Chazal, G., Chudotvorova, I., Pellegrino, C., Corby, S., Ferrand, N., et al. (2011). Enhanced synaptic activity and epileptiform events in the embryonic KCC2 deficient hippocampus. *Front. Cell. Neurosci.* 5:23. doi: 10.3389/fncel.2011.00023

Livnat, I., Finkelshtein, D., Ghosh, I., Arai, H., and Reiner, O. (2010). PAF-AH catalytic subunits modulate the Wnt pathway in developing GABAergic neurons. *Front. Cell. Neurosci.* 4:19. doi: 10.3389/fncel.2010.00019

Nardou, R., Yamamoto, S., Bhar, A., Burnashev, N., Ben-Ari, Y., and Khalilov, I. (2011). Phenobarbital but not diazepam reduces AMPA/kainate receptor mediated currents and exerts opposite actions on initial seizures in the neonatal rat hippocampus. *Front. Cell. Neurosci.* 5:16. doi: 10.3389/fncel.2011.00016

Ormond, J., and Woodin, M. A. (2011). Disinhibition-mediated LTP in the hippocampus is synapse specific. *Front. Cell. Neurosci.* 5:17. doi: 10.3389/fncel.2011.00017

Sale, A., Berardi, N., Spolidoro, M., Baroncelli, L., and Maffei, L. (2010). GABAergic inhibition in visual cortical plasticity. *Front. Cell. Neurosci.* 4:10. doi: 10.3389/fncel.2010.00010

Sernagor, E., Chabrol, F., Bony, G., and Cancedda, L. (2010). GABAergic control of neurite outgrowth and remodeling during development and adult neurogenesis: general rules and differences in diverse systems. *Front. Cell. Neurosci.* 4:11. doi: 10.3389/fncel.2010.00011

Valeeva, G., Abdullin, A., Tyzio, R., Skorinkin, A., Nikolski, E., Ben-Ari, Y., et al. (2010). Temporal coding at the immature depolarizing GABAergic synapse. *Front. Cell. Neurosci.* 4:17. doi: 10.3389/fncel.2010.00017

Young, S. Z., Platel, J.-C., Nielsen, J. V., Jensen, N. A., and Bordey, A. (2010). $GABA_A$ increases calcium in subventricular zone astrocyte-like cells through L- and T-type voltage-gated calcium channels. *Front. Cell. Neurosci.* 4:8. doi: 10.3389/fncel.2010.00008

Received: 20 September 2012; accepted: 28 September 2012; published online: 09 November 2012

Citation: Ben-Ari Y (2012) The yin and yen of GABA in brain development and operation in health and disease. Front. Cell. Neurosci. ***6****:45. doi: 10.3389/fncel.2012.00045*

frontiers in
CELLULAR NEUROSCIENCE

REVIEW ARTICLE
published: 11 March 2010
doi: 10.3389/fncel.2010.00004

Mutations in *ARX* result in several defects involving GABAergic neurons

Gaëlle Friocourt[1,2,3]* and John G. Parnavelas[4]

[1] *U613, Institut National de la Santé et de la Recherche Médicale, Brest, France*
[2] *Laboratory of Molecular Genetics and Histocompatibility, Centre Hospitalier Universitaire Brest, Brest, France*
[3] *Institut Fédératif de Recherche 148, Brest University, Brest, France*
[4] *Department of Cell and Developmental Biology, University College London, London, UK*

Edited by:
Yehezkel Ben-Ari, Institut National de la Santé et de la Recherche Médicale, France

Reviewed by:
Orly Reiner, Weizmann Institute of Science, Israel

****Correspondence:***
Gaëlle Friocourt, U613, Institut National de la Santé et de la Recherche Médicale, 46 rue Félix Le Dantec, CS51819, 29218 Brest Cedex 2, France.
e-mail: gaelle.friocourt@univ-brest.fr

Genetic investigations of X-linked mental retardation have demonstrated the implication of *ARX* in a wide spectrum of disorders extending from phenotypes with severe neuronal migration defects, such as lissencephaly, to mild or moderate forms of mental retardation without apparent brain abnormalities, but with associated features of dystonia and epilepsy. These investigations have in recent years directed attention to the role of this gene in brain development. Analysis of its spatio-temporal localization profile revealed expression in telencephalic structures at all stages of development, mainly restricted to populations of GABA-containing neurons. Furthermore, studies of the effects of *ARX* loss of function either in humans or in lines of mutant mice revealed varying defects, suggesting multiple roles of this gene during development. In particular, *Arx* has been shown to contribute to almost all fundamental processes of brain development: patterning, neuronal proliferation and migration, cell maturation and differentiation, as well as axonal outgrowth and connectivity. In this review, we will present and discuss recent findings concerning the role of *ARX* in brain development and how this information will be useful to better understand the pathophysiological mechanisms of mental retardation and epilepsy associated with *ARX* mutations.

Keywords: ARX, GABA, lissencephaly, epilepsy, interneurons, neuronal migration, basal ganglia

INTRODUCTION

In the last years, defects in transcription regulation have been linked to several monogenic neurodevelopmental disorders resulting, in some cases, in cerebral malformations, mental retardation and/or autism. Such defects may result from mutations located directly in genes encoding transcription factors such as *ZIC2* (*Zinc finger protein of the cerebellum 2*), responsible for holoprosencephaly (Brown et al., 1998). As these transcription factors often have precise spatio-temporal expression profiles as well as multiple trans-acting co-factors, mutations in these genes can have pleiotropic effects. This is, for example, the case for *ARX* (*aristaless-related homeobox gene*), which has been shown in humans to be responsible for a wide spectrum of brain disorders ranging from phenotypes with severe neuronal migration defects, such as lissencephaly, to milder forms of X-linked mental retardation (XLMR) often associated with epilepsy, but without apparent brain abnormalities (for review, see Gécz et al., 2006).

Mental retardation is a heterogeneous group of disorders that result from a variety of acquired and genetic causes. The observation that mental retardation preferentially affects males, has led investigators to focus on genes located on the X-chromosome. XLMR may be: (i) syndromic, characterized by recognizable dysmorphic features, neurological complications and/or metabolic abnormalities, or (ii) non-syndromic, showing no specific features apart from an intelligence quotient (IQ) below 70 with a deficit in adaptive skills (for reviews, see Chelly and Mandel, 2001; Gécz et al., 2009). Lissencephaly, which represents the other end of the spectrum of brain disorders associated with *ARX* mutations, is also a heterogeneous group of cortical malformations resulting from mutations in at least five different genes: *LIS1*, *DCX* (doublecortin), *RELN* (reelin), *ARX* and *TUBA1A* (tubulin alpha1A) (Reiner et al., 1993; des Portes et al., 1998; Gleeson et al., 1998; Hong et al., 2000; Kitamura et al., 2002; Keays et al., 2007). Lissencephaly is caused by abnormal neuronal migration and is characterized by disrupted cytoarchitecture associated with an abnormally thick cortex and absence (agyria) or diminution (pachygyria) of gyri and sulci and, hence, a smooth brain surface (for reviews, see Francis et al., 2006; Guerrini and Parrini, 2009).

ARX encodes a transcription factor which belongs to the class of homeobox genes. Mutations in this class of genes were first described in *Drosophila* and result in the misexpression of body structures in different segments of the fly, demonstrating their important role in specifying the body segments. Since then, homeobox genes were shown to control many cellular processes including proliferation, differentiation, apoptosis, cell shape, cell adhesion, and migration (for review, see Pearson et al., 2005). They are characterized by a 60-amino acid homeobox domain (or homeodomain), which is responsible for DNA-binding. In addition, they often contain other motifs that can contribute to DNA and/or co-factor binding to further define their target gene specificity. These additional motifs, as well as variations in the homeodomain, are used to divide the homeoprotein superfamily into families and subfamilies, such as *Hox*, *Nk*, *Paired*, *Pax*, *Lim*, or *Six*.

The ARX protein belongs to one of the three largest classes of homeoproteins, the paired (Prd) class. This class of homeobox genes are thought to be important regulators of essential events during vertebrate embryogenesis, including the development of the central and peripheral nervous systems (for reviews, see Meijlink et al., 1999; Wigle and Eisenstat, 2008). Three subclasses have been identified based on the nature of a key residue at position 50 within the homeodomain. A serine residue at position 50 (S50) of the homeodomain defines the *Pax*- or *Paired*-type subgroup, whereas a lysine residue at position 50 (K50) defines another subgroup including the *Orthodenticle* gene. The presence of a glutamine at position 50 (Q50) of the homeodomain defines a third subgroup, which contains the *aristaless*-related proteins (Galliot and Miller, 2000). ARX has, in addition to the homeodomain [amino acid (aa) 334–377], a conserved domain located at the C-terminus called the aristaless domain (aa 527–542), an octapeptide domain (aa 27–34) located near the N-terminus, three nuclear localization sequences (aa 82–89, 325–333 and 378–386), a central acidic domain (aa 224–255) and four polyalanine tracts (aa 100–115, 144–155, 275–281 and 432–440) whose function is not well known (**Figure 1**).

ARX MUTATIONS IN HUMAN

ONE SINGLE GENE INVOLVED IN SEVERAL SYNDROMES IN HUMAN

ARX, located on Xp22.13, was first identified in 2002 as being involved in non-syndromic XLMR (OMIM 300382 and 300419) (Bienvenu et al., 2002) as well as in X-linked West syndrome [also called infantile spasms (ISSX)] (OMIM 308350) (Strømme et al., 2002; Kato et al., 2003). Since then, several other mutations have been described and broadened the spectrum of phenotypes resulting from *ARX* mutations (**Figure 1**). These phenotypes can be divided into two groups: (1) a malformation group, which includes X-linked lissencephaly associated with abnormal genitalia (XLAG) (OMIM 300215) (Dobyns et al., 1999; Ogata et al., 2000; Kitamura et al., 2002), hydranencephaly and abnormal genitalia (HYD-AG) (OMIM 300215) and Proud syndrome (OMIM 300004) (Kato et al., 2004); and (2) a non-malformation group including non-syndromic XLMR (Bienvenu et al., 2002), Partington syndrome (PRTS) (OMIM 309510) (Frints et al., 2002; Strømme et al., 2002), various forms of epilepsy including West syndrome (Strømme et al., 2002; Kato et al., 2003), X-linked myoclonic seizures, spasticity and intellectual disability (XMESID) (OMIM 308350) (Scheffer et al., 2002; Strømme et al., 2002), idiopathic infantile epileptic-dyskinetic

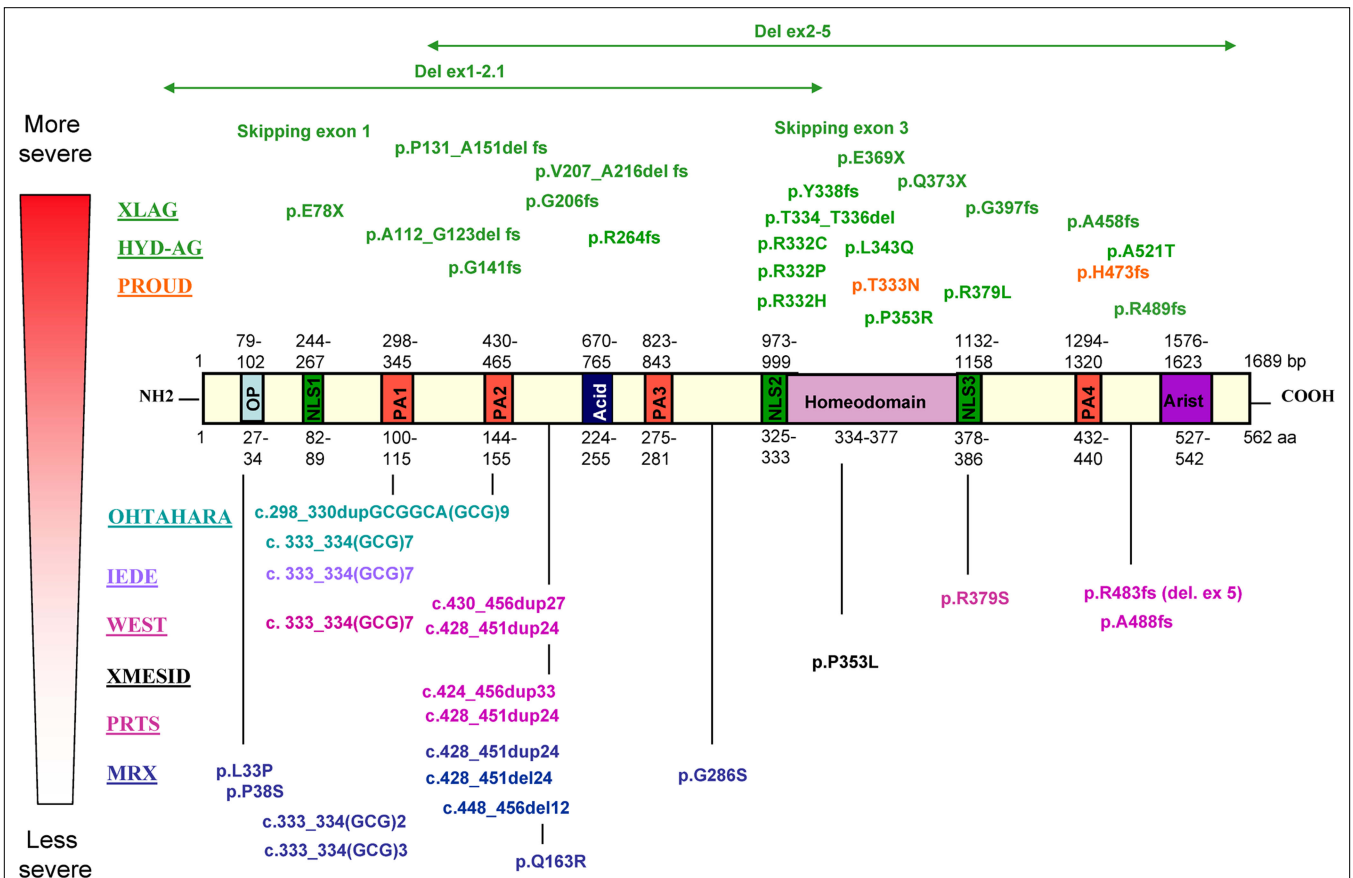

FIGURE 1 | While non-malformation phenotypes [non-specific X-linked mental retardation (MRX), Partington (PRTS) and West syndromes, XMESID, IEDE and Ohtahara syndrome] tend to be caused by pathogenic variations outside the homeodomain or inside the first two polyalanines tracts of ARX, brain and genital malformation phenotypes [XLAG, hydranencephaly with abnormal genitalia (HYD-AG) and Proud syndrome] are associated with pathogenic variations that truncate the ARX protein or alter residues in the highly conserved homeodomain. Interestingly, a non-conservative missense mutation near the C-terminal aristaless domain (p.A521T) causes unusually severe XLAG with microcephaly and mild cerebellar hypoplasia.

encephalopathy (IEDE) (OMIM 308350) (Guerrini et al., 2007) and early infantile epileptic encephalopathy with suppression-burst pattern (EIEE or Ohtahara's syndrome) (OMIM 308350) (Kato et al., 2007) (see **Table 1** for a description of these syndromes).

Phenotype/genotype studies have suggested that there is a correlation between the genotype and the observed phenotype: premature termination mutations [large deletions, frameshift (fs), nonsense mutations or splice sites mutations] lead to the more severe phenotypes in the malformation group. In addition, non-conservative missense mutations within the homeobox or nuclear localization sequences (as for example p.R332C or p.P353R) also cause XLAG, while conservative substitutions in the homeodomain (p.T333N) cause Proud syndrome (**Figure 1**). In contrast, missense mutations outside the homeobox or expansions/deletions of polyalanine tracts lead to the non-malformation group (Sherr, 2003; Kato et al., 2004). Although several studies have generally confirmed this correlation, recent case reports show evidence of strong phenotypic heterogeneity (Hartmann et al., 2004; Van Esch et al., 2004; Kato et al., 2007; Wallerstein et al., 2008; Absoud et al., 2009; Fullston et al., 2010), including in female carriers who have been reported to have in some cases partial or complete agenesis of the corpus callosum, cognitive levels spanning from normal to severely impaired and associated epilepsy (Bonneau et al., 2002; Uyanik et al., 2003; Kato et al., 2004; Okazaki et al., 2008; Wallerstein et al., 2008; Marsh et al., 2009). This phenotypic heterogeneity is probably due to differences in genetic and environmental backgrounds which are specific to each family.

ARX MUTATIONS EXPANDING POLYALANINE TRACTS

The vast majority of *ARX* mutations identified so far affect the two first polyalanine tracts in the ARX protein, and most are expansions that result in highly variable phenotypes (**Figure 1**). In particular, the most frequent and recurrent mutation (representing approximately 45% of all *ARX* mutations reported to date), the in-frame 24 bp duplication (c.428_451dup24), has been associated with PRTS, West syndrome and mental retardation with seizures or non-specific XLMR (Turner et al., 2002; Szczaluba et al., 2006; Guerrini et al., 2007; Laperuta et al., 2007). To date, various types of seizures have been reported in patients with this mutation, including infantile spasms (Strømme et al., 2002; Turner et al., 2002), tonic-clinic seizures (Turner et al., 2002; Partington et al., 2004; Szczaluba et al., 2006), complex partial seizures (Partington et al., 2004) and in one instance, absence of seizures (Szczaluba et al., 2006). Two longer expansions have also been described, a 33- and 27-bp duplication (Demos et al., 2009; Reish et al., 2009). Interestingly, only the 27 bp duplication gives a more severe phenotype when compared to the spectrum of clinical presentations associated with the dup24 bp mutation (Reish et al., 2009).

Similarly, several pathogenic variations have been reported to expand the first polyalanine tract of ARX. In particular, an expansion of seven residues [c.333_334$(GCG)_7$] has been reported to cause X-linked West syndrome (Strømme et al., 2002), IEDE (Guerrini et al., 2007) and Ohtahara syndrome (Absoud et al., 2009). The largest reported expansion, which adds eleven alanines [c.298_330dupGCGGCA$(GCG)_9$], also produces Ohtahara syndrome (Kato et al., 2007). It is interesting to note that despite having only a short expansion of seven alanine residues, the patient described in Absoud's report displays one of the most severe phenotype, Ohtahara syndrome with progressive and severe neurodegeneration, resulting in death during the first year of life. This clinical presentation and course represent a much more severe phenotype than previously described for this mutation, suggesting that there is no real correlation between the expansion length of the polyalanine tract and phenotypic severity.

It has been suggested that these mutations, although recessive, may cause protein aggregation, similar to other polyalanine disorders (for review, see Albrecht and Mundlos, 2005). Indeed, some *ex vivo* data seem to confirm this hypothesis, at least for the c.333_334$(GCG)_7$ mutation (Nasrallah et al., 2004; Friocourt et al., 2006; Shoubridge et al., 2007). *In vitro* transfection of the c.333_334$(GCG)_7$ construct causes protein aggregation, filamentous nuclear inclusions, and an increase in cell death. Similarly,

Table 1 | Short phenotypic description of the syndromes associated with *ARX* mutations.

Non-syndromic XLMR	X-linked mental retardation without any specific features apart from IQ < 70 and a deficit in adaptive skills
Partington syndrome	Mild to moderate X-linked mental retardation and dystonic movements of the hands
XMESID	Myoclonic seizures, spasticity, mental retardation
West syndrome	Infantile spasms (clusters of sudden flexion or extension of the trunks and limbs), specific electroencephalographic pattern of hypsarrhythmia, mental retardation
IEDE	Early-onset infantile spasms, severe generalized dystonia, profound mental retardation
Ohtahara syndrome	Early infantile epileptic encephalopathy (within days of birth or even prenatally) with frequent minor generalized seizures and burst suppressions (high-voltage bursts alternating with almost flat suppression phase) on the electroencephalogram, severe psychomotor retardation, poor prognosis (about one in three patients dies before the second year of life)
Proud syndrome	X-linked mental retardation, agenesis of corpus callosum, abnormal genitalia
HYD-AG	Hydranencephaly, abnormal genitalia
XLAG	Severe congenital or post-natal microcephaly, lissencephaly with a posterior to anterior gradient, agenesis of the corpus callosum, hypothalamic dysfunction (disturbed temperature regulation), pancreatic insufficiency, thalamic/midbrain dysplasia, neonatal-onset intractable epilepsy, severe hypotonia, ambiguous or underdeveloped genitalia in genotypic males (micropenis and cryptorchidism, sometimes retention of testes), death within the first few weeks or months of life

cortical neurons, transfected with this mutant construct using whole-brain electroporation, form neuronal nuclear inclusions *in vivo* (Nasrallah et al., 2004). More recently, Shoubridge et al. (2007) showed that, in addition to increase the propensity of protein aggregation, the c.333_334(GCG)$_7$ mutation results in a shift from nuclear to cytoplasmic localization of ARX protein. Interestingly, two recent reports of knock-in mice for the same mutation show the absence of neuronal inclusions *in vivo* (Kitamura et al., 2009; Price et al., 2009). However, Price et al. (2009) reported that in the parietal cortex of the (GCG) + 7 mutant mice, 45% of cells show cytoplasmic localization of mutated Arx compared to only 28% in wild-type mice. These results suggest that, although protein aggregation is not detectable *in vivo*, polyalanine expansions may cause Arx protein mislocalization in the cytoplasm and thus, a partial loss of function, which may contribute to the pathogenesis.

ARX ACTS AS BOTH A TRANSCRIPTIONAL REPRESSOR AND ACTIVATOR

Both *in vitro* and *in vivo* studies have demonstrated that Arx is a potent transcriptional repressor, but that it can also act as an activator (Collombat et al., 2003; Seufert et al., 2005; McKenzie et al., 2007; Fullenkamp and El-Hodiri, 2008). In particular, the highly conserved octapeptide domain and another C-terminal region (aa 432–483) including the fourth polyalanine tract, have transcriptional repressor activity while the *aristaless*-related domain (aa 527–542) has transcriptional activator activity (McKenzie et al., 2007; Fullenkamp and El-Hodiri, 2008). Some of Arx co-factors have even been identified: the Groucho/transducin-like enhancer (TLE) of split family of co-repressors interacts with Arx octapeptide, whereas repression by the second domain occurs through the interaction with C-terminal binding proteins (CtBPs) (Fullenkamp and El-Hodiri, 2008). Moreover, it was shown that, although the domain encompassing polyalanine tracts 1 and 2 of ARX does not seem to significantly contribute to the repression activity, the expansions of either polyalanine tract 1 or 2 enhance transcriptional repression activity in a manner dependent on the length of the alanine expansion, suggesting that the expansion of ARX polyalanine tracts may be harmful to neurons in a size-dependent manner (McKenzie et al., 2007). Thus, these results suggest that ARX dysfunction due to expanded polyalanine tracts may arise from increased repression activity of the mutant protein. Changes in the transcriptional activity of ARX may thus have subtle effects on neuronal organization and may contribute to the pathogenesis of *ARX*-related disorders.

ARX IS EXPRESSED IN GABAergic CELLS

Pyramidal neurons, the projection cells of the neocortex, derive from the primitive neuroepithelium and, between embryonic day 12 (E12) and the time of birth in mouse, migrate radially as sequential waves to take their positions in the developing cortex in an orderly fashion. The first wave of postmitotic neurons migrates to form a subpial preplate (or primitive plexiform zone). The second wave, which will form the cortical plate (CP), splits the preplate into the superficial molecular layer (or marginal zone) and the deep subplate. Then, the following waves of migrating neurons pass the subplate and generate cell layers in an "inside-out" sequence, such that neurons that are generated early reside in the deepest layers, whereas later-born cells migrate past the existing layers to form the more superficial layers (reviewed in Rakic, 1990; Nadarajah and Parnavelas, 2002; Kriegstein and Noctor, 2004; Ayala et al., 2007). The other neuronal cell type of the cortex, the GABA-containing interneurons, are generated for the most part from progenitors in the medial and caudal ganglionic eminences (MGE and CGE) of the ventral forebrain and reach the cortex by tangential migration (for reviews, see Marin and Rubenstein, 2003; Métin et al., 2006).

In mouse, *Arx* expression is first detectable at the 3-somite stage and, after the 10-somite stage, it appears confined to a specific area in the anterior neural plate (Colombo et al., 2004). At later stages, it is widespread throughout telencephalic structures such as the GE, the cerebral cortex and the hippocampus (Miura et al., 1997; Bienvenu et al., 2002; Colombo et al., 2004; Poirier et al., 2004). No expression is detected in most of the mesencephalic and diencephalic structures, except the ventral thalamus (Bienvenu et al., 2002; Poirier et al., 2004). Outside the brain, Arx is detected in endocrine pancreas, developing testes as well as in heart, skeletal muscle, and liver (Miura et al., 1997; Bienvenu et al., 2002; Kitamura et al., 2002; Collombat et al., 2003; Biressi et al., 2008). In the telencephalon, it is strongly expressed in the subventricular zones (SVZ) and mantle zones of the developing LGE and MGE, but not in the ventricular zones (VZ) of these structures. On the contrary, in the developing cortex, Arx is expressed in progenitors in the VZ/SVZ, as well as in tangentially migrating interneurons emanating from the GE, but not in radially migrating cells. In addition, double-labelling experiments, performed in both dissociated cultures and sections of embryonic or adult cortex, revealed extensive co-localization between Arx and GABA (Colombo et al., 2004; Poirier et al., 2004; Cobos et al., 2005; Friocourt et al., 2006, 2008). The protein is still present in the adult, but is confined primarily in regions that are known to be rich in GABAergic neurons such as the amygdala and the olfactory bulb (Colombo et al., 2004; Poirier et al., 2004). Thus, it has been suggested that the observed seizures in the great majority of patients with *ARX* mutations, probably result from absence and/or dysfunction of GABAergic interneurons. Consistent with these results, *Arx* expression was shown to be regulated by several members of the *Dlx* (*Distal-less*) family of homeobox proteins, particularly *Dlx2* (Cobos et al., 2005; Colasante et al., 2008). Indeed, *Arx* expression is ectopically induced following electroporation of plasmids expressing *Dlx1*, *Dlx2* or *Dlx5* in the chick neural tube and in mouse dorsal thalamus. These results are strengthened by the fact that, *in vivo*, Arx expression is severely reduced in *Dlx1/2* double knockout mice (Cobos et al., 2005).

PLEIOTROPIC ROLES FOR *ARX*

MULTIPLE EFFECTS RESULTING FROM *ARX* LOSS OF EXPRESSION IN MOUSE AND HUMAN

Arx knock-out mice have been shown to display a variety of defects (Kitamura et al., 2002; Colombo et al., 2007). For example, *Arx*-deficient brains were found to be dramatically altered, exhibiting poorly developed olfactory bulbs and reduced volumes of the cerebral cortex and hippocampus (Kitamura et al., 2002). In particular, mutant brain sections revealed an accumulation of newly born interneurons near their proliferative zones in the MGE and CGE, resulting in a major loss of GABAergic interneurons in the cortex,

hippocampus and striatum, similar to the human XLAG (Bonneau et al., 2002; Uyanik et al., 2003; Forman et al., 2005; Okazaki et al., 2008). Colombo et al. (2007) showed that the early differentiation of the basal ganglia appeared normal, whereas subsequent differentiation was impaired, leading to the periventricular accumulation of immature neurons in both LGE and MGE. Neuronal migrations towards the cortex and basal ganglia were greatly reduced in mutants, causing a periventricular accumulation of NPY^+ (neuropeptide Y) or $calretinin^+$ neurons in the MGE. Altogether, these data suggest that *Arx* has major roles in promoting neuronal migration and regulating basal ganglia differentiation in mice. As a likely secondary effect of these malformations, *Arx* mutants also displayed altered connectivity between the cortex and thalamus. In particular, major axonal tracts failed to cross the LGE/MGE border, probably as a result of the loss of LGE corridor cells that guide thalamic axons through the MGE (López-Bendito et al., 2006) and/or the severe reduction of the ventral thalamus and lack of eminentia thalami, an area connecting the diencephalon to the caudoventral telencephalon (Kitamura et al., 2002; Colombo et al., 2007).

In human, XLAG is typically characterized by severe congenital or postnatal microcephaly, lissencephaly with a posterior-to-anterior gradient, an agenesis of the corpus callosum and dysgenesis of the hippocampal dentate gyrus, midbrain malformations, hypothalamic dysfunction, neonatal-onset intractable epilepsy, severe hypotonia and ambiguous or underdeveloped genitalia in genotypic males (Dobyns et al., 1999; Ogata et al., 2000; Kitamura et al., 2002). Histopathological studies revealed poorly delineated and atrophic basal ganglia with small fragmented caudate nuclei and hypodense cavitations within the striatum, the absence or hypoplasia of the olfactory bulbs, hypoplastic optic nerves, a selectively enlarged third ventricle and temporal lobe as well as hippocampal dysplasia. Histological analysis described a cortex organized into 3 distinct layers (a marginal layer, an intermediate layer and a less organized deep layer) instead of the usual six, and a strong decrease in the number, sometimes even a complete absence, of interneurons. Moreover, numerous heterotopic neurons can be observed in the white matter without any clear organization (Bonneau et al., 2002; Uyanik et al., 2003; Forman et al., 2005; Okazaki et al., 2008). These neuropathological features are very similar to those observed in $Arx^{-/y}$ mice (Kitamura et al., 2002; Colombo et al., 2007).

ROLE OF *ARX* IN CELL PROLIFERATION AND NEURONAL MIGRATION

The extensive co-localization between Arx and GABA, its absence of expression in radially migrating neurons, as well as the absence of interneurons documented in the cortex of XLAG patients (Bonneau et al., 2002; Forman et al., 2005; Okazaki et al., 2008) and in *Arx* mutant mice (Kitamura et al., 2002; Colombo et al., 2007) have led to the idea that XLAG syndrome was the result of defective interneuron migration and function, and the proposal of a new term "interneuronopathy" to describe this pathology (Kato and Dobyns, 2005). However, some data suggest that *ARX* expression in cortical progenitors may also be critical for radial migration (Friocourt et al., 2008). Using *in utero* electroporation in mouse to knock-down or overexpress ARX in the developing cortex, we recently showed that targeted inhibition of the gene causes cortical progenitor cells to exit the cell cycle prematurely, whereas overexpression increases the length of the cell cycle, showing that ARX is important to maintain progenitor proliferation. In addition, RNA interference-mediated inactivation of ARX results in decreased neuronal motility, with an accumulation of cells in the SVZ/intermediate zone (IZ) (Friocourt et al., 2008). These results are in agreement with the microcephaly and the misplacement of pyramidal neurons observed in the cortex of *Arx* knockout mice (Kitamura et al., 2002), and in the cortex and white matter of XLAG syndrome (Bonneau et al., 2002).

Interestingly, we observed that arrested cells due to ARX inactivation appeared oval or round in shape, with very few or no processes (Friocourt et al., 2008), very different from the multipolar morphology normally exhibited when cells exit the VZ and enter the lower IZ (Tabata and Nakajima, 2003). Since the first description of the multipolar stage during radial migration, several studies have suggested that the transition into and out of this stage is particularly vulnerable, and that it is disrupted in several disorders of neocortical development, including lissencephaly (LoTurco and Bai, 2006). Cell morphology defects, very similar to those induced by RNAi-mediated inactivation of ARX, have been reported following inactivation of Filamin A (Nagano et al., 2004), Rac1 (Chen et al., 2009) or p27kip1 (Kawauchi et al., 2006) and gain of function of MARK2 (Sapir et al., 2008) or Rnd2 (Heng et al., 2008). Interestingly, all these proteins interact with the actin cytoskeleton or are involved in neuronal polarity, suggesting that ARX may play a role in cell morphology through the regulation of the cytoskeleton. Consistently, we observed that ARX overexpression in radially migrating cells promotes tangentially orientated migration in the SVZ and lower IZ, although these cells do not express GABAergic markers (**Figure 2**). Interestingly, these cells exhibit complex branching and very long processes, which confirm that *ARX* may have a role in cell morphology and especially in process formation (Friocourt et al., 2008).

In *Arx*-null embryos, migration from (i) the LGE to the striatum and other structures and (ii) the MGE to the cortical IZ and MZ are nearly absent, whereas migration through the cortical SVZ is only partially impaired. As a consequence, calbindin- and calretinin-expressing cells are severely reduced and NPY^+ interneurons are nearly absent throughout the brain (Kitamura et al., 2002; Colombo et al., 2007). Defective tangential migration is similarly observed after electroporation into the MGE of rat brain slices (Friocourt et al., 2008). Both inactivation and overexpression of ARX result in impairment of cortical interneuron migration from the MGE. Thus, these results suggest that this defect in tangential migration is cell autonomous and not the consequence of the absence of *Arx* earlier in development (Colombo et al., 2007; Friocourt et al., 2008). Indeed, studies on *Arx* knock-out mice described regional deficiencies and mis- and/or ectopic expression of several transcription factors, potentially important for migration and differentiation of certain population of neurons, as well as abnormal axonal tracts which may have been the reason for the impaired tangential migration (Kitamura et al., 2002; Colombo et al., 2007). Interestingly, we observed that many tangentially migrating neurons overexpressing ARX had one unusually long process (Friocourt et al., 2008). Morphological defects were also observed in migrating interneurons derived from *Arx* mutant mice (Colombo et al., 2007). These authors observed that *Arx*-mutant interneurons failed to migrate from small fragments of mutant LGE to the cortex both on mutant

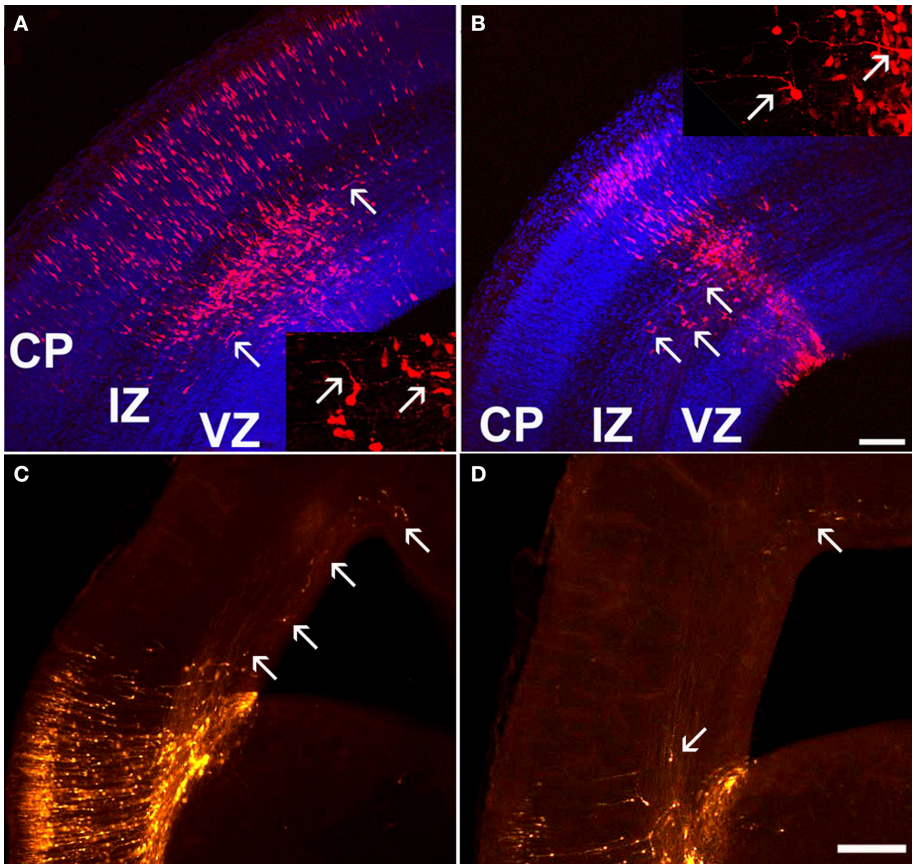

FIGURE 2 | Tangential migration of a few ARX-overexpressing cells in the cortex. (A,B) Examination of coronal sections of E16.5 mouse brains electroporated at E13.5 with an ARX-overexpressing construct. Tangentially orientated cells migrating away from the site of electroporation are detectable in the IZ (see arrows). Some of these cells have long and complex processes, orientated tangentially. **(C,D)** Examination of E18.5 coronal sections of mouse brains electroporated at E13.5 with an ARX-overexpressing construct. Five days after electroporation, the number of tangentially orientated cells observed was reduced, but some had migrated long distances (see arrows). Scale bars: **(A,B)** 100 μm, **(C,D)** 200 μm.

and wild-type slices. Similarly, in Matrigel experiments, *Arx* mutant explants exhibited more than 70% reduction in mean migration distance from the edge of the explant. In addition, the mutant leading processes exhibited an increase in length and branching, further suggesting that *Arx* may regulate the cytoskeleton dynamics during interneuron migration, similar to what was shown for *Dcx* and *Lis1*, two genes responsible for lissencephaly (McManus et al., 2004; Kappeler et al., 2006; Friocourt et al., 2007). It is interesting to note that *Arx* has also been found to be necessary for neuronal migration in the rostral migratory stream, a structure that contains newly generated neurons migrating towards the olfactory bulb (Yoshihara et al., 2005).

Recently, Colasante et al. (2009) performed a gene expression profile analysis comparing E14.5 wild-type and *Arx* mutant ventral telencephalic tissues and identified *Ebf3* among the 35 genes whose expression is consistently altered in *Arx* mutant GE. This gene is normally not (or only marginally) expressed in the developing telencephalon, but it was found strongly misexpressed in the MGE and LGE of *Arx* mutant mice (Colasante et al., 2009). It is also known to be expressed in the developing hindbrain and spinal cord where it promotes neuronal differentiation and radial migration (Garcia-Dominguez et al., 2003). More importantly, these authors observed that electroporation of a construct expressing *Ebf3* into the MGE prevented neuronal tangential migration. Conversely, focal electroporation of a short hairpin RNA (shRNA) targeting *Ebf3* into the MGE of brain slices taken from *Arx* mutants at E14.5 rescued the migration, although only partially. Electroporated cells were found to migrate away from the site of injection and spread following both a radial migration towards the mantle zone of the basal ganglia and a tangential route to the cortex. However, very few cells were able to move through the cortico-striatal boundary and reach the lateral cortex, suggesting that long distance migration capability was not rescued by this means. These results suggest the implication of *Ebf3* in neuronal migration although the underlying mechanisms are still unknown.

ROLE OF *ARX* IN NEURONAL DIFFERENTIATION

Several studies have suggested that *ARX* may play important roles in neuronal maturation and/or differentiation. Indeed, Okazaki et al. (2008) reported the presence of ectopic cells expressing nestin in the SVZ of a patient with XLAG, suggesting some neural maturation defects. Similarly, Colombo et al. (2007) observed that many

immature neurons produced after E11.5 in *Arx* mutants, that had failed to migrate out of the subpallial germinal layers, expressed only weakly MAP2, a marker of differentiated and mature neurons. These cells were also negative for various striatal markers such as *Ebf1* or *enkephalin* mRNAs and calbindin, DARPP32 and dopamine 2 receptor, suggesting that they are unable to differentiate (Colombo et al., 2007). Interestingly, these cells, when dissected from E18.5 LGE and MGE SVZ, expressed MAP2 as well as striatal markers (DARPP32, calbindin, and EBF), suggesting that *Arx* mutant SVZ cells of the LGE are capable of differentiation, and that the maturation defects observed in mutant mice may result from non-adapted local factors in the SVZ.

These observations as well as the high degree of co-localization that exists between Arx and GABA in embryonic and adult brains, and the observation that *Arx* expression is regulated by *Dlx* genes which are strong candidates for regulating the differentiation of most, if not all, telencephalic GABAergic neurons (Stuhmer et al., 2002), have led to the suggestion that Arx might be involved in the specification of the GABAergic phenotype. However, this hypothesis has not been confirmed. In a previous report, we observed that the co-localization of ARX and GABA in cortex or GE is not complete (Friocourt et al., 2008). In particular, we observed that 61–65% of ARX-positive cells expressed GABA and 58–72% of GABAergic cells expressed ARX in dissociated cultures from E16 striatum. Moreover, ARX overexpression in cortical progenitors *in vivo* or in dissociated cultures from E16 rat cortex or GE does not induce GABA or calbindin expression, suggesting that even if *ARX* is involved in GABAergic specification, it does not appear to be sufficient by itself to induce the GABAergic phenotype and thus, it may act in combination with other genes (Friocourt et al., 2008). In addition, the observation that the introduction of an ARX-overexpressing construct into the VZ of the dorsal telencephalon induces tangential migration within the IZ, although these cells do not express GABA (**Figure 2**), suggests that *ARX* may be involved in migration rather than cell specification or differentiation. These results are further reinforced by recent findings which show that Arx re-expression in a *Dlx1/2* mutant background is sufficient to rescue neuronal migration activity. In contrast, *Dlx2* electroporation in *Arx*-deficient brain slices induces GAD65 expression, suggesting that Arx is necessary to promote Dlx-dependent GABAergic cell migration, but is dispensable for Dlx ability to induce GABAergic cell fate commitment (Colasante et al., 2008).

However, it is still possible that *ARX* controls the specification of distinct subsets of GABAergic neurons in the subpallium. Indeed, different studies have reported a decrease in the number of cholinergic neurons in the basal forebrain of *Arx* mutants (Kitamura et al., 2002; Colombo et al., 2007), suggesting that *ARX*, uniquely or in combination with other transcription factors, may play a role in the specification of at least this subpopulation of GABAergic cells. In addition, the observation that ARX is still expressed in GABAergic cells in the mouse adult brain suggests that it may also have a role in more mature neurons. Interestingly, using a genome-wide transcriptomic screen to identify transcriptional changes in the subpallium between wild-type and *Arx* mutant mice, two recent studies isolated genes encoding calbindin and calretinin as up-regulated, suggesting that Arx may repress the expression of these genes (Fulp et al., 2008; Colasante et al., 2009). However, it is also possible that, in the case of calbindin, this up-regulation may result from the accumulation of interneurons which fail to reach the cortex, and that calbindin is not a direct target of Arx. On the contrary, the *Lhx7/8* gene, which is required for cholinergic differentiation and maturation, was found down-regulated in *Arx* mutant striatum, suggesting that Arx normally promotes cholinergic neuron differentiation through the activation of this gene (Colasante et al., 2009).

Recently, Kitamura et al. (2009) published 3 knock-in mice for mutations found in human: P353L (a mutation responsible for XMESID), P353R (a mutation responsible for XLAG), as well as $(GCG)_{+7}$ (expansion in the first polyalanine tract). They observed that the phenotype of the Arx^{P353R} mutant mice is quite severe and very similar to *Arx*-null mice (Kitamura et al., 2002; Colombo et al., 2007). Similarly, the abnormal cortical layer formation, abnormal structure of the striatum, and deficiency of GABAergic neurons in the cortex and striatum caused by P353R mutation closely mimic XLAG (Bonneau et al., 2002; Okazaki et al., 2008). In contrast, the two other mutant lines survived and had milder phenotypes: mice with the $(GCG)_{+7}$ mutation showed severe seizures and impaired learning performance, whereas mice with the P355L mutation exhibited mild seizures and only slightly impaired learning performance. All these mutants exhibited fewer GABAergic and cholinergic neurons in the striatum, medial septum and ventral forebrain nuclei when compared with wild-type mice (**Table 2**).

Interestingly, the severity of the phenotype, as well as the decrease in specific GABAergic subpopulations in mutant brains, seem to correlate quite well with the decreased ability of transcriptional repression (**Figure 3**), suggesting that even subtle transcriptional changes may be a potential basis for the neurological symptoms and cognitive impairment observed in the patients.

PATHOPHYSIOLOGY OF PHENOTYPES RESULTING FROM *ARX* MUTATIONS

To test the hypothesis that the epilepsy phenotype observed in children with *ARX* mutations results primarily from a deficit in forebrain cerebral cortical interneuron function, Marsh and colleagues recently generated a mouse line with a genetic ablation of *Arx* specifically in subpallial derived neurons (Marsh et al., 2009). They found that both male and female mutant mice demonstrated early onset epilepsy resembling the one observed in patients with *ARX* mutations. Although the postnatal brains of these mutant mice appeared grossly normal, they identified interneuron subtype specific defects, again suggesting that *Arx* is necessary for the development of specific populations of interneurons in mice (**Table 2**). The finding that these mutant mice, who have an *Arx* expression left intact in the developing neocortex, recapitulate many key characteristics of *ARX*-related disorders, suggests a critical role for interneurons in the pathogenesis of epilepsy in these patients and strongly support the concept of "interneuronopathy" (Kato and Dobyns, 2005), as the cause of epilepsy, specifically infantile spasms. The proposed pathophysiological mechanism of the observed phenotype in these animals is thus a specific loss of interneurons resulting in an overall increase in excitation.

Indeed GABA, the principal inhibitory neurotransmitter, has been shown to synchronize activity in cortical neuronal circuits, reduce cell hyperexcitability, and prevent epileptiform activity

Table 2 | Summary of the defects reported by studies on different *Arx* mutant lines. The percentages of cells are expressed by comparison to the number of cells in wild-type mice.

Tangential migration from MGE to ctx (Kitamura et al., 2009)	*Arx* KO	E12.5: no initiation of migration	E14.5: stream only in the SVZ	P0: no ARX+ in CP
	Arx P353R	E12.5: no initiation of migration	E14.5: stream only in the SVZ	P0: 28.5% ARX+ in CP
	Arx P353L	E12.5: Initiation of migration	E14.5: streams OK	P0: 92.8% ARX+ in CP
	Arx (GCG) + 7	E12.5: Initiation of migration	E14.5: streams OK	P0: 88.4% ARX+ in CP
Radial + tangential migration in striatum (P0) (Kitamura et al., 2009)	*Arx* KO	Thickened SVZ in striatum		Defect in radial migration
		Loss of GABAergic interneurons in striatum		Defect in tangential migration
	Arx P353R	VZ + SVZ thicker (ARX+/MAP2$^-$)		Defect in radial migration
		Accumulation of SST+ cells in SVZ of ventral striatum, No SST cell in the mantle zone of the striatum		Defect in tangential migration
				Normal radial migration
	Arx P353L	No increase in VZ/SVZ thickness		Defect in tangential migration
		↓ Number of SST+ cells in the mantle zone of the striatum		Normal radial migration
	Arx (GCG) + 7	No increase in VZ/SVZ thickness		Defect in tangential migration
		Most of SST+cells visible in the VZ of the striatum		
Radial migration in ctx (P0) (Kitamura et al., 2009)	*Arx* KO	Thinner CP without severe abnormal structure		Defect in radial migration
	Arx P353R	Tbr1+ deep layer a bit bigger,		Defect in radial migration
		Foxp1+ middle layer abnormal,		
		Satb2+ upper layer thinner		
	Arx P353L	No difference with wild-type		Normal radial migration
	Arx (GCG) + 7	No difference with wild-type		Normal radial migration
Cholinergic neuron differentiation (Kitamura et al., 2009; Price et al., 2009)	*Arx* KO	No ChAT+ cells in the forebrain		
	Arx P353R	No Lhx8 expression at P0		
	Arx P353L	Slight ↓ of Lhx8 expression		
	Arx (GCG) + 7	No Lhx8 expression at P0		
		Severe loss of ChAT+ cells in basal ganglia, 39% in striatum		
		Somatosensory cortex	**Striatum**	
↓ of GABAergic neurons (4–6 weeks post-natal) (Kitamura et al., 2009; Marsh et al., 2009; Price et al., 2009)	*Arx* KO	Absence of NPY+ cells	Loss of NPY+ cells	
		↓↓ in CB+ cells		
		↓CR+ cells		
		No change in PV+ cells		
	Arx P353L	92.7% GAD67+	45% NOS+	
		74% SST+	47.8% SST+	
		100% NPY+	60% MPY+	
		100% PV+	85.2% PV+	
	Arx (GCG) + 7	87.5% GAD67+	45% NOS+	
		100% SST+	52.4% SST+	
		100% NPY+	60–69% NPY+	
		81–100% PV+	70.6% PV+	
		100% CR+		
		58% CB+	47% CB+	
		58–100%ARX+		

Ctx, cortex; KO, knock-out; SST, somatostatin; VZ, ventricular zone; SVZ, subventricular zone; CP, cortical plate; ChAT, choline acetyltransferase; CB, calbindin; CR, calretinin; PV, parvalbumin; NOS, nitric oxide synthase.

in the cerebral cortex and hippocampus. In the developing and newborn rodent brains, it has been shown that this neurotransmitter was excitatory (for review, see Represa and Ben-Ari, 2005). This excitatory action is supposed to play important roles during brain maturation and may transiently regulate neuronal growth, cell proliferation in the germinative zones, neuronal migration and cell differentiation (for reviews, see Represa and Ben-Ari, 2005; Heng et al., 2007). Abnormalities of GABAergic function have already been associated with epilepsy in humans and subcortical structures rich in GABAergic neurons, such as the basal ganglia, have also been implicated in the generation of epileptic spasms (for review, see Dulac, 2001). So, in conclusion, although the precise mechanisms of action of *ARX* and the signalling pathways involved are still unknown, both the descriptions of the patient clinical conditions and the GABAergic defects characterized in different *Arx* mutant lines strongly suggest a functional impairment of GABAergic interneurons in the basal ganglia as the major cause of *ARX*-related phenotypes.

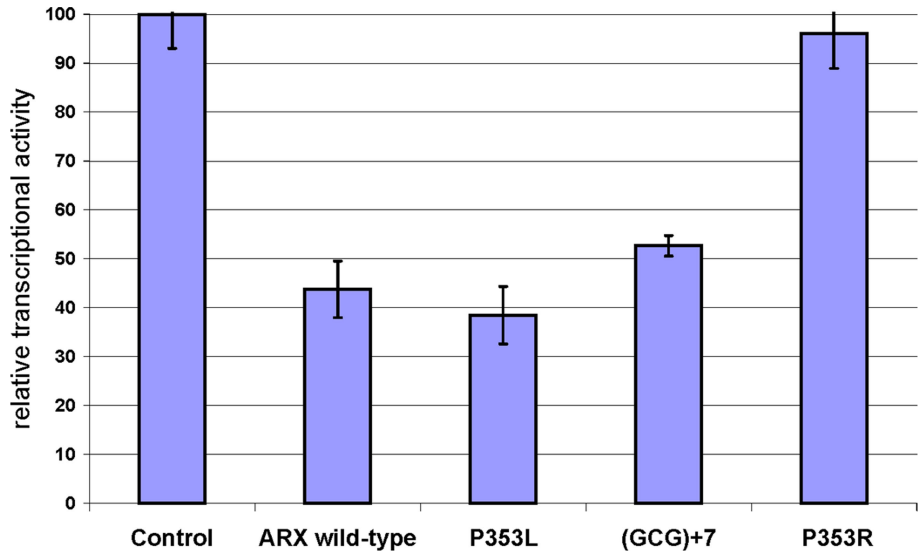

FIGURE 3 | Measure of the transcriptional repression capacity of different *ARX* mutants corresponding to identified mutations in human. The capacity of transcriptional repression of mutant forms of *ARX* was tested on *Lmo1* enhancer, which was cloned upstream TK-luciferase in a similar design as Fulp et al. (2008). *ARX* wild-type or mutant constructs were transfected in Neuro2a cells and the luciferase activity was measured. Luciferase data were normalized to Renilla expression and data are presented as the percentage of transcriptional activity compared to an empty vector control. Although P353L mutation does not have a detectable effect on ARX transcriptional repression, (GCG) + 7 and P353R both decrease ARX capacity to repress expression of the reporter gene.

ACKNOWLEDGMENTS

We wish to thank the Inserm, Fondation Bettencourt-Schueller, Fondation Jerome Lejeune, le Fonds Européen de Développement Régional and the Wellcome Trust (grant number 074549) for support of the work on *ARX*. We also acknowledge the valuable collaboration of Dr S. Kanatani and his colleagues in many of our experiments.

REFERENCES

Absoud, M., Parr, J. R., Halliday, D., Pretorius, P., Zaiwalla, Z., and Jayawant, S. (2009). A novel ARX phenotype: rapid neurodegeneration with Ohtahara syndrome and a dyskinetic movement disorder. *Dev. Med. Child. Neurol.* [Epub ahead of print].

Albrecht, A., and Mundlos, S. (2005). The other trinucleotide repeat: polyalanine expansion disorders. *Curr. Opin. Genet. Dev.* 15, 285–293.

Ayala, R., Shu, T., and Tsai, L. H. (2007). Trekking across the brain: the journey of neuronal migration. *Cell* 128, 29–43.

Bienvenu, T., Poirier, K., Friocourt, G., Bahi, N., Beaumont, D., Fauchereau, F., Ben Jeema, L., Zemni, R., Vinet, M. C., Francis, F., Couvert, P., Gomot, M., Moraine, C., van Bokhoven, H., Kalscheuer, V., Frints, S., Gecz, J., Ohzaki, K., Chaabouni, H., Fryns, J. P., des Portes, V., Beldjord, C., and Chelly, J. (2002). ARX, a novel Prd-class-homeobox gene highly expressed in the telencephalon, is mutated in X-linked mental retardation. *Hum. Mol. Genet.* 11, 981–991.

Biressi, S., Messina, G., Collombat, P., Tagliafico, E., Monteverde, S., Benedetti, L., Cusella De Angelis, M. G., Mansouri, A., Ferrari, S., Tajbakhsh, S., Broccoli, V., and Cossu, G. (2008). The homeobox gene Arx is a novel positive regulator of embryonic myogenesis. *Cell Death Differ.* 15, 94–104.

Bonneau, D., Toutain, A., Laquerrière, A., Marret, S., Saugier-Veber, P., Barthez, M. A., Radi, S., Biran-Mucignat, V., Rodriguez, D., and Gélot, A. (2002). X-linked lissencephaly with absent corpus callosum and ambigous genitalia (XLAG): clinical, magnetic resonance imaging, and neuropathological findings. *Ann. Neurol.* 51, 340–349.

Brown, S. A., Warburton, D., Brown, L. Y., Yu, C., Roeder, E. R., Stengel-Rutkowski, S., Hennekam, R. C. M., and Muenke, M. (1998). Holoprosencephaly due to mutations in ZIC2, a homologue of Drosophila odd-paired. *Nat. Genet.* 20, 180–183.

Chelly, J., and Mandel, J. L. (2001). Monogenic causes of X-linked mental retardation. *Nat. Rev. Genet.* 2, 669–680.

Chen, L., Melendez, J., Campbell, K., Kuan, C. Y., and Zheng, Y. (2009). Rac1 deficiency in the forebrain results in neural progenitor reduction and microcephaly. *Dev. Biol.* 325, 162–170.

Cobos, I., Broccoli, V., and Rubenstein, J. L. (2005). The vertebrate ortholog of Aristaless is regulated by Dlx genes in the developing forebrain. *J. Comp. Neurol.* 483, 292–303.

Colasante, G., Collombat, P., Raimondi, V., Bonanomi, D., Ferrai, C., Maira, M., Yoshikawa, K., Mansouri, A., Valtorta, F., Rubenstein, J. L., and Broccoli, V. (2008). Arx is a direct target of Dlx2 and thereby contributes to the tangential migration of GABAergic interneurons. *J. Neurosci.* 28, 10674–10686.

Colasante, G., Sessa, A., Crispi, S., Calogero, R., Mansouri, A., Collombat, P., and Broccoli, V. (2009). Arx acts as a regional key selector gene in the ventral telencephalon mainly through its transcriptional repression activity. *Dev. Biol.* 334, 59–71.

Collombat, P., Mansouri, A., Hecksher-Sorensen, J., Serup, P., Krull, J., Gradwohl, G., and Gruss, P. (2003). Opposing actions of Arx and Pax4 in endocrine pancreas development. *Genes Dev.* 17, 2591–2603.

Colombo, E., Collombat, P., Colasante, G., Bianchi, M., Long, J., Mansouri, A., Rubenstein, J. L., and Broccoli, V. (2007). Inactivation of Arx, the murine ortholog of the X-linked lissencephaly with ambiguous genitalia gene, leads to severe disorganization of the ventral telencephalon with impaired neuronal migration and differentiation. *J. Neurosci.* 27, 4786–4798.

Colombo, E., Galli, R., Cossu, G., Gécz, J., and Broccoli, V. (2004). Mouse orthologue of ARX, a gene mutated in several X-linked forms of mental retardation and epilepsy, is a marker of adult neural stem cells and forebrain GABAergic neurons. *Dev. Dyn.* 231, 631–639.

Demos, M. K., Fullston, T., Partington, M. W., Gécz, J., and Gibson, W. T. (2009). Clinical study of two brothers with a novel 33 bp duplication in the ARX gene. *Am. J. Med. Genet. A* 149A, 1482–1486.

des Portes, V., Pinard, J. M., Billuart, P., Vinet, M. C., Koulakoff, A., Carrie, A., Gelot, A., Dupuis, E., Motte, J., Berwald-Netter, Y., Catala, M., Kahn, A., Beldjord, C., and Chelly, J. (1998). A novel CNS gene required for neuronal migration and involved in X-linked subcortical laminar heterotopia and lissencephaly syndrome. *Cell* 92, 51–61.

Dobyns, W. B., Berry-Kravis, E., Havernick, N. J., Holden, K. R., and Viskochil, D. (1999). X-linked lissencephaly with absent corpus callosum and ambiguous genitalia. *Am. J. Med. Genet.* 86, 331–337.

Dulac, O. (2001). What is West syndrome? *Brain Dev.* 23, 447–452.

Forman, M. S., Squier, W., Dobyns, W. B., and Golden, J. A. (2005). Genotypically defined lissencephalies show distinct pathologies. *J. Neuropathol. Exp. Neurol.* 64, 847–857.

Francis, F., Meyer, G., Fallet-Bianco, C., Moreno, S., Kappeler, C., Socorro, A. C., Tuy, F. P., Beldjord, C., and Chelly, J. (2006). Human disorders of cortical development: from past to present. *Eur. J. Neurosci.* 23, 877–893.

Frints, S. G., Froyen, G., Marynen, P., Willekens, D., Legius, E., and Fryns, J. P. (2002). Re-evaluation of MRX36 family after discovery of an ARX gene mutation reveals mild neurological features of Partington syndrome. *Am. J. Med. Genet.* 112, 427–428.

Friocourt, G., Kanatani, S., Tabata, H., Yozu, M., Takahashi, T., Antypa, M., Raguénès, O., Chelly, J., Férec, C., Nakajima, K., and Parnavelas, J. G. (2008). Cell-autonomous roles of ARX in cell proliferation and neuronal migration during corticogenesis. *J. Neurosci.* 28, 5794–5805.

Friocourt, G., Liu, J. S., Antypa, M., Rakic, S., Walsh, C. A., and Parnavelas, J. G. (2007). Both doublecortin and doublecortin-like kinase play a role in cortical interneuron migration. *J. Neurosci.* 27, 3875–3883.

Friocourt, G., Poirier, K., Rakic´, S., Parnavelas, J. G., and Chelly, J. (2006). The role of ARX in cortical development. *Eur. J. Neurosci.* 23, 869–876.

Fullenkamp, A. N., and El-Hodiri, H. M. (2008). The function of the Aristaless-related homeobox (Arx) gene product as a transcriptional repressor is diminished by mutations associated with X-linked mental retardation (XLMR). *Biochem. Biophys. Res. Commun.* 377, 73–78.

Fullston, T., Brueton, L., Willis, T., Philip, S., MacPherson, L., Finnis, M., Gecz, J., and Morton, J. (2010). Ohtahara syndrome in a family with an ARX protein truncation mutation (c.81C > G/p.Y27X). *Eur. J. Hum. Genet.* 18, 157–162.

Fulp, C. T., Cho, G., Marsh, E. D., Nasrallah, I. M., Labosky, P. A., and Golden, J. A. (2008). Identification of Arx transcriptional targets in the developing basal forebrain. *Hum. Mol. Genet.* 17, 3740–3760.

Galliot, B., and Miller, D. (2000). Origin of anterior patterning. How old is our head? *Trends Genet.* 16, 1–5.

Garcia-Dominguez, M., Poquet, C., Garel, S., and Charnay, P. (2003). Ebf gene function is required for coupling neuronal differentiation and cell cycle exit. *Development* 130, 6013–6025.

Gécz, J., Cloosterman, D., and Partington, M. (2006). ARX: a gene for all seasons. *Curr. Opin. Genet. Dev.* 16, 308–316.

Gécz, J., Shoubridge, C., and Corbett, M. (2009). The genetic landscape of intellectual disability arising from chromosome X. *Trends Genet.* 25, 308–316.

Gleeson, J. G., Allen, K. M., Fox, J. W., Lamperti, E. D., Berkovic, S., Scheffer, I., Cooper, E. C., Dobyns, W. B., Minnerath, S. R., Ross, M. E., and Walsh, C. A. (1998). Doublecortin, a brain-specific gene mutated in human X-linked lissencephaly and double cortex syndrome, encodes a putative signaling protein. *Cell* 92, 63–72.

Guerrini, R., Moro, F., Kato, M., Barkovich, A. J., Shiihara, T., McShane, M. A., Hurst, J., Loi, M., Tohyama, J., Norci, V., Hayasaka, K., Kang, U. J., Das, S., and Dobyns, W. B. (2007). Expansion of the first PolyA tract of ARX causes infantile spasms and status dystonicus. *Neurology* 69, 427–433.

Guerrini R., and Parrini E. (2009). Neuronal migration disorders. *Neurobiol. Dis.* [Epub ahead of print].

Hartmann, H., Uyanik, G., Gross, C., Hehr, U., Lücke, T., Arslan-Kirchner, M., Antosch, B., Das, A. M., and Winkler, J. (2004). Agenesis of the corpus callosum, abnormal genitalia and intractable epilepsy due to a novel familial mutation in the Aristaless-related homeobox gene. *Neuropediatrics* 35, 157–160.

Heng, J. I., Moonen, G., and Nguyen, L. (2007). Neurotransmitters regulate cell migration in the telencephalon. *Eur. J. Neurosci.* 26, 537–546.

Heng, J. I., Nguyen, L., Castro, D. S., Zimmer, C., Wildner, H., Armant, O., Skowronska-Krawczyk, D., Bedogni, F., Matter, J. M., Hevner, R., and Guillemot, F. (2008). Neurogenin 2 controls cortical neuron migration through regulation of Rnd2. *Nature* 455, 114–118.

Hong, S. E., Shugart, Y. Y., Huang, D. T., Shahwan, S. A., Grant, P. E., Hourihane, J. O., Martin, N. D., and Walsh, C. A. (2000). Autosomal recessive lissencephaly with cerebellar hypoplasia is associated with human RELN mutations. *Nat. Genet.* 26, 93–96.

Kappeler, C., Saillour, Y., Baudoin, J. P., Tuy, F. P., Alvarez, C., Houbron, C., Gaspar, P., Hamard, G., Chelly, J., Métin, C., and Francis, F. (2006). Branching and nucleokinesis defects in migrating interneurons derived from doublecortin knockout mice. *Hum. Mol. Genet.* 15, 1387–1400.

Kato, M., Das, S., Petras, K., Kitamura, K., Morohashi, K., Abuelo, D. N., Barr, M., Bonneau, D., Brady, A. F., Carpenter, N. J., Cipero, K. L., Frisone, F., Fukuda, T., Guerrini, R., Iida, E., Itoh, M., Feldman Lewanda, A., Nanba, Y., Oka, A., Proud, V. K., Saugier-Veber, P., Schelley, S. L., Selicorni, A., Shaner, R., Silengo, M., Stewart, F., Sugiyama, N., Toyama, J., Toutain, A., Lia Vargas, A., Yanazawa, M., Zackai, E. H., and Dobyns, W. B. (2004). Mutations of ARX are associated with striking pleiotropy and consistent genotype-phenotype correlation. *Hum. Mutat.* 23, 147–159.

Kato, M., Das, S., Petras, K., Sawaishi, Y., and Dobyns, WB. (2003). Polyalanine expansion of ARX associated with cryptogenic West syndrome. *Neurology* 61, 267–276.

Kato, M., and Dobyns, W. B. (2005). X-linked lissencephaly with abnormal genitalia as a tangential migration disorder causing intractable epilepsy: proposal for a new term, "interneuronopathy". *J. Child Neurol.* 20, 392–397.

Kato, M., Saitoh, S., Kamei, A., Shiraishi, H., Ueda, Y., Akasaka, M., Tohyama, J., Akasaka, N., and Hayasaka, K. (2007). A longer polyalanine expansion mutation in the ARX gene causes early infantile epileptic encephalopathy with suppression-burst pattern (Ohtahara syndrome). *Am. J. Hum. Genet.* 81, 361–366.

Kawauchi, T., Chihama, K., Nabeshima, Y., and Hoshino, M. (2006). Cdk5 phosphorylates and stabilizes p27kip1 contributing to actin organization and cortical neuronal migration. *Nat. Cell Biol.* 8, 17–26.

Keays, D. A., Tian, G., Poirier, K., Huang, G. J., Siebold, C., Cleak, J., Oliver, P. L., Fray, M., Harvey, R. J., Molnár, Z., Piñon, M. C., Dear, N., Valdar, W., Brown, S. D., Davies, K. E., Rawlins, J. N., Cowan, N. J., Nolan, P., Chelly, J., and Flint, J. (2007). Mutations in alpha-tubulin cause abnormal neuronal migration in mice and lissencephaly in humans. *Cell* 128, 45–57.

Kitamura, K., Itou, Y., Yanazawa, M., Ohsawa, M., Suzuki-Migishima, R., Umeki, Y., Hohjoh, H., Yanagawa, Y., Shinba, T., Itoh, M., Nakamura, K., and Goto, Y. (2009). Three human ARX mutations cause the lissencephaly-like and mental retardation with epilepsy-like pleiotropic phenotypes in mice. *Hum. Mol. Genet.* 18, 3708–3724.

Kitamura, K., Yanazawa, M., Sugiyama, N., Miura, H., Iizuka-Kogo, A., Kusaka, M., Omichi, K., Suzuki, R., Kato-Fukui, Y., Kamiirisa, K., Matsuo, M., Kamijo, S. I., Kasahara, M., Yoshioka, H., Ogata, T., Fukuda, T., Kondo, I., Kato, M., Dobyns, W. B., Yokoyama, M., and Morohashi, K. I. (2002). Mutation of ARX causes abnormal development of forebrain and testes in mice and X-linked lissencephaly with abnormal genitalia in humans. *Nat. Genet.* 32, 359–369.

Kriegstein, A. R., and Noctor, S. C. (2004). Patterns of neuronal migration in the embryonic cortex. *Trends Neurosci.* 27, 392–399.

Laperuta, C., Spizzichino, L., D'Adamo, P., Monfregola, J., Maiorino, A., D'Eustacchio, A., Ventruto, V., Neri, G., D'Urso, M., Chiurazzi, P., Ursini, M. V., and Miano, M. G. (2007). MRX87 family with Aristaless X dup24bp mutation and implication for polyAlanine expansions. *BMC Med. Genet.* 8, 25.

López-Bendito, G., Cautinat, A., Sánchez, J. A., Bielle, F., Flames, N., Garratt, A. N., Talmage, D. A., Role, L. W., Charnay, P., Marín, O., and Garel, S. (2006). Tangential neuronal migration controls axon guidance: a role for neuregulin-1 in thalamocortical axon navigation. *Cell* 125, 127–142.

LoTurco, J. J., and Bai, J. (2006). The multipolar stage and disruptions in neuronal migration. *Trends Neurosci.* 29, 407–413.

Marin, O., and Rubenstein, J. L. (2003). Cell migration in the forebrain. *Annu. Rev. Neurosci.* 26, 441–483.

Marsh, E., Fulp, C., Gomez, E., Nasrallah, I., Minarcik, J., Sudi, J., Christian, S. L., Mancini, G., Labosky, P., Dobyns, W., Brooks-Kayal, A., and Golden, J. A. (2009). Targeted loss of Arx results in a developmental epilepsy mouse model and recapitulates the human phenotype in heterozygous females. *Brain* 132, 1563–1576.

McKenzie, O., Ponte, I., Mangelsdorf, M., Finnis, M., Colasante, G., Shoubridge, C., Stifani, S., Gécz, J., and Broccoli V. (2007). Aristaless-related homeobox gene, the gene responsible for West syndrome and related disorders, is a Groucho/transducin-like enhancer of split dependent transcriptional repressor. *Neuroscience* 146, 236–247.

McManus, M. F., Nasrallah, I. M., Pancoast, M. M., Wynshaw-Boris, A., and Golden, J. A. (2004). Lis1 is necessary for normal non-radial migration of inhibitory interneurons. *Am. J. Pathol.* 165, 775–784.

Meijlink, F., Beverdam, A., Brouwer, A., Oosterveen, T. C., and Berge, D. T. (1999). Vertebrate aristaless-related genes. *Int. J. Dev. Biol.* 43, 651–663.

Métin, C., Baudoin, J. P., Rakic, S. and Parnavelas, J. G. (2006). Cell and molecular mechanisms involved in the migration of cortical interneurons. *Eur. J. Neurosci.* 23, 894–900.

Miura, H., Yanazawa, M., Kato, K., and Kitamura, K. (1997). Expression of a

novel aristaless related homeobox gene '*Arx*' in the vertebrate telencephalon, diencephalon and floor plate. *Mech. Dev.* 65, 99–109.

Nadarajah, B., and Parnavelas, J. G. (2002). Modes of neuronal migration in the developing cerebral cortex. *Nat. Rev. Neurosci.* 3, 423–432.

Nagano, T., Morikubo, S., and Sato, M. (2004). Filamin A and FILIP (Filamin A-Interacting Protein) regulate cell polarity and motility in neocortical subventricular and intermediate zones during radial migration. *J. Neurosci.* 24, 9648–9657.

Nasrallah, I. M., Minarcik, J. C., and Golden, J. A. (2004). A polyalanine tract expansion in Arx forms intranuclear inclusions and results in increased cell death. *J. Cell Biol.* 167, 411–416.

Ogata, T., Matsuo, N., Hiraoka, N., and Hata, J. I. (2000). X-linked lissencephaly with ambiguous genitalia: delineation of further case. *Am. J. Med. Genet.* 94, 174–176.

Okazaki, S., Ohsawa, M., Kuki, I., Kawawaki, H., Koriyama, T., Ri, S., Ichiba, H., Hai, E., Inoue, T., Nakamura, H., Goto, Y., Tomiwa, K., Yamano, T., Kitamura, K., and Itoh, M. (2008). Aristaless-related homeobox gene disruption leads to abnormal distribution of GABAergic interneurons in human neocortex: evidence based on a case of X-linked lissencephaly with abnormal genitalia (XLAG). *Acta Neuropathol.* 116, 453–462.

Partington, M. W., Turner, G., Boyle, J., and Gécz, J. (2004). Three new families with X-linked mental retardation caused by the 428-451dup(24bp) mutation in ARX. *Clin. Genet.* 66, 39–45.

Pearson, J. C., Lemons, D., and McGinnis, W. (2005). Modulating Hox gene functions during animal body patterning. *Nat. Rev. Genet.* 6, 893–904.

Poirier, K., Van Esch, H., Friocourt, G., Saillour, Y., Bahi, N., Backer, S., Souil, E., Castelnau-Ptakhine, L., Beldjord, C., Francis, F., Bienvenu, T., and Chelly, J. (2004). Neuroanatomical distribution of ARX in brain and its localisation in GABAergic neurons. *Mol. Brain Res.* 122, 35–46.

Price, M. G., Yoo, J. W., Burgess, D. L., Deng, F., Hrachovy, R. A., Frost, J. D. Jr., and Noebels, J. L. (2009). A triplet repeat expansion genetic mouse model of infantile spasms syndrome, Arx(GCG)10 + 7, with interneuronopathy, spasms in infancy, persistent seizures, and adult cognitive and behavioral impairment. *J. Neurosci.* 29, 8752–8763.

Rakic, P. (1990). Principles of neural cell migration. *Experientia* 46, 882–891.

Reiner, O., Carrozzo, R., Shen, Y., Wehnert, M., Faustinella, F., Dobyns, W. B., Caskey, C. T., and Ledbetter, D. H. (1993). Isolation of a Miller-Dieker lissencephaly gene containing G protein beta-subunit-like repeats. *Nature* 364, 717–721.

Reish, O., Fullston, T., Regev, M., Heyman, E., and Gecz, J. (2009). A novel de novo 27 bp duplication of the ARX gene, resulting from postzygotic mosaicism and leading to three severely affected males in two generations. *Am. J. Med. Genet. A* 149A, 1655–1660.

Represa, A., and Ben-Ari, Y. (2005). Trophic actions of GABA on neuronal development. *Trends Neurosci.* 28, 278–283.

Sapir, T., Sapoznik, S., Levy, T., Finkelshtein, D., Shmueli, A., Timm, T., Mandelkow, E. M., and Reiner, O. (2008). Accurate balance of the polarity kinase MARK2/Par-1 is required for proper cortical neuronal migration. *J. Neurosci.* 28, 5710–5720.

Scheffer, I. E., Wallace, R. H., Phillips, F. L., Hewson, P., Reardon, K., Parasivam, G., Stromme, P., Berkovic, S. F., Gecz, J., and Mulley, J. C. (2002). X-linked myoclonic epilepsy with spasticity and intellectual disability: mutation in the homeobox gene *ARX*. *Neurology* 59, 348–356.

Seufert, D. W., Prescott, N. L., and El-Hodiri, H. M. (2005). Xenopus aristaless-related homeobox (xARX) gene product functions as both a transcriptional activator and repressor in forebrain development. *Dev. Dyn.* 232, 313–324.

Sherr, E. H. (2003). The ARX story (epilepsy, mental retardation, autism, and cerebral malformations): one gene leads to many phenotypes. *Curr. Opin. Pediatr.* 15, 567–571.

Shoubridge, C., Cloosterman, D., Parkinson-Lawerence, E., Brooks, D., and Gécz, J. (2007). Molecular pathology of expanded polyalanine tract mutations in the Aristaless-related homeobox gene. *Genomics* 90, 59–71.

Strømme, P., Mangelsdorf, M. E., Scheffer, I. E., and Gecz, J. (2002). Infantile spasms, dystonia, and other X-linked phenotypes caused by mutations in Aristaless related homeobox gene, *ARX*. *Brain Dev.* 24, 266–268.

Stuhmer, T., Anderson, S. A., Ekker, M., and Rubenstein, J. L. (2002). Ectopic expression of the Dlx genes induces glutamic acid decarboxylase and Dlx expression. *Development* 129, 245–252.

Szczaluba, K., Nawara, M., Poirier, K., Pilch, J., Gajdulewicz, M., Spodar, K., Chelly, J., Bal, J., and Mazurczak, T. (2006). Genotype–phenotype associations for ARX gene duplication in X-linked mental retardation. *Neurology* 67, 2073–2075.

Tabata, H., and Nakajima, K. (2003). Multipolar migration: the third mode of radial neuronal migration in the developing cerebral cortex. *J. Neurosci.* 23, 9996–10001.

Turner, G., Partington, M., Kerr, B., Mangelsdorf, M., and Gecz, J. (2002). Variable expression of mental retardation, autism, seizures, and dystonic hand movements in two families with an identical ARX gene mutation. *Am. J. Med. Genet.* 112, 405–411.

Uyanik, G., Aigner, L., Martin, P., Gross, C., Neumann, D., Marschner-Schäfer, H., Hehr, U., and Winkler, J. (2003). ARX mutations in X-linked lissencephaly with abnormal genitalia. *Neurology* 61, 232–235.

Van Esch, H., Poirier, K., de Zegher, F., Holvoet, M., Bienvenu, T., Chelly, J., Devriendt, K., and Fryns, J. P. (2004). ARX mutation in a boy with transsphenoidal encephalocele and hypopituitarism. *Clin. Genet.* 65, 503–505.

Wallerstein, R., Sugalski, R., Cohn, L., Jawetz, R., and Friez, M. (2008). Expansion of the ARX spectrum. *Clin. Neurol. Neurosurg.* 110, 631–634.

Wigle, J. T., and Eisenstat, D. D. (2008). Homeobox genes in vertebrate forebrain development and disease. *Clin. Genet.* 73, 212–226.

Yoshihara, S., Omichi, K., Yanazawa, M., Kitamura, K., and Yoshihara, Y. (2005). Arx homeobox gene is essential for development of mouse olfactory system. *Development* 132, 751–762.

Conflict of Interest Statement: The authors declare that the research was conducted in the absence of any commercial or financial relationships that could be construed as a potential conflict of interest.

Received: 08 February 2010; paper pending published: 21 February 2010; accepted: 24 February 2010; published online: 11 March 2010.

Citation: Friocourt G and Parnavelas JG (2010) Mutations in ARX result in several defects involving GABAergic neurons. Front. Cell. Neurosci. ***4****:4. doi: 10.3389/fncel.2010.00004*

frontiers in
CELLULAR NEUROSCIENCE

PERSPECTIVE ARTICLE
published: 31 March 2010
doi: 10.3389/fncel.2010.00009

Inhibitory "noise"

Alain Destexhe*

Unité de Neurosciences, Infomation et Complexité, Centre National de la Recherche Scientifique, Gif-sur-Yvette, France

Edited by:
Yehezkel Ben-Ari, INSERM, France

Reviewed by:
Dominique Debanne,
Université de la Méditerranée, France

****Correspondence:***
Alain Destexhe,
Unité de Neurosciences, Infomation et Complexité, Bat 33, Centre National de la Recherche Scientifique, 1 Avenue de la Terrasse, 91198 Gif-sur-Yvette, France.
e-mail: destexhe@unic.cnrs-gif.fr

Cortical neurons *in vivo* may operate in high-conductance states, in which the major part of the neuron's input conductance is due to synaptic activity, sometimes several-fold larger than the resting conductance. We examine here the contribution of inhibition in such high-conductance states. At the level of the absolute conductance values, several studies have shown that cortical neurons *in vivo* are characterized by strong inhibitory conductances. However, conductances are balanced and spiking activity is mostly determined by fluctuations, but not much is known about excitatory and inhibitory contributions to these fluctuations. Models and dynamic-clamp experiments show that, during high-conductance states, spikes are mainly determined by fluctuations of inhibition, or by inhibitory "noise". This stands in contrast to low-conductance states, in which excitatory conductances determine spiking activity. To determine these contributions from experimental data, maximum likelihood methods can be designed and applied to intracellular recordings *in vivo*. Such methods indicate that action potentials are indeed mostly correlated with inhibitory fluctuations in awake animals. These results argue for a determinant role for inhibitory fluctuations in evoking spikes, and do not support feed-forward modes of processing, for which opposite patterns are predicted.

Keywords: spike-triggered average, conductance, cerebral cortex, dynamic-clamp, computational models

INTRODUCTION

In awake and aroused animals, the cerebral cortex displays low-amplitude and fast electroencephalogram (EEG) activity, which is usually referred to as "desynchronized EEG states" or "activated states". In such states, it was shown that cortical neurons are characterized by very irregular and asynchronous firing activity, which contrasts with the synchronized and slow oscillatory activities seen during slow-wave sleep (Hubel, 1959; Evarts, 1964; Steriade et al., 1974; Destexhe et al., 1999). Because it is during this regime that the main computational tasks are performed, understanding this type of stochastic network state is crucial (Destexhe and Contreras, 2006).

Intracellular measurements in awake animals (Woody and Gruen, 1978; Matsumura et al., 1988; Baranyi et al., 1993; Steriade et al., 2001; Timofeev et al., 2001; Rudolph et al., 2007) have shown that cortical neurons are depolarized (about −60 mV), have a low input resistance and their membrane potential (V_m) is subject to intense fluctuations. These properties were collectively defined as "high-conductance state" (reviewed in Destexhe et al., 2003; Destexhe, 2007), due to the fact that the total membrane conductance is several-fold larger than the resting membrane conductance. High-conductance states are important, because they have a very significant impact on several fundamental integrative properties of neurons, such as the summation of inputs, the temporal precision of the integration, the cell excitability and the global "transfer function" of the neuron (Wolfart et al., 2005; reviewed in Destexhe et al., 2003; Destexhe, 2007).

Various studies in behaving or anesthetized animals have demonstrated the presence of high conductances during either spontaneous activity (Paré et al., 1998; Rudolph et al., 2005, 2007) or responses to sensory inputs (Borg-Graham et al., 1998; Anderson et al., 2000; Monier et al., 2003; Wehr and Zador, 2003; Wilent and Contreras, 2005). Such conductances are usually decomposed from current–voltage relations, into excitatory and inhibitory components, and it was shown that the temporal interplay of excitation and inhibition is determinant to explain the responses of cortical neurons to sensory inputs as well as their selectivity to features such as orientation or direction (Monier et al., 2003; Wehr and Zador, 2003; Wilent and Contreras, 2005).

In parallel to these investigations, it was also shown that the desynchronized and irregular activity of cortical networks is characterized by a balance of excitation and inhibition. In such "balanced states", it is not the absolute conductances that determine the spiking activity, but it is the fluctuations of these conductances (van Vreeswijk and Sompolinsky, 1996; Brunel, 2000). In such fluctuations-driven states, it is thus important to characterize the fluctuations of excitation and inhibition rather than their absolute (or mean) values. Unfortunately, this aspect remains under-characterized in part because of the lack of appropriate methods to characterize conductance fluctuations.

In the present paper, we focus on the measurement and consequences of conductance fluctuations, and in particular for inhibition. We first review techniques to measure conductance fluctuations and the values measured from intracellular recordings *in vivo*. Next, using models and dynamic-clamp experiments, we show that fluctuations of inhibition can be particularly impactful on evoking spikes. We finish by providing evidence that, indeed, this "inhibitory noise" is determinant in awake animals.

METHODS TO CHARACTERIZE CONDUCTANCE FLUCTUATIONS

In contrast to the measurement of mean conductances, for which several methods are possible and were used to measure conductances from experimental data (see Introduction for overview), few

methods are available to estimate the conductance fluctuations. Such information can be obtained from the trial-to-trial variability of sensory responses (see Monier et al., 2008 for a discussion), or using direct methods as we review here. A direct method was proposed to estimate the conductance fluctuations from the fluctuations of the V_m activity. This "VmD method" (Rudolph et al., 2004) consists of measuring the V_m distributions from experiments and fitting these measurements to an analytic expression obtained by a theoretical study in which the V_m is described by stochastic processes (Rudolph and Destexhe, 2003, 2005). Several theoretical studies have focused on the subthreshold V_m fluctuations of a neuron subject to fluctuating conductances g_e and g_i (for excitation and inhibition, respectively). Different analytic approximations have been proposed to describe the steady-state distribution of these V_m fluctuations (Rudolph and Destexhe, 2003, 2005; Richardson, 2004; Lindner and Longtin, 2006; for a comparative study, see Rudolph and Destexhe, 2006). One of these expressions is invertible (Rudolph and Destexhe, 2003, 2005), which enables one to directly estimate the parameters (g_{e0}, g_{i0}, σ_e, σ_i) from experimentally calculated V_m distributions. This constitutes the basis of the VmD method (Rudolph et al., 2004).

One main assumption behind this method is that the conductances variations are Gaussian-distributed, and thus this distribution can be described by the mean (g_{e0}, g_{i0}) and the standard deviations (σ_e, σ_i) for each conductance. Assuming that the V_m fluctuations are also Gaussian-distributed,

$$\rho(V) \sim \exp\left[-\frac{(V-\bar{V})^2}{2\sigma_V^2}\right] \quad (1)$$

where $\bar{V}$ is the average V_m and σ_V its standard deviation. This expression provides an excellent approximation of the V_m distributions obtained from models and experiments (Rudolph et al., 2004), because the V_m distributions obtained experimentally show little asymmetry (for up-states and activated states; for specific examples, see Rudolph et al., 2004, 2005, 2007).

One main advantage of this Gaussian approximation is that it can be inverted, which leads to expressions of the synaptic noise parameters as a function of the V_m measurements, $\bar{V}$ and σ_V. To extract the four parameters, means (g_{e0}, g_{i0}) and standard deviations (σ_e, σ_i), from the V_m requires to measure two V_m distributions obtained at two different constant levels of injected current. In this case, the Gaussian expression (Eq. 1) of the two distributions gives two mean V_m values, $\bar{V}_1$ and $\bar{V}_2$, and two standard deviation values, σ_{V1} and σ_{V2}. The system can be solved for four unknowns, leading to expressions of g_{e0}, g_{i0}, σ_e, σ_i from the values of $\bar{V}_1$, $\bar{V}_2$, σ_{V1} and σ_{V2} (for details, see Rudolph et al., 2004).

This method was tested using controlled conductance injection in neurons using the dynamic-clamp technique, and was shown to provide excellent estimates of the excitatory and inhibitory conductances and their associated variances (Rudolph et al., 2004). It was also applied to intracellular recordings *in vivo* during anesthetized states (Rudolph et al., 2005) and in awake animals (Rudolph et al., 2007), as reviewed here.

In a first study, recordings were performed in cat association cortex under ketamine-xylazine anesthesia, during the slow oscillation typical of this anesthetic and resembling slow-wave-sleep, as well as during prolonged periods of activity, triggered by brain stem (PPT) stimulation, and with activity similar to that of the aroused brain. The VmD method was used to extract synaptic conductance parameters underlying the V_m fluctuations of the up-states of the slow oscillation, as well as those underlying the activated state following PPT stimulation. In both cases, the average estimated inhibitory conductance g_{i0} was markedly higher than the average estimated excitatory conductance g_{e0}, and similarly the estimated variance of inhibition σ_i^2 was higher than the variance of excitation σ_e^2.

In a second study, similar results were obtained across the natural wake-sleep cycle of the cat (**Figure 1**): for a majority of cells, especially during slow-wave-sleep up-states, inhibition dominated in terms of both mean and variance. At the population level, the ratio of inhibition to excitation was higher during slow-wave-sleep up-states compared to the wake state. In three neurons that were recorded across several states, both average conductances together with their variances decreased in the wake state compared to slow-wave-sleep up-states. In addition, especially during the wake state, some cells displayed comparable excitation and inhibition or even a dominant excitation (2 out of 11 cells in the wake state). This study also reported an important diversity in the absolute values of the estimated conductance parameters.

It is important to note that the estimation of conductances for excitation and inhibition relies on a hypothesis about the value of the resting (leak) conductance which can be estimated in various ways (see Discussion in Piwkowska et al., 2008). However, the variance estimates do not depend on the leak conductance, provided that the total conductance is known, which is usually the case.

IMPACT OF FLUCTUATIONS ON SPIKING ACTIVITY

The conductance measurements outlined above show that there is a diversity of combinations of g_e and g_i that underlies the genesis of subthreshold activity in different cells in the association cortex of awake cats. Indeed, an infinite number of combinations of g_e and g_i can give similar V_m activity. **Figure 2A** illustrates two extreme examples out of this continuum using computational models: first a state where both excitatory and inhibitory conductances are of comparable magnitude (**Figure 2A**, left; "Equal conductances"). In this state, both conductances are lower than the resting conductance of the cell and the V_m is fluctuating around −60 mV. Second, similar V_m fluctuations can be obtained when both conductances are of larger magnitude, but in this case, inhibition has to be augmented several-fold to maintain the V_m around −60 mV (**Figure 2A**, right; "Inhibition-dominated"). Such conductance values are more typical of what is usually measured *in vivo* (Rudolph et al., 2005, 2007; Monier et al., 2008). Both conductances are larger than the resting conductance, a situation which can be described as a "high-conductance state".

To determine how these two states differ in their spike selectivity, we evaluated the spike-triggering conductances by averaging the conductance traces collected in 50-ms windows preceding spikes. This spike-triggered average (STA) pattern of conductance variations is shown in **Figure 2B**. For equal-conductance states, there is an increase of total conductance preceding spikes (purple curve in **Figure 2B**, left), as can be expected from the fact that excitation increases (g_e curve in **Figure 2B**, left). In contrast, for inhibition-dominated states, the total conductance decreases prior to the spike

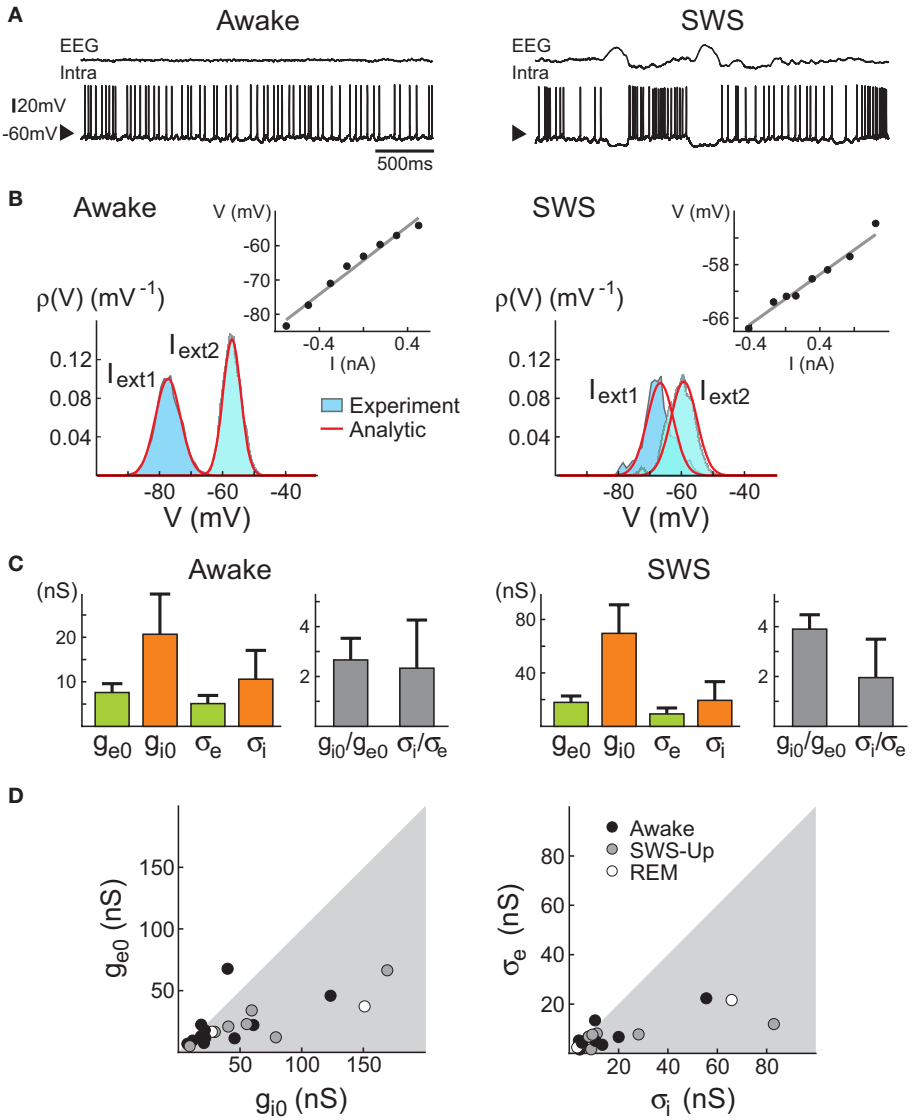

FIGURE 1 | VmD estimation of conductances from intracellular recordings in awake and naturally sleeping cats. (A) Intracellular recordings in awake and naturally sleeping (SWS) cats. Recordings were made in association cortex (area 5–7). **(B)** Examples of V_m distributions computed during wakefulness (Awake) and slow-wave sleep up-states (SWS). The continuous lines show Gaussian fits of the experimental distributions. Insets: current–voltage relations obtained for these particular neurons. **(C)** Conductance values estimated using the VmD method. Results for the means (g_{e0}, g_{i0}) and standard deviations (σ_e, σ_i) of excitatory and inhibitory conductances, respectively, as well as their ratios are shown (error bars: standard deviations obtained by repeating the analysis using different pairs of injected current levels). **(D)** Grouped data showing the means and standard deviations of the conductances for different cells across different behavioral states (REM = Rapid Eye Movement sleep). Figure modified from Rudolph et al. (2007).

(purple curve in **Figure 2B**, right), and this decrease necessarily comes from a similar decrease of inhibitory conductance, which is, in this case, stronger than the increase of excitatory conductance (g_i curve in **Figure 2B**, right). Thus, in such states the spike seems primarily caused by a drop of inhibition.

These patterns of conductance variations preceding spikes were also investigated in real neurons by using dynamic-clamp experiments to inject fluctuating conductances *in vitro*. In this case, performing the same analysis as above revealed similar features: spike-triggered averages (STAs) of the injected conductances displayed either increase or decrease in total conductance, depending on the conductance parameters used (see Piwkowska et al., 2008). It suggested that these features are independent of the spike generating mechanism but rather are caused by subthreshold V_m dynamics.

Further investigation of this system (Piwkowska et al., 2008) led to the conclusion that in an integrate-and-fire neuron with threshold V_t, spikes are associated with increases in total conductance when the following condition is met:

$$\frac{\sigma_e}{\sigma_i} > \sqrt{\frac{V_t - E_i}{E_e - V_t}}$$

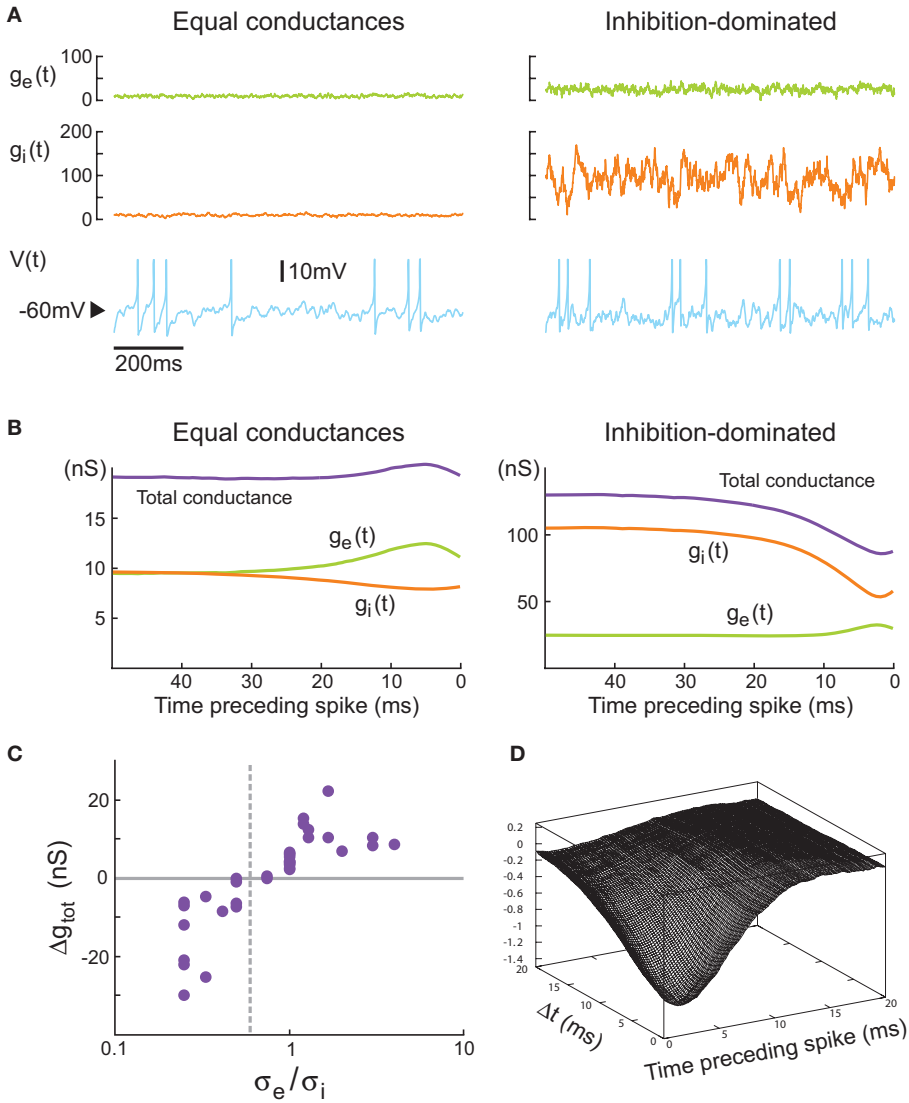

FIGURE 2 | Comparison between equal conductances and inhibition-dominated regimes in models and dynamic-clamp experiments. **(A)** Model with equal conductance (left; $g_{e0} = g_{i0} = 10$ nS, $\sigma_e = \sigma_i = 2.5$ nS) and inhibition-dominated states (right; $g_{e0} = 25$ nS, $g_{i0} = 100$ nS, $\sigma_e = 7$ nS and $\sigma_i = 28$ nS). Excitatory and inhibitory conductances, and the membrane potential, are shown from top to bottom. Action potentials (truncated here) were described by Hodgkin–Huxley type models (Destexhe et al., 2001). **(B)** Average conductance patterns triggering spikes in the model. Spike-triggered averages (STAs) of excitatory, inhibitory and total conductance were computed in a window of 50 ms before the spike. **(C)** Geometrical prediction tested in dynamic-clamp: grouped data showing the total conductance change preceding spikes as a function of the ratio σ_e/σ_i. The dashed line ($\sigma_e/\sigma_i = 0.6$) visualizes the predicted value separating total conductance increase cases from total conductance decrease cases. **(D)** Spike-triggered covariance analysis. The covariance between g_e and g_i (with delay Δt) is represented as a function of the time preceding spike in a dynamic-clamp experiment with inhibition-dominated state. **(A–C)** Modified from Piwkowska et al. (2008), **(D)** unpublished.

where E_e and E_i are the reversal potential for excitation and inhibition, respectively. With the usual values ($V_t = -55$ mV, $E_e = 0$ mV, $E_i = -75$ mV), spikes are associated with increases in total conductance when $\sigma_e > 0.6\sigma_i$ (Piwkowska et al., 2008). This inequality is satisfied in the equal conductances regime and not in the inhibition-dominated regime investigated above.

This conclusion was supported by dynamic-clamp experiments in which these two states were compared using conductance injection (Piwkowska et al., 2008). In eight regular spiking cortical neurons, we scanned different parameter regimes in a total of 36 fluctuating conductance injections. The result of these experiments is displayed in **Figure 2C** where the average total conductance change preceding spikes is represented as a function of the ratio σ_e/σ_i, for all the 36 injections. The vertical dashed line represents the predicted value of $\sigma_e/\sigma_i = 0.6$, which indeed separates all the "conductance drop" configurations from the "conductance increase" configurations. Even though the prediction is based on a simple integrate-and-fire model, the ratio of synaptic variances can predict the sign of the total conductance change triggering spikes in biological cortical neurons subjected to fluctuating excitatory and inhibitory conductances.

Another means of characterization of conductance patterns related to spiking is to calculate the spike-triggered covariance (STC) between g_e and g_i. This covariance, if significant, would allow one to distinguish whether the spike-related increases of g_e and drop of g_i need to be correlated. In other words, is the drop of g_i preceding the spike sufficient to fire the cell, or must this drop occur in conjunction with an increase of g_e. The spike-triggered covariance shows a clear negative correlation between g_e and g_i preceding spikes (**Figure 2D**), suggesting that indeed, the second possibility applies. In contrast, the STC for states with equal conductances did not show significant patterns, suggesting that in this case, the excitation alone is responsible for spiking activity.

In addition, the dynamic-clamp data shows that the average amplitude of change (Δg_e) of each synaptic conductance preceding a spike is related, in a linear way, to the standard deviation of this conductance (Piwkowska et al., 2008). This observation is consistent with the idea that in all the cases studied here, the firing of the cell was driven by fluctuations in the V_m, rather than by a high mean V_m value.

ROLE OF INHIBITORY NOISE *IN VIVO*

The analysis of the preceding section shows that it is not the total conductance that determine the conductance-drop pattern, but the high inhibitory variance – or the high "inhibitory noise" – associated to high-conductance states. This further stresses the need for measuring these features from experimental data.

To estimate the STA of conductances from *in vivo* recordings, one must design methods to extract this information from the V_m activity. We recently designed such a method (Pospischil et al., 2007). The STA of the V_m is calculated first, and the method searches for the "most likely" spike-related conductance time courses ($g_e(t)$, $g_i(t)$) that are compatible with the observed voltage STA. If the conductances are Gaussian-distributed, and if the values of g_{e0}, g_{i0}, σ_e and σ_i are known (as for example following a prior application of the VmD method), then the STA of the V_m can be decomposed into STA of g_e and g_i using a discretization of the time axis (Pospischil et al., 2007). This method was also extended to the case of correlated synaptic conductances (Piwkowska et al., 2008). As for the VmD method, this STA method was successfully tested on models as well as on cortical neurons using dynamic-clamp experiments (see details in Pospischil et al., 2007).

The conductance STA estimation method was used to determine conductance variations preceding spikes during V_m fluctuations *in vivo* (Rudolph et al., 2007). Starting from V_m recordings of spontaneous spiking activity in awake or naturally sleeping cats, we computed the spike-triggered average of the V_m (**Figure 3**). Using values of g_{e0}, g_{i0}, σ_e, σ_i estimated using the VmD method (see above), we computed the most likely conductance traces yielding the observed V_m averages. Most of these analyses (7 out of 10 cells for awake, 6 out of 6 for slow-wave-sleep, 2 out of 2 for REM) revealed conductance dynamics consistent with states dominated by inhibitory variance: there was a drop of the total conductance preceding spikes, due to a strong decrease of the inhibitory conductance (**Figure 3**, right). However, a few cases, in the wake state (3 out of 10 cells), displayed the opposite configuration with the total synaptic conductance increasing before the spike (**Figure 3**, left).

DISCUSSION

In this paper, we have overviewed recent results emphasizing the importance of inhibitory "noise" in cortical neurons. The measurements of excitatory and inhibitory conductances present in different states *in vivo*, in particular in awake animals, show strong conductances in general, as well as strong conductance variances. Because in such balanced states it is the fluctuations that determine spiking activity, it is important to determine which of the conductance fluctuations are most effective in controlling spike activity. The main finding emphasized here is that in most cells recorded, it is the inhibitory fluctuations – or inhibitory noise – that most closely determine spiking activity.

The measurement of the conductance variances is not a simple problem, and different methods have been proposed (Rudolph et al., 2004; Monier et al., 2008). The method illustrated here, the VmD method, is based on decomposing the V_m fluctuations into their excitatory and inhibitory components (σ_e and σ_i) using an analytic expression derived from theoretical work on stochastic processes. The VmD method assumes that the conductances are Gaussian-distributed which seems a reasonable assumption given the large number of inputs involved and the law of large numbers. The VmD analysis reveals that inhibitory noise is generally strong *in vivo* in both anesthetized (up-states) and in awake cats. There was a large diversity of the values measured, with in general dominant inhibition against excitation, for both conductance mean and variances. It is important to note that, contrary to mean conductances, the estimates of σ_e and σ_i do not depend on hypotheses about the leak conductance of the cell.

The role of inhibitory noise was assessed by using spike-triggered averaging methods. Analyses using computational models and dynamic-clamp experiments revealed two different modes of firing according to the conductance patterns involved (Piwkowska et al., 2008). For equal excitatory and inhibitory conductances, spikes are generally associated with a prior increase of total membrane conductance, which is due to an increase of the excitation. In this rather classic regime, the firing is due to an excess of excitation. Another regime is seen when conductances are large (high-conductance state), in which case spikes are preceded by a drop of total membrane conductance. This drop must necessarily come from inhibition, but it is also correlated with an increase of excitation, as shown by the spike-triggered covariance between g_e and g_i (**Figure 2D**). Thus, in this case, the inhibitory fluctuations mostly drive spiking activity and play a permissive role.

These features were predicted by models and also demonstrated in living neurons using dynamic-clamp injection of fluctuating conductances, but it remained to be seen whether these considerations apply to the functioning cerebral cortex *in vivo*. This motivated the development of new methods to determine STA of conductances from V_m recordings (Pospischil et al., 2007). This method uses a maximum likelihood procedure to determine conductance STAs, also based on stochastic processes. The hypothesis is similar to that of the VmD method, the conductance fluctuations are assumed to be Gaussian-distributed. This method was applied to intracellular recordings in awake cats (Rudolph et al., 2007) and showed evidence that spikes are preceded by a drop of membrane conductance, thus arguing for the second firing mode dominated by inhibitory fluctuations. A prominent role for inhibition is also supported by previous intracellular recordings demonstrating a time locking of

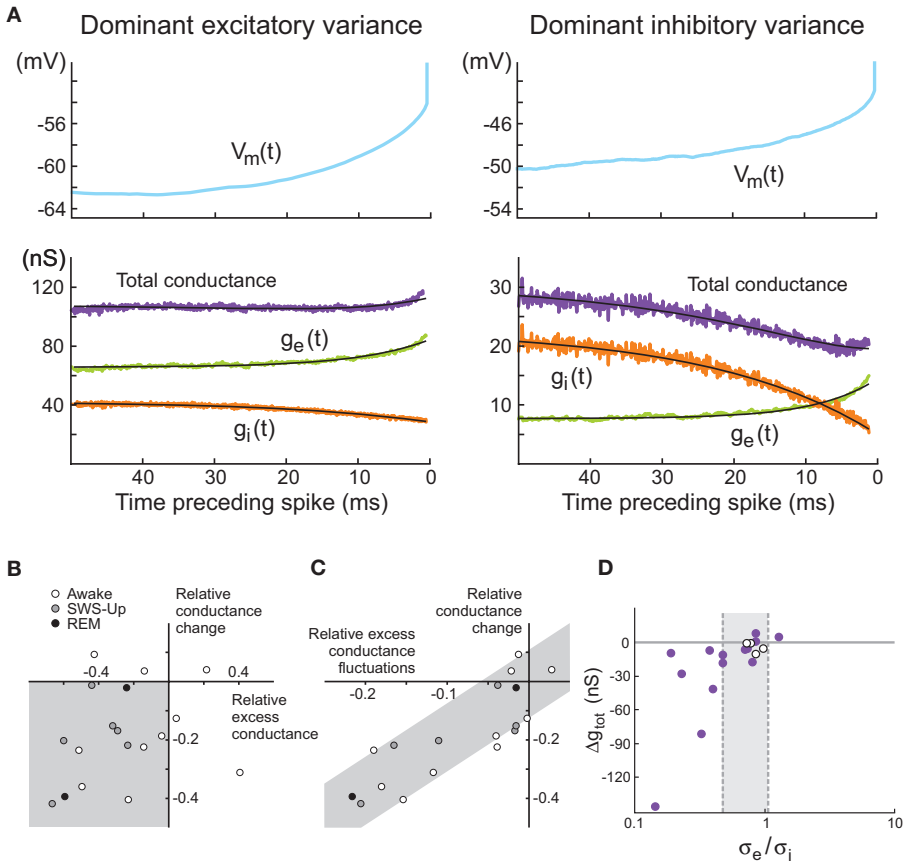

FIGURE 3 | Spike-triggered conductance analysis *in vivo*. (A) STA conductance analysis from intracellular recordings in awake and sleeping cats. Two example cells are shown during wakefulness, and for each, the V_m STA (top) and the extracted conductance STAs (bottom) are shown. In the first cell (left), the total conductance increases before the spike. In the second example cell (right), the total conductance decreases before the spike (black traces are exponential fits to the extracted STAs). This cell represents the majority of the cases. **(B)** Relation between total membrane conductance change before the spike, $(\Delta g_e - \Delta g_i)/(g_{e0} + g_{i0})$ ("relative conductance change"), and the difference of excitatory and inhibitory conductance, $(g_{e0} - \Delta g_{i0})/(g_{e0} + g_{i0})$ ("relative excess conductance"), estimated using the VmD method. Most cells are situated in the lower-left quadrant (gray), indicating a relation between inhibitory-dominant states and a drop of membrane conductance prior to the spike. **(C)** Relation between relative conductance change before the spike and conductance fluctuations, expressed as the difference between excitatory and inhibitory fluctuations, $(\sigma_e - \sigma_i)/(g_{e0} + g_{i0})$ ("relative excess conductance fluctuations"). Here, a clear correlation (gray area) shows that the magnitude of the conductance change before the spike is related to the amplitude of conductance fluctuations. Symbols: wake = open circles, SWS-Up = gray circles, REM = black circles. **(D)** Total conductance change preceding spikes as a function of the ratio σ_e/σ_i. Given the cell-to-cell variability of observed spike thresholds, each cell has a different predicted ratio separating total conductance increase cases from total conductance decrease cases. The two dashed lines (σ_e/σ_i = 0.48 and σ_e/σ_i = 1.07) visualize the two extreme predicted ratios. Cells in white are the ones not conforming to the prediction. **(A–C)** Modified from Rudolph et al. (2007); **(D)** modified from Piwkowska et al. (2008).

inhibitory events with action potentials in awake animals (Timofeev et al., 2001), and the powerful role of inhibitory fluctuations on spiking in anesthetized states (Hasenstaub et al., 2005).

Importantly, a point which was not seen by previous studies, is that it is not the total conductance – or mean conductance – that matters for spiking but it is rather the fluctuations around the mean, or the "conductance noise". The sign of the total conductance change before a spike does not directly depend on the mean synaptic conductances, but is solely determined by the ratio of synaptic conductance variances. It was shown previously that the variance of synaptic conductances is related to the degree of correlation between presynaptic inputs (Destexhe et al., 2001), suggesting that correlations in network activity are particularly effective to control spiking activity.

It is important to note that the predicted pattern of conductance variations, opposite between excitation and inhibition, is contrary to what is expected from feed-forward inputs. A feed-forward drive would predict an increase of excitation closely associated to an increase of inhibition, as seen in many instances of evoked responses during sensory processing (Borg-Graham et al., 1998; Monier et al., 2003; Wehr and Zador, 2003; Wilent and Contreras, 2005). There is no way to account for a concerted g_e increase and g_i drop without invoking recurrent activity, except if the inputs evoked a strong dis-inhibition, but this was so far not observed in conductance measurements. Thus, the present results that inhibitory "noise" is so determinant on firing activity stress the importance of recurrent activity and suggest an unexpected role for inhibitory circuits in information processing.

Future work should address the covariations of conductances *in vivo*. The spike-triggered covariances shown here were obtained from dynamic-clamp experiments in which the injected conductances are known. To estimate this function from V_m recordings would require to design specific methods. It should be possible to extend the previous method to estimate STAs from V_m activity (Pospischil et al., 2007) to spike-triggered covariances, under the same Gaussian assumptions. Another possible extension is to clarify why the inhibition drops in relation to the spike, while it increases in response to sensory inputs. A possibility is that the former pattern is a feature of spontaneous activity in high-conductance states, while the second pattern is specific to evoked inputs. To answer this question, conductances and their variances should be measured in spontaneous activity (as done here) and during evoked responses, but in the same cells. Such experiments are under way.

ACKNOWLEDGMENTS

Thanks to Thierry Bal, Zuzanna Piwkowska and Igor Timofeev for sharing experimental data. Research supported by CNRS, ANR, and the European Community (FACETS grant FP6 15879).

REFERENCES

Anderson, J. S., Carandini, M., and Ferster, D. (2000). Orientation tuning of input conductance, excitation, and inhibition in cat primary visual cortex. *J. Neurophysiol.* 84, 909–926.

Baranyi, A., Szente, M. B., and Woody, C. D. (1993). Electrophysiological characterization of different types of neurons recorded in vivo in the motor cortex of the cat. II. Membrane parameters, action potentials, current-induced voltage responses and electrotonic structures. *J. Neurophysiol.* 69, 1865–1879.

Borg-Graham, L. J., Monier, C., and Frégnac, Y. (1998). Visual input evokes transient and strong shunting inhibition in visual cortical neurons. *Nature* 393, 369–373.

Brunel, N. (2000). Dynamics of sparsely connected networks of excitatory and inhibitory spiking neurons. *J. Comput. Neurosci.* 8, 183–208.

Destexhe, A. (2007). *High-Conductance State. Scholarpedia 2: 1341*. Available at: http://www.scholarpedia.org/article/High-Conductance_State.

Destexhe, A., and Contreras, D. (2006). Neuronal computations with stochastic network states. *Science* 314, 85–90.

Destexhe, A., Contreras, D., and Steriade, M. (1999). Spatiotemporal analysis of local field potentials and unit discharges in cat cerebral cortex during natural wake and sleep states. *J. Neurosci.* 19, 4595–4608.

Destexhe, A., Rudolph, M., Fellous, J.-M., and Sejnowski, T. J. (2001). Fluctuating synaptic conductances recreate in vivo-like activity in neocortical neurons. *Neuroscience* 107, 13–24.

Destexhe, A., Rudolph, M., and Paré, D. (2003). The high-conductance state of neocortical neurons in vivo. *Nat. Rev. Neurosci.* 4, 739–751.

Evarts, E. V. (1964). Temporal patterns of discharge of pyramidal tract neurons during sleep and waking in the monkey. *J. Neurophysiol.* 27, 152–171.

Hasenstaub, A., Shu, Y., Haider, B., Kraushaar, U., Duque, A., and McCormick, D. A. (2005). Inhibitory postsynaptic potentials carry synchronized frequency information in active cortical networks. *Neuron* 47, 423–435.

Hubel, D. (1959). Single-unit activity in striate cortex of unrestrained cats. *J. Physiol.* 147, 226–238.

Lindner, B., and Longtin, A. (2006). Comment on "Characterization of subthreshold voltage fluctuations in neuronal membranes", by M. Rudolph and A. Destexhe. *Neural Comput.* 18, 1896–1931.

Matsumura, M., Cope, T., and Fetz, E. E. (1988). Sustained excitatory synaptic input to motor cortex neurons in awake animals revealed by intracellular recording of membrane potentials. *Exp. Brain Res.* 70, 463–469.

Monier, C., Chavane, F., Baudot, P., Graham, L. J., and Frégnac, Y. (2003). Orientation and direction selectivity of synaptic inputs in visual cortical neurons: a diversity of combinations produces spike tuning. *Neuron* 37, 663–680.

Monier, C., Fournier, J., and Frégnac, Y. (2008). In vitro and in vivo measures of evoked excitatory and inhibitory conductance dynamics in sensory cortices. *J. Neurosci. Meth.* 169, 323–365.

Paré, D., Shink, E., Gaudreau, H., Destexhe, A., and Lang, E. J. (1998). Impact of spontaneous synaptic activity on the resting properties of cat neocortical neurons in vivo. *J. Neurophysiol.* 79, 1450–1460.

Piwkowska, Z., Pospischil, M., Brette, R., Sliwa, J., Rudolph-Lilith, M., Bal, T., and Destexhe, A. (2008). Characterizing synaptic conductance fluctuations in cortical neurons and their influence on spikegeneration. *J. Neurosci. Methods* 169, 302–322.

Pospischil, M., Piwkowska, Z., Rudolph, M., Bal, T., and Destexhe, A. (2007). Calculating event-triggered average synaptic conductances from the membrane potential. *J. Neurophysiol.* 97, 2544–2552.

Richardson, M. J. (2004). Effects of synaptic conductance on the voltage distribution and firing rate of spiking neurons. *Phys. Rev. E Stat. Nonlin. Soft Matter Phys.* 69, 051918.

Rudolph, M., and Destexhe, A. (2003). Characterization of subthreshold voltage fluctuations in neuronal membranes. *Neural Comput.* 15, 2577–2618.

Rudolph, M., and Destexhe, A. (2005). An extended analytic expression for the membrane potential distribution of conductance-based synaptic noise. *Neural Comput.* 17, 2301–2315.

Rudolph, M., and Destexhe, A. (2006). On the use of analytic expressions for the voltage distribution to analyze intracellular recordings. *Neural Comput.* 18, 2917–2922.

Rudolph, M., Pelletier, J.-G., Paré, D., and Destexhe, A. (2005). Characterization of synaptic conductances and integrative properties during electrically-induced EEG-activated states in neocortical neurons in vivo. *J. Neurophysiol.* 94, 2805–2821.

Rudolph, M., Piwkowska, Z., Badoual, M., Bal, T., and Destexhe, A. (2004). A method to estimate synaptic conductances from membrane potential fluctuations. *J. Neurophysiol.* 91, 2884–2896.

Rudolph, M., Pospischil, M., Timofeev, I., and Destexhe, A. (2007). Inhibition determines membrane potential dynamics and controls action potential generation in awake and sleeping cat cortex. *J. Neurosci.* 27, 5280–5290.

Steriade, M., Deschênes, M., and Oakson, G. (1974). Inhibitory processes and interneuronal apparatus in motor cortex during sleep and waking. I. Background firing and responsiveness of pyramidal tract neurons and interneurons. *J. Neurophysiol.* 37, 1065–1092.

Steriade, M., Timofeev, I., and Grenier, F. (2001). Natural waking and sleep states: a view from inside neocortical neurons. *J. Neurophysiol.* 85, 1969–1985.

Timofeev, I., Grenier, F., and Steriade, M. (2001). Disfacilitation and active inhibition in the neocortex during the natural sleep-wake cycle: an intracellular study. *Proc. Natl. Acad. Sci. U.S.A.* 98, 1924–1929.

van Vreeswijk, C., and Sompolinsky, H. (1996). Chaos in neuronal networks with balanced excitatory and inhibitory activity. *Science* 274, 1724–1726.

Wehr, M., and Zador, A. M. (2003). Balanced inhibition underlies tuning and sharpens spike timing in auditory cortex. *Nature* 426, 442–446.

Wilent, W., and Contreras, D. (2005). Dynamics of excitation and inhibition underlying stimulus selectivity in rat somatosensory cortex. *Nat. Neurosci.* 8, 1364–1370.

Wolfart, J., Debay, D., Le Masson, G., Destexhe, A., and Bal, T. (2005). Synaptic background activity controls spike transfer from thalamus to cortex. *Nat. Neurosci.* 8, 1760–1767.

Woody, C. D., and Gruen, E. (1978). Characterization of electrophysiological properties of intracellularly recorded neurons in the neocortex of awake cats: a comparison of the response to injected current in spike overshoot and undershoot neurons. *Brain Res.* 158, 343–357.

Conflict of Interest Statement: The author declares that the research was conducted in the absence of any commercial or financial relationships that could be construed as a potential conflict of interest.

Received: 18 February 2010; paper pending published: 10 March 2010; accepted: 13 March 2010; published online: 31 March 2010.

*Citation: Destexhe A (2010) Inhibitory "noise". Front. Cell. Neurosci. **4**:9. doi: 10.3389/fncel.2010.00009*

frontiers in
CELLULAR NEUROSCIENCE

PERSPECTIVE ARTICLE
published: 31 March 2010
doi: 10.3389/fncel.2010.00010

GABAergic inhibition in visual cortical plasticity

Alessandro Sale[1]*†, Nicoletta Berardi[1,2†], Maria Spolidoro[3], Laura Baroncelli[3] and Lamberto Maffei[1,3]

[1] *Institute of Neuroscience Consiglio Nazionale delle Ricerche, Pisa, Italy*
[2] *Department of Psychology, Florence University, Florence, Italy*
[3] *Laboratory of Neurobiology, Scuola Normale Superiore, Pisa, Italy*

Edited by:
Yehezkel Ben-Ari,
Institut National de la Santé et de la Recherche Médicale, France

Reviewed by:
Rustem Khazipov,
Institut National de la Santé et de la Recherche Médicale, France
Evelyne Sernagor,
Newcastle University, UK

****Correspondence:***
Alessandro Sale,
Institute of Neuroscience Consiglio Nazionale delle Ricerche, Via Moruzzi 1, Pisa I-56124, Italy.
e-mail: sale@in.cnr.it

†Alessandro Sale and Nicoletta Berardi have contributed equally to this work.

Experience is required for the shaping and refinement of developing neural circuits during well defined periods of early postnatal development called critical periods. Many studies in the visual cortex have shown that intracortical GABAergic circuitry plays a crucial role in defining the time course of the critical period for ocular dominance plasticity. With the end of the critical period, neural plasticity wanes and recovery from the effects of visual defects on visual acuity (amblyopia) or binocularity is much reduced or absent. Recent results pointed out that intracortical inhibition is a fundamental limiting factor for adult cortical plasticity and that its reduction by means of different pharmacological and environmental strategies makes it possible to greatly enhance plasticity in the adult visual cortex, promoting ocular dominance plasticity and recovery from amblyopia. Here we focus on the role of intracortical GABAergic circuitry in controlling both developmental and adult cortical plasticity. We shall also discuss the potential clinical application of these findings to neurological disorders in which synaptic plasticity is compromised because of excessive intracortical inhibition.

Keywords: GABA, critical period, ocular dominance plasticity, amblyopia, environmental enrichment

INTRODUCTION

What we are, how we behave, how we talk, how we perceive, crucially depends upon how our brain has developed. Maturation of neural circuits is a protracted phase of brain development which, though initially guided by genetically coded cues, requires in most cases to be shaped and refined by the interaction of the individual with the environment. To allow this shaping action, developing neural circuits exhibit a great degree of plasticity so that they can be modified, functionally and morphologically, in response to experience. Neural plasticity is high during well defined periods of early postnatal development called critical periods (CPs). As experience drives the remodeling of neural connections, determining the maturation of neural circuits and of the corresponding functions, both circuits and functions become progressively less modifiable by experience and CPs draw towards their closure. As a result of this decline in plasticity, recovery from the effects of defective neural circuit development is significantly reduced or lost after the end of the CP. Recent studies, however, reveal that it is possible to enhance neural plasticity in the adult cortex. The visual cortex has long been a paradigmatic model to study the influence of experience on the development and plasticity of neural connections and its molecular basis. Studies in the visual cortex have shown that intracortical GABAergic circuitry is at the core both of developmental plasticity and CP control and of adult cortical plasticity limitations.

INHIBITION IN VISUAL CORTICAL DEVELOPMENT AND DEVELOPMENTAL PLASTICITY

Intracortical GABAergic inhibition (IGI) plays a crucial role in shaping visual cortical receptive fields and their development. Maturation of visual acuity is well correlated with the decrease of mean receptive field size of neurons in the primary visual cortex (Fagiolini et al., 1994) and with the postnatal development of IGI (Huang et al., 1999). Both visual acuity maturation and IGI development are dependent from visual experience: dark rearing, which prevents visual acuity development (Fagiolini et al., 1994), also affects the developmental increase of IGI (Benevento et al., 1995; Gianfranceschi et al., 2003). IGI development has been therefore suggested to contribute to visual acuity development and a direct evidence for this comes from BDNF overexpressing mice (Huang et al., 1999). In these mice BDNF expression in the visual cortex is higher than in wt mice starting from very early postnatal ages and this correlates with a precocious development of IGI, as shown by the faster developmental increase in inhibitory postsynaptic currents and GABA biosynthetic enzyme GAD65 in the perisomatic region of pyramidal cells. This precocious IGI development is accompanied by an accelerated development of visual acuity.

Recently, the use of the environmental enrichment (EE) paradigm has contributed to strengthen the importance of IGI development for the functional development of the visual cortex. EE is a combination of complex sensory-motor stimulation obtained by rearing large groups of animals in wide stimulating environments where a variety of objects are used to promote exploration, cognitive activity, social interaction and physical exercise (for a review, see Sale et al., 2009). EE accelerates (Cancedda et al., 2004; Sale et al., 2004), and prevents dark rearing deleterious effects on, visual acuity development (Bartoletti et al., 2004), promoting the maturation of IGI. In addition, Insuline-like Growth Factor-1 (IGF-1), a possible mediator of EE effects on visual cortex development, is also likely to act targeting IGI development (Ciucci et al., 2007).

The best characterized contribution of IGI to developmental plasticity is that to the opening and closure of the CP for ocular dominance (OD) plasticity (Huang et al., 1999; Hensch, 2005;

Morishita and Hensch, 2008). If vision in one eye is defective in man or experimentally impaired by monocular deprivation (MD) during infancy in mammals, visual acuity of that eye does not develop normally (a condition called amblyopia), binocular vision is impaired, visual cortical neurons become strongly dominated by the non deprived eye (OD shift) and the proportion of binocular neurons greatly decreases (Hubel and Wiesel, 1970; Fagiolini et al., 1994). If the visual deprivation is removed early in development, the ensuing recovery is very good; on the contrary, recovery is very limited if defect removal is delayed to adulthood. Also MD effectiveness in modifying the OD of visual cortical neurons declines with age (Hubel and Wiesel, 1970; Hensch, 2005). Hensch et al. (1998) have shown that inhibitory neurotransmission is necessary for the manifestation of OD plasticity in response to MD. In transgenic mice lacking the 65-kD isoform of the GABA-synthesizing enzyme GAD (GAD65), OD plasticity in response to MD is deficient. OD plasticity in these animals can be rescued if GABAergic transmission is enhanced in the visual cortex by means of benzodiazepines. This suggests that the development of GABAergic intracortical inhibition is an enabling factor for CP opening. Indeed, Fagiolini and Hensch (2000) have shown that precocious enhancement of IGI by the early administration of diazepam to the visual cortex accelerates the opening of the CP (**Figure 1**).

A specific subset of inhibitory interneurons, the parvalbumin-positive large basket cells, seems to be crucial for the control of CP opening (Fagiolini et al., 2004). Moreover, Di Cristo et al. (2007) have shown that premature removal in the visual cortex of polysialic acid (PSA) presented by the neural cell adhesion molecule, results in a precocious maturation of perisomatic innervation by basket interneurons, enhanced inhibitory synaptic transmission, and an earlier onset of OD plasticity (**Figure 1**).

Sugiyama et al. (2008) have demonstrated that another factor might impinge on IGI development to promote CP onset. Otx2 homeoprotein is transported from the retina to the visual cortex in an activity-dependent way and it contributes to the regulation of the onset of visual cortex CP plasticity. Otx2controls maturation of cortical parvalbumin-positive GABAergic interneurons. In addition, it promotes the developmental organization of specific components of the extracellular matrix, the Chondroitin Sulphate Proteoglycans (CSPGs), into tightly woven nets surrounding cor-

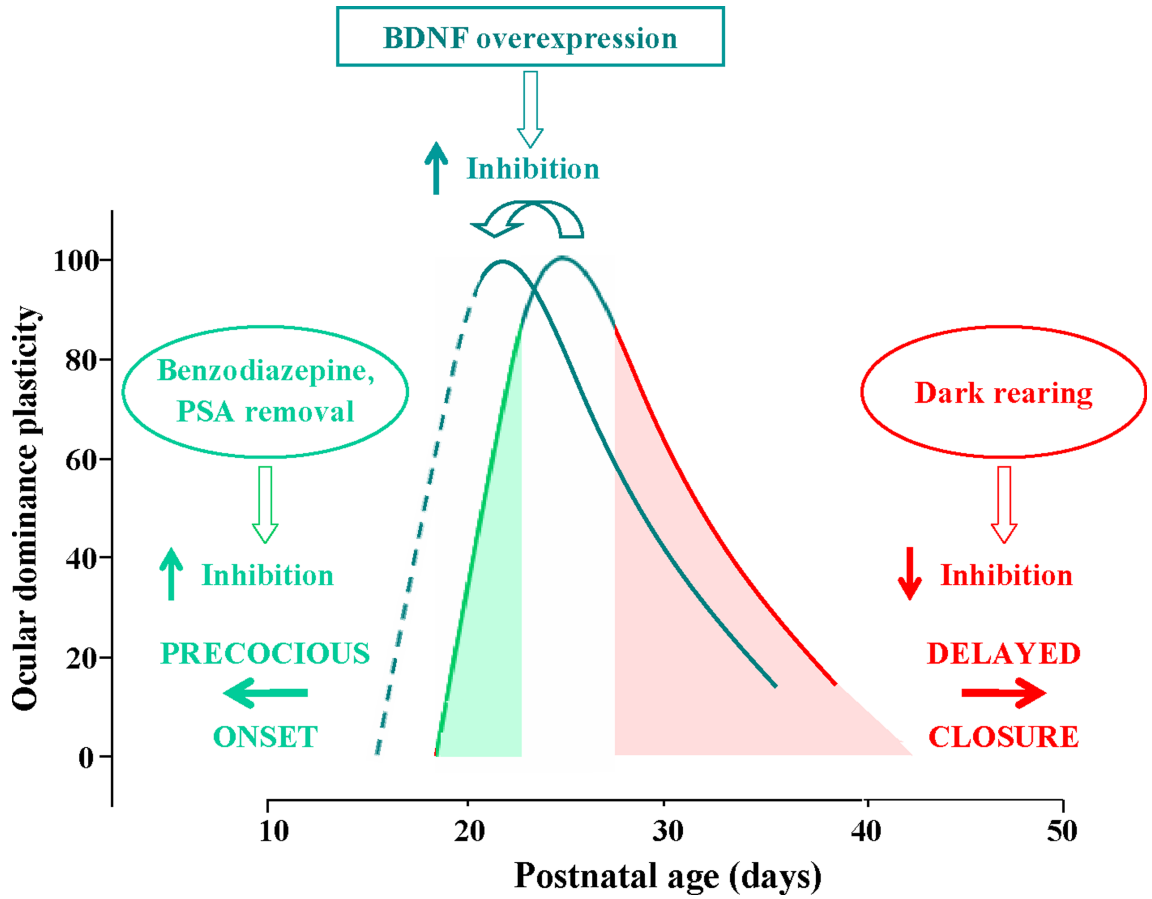

FIGURE 1 |Time course of the critical period (CP) for ocular dominance (OD) plasticity in response to monocular deprivation in rodents; OD plasticity is normalized to the CP peak's level. CP onset can be anticipated by increasing intracortical inhibition through benzodiazepine treatment or PSA (see text) removal (green arrow pointing left). Conversely, the end of the CP can be delayed by preventing the maturation of GABAergic inhibition through dark rearing from birth (red arrow pointing right). The effects of dark rearing can be counteracted by concomitant EE (see text). BDNF over-expression promotes a faster maturation of GABAergic interneurons, acting both on the onset and on the closure of the CP, thus shifting leftward the entire developmental plasticity curve.

tical neurons called perineuronal nets (PNNs). These nets are preferentially found around parvalbumin-positive GABAergic interneurons and might contribute to the development of their functional properties and to the onset of CP, possibly also making Otx-2 available to them.

Development of inhibition seems also to determine the decline of visual cortex plasticity as development proceeds and CPs draw to their end. The results obtained in mice with precocious BDNF expression clearly show that an accelerated development of IGI results in an early closure of the CP for the effects of monocular deprivation (Hanover et al., 1999; Huang et al., 1999) (**Figure 1**). Similarly, animals exposed to EE exhibit a precocious decline of synaptic plasticity in the visual cortex (Cancedda et al., 2004) and EE counteracts the effects of dark rearing on the closure of the CP for OD plasticity, in good correlation with the preserved developmental formation of PNNs around GABAergic interneurons and of GAD65 puncta rings around the cell body of pyramidal cells (Bartoletti et al., 2004). This is in accordance with the well known finding that IGI matures in correspondence with CP progression (see Hensch, 2005) and that dark rearing, which delays CP closure, delays inhibition development (**Figure 1**). They are also in agreement with the data by Fagiolini and Hensch (2000) who observed that, employing long-term monocular deprivation as a probe for OD plasticity, the CP is prolonged into adulthood in GAD65 knock-out mice.

These findings suggest that IGI levels cross two thresholds during development, the first setting the point after which inhibition levels are enough to allow OD plasticity to be expressed (beginning of CP); as development proceeds, the inhibitory tone further increases and crosses a second threshold, after which inhibition drastically reduces the potential for plasticity (closure of CP) (Feldman, 2000).

INTRACORTICAL INHIBITION AND RESTORATION OF PLASTICITY IN THE ADULT VISUAL CORTEX

Recent studies revealed a previously unsuspected plasticity potential for the adult visual cortex, challenging the classic notion that OD plasticity or amblyopia recovery are possible only early in development during the CP. In this new work, the capability to reduce intracortical inhibition levels has emerged as critical for the restoration of plasticity.

The most direct demonstration that GABAergic inhibition actively restricts plasticity in the adult visual cortex derives from the very recent report that a pharmacological reduction of inhibition obtained by intracortical infusion of either mercaptopropionic acid (MPA, an inhibitor of GABA synthesis) or picrotoxin (PTX, a GABAA receptor antagonist), at doses which do not alter visual cortical neuron responsiveness, reactivates OD plasticity in response to MD in adult rats (Harauzov et al., 2010) (**Figure 2**). This is accompanied, in visual cortical slices of MD animals with reduced inhibition, by the reinstatement of white matter-induced LTP in the II-III layer, a form of plasticity normally restricted to the CP due to the maturation of IGI. These results indicate that in normal adult animals, where inhibitory processes have completed their development, a brief reduction of GABAergic inhibition is sufficient to reopen a window of plasticity in the visual cortex well after the normal closure of the CP. This supports the hypothesis that the development of inhibition contributes to CP closure. In the visual cortex of MD animals with reduced inhibition there is a decrease in the expression of CSPGs, which follows the reactivation of OD plasticity. The reduction in PNN density observed in MPA or PTX-treated animals after MD could be an indication that the reactivation of OD plasticity caused by reducing the inhibitory tone sets in motion endogenous mechanisms of extracellular matrix remodelling (Mataga et al., 2002, 2004; Oray et al., 2004; Hensch, 2005). It has to be underlined, however, that the OD shift induced by MD in adult animals with reduced intracortical inhibition (Harauzov et al., 2010) is smaller than that induced during the CP. This suggests that other mechanisms which restrain the expression of OD plasticity are still in place. One of these factors could be the density of PNNs, which are known to develop in correlation with CP closure and have been shown to be non permissive for OD plasticity (Pizzorusso et al., 2002, 2006). The reduction in PNN density in MPA or PTX-treated animals is partial, therefore PNN density remains higher than during the peak of the critical period (Pizzorusso et al., 2002). In addition, the presence of factors limiting chromatin remodelling (Putignano et al., 2007), or signalling from extracellular factors, for example from myelin proteins on Nogo receptors (McGee et al., 2005) as well as the characteristics of adhesion molecules (Hensch, 2005), might contribute to partially restrain the full expression of long-term OD changes in response to MD in animals with reduced intracortical inhibition.

In the attempt to manipulate the balance between excitation and inhibition using non invasive strategies eligible to be transferred to humans, we exploited the paradigm of EE. We found that a 3-weeks exposure of adult amblyopic rats to EE promotes a complete recovery of both visual acuity and OD (**Figure 2**). This striking effect was associated with a threefold reduction in the basal levels of GABA detected by *in vivo* brain microdialysis in the visual cortex contralateral to the previously amblyopic eye (Sale et al., 2007). A reduced cortical inhibition was also detectable at the synaptic plasticity level, since the visual cortical slices of EE rats displayed a full reinstatement of white matter-induced LTP. IGI reduction is crucial for the plasticity enhancement induced by EE, because the recovery of visual functions is completely prevented by cortical infusion of diazepam directly into the primary visual cortex during the EE period (Sale et al., 2007). Consistent with the results of Harauzov et al. (2010), we also found a reduction in PNN density in the animals exposed to EE, a result that strengthens the notion of a possible link between the functional state of the extracellular matrix and the intracortical inhibitory tone. Interestingly, repetitive transcranial magnetic stimulation in humans, which increases cortical excitability, transiently improves contrast sensitivity in adult amblyopes, likely acting on the excitation/inhibition balance (Thompson et al., 2008).

Recent studies reported that exposing adult rats to complete darkness, a treatment qualitatively very different from EE, can favor plasticity in the adult brain (He et al., 2006, 2007) (**Figure 2**). There is indirect evidence that also in this case the enhanced visual cortical plasticity may be related to a reduced expression of GABAA receptors relative to AMPA receptors. This could cause a shift in the balance between inhibition and excitation towards levels more similar to those found in the immature cortex.

With the ambitious goal to search for possible enviromimetics, molecular factors that might be exploited to reproduce the beneficial effects elicited by EE, we came back to the classic observation that

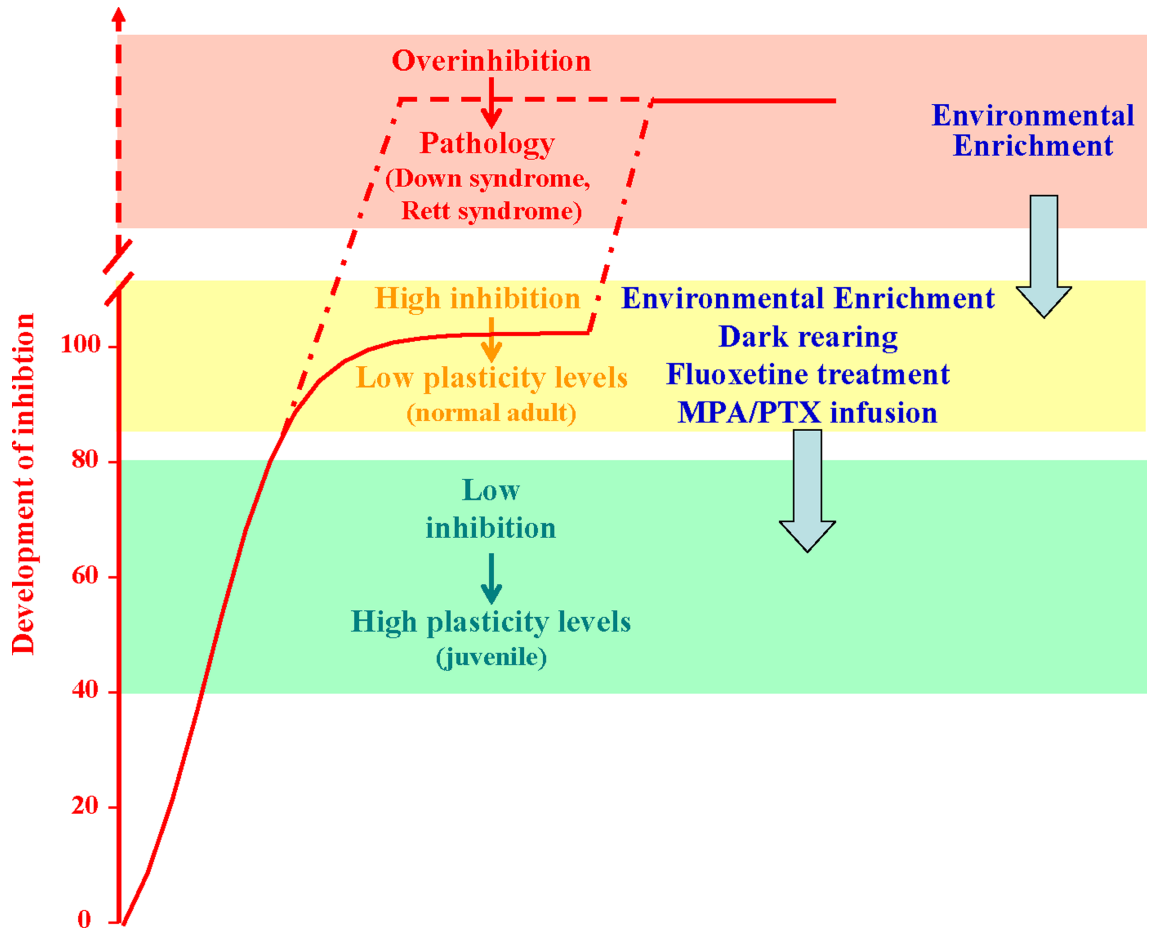

FIGURE 2 | Developmental increase of brain GABAergic inhibition levels (normalized to the normal adult values; red curve) is paralleled by a progressive reduction of experience-dependent plasticity. Plasticity is high during early development (green block) and very low in the adult brain (yellow block). Anomalous increases in the strength of inhibitory neural circuits may lead to over-inhibition linked to permanent deficits in synaptic plasticity and neural development, like in the Rett syndrome and in the Down's syndrome. Reducing GABAergic inhibition with pharmacological (blockers of GABA synthesis or GABA receptor antagonists, fluoxetine) or environmental (EE, and dark exposure) treatments can increase plasticity in the adult brain, enabling OD plasticity and favoring recovery from amblyopia. The capability of EE to reduce GABAergic inhibition makes this paradigm eligible for therapeutic applications also in the treatment of developmental intellectual disabilities.

the neurotransmitter systems characterized by diffuse projections throughout the entire brain, i.e. the serotoninergic, noradrenergic and dopaminergic systems, are all set in motion by EE (see van Praag et al., 2000). These neuromodulators have a great influence on plasticity processes in the adult brain, with a fundamental role in regulating the arousal state and attentional processes (see Gu, 2002), which are important components of the animal response to the enriched experience. Therefore, it should be possible to mimic the EE effects on adult visual cortex plasticity by an artificial modulation of one or more of these transmitters. Widely prescribed drugs for the treatment of depression, the so-called selective serotonin reuptake inhibitors (SSRIs), act by enhancing extracellular serotonin and noradrenalin levels, even if the relationship between acute increases in these neurotrasmitters and the clinical antidepressant effect has remained unclear. We recently showed that chronic treatment with fluoxetine (Prozac), a SSRI used to treat depression, obsessive-compulsive disorder and panic attacks, induces a reinstatement of OD plasticity in response to MD and a full recovery from amblyopia in adult animals (Maya Vetencourt et al., 2008) (**Figure 2**). As found for EE rats, these functional effects are associated with a marked reduction of GABAergic inhibition and are completely prevented by cortical diazepam administration.

The crucial involvement of IGI in limiting adult cortical plasticity could have implications also for other forms of brain repair, emerging as a possible target for behavioural or pharmacological interventions following brain lesions. A change in inhibitory tone has indeed been found in perilesional regions in patients with stroke in the motor cortex; treatment-associated cortical reorganization, which was correlated to the recovery of motor function, was influenced by the distribution of inhibitory properties within the representation area prior to therapy (Liepert et al., 2006).

RESCUING DEVELOPMENTAL INTELLECTUAL DISABILITIES

There is increasing consensus on the concept that not only does brain inhibition control the closure of CPs and adult cortical plasticity, but that it may also be linked to the pathogenesis of

developmental intellectual disabilities (see Fernandez and Garner, 2007 for a recent review). Anomalous increases in the strength of inhibitory neural circuits during brain maturation may lead to permanent deficits in synaptic plasticity and neural development (**Figure 2**). This over-inhibition may be the consequence of environmental disturbances, such as prenatal protein malnutrition (see Morgane et al., 2002) but its etiology is more frequently linked to genetic alterations, with the two paradigmatic examples of Rett syndrome (RS) and Down's syndrome (DS).

RS is an X-linked, severe progressive disorder of CNS development which causes a complex neurological and neurobehavioural phenotype characterized by mild-to-moderate mental retardation and highly disabling dysfunctions in motor coordination skills (Hagberg et al., 1983). The main mutations are found in the gene encoding the methyl-CpG-binding protein (MeCP2) (Amir et al., 1999), a factor critically involved in the epigenetic regulation of the expression of genes essential for plasticity, such as BDNF (Chen et al., 2003; Chang et al., 2006). Electrophysiological studies from MeCP2 transgenic mice reported a reduced neuronal activity in cortical and hippocampal neurons, pointing to a shift in the balance between inhibition and excitation as a likely mechanism underlying the motor and cognitive phenotype (Dani et al., 2005; Asaka et al., 2006; Fernandez and Garner, 2007). Given that persons with RS have an increased sensitivity to sedative drugs which act potentiating GABAergic inhibition (Tofil et al., 2006), it is tempting to speculate that overinhibition may also be present in the brain of human RS patients. Both BDNF overexpression and EE are successful in rescuing or ameliorating the main deficits detectable at the behavioural and electrophysiological level inMeCP2mutant mice (Chang et al., 2006; Kondo et al., 2008; Lonetti et al., 2010). At least for EE, this may directly result from a decrease in the GABAergic tone prompted by exposure to EE stimulation.

DS is caused by triplication of chromosome 21 (Chr21) as result of a misdivision in the sperm or the egg prior to conception, and it is the most diffused genetic cause of mental retardation. The most intensively studied mouse model of DS is the Ts65Dn line, that carries a triplication of a critical segment of Chr16, syntenic with human Chr21 (Gardiner et al., 2003). Ts65dn mice recapitulate all main hallmarks of the DS phenotype (Richtsmeier et al., 2002; Hunter et al., 2003; Driscoll et al., 2004; Wenger et al., 2004). There is increasing evidence that the cognitive deficits displayed by Ts65Dn mice can be attributable to excessive hippocampal inhibition. Accordingly, Fernandez et al. (2007) have shown that the spatial learning disabilities and the failure to induce LTP in the hippocampus observed in Ts65Dn mice can be rescued by administration of non-competitive antagonists of GABAA receptors. It remains unclear whether it is possible to induce a reduction of GABAergic inhibition in Ts65Dn mice through a non-pharmacological approach. The capability of EE to reduce GABAergic inhibition makes this paradigm eligible for therapeutic applications in the treatment of DS (e.g., Martinez-Cué et al., 2002; Dierssen et al., 2003) (**Figure 2**).

In conclusion, intracortical inhibition is a crucial determinant of cortical plasticity, both during development and in the adult. In typical development, it contributes to the maturation of the cortex and of cortex-dependent functions; moreover it might play a role in the intellectual disabilities found in atypical development. In the adult, it limits remodeling of neural connections, tightly controlling neural plasticity and exhibiting spontaneous changes under pathological conditions. Harnessing these changes might favor plasticity and promote functional recovery.

ACKNOWLEDGMENTS

This work was supported by Italian Ministry of the University and Scientific and Technological Research COFIN.

REFERENCES

Amir, R. E., Van den Veyver, I. B., Wan, M., Tran, C. Q., Francke, U., and Zoghbi, H. Y. (1999). Rett syndrome is caused by mutations in X-linked MECP2, encoding methyl-CpG-binding protein 2. *Nat. Genet.* 23, 185–188.

Asaka, Y., Jugloff, D. G., Zhang, L., Eubanks, J. H., and Fitzsimonds, R. M. (2006). Hippocampal synaptic plasticity is impaired in the Mecp2-null mouse model of Rett syndrome. *Neurobiol. Dis.* 21, 217–227.

Bartoletti, A., Medini, P., Berardi, N., and Maffei L. (2004). Environmental enrichment prevents effects of dark-rearing in the rat visual cortex. *Nat. Neurosci.* 7, 215–216.

Benevento, L. A., Bakkum, B. W., and Cohen, R. S. (1995). Gamma-Aminobutyric acid and somatostatin immunoreactivity in the visual cortex of normal and dark-reared rats. *Brain Res.* 21, 172–182.

Cancedda, L., Putignano, E., Sale, A., Viegi, A., Berardi, N., and Maffei, L. (2004). Acceleration of visual system development by environmental enrichment. *J. Neurosci.* 24, 4840–4848.

Chang, Q., Khare, G., Dani, V., Nelson, S., and Jaenisch, R. (2006). The disease progression of Mecp2 mutant mice is affected by the level of BDNF expression. *Neuron* 49, 341–348.

Chen, W. G., Chang, Q., Lin, Y., Meissner, A., West, A. E., Griffith, E. C., Jaenisch, R., and Greenberg, M. E. (2003). Derepression of BDNF transcription involves calcium-dependent phosphorylation of MeCP2. *Science* 302, 885–889.

Ciucci, F., Putignano, E., Baroncelli, L., Landi, S., Berardi, N., and Maffei, L. (2007). Insulin-like growth factor-1 (IGF-1) mediates the effects of enriched environment (EE) on visual cortical development. *PLoS ONE* 2, e475. doi:10.1371/journal.pone.0000475.

Dani, V. S., Chang, Q., Maffei, A., Turrigiano, G. G., Jaenisch, R., and Nelson, S. B. (2005). Reduced cortical activity due to a shift in the balance between excitation and inhibition in a mouse model of Rett syndrome. *Proc. Natl. Acad. Sci. U.S.A.* 102, 12560–12565.

Di Cristo, G., Chattopadhyaya, B., Kuhlman, S. J., Fu, Y., Bélanger, M. C., Wu, C. Z., Rutishauser, U., Maffei, L., and Huang, Z. J. (2007). Activity-dependent PSA expression regulates inhibitory maturation and onset of critical period plasticity. *Nat. Neurosci.* 10, 1569–1577.

Dierssen, M., Benavides-Piccione, R., Martinez-Cue, C., Estivill, X., Florez, J., Elston, G. N., and DeFelipe, J. (2003). Alterations of neocortical pyramidal cell phenotype in the Ts65Dn mouse model of Down syndrome: effects of environmental enrichment. *Cereb. Cortex* 13, 758–764.

Driscoll, L. L., Carroll, J. C., Moon, J., Crnic, L. S., Levitsky, D. A., and Strupp B. J. (2004). Impaired sustained attention and error-induced stereotypy in the aged Ts65Dn mouse: a mouse model of Down syndrome and Alzheimer's disease. *Behav. Neurosci.* 118, 1196–1205.

Fagiolini, M., Fritschy, J. M., Löw, K., Möhler, H., Rudolph, U., and Hensch, T. K. (2004). Specific GABAA circuits for visual cortical plasticity. *Science* 303, 1681–1693.

Fagiolini, M., and Hensch, T. K. (2000). Inhibitory threshold for critical-period activation in primary visual cortex. *Nature* 404, 183–186.

Fagiolini, M., Pizzorusso, T., Berardi, N., Domenici, L., and Maffei, L. (1994). Functional postnatal development of the rat primary visual cortex and the role of visual experience: dark rearing and monocular deprivation. *Vision Res.* 34, 709–720.

Feldman, D. E. (2000). Inhibition and plasticity. *Nat. Neurosci.* 3, 303–304.

Fernandez, F., and Garner C. C. (2007). Over-inhibition: a model for developmental intellectual disability. *Trends Neurosci.* 30, 497–503.

Fernandez, F., Morishita, W., Zuniga, E., Nguyen, J., Blank, M., Malenka, R. C., and Garner C. C. (2007). Pharmacotherapy for cognitive impairment in a mouse model of

Down syndrome. *Nat. Neurosci.* 10, 411–413.

Gardiner, K., Fortna, A., Bechtel, L., and Davisson, M. T. (2003). Mouse models of Down syndrome: how useful can they be? Comparison of the gene content of human chromosome 21 with orthologous mouse genomic regions. *Gene* 318, 137–147.

Gianfranceschi, L., Siciliano, R., Walls, J., Morales, B., Kirkwood, A., Huang, Z. J., Tonegawa, S., and Maffei, L. (2003). Visual cortex is rescued from the effects of dark rearing by overexpression of BDNF. *Proc. Natl. Acad. Sci U.S.A.* 100, 12486–12491.

Gu, Q. (2002). Neuromodulatory transmitter systems in the cortex and their role in cortical plasticity. *Neuroscience* 111, 815–835.

Hagberg, B., Aicardi, J., Dias, K., and Ramos, O. (1983). A progressive syndrome of autism, dementia, ataxia, and loss of purposeful hand use in girls: Rett's syndrome: report of 35 cases. *Ann. Neurol.* 14, 471–479.

Hanover, J. L., Huang, Z. J., Tonegawa, S., and Stryker, M. P. (1999). Brain-derived neurotrophic factor overexpression induces precocious critical period in mouse visual cortex. *J. Neurosci.* 19, RC40.

Harauzov, A., Spolidoro, M., DiCristo, G., De Pasquale, R., Cancedda, L., Pizzorusso, T., Viegi, A., Berardi, N., and Maffei, L. (2010). Reducing intracortical inhibition in the adult visual cortex promotes ocular dominance plasticity. *J. Neurosci.* 30, 361–371.

He, H. Y., Hodos, W., and Quinlan, E. M. (2006). Visual deprivation reactivates rapid ocular dominance plasticity in adult visual cortex. *J. Neurosci.* 26, 2951–2955.

He, H. Y., Ray, B., Dennis, K., and Quinlan, E. M. (2007). Experience-dependent recovery of vision following chronic deprivation amblyopia. *Nat. Neurosci.* 10, 1134–1136.

Hensch, T. K. (2005). Critical period plasticity in local cortical circuits. *Nat. Rev. Neurosci.* 6, 877–888.

Hensch, T. K., Fagiolini, M., Mataga, N., Stryker, M. P., Baekkeskov, S., and Kash, S. F. (1998). Local GABA circuit control of experience-dependent plasticity in developing visual cortex. *Science* 282, 1504–1508.

Huang, Z. J., Kirkwood, A., Pizzorusso, T., Porciatti, V., Morales, B., Bear, M. F., Maffei, L., and Tonegawa, S. (1999). BDNF regulates the maturation of inhibition and the critical period of plasticity in mouse visual cortex. *Cell* 98, 739–755.

Hubel, D. H., and Wiesel, T. N. (1970). The period of susceptibility to the physiological effects of unilateral eye closure in kittens. *J. Physiol. (Lond.)* 206, 419–436.

Hunter, C. L., Bimonte, H. A., and Granholm, A. C. (2003). Behavioral comparison of 4 and 6 month-old Ts65Dn mice: age-related impairments in working and reference memory. *Behav. Brain Res.* 138, 121–131.

Kondo, M., Gray, L. J., Pelka, G. J., Christodoulou, J., Tam, P. P., and Hannan, A. J. (2008). Environmental enrichment ameliorates a motor coordination deficit in a mouse model of Rett syndrome – Mecp2 gene dosage effects and BDNF expression. *Eur. J. Neurosci.* 27, 3342–3350.

Liepert, J., Haevernick, K., Weiller, C., and Barzel, A. (2006). The surround inhibition determines therapy-induced cortical reorganization. *Neuroimage* 32, 1216–1220.

Lonetti, G., Angelucci, A., Morando, L., Boggio, E. M., Giustetto, M., and Pizzorusso, T. (2010). Early environmental enrichment moderates the behavioral and synaptic phenotype of MeCP2 null mice. *Biol. Psychiatry* 67, 85–98.

Martinez-Cué, C., Baamonde, C., Lumbreras, M., Paz, J., Davisson, M. T., Schmidt, C. Dierssen, M., and Flórez, J. (2002). Differential effects of environmental enrichment on behavior and learning of male and female Ts65Dn mice, a model for Down syndrome. *Behav. Brain Res.* 134, 185–200.

Mataga, N., Mizuguchi, Y., and Hensch, T. K. (2004). Experience-dependent pruning of dendritic spines in visual cortex by tissue plasminogen activator. *Neuron* 44, 1031–1041.

Mataga, N., Nagai, N., and Hensch, T. K. (2002). Permissive proteolytic activity for visual cortical plasticity. *Proc. Natl. Acad. Sci. U.S.A.* 99, 7717–7721.

Maya Vetencourt, J. F., Sale, A., Viegi, A., Baroncelli, L., De Pasquale, R., O'Leary, O. F., Castrén, E., and Maffei, L. (2008). The antidepressant fluoxetine restores plasticity in the adult visual cortex. *Science* 320, 385–388.

McGee, A. W., Yang, Y., Fischer, Q. S., Daw, N. W., and Strittmatter, S. M. (2005). Experience-driven plasticity of visual cortex limited by myelin and Nogo receptor. *Science* 309, 2222–2226.

Morgane, P. J., Mokler, D. J., and Galler, J. R. (2002). Effects of prenatal protein malnutrition on the hippocampal formation. *Neurosci. Biobehav. Rev.* 26, 471–483.

Morishita, H., and Hensch, T. K. (2008). Critical period revisited: impact on vision. *Curr. Opin. Neurobiol.* 18, 101–107.

Oray, S., Majewska, A., and Sur, M. (2004). Dendritic spine dynamics are regulated by monocular deprivation and extracellular matrix degradation. *Neuron* 44, 1021–1030.

Pizzorusso, T., Medini, P., Berardi, N., Chierzi, S., Fawcett, J. W., and Maffei, L. (2002). Reactivation of ocular dominance plasticity in the adult visual cortex. *Science* 298, 1248–1251.

Pizzorusso, T., Medini, P., Landi, S., Baldini, S., Berardi, N., and Maffei, L. (2006). Structural and functional recovery from early monocular deprivation in adult rats. *Proc. Natl. Acad. Sci. U.S.A.* 103, 8517–8522.

Putignano, E., Lonetti, G., Cancedda, L., Ratto, G., Costa, M., Maffei, L., and Pizzorusso, T. (2007). Developmental downregulation of histone posttranslational modifications regulates visual cortical plasticity. *Neuron* 53, 747–759.

Richtsmeier, J. T., Zumwalt, A., Carlson, E. J., Epstein, C. J. and Reeves, R. H. (2002). Craniofacial phenotypes in segmentally trisomic mouse models for Down syndrome. *Am. J. Med. Genet.* 107, 317–324.

Sale, A., Berardi, N., and Maffei, L. (2009). Enrich the environment to empower the brain. *Trends Neurosci.* 32, 233–239.

Sale, A., Maya Vetencourt, J. F., Medini, P., Cenni, M. C., Baroncelli, L., De Pasquale, R., and Maffei, L. (2007). Environmental enrichment in adulthood promotes amblyopia recovery through a reduction of intracortical inhibition. *Nat. Neurosci.* 10, 679–681.

Sale, A., Putignano, E., Cancedda, L., Landi, S., Cirulli, F., Berardi, N., and Maffei, L. (2004). Enriched environment and acceleration of visual system development. *Neuropharmacology* 47, 649–660.

Sugiyama, S., Di Nardo, A. A., Aizawa, S., Matsuo, I., Volovitch, M., Prochiantz, A., and Hensch, T. K. (2008). Experience-dependent transfer of Otx2 homeoprotein into the visual cortex activates postnatal plasticity. *Cell* 134, 508–520.

Thompson, B., Mansouri, B., Koski, L., and Hess, R. F. (2008). Brain plasticity in the adult: modulation of function in amblyopia with rTMS. *Curr. Biol.* 18, 1067–1071.

Tofil, N. M., Buckmaster, M. A., Winkler, M. K., Callans, B. H., Islam, M. P., and Percy, A. K. (2006). Deep sedation with propofol in patients with Rett syndrome. *J. Child Neurol.* 21, 210–213.

van Praag, H., Kempermann, G., and Gage, F. H. (2000). Neural consequences of environmental enrichment. *Nat. Rev. Neurosci.* 1, 191–198.

Wenger, G. R., Schmidt, C., and Davisson, M. T. (2004). Operant conditioning in the Ts65Dn mouse: learning. *Behav. Genet.* 34, 105–119.

Conflict of Interest Statement: The authors declare that the research was conducted in the absence of any commercial or financial relationships that could be construed as a potential conflict of interest.

Received: 26 February 2010; paper pending published: 10 March 2010; accepted: 17 March 2010; published online: 31 March 2010.

Citation: Sale A, Berardi N, Spolidoro M, Baroncelli L and Maffei L (2010) GABAergic inhibition in visual cortical plasticity. Front. Cell. Neurosci. ***4****:10. doi: 10.3389/fncel.2010.00010*

frontiers in
CELLULAR NEUROSCIENCE

ORIGINAL RESEARCH ARTICLE
published: 08 April 2010
doi: 10.3389/fncel.2010.00008

$GABA_A$ increases calcium in subventricular zone astrocyte-like cells through L- and T-type voltage-gated calcium channels

Stephanie Z. Young[1], Jean-Claude Platel[1], Jakob V. Nielsen[2], Niels A. Jensen[2] and Angélique Bordey[1]*

[1] *Departments of Neurosurgery and Cellular & Molecular Physiology, Yale University School of Medicine, New Haven, CT, USA*
[2] *Molecular Neurobiology Laboratory, Medical Biotechnology Center, University of Southern Denmark, Odense, Denmark*

Edited by:
Yehezkel Ben-Ari, INSERM, France

Reviewed by:
Enrico Cherubini, International School for Advanced Studies, Italy
Yehezkel Ben-Ari, INSERM, France

***Correspondence:**
Angélique Bordey, Department of Neurosurgery, Yale University School of Medicine, 333 Cedar Street, FMB 422, New Haven, CT 06520-8082, USA.
e-mail: angelique.bordey@yale.edu

In the adult neurogenic subventricular zone (SVZ), the behavior of astrocyte-like cells and some of their functions depend on changes in intracellular Ca^{2+} levels and tonic $GABA_A$ receptor activation. However, it is unknown whether, and if so how, $GABA_A$ receptor activity regulates intracellular Ca^{2+} dynamics in SVZ astrocytes. To monitor Ca^{2+} activity selectively in astrocyte-like cells, we used two lines of transgenic mice expressing either GFP fused to a Gq-coupled receptor or DsRed under the human glial fibrillary acidic protein (*hGFAP*) promoter. $GABA_A$ receptor activation induced Ca^{2+} increases in 40–50% of SVZ astrocytes. $GABA_A$-induced Ca^{2+} increases were prevented with nifedipine and mibefradil, blockers of L- and T-type voltage-gated calcium channels (VGCC). The L-type Ca^{2+} channel activator BayK 8644 increased the percentage of $GABA_A$-responding astrocyte-like cells to 75%, suggesting that the majority of SVZ astrocytes express functional VGCCs. SVZ astrocytes also displayed spontaneous Ca^{2+} activity, the frequency of which was regulated by tonic $GABA_A$ receptor activation. These data support a role for ambient GABA in tonically regulating intracellular Ca^{2+} dynamics through $GABA_A$ receptors and VGCC in a subpopulation of astrocyte-like cells in the postnatal SVZ.

Keywords: GABA, GABA receptors, stem cells, astrocyte, subventricular zone, neurogenesis, progenitor cells, proliferation

INTRODUCTION

Neurogenesis persists in two regions of the adult brain, the SVZ along the lateral ventricle and the subgranular zone in the hippocampal dentate gyrus (Lledo et al., 2006; Zhao et al., 2008). The SVZ contains a mosaic of cell types including neuroblasts ensheathed by cells with astrocytic features such as glial fibrillary acidic protein (GFAP) expression. A subpopulation of these GFAP-expressing cells (also called astrocyte-like cells or SVZ astrocytes) generates intermediate progenitors called transit amplifying cells. The latter generate neuroblasts that differentiate into interneurons in the olfactory bulb. Previous studies have shown that the distinct steps of neurogenesis (i.e. migration, proliferation and differentiation) are influenced by local molecules. These molecules differentially affect intracellular Ca^{2+} dynamics and regulate Ca^{2+}-dependent intracellular pathways (Bordey, 2006; Pathania et al., 2010). One such local molecule is the amino acid γ-aminobutyric acid (GABA) that is synthesized and released by SVZ neuroblasts as shown using immunohistochemistry for glutamic acid decarboxylase (GAD) (the enzyme that catalyzes the decarboxylation of glutamate to GABA) and GABA, and electrophysiology to show functional release from neuroblasts (Stewart et al., 2002; Nguyen et al., 2003; Bolteus and Bordey, 2004; De Marchis et al., 2004; Liu et al., 2005; Gascon et al., 2006; Platel et al., 2008).

GABA acts through specific receptors, $GABA_A$ receptors, which are expressed in both SVZ neuroblasts and astrocytes (Stewart et al., 2002; Nguyen et al., 2003; Wang et al., 2003b; Bolteus and Bordey, 2004; Liu et al., 2005). In developing systems, the $GABA_A$ receptor is thought to regulate the behavior of immature cells through depolarization leading to the canonical activation of VGCCs and intracellular Ca^{2+} increases (Owens and Kriegstein, 2002). Such a mechanism has been reported in SVZ neuroblasts and involves nifedipine-sensitive L-type VGCC (Nguyen et al., 2003; Wang et al., 2003b; Gascon et al., 2006). It has been speculated that this canonical Ca^{2+} increase may not operate in SVZ astrocytes due to their biophysical properties (low input resistance and hyperpolarized resting potential) (Liu et al., 2006; Bordey, 2007). We thus set out to investigate whether and, if so, how $GABA_A$ increases Ca^{2+} in SVZ astrocytes.

One limitation to address this issue has been the inability to distinguish Ca^{2+} indicator-loaded astrocyte-like cells from neuroblasts in acute SVZ slices. To study Ca^{2+} activity selectively in SVZ astrocytes, we used two lines of transgenic mice where astrocyte-like cells express intracellular DsRed or membrane-associated GFP. Using these mice revealed that traditional bath loading of Ca^{2+} indicators preferentially loaded neuroblasts at the slice surface while astrocyte-like cells resided deeper inside the tissue. Using pressure loading of a Ca^{2+} indicator dye inside the tissue, we preferentially loaded astrocyte-like cells. We found that a $GABA_A$ receptor agonist increased Ca^{2+} in a subset of astrocyte-like cells (~50%) through L- and T-type VGCCs. In addition, ambient GABA tonically regulated the frequency of Ca^{2+} activity in ~80% of SVZ astrocytes. GABA increased or decreased the frequency, subdividing the SVZ astrocytes into two subpopulations. For the first time this finding illustrates a functional difference among astrocyte-like cells of the SVZ. Such a $GABA_A$-regulation in selective astrocyte-like cells may impact Ca^{2+}-dependent mechanisms, including proliferation and the release of diffusible molecules (e.g. ATP; Striedinger et al., 2007).

MATERIALS AND METHODS

ANIMALS

Experiments were performed in several lines of transgenic mice: (1) Mice expressing DsRed under the human *GFAP* promoter (*hGFAP*-DsRed mice) were produced by the co-authors, N.A. Jensen and J.V. Nielsen (Noraberg et al., 2007). To generate the *hGFAP*-DsRed transgene, the pDsRed2-1 plasmid (Clontech) was initially modified to introduce a *Pac*I site downstream of the SV40 polyadenylation signal, by filling in an *Afl*II site. Subsequently, the *hGFAP* promoter (Brenner et al., 1994) was cloned into the *Bgl*II and *Sal*I sites, before a rabbit β-globin intron was inserted into the *Bam*HI sites between the *hGFAP* promoter and the DsRed coding sequence. For microinjection, the transgene was excised from the plasmid backbone by digestion with *Bgl*II and *Pac*I, gel-purified and microinjected, at a concentration of 6 ng/μl, into the pronucleus of fertilized B6D2F1 mouse eggs as previously described (Nielsen et al., 2007). Transgenic *hGFAP*-DsRed mice were identified by PCR with primers: 5′-TCTGGGCACAGTGACCTCAGTG and 5′-GGGACATCTTCCCATTCTAAAC. (2) *hGFAP*-DsRed mice were crossed with homozygote mice carrying GFP under the doublecortin promoter (*DCX*-GFP mice, FVB/N strain, a gift from Dr. R. Miller, University of Chicago, originally from Gensat) to generate *hGFAP*-DsRed/*DCX*-GFP mice. These mice were used in 25% of the experiments instead of *hGFAP*-DsRed mice. (3) *hGFAP-tTA/TetO*-MrgA1:GFP mice (called *hGFAP*-MrgA1:GFP mice) were a gift from Dr. Ken McCarthy (University of North Carolina at Chapel Hill). In the absence of doxycycline, astrocytes express MrgA1 receptors fused to GFP (Fiacco et al., 2007). All experimental protocols were approved by the Institutional Animal Care and Use Committees of Yale School of Medicine and by the Danish National Animal Care and Use Committee. Mice were used between postnatal day (P) 20 and P42.

IMMUNOHISTOCHEMISTRY

Slice preparation, immunostaining, and image acquisition and analysis were as previously described (Platel et al., 2009). Primary antibodies included: anti-DCX (goat or rabbit, 1:100, Santa Cruz, SC8066 and SC28939), anti-GFAP (rabbit, 1:1000, Dako, Z0334), anti-EGFR (sheep, 1:100, Millipore, 06-129), and anti-GFP (chicken, 1:500, Abcam). Each staining was replicated at least in four to five slices from three different mice. The appropriate secondary antibodies were Alexa fluor series (1:1000, Invitrogen, USA) or Cyanine series (1:500, Jackson Labs). Z-section images (spaced by 1–2 μm over 10–20 μm) were acquired on a laser-scanning confocal microscope (Olympus FluoView 1000) with a 20× dry objective (N.A. 0.75) or a 60× oil objective (N.A. 1.42). Images were analyzed using Imaris 4.0 (Bitplane AG, Switzerland) and reconstructed in ImageJ 1.39t (Freeware, Wayne Rasband, NIH, USA) and Photoshop CS3 (Adobe, USA).

ACUTE SLICE PREPARATION AND PATCH CLAMP RECORDINGS

Acute coronal or sagittal brain slices (250–300 μm-thick) containing the SVZ were prepared as we previously described (Bolteus and Bordey, 2004; Bolteus et al., 2005). Slices were placed in a flow-through chamber and continuously superfused with oxygenated artificial cerebrospinal fluid (aCSF) containing (in mM): NaCl 125; KCl 2.5; $CaCl_2$ 1.8; $MgCl_2$ 1; $NaHCO_3$ 25; glucose 10. Experiments were performed on an upright Olympus BX61WI microscope equipped with an Olympus FluoView 1000 confocal microscope and a water-immersion Nomarski phase-contrast and fluorescence 60× objective (N.A. 0.9).

Whole-cell patch clamp recordings were obtained as previously described (Wang et al., 2003a,b; Bolteus and Bordey, 2004; Liu et al., 2006). Pipettes had resistances of 6–8 MΩ when filled with an intracellular solution containing the following: 110 mM KCl, 1.0 mM $CaCl_2$, 10 mM EGTA, 10 mM HEPES, 50 μM Alexa Fluor 488 dye and an ATP-regenerating solution that included 4 mM K_2ATP, 20 mM K_2-phosphocreatine, 50 U/ml creatine phosphokinase, and 6 mM $MgCl_2$. The pH and the osmolarity were adjusted to 7.2 and 290 mOsm, respectively. The liquid junction potential (~4 mV) was not corrected. Whole-cell recordings were performed using an Axopatch 200B amplifier, and current signals were low-pass filtered at 2–5 kHz and digitized on-line at 5–20 kHz using a Digidata 1320 digitizing board (Axon Instruments, Foster City, CA, USA). Recorded cells were held at −60 mV. Voltage steps were applied from −100 to +100 mV by 20 mV increment. Capacitive and leak currents were not subtracted.

CALCIUM IMAGING

SVZ cells were loaded by pressure application of Fluo-4 AM (100 μM in aCSF, 0.4% Pluronic acid F-127, Invitrogen). We observed no differences in data obtained with either *hGFAP*-DsRed or *hGFAP*-MrgA1:GFP mice regarding the pharmacology of muscimol responses; we therefore pooled the data. Images were acquired every 2 s with FluoView acquisition software. In acute slices from *hGFAP*-MrgA1:GFP mice, Fluo-4 AM-astrocyte-like cells were distinguished from other SVZ cells due to their enhanced green fluorescence on their cell membrane. In addition, application of a selective peptide agonist of MrgA1 receptors (that has no endogenous receptors) was routinely used to induce Ca^{2+} responses selectively in SVZ astrocytes to identify them at the end of the experiments. ROIs were placed on SVZ cells that responded to the peptide during a 10–20 s application period.

For spontaneous movies, images were acquired every 2 s (0.5 Hz) for 10 min in each condition with 5 min of wash-in or wash-out between each movie. F_0 (i.e. baseline) and F are the mean fluorescence intensities measured throughout all of the regions of interest (ROIs) and in each ROI, respectively. A change in fluorescence was considered to be a Ca^{2+} increase if it was >15% F/F_0 increase. Intracellular Ca^{2+} changes were calculated using Calsignal (Platel et al., 2007) and Clampfit 10. F/F_0 was detected with Calsignal and traces were exported into Clampfit for peak analysis using the threshold detection function. For peak analysis, the baseline for each ROI trace was manually adjusted to zero. In addition, traces from control and drug-treated movies were concatenated and the same threshold for peak detection was used. ROIs were designated as "responding" if the cell was responsive at least 50% of muscimol applications in order to perform subsequent pharmacology. "Non-responsive" cells were cells that displayed no increase in F/F_0.

Data are expressed as mean ± standard error. Statistical analysis used a two-tailed *t*-test except where noted.

PHARMACOLOGY

Ca^{2+} imaging experiments were performed in the presence of the GABA$_B$ blocker CGP 52432 (1 μM) and blockers of glutamate receptors including D-APV (50 μM) for NMDA receptors, NBQX

(20 μM) for AMPA/kainate receptors, MPEP (10 μM) and JNJ 16259685 (100 nM) for group I metabotropic glutamate receptors. We also used for selective experiments: nickel (100 μM) to block N- and R-type VGCCs; nifedipine (10 μM, Sigma-Aldrich) and mibefradil dihydrochloride (10 μM) for blocking L-type and T-type VGCCs, respectively; BayK 8644 (10 μM) to enhance L-type VGCC activity; 2-aminoethoxydiphenyl borate 2-APB (100 μM) for blockade (although non-selective) of IP_3-related signaling. Drugs were from Tocris Biosciences (MO, USA), except where noted.

RESULTS

CHARACTERIZATION OF DsRED-POSITIVE CELLS IN THE SVZ OF *hGFAP*-DsRED MICE

We first verified that DsRed is expressed in astrocyte-like cells of the SVZ. We immunostained for GFAP (blue) in sections from *hGFAP*-DsRed/*DCX*-GFP mice (**Figures 1A,B**). We observed bright DsRed-positive cells, which were GFAP-positive (arrows in **Figure 1B**), and some faint DsRed cells, which were GFAP-negative and *DCX*-GFP-positive (arrowhead in **Figure 1B**). This result was confirmed by staining for both GFAP and DCX in sections from *hGFAP*-DsRed mice (**Figure S1** in Supplementary Material). DsRed-positive cells occasionally stained positive for the transit amplifying cell marker epidermal growth factor receptor (EGFR, **Figure S1B** in Supplementary Material, arrowhead). The known half-life of DsRed (~4 days) allows it to persist at a lower level in daughter cells. These findings are thus in agreement with GFAP-positive cells (*i.e.* SVZ astrocytes) being neural progenitors that generate EGFR-cells and neuroblasts (Doetsch et al., 2002; Platel et al., 2009).

We next performed patch clamp recordings of DsRed-fluorescent cells in acute slices where cells with different fluorescence intensity could be observed (**Figures 1C,D**). Every bright DsRed-fluorescent cell recorded had a hyperpolarized resting potential (mean of −80.8 ± 1.0 mV), low input resistance (57.4 ± 9.1 MΩ, $n = 7$), and a linear current–voltage relationship following depolarizing steps (from −160 to +100 mV, **Figures 1E,F**) from a holding potential of −80 mV. Thus, bright DsRed-fluorescent have characteristics of

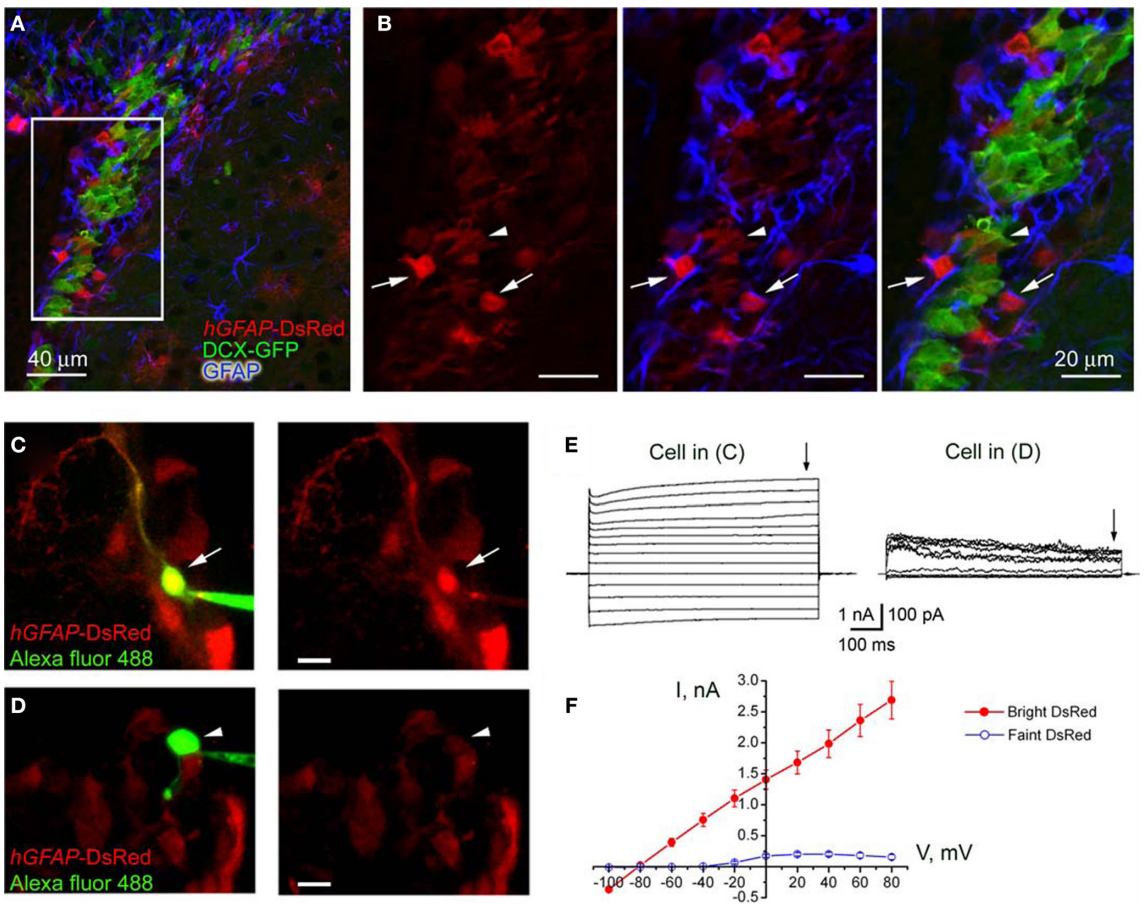

FIGURE 1 | Characterization of *hGFAP*-DsRed-fluorescent cells in the SVZ. **(A)** Confocal images (one optical section) of GFAP immunostaining (blue) in the SVZ contained in a section from a *hGFAP*-DsRed/*DCX*-GFP mouse (P30). **(B)** Higher power photographs of the staining shown in the white square in (A). The arrows point to GFAP-positive DsRed-fluorescent cells while the arrowhead points to GFAP-negative, GFP-fluorescent neuroblasts. **(C and D)** Photographs of Alexa fluor 488-filled bright (C) and faint (D) red cells during patch clamp recording in acute slices from *hGFAP*-DsRed mice. Scale bar: 15 μm. **(E)** Traces of whole cell currents obtained from the cells shown in (C, bright red) and (D, faint red). The cells in (C) and (D) display the current profiles of a GFAP-progenitor and a neuroblast, respectively. **(F)** Mean current–voltage relationships (measured at the end of the voltage steps, arrows in E) of bright cells (red filled circles, $n = 6$) and faint cells (blue open circles, $n = 5$) give reversal potentials of –81 and –43 mV, respectively.

astrocytes of the SVZ (Liu et al., 2006). By contrast, every recorded, faint DsRed-fluorescent cell displayed characteristics of neuroblasts (Wang et al., 2003a; Bolteus and Bordey, 2004). These characteristics include high input resistance (mean of 4.4 ± 1.3 GΩ), depolarized zero-current resting potentials (−42.7 ± 8.7 mV, $n = 5$), and the presence of voltage-dependent outward currents (**Figures 1E,F**). These data suggest that bright and faint DsRed-fluorescent cells can be unambiguously identified as astrocyte-like cells and neuroblasts, respectively, in acute slices.

GFP-POSITIVE CELLS IN THE SVZ OF *hGFAP*-MRGA1:GFP MICE ARE ASTROCYTE-LIKE CELLS

One important limitation of the *hGFAP*-DsRed mice for performing Ca^{2+} imaging is the fact that not every astrocyte-like cell is DsRed-fluorescent (**Figures 1A,B**). This is more apparent in sections from *hGFAP*-DsRed mice crossed with *hGFAP*-GFP mice. While some DsRed-fluorescent cells are GFP-positive (arrows), not all GFP-positive cells are DsRed-fluorescent (arrowheads, **Figures 2A–C**). We thus acquired transgenic mice that express an exogenous Gq-protein coupled receptor (called Mas-related gene A1, MrgA1) in GFAP-expressing cells (*i.e.* astrocytes). MrgA1 has no endogenous ligand in the brain (Fiacco et al., 2007). The MrgA1 receptor fused to GFP was targeted to astrocytes using the inducible tet-off system. Mice expressing the tetracycline transactivator (tTA) under the human *GFAP* promoter were crossed to mice in which the MrgA1:GFP receptor was transcribed using the tet-off (tetO) minimal promoter. In the SVZ of *hGFAP*-tTA/tetO-MrgA1:GFP mice (referred henceforth as *hGFAP*-MrgA1:GFP mice), GFP displays a membrane expression selectively in all astrocyte-like cells (GFAP+ cells, red) but not in neuroblasts (DCX+ cells, blue, **Figures 2D,E**). In addition, SVZ astrocytes loaded with the Ca^{2+} indicator dye Fluo-4 AM can be further identified with a peptide agonist for MrgA1 receptors that does not bind endogenous receptors in the brain. Pressure application of phe-leu-arg-phe amide peptide (FLRFa, 50 μM, 10–20 s) induced Ca^{2+} increases in GFP-decorated cells, i.e. astrocyte-like cells (**Figures 2F,G**).

GABA$_A$ RECEPTOR ACTIVATION LEADS TO CA^{2+} INCREASES IN SVZ ASTROCYTES THROUGH VGCCs

We previously reported that astrocyte-like cells express functional GABA$_A$ receptors using patch clamp recordings (Liu et al., 2005). However, it remained unknown whether these receptors led to Ca^{2+} increases in these cells. We pressure loaded slices with Fluo-4 AM in slices from *hGFAP*-DsRed and *hGFAP*-MrgA1:GFP mice (**Figures 3A,E**, respectively). Application of the GABA$_A$ receptor agonist muscimol (50 μM, 5 s) increased Ca^{2+} in 38.1 ± 4.8% and 51.3 ± 3.5% of SVZ astrocytes from *hGFAP*-DsRed and *hGFAP*-MrgA1:GFP mice (106 cells, $n = 17$ slices and 396 cells, 16 slices, respectively, **Figures 3B,D,F**). Experiments were performed in the presence of glutamate and GABA$_B$ receptor blockers (see Materials and Methods). GABA$_A$-induced Ca^{2+} responses were abolished by either bicuculline or picrotoxin (50 μM), two GABA$_A$ receptor antagonists, in 94 ± 4.67% of the muscimol-responding cells (27 cells, $n = 5$ slices total, **Figures 3C,G and 4E,F**).

GABA$_A$ receptor activation is known to depolarize parenchymal astrocytes (Barakat and Bordey, 2002; Bekar and Walz, 2002). Following GABA$_A$ receptor-induced depolarization, intracellular Ca^{2+} increases in immature cells are also thought to result from the canonical activation of VGCCs (Owens and Kriegstein, 2002; Meier et al., 2008). We thus tested the effects of three VGCC blockers on the percentage of SVZ astrocytes displaying muscimol-induced Ca^{2+} increases in slices from both *hGFAP*-DsRed and *hGFAP*-MrgA1:GFP mice. VGCCs are grouped into three families: (1) the high-voltage activated dihydropyridine (DHP)-sensitive channels (L-type, $Ca_V1.x$), (2) the high-voltage activated DHP-insensitive channels (P-, N- and R-type, $Ca_V2.x$), and (3) the low-voltage activated channels (T-type, $Ca_V3.x$). We tested the following three blockers: Nickel (Ni^{2+}, 100 μM) for R-type $Ca_V2.3$ and T-type $Ca_V3.2$ channels (high sensitivity), and for other T-type channels (low-sensitivity); the DHP antagonist nifedipine (10 μM) for L-type channels, and mibefradil (10 μM) for T-type channels. Ni^{2+} significantly decreased the percentage of muscimol-responding astrocytes but by only 30 ± 9.4% ($n = 50$ cells, six slices, **Figures 4E,F**). Nifedipine and mibefradil significantly decreased the percentage of muscimol-responding astrocytes by 61 ± 10% **Figures 4A,B** and 48 ± 4%, respectively ($n = 217$ cells, six slices, and 78 cells, four slices, respectively, **Figures 4E,F**). When used together, these three VGCC blockers abolished muscimol responses in 90 ± 4% of the responding SVZ astrocytes (**Figures 4E,F**). Of the cells that continue to respond, none of these drugs had any effect on the amplitude or area of the Ca^{2+} responses (**Figure 4G**). These data suggest that GABA$_A$-induced Ca^{2+} responses in astrocyte-like cells of the SVZ are predominately mediated by Ca^{2+} influx through L- and T-type VGCCs.

As illustrated in **Figures 3D and 4E**, 40–50% of SVZ astrocytes display Ca^{2+} increases in response to GABA$_A$ receptor activation. Considering that nearly all SVZ astrocytes tested have been reported to display functional GABA$_A$ currents (Liu et al., 2005), the lack of Ca^{2+} responses could be due to either the absence of functional VGCCs or the fact that GABA$_A$ depolarization does not reach VGCC threshold. We thus tested the L-type VGCC activator BayK 8644. In the presence of BayK 8644, there was a significant increase (to 190% of control) in the % of cells responding to muscimol (from ~35% to 75%, **Figures 4C,D,E,F**). These data suggest that most astrocyte-like cells express DHP-sensitive VGCCs. BayK 8644 also increased the area, but not the amplitude, of muscimol-induced Ca^{2+} increases (**Figure 4G**), suggesting that BayK 3644 prolonged Ca^{2+} responses due to GABA$_A$ receptor activation.

Considering that increases in intracellular Ca^{2+} can further trigger Ca^{2+} increases from intracellular stores, we tested 2-APB, a blocker of inositol-1,4,5-trisphosphate receptors (IP3) and IP3-sensitive intracellular stores, among other channels at 100 μM (Bootman et al., 2002; Peppiatt et al., 2003). Bath application of 2-APB resulted in a 30 ± 9% decrease in the number of muscimol-responding astrocytes, but this decrease was not significant (**Figures 4E,F**, t-test, $p > 0.05$). Nevertheless, when analyzing cells that continue to respond after drug application, 2-APB significantly reduced the amplitude and area of muscimol-induced Ca^{2+} transients, while nifedipine and other VGCC blockers did not (**Figure 4G**). These data suggest that Ca^{2+} release from intracellular stores contributes to the increase in intracellular Ca^{2+} concentration following GABA$_A$ depolarization-induced Ca^{2+} influx through VGCCs.

AMBIENT GABA CONTROLS THE FREQUENCY OF BASELINE CA^{2+} ACTIVITY IN SVZ ASTROCYTES

We previously reported that 60% of SVZ astrocytes recorded with the patch clamp technique displayed a tonic current due to GABA$_A$ receptor activation (Liu et al., 2005). We thus examined whether

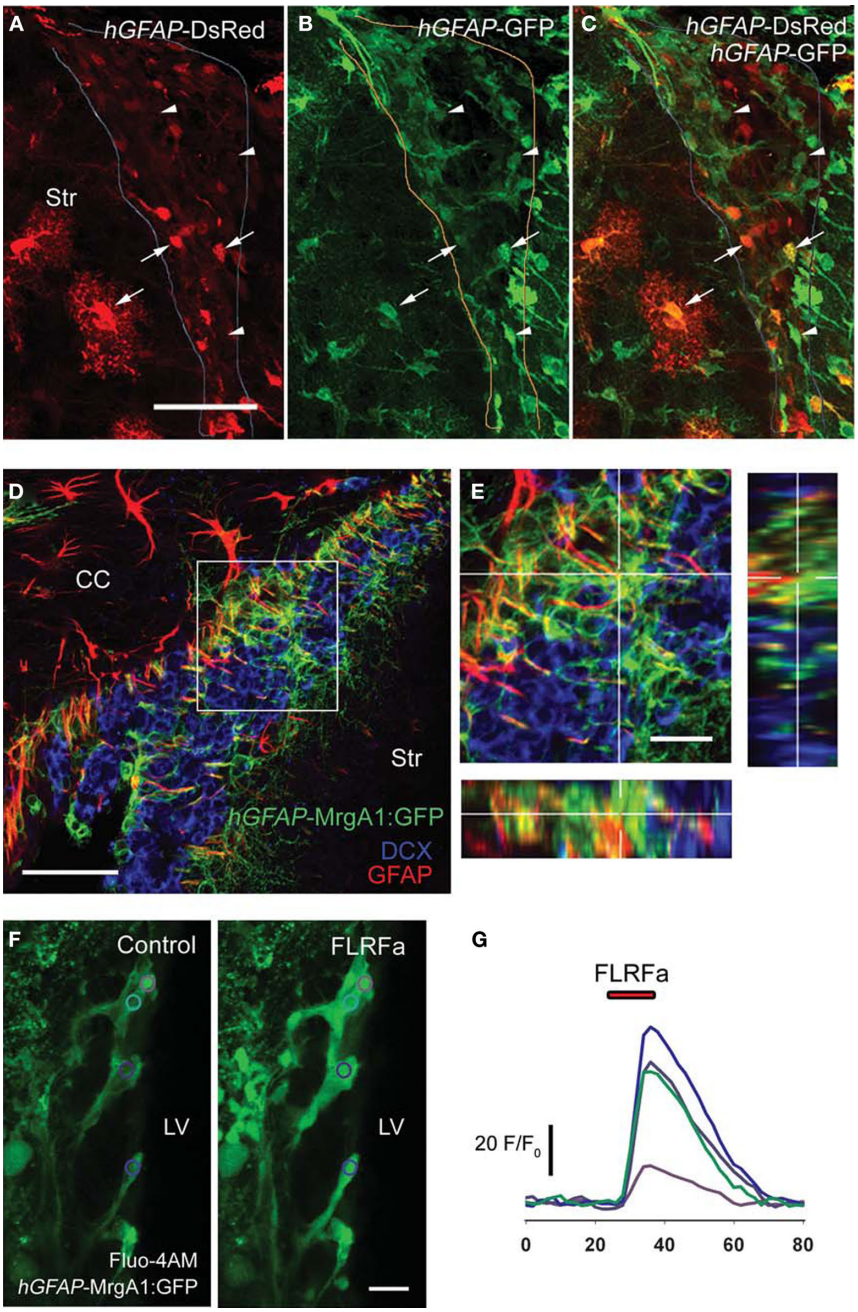

FIGURE 2 | Characterization of *hGFAP*-tTA-MrgA1:GFP mice in the SVZ. **(A–C)** Confocal z-section of a slice from a *hGFAP*-tTA-MrgA1:GFP/*hGFAP*-DsRed mouse. The arrows point to SVZ astrocytes that are both DsRed and GFP-fluroescent, while the arrowheads point to astrocytes that are only GFP-positive. Scale bar = 30 μm. **(D)** A confocal z-stack (four images, spaced by 1.5 μm) of a slice from a *hGFAP*-tTA-MrgA1:GFP mouse. Astrocytes express the MrgA1:GFP. GFP signal colocalized with GFAP (red) but does not colocalize with neuroblast marker DCX (blue). Scale bar = 30 μm **(E)** Higher power image of region indicated by a white box in (D). Scale bar = 10 μm. **(F)** Confocal images of Fluo-AM-loaded slice from a *hGFAP*-tTA-MrgA1:GFP mouse before and during peptide FLRFa application. Regions of interest (ROIs) are indicated by colored circles. Scale bar = 10 μm **(G)** Traces showing F/F_0 from ROIs in (*F*), analyzed in CalSignal. CC = corpus callosum, Str = striatum.

ambient GABA exerted a tonic regulation of Ca^{2+} dynamics in SVZ astrocytes. Recordings were performed in the presence of blockers of GABA$_B$ and glutamate receptors, as described in the Methods. We found that 77.8% of astrocyte-like cells displayed baseline Ca^{2+} activity in the form of Ca^{2+} transients at an average frequency of 0.252 Hz (10 min of recordings, $n = 196$ cells, four slices, see traces in control conditions in **Figure 5D**). To test the effect of drugs on Ca^{2+} activity, a 10-min recording was following by a 5-min drug wash-in and an additional 10-min recording in the presence of the drug. With no drug application (control movies), spontaneous Ca^{2+} activity was

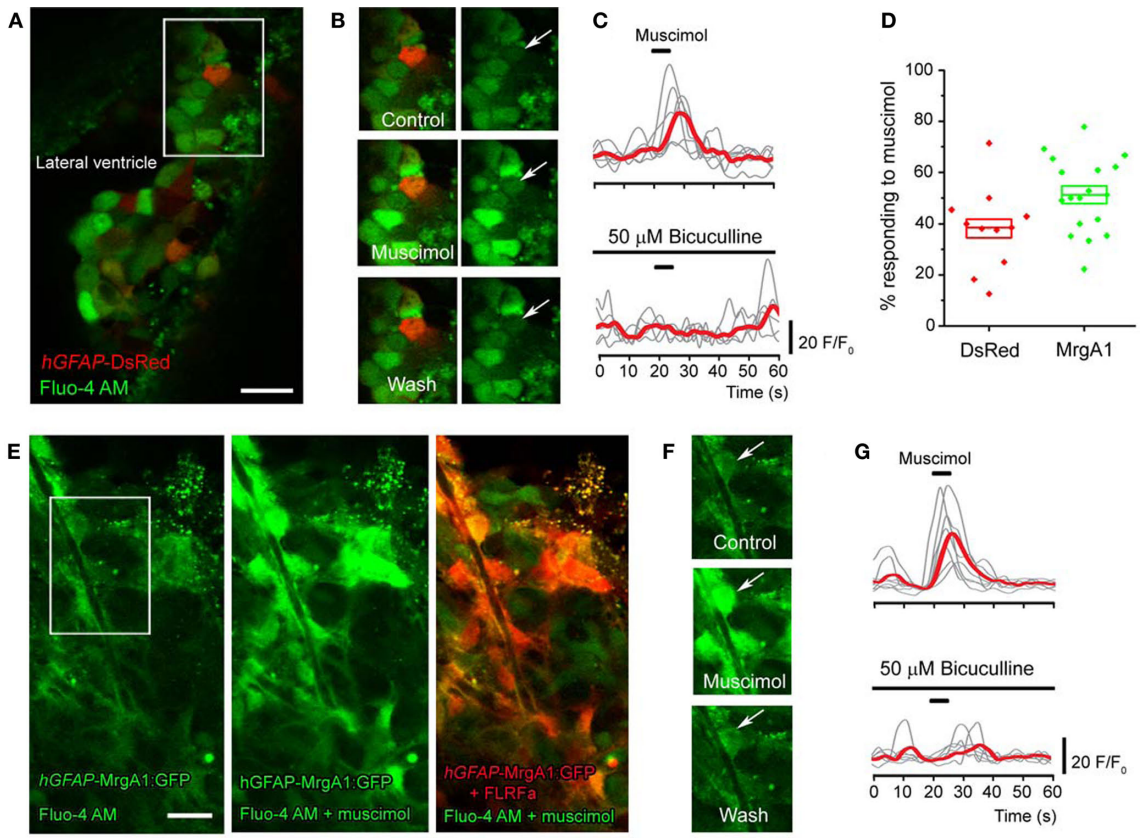

FIGURE 3 | GABA$_A$ receptors regulate Ca^{2+} dynamics in SVZ astrocytes. **(A)** Z-stack confocal image (six images spaced by 1.5 μm) of Fluo-4 AM loaded SVZ cells in a coronal slice from a *hGFAP*-DsRed mouse. Scale bar = 10 μm. **(B)** Confocal image of the same cells shown in the white square in (A) under control conditions, during and following muscimol application. The arrow points to the DsRed-fluorescent cell, which responded to muscimol. **(C)** Representative muscimol-induced Ca^{2+} responses under control and in the presence of bicuculline (a GABA$_A$ receptor blocker). The red trace represents the average of the individual gray traces (n = 7 cells). **(D)** Box plots of the percentage of GFAP-progenitors responding to muscimol in *hGFAP*-DsRed or *hGFAP*-MrgA1:GFP mice (n = 9 and 17 slices, respectively). Box: SEM, bar: median, diamonds: individual slice values. **(E)** Confocal image (one optical section) of Fluo-4 AM loaded SVZ cells (green) in a sagittal slice from a *hGFAP*-MrgA1:GFP mouse. Second panel shows SVZ cells responding to muscimol. The last panel is an overlay of images from responses to FLRFa peptide (orange, indicating SVZ astrocytes) and muscimol (green). Scale bar = 10 μm. **(F)** Confocal image of the same cells shown in the white square in (E) under control conditions, during and following muscimol application. The arrow points to the MrgA1:GFP-fluorescent, FLRFa-responsive cell, which also responded to muscimol. **(G)** Representative muscimol-induced Ca^{2+} responses under control and in the presence of bicuculline in cells from *hGFAP*-MrgA1:GFP slices. The red trace represents the average of the individual gray traces (n = 8 cells).

stable over time. Following analysis of Ca^{2+} frequency in the first and second 10-min periods, we found that 26.3 ± 4.8% and 19.0 ± 2.5% of the cells displayed a non-significant increase and decrease in the frequency of Ca^{2+} transient to 117.0 ± 6.3% and 81.7 ± 6.8% of control, respectively (n = 47 cells, three slices). Spontaneous Ca^{2+} activity was eliminated following 15–20 min of 2-APB application (data not shown), as expected, since regenerative Ca^{2+} transients have been shown to involve Ca^{2+} from internal stores that rely on the activation of IP3 receptors in various cell types (D'Andrea et al., 1993; Ciapa et al., 1994; Liu et al., 2001; Bellamy, 2006). When recorded in the presence of bicuculline (Bic) under baseline conditions, wash-out of bicuculline had two distinct effects on SVZ astrocytes. In 79 ± 3% of the astrocyte-like cells bicuculline wash-out resulted in a significant increase in the frequency of Ca^{2+} transients to 216 ± 39% of control (from 0.154 to 0.36 Hz, n = 90 cells, **Figures 5A,B**, $p < 0.01$). In addition, in 18 ± 6% of the SVZ astrocytes bicuculline wash-out resulted in a significant decrease in the frequency of Ca^{2+} transients to 72.9 ± 4.6% of control (from 0.45 to 0.34 Hz, n = 15/90 cells, **Figure 5B**). Wash-out of SR-95531 (gabazine, 100 nM), a non-competitive GABA$_A$ receptor antagonist, had similar effects (data not shown). Gabazine wash-out increased and decreased the frequency of Ca^{2+} transients in 41% and 27% of the SVZ astrocytes, respectively (n = 3 slices, data not shown). Bath application of bicuculline had the opposite effects to that of bicuculline wash-out, as expected. Bicuculline wash-in significantly decreased the frequency of Ca^{2+} transients to 60 ± 6% of control in 46 ± 8% of astrocyte-like cells (from 0.252 to 0.175 Hz, n = 185 cells) and increased the frequency to 223 ± 32% of control in 31 ± 3% of the cells in the same slices (from 0.10 to 0.25 Hz, n = 185 cells, four slices, **Figures 5C,D**, $p < 0.05$).

DISCUSSION

In this study we first report the use of two transgenic mouse lines to perform Ca^{2+} imaging in astrocyte-like cells of the SVZ. Without these mice, identifying Fluo-4 AM-loaded astrocytes among other

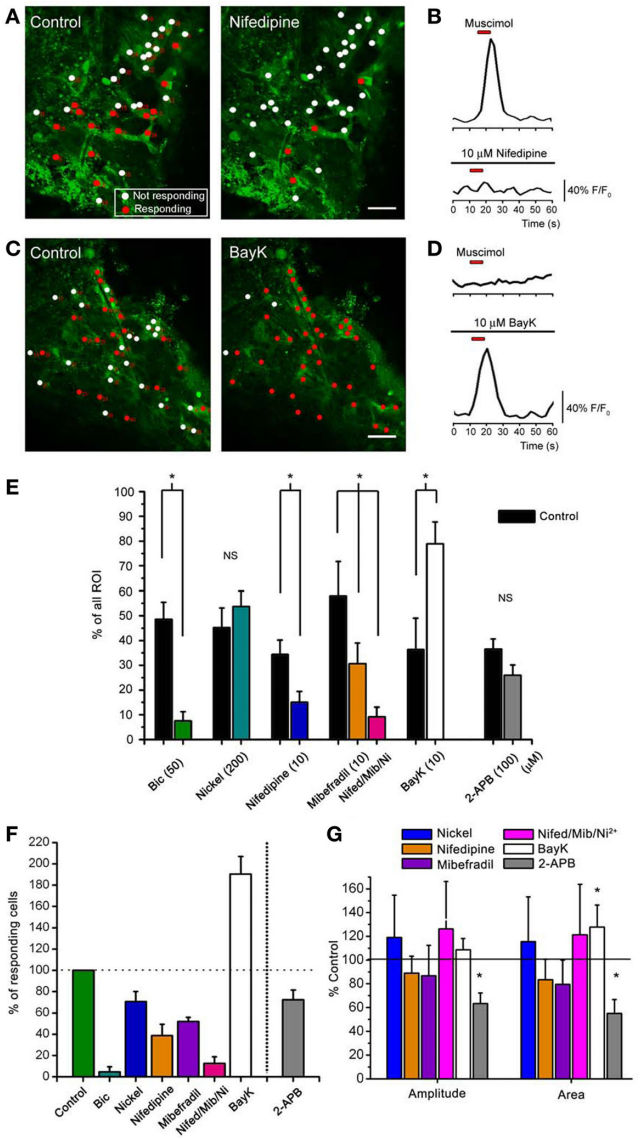

FIGURE 4 | Muscimol responses in SVZ astrocytes are inhibited by L- and T-type Ca^{2+} channel blockers. (A,C) Confocal images of Fluo-4 AM-loaded sagittal slices from *hGFAP*-MrgA1:GFP mice in control and in the presence of nifedipine in (A) (10 μM, an L-type Ca^{2+} channel blocker) or BayK in **(C)** (10 μM, a L-type Ca^{2+} channel enhancer). The red circles indicate muscimol-responsive SVZ astrocytes; the white circles indicate non-responsive cells. More cells respond to muscimol in the presence of BayK (indicated by red circles) while nifedipine silences cells. **(B)** Representative muscimol-induced Ca^{2+} responses from a "responding" cell (red circle) and subsequent block by nifedipine. **(D)** Representative muscimol-induced Ca^{2+} responses after bath application of BayK from a previously "non-responding" cell (white circle). Red bar: 10 s muscimol (20 μM). **(E)** Bar graphs showing the % of cells responding to muscimol from total ROI analyzed. Bic: bicuculline. **(F)** Bar graphs of the % of active cells responding after drug treatment. **(G)** Bar graphs of % of control of amplitude and area from cells that continued to respond after drug treatment. NS = not significant, * = $p < 0.05$.

SVZ cells was not feasible. *hGFAP*-DsRed mice are the most practical mouse line for performing Ca^{2+} imaging with the green fluorescent dye Fluo-4 AM since DsRed fluorescence is readily distinguishable from Fluo-4 fluorescence. However, in these mice not every SVZ astrocyte fluoresces red, and it is unclear whether a sub-population is targeted. In addition, the long half-life of DsRed could be an issue for positive identification. Newly born neuroblasts are DsRed fluorescent but are dimmer than astrocytes. The *hGFAP*-MrgA1:GFP mouse line appears to be the best model to study Ca^{2+} activity in SVZ astrocytes. GFP being fused to the MrgA1 receptor highlights the cell membrane and appears brighter than cytoplasmic Fluo-4 AM-loading. In addition, and perhaps more importantly, SVZ astrocytes can be selectively identified following increases in intracellular Ca^{2+} using the FLRFa peptide. In our system bath loading of the Ca^{2+} indicator Fluo-4 AM resulted in surface labeling of neuroblasts (data not shown). In the SVZ, cells are densely packed, thus limiting dye diffusion inside the tissue. In addition, neuroblasts tend to "bulge out" of the slice surface while astrocytes remain anchored inside the tissue as previously reported (Wang et al., 2003a). Instead, we used pressure loading inside the tissue resulting in preferential loading of SVZ astrocytes. With these experiments, we recommend using *hGFAP*-MrgA1:GFP mice to study Ca^{2+} activity in astrocyte-like cells of the SVZ in future studies.

Next, our pharmacological analyses suggest that the GABA$_A$-mediated Ca^{2+} increases arise from Ca^{2+} influx through L- and T-type VGCCs that are then amplified by Ca^{2+}-induced Ca^{2+} release from internal stores possibly involving IP3 receptors. This pathway is well-described in other neuronal and non-neuronal cell populations, and implies that GABA$_A$ receptor activation results in membrane depolarization that, in turn, activates VGCCs. Indeed, astrocytes are known to be depolarized by GABA$_A$ receptor activation resulting in GABA$_A$-induced Ca^{2+} increases (Bekar and Walz, 2002; Meier et al., 2008). GABA$_A$ depolarization is likely due to high intracellular Cl^- in SVZ astrocytes, although expression of the Cl^- importing transporter $Na^+/K^+/2Cl^-$ (NKCC1) and importantly the absence of the exporting Cl^- transporter $K^+/2Cl^-$ (KCC2) have not been examined in SVZ cells.

Considering the low-activation threshold of T-type VGCCs (as low as −70 mV) (Nilius et al., 2006), it is easily conceivable that these VGCCs can be opened by GABA$_A$-induced depolarization based on the published biophysical properties of SVZ astrocytes. Indeed, GABA$_A$ currents (100 μM GABA) range from −20 to −400 pA in gap-junction coupled SVZ astrocytes held at −84 mV (Liu et al., 2005). The current has a mean of −60 pA in SVZ astrocytes recorded in the presence of a gap junction channel blocker (unpublished data). These cells were recorded with an intracellular solution containing near-physiological chloride concentration. SVZ astrocytes' mean input resistance is 250 MΩ (range from 50 to 500 MΩ) and their mean resting potential is −85 mV ranging from −73 to −95 mV (Liu et al., 2006). Thus, a 60-pA GABA$_A$-current in a 250-MΩ astrocyte would result in a 15-mV depolarization, which is sufficient to reach the threshold for T-type VGCC activation.

L-type VGCCs are high-voltage activated ranging between −50 and −40 mV (Lacinova, 2005). Around ~40–50% of total astrocytes are muscimol-responsive in control conditions (from **Figure 3E**). Of those, ~40% are nifedipine-sensitive (see **Figure 4F**). Therefore, the population of astrocytes that reach the threshold for activation by L-type VGCCs comes to ~16–20% of all SVZ astrocytes. Similarly, SVZ astrocytes with higher input resistances (above 250 MΩ) correspond to ~40% of the total SVZ astrocytes (see Figure 6 in Liu et al., 2006). Of those with higher input resistance, 20% also have

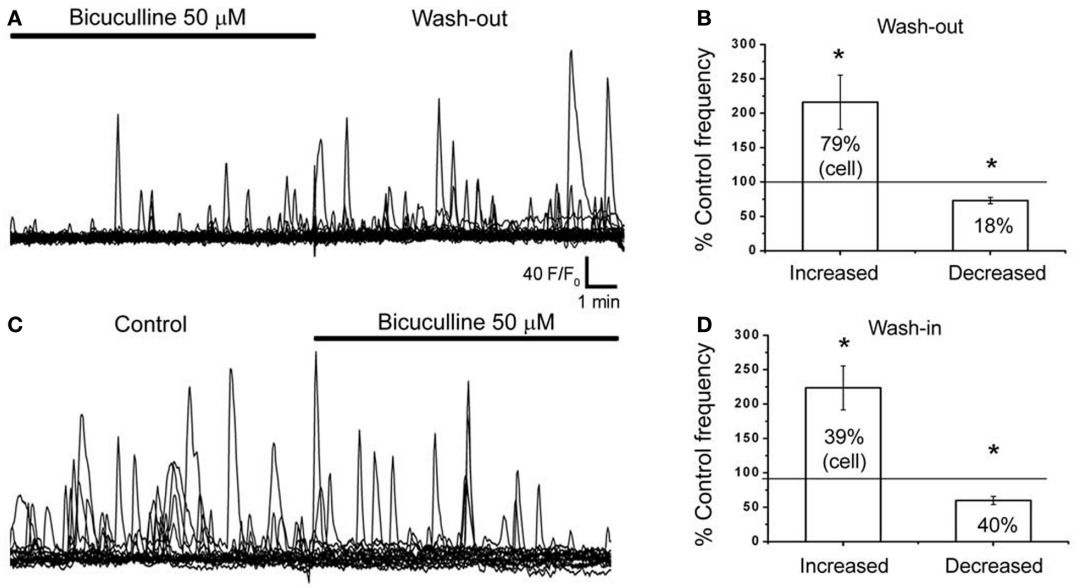

FIGURE 5 | Spontaneous Ca^{2+} activity in SVZ astrocytes are sensitive to GABA$_A$ receptor inhibition. (A,C) Representative traces of spontaneous Ca^{2+} activity from SVZ astrocytes before and after bicuculine (50 μM) wash-out **(A)** or wash-in **(C)**. **(B)** Bar graphs showing that 79% of SVZ astrocytes show an increased frequency to 220% of control during bicuculline wash-out. **(D)** Bar graphs showing that during bicuculline wash-I, 40% of SVZ astrocytes show a decreased 60% in frequency to compared to control. *indicates statistical significance.

resting potentials more depolarized than −80 mV, both of which would be required to reach L-type VGCC activation threshold. In this population, a current of 120 pA or less will be sufficient to reach the activation threshold of L-type VGCCs.

In the non-responding SVZ astrocytes, it is possible that either these cells do not express functional VGCCs or that GABA$_A$-depolarization did not reach the activation threshold for VGCCs. The fact that in the presence of BayK 8644, three-quarters of the SVZ astrocytes responded to muscimol suggests that the majority of, and perhaps all, astrocyte-like cells expresses DHP-sensitive VGCCs. These data suggest that GABA$_A$-depolarization in non-responding astrocyte-like cells does not reach the threshold to open VGCCs.

A question associated with the above data is whether there is enough GABA in the ambient milieu to activate GABA$_A$ receptors and modulate Ca^{2+} activity. GABA is synthesized and released by neuroblasts (Stewart et al., 2002; Nguyen et al., 2003; Bolteus and Bordey, 2004; De Marchis et al., 2004; Liu et al., 2005; Gascon et al., 2006) that may provide a tonic versus a phasic release of GABA (for review and discussion see Bordey, 2007). There are no known phasic or synaptic sources of GABA in the SVZ. It was suggested that ambient GABA levels may be in the μM range in the SVZ (Bolteus and Bordey, 2004; Bolteus et al., 2005). GABA levels are expected to fluctuate over time because neuroblasts migrate, thus changing the microenvironment of astrocyte-like cells. GABA$_A$ receptors in astrocyte-like cells have a reported EC_{50} for GABA of 15 μM and are thus expected to be tonically activated by low μM ambient GABA (Liu et al., 2005). Indeed, based on published data, GABA$_A$ receptors are tonically activated in 60% of the astrocyte-like cells (Liu et al., 2005). It was shown that bicuculline or picrotoxin applications induced a small shift in the current baseline that would correspond to a small depolarization of astrocyte-like cells.

Consistent with the predictions discussed above, we report that astrocyte-like cells of the SVZ display spontaneous Ca^{2+} transients, the activity of which is tonically regulated by ambient GABA acting on GABA$_A$ receptors. In particular, GABA$_A$ receptor inhibition revealed that tonic GABA$_A$ activation had two effects on SVZ astrocyte-like cells, dividing SVZ astrocytes into two functionally distinct populations. In one subpopulation of these cells, tonic GABA$_A$ receptor activation increased the frequency of Ca^{2+} transients while it decreased it in the other subpopulation. This latter GABA$_A$ action may result from a shunting effect of GABA$_A$ conductance in astrocyte-like cells. In future work, it will be important to understand how Ca^{2+} transients are generated in SVZ astrocytes.

In conclusion, tonic regulation of Ca^{2+} activity by ambient GABA could have major implications for the behavior of the Ca^{2+}-dependent release of diffusible molecules from astrocytes such as ATP (Striedinger et al., 2007). Considering that GABA$_A$ receptor activation has been shown to limit SVZ astrocyte proliferation (Liu et al., 2005), it remains to be determined whether GABA$_A$'s effect on proliferation involves L- and/or T-type VGCCs.

ACKNOWLEDGMENTS

This work was supported by grants from the National Institute of Health (NS048256 and DC007681, A.B.), Yale Brown-Coxe fellowship (J.-C.P.), and NRSA 1F31NS063758-01A1 (S.Z.Y.). We thank Tiffany Lin for assistance and discussion on the experiments and analysis. Thank you to M. Morgan Taylor for comments and editing.

SUPPLEMENTARY MATERIAL

The Supplementary Material for this article can be found online at http://www.frontiersin.org/cellularneuroscience/paper/10.3389/fncel.2010.00008/

REFERENCES

Barakat, L., and Bordey, A. (2002). GAT-1 and Reversible GABA Transport in Bergmann Glia in Slices. *J. Neurophysiol.* 88, 1407–1419.

Bekar, L. K., and Walz, W. (2002). Intracellular chloride modulates A-type potassium currents in astrocytes. *Glia* 39, 207–216.

Bellamy, T. C. (2006). Interactions between Purkinje neurones and Bergmann glia. *Cerebellum* 5, 116–126.

Bolteus, A. J., and Bordey, A. (2004). GABA Release and uptake regulate neuronal Precursor Migration in the Postnatal subventricular zone. *J. Neurosci.* 24, 7623–7631.

Bolteus, A. J., Garganta, C., and Bordey, A. (2005). Assays for measuring extracellular GABA levels and cell migration rate in acute slices. *Brain Res. Brain Res. Protoc.* 14, 126–134.

Bootman, M. D., Collins, T. J., Mackenzie, L., Roderick, H. L., Berridge, M. J., and Peppiatt, C. M. (2002). 2-aminoethoxydiphenyl borate (2-APB) is a reliable blocker of store-operated Ca2+ entry but an inconsistent inhibitor of InsP3-induced Ca2+ release. *FASEB J.* 16, 1145–1150.

Bordey, A. (2006). Adult neurogenesis: basic concepts of Signaling. *Cell Cycle* 5, 722–728.

Bordey, A. (2007). Enigmatic GABAergic networks in adult neurogenic zones. *Brain Res. Brain Res. Rev.* 53, 124–134.

Brenner, M., Kisseberth, W. C., Su, Y., Besnard, F., and Messing, A. (1994). GFAP promoter directs astrocyte-specific expression in transgenic mice. *J. Neurosci.* 14, 1030–1037.

Ciapa, B., Pesando, D., Wilding, M., and Whitaker, M. (1994). Cell-cycle calcium transients driven by cyclic changes in inositol trisphosphate levels. *Nature* 368, 875–878.

D'Andrea, P., Zacchetti, D., Meldolesi, J., and Grohovaz, F. (1993). Mechanism of [Ca2+]i oscillations in rat chromaffin cells. Complex Ca(2+)-dependent regulation of a ryanodine-insensitive oscillator. *J. Biol. Chem.* 268, 15213–15220.

De Marchis, S., Temoney, S., Erdelyi, F., Bovetti, S., Bovolin, P., Szabo, G., and Puche, A. C. (2004). GABAergic phenotypic differentiation of a subpopulation of subventricular derived migrating progenitors. *Eur. J. Neurosci.* 20, 1307–1317.

Doetsch, F., Petreanu, L., Caille, I., Garcia-Verdugo, J. M., and Alvarez-Buylla, A. (2002). EGF converts transit-amplifying neurogenic precursors in the adult brain into multipotent stem cells. *Neuron* 36, 1021–1034.

Fiacco, T. A., Agulhon, C., Taves, S. R., Petravicz, J., Casper, K. B., Dong, X., Chen, J., and McCarthy, K. D. (2007). Selective stimulation of astrocyte calcium in situ does not affect neuronal excitatory synaptic activity. *Neuron* 54, 611–626.

Gascon, E., Dayer, A. G., Sauvain, M. O., Potter, G., Jenny, B., De Roo, M., Zgraggen, E., Demaurex, N., Muller, D., and Kiss, J. Z. (2006). GABA regulates dendritic growth by stabilizing lamellipodia in newly generated interneurons of the olfactory bulb. *J. Neurosci.* 26, 12956–12966.

Lacinova, L. (2005). Voltage-dependent calcium channels. *Gen. Physiol. Biophys.* 24(Suppl. 1), 1–78.

Liu, X., Bolteus, A. J., Balkin, D. M., Henschel, O., and Bordey, A. (2006). GFAP-expressing cells in the postnatal subventricular zone display a unique glial phenotype intermediate between radial glia and astrocytes. *Glia* 54, 394–410.

Liu, X., Liao, D., and Ambudkar, I. S. (2001). Distinct mechanisms of [Ca2+]i oscillations in HSY and HSG cells: role of Ca2+ influx and internal Ca2+ store recycling. *J. Membr. Biol.* 181, 185–193.

Liu, X., Wang, Q., Haydar, T. F., and Bordey, A. (2005). Nonsynaptic GABA signaling in postnatal subventricular zone controls proliferation of GFAP-expressing progenitors. *Nat. Neurosci.* 8, 1179–1187.

Lledo, P. M., Alonso, M., and Grubb, M. S. (2006). Adult neurogenesis and functional plasticity in neuronal circuits. *Nat. Rev. Neurosci.* 7, 179–193.

Meier, S. D., Kafitz, K. W., and Rose, C. R. (2008). Developmental profile and mechanisms of GABA-induced calcium signaling in hippocampal astrocytes. *Glia* 56, 1127–1137.

Nguyen, L., Malgrange, B., Breuskin, I., Bettendorff, L., Moonen, G., Belachew, S., and Rigo, J. M. (2003). Autocrine/paracrine activation of the GABA(A) receptor inhibits the proliferation of neurogenic polysialylated neural cell adhesion molecule-positive (PSA-NCAM+) precursor cells from postnatal striatum. *J. Neurosci.* 23, 3278–3294.

Nielsen, J. V., Nielsen, F. H., Ismail, R., Noraberg, J., and Jensen, N. A. (2007). Hippocampus-like corticoneurogenesis induced by two isoforms of the BTB-zinc finger gene Zbtb20 in mice. *Development* 134, 1133–1140.

Nilius, B., Talavera, K., and Verkhratsky, A. (2006). T-type calcium channels: the never ending story. *Cell Calcium* 40, 81–88.

Noraberg, J., Jensen, C. V., Bonde, C., Montero, M., Nielsen, J. V., Jensen, N. A., and Zimmer, J. (2007). The developmental expression of fluorescent proteins in organotypic hippocampal slice cultures from transgenic mice and its use in the determination of excitotoxic neurodegeneration. *Altern. Lab. Anim.* 35, 61–70.

Owens, D. F., and Kriegstein, A. R. (2002). Is there more to GABA than synaptic inhibition? Nat. *Rev. Neurosci.* 3, 715–727.

Pathania, M., Yan, L. D., and Bordey, A. (2010). A symphony of signals conduct early and late stages of adult neurogenesis. Neuropharmacology.

Peppiatt, C. M., Collins, T. J., Mackenzie, L., Conway, S. J., Holmes, A. B., Bootman, M. D., Berridge, M. J., Seo, J. T., and Roderick, H. L. (2003). 2-Aminoethoxydiphenyl borate (2-APB) antagonises inositol 1, 4, 5-trisphosphate-induced calcium release, inhibits calcium pumps and has a use-dependent and slowly reversible action on store-operated calcium entry channels. *Cell Calcium* 34, 97–108.

Platel, J. C., Dave, K. A., and Bordey, A. (2008). Control of neuroblast production and migration by converging GABA and glutamate signals in the postnatal forebrain. *J. Physiol. (Lond.)* 586, 3739–3743.

Platel, J. C., Dupuis, A., Boisseau, S., Villaz, M., Albrieux, M., and Brocard, J. (2007). Synchrony of spontaneous calcium activity in mouse neocortex before synaptogenesis. *Eur. J. Neurosci.* 25, 920–928.

Platel, J. C., Gordon, V., Heintz, T., and Bordey, A. (2009). GFAP-GFP neural progenitors are antigenically homogeneous and anchored in their enclosed mosaic niche. *Glia* 57, 66–78.

Stewart, R. R., Hoge, G. J., Zigova, T., and Luskin, M. B. (2002). Neural progenitor cells of the neonatal rat anterior subventricular zone express functional GABA(A) receptors. *J. Neurobiol.* 50, 305–322.

Striedinger, K., Meda, P., and Scemes, E. (2007). Exocytosis of ATP from astrocyte progenitors modulates spontaneous Ca2+ oscillations and cell migration. *Glia* 55, 652–662.

Wang, D. D., Krueger, D. D., and Bordey, A. (2003a). Biophysical properties and ionic signature of neuronal progenitors of the postnatal subventricular zone in situ. *J. Neurophysiol.* 90, 2291–2302.

Wang, D. D., Krueger, D. D., and Bordey, A. (2003b). GABA depolarizes neuronal progenitors of the postnatal subventricular zone via GABAA receptor activation. *J. Physiol (Lond.)* 550, 785–800.

Zhao, C., Deng, W., and Gage, F. H. (2008). Mechanisms and functional implications of adult neurogenesis. *Cell* 132, 645–660.

Conflict of Interest Statement: The authors declare that the research was conducted in the absence of any commercial or financial relationships that could be construed as a potential conflict of interest.

Received: 02 February 2010; paper pending published: 03 March 2010; accepted: 10 March 2010; published online: 08 April 2010.

Citation: Young SZ, Platel J-C, Nielsen JV, Jensen NA and Bordey A (2010) GABA$_A$ increases calcium in subventricular zone astrocyte-like cells through L- and T-type voltage-gated calcium channels. Front. Cell. Neurosci. ***4****:8. doi: 10.3389/fncel.2010.00008*

frontiers in
CELLULAR NEUROSCIENCE

REVIEW ARTICLE
published: 14 April 2010
doi: 10.3389/fncel.2010.00011

GABAergic control of neurite outgrowth and remodeling during development and adult neurogenesis: general rules and differences in diverse systems

Evelyne Sernagor[1]*, François Chabrol[1], Guillaume Bony[2] and Laura Cancedda[2]

[1] *Institute of Neuroscience, Newcastle University Medical School, Newcastle upon Tyne, UK*
[2] *Department of Neuroscience and Brain Technologies, Italian Institute of Technology, Genoa, Italy*

Edited by:
Yehezkel Ben-Ari, INSERM, France

Reviewed by:
Yehezkel Ben-Ari, INSERM, France

****Correspondence:***
Evelyne Sernagor, Institute of Neuroscience, Newcastle University Medical School, Framlington Place, Newcastle upon Tyne NE2 4HH, UK.
e-mail: evelyne.sernagor@ncl.ac.uk

During development, Gamma-aminobutyric acidergic (GABAergic) neurons mature at early stages, long before excitatory neurons. Conversely, GABA reuptake transporters become operative later than glutamate transporters. GABA is therefore not removed efficiently from the extracellular domain and it can exert significant paracrine effects. Hence, GABA-mediated activity is a prominent source of overall neural activity in developing CNS networks, while neurons extend dendrites and axons, and establish synaptic connections. One of the unique features of GABAergic functional plasticity is that in early development, activation of $GABA_A$ receptors results in depolarizing (mainly excitatory) responses and Ca^{2+} influx. Although there is strong evidence from several areas of the CNS that GABA plays a significant role in neurite growth not only during development but also during adult neurogenesis, surprisingly little effort has been made into putting all these observations into a common framework in an attempt to understand the general rules that regulate these basic and evolutionary well-conserved processes. In this review, we discuss the current knowledge in this important field. In order to decipher common, universal features and highlight differences between systems throughout development, we compare findings about dendritic proliferation and remodeling in different areas of the nervous system and species, and we also review recent evidence for a role in axonal elongation. In addition to early developmental aspects, we also consider the GABAergic role in dendritic growth during adult neurogenesis, extending our discussion to the roles played by GABA during dendritic proliferation in early developing networks versus adult, well established networks.

Keywords: GABA, $GABA_A$ receptor, dendrite, axon, development, adult neurogenesis, paracrine

INTRODUCTION

Gamma-aminobutyric acid (GABA) is the main inhibitory neurotransmitter in mature neural networks. However, there is now a plethora of evidence demonstrating that GABAergic signalling plays important functions in the developing CNS and during adult neurogenesis long before synapse formation, exerting numerous trophic, paracrine roles, ranging from controlling cell proliferation and migration to neurite outgrowth, synapse formation and cell death (for review see Ben-Ari et al., 2007; Ge et al., 2007; Wang and Kriegstein, 2009).

GABA can act on three types of receptors, namely $GABA_A$, $GABA_B$ and $GABA_C$ types. The early trophic effects of GABA are mostly mediated by the activation of ionotropic $GABA_A$ receptor linked to a Cl^- channel. $GABA_A$ receptors are pentomeric complexes composed of several subunits belonging to seven families (α1–6, β1–4, γ1–3, δ, ρ1–2) of membrane proteins, linked to the synaptic anchoring protein gephyrin and to the cytoskeleton. These subunits can assemble in various combinations, which *in vivo* are generally composed of isoforms of α, β and γ subunits, yielding a large variety of $GABA_A$ receptors subtypes (for review see Mohler, 2007). The structural diversity of these isoreceptors determines their functional properties (e.g. channel kinetics, affinity to ligands, desensitization properties), and different cell types can express different $GABA_A$ receptor isoforms. Therefore, these cells can also have different sensitivity to GABAergic activation. The precise composition of $GABA_A$ receptors subunits is not fixed at early developmental stages; it appears to be a rather dynamic process that may be modulated by GABA itself (Cobas et al., 1991). Although the subunit complexes vary in different cell types, general rules apply to developmental changes in the composition of $GABA_A$ receptors. During early development, α2, β2/3 subunits are prominent while the α1 subunit is scarce (Hornung and Fritschy, 1996). As development progresses, there is an increase in α1 subunits with a concomitant decrease in α2 subunits whilst the expression of β2/3 subunits remains unchanged. The switch from α1 to α2 subunits coincides with synapse formation and may be associated with the emergence of synaptic inhibition. The γ2 subunit is highly expressed at early stages, as it is required for postsynaptic, clustering of $GABA_A$ receptors (Essrich et al., 1998). Tonic GABAergic activity as it occurs during early development involves different subunits such as δ or α5 (for review see Farrant and Nusser, 2005).

In the mature brain, $GABA_A$ receptor activation leads to Cl^- influx, resulting in hyperpolarization (inhibition) of the cell. In immature neurons (both during early development and

adulthood), however, $GABA_A$ receptor activation is depolarizing and mainly excitatory (LoTurco et al., 1995; Ben-Ari et al., 2007; Ge et al., 2007; Wang and Kriegstein, 2009). The depolarizing effect of GABA in developing neurons is due to an efflux rather than influx of Cl^- ions following activation of $GABA_A$ receptors, because the intracellular Cl^- concentration is higher than in mature cells. Such reverse Cl^- gradient depends on a high expression of the $Na^+/K^+/Cl^-$ cotransporter NKCC1 (Blaesse et al., 2009), which pumps Cl^- inside the immature neuron, and a low expression of the K^+/Cl^- cotransporter KCC2, which normally extrudes Cl^- from mature neurons (Rivera et al., 1999). This Cl^--mediated depolarization provides a strong excitatory drive that can trigger action potentials (Leinekugel et al., 1997) and opening of voltage-dependent Ca^{2+} channels (VDCCs). This, in turn, leads to Ca^{2+} influx and transient increases in intracellular Ca^{2+} (Yuste and Katz, 1991; Tozuka et al., 2005; Goffin et al., 2008), which will exert a variety of trophic effects. The shift from GABAergic excitation to inhibition occurs as KCC2 expression and functionality increase with maturation. The role of cation-Cl^- co-transporters in controlling the nature of $GABA_A$ responses is a universal phenomenon that is well preserved across development, brain areas and animal species (for review see Blaesse et al., 2009).

Depolarizing GABAergic activity is present at the earliest stages of network activity, long before the onset of sensory experience, when the developing CNS is spontaneously active, neurons extend dendrites and axons, and they establish synaptic connections. This was first reported in the hippocampus, where immature pyramidal cells exhibit GABA-mediated giant depolarizing potentials before the maturation of glutamatergic synapses (Ben-Ari et al., 1989). Early spontaneous GABAergic activity has since been reported in many immature systems including the neocortex, hypothalamus, spinal cord, ventral tegmental area, cerebellum, retina and olfactory bulb (for review see Ben-Ari, 2002) as well as during adult neurogenesis (for review see Bordey, 2007).

The GABAergic transition from excitation to inhibition is activity-dependent. An initial *in vitro* study reported that GABAergic activity regulates its own switch from excitation to inhibition (Ganguly et al., 2001). Although this finding was successively challenged (Ludwig et al., 2003), it was then confirmed in the retina *in vivo* (Leitch et al., 2005). Interestingly, a recent study reported that spontaneous cholinergic nicotinic activity (in chick ciliary ganglion, spinal cord and hippocampus) triggered the GABAergic shift from excitation to inhibition (Liu et al., 2006). Cholinergic nicotinic blockade (in dissociated cultures or in animals knockout for nicotinic cholinergic receptors) prevented $GABA_A$ responses from becoming hyperpolarizing, and this was due to the retention of an immature expression pattern of Cl^- transporters. This early cholinergic nicotinic role may be of particular relevance in the retina where the earliest spontaneous network activity consists of acetylcholine (nicotinic)-mediated waves spreading across the retinal ganglion cell (RGC) layer (for review see Sernagor et al., 2001). Interestingly, depolarizing $GABA_A$ activity becomes involved in controlling the dynamics of the waves at later stages (Sernagor et al., 2003; Syed et al., 2004). Indeed, as it gradually shifts to become inhibitory, it downregulates retinal waves, causing them to slow down and become narrower until they eventually disappear (Sernagor et al., 2003).

The goal of this review is to recapitulate the current knowledge about the role of GABA in neurite outgrowth during development and in adult neurogenesis. Although many studies addressing these important issues have been published, so far little attempt has been made to put all these observations into a common framework in an attempt to understand the general rules that regulate these basic and evolutionary well-conserved processes.

IN VITRO STUDIES

The first evidence that GABA may affect neurite outgrowth was provided by Eins et al. (1983). Indeed, they demonstrated that differentiated C1300 mouse neuroblastoma cells treated with GABA showed an increase in the length and branching of processes (Eins et al., 1983). A large amount of *in vitro* evidence has been provided ever since in several brain areas and diverse species.

CORTEX

GABA treatment promotes neurite length and branching in mixed (inhibitory and excitatory) cortical neurons in embryonic chick and rat cultures (Baloyannis et al., 1983; Spoerri, 1988), and in rat interneurons in cultures from cortical plate and subplate microdissections (Maric et al., 2001). Conversely, treatment of rat neurons in culture with the $GABA_A$ receptor antagonist bicuculline inhibited the extent of neuritic arborization (Ben-Ari et al., 1994; Maric et al., 2001). Interestingly, agents that blocked GABA synthesis caused a reduction of neurite outgrowth. Moreover, in the absence of GABAergic signaling, neuritogenesis was preserved by depolarizing cells and elevating the intracellular Ca^{2+} concentration. Activation of high-threshold L-type Ca^{2+} channels *per se* mimicked the GABA-induced effect. Furthermore, neurite growth could also be antagonized by blocking the Cl^- accumulating pump NKCC1 (Maric et al., 2001). Finally, the effects on neurite outgrowth were absent if the $GABA_A$ agonist was given after the shift of GABAergic signaling from hyperpolarizing to depolarizing had taken place (Maric et al., 2001). All together, these results suggest an involvement of depolarizing GABA and consequent intracellular Ca^{2+} elevation for $GABA_A$-mediated effect on neurite growth.

$GABA_B$ receptors may also play a role in regulating neurite outgrowth as exposure of cortical organotypic slices to a specific $GABA_B$ receptor antagonist resulted in a decrease in the length of the leading process in migrating inhibitory neurons (Lopez-Bendito et al., 2003).

HIPPOCAMPUS

Numerous studies showed that modulation of $GABA_A$-receptor signaling influences neurite growth in hippocampal rodent neurons in cultures. In particular, Barbin et al. (1993) showed a reduction in the number of primary neurites and branching points (resulting in a concomitant decrease of the total neuritic length) upon treatment of cell cultures with bicuculline. Interestingly, the authors reported no effect on neurite outgrowth after treatment with the specific $GABA_A$ receptor agonist muscimol, possibly indicating a role for tonic-GABA signaling in the process (Barbin et al., 1993). In the latter study, authors did not differentiate between excitatory and inhibitory neurons in the cultures. Conversely, muscimol did induce an increase in the number and length of primary dendrites in cultured inhibitory interneurons (Marty et al., 1996).

Notably, application of muscimol reduced the number of primary dendrites when applied 2 weeks after plating (after the excitatory to inhibitory switch of GABA responses takes place), again suggesting the requirement of depolarizing GABA. Interestingly, in a recent paper, a possible involvement of the α5 subunit (but not β2) of the $GABA_A$ receptor was suggested for the GABA-induced effect on neurite outgrowth via lowering of brain-derived neurotrophic factor (BDNF) levels in hamster hippocampal neurons treated with a specific α5 inverse agonist (Giusi et al., 2009). The latter results, again, point to a possible involvement of tonic GABA signaling in neuritogenesis.

CEREBELLUM

GABA treatment triggers dendritic growth and arborization in dissociated cultures of developing cerebellar neurons (Baloyannis et al., 1983). Moreover, cultured cerebellar granule cells (CGCs) have been the focus of further studies demonstrating that GABA has a trophic neuritogenic effect. Indeed, when exposed to GABA for several days, developing CGCs extended significantly more neurites than when grown in control conditions (Hansen et al., 1984). Furthermore, this effect was accompanied by ultrastructural changes such as an increase in the density of cytoskeleton components (neurotubules). Notably, all these effects were not only counteracted, but even severely impaired by depleting the cells of the polyamines putrescine and spermidine (Abraham et al., 1993), indicating that the neuritogenic effects of GABA were linked to protein synthesis and mechanisms regulating cell proliferation. Moreover, the GABAergic effects on immature CGC dendritic proliferation appeared to be triggered by Ca^{2+} influx through the activation of L-type VDCCs, and they were prevented by Ca^{2+} channel blockers such as Mg^{2+} and nifedipine (Fiszman et al., 1999; Borodinsky et al., 2003). Finally, specific blockade of calcium-calmodulin kinase II (CaMKII) and of extracellular signal-regulated kinase 1 and 2 (ERK1/2) also prevented the GABAergic effects on dendritic growth (Borodinsky et al., 2003), indicating the involvement of Ca^{2+} induced activation of various kinases during the differentiation of CGC dendrites (Borodinsky et al., 2003).

Different, and even opposite GABAergic effects on dendritic growth were reported in embryonic rat cerebellar and chick tectum cultures grown in different conditions (Michler, 1990). In serum-containing medium, GABA stimulated neurite growth. Conversely, GABA had the opposite effect in serum-free medium, and $GABA_A$ receptors agonists had the same effect (despite the fact that $GABA_A$ receptors are present in serum-free medium). At the same time, the $GABA_B$ receptor agonist baclofen inhibited neurite elongation in serum-free medium and had no effect in the presence of serum, suggesting that the different action of GABA in serum-free medium may be linked to $GABA_B$ receptor-mediated mechanisms. These studies underscore that one of the main drawbacks of using dissociated cultures is that it is difficult to replicate *in vivo* growth conditions, and that many of the apparent contradictions in *in vitro* studies may be overcome by *in vivo* experiments.

RETINA

The effect of GABA on retinal dendritic growth has not been extensively studied *in vitro*. Spoerri (1988) reported that GABA had a positive effect on dendritic growth in retinal cultures. Like in CGCs in the cerebellum (Hansen et al., 1984), exposure to GABA led to an increase in microtubules density. Moreover, GABA and the $GABA_B$ receptor agonist baclofen both stimulate RGC neurite outgrowth in *Xenopus* cultures (Ferguson and McFarlane, 2002).

OLFACTORY BULB

The olfactory bulb is being widely used for studies on adult neurogenesis (see Effect of GABA on Neurite Extension During Adult Neurogenesis in this review), but few papers also reported GABAergic effects on dendritic growth in immature cultures.

Opposite GABAergic effects to those described in systems outlined in previous sections were reported in primary cultures of embryonic accessory olfactory bulb, where blockade (by bicuculline) rather than activation of $GABA_A$ receptors induces the formation of filopodia in non GABAergic, presumed mitral cells (Kato-Negishi et al., 2003). However, these same cells were quiescent in control conditions and they developed glutamate-mediated sustained Ca^{2+} oscillations in the presence of bicuculline, suggesting that GABA is actually hyperpolarizing in these cultures. Hence, in this case the neuritogenic effect of bicuculline is probably associated with GABAergic disinhinbition and consequently glutamatergic excitation rather than with direct GABAergic effects.

Astrocytes may provide a source of GABA while neurons extend dendrites and establish synaptic connections in cocultures of neurons and astrocytes from the neonatal olfactory bulb (Matsutani and Yamamoto, 1998). Indeed, dendritic branching is inhibited by $GABA_A$ antagonists (and tetrodotoxin) in neurons growing without contact with other neurons but only with astrocytes. The effect was reversed by growing the cultures in the presence of the $GABA_A$ agonist muscimol or by depolarizing the cells with elevated extracellular K^+. However, when neurons were grown on a bed of dead astrocytes, all these effects were absent, demonstrating that astrocytes may exert a paracrine neuritogenic GABAergic effect on neurons growing in their vicinity.

BRAIN STEM

$GABA_A$ activity seems to have differential effects on dendritic growth in different cell types in brainstem cultures (Liu et al., 1997). Indeed, GABA had positive neuritogenic effects on monoamine (serotonergic and noradrenergic) neurons whilst it had negative effects on GABAergic neurons in the same cultures. The results of this pharmacological study were explained by the authors as dependent on the precise composition of the subunits of the $GABA_A$ receptors in different cell subtypes, which may then influence the effect that GABA has on dendritic growth. There is, however, another possible explanation. Indeed, we note that GABA did not appear to be depolarizing in this system because it induced Cl^- influx rather than efflux. Moreover, it is not possible to know whether all three cell types really had GABA-mediated Cl^- influx because the results were presented for a mixed population of brainstem neurons. It may very well be that a more precise analysis of these responses in the three different cell types would reveal significant differences in the extent to which GABA causes hyperpolarization, and in some cases it may even induce membrane depolarization (and thus Ca^{2+} influx). So although the possibility that the precise composition of the subunits of the $GABA_A$ receptors may indeed influence the effect

that GABA has on dendritic growth, it is important first to eliminate the possibility that GABA may exert different levels of depolarization in the three populations of cells. Such differences may explain why the monoamine neurons reacted positively to GABA in terms of dendritic growth whereas the effect on GABAergic neurons was the opposite.

SPINAL CORD

Similar to the earlier study by Michler (1990) in tectum and cerebellum, GABA had an inhibitory effect on dendritic proliferation in spinal cord cultures kept in heat inactivated-serum medium, and the effect was mimicked by the $GABA_B$ agonist baclofen (Bird and Owen, 1998). Here, however, although GABA did not significantly inhibit dendritic growth in serum-containing medium, no $GABA_A$-mediated dendritic proliferation effects were observed. This is the only study that has not reported a $GABA_A$-mediated neuritogenic effect. The reasons are not clear. One possibility is that serum inactivation by heat may have destroyed some essential components in the medium.

Another explanation is that glycine may be the predominant protagonist in the spinal cord during development, playing a role similar to what GABA does in other systems. Indeed, glycine is abundant in the spinal cord, and glycinergic receptors share many developmental similarities with $GABA_A$ receptors with respect to their Cl^--mediated depolarizing responses (Wu et al., 1992). One study on developing spinal cord cultures reported interplay between glycine and GABA in controlling neurite outgrowth (Tapia et al., 2001). In that study, at the time of intense neurite outgrowth (5-day-old cultures) both glycine and GABA induced depolarization and Ca^{2+} influx, and spontaneous synaptic events were predominantly glycinergic (although to a lesser extent also GABAergic). Neurite outgrowth in that system appeared to be promoted only when glycinergic neurotransmission was inhibited, because it was observed either at glycine concentrations that are high enough to desensitize glycine receptors or in the presence of the glycine receptor antagonist strychnine. Interestingly, opening of L-type Ca^{2+}channels via $GABA_A$ receptor activation was necessary for the glycinergic effect. Tapia et al. (2001) suggested that the predominant glycinergic synaptic activity shunted neuronal excitability mediated by $GABA_A$ receptors, hence setting the intracellular Ca^{2+} concentration to suboptimal levels for neurite outgrowth. Glycine receptor desensitization or blockade may therefore relieve the system from its inhibitory state by increasing intracellular Ca^{2+} concentration to optimal levels.

PERIPHERAL NERVOUS SYSTEM

In chick embryonic ciliary ganglion, cholinergic nicotinic activity induces the GABAergic switch from excitation to inhibition, and the effect is linked to KCC2 downregulation (Liu et al., 2006). Concomitantly, when KCC2 expression is forced prematurely *in vitro*, the depolarizing effect of GABA vanishes and neurons loose dendritic processes following prolonged exposure to GABA. Interestingly, these neurons also switched from being multipolar to becoming unipolar, as observed *in vivo* during normal development. If either GABA is omitted from the cultures or KCC2 activity is not induced, neurons remain multipolar. This confirms the neuritogenic role played by GABA while it is depolarizing.

IN VIVO STUDIES

Despite a large body of data indicating a fundamental role for GABA in neurite outgrowth *in vitro*, *in vivo* evidence has been provided only in the last few years.

HIPPOCAMPUS

The first hint came from a study by Groc et al. (2002, 2003), who investigated the role of early GABA and glutamate-driven network activity in the morphological differentiation of CA1 pyramidal cells (by means of neurobiotin filling of electrophysiologically recorded cells). This study reported a strong reduction in the frequency of spontaneous GABA and glutamatergic synaptic currents following injection of tetanus toxin into postnatal day 1 (P1) rat hippocampi. Moreover, consequent blockade of giant depolarizing potentials during the first postnatal week induced a threefold reduction in the total length of basal dendritic trees in pyramidal cells analyzed at the end of the first postnatal week. Interestingly, the apical dendrite, the axons, or the soma grew normally during activity deprivation.

CORTEX

More direct evidence pointing towards a role for $GABA_A$ receptor in neurite outgrowth *in vivo* derived from studies performed in the cortex and retina. Indeed, prematurely shifting the GABA reversal potential to a more hyperpolarizing potential (by knockdown of NKCC1 or overexpression of KCC2) *in utero* resulted in fewer, shorter, and less branched dendrites (Cancedda et al., 2007; Wang and Kriegstein, 2008). The effect seemed to be dependent on the depolarizing action of GABA, as (1) it was mimicked by overexpression of the K^+ inward rectifying channel Kir 2.1, which decreased cell excitability by lowering the resting membrane potential of the cell, and (2) it was absent when a mutated version of KCC2 (which was not able to pump Cl^- ions) was transfected (Cancedda et al., 2007). Conversely, mice lacking the $GABA_A$ receptor α1 subunit, typical of synaptic GABA receptors, displayed dendritic arborization similar to wild type animals (Heinen et al., 2003), once again suggesting that tonic rather than phasic GABAergic transmission may be responsible for the neurogenic effects of GABA.

RETINA

Intense RGC dendritic development occurs while the retina generates spontaneous waves (Sernagor et al., 2001). In turtle, peak RGC dendritic proliferation occurs 1 week before hatching (Mehta and Sernagor, 2006a,b), coinciding with the time depolarizing $GABA_A$ activity becomes involved in controlling the dynamics of the waves (Sernagor et al., 2003). Chronic exposure to bicuculline by means of the slow release polymer Elvax, inserted in the eye from the time GABA starts to modulate retinal waves, resulted in a significant loss of RGC dendritic branches without affecting the overall coverage of dendritic arbors (F. Chabrol and E. Sernagor, unpublished observations). At the same time, chronic GABAergic depletion (by blockade of GABA synthesis) caused severe arbor shrinkage, but dendrites also exhibited numerous very small dendritic branches covering the entire dendritic tree (F. Chabrol and E. Sernagor, unpublished observation). These observations suggest that as in other systems, GABA has a positive neuritogenic effect on dendritic growth. The appearance of numerous small branches covering the entire tree in GABA-depleted retinas

demonstrates that like in the olfactory bulb (Gascon et al., 2006; see Effect of GABA on Neurite Extension During Adult Neurogenesis), GABA has a stabilizing effect on dendritic proliferation.

GABAergic INHIBITION AND DENDRITIC GROWTH

All the studies reported so far have pointed to a possible role for depolarizing GABA in neurite development. A recent paper has addressed the role of GABAergic inhibition on neuronal morphological maturation in *Xenopus* tadpole *in vivo* (Shen et al., 2009). In this paper, authors tested whether inhibitory GABAergic synaptic transmission regulates dendritic arbor development in the *Xenopus* optic tectum by expressing a peptide corresponding to an intracellular loop (ICL) of the γ2 subunit of $GABA_A$ receptor *in vivo*. This peptide completely blocked $GABA_A$-mediated transmission in one third of transfected neurons, and significantly reduced $GABA_A$-mediated synaptic currents in the remaining transfected cells. *In vivo* time-lapse imaging showed that ICL expressing neurons had more sparsely branched dendritic arbors, which nevertheless expanded over larger neuropil areas than in control neurons. Furthermore, analysis of branch dynamics indicated that ICL expression affected arbor growth by reducing rates of branch addition. These intriguing results share common points with the retina, where chronic blockade of $GABA_A$ receptors with bicuculline yield less branched RGC dendritic trees (see previous section). However, in the retina, GABA remained at least partially excitatory in these conditions (Leitch et al., 2005), whereas here GABA appears to be inhibitory, suggesting that GABAergic inhibition normally promotes dendritic growth. One possibility is that extrasynaptic, tonic GABA activity is unaffected because only the γ2 subunit of the $GABA_A$ receptor is impaired, that subunit being mostly specifically associated with synaptic receptors (Farrant and Nusser, 2005). As many examples demonstrate in literature, extrasynaptic GABAergic activity may play important trophic roles, including neuritogenesis. So, in the present case, perhaps extrasynaptic GABAergic signaling is less impaired than assumed. The effects reported on dendritic growth may arise from complex interactions between paracrine GABAergic activity and partially disinhibited glutamatergic synaptic activity.

EFFECT OF GABA ON AXONAL ELONGATION

If on one hand GABA action through $GABA_A$ receptors appears to be a key player in dendritic development, does GABAergic signaling also affect axonal morphological maturation? Recently gathered evidence indicates that this may indeed be the case.

In 2007, Chattopadhyaya et al. demonstrated in organotypic cortical slices that endogenous GABA levels regulate cortical basket-cell axonal branching through the activation of $GABA_A$, and to lesser extent $GABA_B$ receptors during the maturation of inhibitory circuits (Chattopadhyaya et al., 2007). Nevertheless, it is worth noting that this study was performed in the adolescent brain, when GABA is inhibitory (Chattopadhyaya et al., 2007). Furthermore, reversing the Cl^- gradient *in vivo*, from the onset of development, by global KCC2 overexpression in newly fertilized zebrafish embryos reduced the elaboration of axonal tracts (Reynolds et al., 2008).

The effect of GABA on axonal growth may be specifically mediated by the α_2 subunit of the $GABA_A$ receptor, as a α_2 (but not α5) selective agonist strongly reduced axonal sprouting in cell cultures of hamster hippocampal neurons (Giusi et al., 2009). Furthermore, a new study has recently addressed specifically whether GABA signaling may affect axonal morphological maturation both *in vitro* and *in vivo* (Ageta-Ishihara et al., 2009). This study has reported that GABA-mediated increase in intracellular Ca^{2+} via CaMKs influenced axon elongation in cortical neuronal cultures. In particular, two separate branches of the CaMK family, namely CaMKK-CaMK1α and CaMKK-CaMKIγ, respectively guided axonal and dendritic elongation. Indeed, the $GABA_A$ agonist muscimol promoted Ca^{2+} influx and axonal elongation, and this GABAergic axogenic effect was mediated through the CaMKK-CaMKIα cascade. These *in vitro* effects were confirmed *in vivo*, where knockdown of CaMKIα severely impaired the elongation of callosal axonal projections in the somatosensory cortex. Furthermore, $GABA_A$ receptors blockade with bicuculline had an inhibitory effect on axonal elongation, confirming that endogenous GABA was necessary for axonal growth. Finally, lowering the intracellular Cl^- concentration by forced expression of KCC2 abolished the muscimol-induced effect, which corroborated the idea that the effect was mediated through membrane depolarization and Ca^{2+} influx. However, very surprisingly, and in contradiction with previous studies, muscimol did not promote dendritic growth in this study. On the other hand, BDNF specifically induced dendritic growth via the CaMKK-CaMKIγ pathway in the same cultures (Takemoto-Kimura et al., 2007). Interestingly, Ageta-Ishihara et al. (2009) also reported that premature elimination of the excitatory GABA drive by forced expression of KCC2 or NKCC1 downregulation *in vivo* dramatically perturbed the morphological maturation of terminal callosal axonal branches. (H. Mizuno, T. Hirano, and Y. Tagawa, unpublished observation).

EFFECT OF GABA ON NEURITE EXTENSION DURING ADULT NEUROGENESIS

Neurogenesis in the adult brain is a process that occurs throughout life in the mammalian hippocampus and olfactory bulb under physiological conditions (Ma et al., 2009). Adult neurogenesis recapitulates the complete process of neuronal development in a mature CNS environment (e.g. proliferation of neural progenitors, migration and differentiation of neuroblasts, and synaptic integration of newborn neurons). Interestingly, depolarizing GABA, as in the embryonic nervous system, has emerged as a key player in multiple steps of adult neurogenesis. In particular, *in vivo* and *in vitro* studies demonstrated a role for GABA receptor signaling in neuritogenesis of newborn neurons both in the hippocampus and in the olfactory bulb (Ge et al., 2007).

HIPPOCAMPUS

Conversion of GABA-induced depolarization into hyperpolarization in newborn neurons in adult hippocampus leads to marked defects on dendritic development *in vivo* (Ge et al., 2006). Indeed, downregulation of the NKCC1 cotransporter by viral injection reduced the total dendritic length and branch number, as well as dendritic complexity in newborn neurons. In addition, injection of the $GABA_A$ receptor agonist pentobarbital promoted dendrite growth of newborn neurons *in vivo* (Ge et al., 2006). Interestingly, seizure induction, which increases the local hippocampal ambient GABA levels (Ueda and Tsuru, 1995; Patrylo et al., 2001; Cossart et al., 2005; Naylor et al., 2005), greatly accelerated

dendritic development of newborn granule cells in adult mice (Overstreet-Wadiche et al., 2006). It is possible that this GABA-induced effect on neurite outgrowth depends on Ca^{2+} elevation since, as in neonatal development, GABA depolarization increases the intracellular Ca^{2+} concentration in newborn neurons (Tozuka et al., 2005; Goffin et al., 2008). Moreover, GABA-mediated depolarization was also involved in the phosphorylation of CREB during the first 2 weeks of development *in vivo* (Jagasia et al., 2009), and CREB phosphorylation in turn promoted dendritic development (Jagasia et al., 2009). Importantly, developmental defects after the loss of GABA-mediated excitation (by NKCC1 knockdown) could be compensated by enhancement of CREB signaling (Jagasia et al., 2009), indicating that the CREB pathway may influence neuritogenesis downstream of GABA-mediated excitation. Furthermore, CREB signaling may eventually converge onto BDNF pathway for the dendritogenic effect, as dendrite branching, length and complexity was seriously affected in mice with postnatal depletion of BDNF (Chan et al., 2008).

OLFACTORY BULB

Newly generated cells in the subventricular zone (SVZ) of the lateral ventricle migrate to the olfactory bulb trough the rostral migratory stream in adult mammals. GABA mediates the first extrasynaptic responses in these migrating SVZ cells, and at that time, like in immature systems, GABA is depolarizing and opens L-type Ca^{2+} channels (Carleton et al., 2003; Gascon et al., 2006). Ambient GABA appears to induce dendritic proliferation both in dissociated cultures of neonatal SVZ cells and in olfactory bulb slices. This effect was mediated via activation of $GABA_A$ receptors because when the cultures or slices were incubated in the presence of the $GABA_A$ antagonist bicuculline, dendritic growth was severely disrupted (mostly by reducing the number and length of primary dendrites), yielding dendritic arbors with much less complexity (Gascon et al., 2006). This effect was pronounced only on newly generated cells but not on older ones. GABA also caused growth cones to become larger. This early effect is not due to changes in growth cones dynamics (formation and retraction of lamellipodia), but rather to an increase in their lifetime and even in their numbers. GABA had a similar stabilizing effect on newly formed dendrites, while bicuculline increased the frequency of dendritic retraction phases. These neuritogenic GABAergic effects were correlated with the stabilization of microtubules (assayed by measuring the amount of polymerized versus non-polymerized tubulin) in newly formed dendrites. This whole chain of events necessitated Ca^{2+} influx triggered by GABAergic depolarization, because the neuritogenic effects of GABA were abolished when transient increases in intracellular Ca^{2+} were prevented. Interestingly, $GABA_B$ receptor-mediated signaling did not seem to be important for the effect, as the authors found that in dissociated cultures from SVZ-derived neurons of newborn rats, treatment with the $GABA_B$ antagonist CGP54626 resulted in no changes in dendritic arbors and lamellipodia dynamics (Gascon et al., 2006). Conversely, CREB phosphorylation may be important for GABA-dependent neuritogenesis, as (1) although CREB is expressed by the SVZ neuroblasts throughout the neurogenic process, its phosphorylation is transient and parallels neuronal differentiation, increasing in cells entering the olfactory bulb and decreasing after dendrite elongation; (2) inhibitors of different protein kinases involved in CREB phosphorylation in the context of neuronal differentiation block morphological development of SVZ-derived neuroblasts in primary cultures (Giachino et al., 2005).

DISCUSSION AND CONCLUDING REMARKS

This review has gathered evidence for a prominent GABAergic role during neurite growth both in the developing CNS and during adult neurogenesis. Remarkably, the same rules appear to apply to ontogeny and adult neurogenesis, demonstrating universal regulation mechanisms. Type-A GABA activity is the main protagonist, and in a general scheme, it promotes neurite growth through membrane depolarization, Ca^{2+} influx and downstream intracellular effects.

$GABA_B$ receptors may also play a role in neurite outgrowth in some brain areas (but not others; see Fiorentino et al., 2009), but the effects appear to be mediated through fundamentally different metabotropic mechanisms, which do not directly involve changes in membrane potential (e.g., Michler, 1990; Lopez-Bendito et al., 2003). Moreover, no $GABA_B$ effects were reported during neurogenesis in the olfactory bulb (Gascon et al., 2006). Hence, $GABA_B$-mediated effects on neurite growth may be fundamentally different in diverse brain areas and during development vs adult neurogenesis.

TONIC VERSUS PHASIC GABA ACTIVITY

The neuritogenic effects of $GABA_A$ activity appear at very early stages, long before synapse formation (Represa and Ben-Ari, 2005). Several lines of evidence suggest that these effects are mediated by ambient GABA released paracrinally from maturing neurons or from glial cells (Matsutani and Yamamoto, 1998). In the neonatal rat retina, for example, diffuse subunit staining (characteristic of extrasynaptic receptors) for various $GABA_A$ receptor subunits precedes the punctate staining pattern (characteristic of synaptic receptors) by a couple of days (Koulen, 1999).

An indication that this tonic GABAergic release may occur at extrasynaptic sites is the fact that it involves $GABA_A$ receptors that do not express subunits normally constituting synaptic receptors. More specifically, the $\gamma 2$ subunit, which is necessary for clustering of postsynaptic $GABA_A$ receptors, is not highly expressed at extrasynaptic sites at early developmental stages. One study on the development of dendritic arbors in *Xenopus* optic tectum reported that synaptic GABAergic inhibition promotes dendritic growth (Shen et al., 2009). In that study, however, synaptic $\gamma 2$ subunits were specifically impaired, but it is not clear whether tonic release from non-synaptic sites was affected at all, and therefore it is difficult to interpret the results. Finally, knockout of the synaptic $\alpha 1$ subunit had no effect on dendritic growth in the developing visual cortex (Heinen et al., 2003), although it did affect inhibitory activity (Bosman et al., 2002), pointing towards a more prominent role for tonic GABAergic release.

Although in most cases GABA (or $GABA_A$ agonists) were reported to have a direct neuritogenic effect, some *in vitro* studies mentioned that agonists had little or no effect on neurite growth, even though the antagonist bicuculline had a significant inhibitory effect (Barbin et al., 1993; Liu et al., 1997). This suggests that ambient, tonic GABAergic activity plays an important role in promoting neurite growth. It is obvious that there is more ambient GABA in intact tissue, and therefore, in that respect, *in vitro* acute-slice

studies and *in vivo* reports provide a more direct evidence for a neuritogenic role for paracrine GABA activity than cell cultures studies. In support, tonic GABA currents were recorded in acute slices at ages at which forced expression of KCC2 or downregulation of NKCC1 affected neuritogenesis in newborn neurons both during development and in the adult animal, respectively (Ge et al., 2006; Cancedda et al., 2007). Moreover, chronic GABA-synthesis blockade in the developing retina resulted in severe RGC dendritic tree shrinkage and prevented the stabilization of end-branches *in vivo* (F. Chabrol and E. Sernagor, unpublished observation).

GABAergic DEPOLARIZATION OR HYPERPOLARIZATION?

All studies reviewed here unanimously state that the neuritogenic effect of $GABA_A$ signaling is mediated by membrane depolarization (LoTurco et al., 1995; Ben-Ari et al., 2007; Ge et al., 2007; Wang and Kriegstein, 2009), which is generated via Cl^- efflux upon $GABA_A$ receptors activation. This Cl^- outflow originates from a reverse Cl^- gradient. The intracellular Cl^- concentration is indeed higher in immature neurons because of low expression of the KCC2 Cl^- extruding pump (Rivera et al., 1999) and/or high expression of NKCC1 that pumps Cl^- into neurons (Blaesse et al., 2009).

The mere depolarizing action of GABA rather than the GABAergic nature of the depolarization seems to be the major driving force for the neuritogenic effect. Indeed, when GABAergic activity is abolished by GABA synthesis blockade, neurite growth can be rescued by direct depolarization (with high K^+) or by triggering downstream effects such as Ca^{2+} influx (Maric et al., 2001; see next section). Moreover, overexpression of the K^+ inward rectifying Kir 2.1 channel, which strongly decreases membrane excitability *in vivo* prevents membrane depolarization in newborn neurons, mimicking GABA deprivation in these young cells and leading to inhibition of neurite outgrowth (Cancedda et al., 2007). Direct interference with KCC2 or NKCC1 functionality also triggers changes in neurite growth (Maric et al., 2001; Ge et al., 2006; Liu et al., 2006; Cancedda et al., 2007; Wang and Kriegstein, 2008), demonstrating that it is the depolarizing driving force established by the reverse Cl^- gradient that is at work here. Moreover, once GABA has switched to its mature inhibitory role, it can no longer induce neurite growth (Marty et al., 1996; Gascon et al., 2006).

In the few cases where GABA inhibited neurite growth, either direct (Kato-Negishi et al., 2003) or indirect (Liu et al., 1997) evidence demonstrates that the effect was due to hyperpolarizing GABAergic signaling. One study reported that GABAergic inhibition promoted dendritic growth in the *Xenopus* optic tectum (Shen et al., 2009). However, although this study clearly demonstrates that GABAergic synaptic signaling is hyperpolarizing, it is not clear whether the reduction in dendritic proliferation is indeed due to reduced GABAergic inhibition (because of impairment of the $\gamma 2$ subunit of the $GABA_A$ receptor), as the study provides no evidence for what happens at non-synaptic sites.

DOWNSTREAM EFFECTS OF $GABA_A$ SIGNALING ON NEURITE GROWTH

How does GABA depolarization influence morphological maturation of newborn neurons? Increase in intracellular Ca^{2+} due to activation of VDCCs is likely to have a significant role. Indeed, activation of VDCCs mediates GABA-induced promotion of neurite growth in various brain regions, as reported above (Fiszman et al., 1999; Maric et al., 2001; Tapia et al., 2001; Borodinsky et al., 2003; Gascon et al., 2006). Interestingly, all these studies reported that high threshold L-type VDCCs were responsible for the depolarizing GABAergic effect on neurite outgrowth. Nevertheless, as discussed earlier, tonic-GABA signaling appears particularly important for the effect, but only synaptic depolarization seems to be able to reach membrane depolarization levels high enough to activate high-threshold Ca^{2+} channels. One possibility is that in the very first phase of neuritogenesis, when synapses are not yet formed, small changes in the membrane potential (Wang et al., 2003; Ge et al., 2006) resulting from the activation of low affinity non-synaptic GABAergic receptors may open low threshold VDCCs (typically below −57 mV, which is close to the resting membrane potential of immature neurons (Schmidt-Hieber et al., 2004; Ge et al., 2006; Cancedda et al., 2007). Interestingly, the expression of low-threshold T-channels precedes other VDCCs in embryonic hippocampal, sensory and motor neurons (for review see Lory et al., 2006) and in newborn neurons in the dentate gyrus (Schmidt-Hieber et al., 2004), while these cells extend axons and dendrites. Once phasic synaptic GABAergic inputs are established, the depolarization induced by synaptically released GABA could cause sufficient membrane depolarization to activate L-type VDCCs. Therefore, the studies indicating high threshold L-type VDCCs as mediators of the neuritogenic GABA effects were probably undertaken after the onset or completion of synaptogenesis. Specific experiments aimed at investigating neuritogenesis (with application of T-type Ca^{2+} channel blockers) before synapse formation may help to resolve the issue.

Besides directly activating L-type VDCCs, phasic GABA-mediated activation can lead to Ca^{2+} influx by facilitating the opening of NMDA-receptor channels in response to glutamate (Deschenes et al., 1976; Leinekugel et al., 1997; Owens and Kriegstein, 2002; Ben-Ari, 2006; Wang and Kriegstein, 2008), a role taken over by AMPA receptors later in development (Ben-Ari et al., 1997). Indeed, NMDA receptors are functionally silent at negative membrane potentials due to blockade of the channel by Mg^{2+} (Demarque et al., 2004). Nevertheless, there are some indications that the voltage-dependent Mg^{2+} blockade is less efficient in neonatal neurons than in adults (Ben-Ari et al., 1988; Bowe and Nadler, 1990; Kleckner and Dingledine, 1991; Takahashi et al., 1996; Hsiao et al., 2002; but see Khazipov et al., 1995). Interestingly, NMDA (but not AMPA) receptors, can specifically influence initial dendritic arbor growth (Rajan and Cline, 1998), indicating that GABA depolarization may also exert its role on neuritogenesis trough activation of otherwise silent NMDA receptors before AMPAergic transmission takes over. Later, when AMPAergic transmission becomes more prominent, it could act in synergy with GABAergic and NMDA signaling to promote a later phase of neuritogenesis (Ben-Ari et al., 1997), by contributing to removal of the Mg^{2+} block and direct Ca influx, which is enhanced during early developmet in various systems (Otis et al., 1995; Ben-Ari et al., 1997; Gleason and Spitzer, 1998; Ravindranathan et al., 2000; Eybalin et al., 2004; Ni et al., 2007). This hypothesis is favored by the fact that (1) at later developmental stages, both NMDA and AMPA receptors are necessary to enable the completion of neurite development in various systems (Rajan and Cline, 1998; Sin et al., 2002; Haas et al., 2006); (2) AMPAergic transmission is impaired in neurons with downregulation of NKCC1, and these neurons have poorly developed dendrites (Ge et al., 2006; Wang and Kriegstein, 2008).

Interestingly, BDNF may be a downstream effector of depolarizing GABA effect on neurite outgrowth. This is based on two pieces of evidence. (1) BDNF expression and release from target neurons depends on GABAergic depolarization in the first 2 weeks *in vitro*, whereas GABAergic activity reduces the synthesis of BDNF mRNA in mature neurons (Berninger et al., 1995; Marty et al., 1996; Vicario-Abejon et al., 1998; Giusi et al., 2009). (2) BDNF signaling deprivation leads to dendrite growth impairment in newborn neurons during development and in the adult (McAllister et al., 1996; Berghuis et al., 2006; Chen et al., 2006; Takemoto-Kimura et al., 2007; Bergami et al., 2008; Chan et al., 2008; Ageta-Ishihara et al., 2009; Suh et al., 2009). Interestingly, $GABA_B$ receptor can also modulate the production and release of BDNF in an opposite fashion in newborn vs adult neurons (Heese et al., 2000; Ghorbel et al., 2005; Enna et al., 2006; Fiorentino et al., 2009). Despite those indications, however, a direct demonstration that the depolarizing effect of GABA on neurite development depends on BDNF is still missing.

Finally, Ca^{2+} influx may activate downstream effectors relevant to neuritogenesis both acutely through cytoskeleton rearrangement or long-term by activation of kinases and transcriptional programs (e.g., CaMKII, ERK1/2, CREB; Berninger et al., 1995; Owens et al., 1996; Borodinsky et al., 2003; Fiszman and Schousboe, 2004; Ageta-Ishihara et al., 2009; Jagasia et al., 2009).

EXPERIMENTAL APPROACHES

Most studies reported in this review have used *in vitro* pharmacological approaches. The rationale for using such strategy is obvious, as it enables relatively easy manipulation of various components of the chain of factors that influence the way GABA exerts its effects (e.g. blockade of specific receptor subunits or binding site, Cl^- pumps, Ca^{2+} channels etc..), and the results reported in these *in vitro* studies have greatly contributed to our understanding of the mechanisms by which GABA influences neurite outgrowth. Nevertheless, it is still important to address similar questions *in vivo*, where systems are intact and exposed to their natural environment.

In order to interfere with the GABAergic system *in vivo*, either genetically manipulated animals or local pharmacological manipulations must be used. The problem with classic genetic approaches is that animals carrying null mutations for important genes involved in

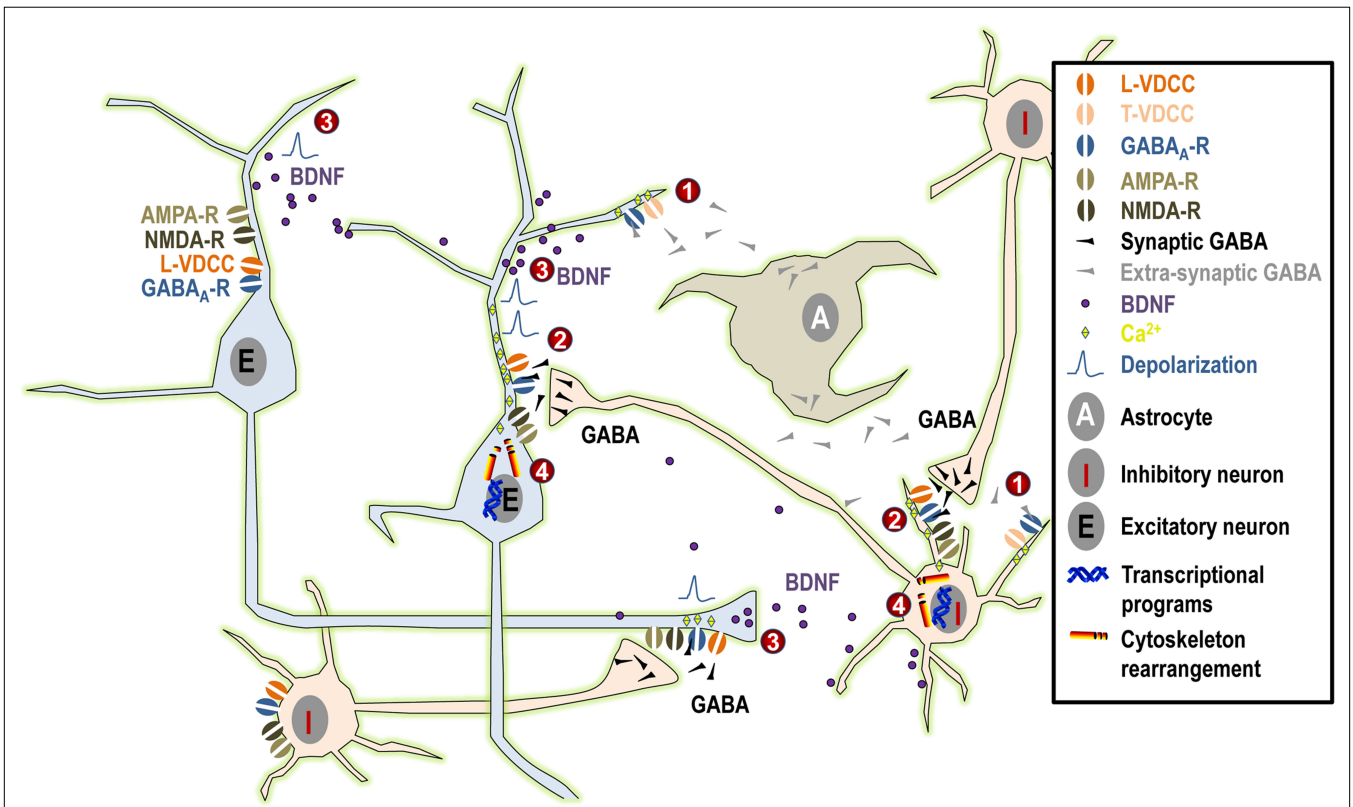

FIGURE 1 | Summary of the possible mechanisms linking $GABA_A$ activity and neurite outgrowth. (1) Under normal physiological conditions, tonic GABAergic release from maturing neurons and/or from astrocytes induces small tonic depolarization that may be sufficient to activate low-threshold T-type VDCCs and to promote the initial phase of neurite growth. **(2)** Subsequently, when synaptic GABA acts in synergy first exclusively with NMDA receptors and at later stages both with AMPA and NMDA receptors, this will result in larger depolarization that may even reach firing threshold. Such larger depolarizing signals may activate high-threshold L-type VDCCs and, together with direct Ca^{2+} influx through NMDA and AMPA receptors, they may contribute to the maturation of neuronal morphology. **(3)** Moreover, GABAergic activity together with NMDA and AMPA receptor signaling (possibly through Ca^{2+} signaling) may influence synthesis and activity-dependent release of BDNF, again influencing dentritic growth. **(4)** Finally, Ca^{2+} influx may activate downstream effectors relevant to neuritogenesis both acutely through cytoskeleton rearrangement or long-term by activation of kinases and transcriptional programs.

GABAergic signaling either die at birth, and if not, they often carry only mild phenotypes into adulthood (perhaps because of functional compensation by other systems (see Owens and Kriegstein, 2002) for an interesting discussion on these issues). Intriguingly, few studies have used classic genetic approaches to investigate how GABA may exert its influence on neurite growth and the reason may well be that many of these models are not inspiring because no obvious phenotype is present in adulthood. Nevertheless, it may well be that more detailed investigation of specific parameters such as dendritic morphometry might reveal important issues in some of these animals. All the same, Heinen et al. (2003) have successfully shown that knockout of the α1 subunit of the $GABA_A$ receptor has no impact on dendritic growth, despite the fact that inhibitory synaptic transmission is impaired in these animals (Bosman et al., 2002). This finding is extremely valuable for our understanding of the tonic versus phasic role played by GABA during neurite outgrowth. Recently, *in utero* electroporation and specific viral infection of newborn neurons in the dentate gyrus have allowed gene expression/knockdown of specific subpopulation of neurons in a time and location restricted fashion, partly avoiding the compensatory mechanisms probably at work in classic genetically modified animals. These new genetic approaches have been successfully used to impair the Cl^- homeostatic control system or to increase K^+ conductance to reduce cell excitability in the rodent brain *in vivo* (Ge et al., 2006; Cancedda et al., 2007; Wang and Kriegstein, 2008). Furthermore, Shen et al. (2009) have successfully applied a similar approach to alter the composition of $GABA_A$ receptors in the developing *Xenopus* optic tectum.

Finally, *in vivo* pharmacological interventions can also contribute to our understanding of the role played by GABA during neurite development. *In vivo* pharmacology is particularly easy in the retina because it is encased in the eye and it is more readily accessible. *In ovo* pharmacological manipulations have been particularly successful in turtle embryos where the eye can easily be exposed by opening the egg shell while the embryo develops (Leitch et al., 2005).

CONCLUSIONS

By triggering a chain of events, GABA appears to exert profound effects on neurite outgrowth in immature neurons during embryonic development and in adult neurogenesis (**Figure 1**).

Long before synapse formation, tonic GABA binds to low affinity extrasynaptic $GABA_A$ receptors and it triggers membrane depolarization through Cl^- efflux (the intracellular concentration of Cl^- being higher than in mature cells because of low expression of the KCC2 pump and high expression of the NKCC1 pump). This, in turn, opens low threshold T-type Ca^{2+} channels, resulting in Ca^{2+} influx and intracellular events that will eventually lead to neurite extension. At later maturational stages, when glutamatergic signaling has developed, GABA may act in concert with NMDA and AMPA neurotransmission, resulting in stronger depolarization and the opening of high-threshold L-type Ca^{2+} channels. This will result in stronger Ca^{2+} influx, which may be important for triggering downstream intracellular events that are responsible for the late phases of neurite growth. This process will come to an end when synaptic inhibition matures (through changes in the composition of the $GABA_A$ receptor subunits and reversal of the Cl^- gradient), leaving the possibility for plastic remodeling of the existing neuritic network by the dynamic balance of neuronal activity resulting from hyperpolarizing GABA and fully developed glutamatergic signaling.

REFERENCES

Abraham, J. H., Hansen, G. H., Seiler, N., and Schousboe, A. (1993). Depletion of polyamines prevents the neurotrophic activity of the GABA-agonist THIP in cultured rat cerebellar granule cells. *Neurochem. Res.* 18, 153–158.

Ageta-Ishihara, N., Takemoto-Kimura, S., Nonaka, M., Adachi-Morishima, A., Suzuki, K., Kamijo, S., Fujii, H., Mano, T., Blaeser, F., Chatila, T. A., Mizuno, H., Hirano, T., Tagawa, Y., Okuno, H., and Bito, H. (2009). Control of cortical axon elongation by a GABA-driven Ca2+/calmodulin-dependent protein kinase cascade. *J. Neurosci.* 29, 13720–13729.

Baloyannis, S. J., Karakatsanis, K., Karathanasis, J., Apostolakis, M., and Diacoyannis, A. (1983). Effects of GABA, glycine, and sodium barbiturate on dendritic growth in vitro. *Acta Neuropathol.* 59, 171–182.

Barbin, G., Pollard, H., Gaiarsa, J. L., and Ben-Ari, Y. (1993). Involvement of GABAA receptors in the outgrowth of cultured hippocampal neurons. *Neurosci. Lett.* 152, 150–154.

Ben-Ari, Y. (2002). Excitatory actions of gaba during development: the nature of the nurture. *Nat. Rev. Neurosci.* 3, 728–739.

Ben-Ari, Y. (2006). Basic developmental rules and their implications for epilepsy in the immature brain. *Epileptic Disord.* 8, 91–102.

Ben-Ari, Y., Cherubini, E., Corradetti, R., and Gaiarsa, J. L. (1989). Giant synaptic potentials in immature rat CA3 hippocampal neurones. *J. Physiol. (Lond.)* 416, 303–325.

Ben-Ari, Y., Cherubini, E., and Krnjevic, K. (1988). Changes in voltage dependence of NMDA currents during development. *Neurosci. Lett.* 94, 88–92.

Ben-Ari, Y., Gaiarsa, J. L., Tyzio, R., and Khazipov, R. (2007). GABA: a pioneer transmitter that excites immature neurons and generates primitive oscillations. *Physiol. Rev.* 87, 1215–1284.

Ben-Ari, Y., Khazipov, R., Leinekugel, X., Caillard, O., and Gaiarsa, J. L. (1997). GABAA, NMDA and AMPA receptors: a developmentally regulated 'menage a trois'. *Trends Neurosci.* 20, 523–529.

Ben-Ari, Y., Tseeb, V., Raggozzino, D., Khazipov, R., and Gaiarsa, J. L. (1994). gamma-Aminobutyric acid (GABA): a fast excitatory transmitter which may regulate the development of hippocampal neurones in early postnatal life. *Prog. Brain Res.* 102, 261–273.

Bergami, M., Rimondini, R., Santi, S., Blum, R., Gotz, M., and Canossa, M. (2008). Deletion of TrkB in adult progenitors alters newborn neuron integration into hippocampal circuits and increases anxiety-like behavior. *Proc. Natl. Acad. Sci. U.S.A.* 105, 15570–15575.

Berghuis, P., Agerman, K., Dobszay, M. B., Minichiello, L., Harkany, T., and Ernfors, P. (2006). Brain-derived neurotrophic factor selectively regulates dendritogenesis of parvalbumin-containing interneurons in the main olfactory bulb through the PLCgamma pathway. *J. Neurobiol.* 66, 1437–1451.

Berninger, B., Marty, S., Zafra, F., da Penha Berzaghi, M., Thoenen, H., and Lindholm, D. (1995). GABAergic stimulation switches from enhancing to repressing BDNF expression in rat hippocampal neurons during maturation in vitro. *Development* 121, 2327–2335.

Bird, M., and Owen, A. (1998). Neurite outgrowth-regulating properties of GABA and the effect of serum on mouse spinal cord neurons in culture. *J. Anat.* 193(Pt 4), 503–508.

Blaesse, P., Airaksinen, M. S., Rivera, C., and Kaila, K. (2009). Cation-chloride cotransporters and neuronal function. *Neuron* 61, 820–838.

Bordey, A. (2007). Enigmatic GABAergic networks in adult neurogenic zones. *Brain Res. Rev.* 53, 124–134.

Borodinsky, L. N., O'Leary, D., Neale, J. H., Vicini, S., Coso, O. A., and Fiszman, M. L. (2003). GABA-induced neurite outgrowth of cerebellar granule cells is mediated by GABA(A) receptor activation, calcium influx and CaMKII and erk1/2 pathways. *J. Neurochem.* 84, 1411–1420.

Bosman, L. W., Rosahl, T. W., and Brussaard, A. B. (2002). Neonatal development of the rat visual cortex: synaptic function of GABAA receptor alpha subunits. *J. Physiol. (Lond.)* 545, 169–181.

Bowe, M. A., and Nadler, J. V. (1990). Developmental increase in the sensitivity to magnesium of NMDA receptors on CA1 hippocampal pyramidal cells. *Brain Res. Dev. Brain Res.* 56, 55–61.

Cancedda, L., Fiumelli, H., Chen, K., and Poo, M. M. (2007). Excitatory GABA action is essential for morphological

maturation of cortical neurons in vivo. *J. Neurosci.* 27, 5224–5235.

Carleton, A., Petreanu, L. T., Lansford, R., Alvarez-Buylla, A., and Lledo, P. M. (2003). Becoming a new neuron in the adult olfactory bulb. *Nat. Neurosci.* 6, 507–518.

Chan, J. P., Cordeira, J., Calderon, G. A., Iyer, L. K., and Rios, M. (2008). Depletion of central BDNF in mice impedes terminal differentiation of new granule neurons in the adult hippocampus. *Mol. Cell. Neurosci.* 39, 372–383.

Chattopadhyaya, B., Di Cristo, G., Wu, C. Z., Knott, G., Kuhlman, S., Fu, Y., Palmiter, R. D., and Huang, Z. J. (2007). GAD67-mediated GABA synthesis and signaling regulate inhibitory synaptic innervation in the visual cortex. *Neuron* 54, 889–903.

Chen, Z. Y., Jing, D., Bath, K. G., Ieraci, A., Khan, T., Siao, C. J., Herrera, D. G., Toth, M., Yang, C., McEwen, B. S., Hempstead, B. L., and Lee, F. S. (2006). Genetic variant BDNF (Val66Met) polymorphism alters anxiety-related behavior. *Science* 314, 140–143.

Cobas, A., Fairen, A., Alvarez-Bolado, G., and Sanchez, M. P. (1991). Prenatal development of the intrinsic neurons of the rat neocortex: a comparative study of the distribution of GABA-immunoreactive cells and the GABAA receptor. *Neuroscience* 40, 375–397.

Cossart, R., Bernard, C., and Ben-Ari, Y. (2005). Multiple facets of GABAergic neurons and synapses: multiple fates of GABA signalling in epilepsies. *Trends Neurosci.* 28, 108–115.

Demarque, M., Villeneuve, N., Manent, J. B., Becq, H., Represa, A., Ben-Ari, Y., and Anikstejn, L. (2004). Glutamate transporters prevent the generation of seizures in the developing rat neocortex. *J. Neurosci.* 24, 3289–3294.

Deschenes, M., Feltz, P., and Lamour, Y. (1976). A model for an estimate in vivo of the ionic basis of presynaptic inhibition: an intracellular analysis of the GABA-induced depolarization in rat dorsal root ganglia. *Brain Res.* 118, 486–493.

Eins, S., Spoerri, P. E., and Heyder, E. (1983). GABA or sodium-bromide-induced plasticity of neurites of mouse neuroblastoma cells in culture. A quantitative study. *Cell Tissue Res.* 229, 457–460.

Enna, S. J., Reisman, S. A., and Stanford, J. A. (2006). CGP 56999A, a GABA(B) receptor antagonist, enhances expression of brain-derived neurotrophic factor and attenuates dopamine depletion in the rat corpus striatum following a 6-hydroxydopamine lesion of the nigrostriatal pathway. *Neurosci. Lett.* 406, 102–106.

Essrich, C., Lorez, M., Benson, J. A., Fritschy, J. M., and Luscher, B. (1998). Postsynaptic clustering of major GABAA receptor subtypes requires the gamma 2 subunit and gephyrin. *Nat. Neurosci.* 1, 563–571.

Eybalin, M., Caicedo, A., Renard, N., Ruel, J., and Puel, J. L. (2004). Transient Ca2+-permeable AMPA receptors in postnatal rat primary auditory neurons. *Eur. J. Neurosci.* 20, 2981–2989.

Farrant, M., and Nusser, Z. (2005). Variations on an inhibitory theme: phasic and tonic activation of GABA(A) receptors. *Nat. Rev. Neurosci.* 6, 215–229.

Ferguson, S. C., and McFarlane, S. (2002). GABA and development of the *Xenopus* optic projection. *J. Neurobiol.* 51, 272–284.

Fiorentino, H., Kuczewski, N., Diabira, D., Ferrand, N., Pangalos, M. N., Porcher, C., and Gaiarsa, J. L. (2009). GABA(B) receptor activation triggers BDNF release and promotes the maturation of GABAergic synapses. *J. Neurosci.* 29, 11650–11661.

Fiszman, M. L., Borodinsky, L. N., and Neale, J. H. (1999). GABA induces proliferation of immature cerebellar granule cells grown in vitro. *Brain Res. Dev. Brain Res.* 115, 1–8.

Fiszman, M. L., and Schousboe, A. (2004). Role of calcium and kinases on the neurotrophic effect induced by gamma-aminobutyric acid. *J. Neurosci. Res.* 76, 435–441.

Ganguly, K., Schinder, A. F., Wong, S. T., and Poo, M. (2001). GABA itself promotes the developmental switch of neuronal GABAergic responses from excitation to inhibition. *Cell* 105, 521–532.

Gascon, E., Dayer, A. G., Sauvain, M. O., Potter, G., Jenny, B., De Roo, M., Zgraggen, E., Demaurex, N., Muller, D., and Kiss, J. Z. (2006). GABA regulates dendritic growth by stabilizing lamellipodia in newly generated interneurons of the olfactory bulb. *J. Neurosci.* 26, 12956–12966.

Ge, S., Goh, E. L., Sailor, K. A., Kitabatake, Y., Ming, G. L., and Song, H. (2006). GABA regulates synaptic integration of newly generated neurons in the adult brain. *Nature* 439, 589–593.

Ge, S., Pradhan, D. A., Ming, G. L., and Song, H. (2007). GABA sets the tempo for activity-dependent adult neurogenesis. *Trends Neurosci.* 30, 1–8.

Ghorbel, M. T., Becker, K. G., and Henley, J. M. (2005). Profile of changes in gene expression in cultured hippocampal neurones evoked by the GABAB receptor agonist baclofen. *Physiol. Genomics* 22, 93–98.

Giachino, C., De Marchis, S., Giampietro, C., Parlato, R., Perroteau, I., Schutz, G., Fasolo, A., and Peretto, P. (2005). cAMP response element-binding protein regulates differentiation and survival of newborn neurons in the olfactory bulb. *J. Neurosci.* 25, 10105–10118.

Giusi, G., Facciolo, R. M., Rende, M., Alo, R., Di Vito, A., Salerno, S., Morelli, S., De Bartolo, L., Drioli, E., and Canonaco, M. (2009). Distinct alpha subunits of the GABA(A) receptor are responsible for early hippocampal silent neuron-related activities. *Hippocampus* 19, 1103–1114.

Gleason, E. L., and Spitzer, N. C. (1998). AMPA and NMDA receptors expressed by differentiating Xenopus spinal neurons. *J. Neurophysiol.* 79, 2986–2998.

Goffin, D., Aarum, J., Schroeder, J. E., Jovanovic, J. N., and Chuang, T. T. (2008). D1-like dopamine receptors regulate GABAA receptor function to modulate hippocampal neural progenitor cell proliferation. *J. Neurochem.* 107, 964–975.

Groc, L., Gustafsson, B., and Hanse, E. (2003). In vivo evidence for an activity-independent maturation of AMPA/NMDA signaling in the developing hippocampus. *Neuroscience* 121, 65–72.

Groc, L., Petanjek, Z., Gustafsson, B., Ben-Ari, Y., Hanse, E., and Khazipov, R. (2002). In vivo blockade of neural activity alters dendritic development of neonatal CA1 pyramidal cells. *Eur. J. Neurosci.* 16, 1931–1938.

Haas, K., Li, J., and Cline, H. T. (2006). AMPA receptors regulate experience-dependent dendritic arbor growth in vivo. *Proc. Natl. Acad. Sci. U.S.A.* 103, 12127–12131.

Hansen, G. H., Meier, E., and Schousboe, A. (1984). GABA influences the ultrastructure composition of cerebellar granule cells during development in culture. *Int. J. Dev. Neurosci.* 2, 247–251, 253–257.

Heese, K., Otten, U., Mathivet, P., Raiteri, M., Marescaux, C., and Bernasconi, R. (2000). GABA(B) receptor antagonists elevate both mRNA and protein levels of the neurotrophins nerve growth factor (NGF) and brain-derived neurotrophic factor (BDNF) but not neurotrophin-3 (NT-3) in brain and spinal cord of rats. *Neuropharmacology* 39, 449–462.

Heinen, K., Baker, R. E., Spijker, S., Rosahl, T., van Pelt, J., and Brussaard, A. B. (2003). Impaired dendritic spine maturation in GABAA receptor alpha1 subunit knock out mice. *Neuroscience* 122, 699–705.

Hornung, J. P., and Fritschy, J. M. (1996). Developmental profile of GABAA-receptors in the marmoset monkey: expression of distinct subtypes in pre- and postnatal brain. *J. Comp. Neurol.* 367, 413–430.

Hsiao, C. F., Wu, N., Levine, M. S., and Chandler, S. H. (2002). Development and serotonergic modulation of NMDA bursting in rat trigeminal motoneurons. *J. Neurophysiol.* 87, 1318–1328.

Jagasia, R., Steib, K., Englberger, E., Herold, S., Faus-Kessler, T., Saxe, M., Gage, F. H., Song, H., and Lie, D. C. (2009). GABA-cAMP response element-binding protein signaling regulates maturation and survival of newly generated neurons in the adult hippocampus. *J. Neurosci.* 29, 7966–7977.

Kato-Negishi, M., Muramoto, K., Kawahara, M., Hosoda, R., Kuroda, Y., and Ichikawa, M. (2003). Bicuculline induces synapse formation on primary cultured accessory olfactory bulb neurons. *Eur. J. Neurosci.* 18, 1343–1352.

Khazipov, R., Ragozzino, D., and Bregestovski, P. (1995). Kinetics and Mg2+ block of *N*-methyl-D-aspartate receptor channels during postnatal development of hippocampal CA3 pyramidal neurons. *Neuroscience* 69, 1057–1065.

Kleckner, N. W., and Dingledine, R. (1991). Regulation of hippocampal NMDA receptors by magnesium and glycine during development. *Brain Res. Mol. Brain Res.* 11, 151–159.

Koulen, P. (1999). Postnatal development of GABAA receptor beta1, beta2/3, and gamma2 immunoreactivity in the rat retina. *J. Neurosci. Res.* 57, 185–194.

Leinekugel, X., Medina, I., Khalilov, I., Ben-Ari, Y., and Khazipov, R. (1997). Ca2+ oscillations mediated by the synergistic excitatory actions of GABA(A) and NMDA receptors in the neonatal hippocampus. *Neuron* 18, 243–255.

Leitch, E., Coaker, J., Young, C., Mehta, V., and Sernagor, E. (2005). GABA type-A activity controls its own developmental polarity switch in the maturing retina. *J. Neurosci.* 25, 4801–4805.

Liu, J., Morrow, A. L., Devaud, L., Grayson, D. R., and Lauder, J. M. (1997). GABAA receptors mediate trophic effects of GABA on embryonic brainstem monoamine neurons in vitro. *J. Neurosci.* 17, 2420–2428.

Liu, Z., Neff, R. A., and Berg, D. K. (2006). Sequential interplay of nicotinic and GABAergic signaling guides neuronal development. *Science* 314, 1610–1613.

Lopez-Bendito, G., Lujan, R., Shigemoto, R., Ganter, P., Paulsen, O., and Molnar, Z. (2003). Blockade of GABA(B) receptors alters the tangential migration of cortical neurons. *Cereb. Cortex* 13, 932–942.

Lory, P., Bidaud, I., and Chemin, J. (2006). T-type calcium channels in differentiation and proliferation. *Cell Calcium* 40, 135–146.

LoTurco, J. J., Owens, D. F., Heath, M. J., Davis, M. B., and Kriegstein, A. R. (1995). GABA and glutamate depolarize cortical progenitor cells and inhibit DNA synthesis. *Neuron* 15, 1287–1298.

Ludwig, A., Li, H., Saarma, M., Kaila, K., and Rivera, C. (2003). Developmental up-regulation of KCC2 in the absence of GABAergic and glutamatergic transmission. *Eur. J. Neurosci.* 18, 3199–3206.

Ma, D. K., Kim, W. R., Ming, G. L., and Song, H. (2009). Activity-dependent extrinsic regulation of adult olfactory bulb and hippocampal neurogenesis. *Ann. N. Y. Acad. Sci.* 1170, 664–673.

Maric, D., Liu, Q. Y., Maric, I., Chaudry, S., Chang, Y. H., Smith, S. V., Sieghart, W., Fritschy, J. M., and Barker, J. L. (2001). GABA expression dominates neuronal lineage progression in the embryonic rat neocortex and facilitates neurite outgrowth via GABA(A) autoreceptor/Cl– channels. *J. Neurosci.* 21, 2343–2360.

Marty, S., Berninger, B., Carroll, P., and Thoenen, H. (1996). GABAergic stimulation regulates the phenotype of hippocampal interneurons through the regulation of brain-derived neurotrophic factor. *Neuron* 16, 565–570.

Matsutani, S., and Yamamoto, N. (1998). GABAergic neuron-to-astrocyte signaling regulates dendritic branching in coculture. *J. Neurobiol.* 37, 251–264.

McAllister, A. K., Katz, L. C., and Lo, D. C. (1996). Neurotrophin regulation of cortical dendritic growth requires activity. *Neuron* 17, 1057–1064.

Mehta, V., and Sernagor, E. (2006a). Early neural activity and dendritic growth in turtle retinal ganglion cells. *Eur. J. Neurosci.* 24, 773–786.

Mehta, V., and Sernagor, E. (2006b). Receptive field structure-function correlates in developing turtle retinal ganglion cells. *Eur. J. Neurosci.* 24, 787–794.

Michler, A. (1990). Involvement of GABA receptors in the regulation of neurite growth in cultured embryonic chick tectum. *Int. J. Dev. Neurosci.* 8, 463–472.

Mohler, H. (2007). Molecular regulation of cognitive functions and developmental plasticity: impact of GABAA receptors. *J. Neurochem.* 102, 1–12.

Naylor, D. E., Liu, H., and Wasterlain, C. G. (2005). Trafficking of GABA(A) receptors, loss of inhibition, and a mechanism for pharmacoresistance in status epilepticus. *J. Neurosci.* 25, 7724–7733.

Ni, X., Sullivan, G. J., and Martin-Caraballo, M. (2007). Developmental characteristics of AMPA receptors in chick lumbar motoneurons. *Dev. Neurobiol.* 67, 1419–1432.

Otis, T. S., Raman, I. M., and Trussell, L. O. (1995). AMPA receptors with high Ca2+ permeability mediate synaptic transmission in the avian auditory pathway. *J. Physiol. (Lond.)* 482(Pt 2), 309–315.

Overstreet-Wadiche, L. S., Bromberg, D. A., Bensen, A. L., and Westbrook, G. L. (2006). Seizures accelerate functional integration of adult-generated granule cells. *J. Neurosci.* 26, 4095–4103.

Owens, D. F., Boyce, L. H., Davis, M. B., and Kriegstein, A. R. (1996). Excitatory GABA responses in embryonic and neonatal cortical slices demonstrated by gramicidin perforated-patch recordings and calcium imaging. *J. Neurosci.* 16, 6414–6423.

Owens, D. F., and Kriegstein, A. R. (2002). Is there more to GABA than synaptic inhibition? *Nat. Rev. Neurosci.* 3, 715–727.

Patrylo, P. R., Spencer, D. D., and Williamson, A. (2001). GABA uptake and heterotransport are impaired in the dentate gyrus of epileptic rats and humans with temporal lobe sclerosis. *J. Neurophysiol.* 85, 1533–1542.

Rajan, I., and Cline, H. T. (1998). Glutamate receptor activity is required for normal development of tectal cell dendrites in vivo. *J. Neurosci.* 18, 7836–7846.

Ravindranathan, A., Donevan, S. D., Sugden, S. G., Greig, A., Rao, M. S., and Parks, T. N. (2000). Contrasting molecular composition and channel properties of AMPA receptors on chick auditory and brainstem motor neurons. *J. Physiol. (Lond.)* 523(Pt 3), 667–684.

Represa, A., and Ben-Ari, Y. (2005). Trophic actions of GABA on neuronal development. *Trends Neurosci.* 28, 278–283.

Reynolds, A., Brustein, E., Liao, M., Mercado, A., Babilonia, E., Mount, D. B., and Drapeau, P. (2008). Neurogenic role of the depolarizing chloride gradient revealed by global overexpression of KCC2 from the onset of development. *J. Neurosci.* 28, 1588–1597.

Rivera, C., Voipio, J., Payne, J. A., Ruusuvuori, E., Lahtinen, H., Lamsa, K., Pirvola, U., Saarma, M., and Kaila, K. (1999). The K+/Cl– co-transporter KCC2 renders GABA hyperpolarizing during neuronal maturation. *Nature* 397, 251–255.

Schmidt-Hieber, C., Jonas, P., and Bischofberger, J. (2004). Enhanced synaptic plasticity in newly generated granule cells of the adult hippocampus. *Nature* 429, 184–187.

Sernagor, E., Eglen, S. J., and Wong, R. O. (2001). Development of retinal ganglion cell structure and function. *Prog. Retin. Eye Res.* 20, 139–174.

Sernagor, E., Young, C., and Eglen, S. J. (2003). Developmental modulation of retinal wave dynamics: shedding light on the GABA saga. *J. Neurosci.* 23, 7621–7629.

Shen, W., Da Silva, J. S., He, H., and Cline, H. T. (2009). Type A GABA-receptor-dependent synaptic transmission sculpts dendritic arbor structure in Xenopus tadpoles in vivo. *J. Neurosci.* 29, 5032–5043.

Sin, W. C., Haas, K., Ruthazer, E. S., and Cline, H. T. (2002). Dendrite growth increased by visual activity requires NMDA receptor and Rho GTPases. *Nature* 419, 475–480.

Spoerri, P. E. (1988). Neurotrophic effects of GABA in cultures of embryonic chick brain and retina. *Synapse* 2, 11–22.

Suh, H., Deng, W., and Gage, F. H. (2009). Signaling in adult neurogenesis. *Annu. Rev. Cell Dev. Biol.* 25, 253–275.

Syed, M. M., Lee, S., Zheng, J., and Zhou, Z. J. (2004). Stage-dependent dynamics and modulation of spontaneous waves in the developing rabbit retina. *J. Physiol. (Lond.)* 560, 533–549.

Takahashi, T., Feldmeyer, D., Suzuki, N., Onodera, K., Cull-Candy, S. G., Sakimura, K., and Mishina, M. (1996). Functional correlation of NMDA receptor epsilon subunits expression with the properties of single-channel and synaptic currents in the developing cerebellum. *J. Neurosci.* 16, 4376–4382.

Takemoto-Kimura, S., Ageta-Ishihara, N., Nonaka, M., Adachi-Morishima, A., Mano, T., Okamura, M., Fujii, H., Fuse, T., Hoshino, M., Suzuki, S., Kojima, M., Mishina, M., Okuno, H., and Bito, H. (2007). Regulation of dendritogenesis via a lipid-raft-associated Ca2+/calmodulin-dependent protein kinase CLICK-III/CaMKIgamma. *Neuron* 54, 755–770.

Tapia, J. C., Mentis, G. Z., Navarrete, R., Nualart, F., Figueroa, E., Sanchez, A., and Aguayo, L. G. (2001). Early expression of glycine and GABA(A) receptors in developing spinal cord neurons. Effects on neurite outgrowth. *Neuroscience* 108, 493–506.

Tozuka, Y., Fukuda, S., Namba, T., Seki, T., and Hisatsune, T. (2005). GABAergic excitation promotes neuronal differentiation in adult hippocampal progenitor cells. *Neuron* 47, 803–815.

Ueda, Y., and Tsuru, N. (1995). Simultaneous monitoring of the seizure-related changes in extracellular glutamate and gamma-aminobutyric acid concentration in bilateral hippocampi following development of amygdaloid kindling. *Epilepsy Res.* 20, 213–219.

Vicario-Abejon, C., Collin, C., McKay, R. D., and Segal, M. (1998). Neurotrophins induce formation of functional excitatory and inhibitory synapses between cultured hippocampal neurons. *J. Neurosci.* 18, 7256–7271.

Wang, D. D., and Kriegstein, A. R. (2008). GABA regulates excitatory synapse formation in the neocortex via NMDA receptor activation. *J. Neurosci.* 28, 5547–5558.

Wang, D. D., and Kriegstein, A. R. (2009). Defining the role of GABA in cortical development. *J. Physiol. (Lond.)* 587, 1873–1879.

Wang, D. D., Krueger, D. D., and Bordey, A. (2003). GABA depolarizes neuronal progenitors of the postnatal subventricular zone via GABAA receptor activation. *J. Physiol. (Lond.)* 550, 785–800.

Wu, W. L., Ziskind-Conhaim, L., and Sweet, M. A. (1992). Early development of glycine- and GABA-mediated synapses in rat spinal cord. *J. Neurosci.* 12, 3935–3945.

Yuste, R., and Katz, L. C. (1991). Control of postsynaptic Ca2+ influx in developing neocortex by excitatory and inhibitory neurotransmitters. *Neuron* 6, 333–344.

Conflict of Interest Statement: The authors declare that the research was conducted in the absence of any commercial or financial relationships that could be construed as a potential conflict of interest.

Received: 03 March 2010; paper pending published: 17 March 2010; accepted: 17 March 2010; published online: 14 April 2010.

Citation: Sernagor E, Chabrol F, Bony G and Cancedda L (2010) GABAergic control of neurite outgrowth and remodeling during development and adult neurogenesis: general rules and differences in diverse systems. Front. Cell. Neurosci. ***4****:11. doi: 10.3389/fncel.2010.00011*

frontiers in
CELLULAR NEUROSCIENCE

ORIGINAL RESEARCH ARTICLE
published: 28 May 2010
doi: 10.3389/fncel.2010.00019

PAF-AH catalytic subunits modulate the Wnt pathway in developing GABAergic neurons

Idit Livnat[1], Danit Finkelshtein[1], Indraneel Ghosh[1], Hiroyuki Arai[2] and Orly Reiner[1]*

[1] *Department of Molecular Genetics, Weizmann Institute of Science, Rehovot, Israel*
[2] *Faculty of Pharmaceutical Sciences, University of Tokyo, Hongo, Bunkyo-ku, Tokyo, Japan*

Edited by:
Yehezkel Ben-Ari,
Institut National de la Santé et de la Recherche Médicale, France

Reviewed by:
John G. Parnavelas,
University College London, UK
Angelique Bordey,
Yale University School of Medicine, USA

****Correspondence:***
Orly Reiner, Department of Molecular Genetics, Weizmann Institute of Science, Rehovot 76100, Israel.
e-mail: Orly.reiner@weizmann.ac.il

Platelet-activating factor acetylhydrolase 1B (PAF-AH) inactivates the potent phospholipid platelet-activating factor (PAF) and is composed of two catalytic subunits (α1 and α2) and a dimeric regulatory subunit, LIS1. The function of the catalytic subunits in brain development remains unknown. Here we examined their effects on proliferation in the ganglionic eminences and tangential migration. In α1 and α2 catalytic subunits knockout mice we noticed an increase in the size of the ganglionic eminences resulting from increased proliferation of GABAergic neurons. Our results indicate that the catalytic subunits act as negative regulators of the Wnt signaling pathway. Overexpression of each of the PAF-AH catalytic subunits reduced the amount of nuclear beta-catenin and provoked a shift of this protein from the nucleus to the cytoplasm. In the double mutant mice, Wnt signaling increased in the ganglionic eminences and in the dorsal part of the cerebral cortex. *In situ* hybridization revealed increased and expanded expression of a downstream target of the Wnt pathway (*Cyclin D1*), and of upstream Wnt components (*Tcf4, Tcf3* and *Wnt7B*). Furthermore, the interneurons in the cerebral cortex were more numerous and in a more advanced position. Transplantation assays revealed a non-cell autonomous component to this phenotype, which may be explained in part by increased and expanded expression of *Sdf1* and *Netrin-1*. Our findings strongly suggest that PAF-AH catalytic subunits modulate the Wnt pathway in restricted areas of the developing cerebral cortex. We hypothesize that modulation of the Wnt pathway is the evolutionary conserved activity of the PAF-AH catalytic subunits.

Keywords: platelet-activating factor acetylhydrolase IB, Wnt, beta-catenin, ganglionic eminences

INTRODUCTION

The proper functioning of the cerebral cortex relies on formation of neural networks that are composed of excitatory neurons and inhibitory interneurons (reviewed by Wonders and Anderson 2006). The excitatory, or projection, neurons are born in proliferating zones of the cerebral cortex, the ventricular zone and the subventricular zone (Noctor et al., 2004; review Gotz and Huttner, 2005). These neurons usually migrate along radial glia to their proper cortical layer (reviews by Hatten, 2002; Ayala et al., 2007). The majority of interneurons, which compose approximately 20% of cortical neurons, are born in the ganglionic eminences (GE) and migrate to the cortex using a tangential mode of migration (reviews by Marin and Rubenstein, 2001; Metin et al., 2006). Following their arrival to the cerebral cortex, the interneurons utilize radial migration to reach the proper laminar position and then they intercalate in the network. Gamma-aminobutyric acid (GABA)-biosynthesizing enzymes preferentially localize to cortical interneurons, which are also known as GABAergic neurons. In the adult mammalian brain, GABA has been associated primarily with the mediation of synaptic inhibition. Imbalance between inhibition and excitation may underlie diseases such as epilepsy (reviewed by Ben-Ari, 2006). Cortical interneurons have also been implicated in developmental processes, including the regulation of neuronal proliferation and migration during corticogenesis and the development of cortical circuitry (reviews by Owens and Kriegstein, 2002; Spitzer, 2006). Identification of molecules and pathways, which regulate the number and migration of GABAergic neurons, is of clear importance when aiming to understand the normal and diseased brain.

Platelet-activating factor-acetyl hydrolaze (PAF-AH) hydrolyzes PAF, an important lipid second messenger. PAF mediates an array of biological processes and is very abundant in the mammalian central nervous system, where it acts as a synaptic messenger, a transcription inducer and is involved in long-term potentiation, a cellular model of memory formation (Kato et al., 1994; Bazan, 1995). PAF deacetylation by PAFAH leads to its inactivation. The PAFAH1B intracellular enzyme is a tetramer composed of two catalytic subunits, α1 (PAFAH1B3) and α2 (PAFAH1B2), and a regulatory dimer of LIS1 (PAFAH1B1) (Hanahan, 1986; Kornecki and Ehrlich, 1988; Koltai et al., 1991; Chao and Olson, 1993; Stafforini et al., 2003; Bazan, 2005). From here forth PAFAH-1B will be referred to as PAF-AH. Deletions or point mutations in the *LIS1* (*Lissencephaly-1*) gene are manifested in humans in a spectrum of abnormal neuronal migration phenotypes ranging between classical lissencephaly and subcortical band heterotopia in humans (Reiner et al., 1993; Barkovich et al., 2005). Impaired neuronal migration has been noticed also in mouse genetic models (Hirotsune et al., 1998; Cahana et al., 2001; McManus et al., 2004b). Further reduction of LIS1 levels using *in utero* electroporation or conditional knock-out results in further impairment of neuronal

migration as well as affects the proliferation of progenitors (Shu et al., 2004; Tsai et al., 2005; Tsai et al., 2007; Hebbar et al., 2008; Yingling et al., 2008). LIS1 dosage is crucial for proper brain development an increased levels of LIS1 affect brain development in human and in mice (Bi et al., 2009). Increased LIS1 levels affect the organization of the ventricular zone and impaired radial and tangential neuronal migration.

Platelet-activating factor-acetyl hydrolaze catalytic subunits knockout mice were generated independently by two groups (Koizumi et al., 2003; Yan et al., 2003). Deletions of only the α2 subunit or both the α1/α2 subunits resulted in severe male infertility. No brain phenotype has been reported for these knockout mice. We further investigated these mice (Koizumi et al., 2003) and detected a moderate increase in the size of the ganglionic eminences. In parallel, we noted that overexpression of the PAF-AH catalytic subunits modulated the Wnt pathway in transfected cells. Conversely, in the double knockout mice Wnt signaling was enhanced. An additional effect on tangential migration was noted: the interneurons in the cerebral cortex were more numerous and in a more advanced position, which was accompanied with earlier development of thalamocortical fibers. Our findings strongly suggest that PAF-AH catalytic subunits modulate the Wnt pathway in restricted areas of the developing cerebral cortex.

MATERIALS AND METHODS

AUTHORIZATION FOR THE USE OF EXPERIMENTAL ANIMALS

The experiments described in this manuscript were approved by the Weizmann Institute IACUC.

PLASMIDS

The expression construct of pDsRedα1 was generated using rat α1 tagged with green fluorescent protein (GFP) digested with *Eco*R1 and *Not*I. The insert was cloned between *Xho*1 and *Sma*I with the *Eco*R1–*Xho*1 adaptors (5′-TCGAGCTACCTGCGGTG-3′ and 5′-AATTCACCGCAGGTAGC-3′) into pDsRed-C1 vector (Clontech, CA, USA). The corresponding Rat α2 tagged with GFP was digested with *Eco*R1 and *Kpn*1 and cloned between *Xho*1 and *Kpn*1 using the same adaptors and vector as described above. pcDNA3-Flagα1 and pcDNA3-Flagα2 expression vectors were generated by subcloning the same fragments into pcDNA3 tagged with a Flag epitope. Cloning was verified by DNA sequence analysis of the plasmids, and Western blot analysis of the transfected expression plasmids in mammalian cells. A plasmid that contains the 3′ UTR of the α1 was generated using a clone isolated from mouse brain cDNA library, inserted into pBS following *Pst*I digestion. pcDNA3-Mycα1 plasmid was received from Prof. Junken Aoki. All GFP-β-catenin constructs, pTOPFLASH-Luc and pFOPFLASH-Luc were kindly provided by Prof. Avri Ben-Ze'ev. pCIG-CA-β-catenin plasmid was a gift from Prof. Andrew P. McMahon (Megason and McMahon, 2002). Flag-Dvl construct was a kind gift from Prof. Marianne Bienz (Schwarz-Romond et al., 2005). pTLHA-CRMP1 was provided by Prof. Erich E. Wanker (Stelzl et al., 2005) and pCDNA-HA-TLE1 was received from Prof. Yoram Groner (Levanon et al., 1998). CXCL12 (*Sdf-1*), inserted into pCMV-SPORT6 vector, was a gift from Prof. John L.R. Rubenstein. pBSc-α2 and *Cyclin D1*, *Tcf3*, *Tcf4* and *Wnt7B* in pFLCI vectors, were provided by the Forchheimer plasmid collection.

ANTIBODIES

Monoclonal antibodies specific for Myc (SC-40) and HA (16B12) were purchased from Santa Cruz, CA, USA, and Convance CA, USA, respectively. Mouse monoclonal anti-Flag (M2), polyclonal antibodies specific for β-catenin and Goat anti-mouse-tubulin (DM1A) were purchased from Sigma (Rehovot, Israel). Mouse monoclonal antibodies for pY489-β-catenin were obtained from the developmental studies hybridoma bank (DSHB). Rabbit polyclonal antibodies for Calbindin were purchased from SWANT (Bellinzona, Switzerland). Polyclonal antibodies specific for Cyclin D1 were purchased from Abcam Cambridge, UK. TAG-1 antibodies were received from Prof. Peles (Horresh et al., 2008). Secondary antibodies used for immunostaining included Cy3- and Cy5-conjugated donkey anti-mouse and anti-rabbit IgG (H + L), and Cy3-conjugated Goat anti-mouse IgM purchased from Jackson ImmunoResearch.

CELL LINES

COS-7 and HEK293 were grown at 37°C, 5% CO_2 in DMEM (Gibco, Auckland, New Zealand) supplemented with 10% fetal bovine serum (FBS), 4 mM glutamine, 100 U/ml penicillin and 0.1 mg/ml streptomycin.

MICE

The single KO PAF-AH catalytic subunit mice were received from Prof. Hiroyki Arai (Koizumi et al., 2003) and were bred to generate the double KO mice. Prof. Yuchio Yanagawa kindly provided the GAD67-GFP (Δneo) mice (Tamamaki et al., 2003). Mice were raised in the Weizmann Institute of Science transgenic facility. Staging of embryos were according to defined developmental stages (Kaufman, 1992). The GAD67-GFP mice were bred with the double KO mice to create triple transgenic mice.

TRANSFECTIONS

COS-7 Cells were transfected using JET PEI (Polyplus-transfection, NY, USA). HEK293 cells were transfected by the calcium phosphate precipitation method (Graham and van der Eb, 1973).

LUCIFERASE REPORTER ASSAYS

Lef/Tcf reporter assays were performed as previously described (Brembeck et al., 2004). Briefly, HEK293 cells were trypsinized 1 day prior to transfection and plated on 24 well plates. Cells were co-transfected with 0.25 μg of pTOPFLASH-Luc or pFOPFLASH-Luc, either 0.5 μg of pCIG-CA-β-catenin or Dvl expression constructs, and either TLE1 or CRMP1, respectively and also with different combinations of either PAF-AH α1 or α2. Empty pcDNA3 was added to keep the plasmid amounts equal in each transfection. Luciferase activity was determined 48 hr after transfection and normalized against β-galactosidase activity. Reporter assays were performed as triple transfections.

IMMUNOSTAINING

COS-7 cells were grown on coverslips (Menzel-Glaser, Braunschweig, Germany). Two days after transfection, cells were washed in PBS (Gibco, Auckland, New Zealand), fixed with 3% paraformaldehyde and permeabilized using 0.1% Triton X-100. After blocking three times in PBS supplemented with 0.1% BSA (Sigma, Rehovot,

Israel), coverslips were incubated with the indicated antibodies, stained with DAPI, mounted with Immu-mount (Thermo Electron Corporation, USA) and examined using the DeltaVision system (Applied Precision, Issaquah, WA, USA).

BRAIN IMMUNOSTAININGS

E13.5 wild-type, heterozygote ($\alpha1^{+/-}\alpha2^{+/-}$), or double KO ($\alpha1^{-/-}\alpha2^{-/-}$) embryos were fixed in 4% paraformaldehyde overnight. The post-fixed embryos were washed three times with PBS and brains were dissected out. The brains were then embedded in 3.5% low-temperature melting point agarose. Coronal sections (60 μm) were cut using a vibratome (Leica) and collected floating in PBS. Sections were permeabilized with PBS-T (1 × PBS, 0.1% Triton X-100), blocked in 10% FCS/PBS-T and then incubated overnight at 4°C with the indicated antibodies. Slides were washed with PBS-T and incubated with secondary antibodies for 1 h RT, washed with PBS-T and mounted using Aqua Poly/Mount (Polysciences. Inc., USA).

IN SITU HYBRIDIZATION

E13.5 embryos (wild-type C57BL/6J, Heterozygote for α1 and α2 ($\alpha1^{+/-}\alpha2^{+/-}$), or double KO ($\alpha1^{-/-}\alpha2^{-/-}$) were collected in ice-cold PBS in a RNase-free environment, then fixed in 4% paraformaldehyde overnight. Isolated brains were gradually dehydrated to 100% methanol and stored at −20°C. After bleaching with 1:5 H_2O_2:methanol, the brains were rehydrated and treated with Proteinase K, then brains were re-fixed and sectioned using a Leica vibratome (150 μm). Antisense digoxigenin-labeled RNA templates were generated by *in vitro* transcription using PCR products (using the appropriate combinations of T7, T3, and SP6 primers) from the corresponding genes. Hybridization was conducted overnight at 60°C, using the riboprobes at a concentration of 1 ng/μl in hybridization buffer [50% formamide (Ambion, Israel), 1.3% SSC, 0.2% Tween-20, 5 mM EDTA, 50 μg/ml yeast tRNA, 100 μg/ml Heparin (Sigma, Israel)]. Immunological detection was done using anti-digoxigenin-AP-conjugate antibodies (Roche, Germany) and NBT/BCIP reagents (Boehringer, Germany).

TRANSPLANTATION TO EXPLANTS

E13.5 GAD67-GFP, wild-type and double KO brains were cut into 250 μm coronal slices and then transferred onto inserts (MilliCell-CM, Millipore) floating on serum free medium (Neurobasal medium supplemented with B27, N2, GlutaMax, glucose, and gentamicin). MGE explants, dissected from E13.5 GAD67-GFP brains, were loaded into a glass micropipette and transplanted into either wild-type or double KO E13.5 MGE. After 24 h of incubation at 37°C, 5% CO_2, grafted neurons were visualized using the DeltaVision system package. Each time-lapse movie lasted 3 h with one frame taken every 2 min.

DiI LABELING

To examine thalamocortical projections, fixed brains (E13.5) were labeled with DiI crystals (1,1′-dioctadecyl-3,3,3′,3′-tetramethylindocarbocyanine perchlorate ('DiI'; DiIC18(3)) *crystalline*, Molecular probes). The crystals were placed within the thalamus and were left to diffuse for 5 days prior to vibratome sectioning (60 μm) that were later imaged using standard fluorescent microscopy.

MICROSCOPY

Images were taken using either the DeltaVision system package (Applied Precision, Issaquah, WA, USA), or confocal microscopy (LSM510, Zeiss).

MEASUREMENTS

Cell counts and neuronal migration speed were analyzed using the MeasurementPro and ImarisTrack modules of Imaris software (Bitplane, Zurich, Switzerland). Area was measured using Adobe Photoshop CS2.

STATISTICAL ANALYSIS

Statistical analysis was conducted using Prism 4 for Macintosh (GraphPad Software, Inc.).

RESULTS

DOUBLE MUTANT MICE EXHIBIT INCREASED GE AREA, WHERE PAF-AH CATALYTIC SUBUNITS ARE EXPRESSED

Analysis of the brains of double mutant embryos (E13.5), revealed a modest increase in the size of the ganglionic eminences (GE). The area of the GE and number of cells at M-phase were determined by anti-phosphohistone H3 (pH3) immunostaining (**Figures 1A,B**). Double KO mice had a significant ($P = 0.0068$) 34 ± 9.4% increase (112600 ± 7579 pixels, $n = 8$) in the area of pH3 positive cells in comparison with the heterozygotes (83860 ± 2371 pixels, $n = 10$). In addition, double KO mice exhibited a 26 ± 7.4% increase in the number of pH3 positive cells (336.4 ± 18.9, $n = 8$, $P = 0.0029$) in comparison with the heterozygotes (266.9 ± 9.3, $n = 10$). When we examined the number of pH3 positive cells in the cerebral cortex there was no difference between the double KO and the heterozygotes, thus suggesting an area specific effect of the mutation. When E12.5 embryos were examined, the area of the proliferation zone in the GE was only slightly and not significantly increased (+4.8%). There was no difference in the number of pH3 positive cells, therefore we focused our studies on E13.5 embryos.

Next, we examined whether the PAF-AH subunits are expressed at this developmental stage in the mouse embryonic brain. *In situ* hybridization showed that both the α1 and the α2 PAF-AH subunits are expressed in the GE as well as in other brain regions such as the developing cerebral cortex and the thalamus (**Figures 1C–F**).

Embryonic expression of the PAF-AH catalytic subunits has been previously noted in the mouse and rat brain (Albrecht et al., 1996; Manya et al., 1998). Our results suggest that the increased number of proliferating cells in the GE observed in double KO at E13.5 may be associated with the lack of expression of PAF-AH catalytic subunits.

PAF-AH SUBUNITS MODULATE THE Wnt PATHWAY

The Wnt pathway participates in the regulation of neuronal proliferation in the ganglionic eminences (Gulacsi and Anderson, 2008). Furthermore, high throughput protein-interaction data suggested possible interactions of the PAF-AH 1B3 (α1) catalytic subunit with several proteins related to the Wnt pathway (Kim et al., 2003; Daniels and Weis, 2005; Stelzl et al., 2005). A schematic presentation of the suggested position of PAF-AH within the Wnt pathway is shown in **Figure 2**.

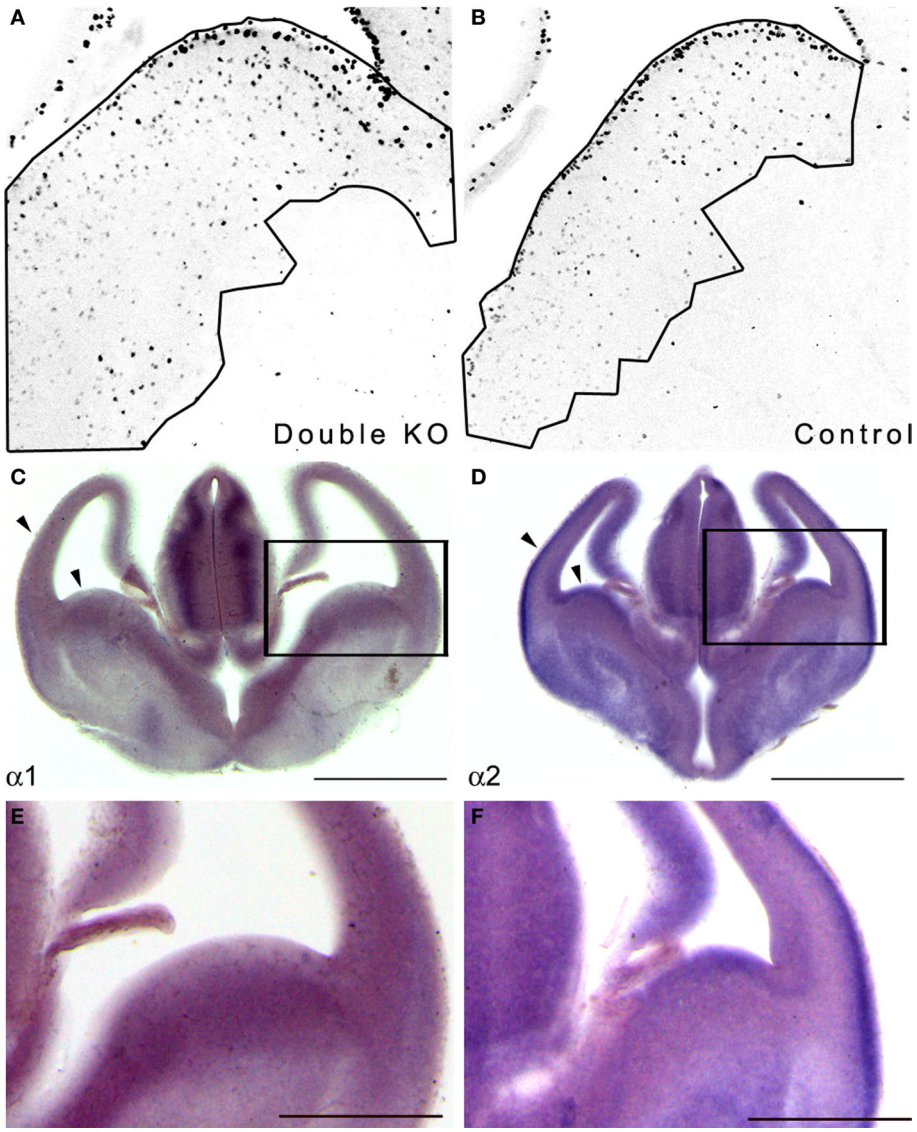

FIGURE 1 | Double KO mice exhibited increased GE area where the PAF-AH catalytic subunit genes are expressed. (A,B) Sections from E13.5 double KO **(A)** or control mice **(B)** were immunostained with anti-pH3. The area of the proliferating zone was marked (black line), and the cells were counted. There were more pH3 positive cells in the double KO mice. **(C,D)** *In situ* hybridization was conducted at E13.5 using PAF-AH α1 **(C)** or α2 **(D)** probes. Scale bar is 1 mm. **(E,F)** High magnification of **(C)** and **(D)**, respectively. Scale bar is 0.5 mm.

As can be seen in the scheme, PAF-AH interacts with multiple components both up and downstream to the canonical Wnt pathway. Although we verified some of the physical interactions in transfected cells using co-immunoprecipitation assays (CRMP1, BRD7 and UNC119, data not shown), we still could not predict how modulation of PAF-AH subunits will affect Wnt-mediated signaling in regard to modulating upstream and/or downstream processes. To test the possible effect of the PAF-AH subunits on the Wnt pathway we conducted cell-based luciferase reporter assays (**Figure 3**). Activation of the Wnt pathway stabilizes β-catenin allowing its entry to the nucleus, thereby activates transcription of genes containing TCF/LEF1 binding sites (Eastman and Grosschedl, 1999). The activation can be induced by addition of a constitutively active (CA) form of β-catenin or by addition of a Disheveled (Dvl) protein. HEK293 cells were co-transfected with either TOPFLASH (positive reporter plasmid with three copies of TCF/LEF-1 binding sites) or FOPFLASH (negative control with mutated binding sites) reporters, along with either CA β-catenin or Dvl (**Figures 3A,B**, respectively). Overexpression of CA β-catenin or Dvl resulted in a significant increase in reporter gene activity ($P < 0.001$). However, when either CRMP1 or TLE1 were co-expressed with Dvl or CA β-catenin, respectively, the increase was significantly smaller ($P < 0.01$). A more pronounced reduction in the reporter activity was accomplished when either PAF-AH α1 or α2 proteins were expressed together with either CRMP1 or TLE1 ($P < 0.001$). Nonetheless, it is important to note that a significant reduction in CA β-catenin- or Dvl-mediated activation was obtained

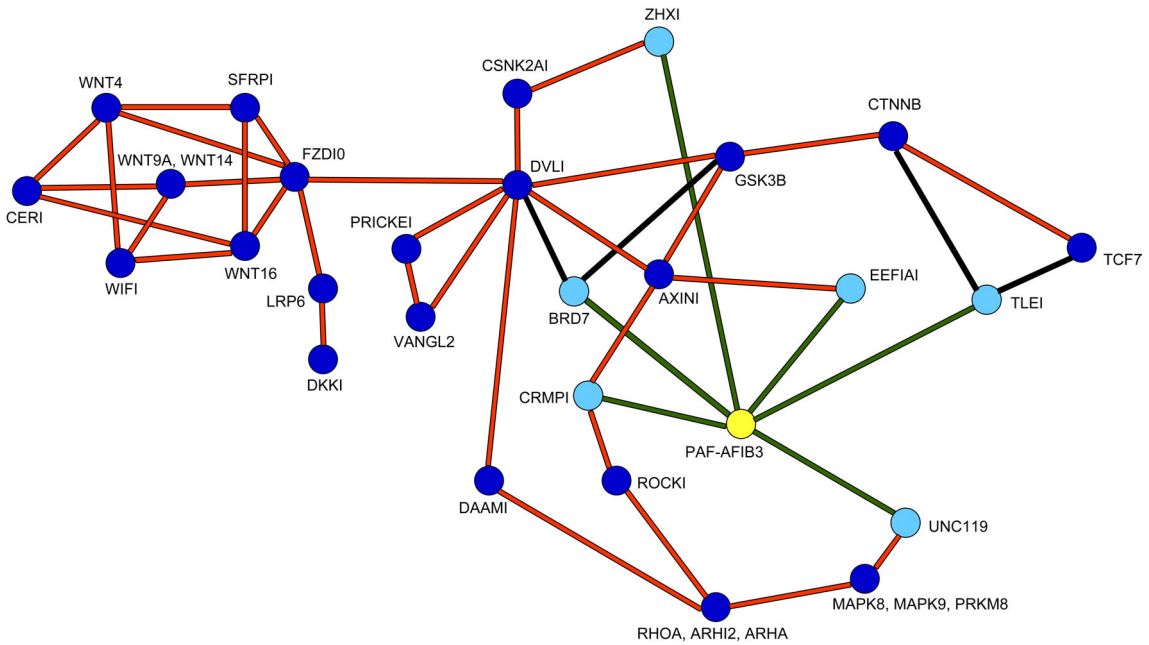

FIGURE 2 | Positioning of PAH-AH in the Wnt pathway. PAF-AH (highlighted in yellow) interacting proteins (highlighted in light blue) connected with green lines were detected in a large yeast two hybrid screen, additional interactions are connected by orange lines (Stelzl et al., 2005) and associated site: http://141.80.164.19/y2h_network/ppi_search.php (enter official gene symbol: pafah1b3). The BRD7 interactions were added from (Kim et al., 2003), and the interactions between CTNNB, TLE1 or TCF proteins were taken from (Daniels and Weis, 2005), these are marked with black lines.

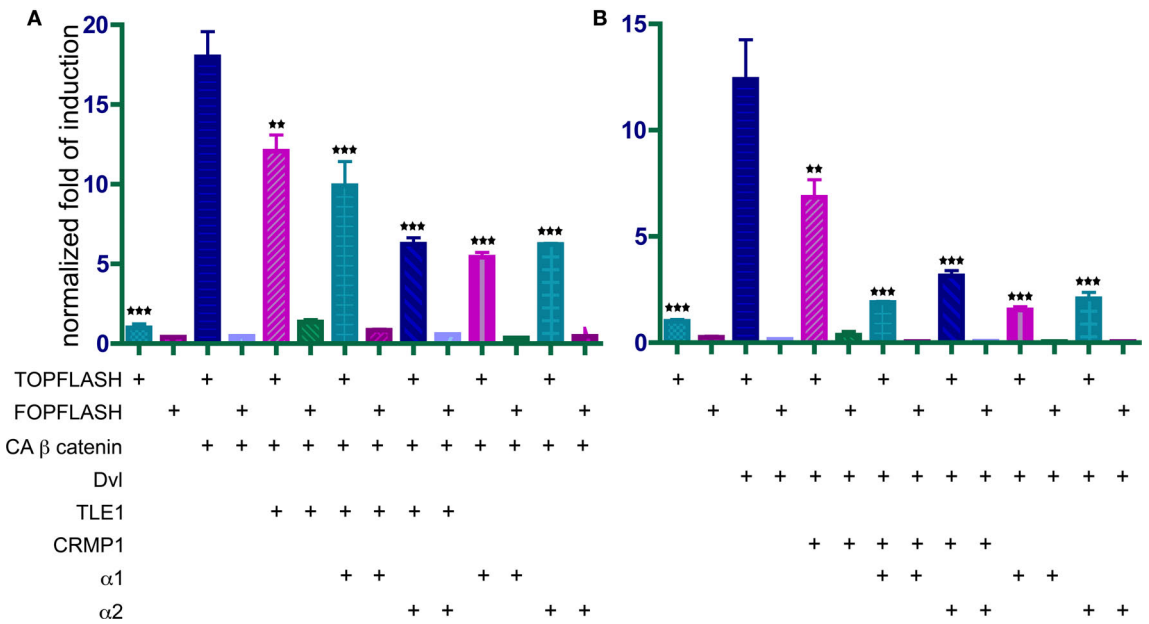

FIGURE 3 | PAFAH α1 and α2 catalytic subunits repress TCF/LEF-dependent transcription induced by CA β-catenin (A) or disheveled (Dvl) (B). HEK293 cells were transfected with either TOPFLASH, a reporter vector for the activation of the Wnt signaling, or FOPFLASH, a negative control reporter. In addition, different combinations of α1 and α2 on top of either TLE1 **(A)**, or CRMP1 **(B)**. Results are normalized as fold of induction relative to basal luciferase activity. Histograms represent the mean of three experiments ± S.E.M. Stars indicate the p values: $^{**}P < 0.01$, $^{***}P < 0.001$.

only when either α1 or α2 were co-expressed with these Wnt pathway activators ($P < 0.001$, ANOVA statistical analysis of luciferase assays with Tukey's multiple comparison test, $n = 3$). Our results verified that CRMP1 and TLE1 are negative regulators of the Wnt signaling pathway as previously reported (Levanon et al., 1998; Stelzl et al., 2005). More importantly, our results demonstrated that the

addition of either PAF-AH catalytic subunits α1 or α2 even without the addition of either CRMP1 or TLE1, repressed gene expression mediated by TCF/LEF1 binding sites.

In summary, expression of either PAF-AH catalytic subunit resulted in a decrease in activation of the Wnt-mediated reporter either following activation with CA β-catenin or following activation of the pathway using Dvl.

The intracellular localization of GFP-tagged CA β-catenin was used as an additional mean to monitor activation of the Wnt pathway. In transfected COS-7 cells CA β-catenin is typically found as puncta in the cell nucleus (**Figure 4A** 92.3 ± 6.2% of the transfected cells) similar to previous reports (Simcha et al., 1998; Giannini et al., 2000). However, the intracellular localization of CA β-catenin shifted to a prominent cytoplasmic localization following transfection with either PAF-AH α1 subunit, where only 35.4 ± 2% of the transfected cells showed nuclear localization (**Figures 4B,C**) or PAF-AH α2 subunit, where 28.5 ± 2.8% of the transfected cells showed nuclear localization (**Figures 4D,E**). In the presence of both subunits a smaller proportion of cells exhibited nuclear localization of CA β-catenin (**Figures 4F,G** 26.2 ± 6.7% of the cells exhibited nuclear localization). The reduction in the percentage of cells exhibiting nuclear β-catenin is statistically significant for all treatments (ANOVA analysis with Dunnett's multiple comparison test, $P < 0.01$, $n = 3$ experiments, 30 cells were quantified for each transfection in each experiment).

The apparent intracellular localization was also verified by cellular fractionation followed by Western blot analysis. Following addition of either PAH-AH α1 or α2 subunit there was a noticeable decrease in the proportion of nuclear β-catenin (data not shown). Interestingly, the catalytic subunits of PAF-AH were found in the nuclear as well as in the cytoplasmic fraction.

In vivo we noticed a dramatic expansion in the area expressing nuclear β-catenin, which was most pronounced in the mantle layer of the lateral cortex (**Figure 5**). There was an almost two fold increase in the number of cells exhibiting nuclear β-catenin staining in the double KO brains in comparison with control sections (192 ± 34% versus 100 ± 7.6%, $n = 4$, $P = 0.04$).

Next, we examined the expression pattern of additional components of the Wnt pathway using *in situ* hybridization (**Figure 6**). The expression pattern of *Cyclin D1*, a downstream target of the Wnt pathway, was increased and expanded in the double KO versus the control mice (**Figures 6A,B**).

Tcf4 and *Tcf3* are members of the T cell factor/Lymphocyte enhancer factor family of transcription factors. Following activation of the Wnt pathway, β-catenin, alone or in association with members of the Tcf/Lef1, can translocate to the nucleus, where it ultimately controls the activity of specific target genes. We noticed an expansion in the expression domains of *Tcf4* (**Figures 6C,D**) and of *Tcf3* (**Figures 6E,F**). It is interesting to note that for the most, the expression pattern of *Tcf4* and *Tcf3* were mutually exclusive. In addition, a striking increase in *Wnt7B* expression was noticed mainly in the lateral cerebral cortex where we have previously noted an increase in nuclear β-catenin (**Figures 6G,H**, arrowhead). Collectively, our data indicate that the double KO mice exhibit increased and expanded expression of upstream and downstream Wnt-pathway components.

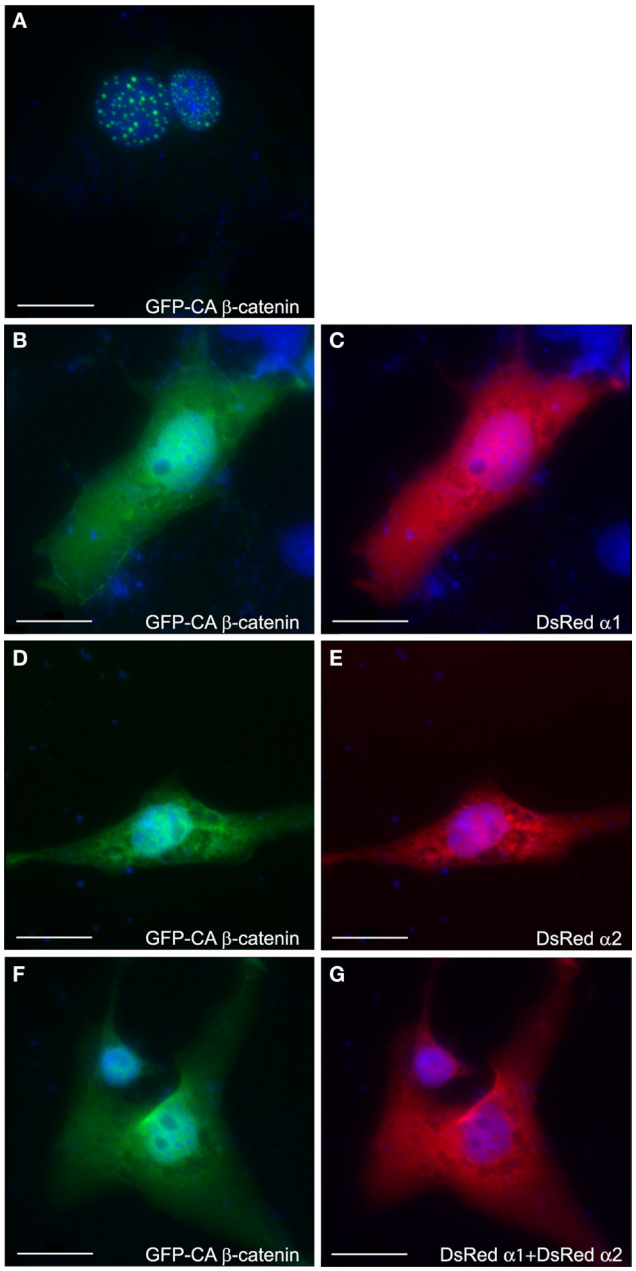

FIGURE 4 | PAFAH subunits affect subcellular localization of GFP-CA β-catenin. COS-7 cells were transfected with GFP-CA β-catenin **(A)** alone or together with DsRedα1 **(B,C)** or DsRedα2 **(D,E)**, or both PAF-AH catalytic subunits **(F,G)**. Cells were fixed 48 h after transfection and nuclear DNA was stained with DAPI (shown in blue). Overexpression of GFP-CA β-catenin demonstrated nuclear localization **(A)**, whereas the addition of either DsRedα1 **(C)** or DsRedα2 **(E)** or both **(G)** shifted β-catenin to the cytoplasm **(B,D,F)**. Scale bars are 20 μm.

PAF-AH DOUBLE KO MICE EXHIBIT ENHANCED TANGENTIAL MIGRATION

The development of the thalamocortical projection depends on the early tangential migration of a population of neurons derived from the ventral telencephalon (Lopez-Bendito et al., 2006). Therefore, we decided to examine whether the double KO

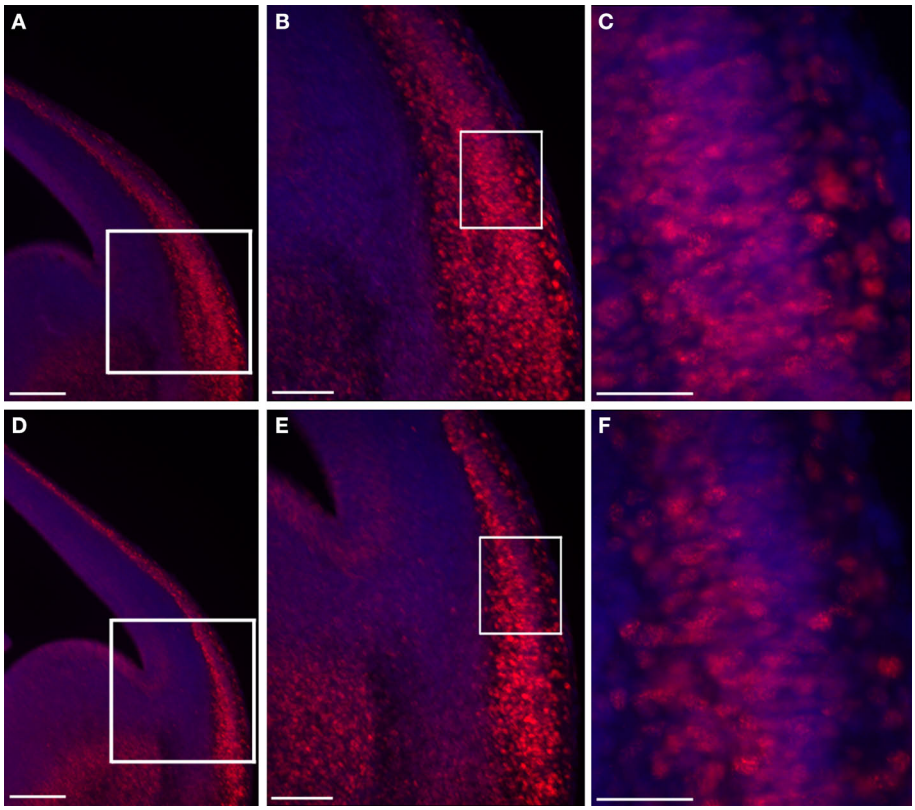

FIGURE 5 | Double KO brain sections exhibit an increased area of nuclear β-catenin. Double KO **(A–C)** exhibit more cells with nuclear β-catenin in comparison with control **(B–F)**. The white boxes define the higher magnifications areas. Scale bars: **(A,D)** 200, **(B,E)** 100, **(C,F)** 40 μm.

mice exhibit any changes in the development of thalamocortical projections. We used TAG-1 immunostaining to visualize the emergence of the corticofugal system in the developing cortex (Denaxa et al., 2001, 2005). Immunohistochemical staining of cortical sections of E13.5 mouse embryos revealed the presence of labeled cells and their axons in the region of the plexiform primordium in wild-type mice (**Figures 7B,D**). In the double mutant mice, intense TAG-1 immunoreactivity was present in fibers of the intermediate zone, the cortical plate as well as the marginal zone of the basolateral cortex (**Figures 7A,C**). In addition, the labeling of thalamocortical fibers by DiI revealed an early development of thalamocortical projections in the double KO brains (**Figure 7E** versus **F**).

The migration of interneurons from the ganglionic eminences towards the cortex was visualized by using fluorescent-based genetic labeling of these cells. We crossed GAD67-GFP knock-in mice (Tamamaki et al., 2003) with the double KO mice. An observable enhancement in interneuron migration to the cortex was noted following elimination of the PAF-AH catalytic subunits (**Figures 8A,B** versus **C,D**). These results were corroborated by an observable increase in the number and relative position of calbindin positive interneurons found in the cerebral cortex in the double KO in comparison with the control (**Figures 8E,F** versus **G,H**).

Next, we monitored neuronal migration by time-lapse movies of neurons. Explants of GAD67-GFP MGE neurons, transplanted on either a wild-type or double knockout substrate, were time-lapsed 24 h after transplantation. GFP-labeled interneurons moved faster on the double knockout slice (20.8 ± 0.6 μm/h $n = 4816$, versus 14.4 ± 0.4 μm/h $n = 7016$, $P < 0.0001$, using unpaired t-test with Welch's correction). The mean and instantaneous velocities of the interneurons fit with previously published results (Tanaka et al., 2003).

These results suggested that the enhanced motility of the interneurons on the double KO substrate may result from a non-cell autonomous phenotype. One secreted protein, which has shown to affect migration of interneurons within this area is SDF-1 (stromal cell-derived factor-1) (Stumm et al., 2003). There was a clear difference in the pattern of *Sdf-1* expression in the cortex; in the double KO it extended from lateral to medial aspect of cortical anlage (**Figure 8I**) in comparison to the normal expression pattern seen in control brains (**Figure 8J**). Next, we examined the expression pattern of *Netrin-1*, which has been shown to affect the migration of interneurons (Stanco et al., 2009). We detected increased expression of *Netrin-1* in the striatum and lateral part of the cerebral cortex in comparison with the expression observed in control brains (**Figures 8K,L**). Collectively, our data indicate that the double KO mice exhibit earlier arrival of thalamocortical fibers, enhanced and faster migration of interneurons to the cortex, which is in part non-cell autonomous.

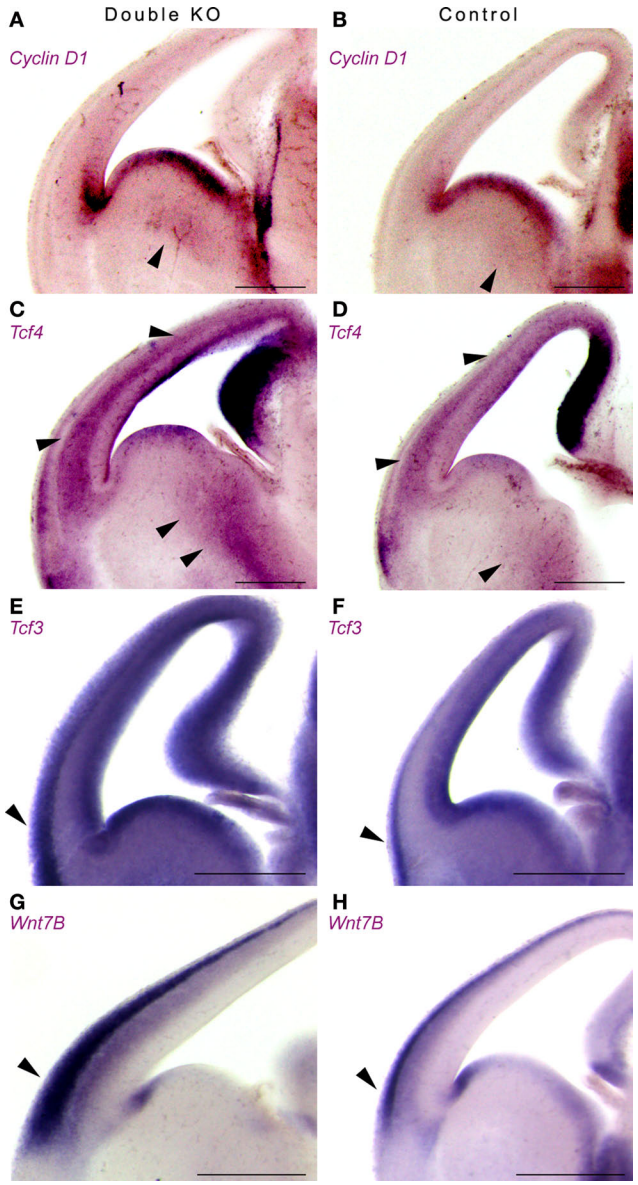

FIGURE 6 | Double KO brains exhibit increased and expanded expression of downstream and upstream components of the Wnt pathway using *in situ* hybridization. (A,B) Expression of *Cyclin D1* in double KO **(A)** or control **(B)**. Note the expansion in the area expressing *Cyclin D1* in the GE. **(C,D)** Expression of *Tcf4* in double KO **(C)** or control **(D)**. Arrowheads mark the comparable GE area, as well as cerebral cortex area **(E,F)** Expression of *Tcf3* in double KO **(E)** or control **(F)**. Note the mutually exclusive pattern of expression between the *Tcf3* and *Tcf4*. **(G,H)** Expression of *Wnt7B* in double KO **(G)** or control **(H)**. The area that expressed high levels of nuclear β-catenin is marked with arrowheads. Scale bars are 0.5 mm.

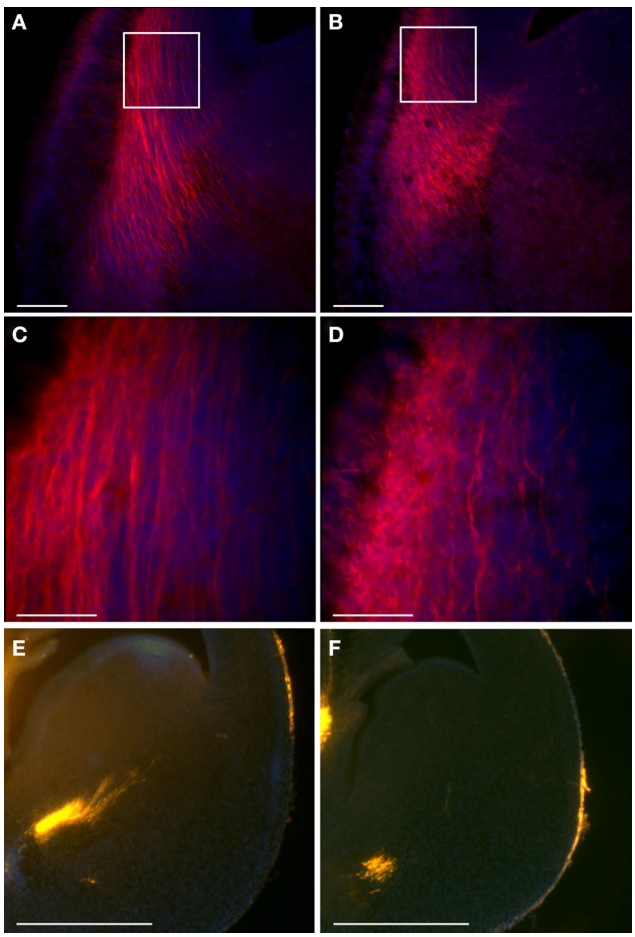

FIGURE 7 | Double KO mice exhibit earlier thalamocortical projections. (A–D) TAG-1 immunostaining of double KO **(A,C)** and control **(B,D)** mice. Scale bars: (**A,B**) – 100; (**C,D**) – 40 μm. The white boxes in **(A)** and **(B)** define the area shown in **(C)** and **(D)**. **(E,F)** DiI stained thalamocortical fibers exhibit earlier projections in double KO brains **(E)** in comparison to the control brains **(F)**. Scale bars are 500 μm.

DISCUSSION

Our study revealed an unexpected activity of the PAF-AH catalytic subunits acting as negative regulators of the Wnt pathway. In addition, deletion of the PAF-AH catalytic subunits increases the proliferation of GABAergic neurons in the ganglionic eminences and affects their migration. The advanced migration of GABAergic neurons is in part a non-cell autonomous effect which may be mediated through the modified expression of Wnts, SDF1 and Netrin1 in the double KO embryos.

PAF-AH CATALYTIC SUBUNITS MODULATE THE Wnt PATHWAY

Increased expression of the PAF-AH subunits repressed gene expression mediated by TCF/LEF1 binding sites following activation with CA β-catenin or following activation of the pathway using Dvl. Subsequent to expression of PAF-AH catalytic subunits, β-catenin was mainly retained in the cytoplasm in a cultured cell line. Conversely, genetic elimination of the PAF-AH catalytic subunits resulted in an increase in the number of cells expressing nuclear β-catenin, increased proliferation in the GE and increased and expanded expression of upstream and downstream Wnt pathway components.

It may be of particular interest to repress the Wnt pathway, which is one of the five major signaling pathways predominating early and late embryonic development (Gerhart, 1999; Nusse,

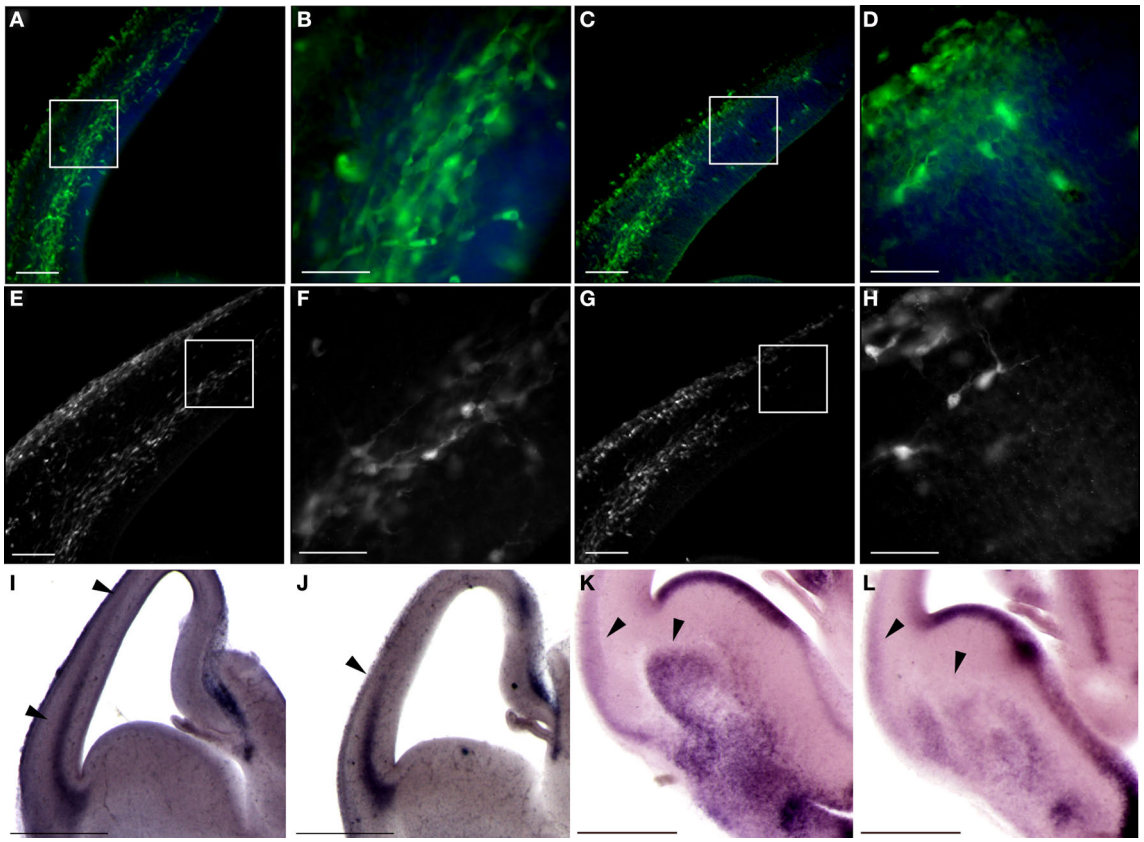

FIGURE 8 | Double KO mice exhibit advanced tangential migration. **(A–D)** GAD67-GFP-labeled interneurons are found in more advanced positions in double KO brain sections **(A,B)** in comparison with control sections **(C,D)**. Scale bars in **(A)** and **(C)** is 100 μm, and in **(B)** and **(D)** is 40 μm. **(E,F)** Calbindin immunostaining, which identifies a subgroup of interneurons, demonstrates advanced positioning of these interneurons in the double KO **(E,F)** versus control **(G,H)**. Scale bars in **(E)** and **(G)** is 100 μm, and in **(F)** and **(H)** is 40 μm. **(I,J)** *Sdf-1* expression by *in situ* hybridization is expanded in the cortex of double KO **(I)** versus the control cortex **(J)**. **(K,L)** *In situ* hybridization of *Netrin-1* reveals an expanded expression in the striatum of double KO **(K)** versus the control striatum **(L)**. Scale bars in **(I–L)** are 0.5 mm.

1999). The Wnt pathway participates in multiple roles as diverse as embryonic segmentation and patterning, gut patterning, nervous system development, formation and patterning of appendages, and stem cell proliferation. Most of the current information involves Wnt signaling through stabilization of β-catenin, which in turn enters the nucleus and controls gene expression (Nelson and Nusse, 2004). The Wnt pathway is highly conserved in evolution (Brown et al., 2008; Croce and McClay, 2008). We hypothesize that the evolutionary conserved function of the PAF-AH catalytic subunits is modulation of the Wnt pathway and not their interaction with LIS1 that acts as cytoplasmic dynein regulator (for review see Reiner, 2000). We are basing this hypothesis on several important observations. On one hand, *Lis1* heterozygote mice exhibit inhibition in radial and tangential migration (Hirotsune et al., 1998; Cahana et al., 2001; McManus et al., 2004b). On the other hand, PAF-AH catalytic subunit KO mice, do not exhibit a cortical phenotype, although they have decreased levels of the LIS1 protein (Koizumi et al., 2003; Yan et al., 2003). Dosage sensitivity of the LIS1 protein is well established. Reduced or increased LIS1 levels exhibit brain phenotypes in mice and in human (Hirotsune et al., 1998; Cahana et al., 2001; Reiner et al., 2002; Bi et al., 2009). Therefore, the finding that PAF-AH catalytic subunit KO mice do not exhibit a cortical phenotype despite the apparent reduction in LIS1 levels was surprising. A possible explanation may be that the reduction in the LIS1 protein levels is just the portion of LIS1, which is required for interaction with the catalytic subunits, and the remaining amount of LIS1 required for other intracellular interactions is normal. An additional argument relates to the evolutionary conservation of the PAF-AH catalytic subunits. We have characterized the fly orthologs of the PAF-AH complex. The *Drosophila* alpha-subunit ortholog lacks two of the three active-site residues and is catalytically inactive against PAF-AH 1B substrates. The beta-subunit (LIS1) ortholog is highly conserved from *Drosophila* to mammals and is able to interact with the mammalian alpha-subunits but is unable to interact with the *Drosophila* alpha-subunit (Sheffield et al., 2000). It will be interesting to investigate the possibility that the *Drosophila* alpha-subunit can modulate the Wnt pathway.

Canonical Wnt signaling mediated by β-catenin has been proposed to function in both neural progenitor cell expansion and neuronal lineage choice (Chenn and Walsh, 2002; Chenn and Walsh, 2003; Zechner et al., 2003; Hirabayashi et al., 2004; Israsena et al.,

2004; Wrobel et al., 2007). The outcome of modulating the Wnt pathway is highly dependent on the brain area and the involvement of other factors (such as FGF2) (Israsena et al., 2004). Furthermore, some of the above mentioned studies used expression of stabilized β-catenin, which is not responsive to normal regulatory mechanisms. Within the medial GE, targeted deletion of β-catenin specifically impaired proliferation without grossly altering differentiation. The phenotype observed there was primarily due to loss of canonical Wnt signaling (Gulacsi and Anderson, 2008). Thus, it may be expected that increased Wnt signaling within the GE will result in increased proliferation as noticed in our studies.

PAF-AH CATALYTIC SUBUNITS AFFECT MIGRATION OF INTERNEURONS

We observed that the double KO mice exhibited increased proliferation in the GE, earlier development of thalamocortical fibers and enhanced and faster migration of interneurons to the cortex, which is in part non-cell autonomous. These phenotypes may be due to activation of the Wnt pathway, nevertheless, we cannot exclude the participation or crosstalk with additional signaling pathways. The phenotypes observed in the PAF-AH double KO mice resemble in part phenotypes of *Robo1*-deficient mice. *Robo1*-KO mice exhibited an increased number of interneurons that was due to increased proliferation. A similar increase in proliferation was observed in *Slit1*(−/−)/*Slit2*(−/−) mutant mice, suggesting that cell division was influenced by Slit-Robo signaling mechanisms (Andrews et al., 2008). In addition, the sonic hedgehog (Shh) pathway participates in proliferation regulation in the GE (Xu et al., 2005; Fuccillo et al., 2006; Gulacsi and Anderson, 2006). It will be interesting to examine the possible involvement of the Slit-Robo and Shh signaling in regulation of the phenotypes observed in the PAF-AH double KO mice.

Furthermore, in *Robo1*-deficient mice more interneurons migrated into the cortex (Andrews et al., 2006). It has been postulated that it was due to migration of the interneurons along the corticothalamic and thalamocortical axons that arrived earlier to their respective targets in the mutant than in the control (Andrews et al., 2006). In the PAF-AH double KO mice we observed earlier arrival of the thalamocortical axons identified by TAG-1 immunostaining. It is known that early born (E11.5–E14.5) GABAergic cells colocalize with TAG-1-positive axons *in vivo*, whereas later-born cells colocalized with TAG-1-negative fibers, suggesting temporal differences in substrate specificity (McManus et al., 2004a). Thus, for the embryonic day we examined (E13.5) TAG-1 should be a good marker for progression of GABAergic cells. In addition, we examined directly the position of the interneurons using GAD67-GFP knock-in mice. The GFP positive interneurons were found in more advanced positions in the PAF-AH double KO mice. When we transplanted wild-type GAD67-GFP interneurons on double KO or wild-type substrates we noticed faster motility on the mutant background. These results suggest a non-cell autonomous activity, which may be attributed to multiple known secreted factors. To date, multiple guidance molecules have been identified (for examples see Lopez-Bendito et al., 2008; Marin and Rubenstein, 2001). In our study, we examined three secreted factors; *Netrin-1, Sdf-1* and *Wnt7B. Netrin-1* was shown to interact with alpha3beta1 integrin to promote interneuronal migration (Stanco et al., 2009). However, *Netrin-1* activity is known to be context dependent and can act as either a chemoattractant or a chemorepellent (Alcantara et al., 2000; Charron et al., 2003; Wilson and Key, 2006). *Netrin-1* expression in the striatum acts as a repulsive factor (Hamasaki et al., 2001). Thus, increased expression of *Netrin-1* in the striatum of double KO may be involved in promoting interneuron migration to the cortex. In addition, *Netrin-1* expression may also influence thalamocortical projections (Powell et al., 2008). SDF-1 regulates migration and positioning of CXCR4-expressing interneurons during cortical development (Stumm et al., 2003; Liapi et al., 2008). Furthermore, localized expression of SDF-1 can induce chemotaxis in migrating neurons and alter their local trajectories (Liapi et al., 2008). The expanded and increased expression of *Sdf-1* in mice lacking PAF-AH catalytic subunits may explain in part the change in the migration rates observed in these mice. In addition, we noted increased and expanded expression of *Wnt7B.* To the best of our knowledge, there are no direct data suggesting for a role of this Wnt family member in regulation of interneuron migration. Nevertheless, the Wnt pathway participates in regulation of cell migration in a very diverse system which is the movement of groups of cells forming the lateral line primordium of the zebrafish (Aman and Piotrowski, 2008). In that system, Wnt/β-catenin works in conjunction with FGF signaling to regulate the expression of SDF-1 chemokine receptors. Thus, despite the long list of known secreted factors guiding and regulating interneuron migration, additional factors may be added. We suggest that possible modulation of the Wnt pathway by the PAF-AH catalytic subunits attenuates interneuron migration to the cerebral cortex.

ACKNOWLEDGMENTS

We thank the following scientists for kindly providing reagents: Profs. Yuchio Yanagawa (Gunma University Graduate School of Medicine, Japan), Hiroyki Arai (University of Tokyo, Japan), Junken Aoki (Tohoku University, Japan), Andrew P. McMahon (Harvard University, USA), Marianne Bienz (MRC Laboratory of Molecular Biology, UK), Erich E. Wanker (Max-Delbrück Center for Molecular Medicine, Germany), John L.R. Rubenstein (University of California at San Francisco, USA), Amos Simon (Tel-Hashomer, Israel) and Avri Ben-Ze'ev, Yoram Groner, and Elior Peles (Weizmann Institute of Science, Israel). We thank Nataly Shvartzman and Yonatan Demeshko for help in genotyping, and Judith Chermesh, Shosh Grossfeld, and Yehuda Melamed from the Veterinary Resources for technical assistance. This research has been supported in part by research grants from the March of Dimes, #6-FY07-388, the Legacy Heritage Biomedical Program of the Israel Science Foundation (grant no. 1062/08), the Benoziyo Center for Neurological Diseases, the Nehemias Gorin foundation, a research grant from Marla Schaefer and the estate of Lela London.

REFERENCES

Albrecht, U., Abu-Issa, R., Ratz, B., Hattori, M., Aoki, J., Arai, H., Inoue, K., and Eichele, G. (1996). Platelet-activating factor acetylhydrolase expression and activity suggest a link between neuronal migration and platelet-activating factor. *Dev. Biol.* 180, 579–593.

Alcantara, S., Ruiz, M., De Castro, F., Soriano, E., and Sotelo, C. (2000). Netrin 1 acts as an attractive or as a repulsive cue for distinct migrating neurons during the development of the cerebellar system. *Development* 127, 1359–1372.

Aman, A., and Piotrowski, T. (2008). Wnt/beta-catenin and Fgf signaling control collective cell migration by restricting chemokine receptor expression. *Dev. Cell* 15, 749–761.

Andrews, W., Barber, M., Hernadez-Miranda, L. R., Xian, J., Rakic, S., Sundaresan, V., Rabbitts, T. H., Pannell, R., Rabbitts, P., Thompson, H., Erskine, L., Murakami, F., and Parnavelas, J. G. (2008). The role of Slit-Robo signaling in the generation, migration and morphological differentiation of cortical interneurons. *Dev. Biol.* 313, 648–658.

Andrews, W., Liapi, A., Plachez, C., Camurri, L., Zhang, J., Mori, S., Murakami, F., Parnavelas, J. G., Sundaresan, V., and Richards, L. J. (2006). Robo1 regulates the development of major axon tracts and interneuron migration in the forebrain. *Development* 133, 2243–2252.

Ayala, R., Shu, T., and Tsai, L. H. (2007). Trekking across the brain: the journey of neuronal migration. *Cell* 128, 29–43.

Barkovich, A. J., Kuzniecky, R. I., Jackson, G. D., Guerrini, R., and Dobyns, W. B. (2005). A developmental and genetic classification for malformations of cortical development. *Neurology* 65, 1873–1887.

Bazan, N. G. (1995). Inflammation. A signal terminator. *Nature* 374, 501–502.

Bazan, N. G. (2005). Lipid signaling in neural plasticity, brain repair, and neuroprotection. *Mol. Neurobiol.* 32, 89–103.

Ben-Ari, Y. (2006). Seizures beget seizures: the quest for GABA as a key player. *Crit. Rev. Neurobiol.* 18, 135–144.

Bi, W., Sapir, T., Shchelochkov, O. A., Zhang, F., Withers, M. A., Hunter, J. V., Levy, T., Shinder, V., Peiffer, D. A., Gunderson, K. L., Nezarati, M. M., Shotts, V. A., Amato, S. S., Savage, S. K., Harris, D. J., Day-Salvatore, D. L., Horner, M., Lu, X. Y., Sahoo, T., Yanagawa, Y., Beaudet, A. L., Cheung, S. W., Martinez, S., Lupski, J. R., and Reiner, O. (2009). Increased LIS1 expression affects human and mouse brain development. *Nat. Genet.* 41, 168–177.

Brembeck, F. H., Schwarz-Romond, T., Bakkers, J., Wilhelm, S., Hammerschmidt, M., and Birchmeier, W. (2004). Essential role of BCL9-2 in the switch between beta-catenin's adhesive and transcriptional functions. *Genes Dev.* 18, 2225–2230.

Brown, F. D., Prendergast, A., and Swalla, B. J. (2008). Man is but a worm: chordate origins. *Genesis* 46, 605–613.

Cahana, A., Escamez, T., Nowakowski, R. S., Hayes, N. L., Giacobini, M., von Holst, A., Shmueli, O., Sapir, T., McConnell, S. K., Wurst, W., Martinez, S., and Reiner, O. (2001). Targeted mutagenesis of Lis1 disrupts cortical development and LIS1 homodimerization. *Proc. Natl. Acad. Sci. USA* 98, 6429–6434.

Chao, W., and Olson, M. S. (1993). Platelet-activating factor: receptors and signal transduction. *Biochem. J.* 292, 617–629.

Charron, F., Stein, E., Jeong, J., McMahon, A. P., and Tessier-Lavigne, M. (2003). The morphogen sonic hedgehog is an axonal chemoattractant that collaborates with netrin-1 in midline axon guidance. *Cell* 113, 11–23.

Chenn, A., and Walsh, C. A. (2002). Regulation of cerebral cortical size by control of cell cycle exit in neural precursors. *Science* 297, 365–369.

Chenn, A., and Walsh, C. A. (2003). Increased neuronal production, enlarged forebrains and cytoarchitectural distortions in beta-catenin overexpressing transgenic mice. *Cereb. Cortex* 13, 599–606.

Croce, J. C., and McClay, D. R. (2008). Evolution of the Wnt pathways. *Methods Mol. Biol.* 469, 3–18.

Daniels, D. L., and Weis, W. I. (2005). Beta-catenin directly displaces Groucho/TLE repressors from Tcf/Lef in Wnt-mediated transcription activation. *Nat. Struct. Mol. Biol.* 12, 364–371.

Denaxa, M., Chan, C. H., Schachner, M., Parnavelas, J. G., and Karagogeos, D. (2001). The adhesion molecule TAG-1 mediates the migration of cortical interneurons from the ganglionic eminence along the corticofugal fiber system. *Development* 128, 4635–4644.

Denaxa, M., Kyriakopoulou, K., Theodorakis, K., Trichas, G., Vidaki, M., Takeda, Y., Watanabe, K., and Karagogeos, D. (2005). The adhesion molecule TAG-1 is required for proper migration of the superficial migratory stream in the medulla but not of cortical interneurons. *Dev. Biol.* 288, 87–99.

Eastman, Q., and Grosschedl, R. (1999). Regulation of LEF-1/TCF transcription factors by Wnt and other signals. *Curr. Opin. Cell Biol.* 11, 233–240.

Fuccillo, M., Joyner, A. L., and Fishell, G. (2006). Morphogen to mitogen: the multiple roles of hedgehog signalling in vertebrate neural development. *Nat. Rev. Neurosci.* 7, 772–783.

Gerhart, J. (1999). 1998 Warkany lecture: signaling pathways in development. *Teratology* 60, 226–239.

Giannini, A. L., Vivanco, M. M., and Kypta, R. M. (2000). Analysis of beta-catenin aggregation and localization using GFP fusion proteins: nuclear import of alpha-catenin by the beta-catenin/Tcf complex. *Exp. Cell Res.* 255, 207–220.

Gotz, M., and Huttner, W. B. (2005). The cell biology of neurogenesis. *Nat. Rev. Mol. Cell Biol.* 6, 777–788.

Graham, F. L., and van der Eb, A. J. (1973). Transformation of rat cells by DNA of human adenovirus 5. *Virology* 54, 536–539.

Gulacsi, A., and Anderson, S. A. (2006). Shh maintains Nkx2.1 *in the MGE by a Gli3*-independent mechanism. *Cereb Cortex* 16 (Suppl 1), i89–i95.

Gulacsi, A. A., and Anderson, S. A. (2008). Beta-catenin-mediated Wnt signaling regulates neurogenesis in the ventral telencephalon. *Nat. Neurosci.* 11, 1383–1391.

Hamasaki, T., Goto, S., Nishikawa, S., and Ushio, Y. (2001). A role of netrin-1 in the formation of the subcortical structure striatum: repulsive action on the migration of late-born striatal neurons. *J. Neurosci.* 21, 4272–4280.

Hanahan, D. J. (1986). Platelet activating factor: a biologically active phosphoglyceride. *Ann. Rev. Biochem.* 55, 483–509.

Hatten, M. E. (2002). New directions in neuronal migration. *Science* 297, 1660–1663.

Hebbar, S., Mesngon, M. T., Guillotte, A. M., Desai, B., Ayala, R., and Smith, D. S. (2008). Lis1 and Ndel1 influence the timing of nuclear envelope breakdown in neural stem cells. *J. Cell Biol.* 182, 1063–1071.

Hirabayashi, Y., Itoh, Y., Tabata, H., Nakajima, K., Akiyama, T., Masuyama, N., and Gotoh, Y. (2004). The Wnt/beta-catenin pathway directs neuronal differentiation of cortical neural precursor cells. *Development* 131, 2791–2801.

Hirotsune, S., Fleck, M. W., Gambello, M. J., Bix, G. J., Chen, A., Clark, G. D., Ledbetter, D. H., McBain, C. J., and Wynshaw-Boris, A. (1998). Graded reduction of Pafah1b1 (Lis1) activity results in neuronal migration defects and early embryonic lethality. *Nat. Genet.* 19, 333–339.

Horresh, I., Poliak, S., Grant, S., Bredt, D., Rasband, M. N., and Peles, E. (2008). Multiple molecular interactions determine the clustering of Caspr2 and Kv1 channels in myelinated axons. *J. Neurosci.* 28, 14213–14222.

Israsena, N., Hu, M., Fu, W., Kan, L., and Kessler, J. A. (2004). The presence of FGF2 signaling determines whether beta-catenin exerts effects on proliferation or neuronal differentiation of neural stem cells. *Dev. Biol.* 268, 220–231.

Kato, K., Clark, G. D., Bazan, N. G., and Zorumski, C. F. (1994). Platelet-activating factor as a potential retrograde messenger in CA1 hippocampal long-term potentiation. *Nature* 367, 175–179.

Kaufman, M. H. (1992). *The Atlas of Mouse Development*. London: Academic Press Limited.

Kim, S., Lee, J., Park, J., and Chung, J. (2003). BP75, bromodomain-containing M(r) 75,000 protein, binds dishevelled-1 and enhances Wnt signaling by inactivating glycogen synthase kinase-3 beta. *Cancer Res.* 63, 4792–4795.

Koizumi, H., Yamaguchi, N., Hattori, M., Ishikawa, T. O., Aoki, J., Taketo, M. M., Inoue, K., and Arai, H. (2003). Targeted disruption of intracellular type I platelet activating factor-acetylhydrolase catalytic subunits causes severe impairment in spermatogenesis. *J. Biol. Chem.* 278, 12489–12494.

Koltai, M., Hosford, D., Guinot, P., Esanu, A., and Braquet, P. (1991). Platelet activating factor (PAF). A review of its effects, antagonists and possible future clinical implications (Part I). *Drugs* 42, 9–29.

Kornecki, E., and Ehrlich, Y. H. (1988). Neuroregulatory and neuropathological actions of the ether-phospholipid platelet-activating factor. *Science* 240, 1792–1794.

Levanon, D., Goldstein, R. E., Bernstein, Y., Tang, H., Goldenberg, D., Stifani, S., Paroush, Z., and Groner, Y. (1998). Transcriptional repression by AML1 and LEF-1 is mediated by the TLE/Groucho corepressors. *Proc. Natl. Acad. Sci. USA* 95, 11590–11595.

Liapi, A., Pritchett, J., Jones, O., Fujii, N., Parnavelas, J. G., and Nadarajah, B. (2008). Stromal-derived factor 1 signalling regulates radial and tangential migration in the developing cerebral cortex. *Dev. Neurosci.* 30, 117–131.

Lopez-Bendito, G., Cautinat, A., Sanchez, J. A., Bielle, F., Flames, N., Garratt, A. N., Talmage, D. A., Role, L. W., Charnay, P., Marin, O., and Garel, S. (2006). Tangential neuronal migration controls axon guidance: a role for neuregulin-1 in thalamocortical axon navigation. *Cell* 125, 127–142.

Lopez-Bendito, G., Sanchez-Alcaniz, J. A., Pla, R., Borrell, V., Pico, E., Valdeolmillos, M., and Marin, O. (2008). Chemokine signaling controls intracortical migration and final distribution of GABAergic interneurons. *J. Neurosci.* 28, 1613–1624.

Manya, H., Aoki, J., Watanabe, M., Adachi, T., Asou, H., Inoue, Y., Arai, H., and Inoue, K. (1998). Switching of platelet-activating factor acetylhydrolase catalytic subunits in developing rat brain. *J. Biol. Chem.* 273, 18567–18572.

Marin, O., and Rubenstein, J. L. (2001). A long, remarkable journey: tangential migration in the telencephalon. *Nat. Rev. Neurosci.* 2, 780–790.

McManus, M. F., Nasrallah, I. M., Gopal, P. P., Baek, W. S., and Golden, J. A. (2004a). Axon mediated interneuron migration. *J. Neuropathol. Exp. Neurol.* 63, 932–941.

McManus, M. F., Nasrallah, I. M., Pancoast, M. M., Wynshaw-Boris, A.,

and Golden, J. A. (2004b). Lis1 is necessary for normal non-radial migration of inhibitory interneurons. *Am. J. Pathol.* 165, 775–784.

Megason, S. G., and McMahon, A. P. (2002). A mitogen gradient of dorsal midline Wnts organizes growth in the CNS. *Development* 129, 2087–2098.

Metin, C., Baudoin, J. P., Rakic, S., and Parnavelas, J. G. (2006). Cell and molecular mechanisms involved in the migration of cortical interneurons. *Eur. J. Neurosci.* 23, 894–900.

Nelson, W. J., and Nusse, R. (2004). Convergence of Wnt, beta-catenin, and cadherin pathways. *Science* 303, 1483–1487.

Noctor, S. C., Martinez-Cerdeno, V., Ivic, L., and Kriegstein, A. R. (2004). Cortical neurons arise in symmetric and asymmetric division zones and migrate through specific phases. *Nat. Neurosci.* 7, 136–144.

Nusse, R. (1999). WNT targets. Repression and activation. *Trends Genet.* 15, 1–3.

Owens, D. F., and Kriegstein, A. R. (2002). Is there more to GABA than synaptic inhibition? *Nat. Rev. Neurosci.* 3, 715–727.

Powell, A. W., Sassa, T., Wu, Y., Tessier-Lavigne, M., and Polleux, F. (2008). Topography of thalamic projections requires attractive and repulsive functions of Netrin-1 in the ventral telencephalon. *PLoS Biol.* 6, e116 doi:10.1371/journal.pbio.0060116.

Reiner, O. (2000). LIS1: let's interact sometimes (part 1). *Neuron* 28, 633–636.

Reiner, O., Cahana, A., Escamez, T., and Martinez, S. (2002). LIS1-no more no less. *Mol. Psychiatry* 7, 12–16.

Reiner, O., Carrozzo, R., Shen, Y., Wehnert, M., Faustinella, F., Dobyns, W. B., Caskey, C. T., and Ledbetter, D. H. (1993). Isolation of a Miller-Dieker lissencephaly gene containing G protein beta-subunit-like repeats. *Nature* 364, 717–721.

Schwarz-Romond, T., Merrifield, C., Nichols, B. J., and Bienz, M. (2005). The Wnt signalling effector dishevelled forms dynamic protein assemblies rather than stable associations with cytoplasmic vesicles. *J. Cell. Sci.* 118, 5269–5277.

Sheffield, P., Garrard, S., Caspi, M., Aoki, J., Inoue, K., Derewenda, U., Suter, B., Reiner, O., and Derewenda, Z. S. (2000). Homologues of the α- and β-subunits of mammalian brain platelet-activating factor acetylhydrolase Ib in the *Drosophila melanogaster* genome. *Proteins* 39, 1–8.

Shu, T., Ayala, R., Nguyen, M. D., Xie, Z., Gleeson, J. G., and Tsai, L. H. (2004). Ndel1 operates in a common pathway with LIS1 and cytoplasmic dynein to regulate cortical neuronal positioning. *Neuron* 44, 263–277.

Simcha, I., Shtutman, M., Salomon, D., Zhurinsky, J., Sadot, E., Geiger, B., and Ben-Ze'ev, A. (1998). Differential nuclear translocation and transactivation potential of beta-catenin and plakoglobin. *J. Cell Biol.* 141, 1433–1448.

Spitzer, N. C. (2006). Electrical activity in early neuronal development. *Nature* 444, 707–712.

Stafforini, D. M., McIntyre, T. M., Zimmerman, G. A., and Prescott, S. M. (2003). Platelet-activating factor, a pleiotrophic mediator of physiological and pathological processes. *Crit. Rev. Clin. Lab. Sci.* 40, 643–672.

Stanco, A., Szekeres, C., Patel, N., Rao, S., Campbell, K., Kreidberg, J. A., Polleux, F., and Anton, E. S. (2009). Netrin-1-alpha3beta1 integrin interactions regulate the migration of interneurons through the cortical marginal zone. *Proc. Natl. Acad. Sci. USA* 106, 7595–7600.

Stelzl, U., Worm, U., Lalowski, M., Haenig, C., Brembeck, F. H., Goehler, H., Stroedicke, M., Zenkner, M., Schoenherr, A., Koeppen, S., Timm, J., Mintzlaff, S., Abraham, C., Bock, N., Kietzmann, S., Goedde, A., Toksoz, E., Droege, A., Krobitsch, S., Korn, B., Birchmeier, W., Lehrach, H., and Wanker, E. E. (2005). A human protein-protein interaction network: a resource for annotating the proteome. *Cell* 122, 957–968.

Stumm, R. K., Zhou, C., Ara, T., Lazarini, F., Dubois-Dalcq, M., Nagasawa, T., Hollt, V., and Schulz, S. (2003). CXCR4 regulates interneuron migration in the developing neocortex. *J. Neurosci.* 23, 5123–5130.

Tamamaki, N., Yanagawa, Y., Tomioka, R., Miyazaki, J., Obata, K., and Kaneko, T. (2003). Green fluorescent protein expression and colocalization with calretinin, parvalbumin, and somatostatin in the GAD67-GFP knock-in mouse. *J. Comp. Neurol.* 467, 60–79.

Tanaka, D., Nakaya, Y., Yanagawa, Y., Obata, K., and Murakami, F. (2003). Multimodal tangential migration of neocortical GABAergic neurons independent of GPI-anchored proteins. *Development* 130, 5803–5813.

Tsai, J. W., Bremner, K. H., and Vallee, R. B. (2007). Dual subcellular roles for LIS1 and dynein in radial neuronal migration in live brain tissue. *Nat. Neurosci.* 10, 970–979.

Tsai, J. W., Chen, Y., Kriegstein, A. R., and Vallee, R. B. (2005). LIS1 RNA interference blocks neural stem cell division, morphogenesis, and motility at multiple stages. *J. Cell Biol.* 170, 935–945.

Wilson, N. H., and Key, B. (2006). Neogenin interacts with RGMa and netrin-1 to guide axons within the embryonic vertebrate forebrain. *Dev. Biol.* 296, 485–498.

Wonders, C. P., and Anderson, S. A. (2006). The origin and specification of cortical interneurons. *Nat. Rev. Neurosci.* 7, 687–696.

Wrobel, C. N., Mutch, C. A., Swaminathan, S., Taketo, M. M., and Chenn, A. (2007). Persistent expression of stabilized beta-catenin delays maturation of radial glial cells into intermediate progenitors. *Dev. Biol.* 309, 285–297.

Xu, Q., Wonders, C. P., and Anderson, S. A. (2005). Sonic hedgehog maintains the identity of cortical interneuron progenitors in the ventral telencephalon. *Development* 132, 4987–4998.

Yan, W., Assadi, A. H., Wynshaw-Boris, A., Eichele, G., Matzuk, M. M., and Clark, G. D. (2003). Previously uncharacterized roles of platelet-activating factor acetylhydrolase 1b complex in mouse spermatogenesis. *Proc. Natl. Acad. Sci. USA* 100, 7189–7194.

Yingling, J., Youn, Y. H., Darling, D., Toyo-Oka, K., Pramparo, T., Hirotsune, S., and Wynshaw-Boris, A. (2008). Neuroepithelial stem cell proliferation requires LIS1 for precise spindle orientation and symmetric division. *Cell* 132, 474–486.

Zechner, D., Fujita, Y., Hulsken, J., Muller, T., Walther, I., Taketo, M. M., Crenshaw, E. B., 3rd, Birchmeier, W., and Birchmeier, C. (2003). beta-Catenin signals regulate cell growth and the balance between progenitor cell expansion and differentiation in the nervous system. *Dev. Biol.* 258, 406–418.

Conflict of Interest Statement: The authors declare that the research was conducted in the absence of any commercial or financial relationships that could be construed as a potential conflict of interest.

Received: 28 February 2010; paper pending published: 10 March 2010; accepted: 10 May 2010; published online: 28 May 2010.

Citation: Livnat I, Finkelshtein D, Ghosh I, Arai H and Reiner O (2010) PAF-AH catalytic subunits modulate the Wnt pathway in developing GABAergic neurons. Front. Cell. Neurosci. ***4****:19. doi: 10.3389/fncel.2010.00019*

frontiers in
CELLULAR NEUROSCIENCE

ORIGINAL RESEARCH ARTICLE
published: 02 June 2010
doi: 10.3389/fncel.2010.00018

GABAergic synapse properties may explain genetic variation in hippocampal network oscillations in mice

Tim S. Heistek[1], A. Jaap Timmerman[1], Sabine Spijker[2], Arjen B. Brussaard[1] and Huibert D. Mansvelder[1]*

[1] *Department of Integrative Neurophysiology, Center for Neurogenomics and Cognitive Research, Neuroscience Campus Amsterdam, VU University, Amsterdam, Netherlands*

[2] *Department of Molecular and Cellular Neuroscience, Center for Neurogenomics and Cognitive Research, Neuroscience Campus Amsterdam, VU University, Amsterdam, Netherlands*

Edited by:
Yehezkel Ben-Ari, Institut National de la Santé et de la Recherche Médicale, France

Reviewed by:
Andreas Frick, Institut National de la Santé et de la Recherche Médicale, France
Igor Timofeev, Laval University, Canada

***Correspondence:**
Huibert D. Mansvelder, Department of Integrative Neurophysiology, Faculty of Earth and Life Sciences, De Boelelaan 1085, 1081 HV Amsterdam, Netherlands.
e-mail: huibert.mansvelder@cncr.vu.nl

Cognitive ability and the properties of brain oscillation are highly heritable in humans. Genetic variation underlying oscillatory activity might give rise to differences in cognition and behavior. How genetic diversity translates into altered properties of oscillations and synchronization of neuronal activity is unknown. To address this issue, we investigated cellular and synaptic mechanisms of hippocampal fast network oscillations in eight genetically distinct inbred mouse strains. The frequency of carbachol-induced oscillations differed substantially between mouse strains. Since GABAergic inhibition sets oscillation frequency, we studied the properties of inhibitory synaptic inputs (IPSCs) received by CA3 and CA1 pyramidal cells of three mouse strains that showed the highest, lowest and intermediate frequencies of oscillations. In CA3 pyramidal cells, the frequency of rhythmic IPSC input showed the same strain differences as the frequency of field oscillations. Furthermore, IPSC decay times in both CA1 and CA3 pyramidal cells were faster in mouse strains with higher oscillation frequencies than in mouse strains with lower oscillation frequency, suggesting that differences in $GABA_A$-receptor subunit composition exist between these strains. Indeed, gene expression of $GABA_A$-receptor β2 (Gabrb2) and β3 (Gabrb2) subunits was higher in mouse strains with faster decay kinetics compared with mouse strains with slower decay kinetics. Hippocampal pyramidal neurons in mouse strains with higher oscillation frequencies and faster decay kinetics fired action potential at higher frequencies. These data indicate that differences in genetic background may result in different $GABA_A$-receptor subunit expression, which affects the rhythm of pyramidal neuron firing and fast network activity through GABA synapse kinetics.

Keywords: fast network oscillations, GABA synapses, heritability, hippocampus, GABA receptor subunits, C57, Balbc, NOD

INTRODUCTION

Variation in cognitive abilities in humans can for a large part be explained by genetic variation. More than 85% of the variation in cognitive ability is of genetic origin (Posthuma et al., 2001a,b). Twin studies have shown that in humans properties of brain oscillations are also highly heritable (Posthuma et al., 2001b; Smit et al., 2005; Linkenkaer-Hansen et al., 2007). Brain oscillations are thought to be involved in cognition and different oscillation frequencies have been related to specific cognitive processes (Gray et al., 1989; Lopes da Silva, 1991; Llinas and Ribary, 1993). For instance, beta- and gamma-band oscillations are increased during working memory and selective attention tasks (Roelfsema et al., 1997; Tallon-Baudry et al., 1998, 2001; Fries et al., 2001; Womelsdorf et al., 2007). Findings in laboratory animals show that gamma-band oscillations in the hippocampus are most likely involved in memory encoding and retrieval (Lisman and Idiart, 1995; Montgomery and Buzsaki, 2007). Phase coupling of gamma oscillations between CA1 and CA3 increases during memory retrieval (Montgomery and Buzsaki, 2007), which occurs at different gamma frequencies than between CA1 and the enthorinal cortex (Colgin et al., 2009). In mice, hippocampal oscillations are affected by genetic background (Jansen et al., 2009). Genetic variation resulting in differences in brain oscillations may give rise to differences in cognition and intelligence in general. However, how genetic differences translate into differences in properties of oscillations and synchronization of neuronal activity is poorly understood.

To address this issue, we studied cellular and synaptic mechanisms underlying hippocampal fast network oscillations in acute brain slices of different mouse strains with known genetic differences. Muscarinic acetylcholine receptor (mAChR) activation in cortical and hippocampal networks acute brain slices induces synchronized activity and network oscillations. During these oscillations, synchronized activity of pyramidal neurons alternates with synchronized activity of inhibitory interneurons (Hajos et al., 2004; Mann et al., 2005; van Aerde et al., 2009). Cellular mechanisms underlying mAChR-induced synchronization depend on synaptic communication between neurons (Fisahn et al., 1998; van Aerde et al., 2008, 2009). Ordered pyramidal and interneuron cell firing and inhibitory synaptic feedback constitute the underlying mechanism underlying oscillating neuronal networks at beta/gamma

frequencies in all cortical areas (Fisahn et al., 1998; Hajos et al., 2004; Mann and Paulsen, 2005; Mann et al., 2005; Oren et al., 2006). Fast network oscillations in hippocampal slices, which resemble gamma frequency oscillations in hippocampus *in vivo* (Csicsvari et al., 2003; Mann et al., 2005), are generated within the CA3 region and depend on fast inhibitory transmission within the stratum pyramidale of CA3 (Mann et al., 2005). Inbred mouse strains show substantial differences in gene expression within the hippocampus (Fernandes et al., 2004; Hovatta et al., 2005) and show clear heritable differences in hippocampal oscillation properties (Jansen et al., 2009). To address the mechanisms underlying genetic variation in network oscillations, we studied CA3 pyramidal neuronal activity and the synaptic inputs they receive in eight different mouse strains during carbachol-induced fast network oscillations. We found that differences in oscillation frequency between mouse strains may be explained by differences in GABAergic synapse properties and $GABA_A$-receptor subunit expression.

MATERIALS AND METHODS

TISSUE PREPARATION

All experimental methods involving animals were approved by the animal welfare committee of our university, and in accordance with Dutch and European law. The eight inbred mouse strains (129S1SvImJ, A/J, Balb/cByJ (Balbc), C3H/HeJ, C57Bl/6J (C57), DBA/2J, FVB/NJ and NOD/LtJ (NOD); **Figure 1A**) were obtained from Jackson Laboratories[1]. All animals were between 13- and 17-days old. After decapitation without anesthesia, brains were quickly removed and stored in ice cold artificial cerebrospinal fluid (ACSF) containing 125 mM NaCl, 25 mM $NaHCO_3$, 3 mM KCl, 1.2 mM NaH_2PO_4, 1 mM $CaCl_2$, 3 mM $MgSO_4$, and 10 mM D(+)-glucose (carboxygenated with 5% CO_2/95% O_2). For RNA isolation, the ventral hippocampus was dissected on ice, and stored at −80°C until further use. For electrophysiology, horizontal slices (400-μm thick)) from the ventral hippocampus were cut using a microtome (Microm[2]). After preparation, slices were stored for at least 1 h in ACSF containing 2 mM $CaCl_2$ and 2 mM $MgSO_4$. To record field potentials, slices were placed on planar eight by eight multi-electrode arrays with 150 μm spacing (MED-P5155, Panasonic[3]) or 200 μm (Multichannel Systems[4]), which were coated with polyethylene (Sigma). Slices were left to properly attach to the electrodes for at least 1 h in a chamber with humidified carbogen gas before they were placed in the recording unit.

ELECTROPHYSIOLOGY

Local field potentials were measured in four slices simultaneous with four recording units at the same time using the multichannel system or in combination with patch-clamp recordings in the MED64 system. During recording slices were perfused with ACSF at a flow rate between 4 and 5 ml/min and were kept at 30°C. Carbamoylcholine chloride (Carbachol, Sigma[5]) was perfused for at least 45 min or added after the mounting of the slices onto the multi-electrode grids. Spontaneous field potentials from all 64 recording electrodes were acquired simultaneously at 20 kHz (MED64 system) or with 60 electrodes at 1 kHz (multichannels systems). In addition to fast network oscillations we also observed low frequency network bursts in some slices of Balbc mice (9 out of 19) which occurred at a frequency of 0.54 ± 0.11 Hz.

Pyramidal cells in CA3 and CA1 neurons were recorded in whole-cell mode using a Multiclamp 700B amplifier (molecular devices[6]). Borosilicate glass (Harvard Apparatus[7]) electrodes with tip resistances of 2–5 MOhm were filled with intracellular solution containing 140 mM K-gluconate, 1 mM KCl, 10 mM HEPES, 4 mM K-phosphocreatine, 4 mM ATP-Mg, and 0.4 mM GTP (pH adjusted to 7.2 with KOH). To ensure temporal alignment between the multi-electrode and single-cell electrophysiological signals, the current or voltage signals from the patch-clamp amplifiers were recorded on one channel of the MED64 amplifier, using an interface (Panasonic). IPSCs were recorded at +20-mV holding potential, while EPSCs were recorded at −70 mV. Internal chloride concentrations were such that at these potentials IPSCs and EPSCs would have a different polarity. As the holding potential might influence the decay time kinetics (Collingridge et al., 1984) mIPSCs were recorded at −70 mV in presence of 25 μM carbachol, 10 μM 6,7-dinitroquinoxaline-2,3(1H, 4H)-dione (DNQX) and 20 μM DL-AP5 and 1 μM TTX and with use of intracellular solution with high chloride concentrations containing: 70 mM Cs-gluconate, 70 mM CsCl, 10 mM HEPES, 5 mM ATP-Mg, and 0.5 mM GTP and 5 mM EGTA (pH adjusted to 7.2 with CsOH). Zolpidem was obtained from Duchefa[8].

RNA ISOLATION, cDNA SYNTHESIS AND REAL-TIME QUANTITATIVE PCR (qPCR)

After isolation of total RNA (Trizol, Invitrogen, San Diego, USA) according to standard procedures, a DNase-I treatment (2 U, Invitrogen Carlsbad, CA, USA) to remove traces of genomic DNA was performed. The amount and purity of RNA was measured using a spectrophotometer (NanoDrop ND–1000 UV-Vis Spectrophotometer, Nanodrop Technologies[9]), and the integrity was analyzed by gel electrophoresis.

For mouse genes encoding $GABA_A$-receptor subunits, transcript-specific primers (**Table 1**) were designed based on Genbank sequence entries using Primer Express software (PE Biosystems[10]; manufacturer's settings). Only primers were taken of which endpoint PCRs showed the amplicon and no primer-dimers as determined by generation of dissociation curves, and which had high amplification efficiencies.

From each tissue sample (n = 4 per strain), random primed (hexamers; Eurogentec[11]) cDNA (1 μg total RNA) was made with reverse transcriptase (200 U; Promega[12]; manufacturer's protocol). cDNA Aliquots were stored at −80°C, because repeated freeze-thaw

[1]www.jax.com
[2]www.microm-online.com
[3]www.med64.com
[4]www.multichannelsystems.com
[5]www.sigmaaldrich.com
[6]www.moleculardevices.com
[7]www.harvardapparatus.com
[8]www.duchefa.com
[9]www.nanodrop.com
[10]www.appliedbiosystems.com
[11]www.eurogentec.com
[12]www.promega.com

Table 1 | Gene specific primers to different $GABA_A$-receptor subunits and housekeeping genes used for real-time qPCR.

Gene	Forward primer 5′–3′	Reverse primer 5′–3′
Gabra1	GTCCTCTGCACCGAGAATTGC	TCAAATTCTTTAGGACAGAGGCAGTA
Gabra2	TGGTTTTTGCTTTGTACAGTCTGACT	GCAAATGCAGGTCTCCTTTAGAG
Gabra3	ATTTCCCGCATCATCTTCCC	TGATAGCTGATTCCCGGTTCAC
Gabra4	GCTCACTTAGCTTCCAGTCCAAA	GATGAAAGACCTCTGGCTGCA
Gabra5	AAAAGACATACAACAGCA	GAAAGTGCCAAACAAGATGGG
Gabra6	TGCTCTTACCAGCCACTGGG	TGCAAAAGCTACTGGGAAGAGAA
Gabrb1	CCTCGCAGCTCAAAGTGAAGA	GAACATTCGGGACCACTTGTCT
Gabrb2	CCCACCTCCGGGAAACTC	GAAGACAAAGCACCCCATTAGG
Gabrb3	AAAGGATCGAGCTCCCACAGT	TGTGGCGAAGACAACATTCC
Gabrg1	TGCTTCGATAGACTGCAGAACTG	GAGTCAATTTTTGCAATGCGTATG
Gabrg2	TCCAAAAAGGCTGATGCTCACT	ACTCGACCATCATTCCAAATTCTC
Gabrg3	GAGGCCGCATCCACATTG	CAGGAAGGATGTCGGGAAGA
Actbr	GCTCCTCCTGAGCGCAAG	CATCTGCTGGAAGGTGGACA
Hptr	ATGGGAGGCCATCACATTGT	ATGTAATCCAGCAGGTCAGCAA
Gapdh	TGCACCACCAACTGCTTAGC	GGCATGGACTGTGGTCATGA

cycles affect measured cycle of threshold (Ct) values. For qPCR measurements (ABI PRISM 7900, Applied Biosystems), PCR conditions (50°C, 2 min; 95°C, 10 min; 40 cycles: 95°C, 10 s, 60°C, 1 min; dissociation curve in 10 min) and SYBR green reagents (Applied Biosystems) were used in a reaction volume of 10 µl using transcript-specific primers (300 nM) on cDNA (~5 ng RNA equivalent).

The obtained Cycle of threshold value for every gene (Ct_x) was used to calculate the relative level of gene expression by normalization to the geometric means of replicated reference controls (Ct_{HK}; Gapdh, Hprt). GAPDH and HPRT were shown as stable expressing genes across strains (Loos et al., 2009). For all graphical representation and statistical calculations, $\log_2$-based values were used for amount of normalized transcript, $C - (Ct_x - Ct_{HK})$ ($C = 5$).

DATA ANALYSIS

Synaptic events were detected using Mini Analysis Program[13]. All other analysis was done using custom made scripts in igorPro 6.04 (Wavematrics[14]) and matlab R2006B (The Mathworks[15]). Data was down sampled to 200 Hz – 2 kHz for analysis. Frequency and power of oscillations were calculated by fitting a Gaussian function to the Fourier transformed data. The average power and frequency of the oscillations were calculated separately in the different layers of the dentate gyrus, CA3 region and CA1 region by taking the average of all electrodes in that region. Synaptic events were selected by a threshold for amplitude and area which were equal across strains. IPSC τ decay times were calculated by fitting an exponential function to the individual IPSCs and only single synaptic events were used for fitting. The τ decay, amplitudes and interval times of a single neuron were put in a histogram and fitted with a lognormal for τ decay and amplitudes, or Gaussian distribution for interval times. The average IPSC/EPSC frequency was calculated as 1/average interval time. Phase coupling factor was calculated by wavelet transforming the local fied potential (LFP) of the electrode closest to the site of the whole-cell recording to determine the phase of the oscillations. Statistical analysis used either the Student's *t* test (paired or unpaired) or an ANOVA with Student Newman Keuls *post hoc* test, as appropriate. For circular statistics we used Hotelling's test for paired comparisons and the Watson Williams test. The Rayleigh test was used to test whether the events showed significant phase-locking to the oscillation. Data are represented as average ± SEM.

RESULTS

Recently, we reported that in eight genetically different inbred mouse strains variation in properties of fast hippocampal network oscillations can be partly explained by genetic differences (Jansen et al., 2009). To test whether these genetic differences are reflected in properties of excitatory and inhibitory synapses in CA3 and CA1, which underlie fast network oscillations in these areas (Whittington et al., 1995; Mann et al., 2005) and information transfer between these areas, we recorded synaptic activity in CA1 and CA3 pyramidal neurons during fast network oscillations. Application of the mAChR agonist carbachol (25 µM) to horizontal slices of the hippocampus induced fast network oscillations (**Figure 1**). The frequency ranged from 13.0 to 30.2 Hz in different mouse strains ($p < 0.05$, ANOVA, **Figures 1A–C**) and *post hoc* analysis revealed a difference in frequency with maximal oscillation power (peak frequency) between Balbc (17.5 ± 0.8 Hz, $n = 13$) and NOD mice (21.6 ± 1.2 Hz, $n = 10$) ($p < 0.05$ **Figure 1E**). As was reported by Jansen et al. (2009), the power of oscillations in specific frequency bands differed between mouse strains (not shown). However, the power at the frequency that showed maximal power (peak power) in CA3 in each mouse strain was not different for the eight inbred strains ($p = 0.43$, ANOVA, **Figure 1E**).

Fast network oscillations in hippocampus are driven by rhythmic hyperpolarizing GABAergic inputs to CA3 pyramidal cells (Mann et al., 2005). To test whether properties of phasic GABAergic inputs to pyramidal cells can affect the frequency of oscillations, we recorded IPSCs in CA3 pyramidal neurons and slowed GABAergic

[13]www.synaptosoft.com

[14]www.wavematrics.com

[15]www.mathworks.com

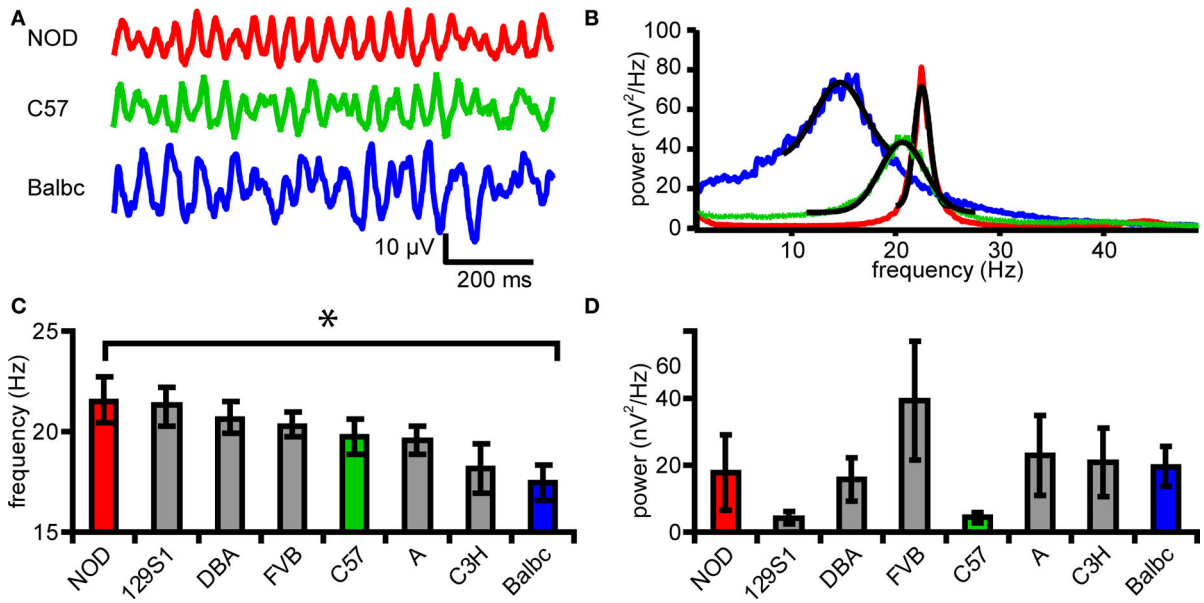

FIGURE 1 | Eight inbred mouse strains differ in frequency of fast network oscilliliations. (A) Example traces of field potential in CA3stratum radiatum from 3 different mouse strains (NOD, C57, Balbc). **(B)** Power spectral density plot corresponding to the traces shown in B. Black lines show the Gaussian fits. **(C)** Peak frequency of oscillations in 8 different mouse strains. **(D)** Peak power of oscillations in 8 different mouse strains. Error bars show SEM.

synaptic kinetics by applying the $GABA_A$-receptor modulator zolpidem during ongoing oscillations (**Figure 2**). Zolpidem (1 μM) reduced the frequency of fast network oscillations in all mouse strains tested (to 82.0 ± 1.8% of control; **Figures 2A–D**). It also strongly increased the power of oscillations (to 234 ± 35%) ($p < 0.05$, $n = 9$, **Figures 2A–D**). These changes in frequency and power were similar in the whole hippocampus (**Figure 2C**). At the synaptic level, zolpidem altered the properties of phasic GABAergic inhibition in NOD and Balbc mice (**Figures 2E–H**; zolpidem data grouped for both strains). Zolpidem decreased the IPSC frequency (to 76 ± 2.5% of control), and increased the decay time constant (178 ± 10%) and IPSC amplitude (175 ± 20%) ($p < 0.05$, $n = 9$, **Figures 2E–H**). We also observed an increased phase-locking of IPSCs to the field potential (163 ± 29%, **Figures 2F,G**) and a shift in the average IPSC phase relative to the field from 1.04 ± 0.17 radials to 0.17 ± 0.30 radials ($p < 0.05$, **Figures 2F,H**). Thus, decreasing IPSC frequency and increasing IPSC decay time constant with zolpidem decreased the frequency of fast network oscillations. The increase in IPSC amplitude and the increase in the power of oscillations may be explained by more precise timing of IPSC inputs in the presence of zolpidem, reflected by an enhanced IPSC phase-locking (**Figure 2G**).

Since GABAergic synaptic properties and IPSC kinetics can strongly affect the frequency of fast network oscillations, we investigated whether differences exist in GABAergic synaptic transmission received by CA3 pyramidal neurons of NOD and Balbc mice. In whole-cell recordings from CA3 pyramidal neurons we monitored both IPSCs (at +20 mV) and EPSC (at −70 mV) during fast network oscillations. The frequency of IPSCs received by CA3 pyramidal cells was significantly higher in NOD mice (24.6 ± 1.0 Hz, $n = 7$) than in Balbc mice (20.6 ± 1.1 Hz, $n = 6$), while in C57 mice pyramidal neurons received IPSCs at intermediate frequencies (21.7 ± 0.9 Hz, $n = 8$) ($p < 0.05$, **Figures 3A–C**). In each mouse strain, the IPSC frequency received by CA3 pyramidal neurons was very similar to the frequency of fast network oscillations in that particular strain (**Figure 3E**). In addition to higher frequencies of IPSCs, GABAergic inputs to CA3 pyramidal neurons in NOD mice also had a significantly faster τ decay time constant (8.3 ± 0.7 ms) compared to Balbc mice (10.7 ± 0.4 ms) ($p < 0.05$, **Figures 3D,E**), while IPSCs in C57 mice showed intermediate decay time constants (9.0 ± 0.7 ms). Just as IPSC frequency, IPSC kinetics paralleled the frequency of oscillations in different mouse strains: NOD mice showed faster network oscillations and faster IPSC decay kinetics, whereas Balbc mice showed slower network oscillations and slower IPSC decay kinetics. IPSC amplitude, phase-locking and IPSC timing relative to the field were not different between different mouse strains ($p > 0.05$, **Figures 3F–I**), in line with the absence of difference between power of fast network oscillations between NOD and Balbc mice (**Figure 1E**). These data suggest that differences in kinetics of GABAergic inhibition received by CA3 pyramidal neurons may explain the differences in fast network oscillations in genetically distinct mouse strains.

We next tested whether differences exist in excitatory glutamatergic transmission received by CA3 pyramidal neurons in NOD and Balbc mice. Spontaneous EPSCs recorded in CA3 pyramidal cells of NOD mice arrived at a similar frequency as in Balbc mice and were timed similarly related to the network oscillations (**Figures 4A–C,E,F**). However, the amplitude of excitatory inputs were larger in Balbc mice (57.5 ± 6.5pA, $n = 6$) than in NOD mice (39.1 ± 2.7pA, $n = 7$; $p < 0.05$, **Figures 4D,E**). Thus, lower frequencies of phasic GABAergic inhibition and fast network oscillations in Balbc mice are not reflected by an altered frequency of excitatory transmission, but by increased amplitudes of EPSCs.

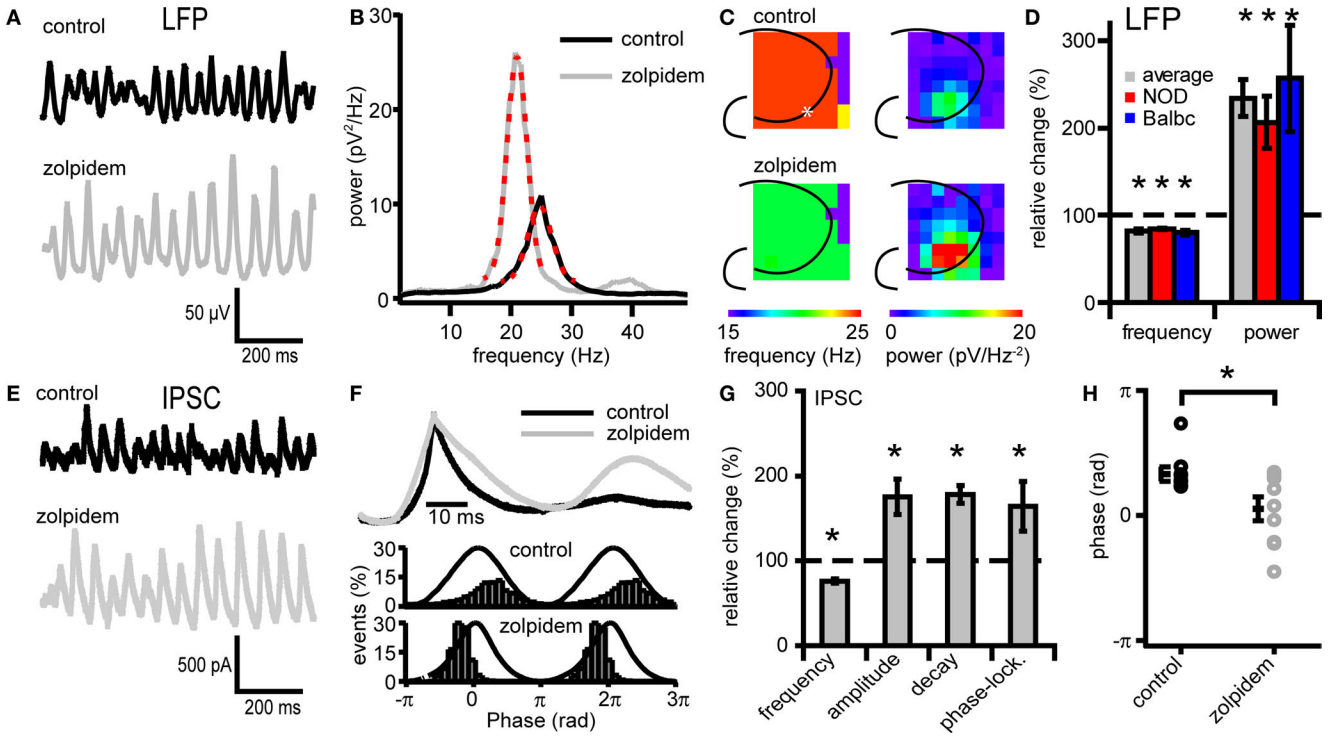

FIGURE 2 | Zolpidem affects both Fast network oscillations and IPSCs on CA3 pyramidal cells. (A) Example traces of oscillations in before and after zolpidem (1 µM) application from a NOD mouse. **(B)** Power spectral density plot corresponding to the traces in **(A)**. Red dotted lines show Gaussian fit. **(C)** Left, frequency of fast network oscillations at control and zolpidem at different electrodes. Right, power of fast network oscillations at control and different concentrations of zolpidem in wild-type mice at different electrodes. The asterix marks the recording site of the LFP **(A)** and IPSCs **(D)**. **(D)** Changes in peak frequency and power by zolpidem. Data are normalized to control data. Zolpidem decreases the frequency and increases the power in both NOD and Balbc mice ($n = 4$ and $n = 5$ respectively, $p < 0.05$). **(E)** Example traces of IPSCs in CA3 pyramidal cells before and after zolpidem application from a NOD mouse. Traces correspond to the field potential traces in **(A)**. **(F)** Average IPSC normalized to peak values from one cell from a NOD mouse. Zolpidem increases the duration of the IPSC. **(G)** Zolpdem effects on IPSC frequency, τ decay times, amplitude and phase-locking relative to the field oscillation ($n = 4$ and $n = 5$ respectively, $p < 0.05$). **(H)** Average phase of IPSCs in control and zolpidem. Zolpidem shifts the occurrence of IPSCs relative to the field ($p < 0.05$). All data are normalized to control data.

Carbachol-induced fast network oscillations in the CA1 area of the hippocampus are driven by rhythmic activity of CA3 circuits (Fisahn et al., 1998; Mann et al., 2005). Physically dissociating CA1 from CA3 in hippocampal slices silences carbachol-induced oscillations in CA1, but not in CA3 (Fisahn et al., 1998). Within a mouse strain, carbachol-induced fast network oscillations in CA1 had the same frequency as oscillations in CA3. Between mouse strains, oscillation frequency in CA1 showed similar differences as was the case for CA3 (NOD: 19.7 ± 0.5 Hz; Balbc: 16.9 ± 0.6 Hz, $p < 0.05$, data not shown). To test whether spontaneous GABAergic inhibition received by CA1 pyramidal cells during ongoing oscillations showed similar differences between NOD and Balbc mice as inhibition received by CA3 pyramidal cells, we recorded IPSCs in CA1 pyramidal neurons. The IPSC inputs to CA1 pyramidal cells were less timed than in CA3 and showed lower phase-locking r values ($p < 0.05$, **Figures 3G,H, and 5D**). Although the IPSC decay kinetics were faster in CA1 compared with CA3 pyramidal cells, we observed a similar difference in decay time constant between NOD (6.4 ± 0.3 ms, $n = 11$) and Balbc (8.8 ± 0.6pA, $n = 7$) ($p < 0.05$, **Figures 5A,B**). We observed no differences in IPSC frequency between NOD and Balbc ($p > 0.05$, **Figure 5C**), neither did we find differences in IPSC amplitude, phase-locking or phase (**Figure 5D,** average data not shown).

Altered decay kinetics of GABAergic synaptic activity most likely results from differences in $GABA_A$-receptor subunit expression in GABAergic synapses (Brussaard et al., 1997; Brussaard and Herbison, 2000; Bosman et al., 2005). To test whether differences in $GABA_A$-receptor subunits exist in hippocampus of NOD and Balbc mice, we compared mRNA levels of different $GABA_A$-receptor subunits in hippocampus. We observed no differences in expression of α or γ subunits, however there was a significant higher expression of the β2 and β3 subunits in NOD mice compared with Balbc mice ($p = 0.008$ and $p = 0.020$, both $n = 4$, **Figure 6A**), suggesting that GABAergic synapses in NOD mice may have a different molecular composition or stoichiometry of subunits.

To test whether differences in $GABA_A$-receptor subunit expression in hippocampus of NOD and Balbc mice was reflected in altered kinetics of single GABAergic synapses, we recorded miniature IPSCs (mIPSCs) from CA3 pyramidal neurons while preventing action potential firing by blocking sodium channels with TTX. In the presence of Carbachol, decay time constants of mIPSCs in NOD mice were faster than in Balbc mice (NOD: 6.8 ± 0.3 ms, $n = 5$; Balbc: 7.8 ± 0.2 ms, $n = 8$; $p < 0.05$, **Figures 6B,C**). The frequency of mIPSCs did not differ between the mouse strains (**Figure 6D**). IPSCs from CA1 pyramidal cells showed a similar difference in decay time constants (data not shown). These data

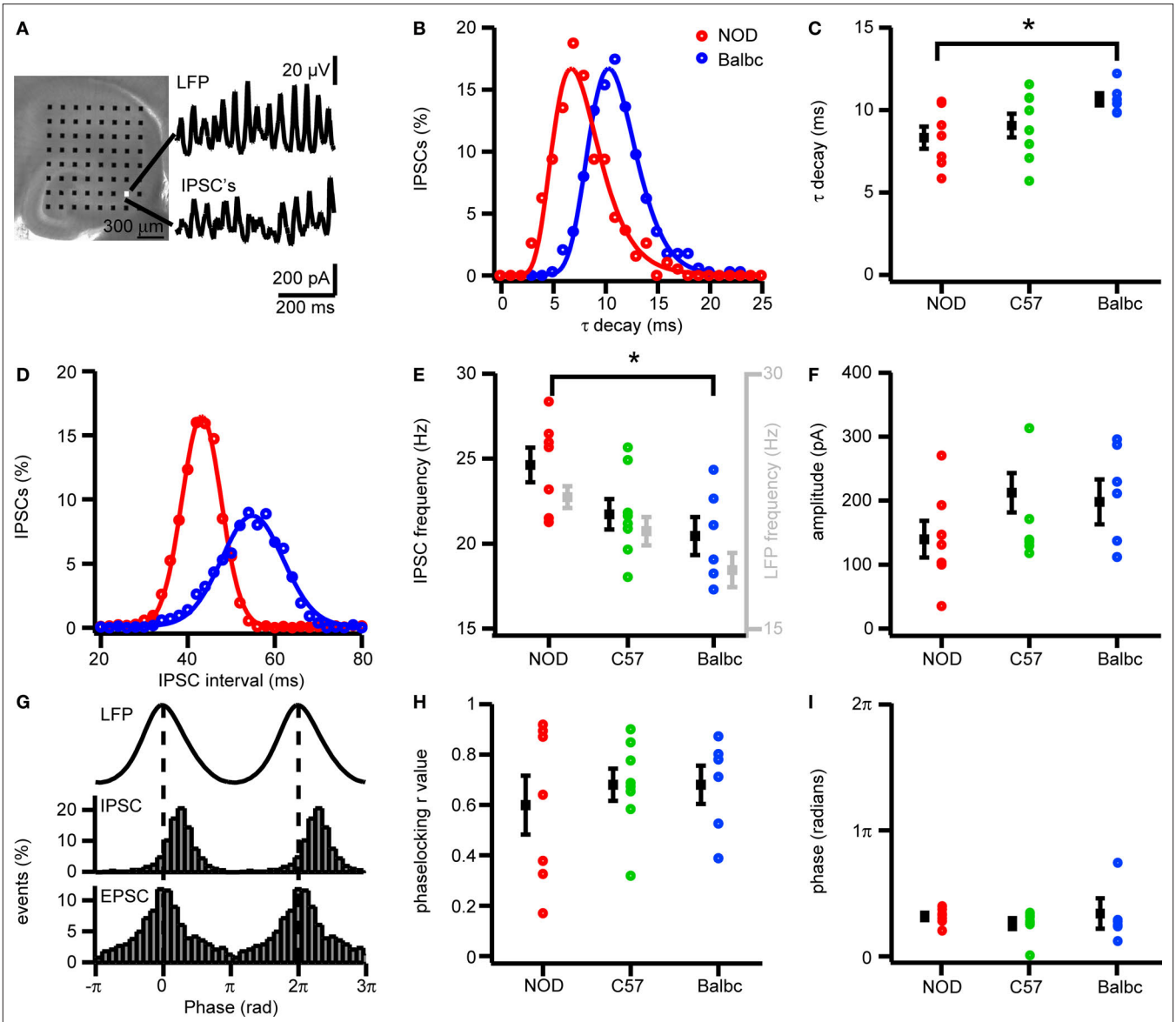

FIGURE 3 | IPSCs in CA3 pyramidal cells of NOD and Balbc mice differ in IPSC frequency and τ decay times. (A) Hippocampal slice placed on a 64 electrode grid and example traces of local field potential and corresponding IPSCs in a CA3 pyramidal cell from an NOD mouse. **(B)** Histogram of decay time constants of IPSCs from NOD (red) and Balbc (blue) mice. Histograms are fitted with lognormal functions. **(C)** Decay time constants of NOD ($n = 7$), C57 ($n = 8$) and Balbc ($n = 6$) mice. NOD mice have faster decay time constants than Balbc mice ($p < 0.05$). Average values are shown in black. **(D)** Histogram of IPSC interval times from cells of NOD and Balbc mice. Histograms are fitted with a Gaussian function. The average IPSC frequency is calculated as 1/average interval time. **(E)** IPSC frequencies of 3 different mouse lines. Average values are shown in black, average frequency of field oscillations are shown in gray. NOD mice have higher IPSC and field potential frequencies than Balbc mice ($p < 0.05$). **(F)** IPSC Amplitudes in 3 different mouse strains. Amplitudes were calculated by fitting a log normal function to the amplitude distribution. **(G)** (top) Average waveform of the field oscillation next to the recording site of the CA3 pyramidal cell. (middle) IPSC event probability histogram at different phases of the oscilation. (bottom) EPSC event probability histogram at different phases of the oscilation from a Balbc mouse. **(H)** IPSC – field potential phase-locking r values for 3 different mouse strains. **(I)** Average phase of IPSCs. Error bars show SEM.

show that GABAergic synapses on hippocampal pyramidal neurons show different kinetics that most likely result from differences in $GABA_A$-receptor subunit expression. These differences in subunit expression may explain the higher frequency of fast network oscillations in hippocampus of NOD mice compared with Balbc mice.

The pyramidal cell-interneuron feedback model for fast network oscillations predicts that the spike timing and spiking probability of pyramidal cells depends on the decay time of inhibitory inputs (Traub et al., 2000). Since decay times of IPSCs differed between NOD and Balbc mice, we tested whether hippocampal pyramidal cells showed differences in action potential firing during fast network oscillations in these mouse strains. In cell-attached recordings during carbachol-induced oscillations, the AP firing frequency of CA3 pyramidal cells was significantly higher in NOD (6.1 ± 1.0 Hz) compared to Balbc mice (3.7 ± 0.6 Hz, $p < 0.05$, **Figures 7A,B**). All CA3 cells showed significant phase-locking to the field oscillations

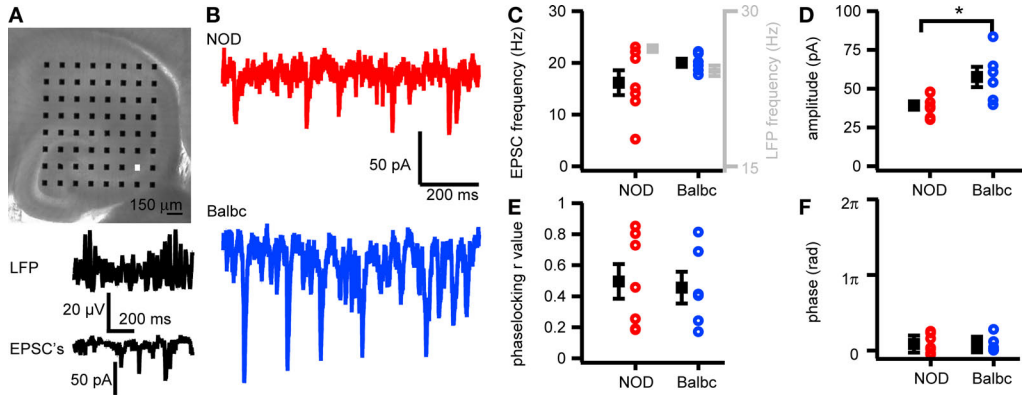

FIGURE 4 | EPSCs in CA3 pyramidal cells in NOD and Balbc mice differ in amplitude. (A) Hippocampal slice placed on a 64 electrode grid and example traces of local field potential and corresponding EPSCs in a CA3 pyramidal cell from a NOD mouse recorded at the in the white colored electrode in the picture. **(B)** Example traces of EPSCs in NOD and Balbc mice. **(C)** EPSC frequency in NOD ($n = 7$) and Balbc ($n = 6$) mice. **(D)** Average EPSC amplitude is higher in Balbc mice compared to NOD mice ($p < 0.05$). **(E)** IPSC – field potential phase-locking r values for NOD and Balbc mice. **(F)** Average phase of IPSCs. Average values + SEM are shown in black.

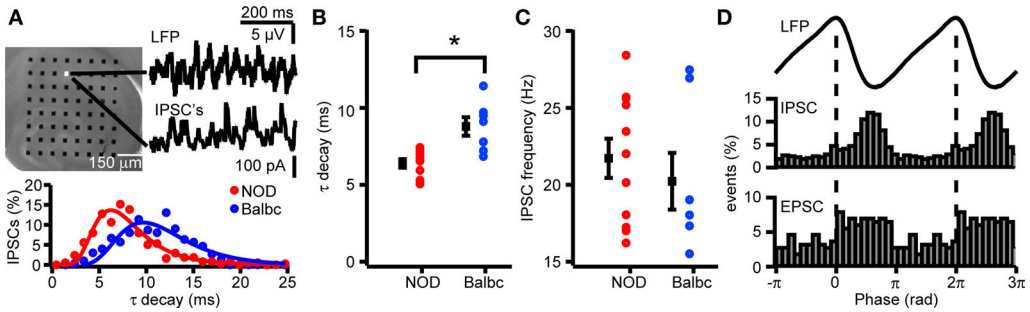

FIGURE 5 | IPSCs in CA1 pyramidal cells of NOD and Balb mice differ in τ decay times. (A) Hippocampal slice (top) placed on a 64 electrode grid and example traces of local field potential and corresponding IPSCs in a CA1 pyramidal cell from an NOD mouse. Histogram (bottom) of decay time constants of IPSCs from NOD and Balbc mice. Histograms are fitted with lognormal functions. **(B)** Decay time constants of NOD ($n = 11$) and Balbc ($n = 7$) mice. NOD mice have faster decay time constants than Balbc mice ($p < 0.05$). **(C)** IPSC frequencies of NOD and Balbc mice. **(D)** (top) Average waveform of the field oscillation next to the recording site of the CA1 pyramidal cell. (middle) IPSC event probability histogram at different phases of the oscilation. (bottom) EPSC event probability histogram at different phases of the oscilation from an NOD mouse. Average values + SEM are shown in black.

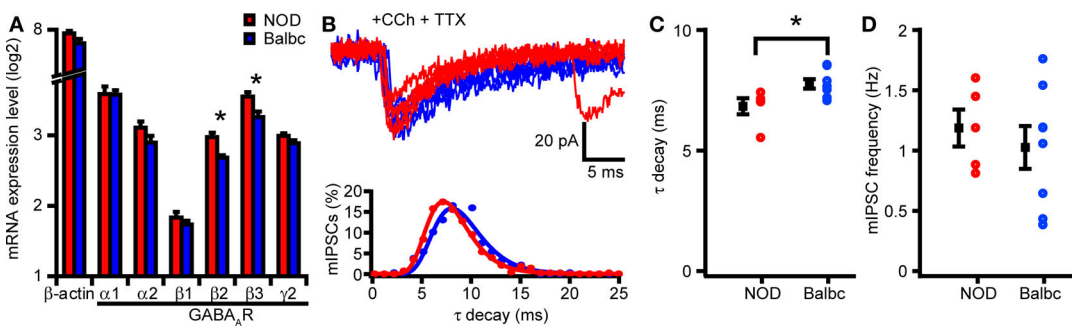

FIGURE 6 | NOD and Balbc mice strains differ in mRNA expression of GABA$_A$-receptor subunits β2 and β3 and mIPSC kinetics. (A) mRNA expression levels of β actin (Actb) and different GABA$_A$-receptor subunits in NOD and Balbc mice in the hippocampus. There is a significant difference in mRNA expression of the GABA$_A$-receptor subunits β2 (Gabrb2) and β3 (Gabrb3) between NOD and Balbc mice (both $n = 4$, $p < 0.05$). **(B)** Example traces of mIPSCs from CA3 pyramidal cells from NOD and Balbc mice (top) and histogram (bottom) of decay time constants of IPSCs from NOD and Balbc mice. Histograms are fitted with lognormal functions. **(C)** Decay time constants of NOD ($n = 5$) and Balbc ($n = 8$) mice. NOD mice have faster decay time constants then Balbc mice ($p < 0.05$). **(D)** Average frequencies of mIPSCs of NOD and Balbc mice. Average values + SEM are shown in black.

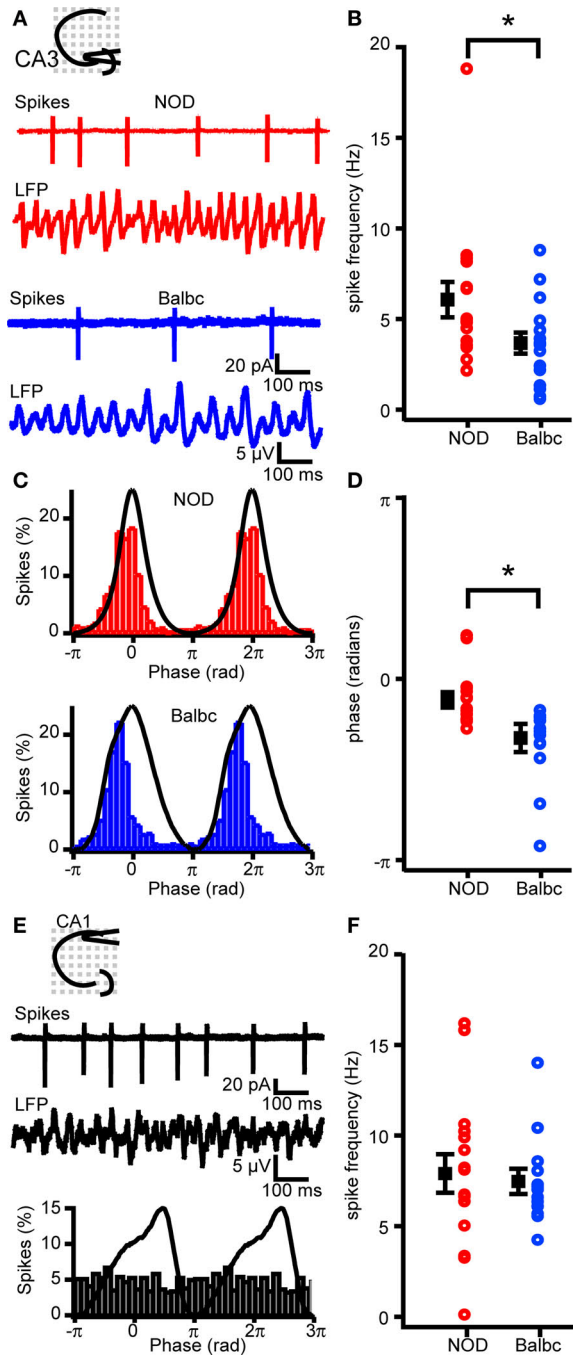

FIGURE 7 | Spike timing and frequency differs between NOD and Balbc mice. (A) Example traces of spikes recorded from CA3 pyramidal cells in cell-attached mode and field potential in NOD and Balbc mice. **(B)** Average firing frequency of CA3 pyramidal cells in NOD ($n = 16$) is higher than in Balbc ($n = 16$, $p < 0.05$) mice. **(C)** Average waveform of the field oscillation spike probability histogram at different phases of the oscilation from a cell from a NOD (top) and a Balbc (bottom) mouse. **(D)** I. Average phase of spikes. Spikes in CA3 pyramidal cells from Balbc mice occur at a earlier phase than in NOD mice ($p < 0.05$). **(E)** Example traces of spikes recorded from CA1 pyramidal cells from a Balbc mouse in cell-attached mode and field potential (top) and average spike probability histogram at different phases of the oscillation (bottom). **(F)** Average firing frequency of CA1 pyramidal cells in NOD and Balbc mice. Average values + SEM are shown in black.

(**Figure 7C**) in both mouse strains. However, the timing of spiking occurred around the peak of the oscillation in pyramidal neurons of NOD mice ($-0.05 \pm 0.02\pi$), while in Balbc mice most spikes occurred before the peak ($-0.16 \pm 0.04\pi$, $p < 0.05$, **Figures 7C,D**). Unlike CA3 pyramidal cells only 4 out of 16 CA1 pyramidal cells in NOD mice and 2 out of 13 CA1 pyramidal cells in Balbc mice fired phase-locked to the oscillations in CA1 (**Figure 7E**). Furthermore, there was no difference in firing frequency between NOD and Balbc mice in CA1 pyramidal cells (**Figure 7F**). These data indicate that the decay kinetics of GABAergic synapses may affect the timing and frequency of CA3 pyramidal cell firing as well as the frequency of fast network oscillations.

DISCUSSION

Brain oscillations are thought to be involved in cognition (Gray et al., 1989; Lopes da Silva, 1991; Llinas and Ribary, 1993), and properties of brain oscillations are also highly heritable (Deary et al., 2010). Little is known about the mechanisms by which genetic variation affects synchronized neuronal activity. In this study, we investigated what mechanisms may give rise to differences in fast network oscillations in hippocampus of genetically distinct inbred mouse strains. Our main findings are that: (1) Genetically distinct mouse lines show differences in the frequency of fast network oscillations that are paralleled by similar differences in the frequency of inhibitory inputs received by CA3 pyramidal neurons. (2) Differences in frequency of oscillations are also paralleled by differences in GABAergic synapse decay kinetics in CA3 and CA1 pyramidal cells. (3) In mouse strains with the highest frequency of oscillations and fastest GABA synapse kinetics, there is more gene expression of $GABA_A$-receptor β2 and β3 subunit mRNA. (4) In NOD mice, which show the fastest field oscillations, CA3 pyramidal cells fire at a higher frequency and at a later phase of the field oscillations than in Balbc mice. Our findings suggest that differences in genetic background result in different $GABA_A$-receptor subunit expression. This may affect GABA synapse kinetics and thereby action potential firing of CA3 pyramidal cells and the frequency of fast network oscillations.

GABAergic inhibition is critical for fast network oscillations, both in hippocampus and neocortex (Whittington et al., 1995; Fisahn et al., 1998; Traub et al., 2000; Mann et al., 2005; Atallah and Scanziani, 2009; van Aerde et al., 2009). Recurrent feedback loops between pyramidal cells and inhibitory interneurons underlie cholinergically-induced gamma oscillations (Fisahn et al., 1998; Traub et al., 2000; Mann et al., 2005). In the CA3 region of the hippocampus, peri-somatic inhibition of CA3 pyramidal neurons appears to dictate the time window during which these neurons fire action potentials (Hajos et al., 2004; Mann et al., 2005). Rapid adjustments in inhibition can instantaneously modulate oscillation frequency (Atallah and Scanziani, 2009). We find that the frequency of inhibitory inputs received by CA3 pyramidal neurons is similar to the frequency of field oscillations. In addition, in genetically different mouse strains the inhibitory input frequency differs to a similar extent as the field oscillations. Therefore, one may predict that the window during which the CA3 pyramidal neuron can escape inhibition and fire an action potential may be shorter in NOD mice due to higher IPSC frequencies.

However, this appears not be the case, since mouse strains that showed higher IPSC frequencies, also showed faster IPSC decay kinetics. In line with other studies (Fisahn et al., 1998; Cope et al., 2005), we found that the modulation of IPSC decay kinetics directly affects the frequency of oscillations. Decay kinetics of peri-somatic inhibition in pyramidal neurons most likely also determines the time window during which the cell can fire action potentials. In cells that receive IPSCs with faster decay kinetics, the episode of inhibition during which the threshold for spiking is elevated will most likely be shorter. Thereby, the combination of IPSCs that arrive more frequent but with faster decay kinetics entrains action potential firing of CA3 pyramidal neurons at higher frequencies. Thus, faster GABAergic synapses may give rise to faster recurrent feedback loops between pyramidal cells and interneurons. Thereby, NOD mice may experience faster field oscillations than Balbc mice. Allosteric enhancement of GABA decay kinetics not only reduced the frequency, but also increased the power of oscillations. In addition to decay times of IPSCs, zolpidem also affected IPSC amplitudes. Since hippocampal field potential oscillations are a reflection of inhibitory synaptic potentials (Oren et al., 2010), this may explain the increase in oscillation power caused by zolpidem. Since we did not observe a different in IPSC amplitude between the mouse strains, this may explain the absence of a difference in oscillation peak power between mouse strains.

Both inhibitory and excitatory synaptic transmission in CA3 are required for rhythm generation. It was shown recently that excitation and inhibition fluctuate in balance during kainate-induced oscillations (Atallah and Scanziani, 2009). However, in carbachol-induced oscillations the phase-locking of excitatory input was much smaller then the phase-locking of inhibitory input, which is in agreement with earlier studies showing that pyramidal cells receive phase-locked inhibition while interneurons receive phase locked excitation during carbachol-induced oscillations (Oren et al., 2006). The amplitude of EPSCs was larger in the mouse strain that showed the slowest oscillation frequency, Balbc. It is unclear what the underlying cause for larger amplitude EPSCs in these mice is. It was recently described that field oscillations are predominantly shaped by inhibitory inputs received by CA3 pyramidal cells (Oren et al., 2010). Therefore, the difference in EPSC amplitude between mouse strains was most likely not reflected in the frequency of field oscillations.

$GABA_A$-receptor subunit distribution in hippocampal synapses has been described to some extend in the CA1 region (Fritschy and Brunig, 2003), however receptor subunit distribution in perisomatic inhibitory synapses in CA3 is not known. We found that NOD mice showed faster IPSC kinetics and had higher mRNA levels of both β2 as well as β3 subunits. $GABA_A$ α and β subunits affect decay time kinetics ((Brussaard et al., 1997; Brussaard and Herbison, 2000; Bosman et al., 2005). In $GABA_A$-receptors containing α5 and γ2 subunits, and β2 and β3 subunits affect GABA currents in opposite directions: receptors with β2 subunits had the highest desensitization rate, while receptors with β3 showed the lowest desensitization rate (Burgard et al., 1996). How increased expression of both β2 and β3 subunits affects GABA receptor kinetics is not clear at this point. Also, it is not known how β subunits affect kinetics of $GABA_A$-receptors expressing other α and γ subunits than α5 and γ2. In transgenic mice lacking β3 subunits, decay time kinetics of IPSCs in cortical and hippocampal neurons are faster (Ramadan et al., 2003; Hentschke et al., 2009), and gamma oscillations in the hippocampus are smaller and faster (Hentschke et al., 2009). However in these mice not only the β3 subunit is lacking, but also the expression of α2 and α3 subunits is reduced, which may affect decay time kinetics (Ramadan et al., 2003). This may suggest that β subunits could affect protein levels of other α subunits, thereby affecting receptor kinetics.

IPSC kinetics in CA1 pyramidal neurons was faster than in CA3 pyramidal neurons. Fritschy and Brunig (2003) showed that in CA1 pyramidal neurons peri-somatic inhibitory synapses predominantly contain α1 subunits. We have evidence that inhibitory inputs to CA3 pyramidal neurons may be mainly mediated by α2 containing receptors (Tim S. Heistek and Huibert D. Mansvelder, unpublished observations), which could explain the differences in IPSC kinetics between these regions. Whether regional differences in β2 and β3 subunit expression exist in hippocampus is not known.

Although it is likely that GABAergic synapse kinetics can account for the observed variation in oscillation frequency between mouse lines, there might be other genes that contribute to differences in properties of fast network oscillations in these strains. While manipulation of ionic channels affecting the excitability of pyramidal cells, such as Im, Ih and Icat (Fisahn et al., 2002; Leao et al., 2009), mainly affects the power of hippocampal oscillations, manipulation of interneuron excitability does affect the frequency of oscillations (Mann and Mody, 2010). Whether differences in interneuron excitability exist between NOD and Balbc mice is not known and Balbc mice show differences in behavior, including anxiety and impulsivity behavior (Fernandes et al., 2004; Hovatta et al., 2005; Loos et al., 2009). It might very well be that genes involved in anxiety and impulsivity also influence neuronal oscillatory activity. Behavioral studies showed that spatial learning and hippocampal LTP are affected in some of these mouse strains (Nguyen et al., 2000; Nguyen and Gerlai, 2002). In recombinant inbred mouse lines there is a high variability in protein kinase C (PKC) levels which correlates with spatial learning (Wehner et al., 1990). PKC activity is known to affect $GABA_A$-receptor functioning and trafficking (Song and Messing, 2005) and could thereby also contribute to the variation in frequency of oscillations.

GENETICS AND HERITABILITY OF OSCILLATIONS

Differences in properties of oscillations might explain heritable variations in cognitive ability. Cognitive functions require the integrated activity of multiple specialized, distributed brain areas. Phase coupling between different areas of the hippocampus and cortex is thought to regulate the information flow between brain areas (Canolty et al., 2006; Sirota et al., 2008; Colgin et al., 2009). Small differences in frequency of oscillations in the hippocampus may lead to a different coupling efficiency and thereby influence spatial and temporal memory processes. Therefore it is likely that genetic variation influencing GABAergic inhibition could impact on neuronal network dynamics and cognition. Indeed in humans there are indications that polymorphisms in $GABA_A$-receptor properties are related with beta- and gamma-band power of neuronal oscillations (Porjesz et al., 2002). Furthermore, in schizophrenia patients there is a decrease in gamma-band activity (Cho et al., 2006) that is correlated with increased expression of the $GABA_A$-receptor α2 subunit and a decrease in GABA transporters(Lewis et al., 2005, 2008). However little is known about variation in frequency

within the gamma band and its implication for cognition. As the frequency range of gamma oscillations *in vivo* is much broader than observed in hippocampal slices, it will be challenging to test whether variation in the frequency range of gamma oscillations exists between individuals.

ACKNOWLEDGMENTS

We thank Hans Lodder and Rik Jansen for excellent technical assistance. Funding for this work was provided by grants from NWO (917.76.360), VU University board (Stg VU-ERC) and Neurobsik (www.neurobsik.nl) to Huibert D. Mansvelder.

REFERENCES

Atallah, B. V., and Scanziani, M. (2009). Instantaneous modulation of gamma oscillation frequency by balancing excitation with inhibition. *Neuron* 62, 566–577.

Bosman, L. W., Heinen, K., Spijker, S., and Brussaard, A. B. (2005). Mice lacking the major adult GABAA receptor subtype have normal number of synapses, but retain juvenile IPSC kinetics until adulthood. *J. Neurophysiol.* 94, 338–346.

Brussaard, A. B., and Herbison, A. E. (2000). Long-term plasticity of postsynaptic GABAA-receptor function in the adult brain: insights from the oxytocin neurone. *Trends Neurosci.* 23, 190–195.

Brussaard, A. B., Kits, K. S., Baker, R. E., Willems, W. P., Leyting-Vermeulen, J. W., Voorn, P., Smit, A. B., Bicknell, R. J., and Herbison, A. E. (1997). Plasticity in fast synaptic inhibition of adult oxytocin neurons caused by switch in GABA(A) receptor subunit expression. *Neuron* 19, 1103–1114.

Burgard, E. C., Tietz, E. I., Neelands, T. R., and Macdonald, R. L. (1996). Properties of recombinant gamma-aminobutyric acid A receptor isoforms containing the alpha 5 subunit subtype. *Mol. Pharmacol.* 50, 119–127.

Canolty, R. T., Edwards, E., Dalal, S. S., Soltani, M., Nagarajan, S. S., Kirsch, H. E., Berger, M. S., Barbaro, N. M., and Knight, R. T. (2006). High gamma power is phase-locked to theta oscillations in human neocortex. *Science* 313, 1626–1628.

Cho, R. Y., Konecky, R. O., and Carter, C. S. (2006). Impairments in frontal cortical gamma synchrony and cognitive control in schizophrenia. *Proc. Natl. Acad. Sci. U.S.A.* 103, 19878–19883.

Colgin, L. L., Denninger, T., Fyhn, M., Hafting, T., Bonnevie, T., Jensen, O., Moser, M. B., and Moser, E. I. (2009). Frequency of gamma oscillations routes flow of information in the hippocampus. *Nature* 462, 353–357.

Collingridge, G. L., Gage, P. W., and Robertson, B. (1984). Inhibitory postsynaptic currents in rat hippocampal CA1 neurones. *J. Physiol. (Lond.)* 356, 551–564.

Cope, D. W., Halbsguth, C., Karayannis, T., Wulff, P., Ferraguti, F., Hoeger, H., Leppa, E., Linden, A. M., Oberto, A., Ogris, W., Korpi, E. R., Sieghart, W., Somogyi, P., Wisden, W., and Capogna, M. (2005). Loss of zolpidem efficacy in the hippocampus of mice with the GABAA receptor gamma2 F77I point mutation. *Eur. J. Neurosci.* 21, 3002–3016.

Csicsvari, J., Jamieson, B., Wise, K. D., and Buzsaki, G. (2003). Mechanisms of gamma oscillations in the hippocampus of the behaving rat. *Neuron* 37, 311–322.

Deary, I. J., Penke, L., and Johnson, W. (2010). The neuroscience of human intelligence differences. *Nat. Rev. Neurosci.* 11, 201–211.

Fernandes, C., Paya-Cano, J. L., Sluyter, F., D'Souza, U., Plomin, R., and Schalkwyk, L. C. (2004). Hippocampal gene expression profiling across eight mouse inbred strains: towards understanding the molecular basis for behaviour. *Eur. J. Neurosci.* 19, 2576–2582.

Fisahn, A., Pike, F. G., Buhl, E. H., and Paulsen, O. (1998). Cholinergic induction of network oscillations at 40 Hz in the hippocampus *in vitro*. *Nature* 394, 186–189.

Fisahn, A., Yamada, M., Duttaroy, A., Gan, J. W., Deng, C. X., McBain, C. J., and Wess, J. (2002). Muscarinic induction of hippocampal gamma oscillations requires coupling of the M1 receptor to two mixed cation currents. *Neuron* 33, 615–624.

Fries, P., Reynolds, J. H., Rorie, A. E., and Desimone, R. (2001). Modulation of oscillatory neuronal synchronization by selective visual attention. *Science* 291, 1560.

Fritschy, J. M., and Brunig, I. (2003). Formation and plasticity of GABAergic synapses: physiological mechanisms and pathophysiological implications. *Pharmacol. Ther.* 98, 299–323.

Gray, C. M., Konig, P., Engel, A. K., and Singer, W. (1989). Oscillatory responses in cat visual cortex exhibit inter-columnar synchronization which reflects global stimulus properties. *Nature* 338, 334–337.

Hajos, N., Palhalmi, J., Mann, E. O., Nemeth, B., Paulsen, O., and Freund, T. F. (2004). Spike timing of distinct types of GABAergic interneuron during hippocampal gamma oscillations *in vitro*. *J. Neurosci.* 24, 9127–9137.

Hentschke, H., Benkwitz, C., Banks, M. I., Perkins, M. G., Homanics, G. E., and Pearce, R. A. (2009). Altered GABAA,slow inhibition and network oscillations in mice lacking the GABAA receptor beta3 subunit. *J. Neurophysiol.* 102, 3643–3655.

Hovatta, I., Tennant, R. S., Helton, R., Marr, R. A., Singer, O., Redwine, J. M., Ellison, J. A., Schadt, E. E., Verma, I. M., Lockhart, D. J., and Barlow, C. (2005). Glyoxalase 1 and glutathione reductase 1 regulate anxiety in mice. *Nature* 438, 662–666.

Jansen, R., Linkenkaer-Hansen, K., Heistek, T., Timmerman, J., Mansvelder, H. D., Brussaard, A. B., de Gunst, M., and van Ooyen, A. (2009). Inbred mouse strains differ in multiple hippocampal activity traits. *Eur. J. Neurosci.* 30, 1092–1100.

Leao, R. N., Tan, H. M., and Fisahn, A. (2009). Kv7/KCNQ channels control action potential phasing of pyramidal neurons during hippocampal gamma oscillations *in vitro*. *J. Neurosci.* 29, 13353–13364.

Lewis, D. A., Cho, R. Y., Carter, C. S., Eklund, K., Forster, S., Kelly, M. A., and Montrose, D. (2008). Subunit-selective modulation of GABA type A receptor neurotransmission and cognition in schizophrenia. *Am. J. Psychiatry* 165, 1585–1593.

Lewis, D. A., Hashimoto, T., and Volk, D. W. (2005). Cortical inhibitory neurons and schizophrenia. *Nat. Rev. Neurosci.* 6, 312–324.

Linkenkaer-Hansen, K., Smit, D. J., Barkil, A., van Beijsterveldt, T. E., Brussaard, A. B., Boomsma, D. I., van Ooyen, A., and de Geus, E. J. (2007). Genetic contributions to long-range temporal correlations in ongoing oscillations. *J. Neurosci.* 27, 13882–13889.

Lisman, J. E., and Idiart, M. A. (1995). Storage of 7 ± 2 short-term memories in oscillatory subcycles. *Science* 267, 1512–1515.

Llinas, R., and Ribary, U. (1993). Coherent 40-Hz oscillation characterizes dream state in humans. *Proc. Natl. Acad. Sci. U.S.A.* 90, 2078–2081.

Loos, M., van der Sluis, S., Bochdanovits, Z., van Zutphen, I. J., Pattij, T., Stiedl, O., Smit, A. B., and Spijker, S. (2009). Activity and impulsive action are controlled by different genetic and environmental factors. *Genes Brain Behav.* 8, 817–828.

Lopes da Silva, F. (1991). Neural mechanisms underlying brain waves: from neural membranes to networks. *Electroencephalogr. Clin. Neurophysiol.* 79, 81–93.

Mann, E. O., and Mody, I. (2010). Control of hippocampal gamma oscillation frequency by tonic inhibition and excitation of interneurons. *Nat. Neurosci.* 13, 205–212.

Mann, E. O., and Paulsen, O. (2005). Mechanisms underlying gamma ('40 Hz') network oscillations in the hippocampus–a mini-review. *Prog. Biophys. Mol. Biol.* 87, 67–76.

Mann, E. O., Suckling, J. M., Hajos, N., Greenfield, S. A., and Paulsen, O. (2005). Perisomatic feedback inhibition underlies cholinergically induced fast network oscillations in the rat hippocampus *in vitro*. *Neuron* 45, 105–117.

Montgomery, S. M., and Buzsaki, G. (2007). Gamma oscillations dynamically couple hippocampal CA3 and CA1 regions during memory task performance. *Proc. Natl. Acad. Sci. U.S.A.* 104, 14495–14500.

Nguyen, P. V., Abel, T., Kandel, E. R., and Bourtchouladze, R. (2000). Strain-dependent differences in LTP and hippocampus-dependent memory in inbred mice. *Learn. Mem.* 7, 170–179.

Nguyen, P. V., and Gerlai, R. (2002). Behavioural and physiological characterization of inbred mouse strains: prospects for elucidating the molecular mechanisms of mammalian learning and memory. *Genes Brain Behav.* 1, 72–81.

Oren, I., Hajos, N., and Paulsen, O. (2010). Identification of the current generator underlying cholinergically induced gamma frequency field potential oscillations in the hippocampal CA3 region. *J. Physiol.* 588, 785–797.

Oren, I., Mann, E. O., Paulsen, O., and Hajos, N. (2006). Synaptic currents in anatomically identified CA3 neurons during hippocampal gamma oscillations *in vitro*. *J. Neurosci.* 26, 9923–9934.

Porjesz, B., Almasy, L., Edenberg, H. J., Wang, K., Chorlian, D. B., Foroud, T., Goate, A., Rice, J. P., O'Connor, S. J., Rohrbaugh, J., Kuperman, S., Bauer, L. O., Crowe, R. R., Schuckit, M. A., Hesselbrock, V., Conneally, P. M., Tischfield, J. A., Li, T. K., Reich, T., and Begleiter, H. (2002). Linkage disequilibrium between the beta frequency of the human EEG and a GABAA receptor gene locus. *Proc. Natl. Acad. Sci. U.S.A.* 99, 3729–3733.

Posthuma, D., de Geus, E. J., and Boomsma, D. I. (2001a). Perceptual speed and IQ are associated through common genetic factors. *Behav. Genet.* 31, 593–602.

Posthuma, D., Neale, M. C., Boomsma, D. I., and de Geus, E. J. (2001b). Are smarter brains running faster? Heritability of alpha peak frequency, IQ, and their interrelation. *Behav. Genet.* 31, 567–579.

Ramadan, E., Fu, Z., Losi, G., Homanics, G. E., Neale, J. H., and Vicini, S. (2003). GABA(A) receptor beta3 subunit deletion decreases alpha2/3 subunits and IPSC duration. *J. Neurophysiol.* 89, 128–134.

Roelfsema, P. R., Engel, A. K., König, P., and Singer, W. (1997). Visuomotor integration is associated with zero time-lag synchronization among cortical areas. *Nature* 385, 157–161.

Sirota, A., Montgomery, S., Fujisawa, S., Isomura, Y., Zugaro, M., and Buzsaki, G. (2008). Entrainment of neocortical neurons and gamma oscillations by the hippocampal theta rhythm. *Neuron* 60, 683–697.

Smit, D. J., Posthuma, D., Boomsma, D. I., and Geus, E. J. (2005). Heritability of background EEG across the power spectrum. *Psychophysiology* 42, 691–697.

Song, M., and Messing, R. O. (2005). Protein kinase C regulation of GABAA receptors. *Cell. Mol. Life Sci.* 62, 119–127.

Tallon-Baudry, C., Bertrand, O., and Fischer, C. (2001). Oscillatory synchrony between human extrastriate areas during visual short-term memory maintenance. *J. Neurosci.* 21, RC177.

Tallon-Baudry, C., Bertrand, O., Peronnet, F., and Pernier, J. (1998). Induced gamma-band activity during the delay of a visual short-term memory task in humans. *J. Neurosci.* 18, 4244–4254.

Traub, R. D., Bibbig, A., Fisahn, A., LeBeau, F. E., Whittington, M. A., and Buhl, E. H. (2000). A model of gamma-frequency network oscillations induced in the rat CA3 region by carbachol *in vitro*. *Eur. J. Neurosci.* 12, 4093–4106.

van Aerde, K. I., Heistek, T. S., and Mansvelder, H. D. (2008). Prelimbic and infralimbic prefrontal cortex interact during fast network oscillations. *PLoS ONE* 3, e2725. doi: 10.1371/journal.pone.0002725.

van Aerde, K. I., Mann, E. O., Canto, C. B., Heistek, T. S., Linkenkaer-Hansen, K., Mulder, A. B., van der Roest, M., Paulsen, O., Brussaard, A. B., and Mansvelder, H. D. (2009). Flexible spike timing of layer 5 neurons during dynamic beta oscillation shifts in rat prefrontal cortex. *J. Physiol. (Lond.)* 587, 5177–5196.

Wehner, J. M., Sleight, S., and Upchurch, M. (1990). Hippocampal protein kinase C activity is reduced in poor spatial learners. *Brain Res.* 523, 181–187.

Whittington, M. A., Traub, R. D., and Jefferys, J. G. (1995). Synchronized oscillations in interneuron networks driven by metabotropic glutamate receptor activation. *Nature* 373, 612–615.

Womelsdorf, T., Schoffelen, J. M., Oostenveld, R., Singer, W., Desimone, R., Engel, A. K., and Fries, P. (2007). Modulation of neuronal interactions through neuronal synchronization. *Science* 316, 1609.

Conflict of Interest Statement: The authors declare that the research was conducted in the absence of any commercial or financial relationships that could be construed as a potential conflict of interest.

Received: 23 February 2010; paper pending published: 10 March 2010; accepted: 06 May 2010; published online: 02 June 2010.

*Citation: Heistek TS, Timmerman AJ, Spijker S, Brussaard AB and Mansvelder HD (2010) GABAergic synapse properties may explain genetic variation in hippocampal network oscillations in mice. Front. Cell. Neurosci. **4**:18. doi: 10.3389/fncel.2010.00018*

frontiers in
CELLULAR NEUROSCIENCE

ORIGINAL RESEARCH ARTICLE
published: 10 June 2010
doi: 10.3389/fncel.2010.00016

Developmental changes in GABAergic mechanisms in human visual cortex across the lifespan

Joshua G.A. Pinto[1], Kyle R. Hornby[1], David G. Jones[1] and Kathryn M. Murphy[1,2]*

[1] *McMaster Integrative Neuroscience Discovery and Study Program, McMaster University, Hamilton, ON, Canada*
[2] *Department of Psychology, Neuroscience and Behaviour, McMaster University, Hamilton, ON, Canada*

Edited by:
Yehezkel Ben-Ari, Institut National de la Santé et de la Recherche Médicale, France

Reviewed by:
Peter C. Kind, University of Edinburgh, UK

****Correspondence:***
Kathryn M. Murphy, McMaster Integrative Neuroscience Discovery and Study (MiNDS), McMaster University, 1280 Main Street West, L8S 4K1, Hamilton, ON, Canada.
e-mail: kmurphy@mcmaster.ca

Functional maturation of visual cortex is linked with dynamic changes in synaptic expression of GABAergic mechanisms. These include setting the excitation–inhibition balance required for experience-dependent plasticity, as well as, intracortical inhibition underlying development and aging of receptive field properties. Animal studies have shown that there is developmental regulation of GABAergic mechanisms in visual cortex. In this study, we show for the first time how these mechanisms develop in the human visual cortex across the lifespan. We used Western blot analysis of postmortem tissue from human primary visual cortex ($n = 30$, range: 20 days to 80 years) to quantify expression of eight pre- and post-synaptic GABAergic markers. We quantified the inhibitory modulating cannabinoid receptor (CB1), GABA vesicular transporter (VGAT), GABA synthesizing enzymes (GAD65/GAD67), $GABA_A$ receptor anchoring protein (Gephyrin), and $GABA_A$ receptor subunits ($GABA_A\alpha1$, $GABA_A\alpha2$, $GABA_A\alpha3$). We found a complex pattern of different developmental trajectories, many of which were prolonged and continued well into the teen, young adult, and even older adult years. These included a monotonic increase or decrease ($GABA_A\alpha1$, $GABA_A\alpha2$), a biphasic increase then decrease (GAD65, Gephyrin), or multiple increases and decreases (VGAT, CB1) across the lifespan. Comparing the balances between the pre- and post-synaptic markers we found three main transition stages (early childhood, early teen years, aging) when there were rapid switches in the composition of the GABAergic signaling system, indicating that functioning of the GABAergic system must change as the visual cortex develops and ages. Furthermore, these results provide key information for translating therapies developed in animal models into effective treatments for amblyopia in humans.

Keywords: GABA, development, human, aging, visual cortex, inhibition, plasticity

INTRODUCTION

Functional maturation of the visual cortex is linked with dynamic changes in synaptic expression of GABAergic signaling mechanisms. Even small changes in the relative amounts of excitation and inhibition can dramatically alter experience-dependent plasticity (Kirkwood and Bear, 1994; Hensch et al., 1998; Iwai et al., 2003). During development, specific components of the GABAergic signaling affect ocular dominance plasticity (Hensch et al., 1998; Fagiolini et al., 2004; Hensch, 2005) and orientation selectivity (Tsumoto and Sato, 1985; Fagiolini et al., 2004). Furthermore, the emergence of normal binocular visual function depends on interocular inhibition that is mediated by GABAergic inhibitory circuitry in visual cortex (Sengpiel and Vorobyov, 2005). In adult visual cortex, activity regulates $GABA_A$ receptor expression (Hendry et al., 1994) and during aging the loss of orientation tuning in visual cortical receptive fields (Leventhal et al., 2003) and changes in visual perception (Betts et al., 2005) have been linked with an overall loss of GABA.

When GABAergic signaling in visual cortex is manipulated to shift the excitatory-inhibitory balance, the effect can either enhance or reduce experience-dependent plasticity (Kirkwood and Bear, 1994; Iwai et al., 2003; Maffei et al., 2004; Hensch and Fagiolini, 2005). This approach has been extended in a series of recent studies using pharmacological manipulations of GABA signaling, such as fluoxetine, to reinstate ocular dominance plasticity in adult visual cortex and facilitate recovery from amblyopia (Maya Vetencourt et al., 2008; Harauzov et al., 2010). Taken together, these studies are providing a better understanding for the role of GABAergic signaling in the maturation and function of the visual cortex, and have opened the door for the development of new treatments for neurodevelopmental disorders such as amblyopia.

The GABAergic synapse is a complex structure with a large set of pre- and post-synaptic proteins, many of which have been linked with experience-dependent plasticity in the cortex. On the pre-synaptic side these include: the two isoforms of the GABA synthesizing enzyme glutamic acid decarboxylase (GAD), GAD65 and GAD67; the CB1 receptor that modulates GABA release; and the vesicular transporter VGAT that is responsible for loading GABA into synaptic vesicles (McIntire et al., 1997; Sagne et al., 1997). GAD65 is localized in the axon terminals and synthesizes the on-demand pool of GABA, while GAD67 is located in the cell body and synthesizes the basal pool of GABA (Feldblum et al., 1993, 1995). Knocking out GAD65 leads to a loss of critical period ocular dominance plasticity, however, it can be rescued by infusion of diazepam (Iwai et al., 2003). Activation of CB1 receptors is involved in regulating activity-dependent synaptic plasticity (Sjöström et al., 2003; Jiang

et al., 2010) and blocking CB1 receptors during the critical period alters activity patterns (Bernard et al., 2005). Finally, VGAT contributes to an efficient up- and down-regulation of vesicular GABA content that effects post-synaptic currents and the fine-tuning of inhibitory strength (Engel et al., 2001).

On the post-synaptic side many components of the ionotropic $GABA_A$ receptor complex contribute to experience-dependent plasticity. Gephyrin is the $GABA_A$ receptor anchoring protein. Gephyrin clusters $GABA_A$ receptors (Essrich et al., 1998; Kneussel et al., 1999), and it seems to fulfill a modulator role for changes in synaptic activity and structure. Furthermore, expression levels of Gephyrin give an indication of the total amount of $GABA_A$ receptors at a given time. The $GABA_A$ receptor is a pentameric structure and is functionally diverse, with 20 known subunits. Three subunits are of particular interest, α1, α2, and α3, because they are developmentally regulated (Hendrickson et al., 1994; Chen et al., 2001; Bosman et al., 2002), they affect receptor kinetics (Laurie et al., 1992; Gingrich et al., 1995), and the α subunit is the interface for binding GABA (Smith and Olsen, 1995) and benzodiazepine (Sigel, 2002). Both α1 and α2 subunits play key functional roles, with α2 involved in regulating cell firing, and α1 necessary for critical period plasticity (Fagiolini et al., 2004). The α1 subunit also has high-affinity for binding GABA and benzodiazepine receptor ligands (Pritchett et al., 1989).

Although there have been many animal studies of developmental and aging changes in expression of GABAergic signaling components in visual cortex (e.g., Shaw et al., 1991; Hendrickson et al., 1994; Hornung and Fritschy, 1996; Guo et al., 1997; Leventhal et al., 2003; Minelli et al., 2003), there have been relatively few studies of human visual cortex (Murphy et al., 2005). This poses a challenge when considering how to translate GABAergic drug treatments for amblyopia from animal models to human trials. To fill this gap, we have carried out a comprehensive study of changes in the expression of a collection of pre- and post-synaptic GABAergic signaling mechanisms in human visual cortex across the lifespan. Using Western blot analysis we quantified the developmental trajectories for four pre- and four post-synaptic components of GABA signaling. These results show a complex pattern of different developmental trajectories among the GABA signaling mechanisms in human visual cortex. Many of the changes are prolonged, highlighting a long time course for the development of GABA signaling in human visual cortex, much longer than would be predicted from animal studies. Furthermore, there are three transition stages when there are rapid switches in the relative amounts of the different components, indicating that functioning of the GABAergic system must change as the visual cortex develops and ages. A portion of these data has been presented previously (Pinto et al., 2008).

MATERIALS AND METHODS

SAMPLES AND TISSUE

Tissue samples were obtained from the Brain and Tissue Bank for Developmental Disorders at the University of Maryland (Baltimore, MD, USA). The samples were from the posterior pole of the left hemisphere of human visual cortex, including both superior and inferior portions of the calcarine fissure where the central visual field is represented in primary visual cortex (V1) according to the gyral and sulcal landmarks. The samples were from 28 individuals ranging in age from 20 days to 80 years (**Table 1**). All samples were obtained within 23 h postmortem, and at the Brain and Tissue Bank were fresh frozen after being sectioned coronally in 1-cm intervals, rinsed with water, blotted dry, placed in a quick-freeze bath (dry ice and isopentane), and stored frozen (−70°C). The individuals had no history of neurological or mental health disorders.

Table 1 | Human tissue samples. The age group, age, postmortem interval and cause of death for each of the human cortical tissue samples.

Age group	Age	Postmortem interval (hours)	Sex	Cause of death
Neonates	20 days	14	F	Pneumonia
Neonates	86 days	23	F	Not known
Neonates	96 days	12	M	Bronchopneumonia
Neonates	98 days	16	M	Cardiovascular disorder
Neonates	119 days	22	M	Bronchopneumonia
Neonates	120 days	23	M	Pneumonia
Neonates	133 days	16	M	Accidental
Neonates	136 days	11	F	Pneumonia
Neonates	273 days	10	M	Sudden infant death syndrome
Infants	1.34 years	21	M	Dehydration
Infants	2.16 years	21	F	Cardiovascular disorder
Infants	2.21 years	11	F	Accidental
Young children	3.34 years	11	F	Drowning
Young children	4.56 years	15	M	Accidental
Young children	4.71 years	17	M	Drowning
Older children	5.40 years	17	M	Accidental
Older children	8.14 years	20	F	Accidental
Older children	8.59 years	20	F	Cardiovascular disorder
Teens	12.45 years	22	M	Cardiovascular disorder
Teens	13.27 years	5	M	Asphyxia
Teens	15.22 years	16	M	Multiple injuries
Young adults	22.98 years	4	M	Multiple injuries
Young adults	32.61 years	13	M	Cardiovascular disorder
Young adults	50.43 years	8	M	Cardiovascular disorder
Young adults	53.90 years	5	F	Cardiovascular disorder
Older adults	69.30 years	12	M	Cardiovascular disorder
Older adults	71.91 years	9	F	Multiple medical disorders
Older adults	79.50 years	14	F	Drug overdose

TISSUE SAMPLE PREPARATION

Tissue samples (50–100 mg) were cut from the frozen block of V1 and suspended in cold homogenization buffer (1 ml buffer:50 mg tissue, 0.5 mM DTT, 1 mM EDTA, 2 mM EGTA, 10 mM HEPES, 10 mg/L leupeptin, 100 nM microcystin, 0.1 mM PMSF, 50 mg/L soybean trypsin inhibitor). The tissue samples were homogenized in a glass-glass Dounce homogenizer (Kontes, Vineland, NJ, USA). A subcellular fractionation procedure (synaptoneurosomes) (Hollingsworth et al., 1985; Titulaer and Ghijsen, 1997; Quinlan et al., 1999) was performed to obtain protein samples that were enriched for synaptic proteins. The synaptoneurosome was obtained by passing the homogenized sample through a coarse (100 μm) pore nylon-mesh filter followed by a fine (5 μm) pore hydrophilic mesh filter (Millipore, Bedford, MA, USA), then centrifuged at $1000 \times g$ for 10 min to obtain the synaptic fraction of the membrane. The synaptic pellet was resuspended in boiling 1% sodium-dodecyl-sulfate (SDS) and stored at −80°C. Protein concentrations were determined using the bicinchonic acid (BCA) assay guidelines (Pierce, Rockford, IL, USA). A control sample was made by combining a small amount of the prepared tissue sample from each of the cases.

IMMUNOBLOTTING

The samples (20 μg) were separated on sodium-dodecyl-sulfate polyacrylamide gels (SDS-PAGE) and transferred to polyvinylidene difluoride (PVDF-FL) membranes (Millipore, Billerica, MA, USA). Each sample was run multiple times. Blots were pre-incubated in blocking buffer [Odyssey Blocking Buffer 1:1 with phosphate buffered saline (PBS)] for 1 h (LI-COR Biosciences; Lincoln, NE, USA), then incubated in primary antibody overnight at 4°C using the following concentrations: GAD65, 1:500 (Chemicon International, Temecula, CA, USA); GAD67, 1:1000 (Chemicon International, Temecula, CA, USA); VGAT, 1:1000 (Synaptic Systems, Göttingen, Germany); CB1, 1:1000 (Cayman, Ann Arbor, MI, USA); Gephyrin, 1:500 (Chemicon International, Temecula, CA, USA); $GABA_A\alpha1$, 1:500 (Imgenex, San Diego, CA, USA); $GABA_A\alpha2$, 1:1000 (Imgenex, San Diego, CA, USA); $GABA_A\alpha3$, 1:1000 (Imgenex, San Diego, CA, USA). The blots were washed with PBS containing 0.05% Tween (PBS-T, Sigma, St. Louis, MO, USA) (3×10 min), incubated (1 h, room temperature) with the appropriate IRDye labeled secondary antibody, (Anti-Mouse, 1:8000, Anti-Rabbit, 1:10,000) (LI-COR Biosciences; Lincoln, NE, USA), and washed in PBS-T (3×10 min). The blots were visualized using the Odyssey scanner (LI-COR Biosciences; Lincoln, NE). The blots were stripped and prepared to be re-probed with additional antibodies (Blot Restore Membrane Rejuvenation kit, Chemicon International, Temecula, CA, USA).

ANALYSIS

To analyze the bands, we scanned the blots (Odyssey Infrared Scanner) and quantified the bands using densitometry (LI-COR Odyssey Software version 3.0; LI-COR Biosciences; Lincoln, NE, USA). Density profiles were determined by performing a subtraction of the background, integrating the pixel intensity across the area of the band, and dividing the intensity by the width of the band to control for variations in band size. A control sample (a mixture of all the samples) was run on all of the gels and the density of each sample was measured relative to that control (sample density/control density).

To visualize changes in expression of the GABAergic signaling mechanisms, the results were plotted in two ways. This was done to facilitate analysis of changes between developmental stages, to describe the pattern of changes, and to be able to quantify the time course of changes. First, the samples were grouped into developmental ages (<1 year neonates, 1–2 years infants, 3–4 years young children, 5–11 years older children, 12–20 years teens, 21–55 years young adults, and >55 years older adults) with three or more cases in each group and following the age groups used by Law et al. (2003) and Duncan et al. (2010). Group mean values and standard errors were calculated for each antibody and normalized to the mean level of expression for the youngest group. Second, we plotted scattergrams for each antibody that included both the average expression level (black symbols) for each case and every point from all runs (gray symbols). To help describe the pattern of change in expression across the lifespan, a weighted average curve was fit to each scatter plots using the locally weighted least squares method at 50% (dotted lines). In addition, an exponential decay function (solid lines) was fit to the scattergrams when there was a clear monotonic increase or decrease in the expression across the lifespan. The goodness of fit was determined (R) and the time constant (τ) for the rise or fall of expression level was calculated from the exponential decay function. The age when adult levels were reached was defined as 3τ. This provides an objective measure, representing the age at which expression had reached 87.5% of their asymptotic level.

Four indices were calculated to quantify relative changes in expression levels of the GABAergic signaling components: maturation of receptor composition {$GABA_A\alpha1$:$GABA_A\alpha2$ ([$GABA_A\alpha1$ − $GABA_A\alpha2$]/[$GABA_A\alpha1$ + $GABA_A\alpha2$]); $GABA_A\alpha1$:$GABA_A\alpha3$ ([$GABA_A\alpha1$ − $GABA_A\alpha3$]/[$GABA_A\alpha1$ + $GABA_A\alpha3$]); changes in pre-synaptic production versus trafficking, GAD65:VGAT ([GAD65 − VGAT]/[GAD65 + VGAT]); and changes in pre- versus post-synaptic GABAergic signaling, GAD65:Gephyrin ([GAD65 − Gephyrin]/[GAD65 + Gephyrin])}.

Statistical comparisons of differences in expression levels between the age groups were calculated using Kruskal–Wallis nonparametric analysis of variance and planned pairwise comparisons using a Tukey's HSD test ($p < 0.05$).

RESULTS

The tissue samples were collected over a range (4–23 h) of postmortem intervals and the first step was to determine if that interval affected expression of any of the GABAergic proteins. There were no significant correlations (p values >0.1) between postmortem interval and the expression level for any of the antibodies (GAD65, $R = 0.26$; GAD67, $R = 0.08$; VGAT, $R = 0.20$; $GABA_A\alpha1$, $R = 0.04$; $GABA_A\alpha2$, $R = 0.25$; $GABA_A\alpha3$, $R = 0.17$; Gephyrin, $R = 0.17$; CB1, $R = 0.19$).

CHANGES IN PRE-SYNAPTIC GABAergic COMPONENTS

Expression levels of the two GABA synthesizing enzymes (GAD65 and GAD67) were quantified in human V1 across the lifespan. GAD65 is the isoform that localizes in the axon terminals and is responsible for supplying the "on-demand" pool of GABA. GAD67 is the isoform that is predominant in the cell body and supplies the basal pool of GABA (Feldblum et al., 1993; Esclapez et al., 1994).

Expression levels of GAD67 did not change across the lifespan (**Figures 1A,B**). In contrast, developmental changes were found for GAD65 expression levels ($p < 0.0002$; **Figures 1C,D**). GAD65 showed a progressive 60% increase in expression levels from early in life (<4 years) to the teenage and adult years ($p < 0.05$), with a slight decline into older adults (>55 years). The difference in the developmental trajectories of these two enzymes indicates that the basal pool of GABA is maintained across the lifespan, whereas the axonal pool has a time window of heightened production capacity.

To further examine how the pre-synaptic components of the GABAergic system change across the lifespan in human V1, we quantified the expression of two key inhibitory proteins, CB1 and VGAT (**Figure 2**). CB1 is a pre-synaptic receptor involved in modulating GABA release (Hajos and Freund, 2002); over the lifespan there were significant changes in the expression of CB1 in human V1 ($p < 0.0002$). In infants (<1 year) and pre-teens (5–11 years), CB1 expression was high, but in young children (1–2 years), adults (21–55 years), and older adults (>55 years) it was about 40% less ($p < 0.05$; **Figures 2A,B**). The GABA vesicular transporter VGAT showed a similar pattern of expression levels across the lifespan ($p < 0.002$). VGAT expression was highest in infants (<1 year) and pre-teens (5–11 years), and had about 32% less expression in adults (21–55 years; $p < 0.02$; **Figures 2C,D**).

To quantify changes in the balance between the mechanisms that produce and traffic GABA in the pre-synaptic terminal, we calculated an index of GAD65:VGAT expression. There were significant changes in the balance between GAD65:VGAT across the lifespan ($p < 0.0005$). There was more VGAT expression in both young children (<11 years) and older adults (>55 years; **Figure 3**). In contrast, there was an abrupt switch to much more GAD65 during the teenage ($p < 0.02$) and young adult years ($p < 0.001$). These shifts in the balance between GAD65 and VGAT indicate that the rate limiting component regulating GABA transmission changes across the lifespan (**Figure 3**).

POST-SYNAPTIC CHANGES IN GABA$_A$ RECEPTORS

Expression levels for three subunits of the ionotropic GABA$_A$ receptor were quantified (GABA$_A$α1, GABA$_A$α2, GABA$_A$α3). Each subunit exhibited a unique developmental trajectory across the lifespan (**Figure 4**). Quantification of GABA$_A$α1 expression in human V1

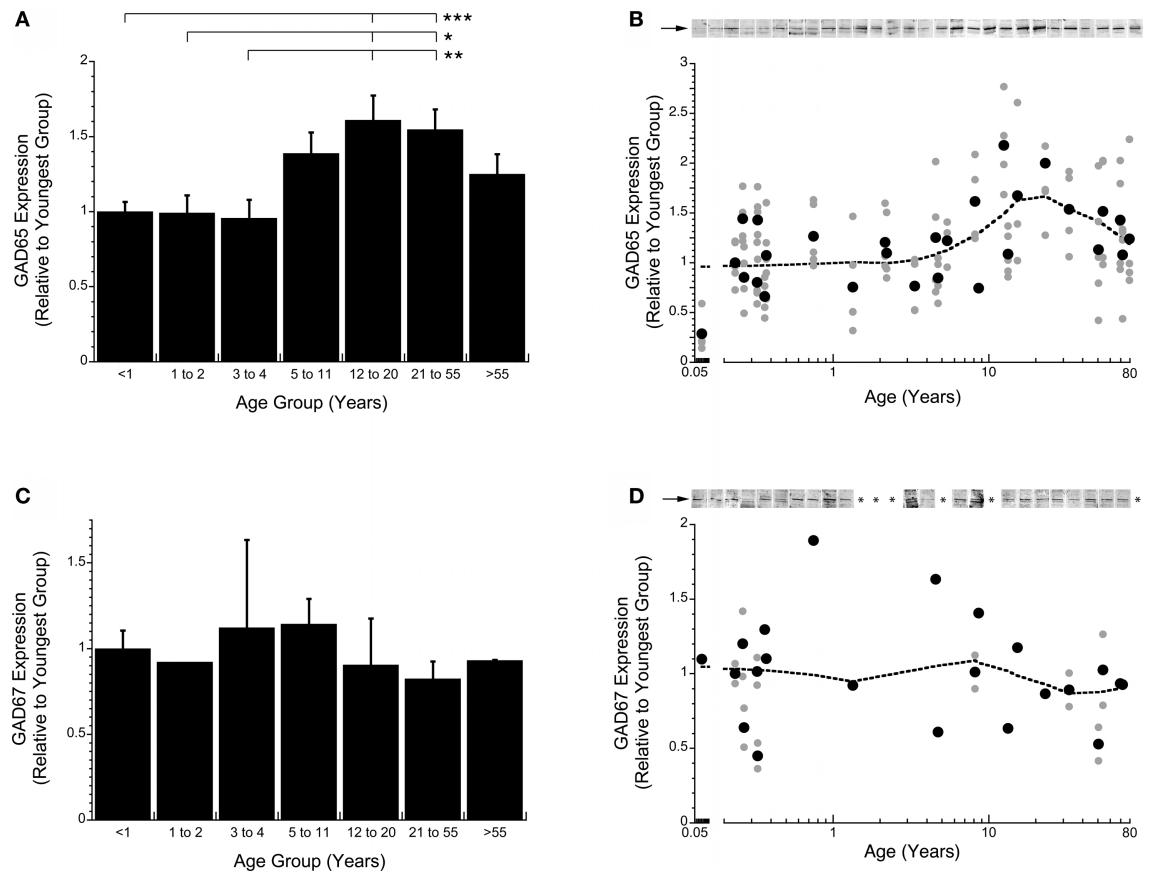

FIGURE 1 | Developmental changes in GAD65 (A,B) and GAD67 (C,D) expression in human visual cortex across the lifespan plotted relative to the youngest age group (<1 year) for the grouped means and scattergrams (• average expression for each case; • all runs). Example blots for each case are presented above the scattergrams **(B,D)**. The arrow indicates the band that was quantified. A weighted average curve was fit to each scatter plots using the locally weighted least squares method at 50% (dotted line). GAD65 showed a significant change across the lifespan (Kruskal–Wallis, $p < 0.0001$) with progressive increase in expression levels into the teenage and adult years then a loss with aging **(A,B)**. There was no change in expression levels of GAD67 across the lifespan **(C,D)**. The lines above the histograms identify the groups that were significantly different (Tukey's *post hoc* HSD, $*p < 0.05$, $**p < 0.02$, $***p < 0.001$).

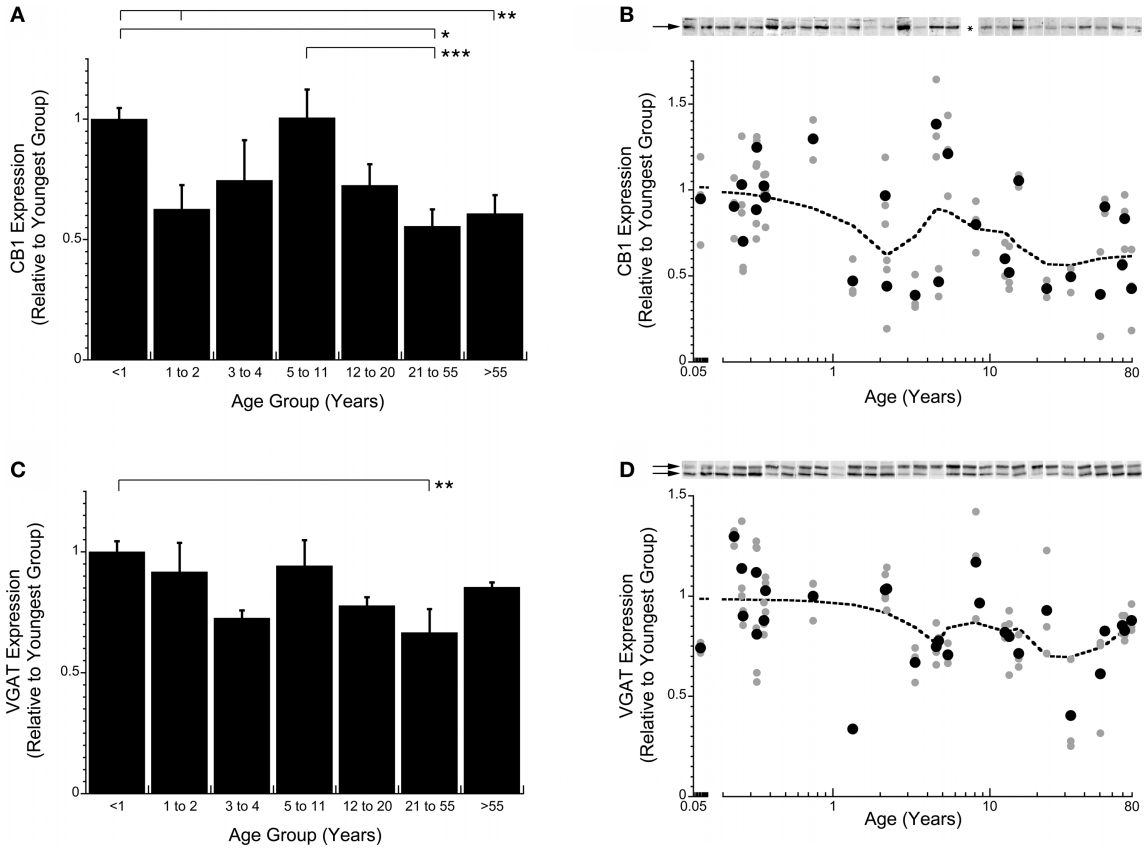

FIGURE 2 | Quantification of changes in expression levels of CB1 (A,B) and VGAT (C,D) in human visual cortex across the lifespan. The graphs follow the same conventions as described in **Figure 1**. CB1 levels are high in infants (<1 year) then fall into young children (1–2 years) before rising again in pre-teens (5–11 years) and falling again in teens (12–20 years) and leveling off (Kruskal–Wallis, $p < 0.0001$) **(A,B)**. For VGAT 2 bands were quantified (arrows at 50 and 57 kDa). VGAT levels are highest in infants (<1 year) then gradually fall into children (3–4 years) before rising again into pre-teens (5–11 years) then falling into adults (21–55 years) before finally rising again in older adults (>55 years) (Kruskal–Wallis, $p < 0.005$) **(C,D)**. The lines above the histograms identify the groups that were significantly different (Tukey's *post hoc* HSD, $*p < 0.05$, $**p < 0.02$, $***p < 0.001$) (• average expression for each case; • all runs; dotted line is the weighted average).

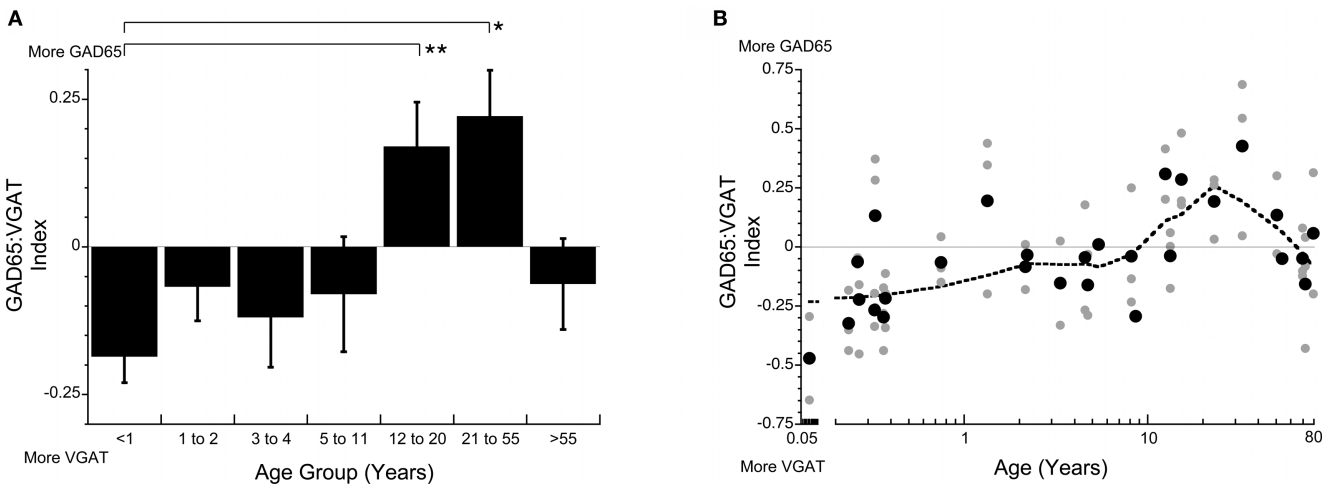

FIGURE 3 | The index of GAD65:VGAT (A,B) gives insight into the relative balance between production and trafficking of GABA. The balance is in favor of VGAT early (<11 years) and late (>55 years) in development, but there is much more GAD65 during the teenage to adult years (12–55 years) (Kruskal–Wallis, $p < 0.0002$) **(A,B)**. The lines above the histograms identify the groups that were significantly different (Tukey's *post hoc* HSD, $*p < 0.05$, $**p < 0.02$, $***p < 0.001$) (• average expression for each case; • all runs; dotted line is the weighted average).

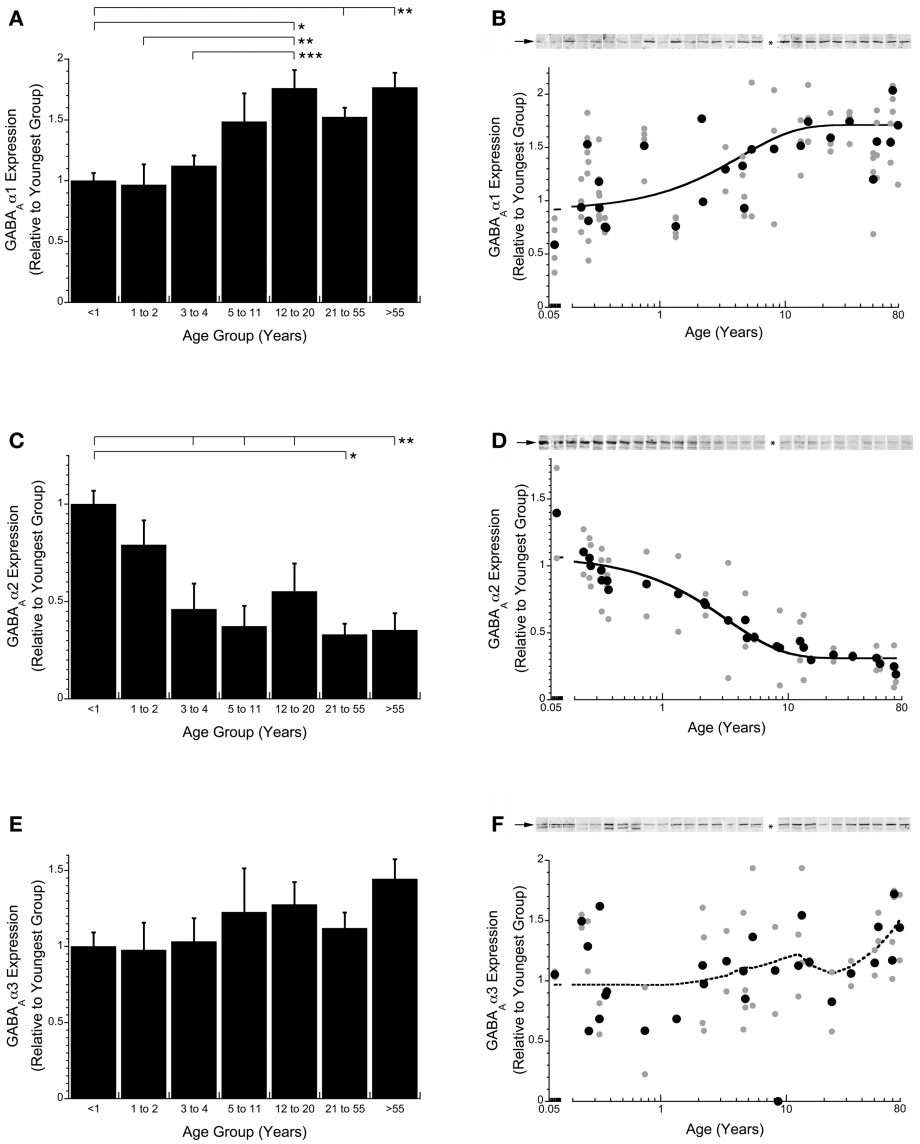

FIGURE 4 | Changes in expression of GABA$_A$ receptor subunits GABA$_A$α1 (A,B), GABA$_A$α2 (C,D), and GABA$_A$α3 (E,F) during postnatal development. An exponential decay function (solid line) was fit to the expression levels for GABA$_A$α1 and GABA$_A$α2 and the time constants (τ) were calculated with adult levels defined as 3τ. GABA$_A$α1 expression increased until early teens when it leveled off (3τ = 13.5 years, τ = 4.50 years, $R = 0.67$; $p < 0.0001$; **B**). GABA$_A$α2 expression decreased until older childhood when it leveled off (3τ = 10 years of age, τ = 3.34 years, $R = 0.96$; $p < 0.0001$; **D**). GABA$_A$α3 expression levels did not change significantly throughout the lifespan **(E,F)** (dotted line is the weighted average). The lines above the histograms identify the groups that were significantly different (Tukey's *post hoc* HSD, $*p < 0.05$, $**p < 0.02$, $***p < 0.001$) (• average expression for each case; • all runs).

showed a prolonged development profile, increasing about 75% to reach adult levels at 13.5 years of age (3τ, τ = 4.50 years, $R = 0.67$; $p < 0.0001$; **Figure 4B**). GABA$_A$α2 expression changed in the opposite direction and had a slightly more rapid developmental profile, decreasing by about 65% to reach adult levels at 10 years of age (3τ, τ = 3.34 years, $R = 0.96$; $p < 0.0001$; **Figure 4D**). GABA$_A$α3 had no significant change in expression levels across the lifespan ($p > 0.36$; **Figures 4E,F**).

The three GABA$_A$ receptor subunits that we quantified are classified into two categories, immature (GABA$_A$α2, GABA$_A$α3) and mature (GABA$_A$α1), with the mature subunit conferring faster receptor decay times and great affinity for GABA compared with the immature subunits. To determine the magnitude and time course of receptor maturation we calculated two indices (GABA$_A$α1:GABA$_A$α2, GABA$_A$α1:GABA$_A$α3). The GABA$_A$α1:GABA$_A$α2 balance was initially in favor of GABA$_A$α2, then progressively shifted toward more GABA$_A$α1 (**Figure 5**). We fit a tau (τ) function to the index to quantify the time course of the switch in receptor composition. The mature balance was reached at 4.5 years of age (3τ, τ = 1.50 years, $R = 0.84$; $p < 0.0001$; **Figure 5B**). The GABA$_A$α1:GABA$_A$α3 switch was smaller in magnitude and much more abrupt. There was initially more GABA$_A$α3, but that switched within the first year to slightly more GABA$_A$α1, and reached mature levels at about 8 months of age (3τ, τ = 0.23 years, $R = 0.65$; $p < 0.0001$; **Figure 5D**).

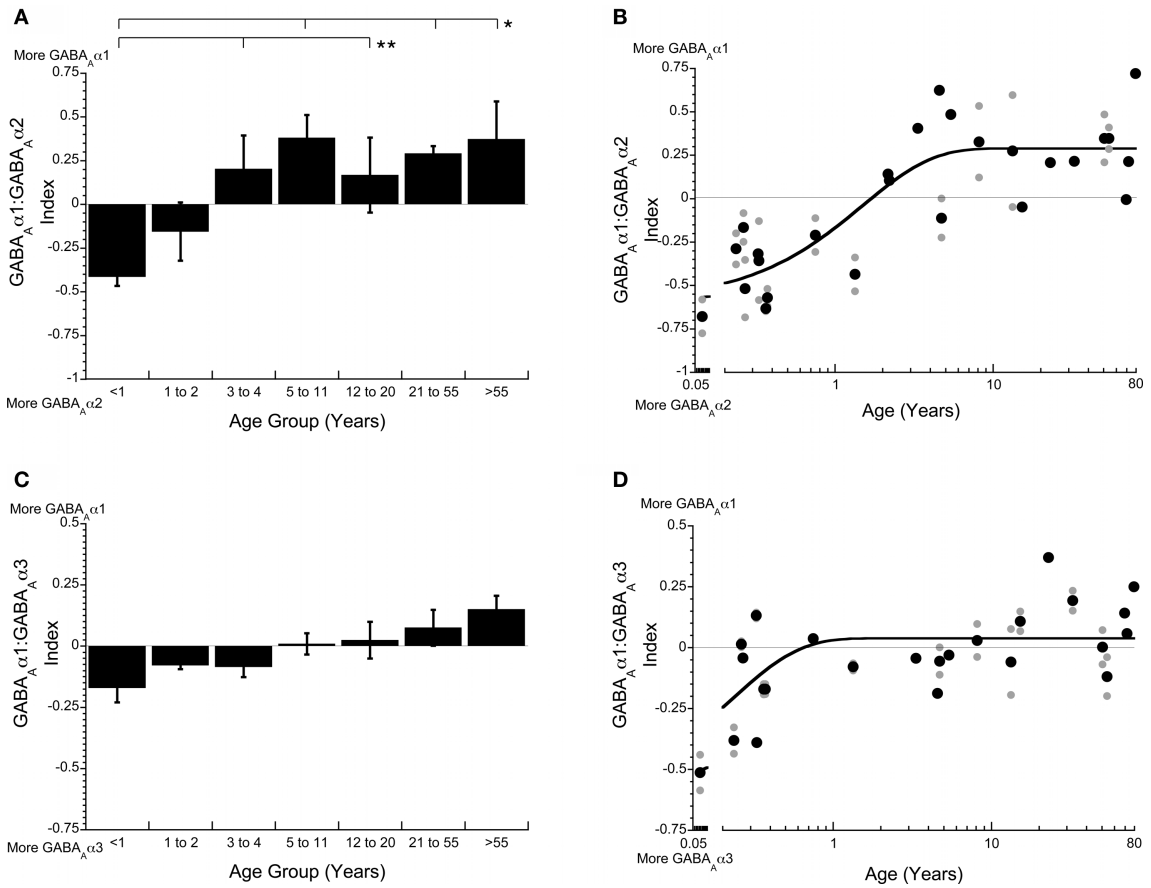

FIGURE 5 | The indices of GABA$_A$α1:GABA$_A$α2 (A,B) and GABA$_A$α1:GABA$_A$α3 (C,D) are important for determining the kinetics and maturation of the GABA$_A$ receptor. The GABA$_A$α1:GABA$_A$α2 index starts in favor of GABA$_A$α2, then shifts to more GABA$_A$α1 in children (3–4 years), reaching the adult balance in younger childhood ($3\tau = 4.5$ years of age, $\tau = 1.50$ years, $R = 0.84$; $p < 0.0001$; **B**). The GABA$_A$α1: GABA$_A$α3 index starts out with more GABA$_A$α3 very early, then quickly shifts to slightly more GABA$_A$α1, reaching adult levels within the first year ($3\tau = 0.69$ years of age, $\tau = 0.23$ years, $R = 0.65$; $p < 0.0001$; **D**). The lines above the histograms identify the groups that were significantly different (Tukey's *post hoc* HSD, $^*p < 0.05$, $^{**}p < 0.02$, $^{***}p < 0.001$) (• average expression for each case; • all runs; solid lines are exponential decay functions).

Both indices showed a shift to more GABA$_A$α1, however, there was a greater change for the shift from more GABA$_A$α2 to more GABA$_A$α1.

To examine the overall levels of GABA$_A$ receptors in human V1, we quantified the expression of Gephyrin across the lifespan. Gephyrin is the GABA$_A$ receptor anchoring protein and these expression levels provide an indication of total GABA$_A$ receptor expression. There were significant changes in Gephyrin expression across the lifespan ($p < 0.002$). Early in development (<1 year) and for older adults (>55 years), the expression levels for Gephyrin were low. In contrast, during the rest of the lifespan, Gephyrin expression was significantly higher (~120% increase) and had a peak in expression during childhood (5–11 years; $p < 0.05$; **Figure 6A**).

PRE- VERSUS POST-SYNAPTIC DEVELOPMENT

To determine the relative contribution of pre- versus post-synaptic components of GABAergic signaling across the lifespan, we calculated a index of Gephyrin:GAD65 expression (**Figure 6**). In young infants (<1 year) this pre- versus post-synaptic balance was in favor of more GAD65, the pre-synaptic side ($p < 0.01$). This switched to more Gephyrin during childhood (1–11 years of age), then a balance during the teenage and adult years, followed by an abrupt switch to relatively more GAD65 in older adults ($p < 0.05$; **Figures 6C,D**). These changes represent a shift in GABAergic signaling mechanisms from more pre-synaptic, to more post-synaptic, to a balance, to substantially more pre-synaptic. This index captures an important aspect of the changing nature of the pre- and post-synaptic GABAergic signaling mechanisms in human V1 across the lifespan. There is not a single balance that is maintained across the lifespan.

DISCUSSION

Our study is the first to characterize changes in pre- and post-synaptic components of the GABAergic signaling system across the lifespan in human primary visual cortex. We found a complex pattern of different developmental trajectories among these GABAergic signaling mechanisms. Many of the changes were prolonged and continued well into the teen, young adult, and even older adult years. For example, the peak of GAD65 expression was not reached until the teen to young adult years before

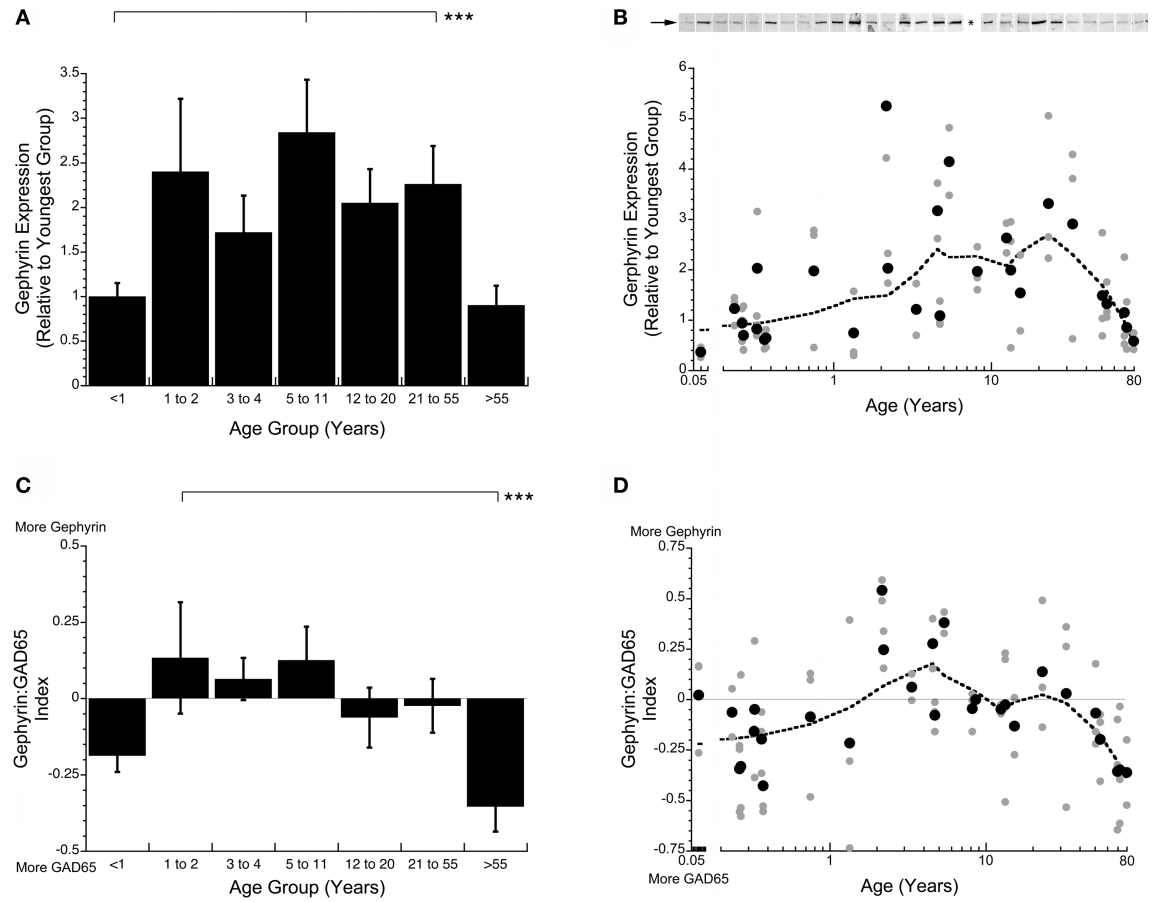

FIGURE 6 | Changes in expression of Gephyrin (A,B) and the index of Gephyrin:GAD65 (C,D) during postnatal development. Expression levels of Gephyrin are lowest in infants (<1 year) and older adults (<55 years) and higher for the rest of the lifespan (Kruskal–Wallis, $p < 0.005$) **(A)**. The Gephyrin:GAD65 index shows a shift from more GAD65 in infants (<1 year) to more Gephyrin in children (1–11 years) to a balance from the teenage to adult years (12–55) then a switch to much more GAD65 in aging (>55 years) (Kruskal–Wallis, $p < 0.008$) **(C)**. The lines above the histograms identify the groups that were significantly different (Tukey's *post hoc* HSD, $*p < 0.05$, $**p < 0.02$, $***p < 0.001$) (• average expression for each case; • all runs; dotted line is the weighted average).

falling off in aging. Thus, the potential to produce the on-demand pool of GABA, which enables repeated waves of phasic inhibition and experience-dependent plasticity, must have a very long developmental time course in human visual cortex. Changes in expression of $GABA_A\alpha1$ and $GABA_A\alpha2$ subunits were also prolonged and increased or decreased, respectively, into the teenage years. Comparing the balance between these subunits, however, showed that the switch from relatively more $GABA_A\alpha2$ to more $GABA_A\alpha1$ occurred during childhood. This switch is important for understanding changes in GABAergic signaling, since it is the relative balance of the $GABA_A$ subunits that influences the shift to more phasic inhibition (Prenosil et al., 2006). The current results extend our previous study that focused on synaptic changes during the first 5 years of life (Murphy et al., 2005). In addition, we found a number of changes in GABAergic signaling during aging. Gephyrin and GAD65 declined into aging, highlighting that there are both pre- and post-synaptic losses of GABAergic signaling in the aging visual cortex. The changes across the life span in expression of these components of GABA signaling undoubtedly affects experience-dependent plasticity (Hensch, 2005), development and tuning of cortical receptive fields (Leventhal et al., 2003; Fagiolini et al., 2004), and visual perception (Betts et al., 2005; Edden et al., 2009).

There is a heterogenous array of GABAergic neurons and circuits in primate visual cortex (Jones, 1993). The diversity of anatomical and physiological characteristics points to 14–19 different types of GABAergic neurons in the cortex (Gupta et al., 2000). They are spread across all layers of the cortex and in primate visual cortex the largest concentration is in layers II–III and IVa (Beaulieu et al., 1992). The $GABA_A$ receptor is also very diverse. This pentameric receptor has at least 20 different subunits, including α, β, γ, σ, ε, θ, and π, that combine to make a very wide range of different $GABA_A$ receptors (Sieghart, 1995; Cherubini and Conti, 2001; Rudolph et al., 2001). GABAergic interneurons make connections onto specific compartments of cortical pyramidal neurons. Synapses containing α-subunits are differentially distributed across pyramidal neurons with all types of α-subunits found at synapses on dendrites, $\alpha1$ and $\alpha2$ are also found on the soma, and only $\alpha2$ is on the axon initial segment. This diversity of morphologies, receptor compositions, and connectivity patterns confers a wide range of specific

functions to the different GABAergic circuits (Hensch, 2005). This heterogeneity poses a challenge for understanding the organization and function of GABAergic signaling.

The diversity in the GABAergic system introduces a number of sources of variability. We found substantial inter-individual variability for expression of the GABAergic proteins in human visual cortex and this probably reflects the heterogeneous nature of the GABAergic system. In addition, we also found substantial variability when measuring the expression levels of the GABAergic proteins from individuals. This measurement variability likely arises because the GABAergic system represents a smaller fraction of the total number of neurons and synapses in visual cortex compared to the excitatory system. This smaller sample size will contribute to increased measurement variability when quantifying GABAergic expression. For example, GABAergic signaling in primate visual cortex comprises about 20% of the total number of neurons (Beaulieu et al., 1992; Jones, 1993), and an even smaller portion (17%) of the total number of synapses (Beaulieu et al., 1992). Based on the difference in proportion of excitatory versus inhibitory synapses, statistics predicts that there should be about 4.8 times more measurement variability when quantifying expression of GABAergic synaptic proteins. This is very close to the larger measurement variability that we have found when quantifying the expression of inhibitory (gephyrin) versus excitatory (PSD-95) anchoring proteins in rat cortex (Pinto and Murphy, unpublished results). Additional variability in higher mammals will arise from inter-individual differences in the number of inhibitory synapses (Beaulieu and Colonnier, 1985), and the relatively smaller number of inhibitory synapses per neuron in primates compared with rats (Beaulieu et al., 1992). Taken together, the diversity and smaller proportion of GABAergic synapses predicts that there must be substantial variability when measuring expression of GABAergic synaptic proteins. Furthermore, previous studies suggest that there is greater synaptic specialization in non-human primates (Beaulieu et al., 1992) raising the possibility of even greater diversity in human cortex. In spite of these inherent sources of variability, our large data set makes it clear that there are significant changes in GABAergic expression in human visual cortex across the lifespan.

Monyer and Markram (2004) aptly describe studying GABAergic interneurons as a daunting task because of the diverse nature of this system. They also point out that combinatorial approaches are helping to clarify the diversity of GABAergic interneurons. In our study, we used a large number of samples from human visual cortex covering the lifespan to quantify the expression and developmental trajectories of eight components of the GABAergic system. The number of proteins quantified allowed us to capture a unique perspective on both pre- and post-synaptic development that would be missed by studying a smaller set of synaptic proteins. Furthermore, by quantifying the expression of GABAergic proteins in a preparation enriched for synaptic proteins (Hollingsworth et al., 1985; Titulaer and Ghijsen, 1997; Quinlan et al., 1999), we are able to tie the current findings closer to functional changes at the synapse. This is especially important for changes that affect experience-dependent plasticity (Quinlan et al., 1999). This contrasts with other approaches, such as measuring mRNA expression of GABAergic components (e.g., Duncan et al., 2010), because it is hard to make the link between mRNA expression and the level of protein expression at the synapse. Finally, the developmental trajectories that we describe reflect the average across the whole group of samples and this type of cross sectional design cannot address how the levels of these GABAergic markers change in an individual. The higher level of variability in expression that we found for older children through young adults suggests that the timing of rapid changes may vary across individuals.

The immunoblotting technique used for the current study does not allow for an analysis of developmental changes in the variety of different morphological types of GABAergic interneurons, specific intracortical inhibitory circuits, or locations of receptor subunits on different compartments of the post-synaptic neuron. It will be important for future studies to extend this work to include anatomical methods that describe and quantify laminar and morphological changes in GABAergic neurons, as well as tracing the specific locations of GABAergic synapses in cortical circuits. These will be challenging studies because of the difficulty obtaining postmortem tissue that is both appropriate for anatomical investigations and covers a wide range of ages. Despite these obstacles they should be a priority, especially since site-specific optimization of GABA synapses may trigger experience-dependent plasticity in visual cortex (Katagiri et al., 2007).

TRANSITIONAL STAGES IN GABAergic SIGNALING

The pattern of changes in expression of the GABAergic signaling mechanisms was complex and there was not one or two key components driving these changes. Instead, each pre- and post-synaptic mechanisms followed different developmental trajectory that combine to create a complex pattern of overall changes. The expression patterns for individual proteins can be characterized as either no change (GAD67, $GABA_A\alpha3$), a monotonic increase or decrease ($GABA_A\alpha1$, $GABA_A\alpha2$), a biphasic increase then decrease (GAD65, Gephyrin), or multiple increases and decreases (VGAT, CB1) across the lifespan. These different developmental trajectories may be linked to functional changes and the different roles that these synaptic proteins play in GABAergic signaling. For example, the multiple increases and decreases found for CB1 may reflect the multiple roles that it has in synaptic development, plasticity, and regulating GABA release (Hajos and Freund, 2002). By calculating a series of indices to quantify the balance between the various pre- and post-synaptic GABAergic mechanisms, we found three transitional stages during early development, teen years, or aging when there were large switches in the relative amounts of the components of the GABAergic signaling system. The three distinct transitional stages in GABAergic signaling reflect important times during the lifespan when there must be significant changes in the function of GABAergic inhibition. Interestingly, these transition stages line up with time points when visual functions are changing and when the visual system is sensitive to experience-dependent change (Faubert, 2002; Lewis and Maurer, 2005; Maurer et al., 2007a,b).

The first stage reflects an early developmental transition between neonates/infants (<2 years) and young children (3–5 years) when there was a switch in composition of the $GABA_A$ receptor. The relative expression switched from more of the immature subunits ($GABA_A\alpha2$ and $GABA_A\alpha3$) to more of the mature ($GABA_A\alpha1$) subunit. The $GABA_A\alpha1$ subunit has a special role in development of the visual cortex driving experience-dependent plasticity whereas $GABA_A\alpha2$ modulates neuronal firing (Fagiolini et al., 2004). The kinetics of the $GABA_A$ receptor speed up threefold when the

$GABA_A\alpha1$ subunit dominates (Gingrich et al., 1995) and gamma bursts depend on circuits dominated by $GABA_A\alpha1$ (Cardin et al., 2009; Sohal et al., 2009). Furthermore, the switch has pharmacological implications as the α2 subunit exhibits the anxiolytic effects of benzodiazepines, whereas α1, α3, and α5 mediate the sedative and amnesic effects (Rudolph et al., 1999; Löw et al., 2000). This developmental switch in $GABA_A$ receptor subunits also occurs in rats (Bosman et al., 2002), cats (Chen et al., 2001), and macaque monkeys (Hendrickson et al., 1994). For these species, however, the switch is correlated with different aspects of the critical period. In rats, the switch occurs before the start of the critical period (Heinen et al., 2004), but in cats and macaque monkeys the switch overlaps the critical period for ocular dominance plasticity (Hendrickson et al., 1994; Chen et al., 2001). The current results show that in human V1 this transitional switch in expression of $GABA_A$ receptor subunits spans the critical period, when disrupting vision can cause long lasting changing in visual acuity (Lewis and Maurer, 2005). Perhaps this first stage defines the period of ocular dominance plasticity in human V1.

In the second stage, the teenage transition was a switch from a greater capacity for trafficking GABA (more VGAT) to a greater capacity to produce the on-demand pool of GABA (more GAD65). In addition, there was a high level of $GABA_A\alpha1$ expression during this stage. These suggest that in teens and young adults the pool of on-demand GABA can be readily replenished and binds with α1 containing receptors to maintain a high level of phasic inhibition. Perhaps this combination is needed for optimal coding of neural signals, especially during periods of sustained neural activity. Optimal orientation tuning of receptive fields (Leventhal et al., 2003) and perceptual performance on orientation discrimination (Edden et al., 2009) depend on the level of GABA concentration. It seems likely that the high levels of GAD65 and $GABA_A\alpha1$ at this stage are contributing to optimal visual performance on tasks such as orientation discrimination.

In the third stage, during the transition to older adults, there were two switches in the balance between components of the GABAergic signaling system: from greater capacity to produce GABA (more GAD65) to greater capacity to traffic GABA to the synapse (more VGAT); and from relatively more post-synaptic (more Gephyrin) to more pre-synaptic (more GAD65) expression. Both of these changes were large switches from those found for young adults and point to significant changes in functioning of GABAergic synapses in the aging visual cortex. Furthermore, the time course of the GABAergic changes in aging is similar to the decline of visual abilities. The changes could contribute to the loss of orientation tuning (Leventhal et al., 2003) and processing of complex visual stimuli that are particularly vulnerable during aging (Habak and Faubert, 2000; Faubert, 2002). For example, the perception of a moving stimulus in the context of a moving surround is particularly affected in aging (Betts et al., 2005) and a loss of GABA inhibition has been suggested as the mechanism underlying this perceptual loss. It seems likely that the changes in the balance of GABAergic components at aging synapses contribute to the visual losses that accompany aging.

LINKS WITH EXPERIENCE-DEPENDENT PLASTICITY

Previous studies have shown that a specific excitatory-inhibitory balance and expression of the $GABA_A\alpha1$ subunit are required for ocular dominance plasticity in the developing rodent visual cortex (Hensch et al., 1998; Fagiolini et al., 2004). Furthermore, inhibition is abnormal in visual cortex of monocularly deprived (Burchfiel and Duffy, 1981) and strabismic cats (Singer et al., 1980). Our findings suggest that the period of ocular dominance plasticity in the human visual cortex is prolonged. If ocular dominance plasticity follows the development of $GABA_A\alpha1$ then it would extend through childhood into teenage and possibly even to young adult years. This idea is consistent with the prolonged period of visual changes found in children with cataracts (Lewis and Maurer, 2005; Maurer et al., 2007a,b). Importantly, the current findings indicate that primary visual cortex continues to have the necessary balance of GABAergic signaling mechanisms to mediate experience-dependent plasticity well into the teenage years. In addition, because the development of GAD65 expression may extend into the young adult years it is possible that this affects plasticity in primary visual cortex and contributes to visual recovery promoted by perceptual learning treatment in adults with amblyopia (Levi and Li, 2009). Finally, the losses in aging may contribute to reduced synaptic plasticity and may be part of a more generalized change in the balance of synaptic proteins (Williams et al., 2010) in the aging cortex that could underlie age-related perceptual and cognitive declines.

The prolonged window of GABA changes in human visual cortex provides an opportunity to translate experimental treatments that target GABAergic signaling in the visual system into therapeutics that may even be useful in treating amblyopia in young adults. For example, new studies have shown that fluoxetine can reinstate ocular dominance plasticity in the adult cortex by reducing intracortical inhibition (Maya Vetencourt et al., 2008; Harauzov et al., 2010). The current study provides the necessary information about GABAergic signaling in human cortex to begin the process of translating the exciting therapies being developed in animal models into effective treatments for amblyopia in humans.

ACKNOWLEDGMENTS

This research was supported by grants from NSERC and CIHR to Kathryn M. Murphy and David G. Jones. Joshua G.A. Pinto is the recipient of an OGSST PhD award.

REFERENCES

Beaulieu, C., and Colonnier, M. (1985). A laminar analysis of the number of round-asymmetrical and flat-symmetrical synapses on spines, dendritic trunks, and cell bodies in area 17 of the cat. *J. Comp. Neurol.* 231, 180–189.

Beaulieu, C., Kisvarday, Z., Somogyi, P., Cynader, M., and Cowey, A. (1992). Quantitative distribution of GABA-immunopositive and -immunonegative neurons and synapses in the monkey striate cortex (area 17). *Cereb. Cortex* 2, 295–309.

Bernard, C., Milh, M., Morozov, Y. M., Ben-Ari, Y., Freund, T. F., and Gozlan, H. (2005). Altering cannabinoid signaling during development disrupts neuronal activity. *Proc. Natl. Acad. Sci. U.S.A.* 102, 9388–9393.

Betts, L. R., Taylor, C. P., Sekuler, A. B., and Bennett, P. J. (2005). Aging reduces center-surround antagonism in visual motion processing. *Neuron* 45, 361–366.

Bosman, L. W., Rosahl, T. W., and Brussaard, A. B. (2002). Neonatal development of the rat visual cortex: synaptic function of GABAA receptor alpha subunits. *J. Physiol.* 545(Pt 1), 169–181.

Burchfiel, J. L., and Duffy, F. H. (1981). Role of intracortical inhibition in deprivation amblyopia: reversal by microiontophoretic bicuculline. *Brain Res.* 206, 479–484.

Cardin, J. A., Carlen, M., Meletis, K., Knoblich, U., Zhang, F., Deisseroth, K., Tsai, L. H., and Moore, C. I. (2009). Driving fast-spiking cells induces gamma rhythm and controls

sensory responses. *Nature* 459, 663–667.

Chen, L., Yang, C., and Mower, G. D. (2001). Developmental changes in the expression of GABA(A) receptor subunits (alpha(1), alpha(2), alpha(3)) in the cat visual cortex and the effects of dark rearing. *Brain Res. Mol. Brain Res.* 88, 135–143.

Cherubini, E., and Conti, F. (2001). Generating diversity at GABAergic synapses. *Trends Neurosci.* 24, 155–162.

Duncan, C. E., Webster, M. J., Rothmond, D. A., Bahn, S., Elashoff, M., and Weickert, C. S. (2010). Prefrontal GABA(A) receptor alpha-subunit expression in normal postnatal human development and schizophrenia. *J. Psychiatr. Res.* [Epub ahead of print].

Edden, R. A., Muthukumaraswamy, S. D., Freeman, T. C., and Singh, K. D. (2009). Orientation discrimination performance is predicted by GABA concentration and gamma oscillation frequency in human primary visual cortex. *J. Neurosci.* 29, 15721–15726.

Engel, D., Pahner, I., Schulze, K., Frahm, C., Jarry, H., Ahnert-Hilger, G., and Draguhn, A. (2001). Plasticity of rat central inhibitory synapses through GABA metabolism. *J. Physiol.* 535(Pt 2), 473–482.

Esclapez, M., Tillakaratne, N. J., Kaufman, D. L., Tobin, A. J., and Houser, C. R. (1994). Comparative localization of two forms of glutamic acid decarboxylase and their mRNAs in rat brain supports the concept of functional differences between the forms. *J. Neurosci.* 14(Pt 2), 1834–1855.

Essrich, C., Lorez, M., Benson, J. A., Fritschy, J. M., and Luscher, B. (1998). Postsynaptic clustering of major GABAA receptor subtypes requires the gamma 2 subunit and gephyrin. *Nat. Neurosci.* 1, 563–571.

Fagiolini, M., Fritschy, J. M., Low, K., Mohler, H., Rudolph, U., and Hensch, T. K. (2004). Specific GABAA circuits for visual cortical plasticity. *Science* 303, 1681–1683.

Faubert, J. (2002). Visual perception and aging. *Can. J. Exp. Psychol.* 56, 164–176.

Feldblum, S., Dumoulin, A., Anoal, M., Sandillon, F., and Privat, A. (1995). Comparative distribution of GAD65 and GAD67 mRNAs and proteins in the rat spinal cord supports a differential regulation of these two glutamate decarboxylases in vivo. *J. Neurosci. Res.* 42, 742–757.

Feldblum, S., Erlander, M. G., and Tobin, A. J. (1993). Different distributions of GAD65 and GAD67 mRNAs suggest that the two glutamate decarboxylases play distinctive functional roles. *J. Neurosci. Res.* 34, 689–706.

Gingrich, K. J., Roberts, W. A., and Kass, R. S. (1995). Dependence of the GABAA receptor gating kinetics on the alpha-subunit isoform: implications for structure-function relations and synaptic transmission. *J. Physiol.* 489(Pt 2), 529–543.

Guo, Y., Kaplan, I. V., Cooper, N. G., and Mower, G. D. (1997). Expression of two forms of glutamic acid decarboxylase (GAD67 and GAD65) during postnatal development of the cat visual cortex. *Brain Res. Dev. Brain Res.* 103, 127–141.

Gupta, A., Wang, Y., and Markram, H. (2000). Organizing principles for a diversity of GABAergic interneurons and synapses in the neocortex. *Science* 287, 273–278.

Habak, C., and Faubert, J. (2000). Larger effect of aging on the perception of higher-order stimuli. *Vision Res.* 40, 943–950.

Hajos, N., and Freund, T. F. (2002). Distinct cannabinoid sensitive receptors regulate hippocampal excitation and inhibition. *Chem. Phys. Lipids* 121, 73–82.

Harauzov, A., Spolidoro, M., DiCristo, G., De Pasquale, R., Cancedda, L., Pizzorusso, T., Viegi, A., Berardi, N., and Maffei, L. (2010). Reducing intracortical inhibition in the adult visual cortex promotes ocular dominance plasticity. *J. Neurosci.* 30, 361–371.

Heinen, K., Bosman, L. W., Spijker, S., van Pelt, J., Smit, A. B., Voorn, P., Baker, R. E., and Brussaard, A. B. (2004). GABAA receptor maturation in relation to eye opening in the rat visual cortex. *Neuroscience* 124, 161–171.

Hendrickson, A., March, D., Richards, G., Erickson, A., and Shaw, C. (1994). Coincidental appearance of the alpha 1 subunit of the GABA-A receptor and the type I benzodiazepine receptor near birth in macaque monkey visual cortex. *Int. J. Dev. Neurosci.* 12, 299–314.

Hendry, S. H., Huntsman, M. M., Viñuela, A., Möhler, H., de Blas, A. L., and Jones, E. G. (1994). GABAA receptor subunit immunoreactivity in primate visual cortex: distribution in macaques and humans and regulation by visual input in adulthood. *J. Neurosci.* 14, 2383–2401.

Hensch, T. K. (2005). Critical period mechanisms in developing visual cortex. *Curr. Top. Dev. Biol.* 69, 215–237.

Hensch, T. K., and Fagiolini, M. (2005). Excitatory-inhibitory balance and critical period plasticity in developing visual cortex. *Prog. Brain Res.* 147, 115–124.

Hensch, T. K., Fagiolini, M., Mataga, N., Stryker, M. P., Baekkeskov, S., and Kash, S. F. (1998). Local GABA circuit control of experience-dependent plasticity in developing visual cortex. *Science* 282, 1504–1508.

Hollingsworth, E. B., McNeal, E. T., Burton, J. L., Williams, R. J., Daly, J. W., and Creveling, C. R. (1985). Biochemical characterization of a filtered synaptoneurosome preparation from guinea pig cerebral cortex: cyclic adenosine 3′:5′-monophosphate-generating systems, receptors, and enzymes. *J. Neurosci.* 5, 2240–2253.

Hornung, J. P., and Fritschy, J. M. (1996). Developmental profile of GABAA-receptors in the marmoset monkey: expression of distinct subtypes in pre- and postnatal brain. *J. Comp. Neurol.* 367, 413–430.

Iwai, Y., Fagiolini, M., Obata, K., and Hensch, T. K. (2003). Rapid critical period induction by tonic inhibition in visual cortex. *J. Neurosci.* 23, 6695–6702.

Jiang, B., Huang, S., de Pasquale, R., Millman, D., Song, L., Lee, H., Tsumoto, T., and Kirkwood, A. (2010). The maturation of GABAergic transmission in the visual cortex requires endocannabinoid-mediated LTD of inhibitory inputs during a critical period. *Neuron* 66, 248–259.

Jones, E. G. (1993). GABAergic neurons and their role in cortical plasticity in primates. *Cereb. Cortex* 3, 361–372.

Katagiri, H., Fagiolini, M., and Hensch, T. K. (2007). Optimization of somatic inhibition at critical period onset in mouse visual cortex. *Neuron* 53, 805–812.

Kirkwood, A., and Bear, M. F. (1994). Hebbian synapses in visual cortex. *J. Neurosci.* 14(Pt 2), 1634–1645.

Kneussel, M., Brandstatter, J. H., Laube, B., Stahl, S., Muller, U., and Betz, H. (1999). Loss of postsynaptic GABA(A) receptor clustering in gephyrin-deficient mice. *J. Neurosci.* 19, 9289–9297.

Laurie D. J., Wisden W., and Seeburg P. H. (1992). The distribution of thirteen GABAA receptor subunit mRNAs in the rat brain. III. Embryonic, and postnatal development. *J. Neurosci.* 12, 4151–4172.

Law, A. J., Weickert, C. S., Webster, M. J., Herman, M. M., Kleinman, J. E., and Harrison, P. J. (2003). Expression of NMDA receptor NR1, NR2A and NR2B subunit mRNAs during development of the human hippocampal formation. *Eur. J. Neurosci.* 18, 1197–1205.

Leventhal, A. G., Wang, Y., Pu, M., Zhou, Y., and Ma, Y. (2003). GABA and its agonists improved visual cortical function in senescent monkeys. *Science* 300, 812–815.

Levi, D. M., and Li, R. W. (2009). Perceptual learning as a potential treatment for amblyopia: a mini-review. *Vision Res.* 49, 2535–2549.

Lewis, T. L., and Maurer, D. (2005). Multiple sensitive periods in human visual development: evidence from visually deprived children. *Dev. Psychobiol.* 46, 163–183.

Löw, K., Crestani, F., Keist, R., Benke, D., Brünig, I., Benson, J. A., Fritschy, J. M., Rülicke, T., Bluethmann, H., Möhler, H., and Rudolph, U. (2000). Molecular and neuronal substrate for the selective attenuation of anxiety. *Science* 290, 131–134.

Maffei, A., Nelson, S. B., and Turrigiano, G. G. (2004). Selective reconfiguration of layer 4 visual cortical circuitry by visual deprivation. *Nat. Neurosci.* 7, 1353–1359.

Maurer, D., Mondloch, C. J., and Lewis, T. L. (2007a). Effects of early visual deprivation on perceptual and cognitive development. *Prog. Brain Res.* 164, 87–104.

Maurer, D., Mondloch, C. J., and Lewis, T. L. (2007b). Sleeper effects. *Dev. Sci.* 10, 40–47.

Maya Vetencourt, J. F., Sale, A., Viegi, A., Baroncelli, L., De Pasquale, R., O'Leary, O. F., Castren, E., and Maffei, L. (2008). The antidepressant fluoxetine restores plasticity in the adult visual cortex. *Science* 320, 385–388.

McIntire, S. L., Reimer, R. J., Schuske, K., Edwards, R. H., and Jorgensen, E. M. (1997). Identification and characterization of the vesicular GABA transporter. *Nature* 389, 870–876.

Minelli, A., Alonso-Nanclares, L., Edwards, R. H., DeFelipe, J., and Conti, F. (2003). Postnatal development of the vesicular GABA transporter in rat cerebral cortex. *Neuroscience* 117, 337–346.

Monyer, H., and Markram, H. (2004). Interneuron diversity series: molecular and genetic tools to study GABAergic interneuron diversity and function. *Trends Neurosci.* 27, 90–97.

Murphy, K. M., Beston, B. R., Boley, P. M., and Jones, D. G. (2005). Development of human visual cortex: a balance between excitatory and inhibitory plasticity mechanisms. *Dev. Psychobiol.* 46, 209–221.

Pinto, J. A. G., Hornby, K. R., Jones, D. G., and Murphy, K. M. (2008). "Developmental changes in GABAergic inhibitory mechanisms in human primary visual cortex," in *International Society for Developmental Neuroscience Meeting*, 1–4 June 2008, Asilomar, CA.

Prenosil, G. A., Schneider Gasser, E. M., Rudolph, U., Keist, R., Fritschy, J. M., and Vogt, K. E. (2006). Specific subtypes of GABAA receptors mediate phasic and tonic forms of inhibition in hippocampal pyramidal neurons. *J. Neurophysiol.* 96, 846–857.

Pritchett, D. B., Sontheimer, H., Shivers, B. D., Ymer, S., Kettenmann, H.,

Schofield, P. R., and Seeburg, P. H. (1989). Importance of a novel GABAA receptor subunit for benzodiazepine pharmacology. *Nature* 338, 582–585.

Quinlan, E. M., Olstein, D. H., and Bear, M. F. (1999). Bidirectional, experience-dependent regulation of N-methyl-D-aspartate receptor subunit composition in the rat visual cortex during postnatal development. *Proc. Natl. Acad. Sci. U.S.A.* 96, 12876–12880.

Rudolph, U., Crestani, F., Benke, D., Brünig, I., Benson, J. A., Fritschy, J. M., Martin, J. R., Bluethmann, H., and Möhler, H. (1999). Benzodiazepine actions mediated by specific gamma-aminobutyric acid (A) receptor subtypes. *Nature* 401, 796–800.

Rudolph, U., Crestani, F., and Möhler, H. (2001). GABA(A) receptor subtypes: dissecting their pharmacological functions. *Trends Pharmacol. Sci.* 22, 188–194.

Sagne, C., El Mestikawy, S., Isambert, M. F., Hamon, M., Henry, J. P., Giros, B., and Gasnier, B. (1997). Cloning of a functional vesicular GABA and glycine transporter by screening of genome databases. *FEBS Lett.* 417, 177–183.

Sengpiel, F., and Vorobyov, V. (2005). Intracortical origins of interocular suppression in the visual cortex. *J. Neurosci.* 25, 6394–6400.

Shaw, C., Cameron, L., March, D., Cynader, M., Zielinski, B., and Hendrickson, A. (1991). Pre- and postnatal development of GABA receptors in *Macaca* monkey visual cortex. *J. Neurosci.* 11, 3943–3959.

Sieghart, W. (1995). Structure and pharmacology of gamma-aminobutyric acid A receptor subtypes. *Pharmacol. Rev.* 47, 181–232.

Sigel, E. (2002). Mapping of the benzodiazepine recognition site on GABA(A) receptors. *Curr. Top. Med. Chem.* 2, 833–839.

Singer, W., von Grünau, M., and Rauschecker, J. (1980). Functional amblyopia in kittens with unilateral exotropia. I. Electrophysiological assessment. *Exp. Brain Res.* 40, 294–304.

Sjöström, P. J., Turrigiano, G. G., and Nelson, S. B. (2003). Neocortical LTD via coincident activation of presynaptic NMDA and cannabinoid receptors. *Neuron* 39, 641–654.

Smith, G. B., and Olsen, R. W. (1995). Functional domains of GABAA receptors. *Trends Pharmacol. Sci.* 16, 162–168.

Sohal, V. S., Zhang, F., Yizhar, O., and Deisseroth, K. (2009). Parvalbumin neurons and gamma rhythms enhance cortical circuit performance. *Nature* 459, 698–702.

Titulaer, M. N., and Ghijsen, W. E. (1997). Synaptoneurosomes. A preparation for studying subhippocampal GABAA receptor activity. *Methods Mol. Biol.* 72, 49–59.

Tsumoto, T., and Sato, H. (1985). GABAergic inhibition and orientation selectivity of neurons in the kitten visual cortex at the time of eye opening. *Vision Res.* 25, 383–388.

Williams, K., Irwin, D. A., Jones, D. G., and Murphy, K. M. (2010). Dramatic loss of Ube3A expression during aging of the mammalian cortex. *Front. Aging Neurosci.* 2:18. doi: 10.3389/fnagi.2010.00018.

Conflict of Interest Statement: The authors declare that the research was conducted in the absence of any commercial or financial relationships that could be construed as a potential conflict of interest.

Received: 06 February 2010; paper pending published: 28 March 2010; accepted: 26 April 2010; published online: 10 June 2010.

*Citation: Pinto JGA, Hornby KR, Jones DG and Murphy KM (2010) Developmental changes in GABAergic mechanisms in human visual cortex across the lifespan. Front. Cell. Neurosci. **4**:16. doi: 10.3389/fncel.2010.00016*

frontiers in
CELLULAR NEUROSCIENCE

ORIGINAL RESEARCH ARTICLE
published: 21 June 2010
doi: 10.3389/fncel.2010.00015

Contribution of GABAergic interneurons to the development of spontaneous activity patterns in cultured neocortical networks

Thomas Baltz, Ana D. de Lima and Thomas Voigt*

Institute of Physiology, Otto-von-Guericke-University Magdeburg, Magdeburg, Germany

Edited by:
Yehezkel Ben-Ari, Institut National de la Santé et de la Recherche Médicale, France

Reviewed by:
Rustem Khazipov, Institut National de la Santé et de la Recherche Médicale, France
Yehezkel Ben-Ari, Institut National de la Santé et de la Recherche Médicale, France

****Correspondence:***
Thomas Voigt, Institut für Physiologie, Medizinische Fakultät, Otto-von-Guericke-University, Leipziger Str. 44, D-39120 Magdeburg, Germany.
e-mail: thomas.voigt@med.ovgu.de

Periodic synchronized events are a hallmark feature of developing neuronal networks and are assumed to be crucial for the maturation of the neuronal circuitry. In the developing neocortex, the early network oscillations coincide with an excitatory action of the neurotransmitter gamma-aminobutyric acid (GABA). A relationship between the emerging inhibitory action of GABA and the gradual disappearance of early synchronized network activity has been previously suggested. Therefore we investigate the interplay between the action of GABA and spontaneous activity in cultured networks of the lateral or dorsal embryonic rat neocortex, which show considerable difference in the content of GABAergic neurons. Here we present the results of long-term monitoring of spontaneous electrical activity of cultured networks growing on microelectrode arrays and the time course of changes in GABA action using calcium imaging. All cultures studied displayed stereotyped synchronized burst events at the end of the first week *in vitro*. As the $GABA_A$ depolarizing action decreases, naturally or after bumetanide treatment, network activity in lateral cortex cultures changed from stereotypic bursting to more clustered and asynchronous activity patterns. Dorsal cortex cultures and cultures lacking $GABA_A$-receptor mediated synaptic transmission, retained an immature synchronous firing pattern, but developed prominent intraburst oscillations (~3–10 Hz). Large, mostly parvalbumin positive, GABAergic neurons dominate the GABAergic population in lateral cortex cultures. These large interneurons were virtually absent in dorsal cortex cultures. Based on these results, we suggest that the richly interconnected large GABAergic neurons contribute to desynchronize and temporally differentiate the spontaneous activity of cultured cortical networks.

Keywords: MEA, gamma-aminobutyric acid, neocortex, cerebral cortex, oscillations, network activity, rat, cell culture

INTRODUCTION

The electrical activity of immature neuronal networks is characterized by recurrent correlated activity, which has been observed in many structures and experimental conditions (O'Donovan, 1999; Ben-Ari, 2001; Blankenship and Feller, 2010), including the cerebral cortex *in vivo* (Chiu and Weliky, 2001; Minlebaev et al., 2007; Yang et al., 2009), in slices (Garaschuk et al., 2000; McCabe et al., 2006; Allene et al., 2008) and in culture preparations (Kamioka et al., 1996; Opitz et al., 2002; Giugliano et al., 2004; Van Pelt et al., 2004; Chiappalone et al., 2006; Eytan and Marom, 2006; Wagenaar et al., 2006a; Pasquale et al., 2008). The slow synchronous oscillatory activity has functional relevance during the formation of connections within the network (Ben-Ari, 2002; Owens and Kriegstein, 2002; Angenstein et al., 2004; Voigt et al., 2005; Ben-Ari et al., 2007).

GABAergic signaling and therefore gamma-aminobutyric acid (GABA) interneurons play an important role in the generation of spontaneous network oscillations in the developing neocortex and hippocampus (Moody and Bosma, 2005; Ben-Ari et al., 2007). Specifically, the emergence of early network activity in hippocampal slices depends on depolarizing action of GABA (Ben-Ari, 2001). The highly synchronous network activity recorded in acute cortical slices [cortical early network oscillations (cENOs)] is apparently not dependent on GABAergic drive (Garaschuk et al., 2000; Allene et al., 2008), but the developmental shift of GABAergic signaling has been postulated to induce their gradual disappearance (Garaschuk et al., 2000), with the subsequent appearance of a GABA-driven pattern [cortical giant depolarizing potentials (cGDPs)] with higher frequency and lower synchronization (Allene et al., 2008).

In a recent study Lischalk et al. (2009) suggest that temporal areas of the cortex function as pacemakers for the early network transients, which then propagate to the rest of the cortex (see also Garaschuk et al., 2000). Interestingly, lateral and dorsal regions of the cortex embryo differ in the developmental properties of their early neurons (Bellion et al., 2003). While lateral cortex explants hold GABAergic neurons with migrating characteristics of the ganglionic eminence lineage (Marin and Rubenstein, 2001; Wonders and Anderson, 2006), the dorsal cortex differentiates small bipolar GABAergic neurons, possibly of cortical origin, which migrated along axons *in vitro* (Letinic et al., 2002; Bellion et al., 2003). Because GABAergic neurons of different lineages also develop distinct physiological features (Butt et al., 2005; Batista-Brito and Fishell, 2009), neurons of the lateral cortex might form networks with physiological features and development different from those of dorsal cortex cultures. This leads to the question if the pacemaker function of the temporal cortex could be mediated by a unique development of the GABAergic circuitry. This is of interest because,

first, the immature network patterns (cENOs) recorded in slices of the cerebral cortex occur in absence of GABAergic signaling (Garaschuk et al., 2000; Allene et al., 2008). Secondly, although cultured networks have been extensively used as models for cortical network studies (Feinerman et al., 2007; Le et al., 2007; Rolston et al., 2007; Bakkum et al., 2008; Baruchi et al., 2008; Chao et al., 2008; Pasquale et al., 2008; Raichman and Ben-Jacob, 2008; Shahaf et al., 2008), generating cultured cortical networks with a predictable activity pattern development has been difficult (Wagenaar et al., 2006a). Finally, although early synchronized network activity is described as extremely robust behavior, due to homeostatic regulation of intrinsic features (Marder and Goaillard, 2006; Blankenship and Feller, 2010), the limits of homeostasis might be reached along maturation if the local circuitry is abnormally constructed. In fact, many developmental neuropathologies show both network oscillations abnormalities and alterations of interneuronal circuitry (Chagnac-Amitai and Connors, 1989; Lewis et al., 2005; Sudbury and Avoli, 2007; Gonzalez-Burgos and Lewis, 2008; Rheims et al., 2008; Uhlhaas et al., 2008).

In the present study we compared the early synchronized activity of neocortical cultures generated from the lateral or dorsal embryonic rat cortex growing on substrate integrated micro-electrode arrays (MEAs). Additionally, we asked if developmental alterations of the network activity are correlated with the GABA shift (Rivera et al., 2005; Blaesse et al., 2009) and if they are modified by the $GABA_A$ receptor ($GABA_AR$) signaling or by the structure of the GABAergic network. We show that the development of a variable, less synchronized burst activity correlates with the gradual maturation of $GABA_AR$ signaling and depends on the presence of large GABAergic neurons with widespread connections in cultured networks.

MATERIALS AND METHODS

CELL CULTURE

Monolayer neuronal cultures were prepared from cerebral cortices of Sprague Dawley rats at embryonic day E16 (day after insemination was E1; birth = E22). We plated cells either on Petri dishes or on microelectrode arrays (see below). To keep culture conditions between MEA and Petri dish cultures as close as possible, these cultures were derived from the same preparations (i.e., sister cultures). All experimental procedures were approved by local government (Landesverwaltungsamt Halle, Germany).

Petri dish cultures

For Petri dish cultures each plasma cleaned (Harrick Plasma, Ithaca, NY, USA) cover slip was fitted to a 20-mm hole in the bottom of a 60-mm Petri dish. A 30-mm acrylic glass ring was glued with silicon grease around the hole, to restrict the culture size and the volume of necessary media. The cover slips were treated overnight with poly-D-lysine (0.1 mg/ml in borate buffer, pH 8.5, 36°C). Astroglial cultures were prepared from cerebral hemispheres of P0-P3 Sprague Dawley rats as reported in detail previously (de Lima and Voigt, 1999). Purified astroglial cells were plated in the inner portion of the Petri dish (500 cells/mm^2 inside the acrylic glass ring) 5 days before the neurons. The astroglia has neurotrophic effects and strongly reduces cell proliferation in culture (Schmalenbach and Müller, 1993; de Lima and Voigt, 1999). We used upper (dCtx) and lateral portions (vCtx) of the dorsal telencephalic vesicles (excluding hippocampal and basal telencephalic anlagen) as neuronal donor tissue for the two distinct culture types. Neurons for dCtx and vCtx cultures were dissected from the dorsal and lateral aspects of the presumptive dorsal pallium domain (Puelles and Rubenstein, 2003). Both donor regions were clearly situated above the pallial/subpallial boundary (Campbell, 2003). The dorsal cortex, used as donor for dCtx cultures, included the whole antero-posterior extension of the sensorimotor neocortical anlage. The lateral side of the dorsal pallium, used as donor for vCtx cultures, included also temporal cortical areas and prospective limbic subdivisions, i.e., perirhinal, entorhinal and insular cortices (Barbe and Levitt, 1991; Ferri and Levitt, 1995; Bellion et al., 2003). Similar to explants of the mouse cortex (Bellion et al., 2003; Bellion and Metin, 2005), networks derived from the dorsal and lateral regions of the rat embryonic cortex showed differences in their GABAergic neuronal populations (see Results).

The neocortical tissue was dissociated with trypsin/EDTA and seeded onto the poly-D-lysine coated glass cover slips in N2 medium (75% DMEM, 25% Ham's F12, and N2 supplement; Invitrogen, Carlsbad, CA, USA). All cultures were maintained in a humidified 5% CO2/95% air atmosphere at 36°C.

MEA cultures

After plasma cleaning, each MEA dish was treated with poly-D-lysine, followed by the same glial and neuronal culture procedures as described above. Cells were seeded at densities ranging from 800 to 1300 cells/mm^2, but the same density was used for different culture types within a preparation. No differences were observed in electrical activity patterns (i.e., irregular vs. regular bursting, see Results) among preparations within the cell density range used. The culture chamber was sealed by a screw cap to prevent infection and evaporation. Within the incubator the cap was loosened to allow gas circulation. Some MEA cultures were raised in the presence of the specific $GABA_AR$ blocker gabazine (20 μM), added 3 h after plating.

MEA RECORDING AND DATA ANALYSIS

Recording of electrical activity was carried out by using microelectrode arrays [MEAs, Multi Channel Systems (MCS), Reutlingen, Germany] with 59 substrate embedded titanium nitride recording electrodes, arranged in a 10 × 6 rectangular array with one electrode missing in the first column. The electrodes, 30 μm in diameter, had an inter-electrode distance (center to center) of 500 μm. Signals were amplified 1100× and sampled at 25 kHz using a preamplifier (MEA1060-Inv-BC) and data acquisition card (both MCS). The spontaneous activity of individual cultures was monitored at 36°C for 20 min/day *in vitro* using MC_Rack software (MCS) at different stages of development (usually every 1–3 days, starting at 5 DIV) until at least 3 weeks after plating (i.e., ≥21 DIV). Recordings for different culture conditions (e.g., vCtx and dCtx cultures) within a preparation were always age-matched.

Spike detection

Spikes were detected on-line on the band-pass filtered (0.15–3.5 kHz) signal, using a threshold of −5× standard deviation from background noise. Spike waveforms were stored and analyzed

off-line. Overlapping spike waveforms were commonly seen during bursts, supposedly due to high action potential firing of several cells near a particular electrode. Given that the cells rarely fired between bursts, automatic spike sorting procedures were less reliable. Spike sorting was therefore not attempted in the present study.

Data processing

Custom written MATLAB (version 2007b, MathWorks, Natick, USA) programs were used for off-line analysis. Different parameters (e.g., burst frequency, see below) were extracted from 20-min recordings. We divided the recordings in three distinct age groups, following developmental properties, i.e., the change in GABAergic synaptic transmission [before (5–10 DIV), during (11–17 DIV), and after (18–24 DIV) the GABA shift]. Generally, evaluated parameters for a given culture condition and age varied more between different preparations than between sister cultures (i.e., within a preparation) (see also Wagenaar et al., 2006a). Therefore, for each age and preparation the data was normalized by the mean of untreated vCtx networks and ultimately pooled for the different preparations. However, absolute datasets are given in **Tables 1 and 2**.

Burst detection

Recurrent population burst is the most common activity pattern seen in developing cortical networks (Robinson et al., 1993; Maeda et al., 1995; Voigt et al., 2001; Marom and Shahaf, 2002; Opitz et al., 2002; Wagenaar et al., 2006a). The preposition 'population' indicates that the activity of several, up to all, neurons in the network is modulated in synchrony into a 'burst state', whereas individual spikes are not necessarily synchronized (see **Figure 2**, for example). If not otherwise stated, such population bursts are simply called bursts. More precisely, we define bursts as transient episodes of repetitive spiking >400 ms apart, which show some distribution across the network. The detection of burst then was accomplished by a top-down heuristic approach as follows. We first merged the spike times of all 59 electrodes onto a single virtual electrode, which accordingly contained all spike times for a given recording. We then searched on this virtual electrode for clusters of spikes with a maximal inter spike interval of 60 ms. If a cluster included at least 30 spikes and was a result of spikes detected on at least three electrodes, a burst was defined. The contribution of an electrode to a burst was assessed to be significant when at least three spikes were detected. This approach reliably detected bursts in our datasets, even in young cultures where the spike frequency during bursts was relatively low. The following parameters were quantified: the frequency of burst discharges, the coefficient of variation of the interburst interval (CV IBI), and the number of electrodes with spiking activity during bursts ('electrode attendance'). The latter was used as a measurement for the distribution of the activity through the network, i.e., synchronization of the bursts discharges along the electrode array.

CALCIUM IMAGING

We used calcium imaging to investigate developmental changes in $GABA_A$R mediated synaptic transmission (Chen et al., 1996; Owens et al., 1996; Ganguly et al., 2001). Petri dish cultures were incubated in 5 μM fluo-3 pentacetoxy-methylester (Molecular Probes; purchased from MoBiTec, Goettingen, Germany) dissolved in DMSO (Molecular Probes, Eugene, OR, USA) for 1 h, followed by several washes with artificial cerebrospinal fluid (aCSF). The ionic composition of the aCSF was (mM): 140 NaCl, 5 KCl, 1.5 $CaCl_2$, 0.75 $MgCl_2$, 1.25 NaH_2PO_4, 20 D-glucose and 15 HEPES/NaOH (pH 7.4), and resembled the main components of the N2 culture medium except the pH buffering system (HEPES vs. bicarbonate). The culture dishes were transferred to an inverted microscope (Axiovert S100 TV, Zeiss, Oberkochen, Germany) equipped with a charge-coupled device camera (Cool Snap ES, Visitron Systems, Puchheim,

Table 1 | All values are mean ± SEM of values pooled from different cultures. See **Figure 8** for number of experiments, cultures and preparations.

Network	vCtx control			vCtx blocked		
Age (DIV)	5–10	11–17	18–24	5–10	11–17	18–24
Burst frequency (Hz)	0.010 ± 0.001	0.045 ± 0.006	0.200 ± 0.016	0.009 ± 0.001	0.029 ± 0.004	0.048 ± 0.003
Total spike frequency (Hz)	7.86 ± 1.30	54.27 ± 7.22	117.28 ± 12.13	5.97 ± 0.98	49.21 ± 5.06	129.57 ± 9.92
Burst duration (ms)	1431.35 ± 74.49	1348.78 ± 66.29	1078.71 ± 80.42	1110.92 ± 40.25	993.64 ± 53.10	1718.29 ± 127.29
CV IBI	0.39 ± 0.04	0.49 ± 0.05	2.39 ± 0.22	0.34 ± 0.04	0.39 ± 0.02	0.29 ± 0.04
Mean electrodes in bursts	15.35 ± 1.52	29.81 ± 1.18	23.04 ± 1.39	13.06 ± 1.72	36.66 ± 1.27	42.38 ± 1.70
Max electrodes in bursts	18.13 ± 1.57	38.15 ± 1.49	41.30 ± 2.34	15.46 ± 1.82	40.00 ± 1.20	45.44 ± 1.80

Table 2 | All values are mean ± SEM of values pooled from different cultures. See **Figure 11** for number of experiments, cultures and preparations.

Network	vCtx			dCtx		
Age (DIV)	5–10	11–17	18–24	5–10	11–17	18–24
Burst frequency (Hz)	0.001 ± 0.001	0.045 ± 0.004	0.213 ± 0.012	0.002 ± 0.0004	0.018 ± 0.002	0.065 ± 0.005
Total spike frequency (Hz)	5.95 ± 0.88	48.07 ± 5.14	143.06 ± 11.87	2.92 ± 0.56	21.36 ± 1.89	58.19 ± 5.64
Burst duration (ms)	1172.56 ± 62.19	1336.04 ± 43.24	961.61 ± 51.96	1349.75 ± 46.36	1233.94 ± 27.20	1031.02 ± 52.75
CV IBI	0.37 ± 0.02	0.42 ± 0.03	1.90 ± 0.16	0.40 ± 0.05	0.38 ± 0.03	0.43 ± 0.05
Mean electrodes in bursts	13.96 ± 1.22	26.30 ± 1.9	24.68 ± 1.28	16.78 ± 0.92	27.26 ± 1.09	30.38 ± 1.65
Max electrodes in bursts	16.58 ± 1.30	33.12 ± 1.53	40.43 ± 1.79	17.65 ± 0.96	31.32 ± 1.15	35.53 ± 1.6

Germany) and allowed to equilibrate for 20 min, a time when de-esterification of the dye takes place. Recording fields (usually 890 × 665 μm², 5–10 for each culture dish) were chosen randomly and sometimes marked with a diamond tool when repeated imaging was required. Fluorescence images were obtained with a frequency of 2 Hz during 90-s-long sessions using MetaMorph 7.0 software (Universal Imaging Corp., West Chester, PA, USA). Excitation wavelength was 470 ± 20 nm (Chroma Technology, Brattleboro, VT, USA). A differential interference contrast (DIC) image of each field was also acquired for later cell identification. During each recording session cells were locally perfused with an aCSF containing either high potassium (KCl, 60 mM) or the $GABA_A$R agonist muscimol (200 μM) using a multibarreled perfusion system. The local application lasted 2 s, resembling prolonged activation as during population burst activity. In young cultures muscimol elicits a large intracellular calcium response in many neurons (see Results), which was blocked by simultaneous application of high concentrations of the $GABA_A$R antagonist gabazine (200–400 μM) (not shown). A second application of high potassium served as a control against possible bleaching of the dye during the recording session. Time points of pharmacological application are indicated by bars in **Figure 4B**. Images were processed off-line using MetaMorph software and custom written MATLAB programs. We calculated the maximal emitted fluorescence in response to local pharmacological application for each cell. These values were called F_{K1}, F_M and F_{K2} (a.u.) (see **Figure 4B**). The trace (ΔF) then was normalized with respect to F_{K1} ($F_N = \Delta F/F_{K1}$). A cell was considered responsive to muscimol if the change of the normalized fluorescence (F_N) was larger than an empirically determined threshold ($F_N/dt \geq 0.05$). Using the change in fluorescence, rather than F_M itself, rules out false positive detection in case a cell showed very slow recovery from the preceding potassium application (this was observed rarely). All imaging experiments were carried out in the presence of glutamatergic blockers [D(−)-AP-5 12.5 μM, 6-cyano-7-nitroquinoxaline-2,3-dione disodium (CNQX) 2.5 μM], to suppress the spontaneous bursting.

DRUGS AND DRUG APPLICATION

All drugs were dissolved to 100–1000× stocks, stored at −20°C, and diluted to final concentration just before application. We purchased 5-aminomethyl-3-hydroxyisoxazole hydrobromide (muscimol) and (−)-bicuculline methiodide (bicuculline) from RBI (RBI/Sigma, Deisenhofen, Germany), and D-2-amino-5-phosphonopentanoic acid (D(−)-AP-5), 6-imino-3-(4-methoxyphenyl)-1(6*H*)-pyridazinebutanoic acid hydrobromide (gabazine) and CNQX and 3-(aminosulfonyl)-5-(butylamino)-4-phenoxybenzoic acid (bumetanide) from Tocris Cookson (Biotrend, Cologne, Germany). Drugs were applied either directly from the stocks in case of MEA recordings or via a magnetic valve controlled gravity-fed perfusion system (ALA Scientific Instruments, New York, NY, USA) during the calcium imaging experiments.

IMMUNOCYTOCHEMISTRY

GABA immunocytochemistry was carried out as described previously (de Lima and Voigt, 1997, 1999; Voigt et al., 2001; de Lima et al., 2007). Briefly, Petri dish cultures were fixed for 30 min at 36°C by adding 70% glutaraldehyde to the culture medium to make a final concentration of 3.5%. Aldehyde-fixed cultures were then thoroughly washed in 0.05 M Tris buffer containing 0.85% sodium metabisulfite (pH 7.5), and preincubated for 3 h at room temperature with 3% bovine serum albumin, 10% normal goat serum and 0.6% Triton X-100 in Tris/metabisulfite solution. After washing, successive antibody incubations were performed: mouse anti-GABA (Chemicon, Temecula, CA, USA; 1:200) in Tris/metabisulfite solution containing 3% bovine serum albumin, 10% normal goat serum, 0.6% Triton X-100 overnight at room temperature; goat anti-mouse and mouse peroxidase-anti-peroxidase (1:200 in PBS containing 10% normal goat serum, 2% bovine serum albumin, 5% sucrose and 0.3% Triton X-100, 2 h, room temperature, Sternberger, Baltimore, MD, USA). After the primary antibodies, all washes were performed with PBS (0.1 M, pH 7.4). Peroxidase-anti-peroxidase antibody complexes were made visible by incubating with a solution containing 0.01% 3,3′-diaminobenzidine tetrahydrochloride, 0.004% H_2O_2, 1% nickel ammonium sulfate and 50 mM imidazole in 50 mM Tris–HCl saline buffer. After a final PBS wash, coverslips were dehydrated in an ethanol series, cleared in two changes of xylene and mounted over clean slides with Fluoromount (BDH Laboratory Supplies, Poole, UK).

For double-immunofluorescence labeling, coverslips were fixed with 4% paraformaldehyde and 0.005% glutaraldehyde (20 min, 36°C). GABA immunocytochemistry was performed as described above, except that anti-mouse-Cy3 (1:400; Jackson ImmunoResearch, Dianova, Hamburg) was used as secondary antibody. After washing, coverslips were fixed again with 4% paraformaldehyde and stained for parvalbumin (polyclonal rabbit anti-parvalbumin, 1:5000, Swant, Bellinzona) followed by anti-rabbit-Cy2 (1:400; Jackson ImmunoResearch). Coverslips were shortly dehydrated and embedded with Fluoromount. Only cells with an intense GABA staining of soma and dendrites were considered for the analysis.

To estimate the density of GABAergic cells we counted GABA positive neurons at 200× magnification using bright field microscopy with the aid of a grid in the microscope eyepiece on an inverse microscope equipped with a CCD camera (Axiophot, Zeiss, Oberkochen, Germany) (12 fields per cover slip, chosen at regularly spaced points over the cover slip surface). For each field the total cell number was counted at 400× magnification and phase contrast optics. We also quantified the overall intensity of GABAergic staining by taking digital images and computing the average luminance for each image. The data obtained from vCtx and dCtx cultures were normalized by the mean luminance of all dCtx cultures (see Results). All images were taken on the same day and microscope; no contrast or brightness correction was made. Cell soma size was estimated using 400× magnification with the aid of MetaMorph software.

RESULTS

First we describe the development of spontaneous activity in lateral cortex networks (vCtx) in control conditions (**Figures 1 and 2A**). Then we compare this development (a) with the spontaneous activity development of similar vCtx networks chronically blocked with a $GABA_A$R antagonist (**Figures 2B, 7 and 8**, **Table 1**), and (b) with the spontaneous activity development of dorsal cortex networks (dCtx), grown in control conditions (**Figures 9–11**, **Table 2**). The

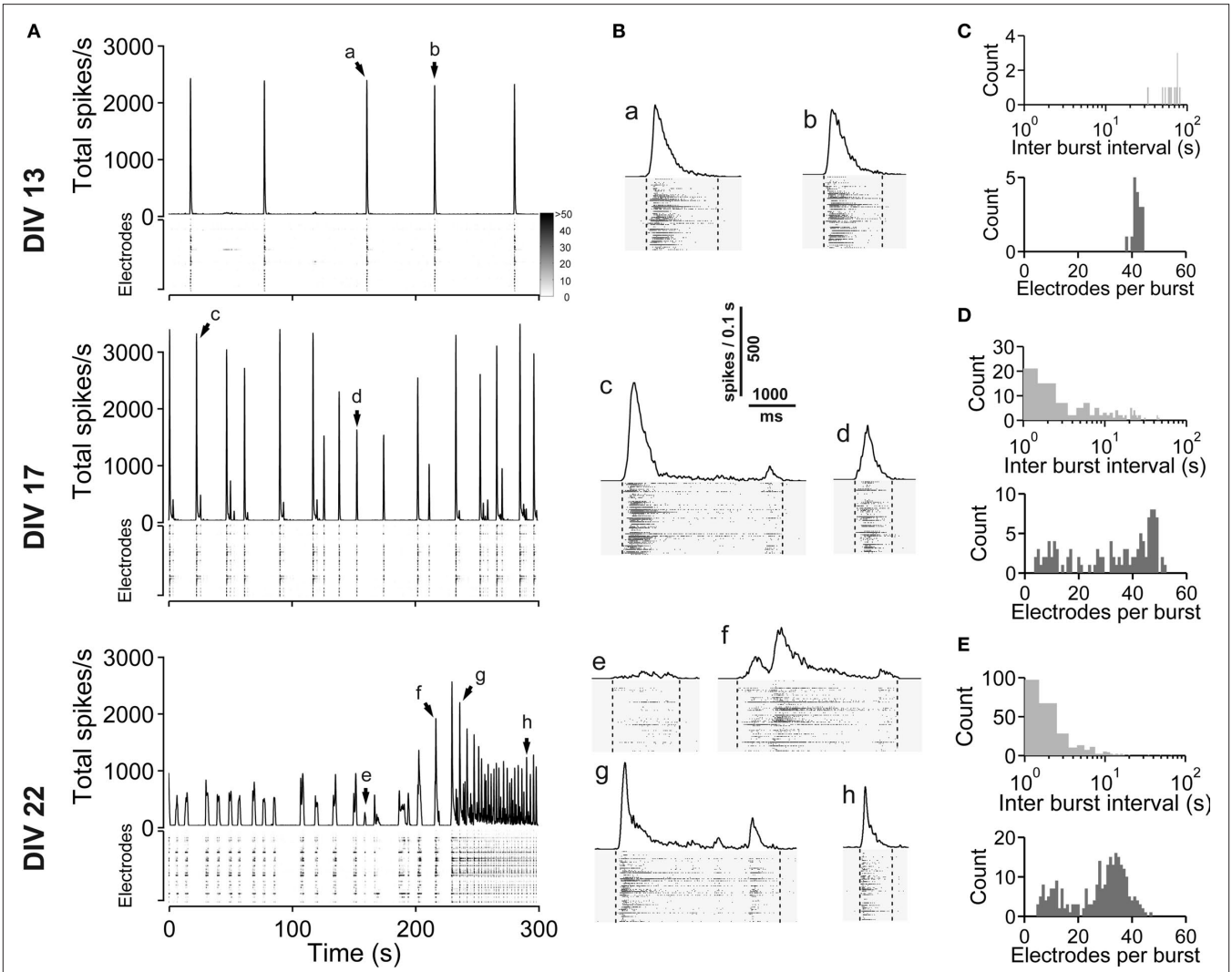

FIGURE 1 | Spontaneous network activity development of lateral cortex cultures (vCtx). (A) The total spike frequency is shown over time for the same culture at different stages of development (DIV, see labeling on the left side). vCtx cultures develop a heterogeneous pattern of burst discharges when maintained several weeks *in vitro*. The upper part of each graph indicates the global firing rate, which is defined as the number of detected spikes through all MEA electrodes per time unit (second). Spikes detected by individual electrodes are indicated by gray levels in the lower part. The same scale (see gray scale at 13 DIV) was used for all graphs. Each of the vertically stacked horizontal lines corresponds to one electrode. For clarity only 5 min out of the 20-min recording sessions are shown. Arrows indicate bursts which are shown in higher temporal resolution in **(B)**. **(B)** Individual population bursts in higher time resolution. Lower case letters correspond to labeling in **(A)**. Dotted lines indicate detected burst limits. Time unit for the global firing rate is 0.1 s. **(C)** Histograms of the interburst interval (top) and electrode attendance in bursts (bottom) for a 20-min recording session for the culture shown in **(A)** at 13 DIV. Note the log scale for the interburst interval histogram (bin size is 1 s). **(D)** Same as **(C)** except for 17 DIV. **(E)** Same as **(C)** except for 22 DIV.

GABAergic neurons developing in vCtx and dCtx networks are described in **Figure 6**. **Figures 4, 5 and 12** show the developmental GABA shift in vCtx and dCtx networks.

SPONTANEOUS ACTIVITY DEVELOPMENT IN vCtx NETWORKS

Spontaneous electrical activity of cultures obtained from lateral cortex at embryonic day 16 (E16) was monitored by means of 59 substrate-integrated electrodes. At the earliest age studied (5 DIV) sporadic single spikes were detected on a few (~1–5) electrodes. Afterwards spontaneous activity increased steadily. **Figure 1A** shows exemplar recordings of spontaneous activity in cortical networks from 13-, 17- and 22-day-old vCtx networks. The total spike frequency (integrated over all electrodes) increased from an average 7.86 ± 1.30 Hz at 5–10 DIV (mean ± SEM, $n = 28$ recordings, eight cultures, three preparations) to 54.27 ± 7.22 Hz ($n = 33$) and 117.28 ± 12.13 Hz ($n = 20$) at 11–17 and 18–24 DIV, respectively (**Table 1**). By the end of the first week *in vitro* the cultures developed recurrent synchronous burst discharges, i.e., transient clusters of spikes, which spread over several electrodes (see Materials and Methods; **Figures 1 and 2A**). Bursts that occurred at regular intervals were observed until about the end of the second week *in vitro* (**Figure 1A**, DIV 13). Later bursts became irregular in their occurrence and synchronization along the electrode array (**Figure 1A**, DIV 17, DIV 22). During the first 3 weeks *in vitro* the interburst

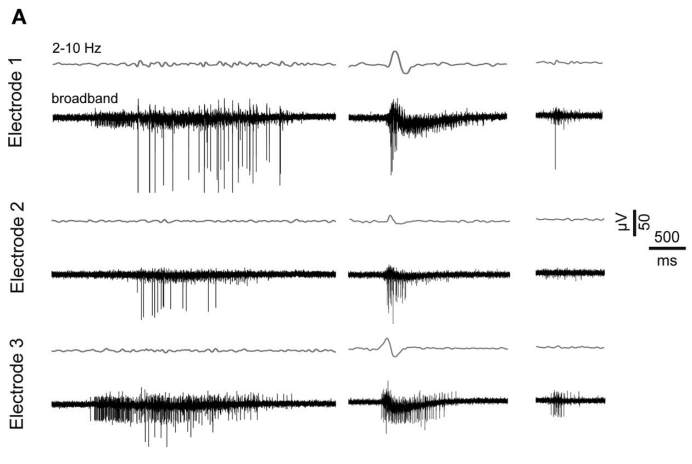

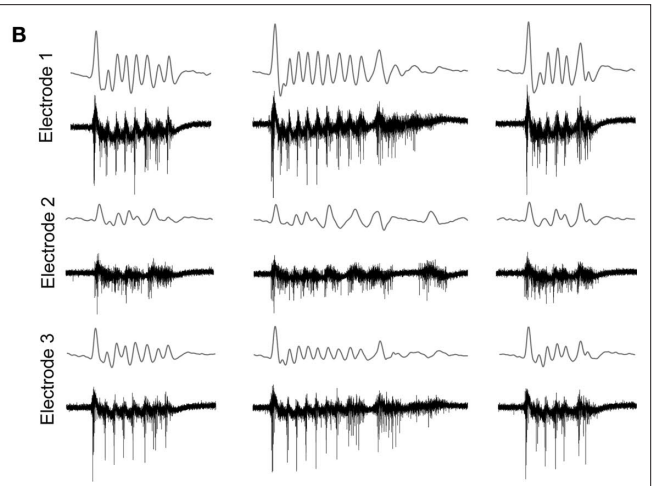

FIGURE 2 | Features of spontaneous activity of vCtx networks. (A) Extracellularly recorded signals show three burst events of different magnitude from a 21-day-old vCtx culture. Gray lines above each raw trace indicate the band-pass filtered signal (2–10 Hz). The same burst event is shown on three different electrodes 1–2 mm apart. **(B)** Same as in **(A)**, except that the vCtx culture was chronically blocked with gabazine (20 μM, added at 0 DIV).

interval (IBI) distribution steadily shifted toward lower values (**Figures 1C–E**, top graphs). The burst frequency was on average 0.010 ± 0.001 Hz in 5- to 10-day-old vCtx cultures and increased to 0.05 ± 0.01 Hz and 0.20 ± 0.02 Hz in 11–17 DIV and 18- to 24-day-old cultures, respectively. During the IBIs, in the range of seconds to minutes, neurons showed virtually no spiking activity. The increase of variability of burst timing during the development is reflected in the CV IBI. The CV IBI was initially 0.39 ± 0.04 in 5- to 10-day-old vCtx cultures and increased to 0.49 ± 0.05 and 2.39 ± 0.23 in 11- to 17- and 18- to 24-day-old cultures, respectively. Burst duration was on average 1431.35 ± 74.49 ms in 5- to 10-day-old vCtx cultures, and 1348.78 ± 66.29 ms and 1078.71 ± 80.42 ms in 11- to 17- and 18- to 24-day-old vCtx cultures, respectively.

As a measure for burst synchrony, i.e., spread of burst firing across the electrode array, we determined the burst electrode attendance, i.e., the number of electrodes with spiking activity during each burst event. Note that the term synchronization does not apply at a time scale of single spikes, but on a longer time scale, i.e., firing rates of many cells are modulated in synchrony (see **Figure 2A**). The mean electrode attendance was on average 15.35 ± 1.52 electrodes in 5- to 10-day-old vCtx cultures, increased to 29.81 ± 1.18 electrodes at 11–17 DIV and decreased significantly ($p < 0.001$, *t*-test) to 23.04 ± 1.39 electrodes in 18- to 24-day-old cultures. The maximal electrode attendance during the recording session shows a steady increase from initially 18.13 ± 1.57 electrodes at 5–10 DIV to 38.15 ± 1.49 and 41.30 ± 2.34 electrodes at 11–17 DIV and 18–24 DIV, respectively. Thus, the decreased mean burst synchrony in 18–24 DIV old cultures is not due to a declining of neuronal health. An initial single peak in the histogram of the electrode attendance in 2-week-old cultures (**Figure 1C**, bottom) became broader and at least two peaks could be identified after approximately 3 weeks *in vitro* (**Figure 1E**, bottom). That is, the network activity ultimately comprised both very synchronous and partially synchronized bursts.

The spontaneous population burst activity was fully blocked by application of AMPA and NMDA glutamate receptor blockers (CNQX, 10 μM, and D(−)-AP-5, 50 μM, respectively) in 3-week-old vCtx cultures ($n = 3$; one preparation, not shown). The acute $GABA_AR$ blockade with bicuculline (5 μM) changed the variable burst discharges of vCtx cultures (>21 DIV) to more regular, stereotyped bursts (**Figure 3A**). Compared with unblocked controls the burst frequency was decreased by 61.71 ± 4.05% ($p < 0.001$), the number of electrodes in bursts was increased by 60.79 ± 9.17% ($p < 0.001$), the burst duration was increased by 144.08 ± 62.75% ($p < 0.05$), the overall spike frequency was increased by 55.02 ± 16.85% ($p < 0.05$), and the CV IBI was decreased by 69.75 ± 9.29% ($p < 0.001$, $n = 8$ cultures, three preparations, *t*-test, **Figures 3C–G**, dark gray bars).

Next we asked if the maturation of the network activity pattern is correlated with the GABA shift. Early bursting activity in cortical neurons is accompanied by an increase of intracellular calcium (Opitz et al., 2002). Small increases of intracellular calcium concentration are usually associated with single spiking or subthreshold activation, whereas bursting leads to a very strong increase of intracellular calcium (Opitz et al., 2002; Cossart et al., 2005). The local application of the $GABA_AR$ agonist muscimol early in network development evokes a calcium transient due to the depolarizing action of GABA (Yuste and Katz, 1991; Lin et al., 1994; LoTurco et al., 1995; Garaschuk et al., 2000; Ganguly et al., 2001). In this set of experiments we locally applied short puffs of either high potassium (60 mM) or muscimol (200 μM, **Figure 4**), and recorded calcium transients by Fluo-3 imaging. The time course of the pharmacological applications is shown in **Figure 4B**. In vCtx cultures, we found that the amplitude of intracellular calcium transients and the number of neurons with a significant increase of intracellular calcium decreased with development (**Figures 4D–G**). The fraction of cells that showed a significant increase of intracellular calcium in response to muscimol decreased from initially 95.98 ± 1.23% at 5 DIV to 45.22 ± 4.10% at 29 DIV (**Figure 4E**). Interestingly, some cells already showed very weak response to muscimol as early as DIV 5 (**Figure 4G**). Moreover, concurrent with observations in cortical slices (Garaschuk et al., 2000), after the GABA shift >40% of neurons showed a small, but significant increase of intracellular calcium in response to the GABA agonist muscimol (**Figures 4E–G**).

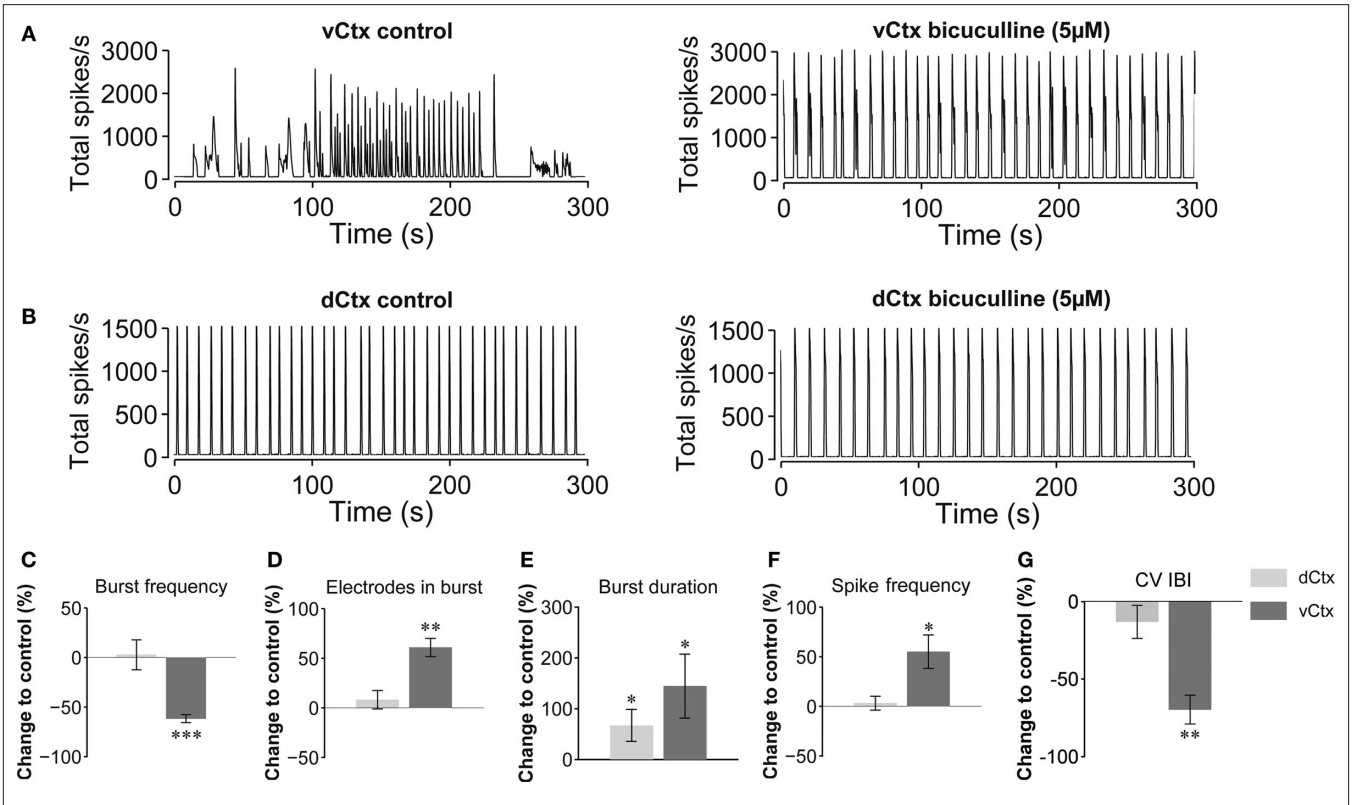

FIGURE 3 | Acute GABA$_A$R blockade of 3-week-old networks. (A) Bursting activity of a 21-day-old vCtx culture under control conditions (left) and during the presence of the GABA$_A$R blocker bicuculline (5 μM) in the culture media (right). **(B)** Same as in **(A)** but for dCtx networks (see **Figures 9–11**). **(C–G)** Dark gray bars in summary graphs show changes of burst properties of vCtx cultures in blocked compared with control conditions. Light gray bars show equivalent quantitative results for acutely blocked dCtx compared with control dCtx networks. Data were obtained from 20-min recording sessions of 20- to 28-day-old cultures (vCtx cultures: $n = 8$, dCtx cultures: $n = 7$, three preparations, asterisks indicate significance: $*p < 0.05$; $**p < 0.001$; $***p < 0.0001$; *t*-test).

The results above suggest a causal relationship between the development of the hyperpolarizing postsynaptic effect of GABA and the network activity heterogeneity in mature (~3-week-old) vCtx cultures. In the following we tested if a change in the polarity of GABA action can evoke a premature network activity differentiation in young cultures. The depolarizing effect of GABA in immature neurons is due to high intracellular chloride provided by the Na^+, K^+-$2Cl^-$ cotransporter NKCC1 (Ben-Ari, 2002; Yamada et al., 2004; Dzhala et al., 2005; Ben-Ari et al., 2007). A blockade of NKCC1 with bumetanide in young neurons results in a hyperpolarization shift of the GABA$_A$ reversal potential (Dzhala et al., 2005, 2008; Sipila et al., 2006; Balena and Woodin, 2008). In vCtx cultures (9–11 DIV) we blocked the NKCC1 function with bumetanide (10 μM) and quantified the regularity of burst firing by the coefficient of variation of the intraburst frequency (CV IBF) and the CV IBI. NKCC1 blockade led to a significant increase of bursting variability (**Figure 5**). Compared with controls the CV IBI (**Figure 5G**) and CV IBF (**Figure 5H**) were increased by $105.85 \pm 34.84\%$ ($p < 0.05$) and $41.05 \pm 14.87\%$ ($p < 0.05$), respectively. Thus, a shift of the postsynaptic effect of GABA from depolarizing into the hyperpolarizing direction induced a change of the network activity from regular, highly synchronized bursting to less synchronized and irregular bursting in vCtx cultures.

In vCtx cultures, $4.68 \pm 0.21\%$ of the neurons at 1 DIV and $3.56 \pm 0.54\%$ of the neurons at 21 DIV (mean ± SEM, $n = 8$ cultures, three preparations) were labeled with GABA antibodies. The soma size of GABAergic neurons (21–22 DIV) showed a bimodal distribution (**Figures 6A,D**), and, on average, $72.25 \pm 5.45\%$ (434 of 578 analyzed cells) of the GABAergic neurons had a soma area above 100 μm^2 and 27.75% (144 cells) had a soma area below 100 μm^2. Most large GABAergic cells in 21- to 22-day-old vCtx cultures were parvalbumin positive ($77.11 \pm 1.69\%$, 714 of 926 cells, eight cultures, three preparations, **Figure 6C**). In contrast, small GABAergic neurons were invariably parvalbumin negative (**Figure 6C**). The morphological and immunocytochemical characterization of GABAergic neurons are in line with previous findings in young neocortical cultures (de Lima and Voigt, 1997; de Lima et al., 2004, 2009).

SPONTANEOUS NETWORK ACTIVITY DEVELOPMENT WITH BLOCKED GABA$_A$ SIGNALING

After the GABA shift, the synchronization and regularity of spontaneous bursting decreases significantly (see above). The acute blockade of GABA$_A$R signaling increased network activity synchronization and regularity. Here we ask if the chronic blockade of GABA$_A$Rs can prevent the maturation of the spontaneous activity pattern in vCtx networks.

We examined the effect of GABA$_A$ergic signaling by comparing the spontaneous activity development of GABA$_A$R-blocked vCtx cultures (gabazine 20 μM, added 3 h after plating, **Figures 7 and 8**, **Table 1**) with control vCtx sister cultures (see above, **Figures 1 and 2**).

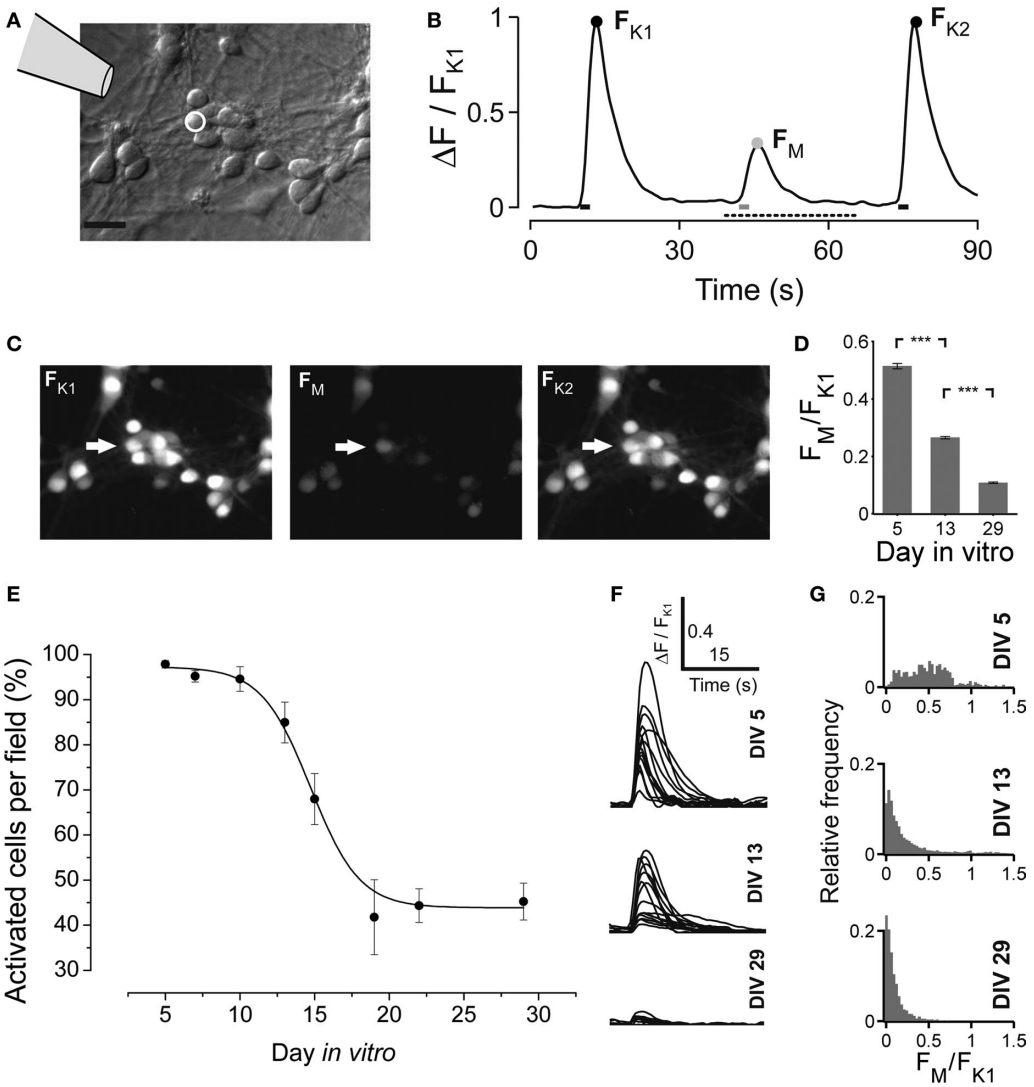

FIGURE 4 | Developmental change of the $GABA_A$R mediated calcium response in vCtx cultures. (A) Schematic drawing indicates the local drug application pipette over the differential interference contrast image of a 5-day-old culture (Scale bar = 20 μm). **(B)** Fluorescence changes of an individual cell [white circle in **(A)**] in response to a short pulse of either a solution containing high potassium (60 mM) or the $GABA_A$R agonist muscimol (200 μM). The three calcium transients correspond to the time points of drug application, indicated by bars at the bottom. The black dots denote the maximum fluorescence in response to the K^+ pulses (F_{K1} and F_{K2}). The gray dot denotes the maximum fluorescence in response to local muscimol application (F_M). **(C)** Fluo-3 fluorescence of the cells shown in **(A)** at F_{K1}, F_M and F_{K2}. **(D)** Average ratio of the evoked calcium responses F_M and F_{K1} at DIV 5, DIV 13 and DIV 29 (n = 1834, 1922 and 1643 cells, respectively; each from three independent preparations; asterisks indicate significance, $p < 0.0001$; t-test). **(E)** The fraction of cells with a significant increase of fluorescence in response to muscimol in each recorded field is shown as a function of time. Each dot represents the average of several recorded fields (>15), pooled from three cultures per DIV, three preparations. Solid line is a Boltzmann fitted sigmoid. **(F)** Example traces of muscimol elicited calcium transients for different ages for the time interval indicated by a dotted line in **(B)**. **(G)** Histograms of the ratio F_M and F_{K1} at the indicated days *in vitro*.

Similar to controls, $GABA_A$R-blocked vCtx cultures showed regular bursting at the end of the first week *in vitro*. Unlike control cultures, regular bursting persisted in the $GABA_A$R-blocked cultures (**Figure 7A**). Interestingly, spontaneous bursts in older cultures showed prominent oscillatory discharges (circa 3–15 discharges, ~3–10/s) (**Figures 2B and 7B**).

Compared with control cultures, the total spike frequency was lower in the blocked networks until the middle of the second week *in vitro* (72.89 ± 5.99% of controls, $p < 0.05$, **Figures 8D,I**). In the following weeks total spike frequency was not significantly different from control networks ($p = 0.08$, 11–17 DIV; $p = 0.21$, 18–24 DIV, **Figures 8D,I**). The burst frequency of chronically blocked cultures did not differ significantly from that of the unblocked cultures until about the middle of the second week *in vitro* (5–10 DIV, $p = 0.74$, $n = 28$ recordings from eight unblocked cultures, $n = 27$ recordings from eight blocked cultures, three preparations, t-test, **Figures 8A,F**). In older cultures, the burst frequency was decreased under the chronic $GABA_A$R blockade (11–17 DIV: 73.20 ± 13.41% of controls, $n = 33$ recordings of unblocked cultures, $n = 30$ recordings of blocked cultures, $p < 0.001$; 18–24 DIV: 24.98 ± 1.72% of

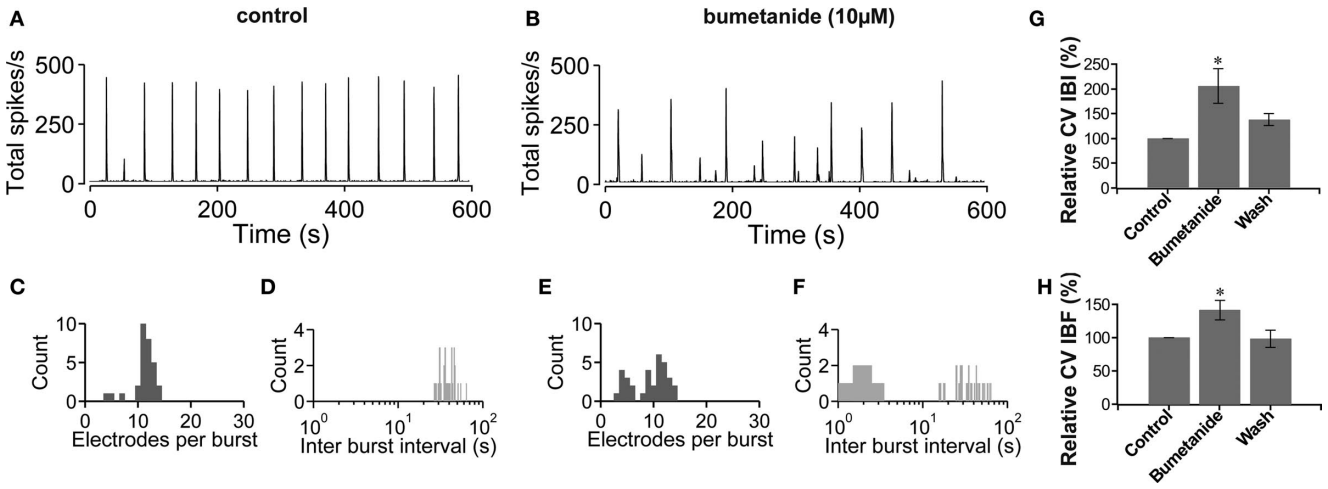

FIGURE 5 | Blockade of NKCC1 function by bumetanide. (A,B) The total network spike frequency over time is shown for a 9-day-old vCtx culture in control conditions **(A)** and in the presence of bumetanide (10 μM) in the culture media **(B)**. **(C,D)** Histograms of the electrode attendance during bursts **(C)** and interburst interval **(D)** for a 20-min recording period, of which 600 s are shown in **(A)**. Note the log scale for the interburst interval histogram (bin size is 1 s). **(E,F)** Same as **(C,D)** except for the recording shown in **(B)**. **(G,H)** Bumetanide induced changes in the variability of the interburst interval (G) and intraburst frequency (H). Asterisks indicate statistical significance: $*p < 0.05$, $n = 7$, two preparations, *t*-test).

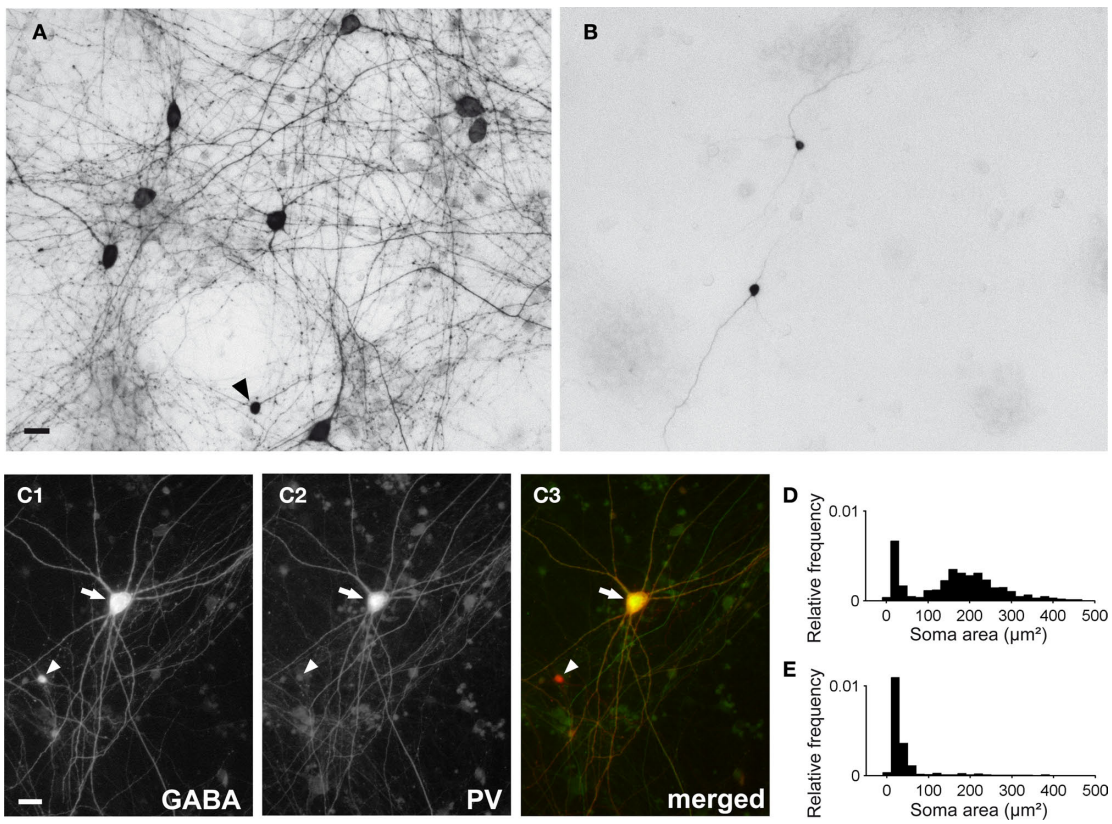

FIGURE 6 | GABAergic neurons in 3-week-old cultured networks. (A) The bright field image shows several large GABA immunostained neurons in a 21-day-old vCtx culture (DAB staining). The arrowhead indicates a small GABAergic neuron. **(B)** Same as **(A)** except for dCtx culture. Two small GABAergic neurons can clearly be identified. **(C_{1-3})** Colocalization of gamma-aminobutyric acid (GABA) and parvalbumin (PV) immunofluorescence in a large GABAergic neuron (arrow) in a 21-day-old vCtx culture. The arrowhead indicates a small GABA+/PV– neuron. Scale bar is 20 μm. **(D)** Distribution of the soma size of GABAergic neurons in vCtx cultures (see main text for details). **(E)** Same as **(D)** except for dCtx cultures.

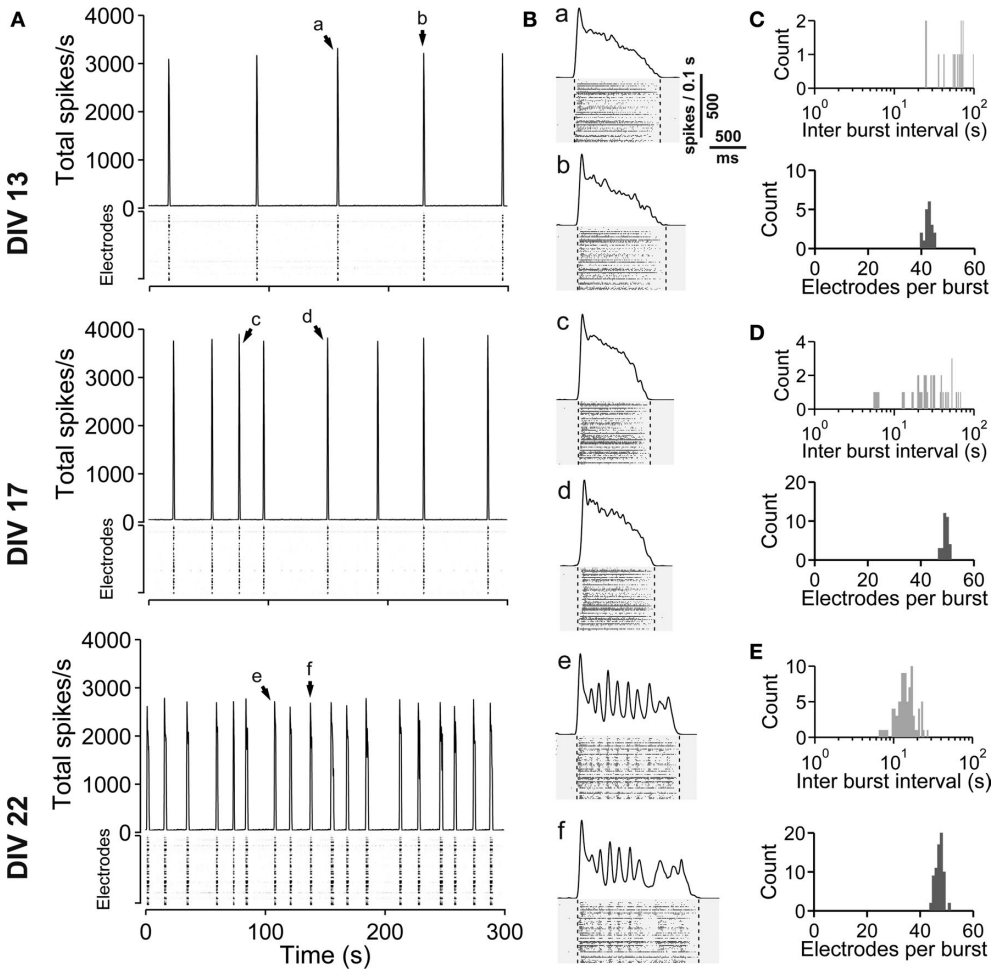

FIGURE 7 | Spontaneous activity development of vCtx networks with chronically blocked $GABA_A$ receptors. (A) The total spike frequency is shown over time for vCtx cultures chronically treated with gabazine (20 μM, added at 0 DIV) at different stages of development (13, 17, 22 DIV). These networks develop a regular bursting pattern, which persists throughout their lifetime. See **Figure 1** for graph description. Arrows indicate bursts which are shown in higher temporal resolution in **(B)**. **(B)** Individual population bursts in higher time resolution. Oscillatory discharges emerge during the third week *in vitro*. Lower case letters correspond to labeling in **(A)**. Dotted lines indicate detected burst limits. Time unit for the global firing rate is 0.1 s. **(C)** Histograms of the interburst interval (top) and electrode attendance in bursts (bottom) for a 20-min recording session for the culture shown in **(A)** at 13 DIV. Note the log scale for the interburst interval histogram (bin size is 1 s). **(D)** Same as **(C)** except for 17 DIV. **(E)** Same as **(C)** except for 22 DIV.

controls, $n = 20$ recordings of unblocked cultures, $n = 18$ recordings of blocked cultures, $p < 0.0001$). The CV IBI in 5- to 10- and 11- to 17-day-old blocked cultures did not differ significantly from age-matched controls (**Figures 8C,H**). In 18- to 24-day-old blocked cultures, however, the CV IBI was significantly decreased ($12.58 \pm 1.88\%$ of controls; $p < 0.0001$). Furthermore, while the mean burst duration of blocked vCtx cultures was decreased at 5–10 and 11–17 DIV ($80.54 \pm 4.25\%$, $p < 0.001$ and $76.51 \pm 2.69\%$, $p < 0.001$, respectively), burst duration was increased in 18- to 24-day-old blocked cultures compared with aged matched controls ($154.64 \pm 10.63\%$, $p < 0.0001$) (**Figure 8E**).

In contrast to the development in control cultures, the average electrode attendance during bursts increased during the first 2 weeks *in vitro* and remained stable afterwards in cultures with blocked $GABA_A$Rs (**Figure 8B**). The electrode attendance of blocked vCtx cultures was lower than controls ($77.65 \pm 4.83\%$ of controls, $p < 0.001$) until the middle of the second week *in vitro*. This reversed with further development of the cultures. The average electrode attendance was $127.92 \pm 5.53\%$ ($p < 0.0001$) of control in 11–17 DIV old blocked vCtx cultures and $184.10 \pm 9.72\%$ ($p < 0.0001$) of controls in 18- to 24-day-old cultures (**Figures 8B,G**). The maximal electrode attendance showed no significant differences ($p = 0.11$) between blocked and unblocked 3-week-old networks (**Figure 8J**). The single peak in the electrode attendance histogram of blocked cultures mirrors the temporal regularity of burst firing and suggests the recruitment of the whole network during each burst event (see **Figures 7C–E**, bottom plots).

The population of GABAergic neurons in cultures grown under $GABA_A$R blockade was similar to control cultures (not shown). This is in accordance with previous results showing that the chronic blockade of $GABA_A$R did not decrease the density of GABAergic neurons (de Lima et al., 2004, 2007).

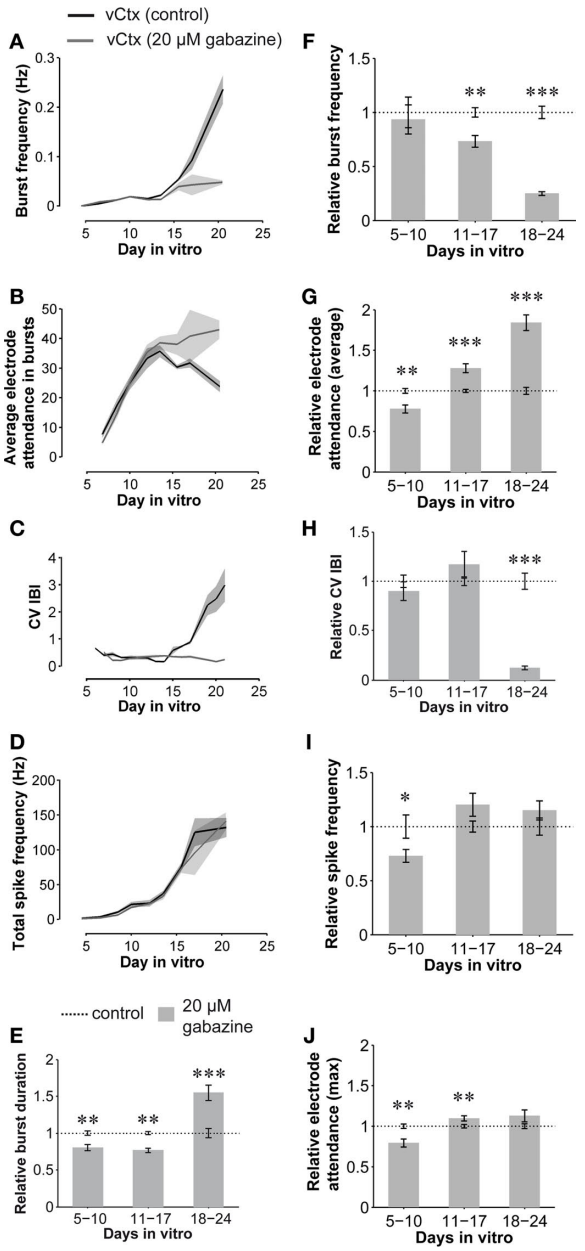

FIGURE 8 | Quantitative features of spontaneous activity development: GABA$_A$R-blocked compared with control vCtx networks. (A–D) Graphs show the development of spontaneous network activity features in control vCtx cultures and in sister vCtx cultures grown with GABA$_A$R blocker gabazine (20 μM) added to the medium. **(A)** Shows the development of the burst frequency, **(B)** the average number of spiking electrodes during a burst event, **(C)** the coefficient of variation of the interburst interval (CV IBI) and **(D)** the total spike frequency for cultures obtained from one preparation. (**A–D**, $n = 4$, cultures per age group, shaded areas in this and subsequent figures indicate SEM). **(E–J)** Summary graphs of parameters of spontaneous activity development of blocked vCtx cultures pooled from different preparations normalized to values of age-matched control cultures in each preparation. Data were obtained from 20-min recording sessions per day *in vitro*. Asterisks indicate significance: $*p < 0.05$; $**p < 0.001$; $***p < 0.0001$; *t*-test; 5–10 DIV $n = 28$ recordings of unblocked cultures/$n = 27$ recordings of blocked cultures; 11–17 DIV $n = 33/n = 30$; 18–24 DIV $n = 20/n = 18$; eight cultures per group; three preparations. Data are given in mean ± SEM.

SPONTANEOUS ACTIVITY DEVELOPMENT OF dCtx NETWORKS

In the previous experiments, the embryonic tissue dissociated from the lateral cortex was limited to the lateral aspect of the neocortex, which, at E16, was populated by GABAergic neurons migrating upwards from the ventral telencephalic origins. Here we compared a set of vCtx cultures with sister cultures grown from more dorsal cortical tissue (dCtx cultures) (**Figures 9–11**, **Table 2**). The development of spontaneous network activity of this set of vCtx cultures was indistinguishable from the control vCtx cultures described above (**Figures 1 and 2A**). In contrast to vCtx cultures, the network activity in dCtx cultures comprised regular burst firing throughout the culture period (**Figure 9A**) and, similarly to experiments with chronic GABA$_A$R blockade, intraburst oscillations emerged at an age of approximately 3 weeks *in vitro* (**Figures 9B and 10**).

When compared with vCtx cultures, the overall spike rate was low in dCtx networks (54.54 ± 4.80% of vCtx cultures, 5–10 DIV, $p < 0.0001$; 65.01 ± 7.61%, 11–17 DIV, $p < 0.0001$ and 57.82 ± 7.45%, 18–24 DIV, $p < 0.0001$) (**Figure 11G**). Similarly, the burst frequency of dCtx networks was lower than in vCtx networks throughout the culturing period ($p < 0.0001$, 5–10 DIV; $p < 0.0001$, 11–17 DIV; $p < 0.0001$, 18–24 DIV; **Figures 11A,E**). The CV IBI of dCtx cultures did not differ significantly from vCtx controls in 5–10 DIV and 11–17 DIV old cultures, but was significantly lower in 18- to 24-day-old cultures (27.18 ± 3.81% of vCtx cultures, $p < 0.0001$, **Figure 11H**).

The histogram of electrode attendance during burst firing had a single peak (**Figures 9C–E**, bottom plots), suggesting little variability in the synchronization of the burst discharges along the electrode array compared with vCtx cultures (**Figures 1C–E**). The average number of electrodes with spikes during burst was higher than in vCtx cultures (**Figures 11B,F**), indicating more synchronized burst firing in dCtx cultures. The average electrode attendance of dCtx cultures at 5–10 DIV was 124.32 ± 10.05% of age-matched vCtx cultures' electrode attendance ($p < 0.05$, *t*-test, $n = 36$ recordings from 12 vCtx cultures, $n = 31$ recordings from 12 dCtx cultures, five preparations), 119.65 ± 6.42% of vCtx cultures attendance at 11–17 DIV ($p < 0.05$, $n = 56$ recordings from vCtx cultures, $n = 59$ recordings of dCtx cultures) and 133.39 ± 7.85% of vCtx cultures attendance at 18–24 DIV ($p < 0.001$, $n = 44$ recordings from vCtx cultures, $n = 47$ recordings of dCtx cultures). The maximum electrode attendance in dCtx and vCtx cultures did not differ significantly ($p = 0.31$, 5–10 DIV; $p = 0.09$, 11–17 DIV; $p = 0.39$, 18–24 DIV, **Figure 11C**). The mean burst duration of dCtx cultures was significantly higher than in vCtx cultures at 5–10 DIV (116.55 ± 6.22% of vCtx cultures, $p < 0.05$) and 18–24 DIV (154.636 ± 10.626% of vCtx cultures, $p < 0.05$) (**Figure 11D**).

The spontaneous population burst activity in 3-week-old dCtx networks was fully blocked by application of the glutamate receptor blockers CNQX (10 μM) and D(−)-AP-5 (50 μM; not shown, $n = 2$, one preparation). The acute blockade of GABA$_A$R signaling in dCtx cultures with bicuculline (5 μM) had no significant effects on burst frequency ($p = 0.87$), total spike frequency ($p = 0.67$), spikes in bursts ($p = 0.16$), electrode attendance in burst ($p = 0.41$) and CV IBI ($p = 0.26$), but significantly increased the burst duration ($p < 0.05$, $n = 7$ cultures, 21 DIV, three preparations, *t*-test) (**Figures 3B–G**, light gray bars).

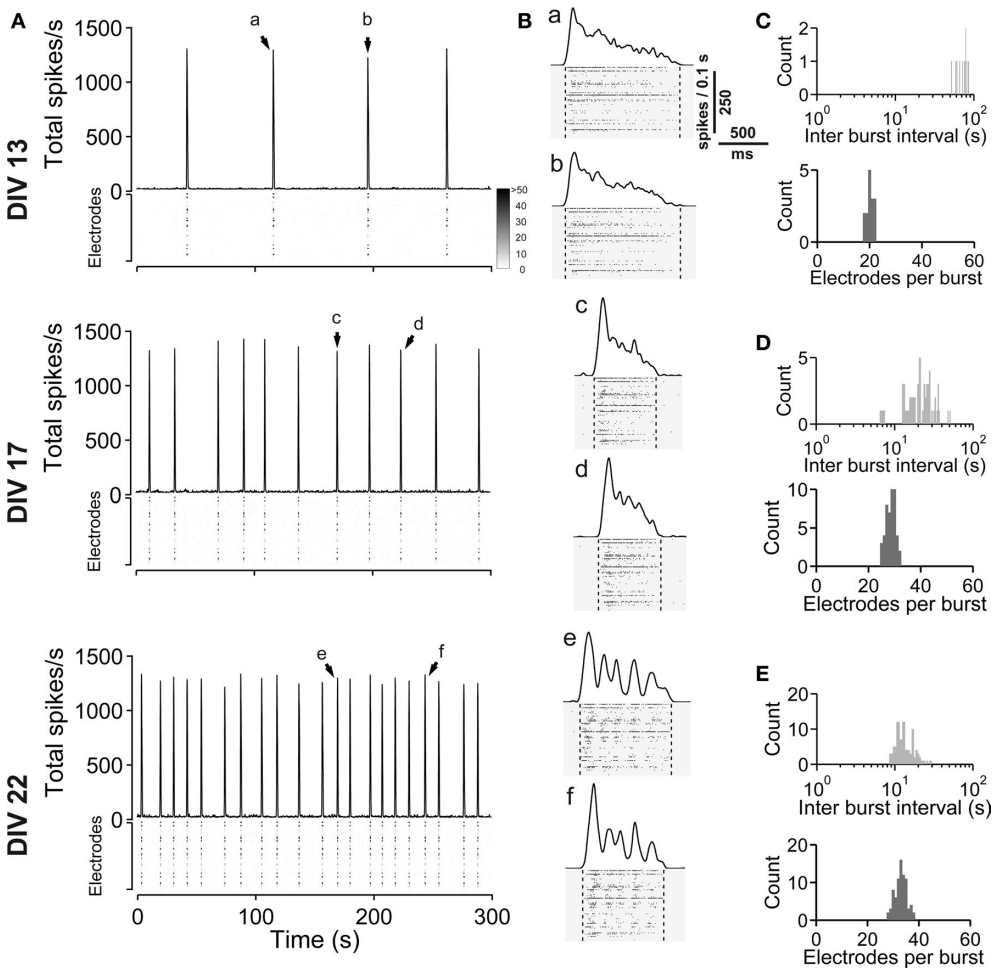

FIGURE 9 | Spontaneous network activity development of dorsal cortex (dCtx) cultures. (A) The total spike frequency is shown over time for the same culture at different stages of development (DIV, see labeling on the left side). dCtx cultures develop a regular bursting pattern, which persists throughout their lifetime. See **Figure 1** for graph description. Arrows indicate bursts which are shown in higher temporal resolution in **(B)**. **(B)** Individual population bursts in higher time resolution. Oscillatory discharges emerge approximately during the third week *in vitro*. Lower case letters correspond to labeling in **(A)**. Dotted lines indicate detected burst limits. Time unit for the global firing rate is 0.1 s. **(C)** Histograms of the interburst interval (top) and electrode attendance in bursts (bottom) for a 20-min recording session for the culture shown in **(A)** at 13 DIV. Note the log scale for the interburst interval histogram (bin size is 1 s). **(D)** Same as **(C)** except for 17 DIV. **(E)** Same as **(C)** except for 22 DIV.

With Fluo-3 imaging, we monitored the GABA shift in dCtx cultures. We quantified the amplitude of the transients elicited by locally applied short puffs of either a solution containing high potassium (60 mM) or muscimol (200 μM, **Figure 12**), and counted the cells showing calcium transients. Similar to what was observed in vCtx cultures (see **Figure 4**), in dCtx networks the amplitude of intracellular calcium transients decreased between 10 and 17 DIV (**Figure 12**). The fraction of cells showing a calcium transient in response to muscimol decreased from initially 94.17 ± 0.86% to 14.87 ± 1.86% (**Figure 12A**). The data shows that GABA action changes in dCtx cultures, despite a reduced amount of GABAergic neurons (see below). Interestingly, the percentage of cells showing a calcium transient after muscimol application was lower than in vCtx cultures (**Figures 4E and 12A**). Whether this discrepancy is due to a homeostatic regulation due to GABA signaling differences, or due to a GABA independent mechanism, remains to be investigated.

The immunocytochemical analysis showed that in 1-day-old dCtx cultures, no more than 0.04 ± 0.02% of the neurons were GABAergic (six cultures, three preparations). At 21–22 DIV, 1.79 ± 0.49% of the cells were GABAergic (seven cultures; three preparations). The vast majority of these GABAergic neurons had a very small soma size, a fusiform or bipolar morphology, and were not parvalbumin immunoreactive. The soma size distribution of GABAergic neurons was unimodal (21–22 DIV, **Figures 6B,E**). On average 91.61 ± 2.97% (496 of 548 analyzed cells) of GABAergic neurons had a soma area below 100 μm^2 and only 8.39% (52 cells) had a soma area above 100 μm^2. The developmental increase of the smaller GABAergic neurons' fraction concurs with the finding that GABAergic precursors are mitotically active in culture (de Lima and Voigt, 1997, 1999).

Besides counting GABAergic somata, we compared the staining intensity of the GABAergic neuropil of dCtx and vCtx cultures. We determined the average staining intensity for each culture type

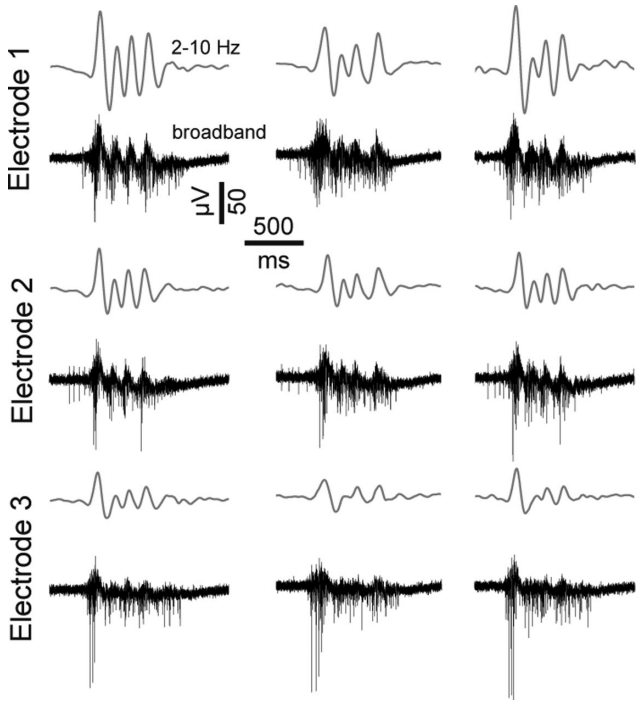

FIGURE 10 | Features of dCtx spontaneous network activity. Extracellularly recorded signals from three burst events of a recording from a dCtx culture (21 DIV). Gray lines above each raw trace indicate the band-pass filtered signal (2–10 Hz). The same burst event is shown on three different electrodes.

(i.e., the attenuation of the light intensity due to stained regions) and normalized to the average values of dCtx cultures. We found that the GABA staining of vCtx cultures was on average 8.05 ± 0.73 times stronger than that of dCtx cultures (19–22 DIV, $p < 0.0001$, *t*-test; $n = 55$ and 58 fields of dCtx and vCtx cultures, respectively).

DISCUSSION

PATTERNS OF NETWORK ACTIVITY

In all cultured networks recurrent network bursting started approximately at the end of the first week *in vitro*, continued throughout the culturing period and was absent in the presence of AMPA and NMDA glutamatergic receptor blockers. This is in line with previous observations on similar E16-donor cultures (Voigt et al., 2001, 2005; Opitz et al., 2002) or cultures grown from older cortices (Maeda et al., 1995; Kamioka et al., 1996; Marom and Shahaf, 2002; Chiappalone et al., 2006; Wagenaar et al., 2006a,b; Shahaf et al., 2008). Early large scale bursts characteristically have IBIs up to minutes and reach maximal neuronal attendance during the second week *in vitro*. These large scale network bursts resemble the immature bursting activity in slices of the neonatal rodent cortex, called 'cortical early network oscillations' (cENOs) (Garaschuk et al., 2000), recorded by calcium imaging or patch clamp in acute or cultured slices of the cerebral cortex (Garaschuk et al., 2000; Corlew et al., 2004; McCabe et al., 2006; Allene et al., 2008; Sheroziya et al., 2009).

Population bursts with lower neuronal attendance and hence with decreased overall spiking appeared in culture several days after the appearance of the first large transients, and were unique to mature vCtx cultures (~3-week-old). This kind of activity was blocked by acute application of $GABA_A$R antagonists and was absent in cultures lacking large interneurons or in cultures chronically blocked by $GABA_A$R antagonists. Notably, also in acute neocortical slices network events with small amplitudes and less participating neurons, cGDPs, develop later than the early network oscillations (cENOs) and were compared to the GDPs described in the hippocampus (Allene et al., 2008).

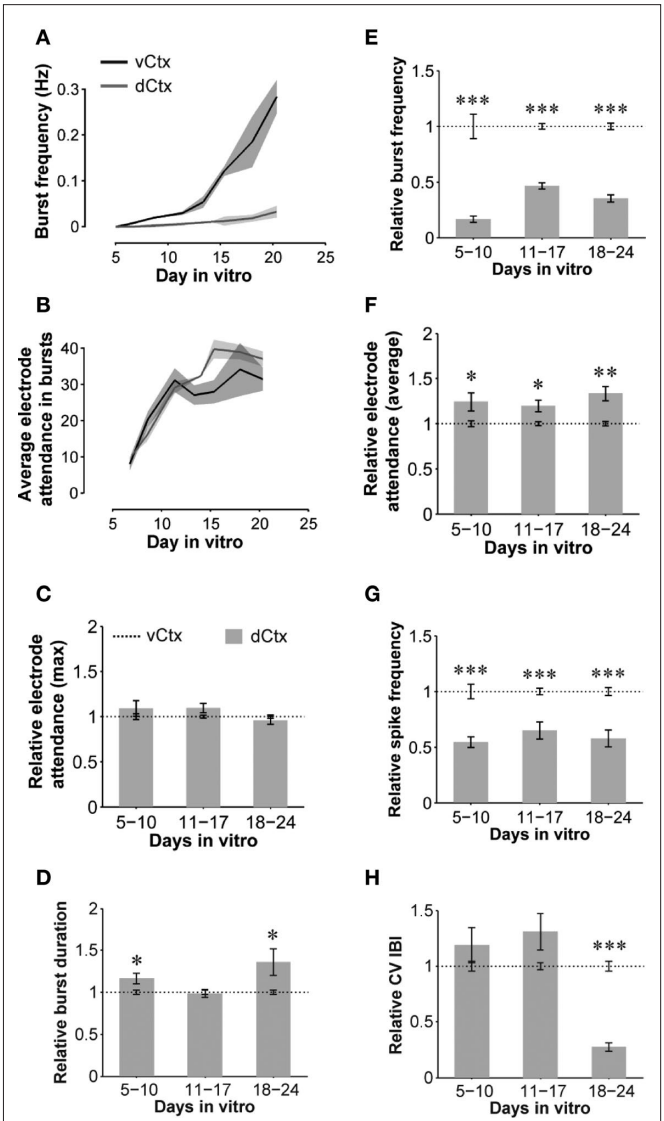

FIGURE 11 | Quantitative features of spontaneous activity development: dCtx compared with vCtx networks. (A,B) Graphs show the development of spontaneous network activity features in control vCtx and in sister dCtx cultures from one preparation ($n = 3$ cultures per culture type). **(A)** shows the development of the burst frequency and **(B)** the electrode number in burst events as a function of time. **(C–H)** Summary graphs of parameters of spontaneous activity development of dCtx cultures pooled from different preparations normalized to values of age-matched vCtx sister cultures in each preparation. Data are obtained from 20-min recording sessions per day *in vitro*. Asterisks indicate significance: $*p < 0.05$; $**p < 0.001$; $***p < 0.0001$; *t*-test; 5–10 DIV $n = 36$ recordings of vCtx cultures/$n = 31$ recordings of dCtx cultures; 11–17 DIV $n = 56/n = 59$; 18–24 DIV $n = 44/n = 47$; 12 cultures per group; five preparations.

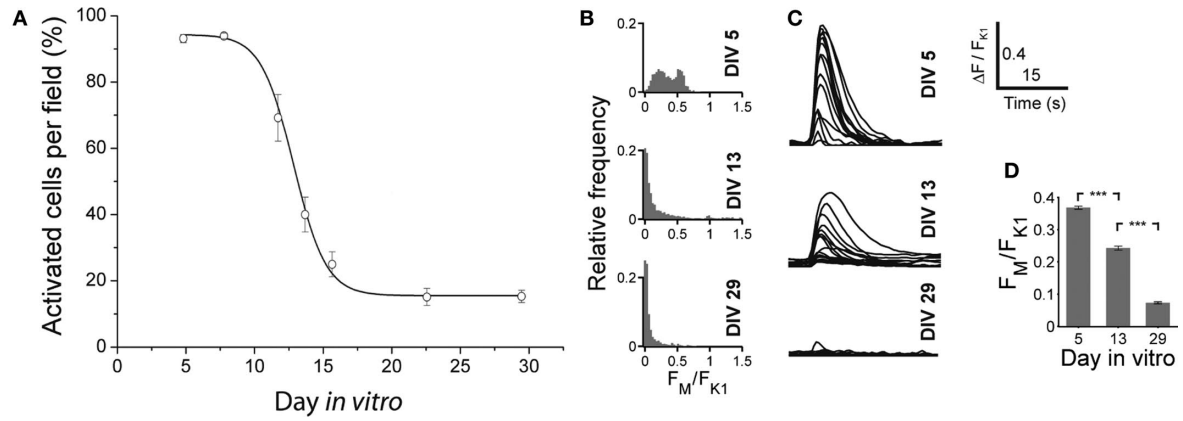

FIGURE 12 | Developmental change of the $GABA_AR$ mediated calcium response in dCtx cultures. (A) Graph shows the fraction of neurons in dCtx cultures with a significant increase of fluorescence in response to muscimol, as a function of time. Each dot represents the average of several recorded fields (>15), pooled from three cultures from three preparations per time point. Solid line is a Boltzmann fitted sigmoid (see also **Figure 4** for a more detailed description of the experimental configuration). **(B)** Histograms of the ratio F_M and F_{K1} at the indicated days *in vitro*. **(C)** Example traces of muscimol elicited calcium fluorescence at the indicated ages. **(D)** Average ratio of the evoked calcium responses F_M and F_{K1} at DIV 5, DIV 13 and DIV 29 (n = 1297, 2142 and 1613 cells, respectively; each from three independent preparations; asterisks indicate significance, $p < 0.0001$; t-test).

Characteristic of mature dCtx cultures and $GABA_AR$-blocked vCtx cultures was a regular burst pattern with widespread burst synchrony (**Figures 7 and 9**) and intraburst oscillatory discharges (see **Figures 2B and 10**). These bursts are mediated by ionotropic glutamatergic receptors activity and are reminiscent of intraburst oscillatory activity in spinal cord slices or disinhibited spinal cord cultures (Streit, 1993; Bracci et al., 1996; Yvon et al., 2007), picrotoxin induced afterdischarges in hippocampal slices (Miles et al., 1984) or endogenous spindle-burst activity in developing neocortex *in vivo* (Minlebaev et al., 2007, 2009). In the neonatal barrel cortex, GABAergic synapses contribute minimally to the pace of the ubiquitous spindle-bursts activity (Minlebaev et al., 2007). Yvon et al. (2007) suggested that this kind of intraburst oscillation might be generated by the depolarization-induced modulation of inactivation dynamics of Na^+ channels. This is in line with the observation that during oscillatory discharges the spike amplitudes progressively decrease during each intraburst episode and partially recovers until the next episode (**Figures 2B and 10**).

TEMPORAL CLUSTERING OF NETWORK ACTIVITY IN LATERAL CORTEX CULTURES

In all vCtx cultures older than 17–20 DIV a gradual but predictable change in the network activity was observed, consisting of alternating periods of higher and lower burst incidence. Periods characterized by high burst incidence were observed in long-term E18 cortical cultures by Wagenaar et al. (2006a), who termed such events 'superbursts', and in mega-slice co-cultures by Baker et al. (2006) who called them 'network bursts'. The appearance of organized clustering of bursting activity in cultured cortical networks, however, hardly followed a predictable growing condition (Wagenaar et al., 2006a).

Burst clustering in E16 cultures of the neocortex reliably develops in the presence of large GABAergic neurons and functional $GABA_AR$ mediated synaptic transmission. This activity pattern radically differed from network activity of vCtx cultures under chronic or acute pharmacological blockade of the $GABA_ARs$ or from cultures lacking large GABAergic cells. In these cultures, bursting was stereotyped with little IBI variation. Therefore, GABAergic signaling provided by the large GABAergic neurons, either alone or together with other GABAergic neurons, promotes temporally clustered network activity.

TIMING OF NETWORK ACTIVITY DIFFERENTIATION

In cultured networks, the differentiation of early network activity, i.e., the increase of bursting frequency has been correlated with the increase of synaptogenesis and the functional maturation of synapses (Muramoto et al., 1993; Voigt et al., 2005). In slices and slice cultures, the regression of calcium transients with high attendance (Corlew et al., 2004), the disappearance of large scale calcium transients (Garaschuk et al., 2000), and the sequential development of more localized activity (Allene et al., 2008) have been described. The GABA shift, which occurs temporally correlated with these changes (Garaschuk et al., 2000), was proposed as the mechanism triggering spontaneous activity maturation.

The decrease in the number of neurons showing intracellular calcium transients upon $GABA_AR$ activation with muscimol (**Figures 4 and 12**) reflects the time course of the GABA shift (Lin et al., 1994; LoTurco et al., 1995; Chen et al., 1996; Owens et al., 1996; Garaschuk et al., 2000; Ganguly et al., 2001), which is typical for the early postnatal development of cortical and hippocampal networks (Ben-Ari et al., 2007; Blaesse et al., 2009). Our results show that both the decrease in large-scale synchronicity and the appearance of clustered burst activity with age were temporally correlated with the GABA shift. Accordingly, we asked if in cultures the maturation of network activity patterns might depend on the development of the GABA action.

The developmental change of the mode of GABA action is mediated by a decreased expression of the sodium-potassium-chloride cotransporter NKCC1, which accumulates chloride in young neurons, and an increased expression of the potassium-chloride

cotransporter KCC2, which extrudes chloride from mature neurons (Ben-Ari et al., 2007; Blaesse et al., 2009). Bumetanide, at doses that selectively block the chloride-importing by NKCC1, results in a hyperpolarization shift of the $GABA_A$R reversal potential (Dzhala et al., 2005, 2008; Sipila et al., 2006; Balena and Woodin, 2008; Zhu et al., 2008). The blockade of the NKCC1 function in young vCtx cultures induced a premature attenuation of burst regularity, including the appearance of less synchronized events (**Figures 5B,E**). Taken together, these data suggest that the depolarizing to hyperpolarizing shift of GABA contributes significantly in shaping the early synchronized activity of neocortical networks *in vitro*.

$GABA_A$ SIGNALING AND GABA SHIFT

Previous studies provide conflicting evidence as to the role of $GABA_A$ signaling in the causation of the GABA shift (for a review see: Ben-Ari et al., 2007). In the model put forward by Ganguly et al. (2001), $GABA_A$ signaling acts as a self-limiting trophic factor during hippocampus development, causing its own shift from depolarizing to hyperpolarizing. According to this model, $GABA_A$ depolarization increases KCC2 expression, which then diminishes the intracellular chloride concentration. Although the general idea of the shift being modulated by depolarizing activity has been confirmed (Sernagor et al., 2003; Leitch et al., 2005), the concept that KCC2 expression and the GABA shift specifically depend on GABA signaling and $GABA_A$ mediated depolarization remains controversial (Ludwig et al., 2003; Titz et al., 2003; Wojcik et al., 2006; Sipila et al., 2009).

In the present study the dCtx networks show rare GABAergic neurons and $GABA_A$ signaling had only minor effects on the network activity. According to the Ganguly model, a GABA shift should be impaired or delayed in the absence of GABAergic neurons, as in dCtx networks. Contrary to this prediction, a shift of GABAergic action occurs in both vCtx and dCtx networks, independently of the GABAergic neuronal content. This is in line with previous results in hippocampal and midbrain cultures showing that a GABA shift and the up-regulation of KCC2 expression can take place in the complete absence of $GABA_A$R signaling (Ludwig et al., 2003; Titz et al., 2003; Wojcik et al., 2006), or of depolarizing GABA signaling (Sipila et al., 2009).

CONTRIBUTION OF GABAergic NEURONS TO NETWORK ACTIVITY PATTERNS

The activity dynamics of mature vCtx cultures with a well developed network of large GABAergic neurons remarkably differed from that of dCtx cultures with deficient GABAergic innervation. The presence of GABA interneurons with long-range connection seems necessary for the development of less synchronized and temporally clustered network activity pattern. With an exceptionally high density of synapses onto their dendrites and a widespread axonal arborization, large GABAergic neurons can effectively integrate inputs from presynaptic cells and propagate their output to close-by and distant neurons simultaneously (Voigt et al., 2001).

At this point it is not entirely clear if the small fraction of bipolar/bitufted GABAergic neurons contribute to the network activity development in vCtx or dCtx cultures. In dCtx cultures, small GABAergic neurons are present in very low density and fail to build a continuous network. dCtx networks thus represent a prototype of an immature network with predominantly glutamatergic circuitry that becomes spontaneously active with a local deficiency in GABAergic neurons from the ventral telencephalic lineage. Besides providing information about the role of GABAergic signaling to the development of network activity, these networks might be used to interrogate how the earlier development of the more lateral regions influences the development of dorsal regions. Lischalk et al. (2009) showed that temporal areas of the cortex may function as pacemakers for the early network transients, which then propagate to the rest of the cortex. Because GABAergic neurons invade the cortex from ventral to dorsal (Marin and Rubenstein, 2001), it is feasible to assume that these neurons differentiate faster in more lateral parts of the cortex, e.g., the temporal cortex. Given that vCtx cultures develop a faster pace of recurrent burst activity than age-matched dCtx cultures, more lateral cortical regions could prematurely drive the more dorsal cortex. If vCtx and dCtx cultures are grown in separate compartments, they connect to each other (see Voigt et al., 2005), and dCtx cultures show similar patterns of activity as vCtx cultures (de Lima and Voigt, unpublished results). Also in a local cortical network, this type of early functional interaction might be relevant for the development of, for example, layers of neurons with different GABAergic populations.

The development of spontaneous activity in cultures obtained from the embryonic cortex consistently varies in correlation with the content of GABAergic neurons. Although differences between the developing vCtx and dCtx cultures might not be limited to the GABAergic system (Bellion et al., 2003), our data suggest that the early GABAergic system sculptures early network activity dynamics, predictably influencing the microstructure and regularity of burst firing.

ACKNOWLEDGMENTS

The authors thank Ms. B. Adam and Ms. A. Ritter for expert technical assistance. This work was supported by the Bundesministerium für Bildung und Forschung (grant BMBF/BNCN 016Q0702) and the Land Sachsen Anhalt (grant LSA 3431A/0302M).

REFERENCES

Allene, C., Cattani, A., Ackman, J. B., Bonifazi, P., Aniksztejn, L., Ben-Ari, Y., and Cossart, R. (2008). Sequential generation of two distinct synapse-driven network patterns in developing neocortex. *J. Neurosci.* 28, 12851–12863.

Angenstein, F., Niessen, H. G., Goldschmidt, J., Vielhaber, S., Ludolph, A. C., and Scheich, H. (2004). Age-dependent changes in MRI of motor brain stem nuclei in a mouse model of ALS. *Neuroreport* 15, 2271–2274.

Baker, R. E., Corner, M. A., and van Pelt, J. (2006). Spontaneous neuronal discharge patterns in developing organotypic mega-co-cultures of neonatal rat cerebral cortex. *Brain Res.* 1101, 29–35.

Bakkum, D. J., Chao, Z. C., and Potter, S. M. (2008). Spatio-temporal electrical stimuli shape behavior of an embodied cortical network in a goal-directed learning task. *J. Neural Eng.* 5, 310–323.

Balena, T., and Woodin, M. A. (2008). Coincident pre- and postsynaptic activity downregulates NKCC1 to hyperpolarize E(Cl) during development. *Eur. J. Neurosci.* 27, 2402–2412.

Barbe, M. F., and Levitt, P. (1991). The early commitment of fetal neurons to the limbic cortex. *J. Neurosci.* 11, 519–533.

Baruchi, I., Volman, V., Raichman, N., Shein, M., and Ben-Jacob, E. (2008). The emergence and properties of mutual synchronization in in vitro

coupled cortical networks. *Eur. J. Neurosci.* 28, 1825–1835.
Batista-Brito, R., and Fishell, G. (2009). The developmental integration of cortical interneurons into a functional network. *Curr. Top. Dev. Biol.* 87, 81–118.
Bellion, A., and Metin, C. (2005). Early regionalisation of the neocortex and the medial ganglionic eminence. *Brain Res. Bull.* 66, 402–409.
Bellion, A., Wassef, M., and Metin, C. (2003). Early differences in axonal outgrowth, cell migration and GABAergic differentiation properties between the dorsal and lateral cortex. *Cereb. Cortex* 13, 203–214.
Ben-Ari, Y. (2001). Developing networks play a similar melody. *Trends Neurosci.* 24, 353–360.
Ben-Ari, Y. (2002). Excitatory actions of gaba during development: the nature of the nurture. *Nat. Rev. Neurosci.* 3, 728–739.
Ben-Ari, Y., Gaiarsa, J. L., Tyzio, R., and Khazipov, R. (2007). GABA: a pioneer transmitter that excites immature neurons and generates primitive oscillations. *Physiol. Rev.* 87, 1215–1284.
Blaesse, P., Airaksinen, M. S., Rivera, C., and Kaila, K. (2009). Cation-chloride cotransporters and neuronal function. *Neuron* 61, 820–838.
Blankenship, A. G., and Feller, M. B. (2010). Mechanisms underlying spontaneous patterned activity in developing neural circuits. *Nat. Rev. Neurosci.* 11, 18–29.
Bracci, E., Ballerini, L., and Nistri, A. (1996). Spontaneous rhythmic bursts induced by pharmacological block of inhibition in lumbar motoneurons of the neonatal rat spinal cord. *J. Neurophysiol.* 75, 640–647.
Butt, S. J., Fuccillo, M., Nery, S., Noctor, S., Kriegstein, A., Corbin, J. G., and Fishell, G. (2005). The temporal and spatial origins of cortical interneurons predict their physiological subtype. *Neuron* 48, 591–604.
Campbell, K. (2003). Dorsal–ventral patterning in the mammalian telencephalon. *Curr. Opin. Neurobiol.* 13, 50–56.
Chagnac-Amitai, Y., and Connors, B. W. (1989). Horizontal spread of synchronized activity in neocortex and its control by GABA-mediated inhibition. *J. Neurophysiol.* 61, 747–758.
Chao, Z. C., Bakkum, D. J., and Potter, S. M. (2008). Shaping embodied neural networks for adaptive goal-directed behavior. *PLoS Comput. Biol.* 4, e1000042. doi: 10.1371/journal.pcbi.1000042.
Chen, G., Trombley, P. Q., and van den Pol, A. N. (1996). Excitatory actions of GABA in developing rat hypothalamic neurones. *J. Physiol. (Lond.)* 494, 451–464.
Chiappalone, M., Bove, M., Vato, A., Tedesco, M., and Martinoia, S. (2006). Dissociated cortical networks show spontaneously correlated activity patterns during in vitro development. *Brain Res.* 1093, 41–53.
Chiu, C., and Weliky, M. (2001). Spontaneous activity in developing ferret visual cortex in vivo. *J. Neurosci.* 21, 8906–8914.
Corlew, R., Bosma, M. M., and Moody, W. J. (2004). Spontaneous, synchronous electrical activity in neonatal mouse cortical neurones. *J. Physiol.* 560, 377–390.
Cossart, R., Ikegaya, Y., and Yuste, R. (2005). Calcium imaging of cortical networks dynamics. *Cell Calcium* 37, 451–457.
de Lima, A. D., Gieseler, A., and Voigt, T. (2009). Relationship between GABAergic interneurons migration and early neocortical network activity. *Dev Neurobiol* 69, 105–123.
de Lima, A. D., Lima, B. D., and Voigt, T. (2007). Earliest spontaneous activity differentially regulates neocortical GABAergic interneuron subpopulations. *Eur. J. Neurosci.* 25, 1–16.
de Lima, A. D., Opitz, T., and Voigt, T. (2004). Irreversible loss of a subpopulation of cortical interneurons in the absence of glutamatergic network activity. *Eur. J. Neurosci.* 19, 2931–2943.
de Lima, A. D., and Voigt, T. (1997). Identification of two distinct populations of GABAergic neurons in cultures of the rat cerebral cortex. *J. Comp. Neurol.* 388, 526–541.
de Lima, A. D., and Voigt, T. (1999). Astroglia inhibit the proliferation of neocortical cells and prevent the generation of small GABAergic neurons in vitro. *Eur. J. Neurosci.* 11, 3845–3856.
Dzhala, V. I., Brumback, A. C., and Staley, K. J. (2008). Bumetanide enhances phenobarbital efficacy in a neonatal seizure model. *Ann. Neurol.* 63, 222–235.
Dzhala, V. I., Talos, D. M., Sdrulla, D. A., Brumback, A. C., Mathews, G. C., Benke, T. A., Delpire, E., Jensen, F. E., and Staley, K. J. (2005). NKCC1 transporter facilitates seizures in the developing brain. *Nat. Med.* 11, 1205–1213.
Eytan, D., and Marom, S. (2006). Dynamics and effective topology underlying synchronization in networks of cortical neurons. *J. Neurosci.* 26, 8465–8476.
Feinerman, O., Segal, M., and Moses, E. (2007). Identification and dynamics of spontaneous burst initiation zones in unidimensional neuronal cultures. *J. Neurophysiol.* 97, 2937–2948.
Ferri, R. T., and Levitt, P. (1995). Regulation of regional differences in the differentiation of cerebral cortical neurons by EGF family-matrix interactions. *Development* 121, 1151–1160.
Ganguly, K., Schinder, A. F., Wong, S. T., and Poo, M. (2001). GABA itself promotes the developmental switch of neuronal GABAergic responses from excitation to inhibition. *Cell* 105, 521–532.
Garaschuk, O., Linn, J., Eilers, J., and Konnerth, A. (2000). Large-scale oscillatory calcium waves in the immature cortex. *Nat. Neurosci.* 3, 452–459.
Giugliano, M., Darbon, P., Arsiero, M., Luscher, H. R., and Streit, J. (2004). Single-neuron discharge properties and network activity in dissociated cultures of neocortex. *J. Neurophysiol.* 92, 977–996.
Gonzalez-Burgos, G., and Lewis, D. A. (2008). GABA neurons and the mechanisms of network oscillations: implications for understanding cortical dysfunction in schizophrenia. *Schizophr. Bull.* 34, 944–961.
Kamioka, H., Maeda, E., Jimbo, Y., Robinson, H. P. C., and Kawana, A. (1996). Spontaneous periodic synchronized bursting during formation of mature patterns of connections in cortical cultures. *Neurosci. Lett.* 206, 109–112.
Le, F. J., Rutten, W. L., Stegenga, J., Wolters, P. S., Ramakers, G. J., and van, P. J. (2007). Conditional firing probabilities in cultured neuronal networks: a stable underlying structure in widely varying spontaneous activity patterns. *J. Neural Eng.* 4, 54–67.
Leitch, E., Coaker, J., Young, C., Mehta, V., and Sernagor, E. (2005). GABA type-A activity controls its own developmental polarity switch in the maturing retina. *J. Neurosci.* 25, 4801–4805.
Letinic, K., Zoncu, R., and Rakic, P. (2002). Origin of GABAergic neurons in the human neocortex. *Nature* 417, 645–649.
Lewis, D. A., Hashimoto, T., and Volk, D. W. (2005). Cortical inhibitory neurons and schizophrenia. *Nat. Rev. Neurosci.* 6, 312–324.
Lin, M. H., Takahashi, M. P., Takahashi, Y., and Tsumoto, T. (1994). Intracellular calcium increase induced by GABA in visual cortex of fetal and neonatal rats and its disappearance with development. *Neurosci. Res.* 20, 85–94.
Lischalk, J. W., Easton, C. R., and Moody, W. J. (2009). Bilaterally propagating waves of spontaneous activity arising from discrete pacemakers in the neonatal mouse cerebral cortex. *Dev Neurobiol* 69, 407–414.
LoTurco, J. J., Owens, D. F., Heath, M. J. S., Davis, M. B. E., and Kriegstein, A. R. (1995). GABA and glutamate depolarize cortical progenitor cells and inhibit DNA synthesis. *Neuron* 15, 1287–1298.
Ludwig, A., Li, H., Saarma, M., Kaila, K., and Rivera, C. (2003). Developmental up-regulation of KCC2 in the absence of GABAergic and glutamatergic transmission. *Eur. J. Neurosci.* 18, 3199–3206.
Maeda, E., Robinson, H. P. C., and Kawana, A. (1995). The mechanisms of generation and propagation of synchronized bursting in developing networks of cortical neurons. *J. Neurosci.* 15, 6834–6845.
Marder, E., and Goaillard, J. M. (2006). Variability, compensation and homeostasis in neuron and network function. *Nat. Rev. Neurosci.* 7, 563–574.
Marin, O., and Rubenstein, J. L. (2001). A long, remarkable journey: tangential migration in the telencephalon. *Nat. Rev. Neurosci.* 2, 780–790.
Marom, S., and Shahaf, G. (2002). Development, learning and memory in large random networks of cortical neurons: lessons beyond anatomy. *Q. Rev. Biophys.* 35, 63–87.
McCabe, A. K., Chisholm, S. L., Picken-Bahrey, H. L., and Moody, W. J. (2006). The self-regulating nature of spontaneous synchronized activity in developing mouse cortical neurones. *J. Physiol.* 577, 155–167.
Miles, R., Wong, R. K., and Traub, R. D. (1984). Synchronized afterdischarges in the hippocampus: contribution of local synaptic interactions. *Neuroscience* 12, 1179–1189.
Minlebaev, M., Ben-Ari, Y., and Khazipov, R. (2007). Network mechanisms of spindle-burst oscillations in the neonatal rat barrel cortex in vivo. *J. Neurophysiol.* 97, 692–700.
Minlebaev, M., Ben-Ari, Y., and Khazipov, R. (2009). NMDA receptors pattern early activity in the developing barrel cortex in vivo. *Cereb. Cortex* 19, 688–696.
Moody, W. J., and Bosma, M. M. (2005). Ion channel development, spontaneous activity, and activity-dependent development in nerve and muscle cells. *Physiol. Rev.* 85, 883–941.
Muramoto, K., Ichikawa, M., Kawahara, M., Kobayashi, K., and Kuroda, Y. (1993). Frequency of synchronous oscillations of neuronal activity increases during development and is correlated to the number of synapses in cultured cortical neuron networks. *Neurosci. Lett.* 163, 163–165.
O'Donovan, M. J. (1999). The origin of spontaneous activity in developing networks of the vertebrate nervous system. *Curr. Opin. Neurobiol.* 9, 94–104.

Opitz, T., de Lima, A. D., and Voigt, T. (2002). Spontaneous development of synchronous oscillatory activity during maturation of cortical networks in vitro. *J. Neurophysiol.* 88, 2196–2206.

Owens, D. F., Boyce, L. H., Davis, M. B. E., and Kriegstein, A. R. (1996). Excitatory GABA responses in embryonic and neonatal cortical slices demonstrated by gramicidin perforated-patch recordings and calcium imaging. *J. Neurosci.* 16, 6414–6423.

Owens, D. F., and Kriegstein, A. R. (2002). Is there more to GABA than synaptic inhibition? *Nat. Rev. Neurosci.* 3, 715–727.

Pasquale, V., Massobrio, P., Bologna, L. L., Chiappalone, M., and Martinoia, S. (2008). Self-organization and neuronal avalanches in networks of dissociated cortical neurons. *Neuroscience* 153, 1354–1369.

Puelles, L., and Rubenstein, J. L. (2003). Forebrain gene expression domains and the evolving prosomeric model. *Trends Neurosci.* 26, 469–476.

Raichman, N., and Ben-Jacob, E. (2008). Identifying repeating motifs in the activation of synchronized bursts in cultured neuronal networks. *J. Neurosci. Methods* 170, 96–110.

Rheims, S., Represa, A., Ben-Ari, Y., and Zilberter, Y. (2008). Layer-specific generation and propagation of seizures in slices of developing neocortex: role of excitatory GABAergic synapses. *J. Neurophysiol.* 100, 620–628.

Rivera, C., Voipio, J., and Kaila, K. (2005). Two developmental switches in GABAergic signalling: the K+-Cl– cotransporter KCC2 and carbonic anhydrase CAVII. *J. Physiol.* 562, 27–36.

Robinson, H. P. C., Kawahara, M., Jimbo, Y., Torimitsu, K., Kuroda, Y., and Kawana, A. (1993). Periodic synchronized bursting and intracellular calcium transients elicited by low magnesium in cultured cortical neurons. *J. Neurophysiol.* 70, 1606–1616.

Rolston, J. D., Wagenaar, D. A., and Potter, S. M. (2007). Precisely timed spatiotemporal patterns of neural activity in dissociated cortical cultures. *Neuroscience* 148, 294–303.

Schmalenbach, C., and Müller, H. W. (1993). Astroglia–neuron interactions that promote long-term neuronal survival. *J. Chem. Neuroanat.* 6, 229–237.

Sernagor, E., Young, C., and Eglen, S. J. (2003). Developmental modulation of retinal wave dynamics: shedding light on the GABA saga. *J. Neurosci.* 23, 7621–7629.

Shahaf, G., Eytan, D., Gal, A., Kermany, E., Lyakhov, V., Zrenner, C., and Marom, S. (2008). Order-based representation in random networks of cortical neurons. *PLoS Comput. Biol.* 4:e1000228. doi: 10.1371/journal.pcbi.1000228.

Sheroziya, M. G., von Bohlen Und, H. O., Unsicker, K., and Egorov, A. V. (2009). Spontaneous bursting activity in the developing entorhinal cortex. *J. Neurosci.* 29, 12131–12144.

Sipila, S. T., Huttu, K., Yamada, J., Afzalov, R., Voipio, J., Blaesse, P., and Kaila, K. (2009). Compensatory enhancement of intrinsic spiking upon NKCC1 disruption in neonatal hippocampus. *J. Neurosci.* 29, 6982–6988.

Sipila, S. T., Schuchmann, S., Voipio, J., Yamada, J., and Kaila, K. (2006). The cation-chloride cotransporter NKCC1 promotes sharp waves in the neonatal rat hippocampus. *J. Physiol.* 573, 765–773.

Streit, J. (1993). Regular oscillations of synaptic activity in spinal networks in vitro. *J. Neurophysiol.* 70, 871–878.

Sudbury, J. R., and Avoli, M. (2007). Epileptiform synchronization in the rat insular and perirhinal cortices in vitro. *Eur. J. Neurosci.* 26, 3571–3582.

Titz, S., Hans, M., Kelsch, W., Lewen, A., Swandulla, D., and Misgeld, U. (2003). Hyperpolarizing inhibition develops without trophic support by GABA in cultured rat midbrain neurons. *J. Physiol.* 550, 719–730.

Uhlhaas, P. J., Haenschel, C., Nikolic, D., and Singer, W. (2008). The role of oscillations and synchrony in cortical networks and their putative relevance for the pathophysiology of schizophrenia. *Schizophr. Bull.* 34, 927–943.

Van Pelt, J., Corner, M. A., Wolters, P. S., Rutten, W. L., and Ramakers, G. J. (2004). Longterm stability and developmental changes in spontaneous network burst firing patterns in dissociated rat cerebral cortex cell cultures on multielectrode arrays. *Neurosci. Lett.* 361, 86–89.

Voigt, T., Opitz, T., and de Lima, A. D. (2001). Synchronous oscillatory activity in immature cortical network is driven by GABAergic preplate neurons. *J. Neurosci.* 21, 8895–8905.

Voigt, T., Opitz, T., and de Lima, A. D. (2005). Activation of early silent synapses by spontaneous synchronous network activity limits the range of neocortical connections. *J. Neurosci.* 25, 4605–4615.

Wagenaar, D. A., Pine, J., and Potter, S. M. (2006a). An extremely rich repertoire of bursting patterns during the development of cortical cultures. *BMC Neurosci.* 7, 11.

Wagenaar, D. A., Pine, J., and Potter, S. M. (2006b). Searching for plasticity in dissociated cortical cultures on multi-electrode arrays. *J. Negat. Results Biomed.* 5, 16.

Wojcik, S. M., Katsurabayashi, S., Guillemin, I., Friauf, E., Rosenmund, C., Brose, N., and Rhee, J. S. (2006). A shared vesicular carrier allows synaptic corelease of GABA and glycine. *Neuron* 50, 575–587.

Wonders, C. P., and Anderson, S. A. (2006). The origin and specification of cortical interneurons. *Nat. Rev. Neurosci.* 7, 687–696.

Yamada, J., Okabe, A., Toyoda, H., Kilb, W., Luhmann, H. J., and Fukuda, A. (2004). Cl– uptake promoting depolarizing GABA actions in immature rat neocortical neurones is mediated by NKCC1. *J. Physiol.* 557, 829–841.

Yang, J. W., Hanganu-Opatz, I. L., Sun, J. J., and Luhmann, H. J. (2009). Three patterns of oscillatory activity differentially synchronize developing neocortical networks in vivo. *J. Neurosci.* 29, 9011–9025.

Yuste, R., and Katz, L. C. (1991). Control of postsynaptic Ca^{2+} influx in developing neocortex by excitatory and inhibitory neurotransmitters. *Neuron* 6, 333–344.

Yvon, C., Czarnecki, A., and Streit, J. (2007). Riluzole-induced oscillations in spinal networks. *J. Neurophysiol.* 97, 3607–3620.

Zhu, L., Polley, N., Mathews, G. C., and Delpire, E. (2008). NKCC1 and KCC2 prevent hyperexcitability in the mouse hippocampus. *Epilepsy Res.* 79, 201–212.

Conflict of Interest Statement: The authors declare that the research was conducted in the absence of any commercial or financial relationships that could be construed as a potential conflict of interest.

Received: 16 February 2010; paper pending published: 10 March 2010; accepted: 16 April 2010; published online: 21 June 2010.

*Citation: Baltz T, de Lima AD and Voigt T (2010) Contribution of GABAergic interneurons to the development of spontaneous activity patterns in cultured neocortical networks. Front. Cell. Neurosci. **4**:15. doi: 10.3389/fncel.2010.00015*

frontiers in
CELLULAR NEUROSCIENCE

ORIGINAL RESEARCH ARTICLE
published: 14 July 2010
doi: 10.3389/fncel.2010.00017

Temporal coding at the immature depolarizing GABAergic synapse

Guzel Valeeva[1,2†], Azat Abdullin[1,2,3†], Roman Tyzio[1†], Andrei Skorinkin[2,4], Evgeny Nikolski[2], Yehezkiel Ben-Ari[1] and Rustem Khazipov[1]*

[1] *Institut de Neurobiologie de la Méditerranée-Institut National de la Santé et de la Recherche Médicale U901, Universite Mediterranean Aix-Marseille II, Marseille, France*
[2] *Kazan Institute of Biochemistry and Biophysics, Russian Academy of Sciences, Kazan, Russia*
[3] *Tatar State University of Humanities and Education, Kazan, Russia*
[4] *Kazan Federal University, Kazan, Russia*

Edited by:
Enrico Cherubini, International School for Advanced Studies, Italy

Reviewed by:
Enrico Cherubini, International School for Advanced Studies, Italy
Ivan Soltesz, University of California at Irvine, USA

***Correspondence:**
Rustem Khazipov, Institut de Neurobiologie de la Méditerranée-Institut National de la Santé et de la Recherche Médicale U901, 163 route de Luminy, Marseille 13273, France. e-mail: khazipov@inmed.univ-mrs.fr

†Guzel Valeeva, Azat Abdullin, and Roman Tyzio have contributed equally to this work.

In the developing hippocampus, GABA exerts depolarizing and excitatory actions and contributes to the generation of neuronal network driven giant depolarizing potentials (GDPs). Here, we studied spike time coding at immature GABAergic synapses and its impact on synchronization of the neuronal network during GDPs in the neonatal (postnatal days P2–6) rat hippocampal slices. Using extracellular recordings, we found that the delays of action potentials (APs) evoked by synaptic activation of GABA(A) receptors are long (mean, 65 ms) and variable (within a time window of 10–200 ms). During patch-clamp recordings, depolarizing GABAergic responses were mainly subthreshold and their amplification by persistent sodium conductance was required to trigger APs. AP delays at GABAergic synapses shortened and their variability reduced with an increase in intracellular chloride concentration during whole-cell recordings. Negative shift of the GABA reversal potential (E_{GABA}) with low concentrations of bumetanide, or potentiation of GABA(A) receptors with diazepam reduced GDPs amplitude, desynchronized neuronal firing during GDPs and slowed down GDPs propagation. Partial blockade of GABA(A) receptors with bicuculline increased neuronal synchronization and accelerated GDPs propagation. We propose that spike timing at depolarizing GABA synapses is determined by intracellular chloride concentration. At physiological levels of intracellular chloride GABAergic depolarization does not reach the action potential threshold and amplification of GABAergic responses by non-inactivating sodium conductance is required for postsynaptic AP initiation. Slow and variable excitation at GABAergic synapse determines the level of neuronal synchrony and the rate of GDPs propagation in the developing hippocampus.

Keywords: gamma aminobutyric acid, development, neonatal, hippocampus

INTRODUCTION

Gamma aminobutyric acid is the main inhibitory neurotransmitter in the adult brain. Synchronous inhibition by hyperpolarization and shunt provided by GABAergic interneurons is instrumental for the generation of various network activity patterns in the adult brain (Freund and Buzsaki, 1996). However, early in development, GABA acting via chloride-permeable GABA(A) channels, exerts depolarizing and excitatory action due to elevated intracellular chloride concentration in immature neurons (Ben Ari et al., 2007). Depolarizing GABA is involved in the generation of primitive pattern of neuronal network activity in the immature hippocampus – so called GDPs (Ben-Ari et al., 1989; Khazipov et al., 2004; Dzhala et al., 2005; Sipila et al., 2005). During GDPs, both pyramidal cells and interneurons fire within a time window of a few hundreds of milliseconds. GDPs are initiated in CA3 hippocampal region and propagate, in a wave-like manner, to CA1, dentate gyrus, and along hippocampus in a septo-temporal direction. Slow wave-like propagation of GDPs along the intact hippocampus *in vitro* may take almost a second (Leinekugel et al., 1998). Excitation to pyramidal cells and interneurons during GDPs is brought by synergistic excitatory actions of GABA and glutamate (Menendez de la et al., 1996; Khazipov et al., 1997; Leinekugel et al., 1997; De la Prida et al., 1998; Bolea et al., 1999; Lamsa et al., 2000). By providing a coincidence between pre- and postsynaptic neurons, GDPs are thought to be involved in activity-dependent spike timing dependent plasticity (Kasyanov et al., 2004; Mohajerani and Cherubini, 2006), which is particularly robust during the early developmental period (Isaac et al., 1995; Durand et al., 1996). However, factors determining spatio-temporal characteristics of GPDs and spike timing during GDPs are not completely understood.

While excitatory actions of GABA on immature neurons have been well documented in virtually all brain structures using variety of electrophysiological and imaging techniques, an important question of postsynaptic action potential (AP) time coding at the GABAergic synapse has not been addressed. AP temporal coding is a major characteristic of excitatory synapse, which implies a delay of APs and its variability in the postsynaptic cell receiving an excitatory input. AP temporal coding is determined by kinetics of transmitter release, kinetics of postsynaptic receptor mediated excitatory currents, and postsynaptic membrane properties including voltage-gated conductances which shape and amplify or inhibit postsynaptic potentials (PSPs) (Fricker and Miles, 2000). In

glutamatergic synapses, synchronous activation of multiple glutamatergic inputs generates suprathreshold EPSPs that evoke APs with short and reliable delays that synchronizes neuronal population giving rise to population spike. Upon removal of GABAergic inhibition, synchronization of neuronal population via recurrent collateral glutamatergic synapses also enables generation of high-frequency oscillations (Miles and Wong, 1986, 1987). However, small near-threshold excitatory postsynaptic potentials (EPSPs) evoke postsynaptic APs with long and variable delays due to activation of the voltage-gated potassium conductance and amplification of EPSPs by non-inactivating sodium conductance in pyramidal cells (Fricker and Miles, 2000). Thus, the AP timing at glutamatergic synapses strongly depends on the amount of glutamatergic conductance activated in the postsynaptic cell. In contrast, at immature GABAergic synapses E_{GABA} is likely to be the critical factor determining the AP timing as E_{GABA} is set by chloride transporters not far from the AP threshold (AP_{thr}) (Ben-Ari et al., 1989; Hollrigel et al., 1998; Sipila et al., 2005; Rheims et al., 2008). In the present study, we provide evidence that (i) GABAergic interneurons excite CA3 pyramidal cells with long and variable delays; (ii) the AP timing at GABAergic synapses depends on intracellular chloride concentration in the postsynaptic neuron; and (iii) in physiological conditions, GABAergic depolarization is mainly subthreshold and requires activation of persistent sodium conductance to trigger APs. We also show that slow and variable spike timing at depolarizing GABAergic synapses shapes GDPs by reducing neuronal synchronization and slowing down their propagation.

MATERIALS AND METHODS

Hippocampal slices were prepared from Wistar rats of both sexes (Postnatal days [P]2–6). All animal use protocols conformed to the INSERM guidelines on the use of laboratory animals. Transverse (perpendicular to the longitudinal hippocampal axis) slices (350–500 μm) were cut from the middle third of hippocampus using Vibratome (VT 1000E; Leica, Nussloch, Germany). Slices were kept in oxygenated (95% O_2/5% CO_2) artificial cerebrospinal fluid (ACSF) of the following composition (in mM): NaCl 126, KCl 3.5, $CaCl_2$ 2.0, $MgCl_2$ 1.3, $NaHCO_3$ 25, NaH_2PO_4 1.2 and glucose 11 (pH 7.4) at room temperature (20–22°C) at least 1 h before use. For recordings, slices were placed into a conventional fully submerged chamber superfused with ACSF at a rate of 2–3 ml/min.

Extracellular field potentials and multiple unit activity (MUA) were recorded using 64-electrodes planar arrays (MCA, Germany) or 2–3 electrodes made from tungsten wire of diameter 50 μm (California Fine Wire, Grover Beach, CA, USA) placed in CA3 and CA1 pyramidal cell layer. Signals were amplified (×1000, bandpass 0.1 Hz–4 kHz) and digitized at 10 kHz. Patch-clamp recordings were performed using Axopatch 200A (Axon Instruments, Union City, CA, USA) and EPC-9 (HEKA Elektronik Dr. Schulze GmbH, Lambrecht/Pfalz, Germany) amplifiers. Patch electrodes were made from borosilicate glass capillaries (GC150F-15, Clark Electromedical Instruments). For recordings of single GABA(A) channels, patch pipette solution contained (in mM): NaCl 120, TEA–Cl 20, KCl 5, 4-aminopyridine 5, $CaCl_2$ 0.1, $MgCl_2$ 10, glucose 10, Hepes–NaOH 10 buffered to pH 7.2–7.3 and GABA (1–5 μM) was added at the day of experiment from 1 mM frozen stock solution. Driving force for GABA(A) receptor mediated currents was determined from the current–voltage relationships of the currents through single GABA(A) channels as described earlier (Tyzio et al., 2006) and corrected for an error of 2 mV (Tyzio et al., 2008). Membrane potential was estimated using cell-attached recordings of single NMDA channels as described before (Leinekugel et al., 1997; Tyzio et al., 2003). For recordings of single NMDA channels pipette solution contained nominally Mg^{2+} free ACSF with NMDA (10 μM), glycine (1 μM), and strychnine (1 μM). Patch pipette solution for whole-cell recordings contained (in mM): potassium gluconate (0–135) or KCl (0–135); $MgCl_2$, 2; Hepes, 10; Mg–ATP, 4; Na–GTP, 0.3; equilibrated at pH 7.3 with KOH. In current-clamp recordings, membrane potential was maintained at values between −75 and −80 mV by injection of constant negative current. Synaptic GABA(A) receptor mediated responses were evoked by electrical stimulation in the presence of the antagonists of glutamate ionotropic receptors CNQX (10 μM) and D-APV (40 μM), and GABA(B) receptors CGP55845 (1 μM). Simulated GABA–PSPs were evoked by injection of GABA-PSCs waveform obtained by averaging one hundred spontaneous GABA-PSCs recorded in voltage-clamp mode in the presence of glutamate ionotropic receptor antagonists. The amplitude of GABA-PSPs was adjusted to evoke near-threshold responses. Action potential threshold (AP_{thr}) was determined offline using the custom-made software (IGOR Pro, WaveMetrics) as a value of membrane potential at which dU/dt exceeded 10 V/s (Stuart et al., 1997; Fricker et al., 1999). AP delays were measured as a time between the stimulus and AP peak. Recordings were digitized (10 kHz) online with Digidata 1200/1322 interface cards (Axon Instruments, Union City, CA, USA) and analyzed offline with Axon package, miniAnalysis (Synaptosoft), IGOR Pro (WaveMetrics) and Origin 5.0 (Microcal Software, Northampton, MA, USA). Group measures are expressed as means ± SE unless indicated; error bars also indicate SE. The statistical significance of differences was assessed with the Students *t*-test and Kolmogorov–Smirnov test. The level of significance was set at $P < 0.05$.

RESULTS

ACTION POTENTIAL DELAYS AT THE EXCITATORY GABAergic SYNAPSE

Experiments were performed in hippocampal slices obtained from P2–6 neonatal rats. To asses temporal characteristics of GABAergic excitation we determined the AP delays in CA3 pyramidal cells in response to synaptic activation of GABA(A) receptors. Synaptic GABA(A) receptor mediated responses were elicited by electrical slice stimulation using bipolar electrodes or glass pipette positioned in a vicinity of the recording site (separation distance <0.5 mm) in the presence of ionotropic glutamate (10 μM CNQX, 40 μM D-APV) and GABA(B) (1 μM CGP55845) receptor antagonists (Davies et al., 1990; Khazipov et al., 1993).

In the first experiment, we used extracellular recordings of MUA that is action currents from tens of neurons nearby the recording site (Cohen and Miles, 2000). Synaptic activation of GABA(A) receptors invariably increased MUA in CA3 pyramidal cell layer (**Figure 1**), and the response was suppressed by the GABA(A) receptor antagonist bicuculline (10 μM; see also **Figure 4**). In certain cases, short-latency spikes persisted in the presence of bicuculline, probably due to the direct stimulation of axons of the recorded neurons (not shown); these experiments were discarded from the analysis. In the experiments, in which bicuculline completely

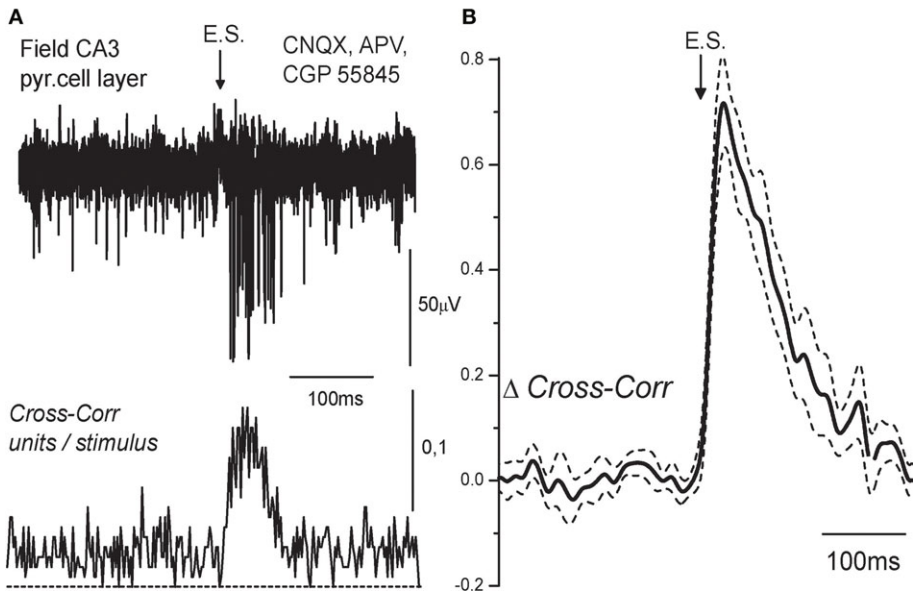

FIGURE 1 | Temporal characteristics of excitation at GABAergic synapses using extracellular recordings. (A) Extracellular recordings of the action potentials (APs) evoked by electrical stimulation (ES) in the presence of the AMPA, NMDA, and GABA(B) receptor antagonists (10 μM CNQX, 40 μM D-APV, 1 μM CGP55845) in the CA3 layer of P5 rat hippocampus. Five traces are superimposed. Below: cross-correlogram of the APs times versus stimulus. **(B)** Average cross-correlogram of the APs versus stimulus obtained from eight slices (P2–5 rats). Dashed lines show SEM.

suppressed synaptic MUA response, MUA was cross-correlated with stimulus and the time course of MUA response has been analyzed. MUA peaked at 28 ± 6 ms after the stimulus and decayed with a decay time constant of 76 ± 18 ms; half-width of MUA elevation was of 71 ± 13 ms (mean ± S.D.; $n = 8$ slices). Mean value of APs delay was of 65 ± 12 ms ($n = 8$). In none of recorded slices, activation of GABA(A) receptors evoked population spikes, that are a characteristic response to the collective activation of glutamatergic synapses. These results indicate that the AP delays at excitatory GABAergic synapses in the immature CA3 pyramidal cells are long and variable.

DEPENDENCE OF THE TEMPORAL CHARACTERISTICS OF GABA-MEDIATED EXCITATION ON $[Cl^-]_i$

We hypothesized that slow kinetics of GABAergic excitation results from relatively small driving force (DF_{GABA}) of the GABA(A) receptor mediated responses. Therefore, we next studied the temporal characteristics of GABAergic excitation as a function of intracellular chloride concentration. In this aim, we investigated AP delays of evoked by synaptic GABA(A) receptor mediated responses using current-clamp whole-cell recordings from CA3 pyramidal cells with chloride concentration of $[Cl^-]_p$ = 18, 30, 50, and 140 mM in the recording pipette (**Figure 2**). Membrane potential was maintained at −70/−80 mV by injection of the constant negative current to compensate for the leakage through the gigaseal contact between the membrane and pipette (Tyzio et al., 2003). Under these conditions, synaptic activation of GABA(A) receptors evoked depolarizing post-synaptic potentials (GABA-PSPs) which were completely blocked by bicuculline (20 μM). In keeping with the results of previous studies using intracellular recordings with sharp electrodes (Ben-Ari et al., 1989), GABA-PSPs often triggered APs in pyramidal cells. In each neuron, AP probability and delays were analyzed from a hundred of evoked GABA-PSPs. With $[Cl^-]_p$ of 18 mM, GABA-PSPs evoked APs in two of 12 neurons. With $[Cl^-]_p$ of 30, 50, and 140 mM probability of GABA-PSPs to evoke APs increased to 39 ± 8% ($n = 11$), 30 ± 2% ($n = 2$) and 70 ± 7% ($n = 8$), respectively. AP delays and their variability also strongly depended on $[Cl^-]_p$ (**Figure 3**). At $[Cl^-]_p$ of 18 mM, mean AP delay and dispersion attained 56 ± 8 and 14 ± 1 ms, respectively ($n = 2$; **Figure 2A**, left), that was close to the values obtained using extracellular recordings. At $[Cl^-]_p$ = 30 mM, APs delays varied within a range from 8 to 145 ms, with a mean of 38 ± 21 ms ($n = 14$); AP delays were highly variable with standard deviation varying from 8 to 44 ms in individual cells, and with a mean SD of 17 ± 2 ms ($n = 14$). With symmetrical chloride ($[Cl^-]_p$ = 140 mM), AP delays and their dispersion reduced to 12 ± 2 and 4 ± 0.5 ms, respectively ($n = 8$; **Figure 3**, right). Interestingly, at lower $[Cl^-]_p$ values APs barely emerged at the rising phase or peak of GABA-PSPs but rather from an additional depolarization, which prolonged and amplified synaptic potentials. With elevated intracellular chloride concentration, APs typically emerged at the rising phase of GABA-PSPs.

In the immature cortical neurons, elevated $[Cl^-]_i$ is set by NKCC1 chloride co-transporter (Payne et al., 2003; Yamada et al., 2004; Dzhala et al., 2005; Tyzio et al., 2006). We therefore hypothesized that reduction of NKCC1 activity, via reduction in $[Cl^-]_i$ and negative shift in E_{GABA}, will increase GABA-evoked AP delays and their variability. Using extracellular recordings of MUA responses evoked by pharmacologically isolated GABA-PSPs we found that indeed, low concentrations of bumetanide (0.3–0.6 μM) cause significant increase in the AP delays and their variability, that was manifested by an increase in the mean AP delay, half-width and decay time constant of the MUA response. Bumetanide also reduced APs number in MUA response evoked by GABA-PSPs (**Figure 4**). Thus, the

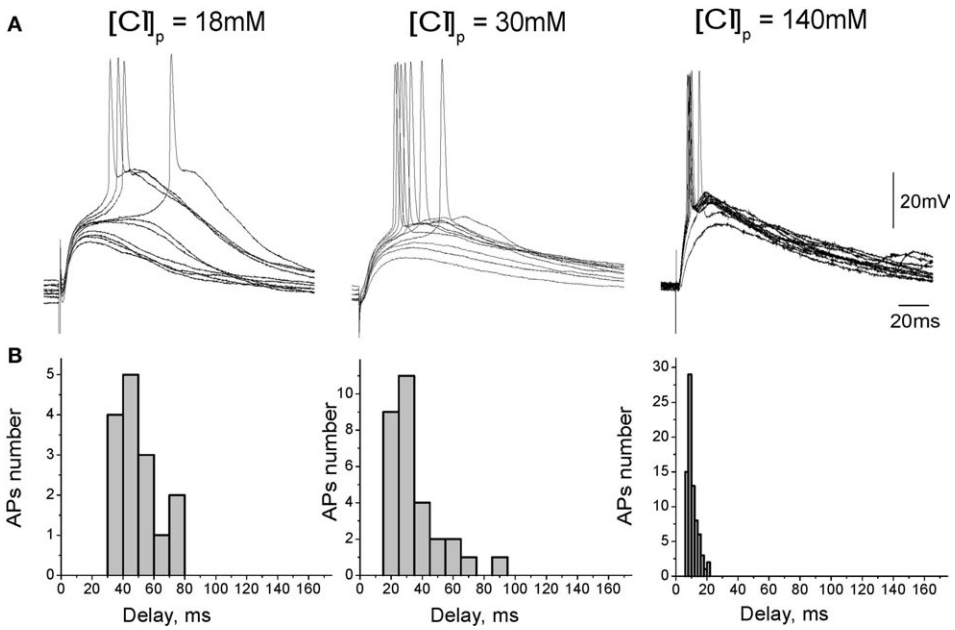

FIGURE 2 | Dependence of depolarizing GABAergic postsynaptic responses on chloride concentration in the recording pipette. (A) GABA(A) receptor mediated postsynaptic potentials recorded from CA3 pyramidal cells in whole-cell current-clamp configuration at different $[Cl^-]_p$. GABA-PSPs were evoked by electrical stimulation in the presence of the glutamate and GABA(B) receptors blockers. **(B)** Corresponding histograms of the GABA-PSP-triggered AP delays.

results of whole-cell recordings with different $[Cl^-]_p$ and the effects of low-bumetanide on MUA responses indicate that AP timing at GABAergic synapses is strongly dependent on $[Cl^-]_i$ in the postsynaptic neuron.

GABA DRIVING FORCE, RESTING MEMBRANE POTENTIAL AND ACTION POTENTIAL THRESHOLD

We further measured three parameters on which depends excitatory action of GABA: GABA driving force (DF_{GABA}), resting membrane potential (E_m) and AP_{thr} in CA3 pyramidal cells (**Figure 5**). DF_{GABA} was measured using cell-attached recordings of single GABA(A) channels, that do not affect intracellular chloride (Tyzio et al., 2006). Deduced from the current–voltage relationships of the currents through GABA(A) channels, DF_{GABA} in P2–5 CA3 pyramidal cells was of 16.5 ± 1.6 mV (n = 32 cells; **Figure 5A**), which is close to the previously reported values (Tyzio et al., 2008). Resting potential was measured using NMDA channels in cell-attached recordings as voltage sensors (Tyzio et al., 2003). We found that E_m in P2–5 CA3 pyramidal cells is of −78.8 ± 3.1 mV (n = 14; **Figure 5B**). Knowing these values we further estimated E_{GABA} ($E_{GABA} = E_m + DF_{GABA}$) in P2–5 CA3 pyramidal cells of −61.4 ± 5.4 mV. Corresponding Nernst values of $[Cl^-]_i$ ranged from 7 to 30 mM (see also Tyzio et al., 2007, 2008).

Threshold of APs triggered by GABA-PSPs was measured as a value of membrane potential at which dU/dt exceeded 10 V/s in whole-cell current-clamp recordings. AP_{thr} varied from −63 to −34 mV, with a mean of −45.9 ± 6.5 mV (n = 11 cells; **Figure 5C**). As summarized on **Figure 5D**, there is only small overlap between E_{GABA} and E_m, and in the vast majority of neurons E_{GABA} is essentially subthreshold and barely attains AP_{thr}. These findings are in agreement with the results obtained using whole-cell recordings, which suggested that excitatory action of GABA requires activation of additional subthreshold conductance, which amplifies GABA-PSPs and brings potential to the AP_{thr}.

ROLE OF PERSISTENT NA^+ CURRENTS IN THE GABAergic EXCITATION

In the previous studies, persistent Na^+ current (INap), which is activated at ≈−60 mV was shown to account for the slow regenerative depolarization triggering spontaneous bursting in the immature CA3 pyramidal neurons (Sipila et al., 2005, 2006). Because E_{GABA} is close to the activation threshold of INap, we hypothesized that INap amplifies GABA-PSPs and contributes to the excitatory action of GABA. To test this hypothesis, we studied the effects of sodium channel blockers TTX and phenytoin on GABA-PSPs. Because blockade of sodium channels causes presynaptic inhibition, we examined simulated GABA-PSPs (simGABA-PSPs) evoked by injection of GABA-PSCs waveform, which was obtained in voltage-clamp recordings similar to the procedure previously described for glutamatergic synapses (Fricker and Miles, 2000). The amplitude of GABA-PSCs was adjusted in each neuron to evoke near-threshold responses. The experiments were performed in the presence of the GABA and glutamate receptor antagonists to suppress ongoing synaptic activity. As illustrated by **Figure 6**, simulated GABA responses were amplified and prolonged by voltage-gated conductance, and triggered APs with long and variable delays similarly to synaptic GABA-PSPs with a mean AP delay of 69 ± 4 ms and standard deviation of 10 ± 1 ms (n = 20). Application of voltage-gated sodium channels blocker TTX (1 μM) not only inhibited APs evoked by simGABA-PSPs but also suppressed the amplification of simGABA-PSPs by subthreshold voltage-gated conductance (**Figure 7A**). Integral

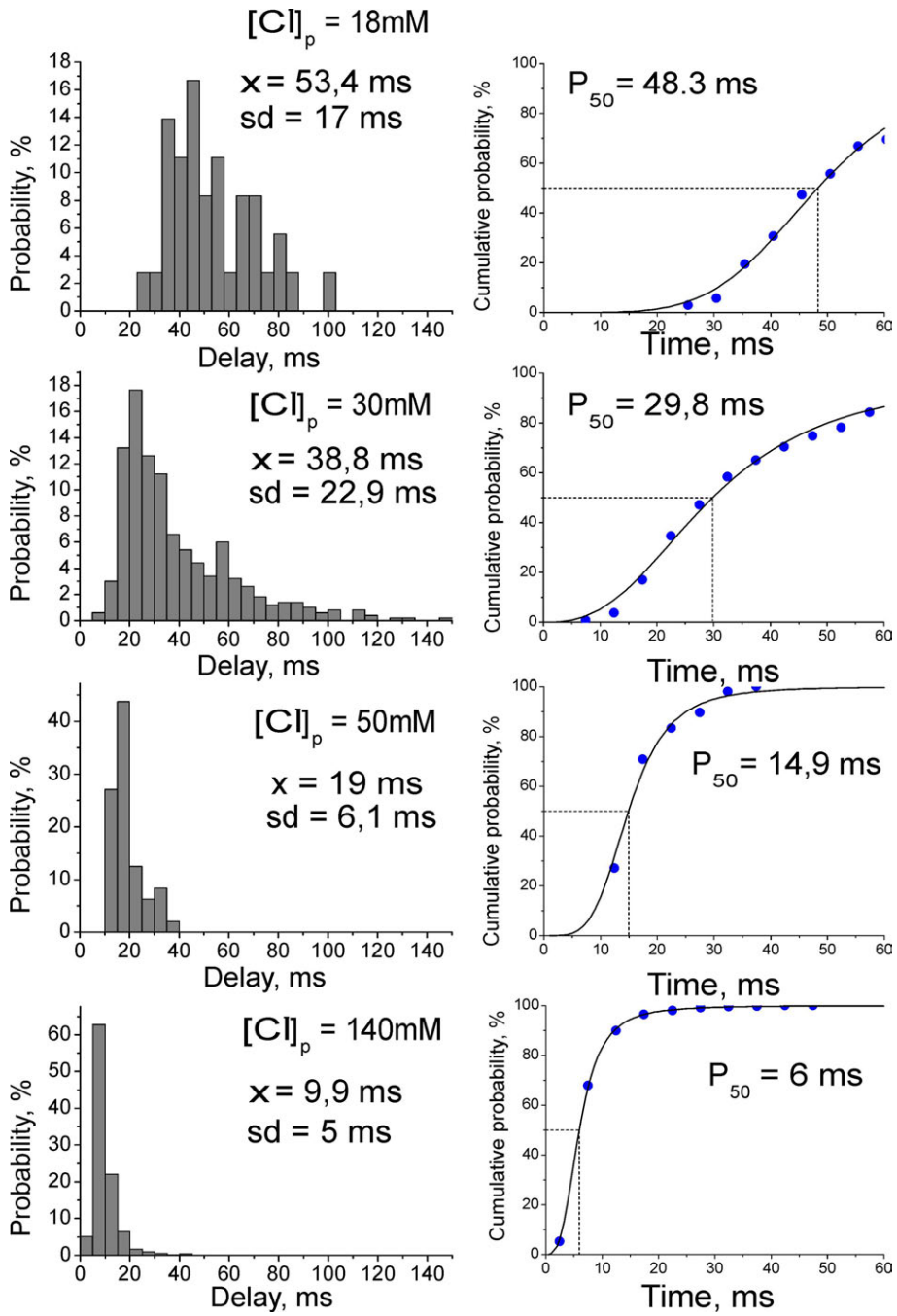

FIGURE 3 | Dependence of spike timing at GABAergic synapse on intracellular chloride concentration. Left: Average histograms of the AP delays at different $[Cl^-]_p$ in whole-cell recordings. Right: Cumulative curves for the AP delays fitted by Hill equation.

response calculated as a surface of simGABA-PSPs was reduced by TTX from 4851 ± 591 μVs (calculated for selected simGABA-PSPs which did not evoke APs) to 3536 ± 574 μVs, that is to 70 ± 5% of the control values ($n = 6$; $P = 0.004$). TTX also reduced the half-width of simGABA-PSPs from 132 ± 15 to 110 ± 11 ms, that is to 85 ± 5% of the control values ($n = 6$; $P = 0.0003$). Antiepileptic drug phenytoin (200 μM) that preferentially blocks repeated Na^+ cannel openings and INap (Kuo and Bean, 1994; Segal and Douglas, 1997) also blocked amplification of simGABA-PSPs, reducing the integral response to 70 ± 5% (from 7585 ± 549 to 5239 ± 555 μVs; $n = 3$; $P = 0.005$) and the half-width from 182 ± 10 to 146 ± 2 ms; $n = 3$; $P = 0.003$; **Figure 7B**). Phenytoin completely suppressed APs evoked by simGABA-PSPs. Phenytoin also inhibited APs triggered by synaptically evoked GABA-PSPs ($n = 4$, **Figure 7C**). However, phenytoin also increased the number of failures of the synaptically evoked responses suggesting an additional presynaptic effect. Taken

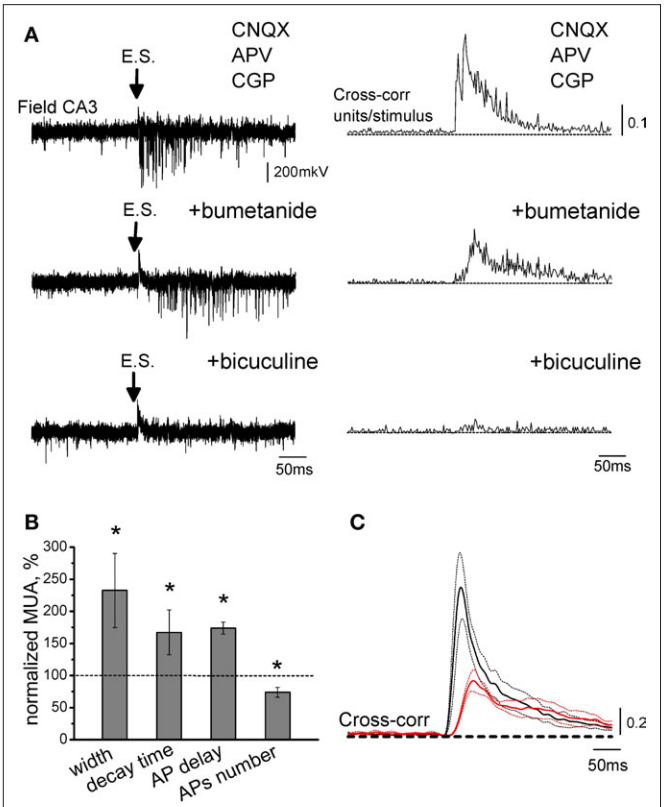

FIGURE 4 | Effect of partial blockade of NKCC1 co-transporter on action potential delays at GABAergic synapses. (A) Extracellular recordings of MUA evoked by electrical stimulation (E.S.) in the presence of the glutamate and GABA(B) receptor antagonists from the CA3 layer of P5 rat hippocampus (top: control, middle: 0.3 μM bumetanide and bottom: 20 μM bicuculline). On the right are shown corresponding cross-correlograms of the AP times versus stimulus. **(B)** Summary plot of the effects of low-bumetanide on synaptic GABA-evoked MUA. **(C)** Average cross-correlograms in control conditions (black) and in the presence of 0.3–0.6 μM bumetanide (red) ($n = 4$ slices; P2–5 rats). Dashed lines show SEM. Note that partial blockade of NKCC1 co-transporter increases AP delays and their jitter, and decreases APs number.

together, these results indicate that INap participates in the amplification of depolarizing subthreshold GABA-PSPs and that this amplification is involved in excitatory action of GABA in immature CA3 pyramidal neurons. It should be noted that simGABA-PSPs under standard current-clamp conditions may differ from natural responses as DF_{GABA} decreases during depolarizing GABA-PSPs; this should result in an acquisition of a "plateau" shape of the response and favor the role of near-threshold activated conductances. Use of dynamic clamp would be useful to address these questions in future studies.

IMPLICATION OF "SLOW" GABA(A)-MEDIATED EXCITATION FOR GDPs

Essential features of GDPs are relatively low level of neuronal firing synchrony within the temporal window of GDPs (Ben-Ari et al., 1989; Khazipov et al., 1997; Strata et al., 1997; Hollrigel et al., 1998; Menendez de la and Sanchez-Andres, 2000; Sipila et al., 2006) and slow wave-like propagation of GDPs between the hippocampal regions and along the hippocampus (Leinekugel et al., 1998; Menendez de la et al., 1998). We suggested that low level of synchrony and slow propagation of GDPs involves slow and asynchronous spiking at excitatory GABAergic synapses. To verify our assumption, we tested effects of drugs that modulate E_{GABA} (low-bumetanide) and efficacy of GABAergic transmission (bicuculline, diazepam) on synchronization of neuronal network during generation of GDPs. Extracellular recordings were performed using two to three wire electrodes placed in CA3 and CA1 pyramidal cell layer with 300–600 μm separation distance or 64-sites recordings using planar electrode arrays with a 200-μm separation distance. Neuronal synchrony was quantified by measuring: (i) GDPs parameters at a single recording site in CA3 pyramidal cell layer including amplitude and duration of the local field potential, duration of MUA bursts associated with GDPs and GDPs frequency, and (ii) velocity of GDPs propagation (**Figure 8**).

In control conditions, field GDPs had 149 ± 35 μV amplitude, 101 ± 6 ms half-width and occurred at 0.2 ± 0.03 s^{-1}. GDPs typically originated from CA3a or CA3b and propagated towards CA1 and CA3c, at a rate of 25 ± 5 mm/s ($n = 20$). Because of variability in GDPs parameters between slices and rats, the effects of drugs were studied in paired experiments, and the results were normalized to control values in each given slice. Partial blockade of GABA(A) receptors with low doses of bicuculline (2–5 μM), that causes nearly half-reduction of the GABA-PSCs in the hippocampal slices (Whittington et al., 1995), caused transformation of GDPs into super synchronous neuronal network discharges with tremendously high amplitude (916 ± 315% of control values; $P < 0.05$) and short duration (57 ± 12 ms versus 226 ± 22 ms in control conditions; $P < 0.001$). This was accompanied by five-fold shortening of delays of GDP in neighboring recording sites (21 ± 6% of control values; $P < 0.01$), therefore increasing propagation rate by 282 ± 81% ($P < 0.01$; $n = 7$). Yet the frequency of GDPs decreased when GABA receptors were partially blocked, probably because of more powerful activation of the inhibitory conductances (GABA(B) and Ca^{2+}-activated potassium channels) which control inter-GDPs intervals (Gaiarsa et al., 1995; Sipila et al., 2006). In contrast to the effects caused by suppression of GABA(A) receptors, enhancement of GABA action by positive allosteric modulator of GABA(A) receptors diazepam (2 μM) had desynchronizing effect on GDPs. Local field potentials associated with GDPs reduced so that they could be hardly measured from the baseline noise, and duration of MUA bursts associated with GDPs increased to 147 ± 22% of control values. Propagation of GDPs was delayed by 282 ± 73% ($P < 0.05$; $n = 4$). These results suggest that GABAergic synapses desynchronize hippocampal network during generation of GDPs, and slow down GDPs propagation.

GABAergic and glutamatergic synapses are co-activated in CA3 pyramidal cells during GDPs (Leinekugel et al., 1997; Bolea et al., 1999; Lamsa et al., 2000). To determine the role of fast AMPA receptor mediated synaptic transmission in the network synchronization during GDPs we tested low doses of the AMPA receptor antagonist CNQX (1 μM, that causes nearly 50% reduction in the amplitude of field EPSPs (Andreasen et al., 1989). After CNQX application, field GDPs reduced to baseline noise levels and duration of associated with GDPs MUA bursts prolonged by 100 ± 49% ($P < 0.05$), while GDP frequency and propagation rate decreased respectively by 78 ± 11 and 86 ± 3% ($P < 0.05$; $n = 5$).

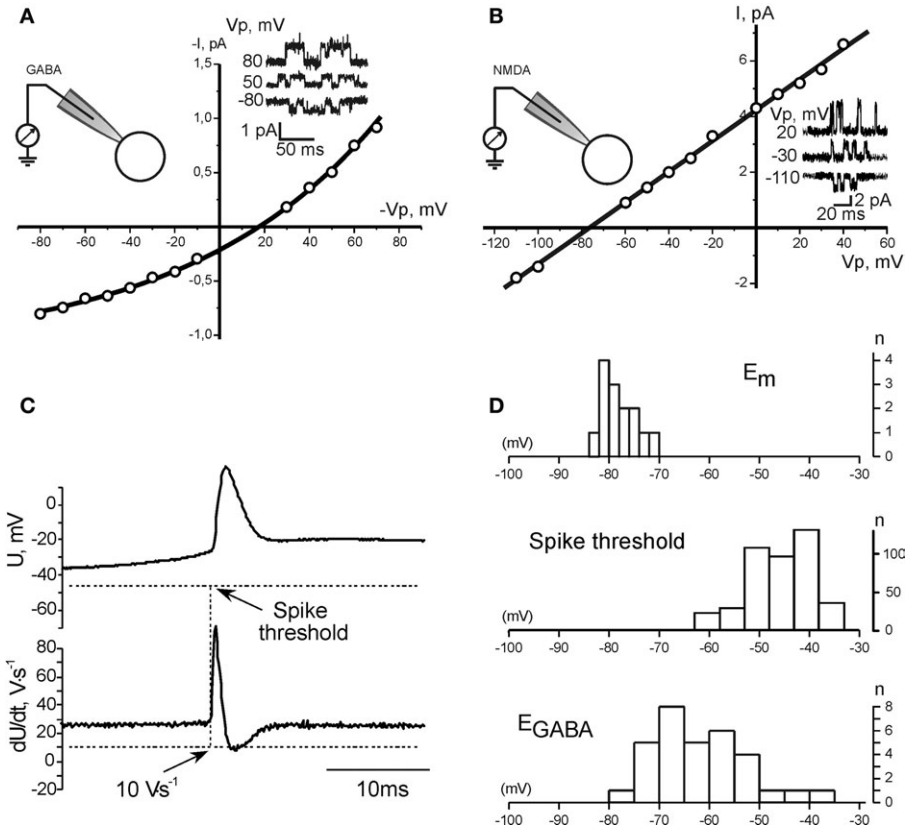

FIGURE 5 | GABA driving force, resting membrane potential, and the action potential threshold in neonatal CA3 pyramidal cells. (A, B) Measurements of the GABA driving force **(A)** and membrane potential **(B)** using cell-attached recordings of GABA and NMDA channels, respectively. Example traces of single channel openings at different pipette potentials (V_p) are shown in insets. **(C)** Measurement of the action potential threshold in whole-cell current-clamp recordings. **(D)** Summary plot of the resting membrane potential, GABA reversal potential and the action potential threshold in P2–5 CA3 pyramidal neurons.

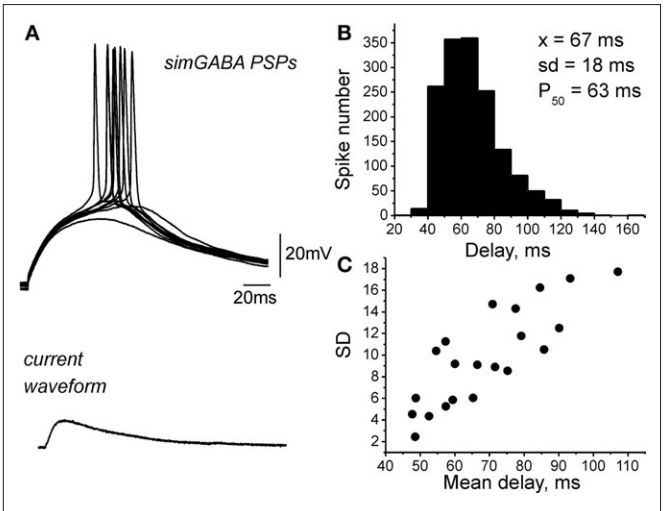

FIGURE 6 | Responses elicited by injection of synaptic GABAergic current waveform. (A) Example traces of the responses (top traces) elicited by injection of the current waveform of GABA-PSCs (bottom trace) recorded in current-clamp mode in the presence of the GABA and glutamate receptor antagonists. **(B)** Histogram of AP delays distribution over 20 cells. **(C)** Plot of standard deviation (SD) versus mean AP delay value; each point corresponds to an individual neuron.

We further investigated how modulation of E_{GABA} affects GDPs using NKCC1 inhibitor bumetanide (**Figure 9**). At 5–10 μM, bumetanide completely blocked GDPs in agreement with previous reports (Dzhala et al., 2005; Nardou et al., 2009; Sipila et al., 2009). At lower doses (0.3–1 μM), at which bumetanide caused an increase in AP delays and their variability (**Figure 4**), we observed a decrease in GDPs frequency and the level of neuronal firing during GDPs. Field GDPs reduced to baseline noise levels, duration of GDPs-associated MUA bursts increased from 228 ± 47 to 278 ± 52 ms ($n = 6$; $P < 0.01$) and propagation rate of GDPs decreased by 63 ± 6% ($n = 6$; $P < 0.05$). In the presence of low-bumetanide, we often observed compartmentalized GDPs that were restricted to one electrode and failed to propagate to the neighboring sites (not shown).

DISCUSSION

The main findings of the present study are the following: (i) delays of APs evoked by synaptic GABA in neonatal CA3 pyramidal cells are long and variable, and depend on intracellular chloride concentration; (ii) at physiological conditions, depolarization produced by GABA is typically more negative than the AP_{thr}, and activation of subthreshold voltage-gated INap is required to trigger APs; (iii) while depolarizing action of GABA is required for GDPs generation, slow and variable AP delays in GABAergic synapses reduce neuronal synchrony during generation of GDPs and slow down GDPs propagation.

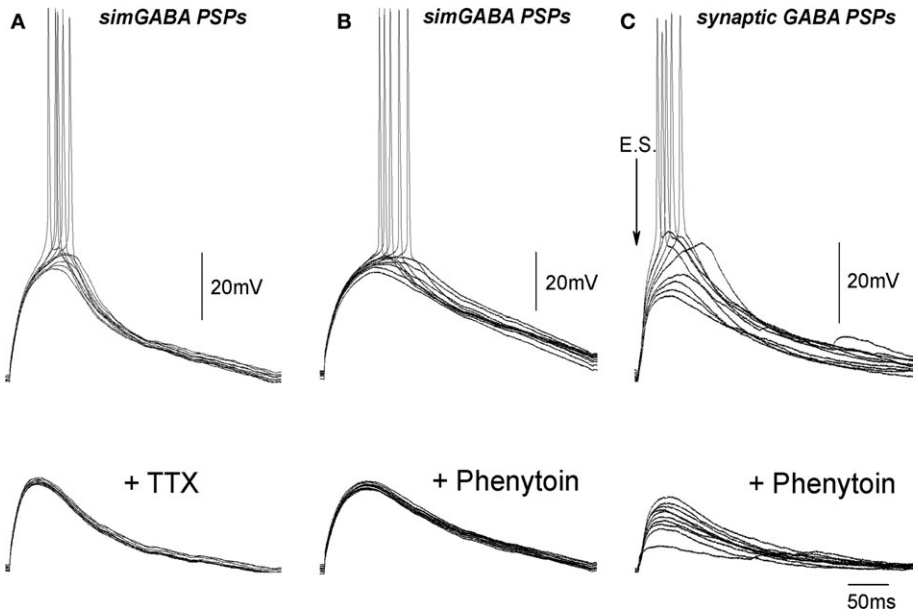

FIGURE 7 | Na⁺ channel blockers inhibit subthreshold voltage-gated conductance and the action potentials evoked by simulated and synaptic GABA-PSPs. **(A, B)** Example traces of simGABA-PSPs evoked by injection of GABA-PSC waveform in control conditions (upper traces) and in the presence of 1 μM TTX **(A)** and 200 μM phenytoin **(B)** (bottom traces). **(C)** Synaptic GABA-PSPs in control conditions (upper traces) and in the presence of 100 μM phenytoin (bottom traces).

Although excitatory actions of GABA in the immature neurons have been well documented in various brain structures (Ben Ari et al., 2007), the temporal AP coding aspect of GABAergic excitation until present study has not been analyzed. Our central finding is that transmission of excitation in the immature depolarizing GABAergic synapses is slow and highly variable. This was observed using non-invasive extracellular MUA recordings, that affect neither membrane potential nor intracellular chloride, and whole-cell recordings with elevated chloride concentration in the pipette solution. These observations are in agreement with the results of previous studies, in which representative traces show similar long and variable latency APs evoked by stimulation of synaptic GABAergic inputs, using cell-attached recordings from CA3 pyramidal cells (Leinekugel et al., 1997), interneurons (Khazipov et al., 1997), and neocortical pyramidal and stellate cells (Rheims et al., 2008). These findings are important because GABAergic synapses are the first synapses established in the hippocampal neurons, both in rodents and primates (Tyzio et al., 1999; Khazipov et al., 2001) and GABAergic conductance is predominant in GDPs (Ben-Ari et al., 1989; Khazipov et al., 1997; Leinekugel et al., 1997; Hollrigel et al., 1998). We have shown that the temporal coding at GABA synapse is strongly dependent on intracellular chloride concentration in the postsynaptic neuron: AP delays and their variability strongly decreased with an artificial elevation of $[Cl^-]_i$ during whole-cell recordings, and increased in the conditions of partial blockade of NKCC1 using low concentration of bumetanide. Comparison of the physiological values of E_m, DF_{GABA} and AP_{thr} lead us to conclusion that at physiological levels of $[Cl^-]_i$, depolarizing GABA-PSPs do not attain the action potential threshold, and that the activation of intermediate subthreshold voltage-gated conductance is required to trigger APs. This is in keeping with findings in immature granular cells, in which E_{GABA} is slightly, by ~5 mV, is more negative than the action potential threshold (−46 and −42 mV, respectively), yet granular cells discharge, typically one action potential, during pure GABAergic GDPs (Hollrigel et al., 1998; see also Brickley et al., 1996). This intermediate step in AP initiation is likely the key factor contributing to slow AP delays in GABAergic synapse. Several lines of evidence indicate that persistent Na^+ current INap contributes to the amplification of GABA-PSPs and excitatory action of GABA. INap is present in the immature CA3 pyramidal cells (McBain and Dingledine, 1992) and promotes their spontaneous bursting (Sipila et al., 2005, 2006). Activation threshold of INap is near −60 mV (Sipila et al., 2006), that is close to the depolarization attained by GABA-PSPs. In adult CA1 pyramidal cells, which also express INap (Azouz et al., 1996), small glutamatergic EPSPs evoked from subthreshold potentials initiate firing with long and variable latencies due to INap-mediated plateau potentials that amplify and prolong EPSPs (Fricker and Miles, 2002). Thus, present findings significantly modify traditional view on GABAergic excitation which assumed that GABA reaches AP_{thr} and directly activates APs (Ben Ari, 2002; Ben Ari et al., 2007). It appears that in P2–5 CA3 pyramidal cells, GABAergic depolarization *per se* typically does not attain AP_{thr}, and that amplification of GABA-PSPs by INap is required for postsynaptic excitation. That GDPs are inhibited by INap blockers phenytoin and riluzole (Sipila et al., 2006) is in agreement with these findings. Interestingly, similar mechanisms may operate in the immature neocortex, in which delays of GABA-evoked APs are also long and variable, and E_{GABA} barely attains AP_{thr} (Rheims et al., 2008). Variability of AP delays, which is also observed using simGABA-PSPs, likely reflects dynamic changes in the state of the

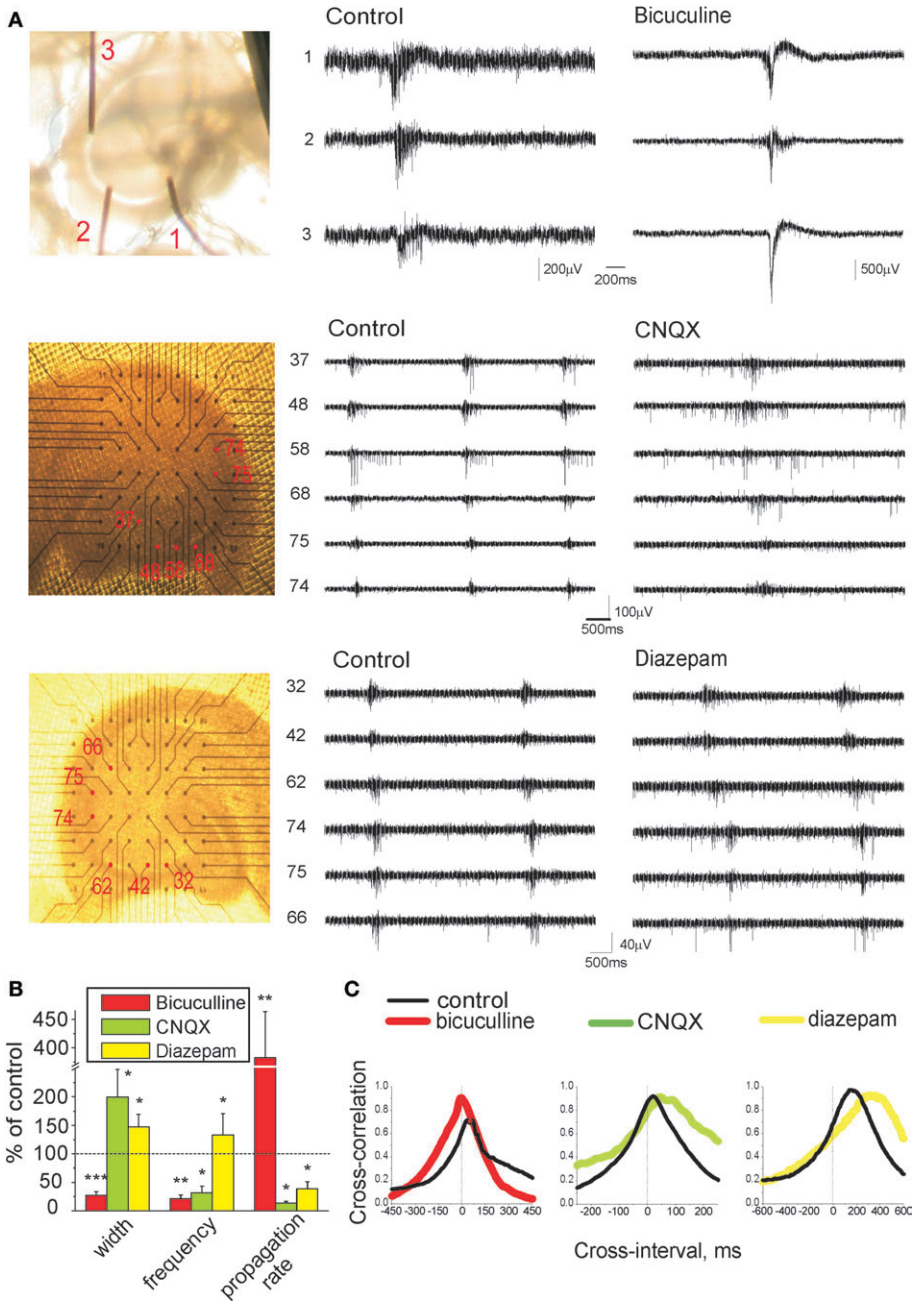

FIGURE 8 | Effects of drugs modulating efficacy of GABAergic and glutamatergic transmission on network synchronization during GDPs. **(A)** Left: recording field electrodes arrangement in pyramidal layer of hippocampus for concomitant recordings from different sites. Middle and right: traces representing extracellular GDP recordings in control conditions and after drug application (top traces, 3 μM bicuculline; middle traces, 1 μM CNQX; bottom traces, 2 μM diazepam). **(B)** GDPs half-width, frequency, and propagation rate in the presence of drugs normalized to the control values. **(C)** Cross-correlograms of unitary APs between two distinct CA regions (CA3 and CA1, or within CA3) in control conditions (black) and in the presence of the drug. **(B, C)** represent pooled data obtained in the presence of bicuculline ($n = 7$); CNQX ($n = 5$); diazepam ($n = 4$).

voltage-gated conductances (INap, potassium channels, Ih, etc.). At the level of population, variability is multiplied by heterogeneity in $[Cl^-]_i$ that also strongly affects AP delays. However, we do not claim that amplification of GABA-PSPs by intrinsic membrane conductances is a general mechanism required for GABAergic excitation. It is plausible that a situation with $E_{GABA} \geq AP_{thr}$ may also take place, for instance in cells with very positive E_{GABA} at very early developmental stages (LoTurco et al., 1995) or as a result of epileptogenic process (Cohen et al., 2002; Khalilov et al., 2003; Huberfeld et al., 2007), trauma (van den Pol et al., 1996; Pieraut et al., 2007), or in the neurons with relatively negative AP_{thr}, such as neocortical interneurons (Rheims et al., 2008).

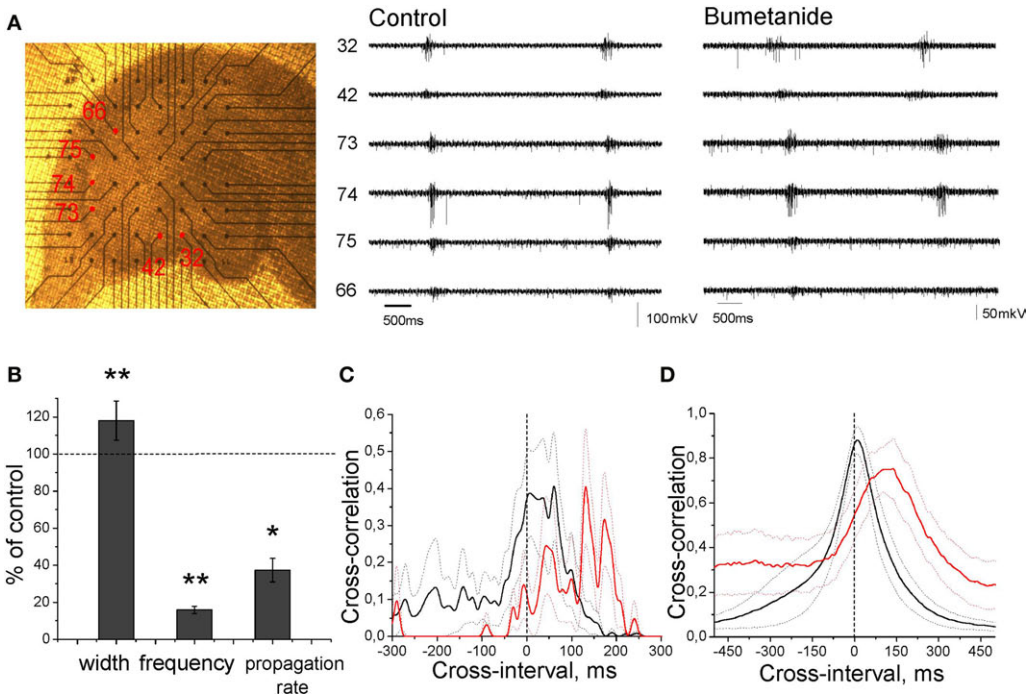

FIGURE 9 | Effect of partial blockade of NKCC1 on GDPs. (A) Photograph of the recording setup and extracellular GDP recordings in control conditions (left traces) and in the presence of 0.3 μM bumetanide (right traces). **(B)** Normalized GDPs width, frequency, and propagation rate in the presence of 0.3 μM bumetanide. **(C, D)** Cross-correlograms of unitary APs **(C)** and GDPs **(D)** between two distinct CA regions (CA3 and CA1, or within CA3) in control conditions (black) and in the presence of bumetanide (red). Dashed lines show SEM. **(B–D)** Pooled data from four slices.

Present results suggest that slow and variable AP delays at GABAergic synapses have major impact on synchronization of neuronal network during generation and propagation of GDPs. Decrease of depolarizing driving force for GABA by low-bumetanide desynchronized neuronal network during generation of GDPs. On the other hand, reduction of GABAergic conductance with low-bicuculline and its augmentation with diazepam increased and decreased neuronal synchronization during GDPs, respectively. In keeping with the major contribution of GABAergic conductance to GDPs (Ben-Ari et al., 1989; Khazipov et al., 1997; Leinekugel et al., 1997; Strata et al., 1997), slow and variable AP delays at GABAergic synapses seem to play an important role in determining the level of neuronal synchrony during GDPs and the rate of their propagation. Yet GABA is not the only factor contributing to neuronal excitation during GDPs. Less prominent, but possessing stronger driving force glutamatergic component provided by recurrent collateral synapses plays equally important role in GDPs generation (Khazipov et al., 1997; Leinekugel et al., 1997; Bolea et al., 1999), as glutamate receptor antagonists reduce neuronal synchrony, according to present study, and block GDPs when glutamate receptors are fully blocked (Ben-Ari et al., 1989). After partial blockade of GABA receptors, increase in neuronal synchronization is likely determined by glutamatergic synapses which provide faster and less variable conduction of excitation than GABAergic synapses. The difference in excitation provided by GABA and glutamate is likely due to the difference in the level of depolarization, which is secondary to the amount and driving force of these two conductances. Small glutamatergic EPSPs evoked from just subthreshold potentials are amplified by INap-mediated plateau potentials and evoke postsynaptic spikes with long and variable delays in adult pyramidal cells (Fricker and Miles, 2002), that is similar to the present observations with GABA-PSPs. Because glutamate-driving force is close to 0 mV, increase in glutamatergic conductance provides stronger depolarization which exceeds AP_{thr} and postsynaptic cells fire APs at short delays with little variability. By an order higher input resistance and smaller capacitance of the immature neurons (Tyzio et al., 2003) also should be taken into account, because both factors should provide larger depolarization in response to even weak input. In contrast, GABAergic depolarization is limited by small driving force, and its level can not exceed E_{GABA} despite of the large GABAergic conductance activated during GDPs. GABAergic depolarization also potentiates NMDA receptors via attenuation of their voltage-dependent magnesium block, and in keeping with their slow kinetics, NMDA receptor mediated depolarization could be an additional factor contributing to delayed firing (Khazipov et al., 1995; Leinekugel et al., 1997).

Present results suggest that slow and variable excitation in GABAergic synapses is an important factor controlling spike timing during GDPs. By providing a coincidence between pre- and postsynaptic neurons, GDPs are thought to be involved in activity-dependent plasticity in the hippocampal network (Kasyanov et al., 2004; Mohajerani and Cherubini, 2006). Synaptic plasticity is particularly robust during the early developmental period (Isaac et al., 1995; Durand et al., 1996), and similarly to adult forms of plasticity, it depends on timing of firing in pre- and postsynaptic neurons both in glutamatergic and GABAergic synapses. Because all neurons fire action potentials during GDPs, entire network is

activated and all synaptic inputs are imposed to plasticity, which direction (potentiation or depression) should depend on the spike timing in the synaptically coupled neurons. In the future studies it would also be important to determine the role of slow spike timing at GABAergic synapses in the generation of the early patterns of hippocampal activity in the intact animals *in vivo*.

ACKNOWLEDGMENTS

Financial support from EU (EC contract number LSH-CT-2006-037315 (EPICURE) FP6 -Thematic priority LIFESCIHEALTH), INSERM, ANR, FRM, LFCE, Rothschild/ Inserm "interface" program and "co-tutelle" grant by the French Government and RFBR are acknowledged.

REFERENCES

Andreasen, M., Lambert, J. D. C., and Jensen, M. S. (1989). Effects of new non-N-methyl-D-aspartate antagonists on synaptic transmission in the in vitro rat hippocampus. *J. Physiol. (Lond.)* 414, 317–336.

Azouz, R., Jensen, M. S., and Yaari, Y. (1996). Ionic basis of spike after-depolarization and burst generation in adult rat hippocampal CA1 pyramidal cells. *J. Physiol (Lond.)* 492, 211–223.

Ben Ari, Y. (2002). Excitatory actions of GABA during development: the nature of the nurture. *Nat. Rev. Neurosci.* 3, 728–739.

Ben-Ari, Y., Cherubini, E., Corradetti, R., and Gaïarsa, J.-L. (1989). Giant synaptic potentials in immature rat CA3 hippocampal neurones. *J. Physiol. (Lond.)* 416, 303–325.

Ben Ari, Y., Gaiarsa, J. L., Tyzio, R., and Khazipov, R. (2007). GABA: a pioneer transmitter that excites immature neurons and generates primitive oscillations. *Physiol. Rev.* 87, 1215–1284.

Bolea, S., Avignone, E., Berretta, N., Sanchez-Andres, J. V., and Cherubini, E. (1999). Glutamate controls the induction of GABA-mediated giant depolarizing potentials through AMPA receptors in neonatal rat hippocampal slices. *J. Neurophysiol.* 81, 2095–2102.

Brickley, S. G., Cull-Candy, S. G., and Farrant, M. (1996). Development of a tonic form of synaptic inhibition in rat cerebellar granule cells resulting from persistent activation of GABAA receptors. *J. Physiol. (Lond.)* 497, 753–759.

Cohen, I., and Miles, R. (2000). Contributions of intrinsic and synaptic activities to the generation of neuronal discharges in in vitro hippocampus. *J. Physiol. (Lond.)* 524, 485–502.

Cohen, I., Navarro, V., Clemenceau, S., Baulac, M., and Miles, R. (2002). On the origin of interictal activity in human temporal lobe epilepsy in vitro. *Science* 298, 1418–1421.

Davies, C. H., Davies, S. N., and Collingridge, G. L. (1990). Paired-pulse depression of monosynaptic GABA-mediated inhibitory postsynaptic responses in rat hippocampus. *J. Physiol. (Lond.)* 424, 513–531.

De la Prida, L. M., Bolea, S., and Sanchez-Andres, J. V. (1998). Origin of the synchronized network activity in the rabbit developing hippocampus. *Eur. J. Neurosci.* 10, 899–906.

Durand, G. M., Kovalchuk, Y., and Konnerth, A. (1996). Long-term potentiation and functional synapse induction in developing hippocampus. *Nature* 381, 71–75.

Dzhala, V. I., Talos, D. M., Sdrulla, D. A., Brumback, A. C., Mathews, G. C., Benke, T. A., Delpire, E., Jensen, F. E., and Staley, K. J. (2005). NKCC1 transporter facilitates seizures in the developing brain. *Nat. Med.* 11, 1205–1213.

Freund, T., and Buzsaki, G. (1996). Interneurons of the hippocampus. *Hippocampus* 6, 345–470.

Fricker, D., and Miles, R. (2000). EPSP amplification and the precision of spike timing in hippocampal neurons. *Neuron* 28, 559–569.

Fricker, D., and Miles, R. (2002). EPSP amplification and the precision of spike timing in hippocampal neurons. *Neuron* 28, 559–569.

Fricker, D., Verheugen, J. A., and Miles, R. (1999). Cell-attached measurements of the firing threshold of rat hippocampal neurones. *J. Physiol. (Lond.)* 517, 791–804.

Gaiarsa, J. L., McLean, H., Congar, P., Leinekugel, X., Khazipov, R., Tseeb, V., and Ben-Ari, Y. (1995). Postnatal maturation of gamma-aminobutyric acidA and B-mediated inhibition in the CA3 hippocampal region of the rat. *J. Neurobiol.* 26, 339–349.

Hollrigel, G. S., Ross, S. T., and Soltesz, I. (1998). Temporal patterns and depoarizing actions of spontaneous GABAA receptor activation in granule cells of the early postnatal dentate gyrus. *J. Neurophysiol.* 80, 2340–2351.

Huberfeld, G., Wittner, L., Clemenceau, S., Baulac, M., Kaila, K., Miles, R., and Rivera, C. (2007). Perturbed chloride homeostasis and GABAergic signaling in human temporal lobe epilepsy. *J. Neurosci.* 27, 9866–9873.

Isaac, J. T., Nicoll, R. A., and Malenka, R. C. (1995). Evidence for silent synapses: implications for the expression of LTP. *Neuron* 15, 427–434.

Kasyanov, A. M., Safiulina, V. F., Voronin, L. L., and Cherubini, E. (2004). GABA-mediated giant depolarizing potentials as coincidence detectors for enhancing synaptic efficacy in the developing hippocampus. *Proc. Natl. Acad. Sci. U.S.A.* 101, 3967–3972.

Khalilov, I., Holmes, G. L., and Ben Ari, Y. (2003). In vitro formation of a secondary epileptogenic mirror focus by interhippocampal propagation of seizures. *Nat. Neurosci.* 6, 1079–1085.

Khazipov, R., Bregestovski, P., and Ben-Ari, Y. (1993). Hippocampal inhibitory interneurons are functionally disconnected from excitatory inputs by anoxia. *J. Neurophysiol.* 70, 2251–2259.

Khazipov, R., Esclapez, M., Caillard, O., Bernard, C., Khalilov, I., Tyzio, R., Hirsch, J., Dzhala, V., Berger, B., and Ben-Ari, Y. (2001). Early development of neuronal activity in the primate hippocampus in utero. *J. Neurosci.* 21, 9770–9781.

Khazipov, R., Khalilov, I., Tyzio, R., Morozova, E., Ben Ari, Y., and Holmes, G. L. (2004). Developmental changes in GABAergic actions and seizure susceptibility in the rat hippocampus. *Eur. J. Neurosci.* 19, 590–600.

Khazipov, R., Leinekugel, X., Khalilov, I., Gaïarsa, J.-L., and Ben-Ari, Y. (1997). Synchronization of GABAergic interneuronal network in CA3 subfield of neonatal rat hippocampal slices. *J. Physiol. (Lond.)* 498, 763–772.

Khazipov, R., Ragozzino, D., and Bregestovski, P. (1995). Kinetics and Mg^{2+} block of N-methyl-D-aspartate receptor channels during postnatal development of hippocampal CA3 pyramidal neurons. *Neuroscience* 69, 1057–1065.

Kuo, C. C., and Bean, B. P. (1994). Na^{+} channels must deactivate to recover from inactivation. *Neuron* 12, 819–829.

Lamsa, K., Palva, J. M., Ruusuvuori, E., Kaila, K., and Taira, T. (2000). Synaptic GABA(A) activation inhibits AMPA-kainate receptor-mediated bursting in the newborn (P0-P2) rat hippocampus. *J. Neurophysiol.* 83, 359–366.

Leinekugel, X., Khalilov, I., Ben-Ari, Y., and Khazipov, R. (1998). Giant depolarizing potentials: the septal pole of the hippocampus paces the activity of the developing intact septohippocampal complex in vitro. *J. Neurosci.* 18, 6349–6357.

Leinekugel, X., Medina, I., Khalilov, I., Ben-Ari, Y., and Khazipov, R. (1997). Ca^{2+} oscillations mediated by the synergistic excitatory actions of GABAA and NMDA receptors in the neonatal hippocampus. *Neuron* 18, 243–255.

LoTurco, J. J., Owens, D. F., Heath, M. J., Davis, M. B., and Kriegstein, A. R. (1995). GABA and glutamate depolarize cortical progenitor cells and inhibit DNA synthesis. *Neuron* 15, 1287–1298.

McBain, C., and Dingledine, R. (1992). Dual-component miniature excitatory synaptic currents in rat hippocampal CA3 pyramidal neurons. *J. Neurophysiol.* 68, 16–27.

Menendez de la, P. L., and Sanchez-Andres, J. V. (2000). Heterogenous populations of cells mediate spontaneous synchronous bursting in the developing hippocampus though a frequency-dependent mechanism. *Neuroscience* 97, 227–241.

Menendez, de la, P. L., Bolea, S., and Sanchez-Andres, J. V. (1996). Analytical characterization of spontaneous activity evolution during hippocampal development in the rabbit. *Neurosci. Lett.* 218, 185–187.

Menendez, de la, P. L., Bolea, S., and Sanchez-Andres, J. V. (1998). Origin of the synchronized network activity in the rabbit developing hippocampus. *Eur. J. Neurosci.* 10, 899–906.

Miles, R., and Wong, R. K. S. (1986). Excitatory synaptic interactions between CA3 neurones in the guinea-pig hippocampus. *J. Physiol. (Lond.)* 373, 397–418.

Miles, R., and Wong, R. K. S. (1987). Inhibitory control of local excitatory circuits in the guinea- pig hippocampus. *J. Physiol. (Lond.)* 388, 611–629.

Mohajerani, M. H., and Cherubini, E. (2006). Role of giant depolarizing potentials in shaping synaptic currents in the developing hippocampus. *Crit. Rev. Neurobiol.* 18, 13–23.

Nardou, R., Ben-Ari, Y., and Khalilov, I. (2009). Bumetanide, an NKCC1 antagonist, does not prevent formation of epileptogenic focus but blocks epileptic focus seizures in immature rat hippocampus. *J. Neurophysiol.* 101, 2878–2888.

Payne, J. A., Rivera, C., Voipio, J., and Kaila, K. (2003). Cation-chloride co-transporters in neuronal communication, development and trauma. *Trends Neurosci.* 26, 199–206.

Pieraut, S., Laurent-Matha, V., Sar, C., Hubert, T., Mechaly, I., Hilaire, C., Mersel, M., Delpire, E., Valmier, J., and Scamps, F. (2007). NKCC1 phosphorylation stimulates neurite growth of injured adult sensory neurons. *J. Neurosci.* 27, 6751–6759.

Rheims, S., Minlebaev, M., Ivanov, A., Represa, A., Khazipov, R., Holmes, G. L., Ben Ari, Y., and Zilberter, Y. (2008). Excitatory GABA in rodent developing neocortex in vitro. *J. Neurophysiol.* 100, 609–619.

Segal, M. M., and Douglas, A. F. (1997). Late sodium channel openings underlying epileptiform activity are preferentially diminished by the anticonvulsant phenytoin. *J. Neurophysiol.* 77, 3021–3034.

Sipila, S. T., Huttu, K., Soltesz, I., Voipio, J., and Kaila, K. (2005). Depolarizing GABA acts on intrinsically bursting pyramidal neurons to drive giant depolarizing potentials in the immature hippocampus. *J. Neurosci.* 25, 5280–5289.

Sipila, S. T., Huttu, K., Voipio, J., and Kaila, K. (2006). Intrinsic bursting of immature CA3 pyramidal neurons and consequent giant depolarizing potentials are driven by a persistent Na current and terminated by a slow Ca-activated K current. *Eur. J. Neurosci.* 23, 2330–2338.

Sipila, S. T., Huttu, K., Yamada, J., Afzalov, R., Voipio, J., Blaesse, P., and Kaila, K. (2009). Compensatory enhancement of intrinsic spiking upon NKCC1 disruption in neonatal hippocampus. *J. Neurosci.* 29, 6982–6988.

Strata, F., Atzori, M., Molnar, M., Ugolini, G., Tempia, F., and Cherubini, E. (1997). A pacemaker current in dye-coupled hilar interneurons contributes to the generation of giant GABAergic potentials in developing hippocampus. *J. Neurosci.* 17, 1435–1446.

Stuart, G., Schiller, J., and Sakmann, B. (1997). Action potential initiation and propagation in rat neocortical pyramidal neurons. *J. Physiol. (Lond.)* 505, 617–632.

Tyzio, R., Cossart, R., Khalilov, I., Minlebaev, M., Hubner, C. A., Represa, A., Ben Ari, Y., and Khazipov, R. (2006). Maternal oxytocin triggers a transient inhibitory switch in GABA signaling in the fetal brain during delivery. *Science* 314, 1788–1792.

Tyzio, R., Holmes, G. L., Ben-Ari, Y., and Khazipov, R. (2007). Timing of the developmental switch in GABA(A) mediated signalling from excitation to inhibition in CA3 rat hippocampus using gramicidin perforated patch and extracellular recordings. *Epilepsia* 48, 96–105.

Tyzio, R., Ivanov, A., Bernard, C., Holmes, G. L., Ben Ari, Y., and Khazipov, R. (2003). Membrane potential of CA3 hippocampal pyramidal cells during postnatal development. *J. Neurophysiol.* 90, 2964–2972.

Tyzio, R., Minlebaev, M., Rheims, S., Ivanov, A., Jorquera, I., Holmes, G. L., Zilberter, Y., Ben Ari, Y., and Khazipov, R. (2008). Postnatal changes in somatic gamma-aminobutyric acid signalling in the rat hippocampus. *Eur. J. Neurosci.* 27, 2515–2528.

Tyzio, R., Represa, A., Jorquera, I., Ben-Ari, Y., Gozlan, H., and Aniksztejn, L. (1999). The establishment of GABAergic and glutamatergic synapses on CA1 pyramidal neurons is sequential and correlates with the development of the apical dendrite. *J. Neurosci.* 19, 10372–10382.

van den Pol, A. N., Obrietan, K., and Chen, G. (1996). Excitatory actions of GABA after neuronal trauma. *J. Neurosci.* 16, 4283–4292.

Whittington, M. A., Traub, R. D., and Jefferys, J. G. R. (1995). Erosion of inhibition contributes to the progression of low magnesium bursts in rat hippocampal slices. *J. Physiol. (Lond.)* 486, 723–734.

Yamada, J., Okabe, A., Toyoda, H., Kilb, W., Luhmann, H. J., and Fukuda, A. (2004). Cl-uptake promoting depolarizing GABA actions in immature rat neocortical neurones is mediated by NKCC1. *J. Physiol. Online* 557, 829–841.

Conflict of Interest Statement: The authors declare that the research was conducted in the absence of any commercial or financial relationships that could be construed as a potential conflict of interest.

Received: 22 February 2010; paper pending published: 26 March 2010; accepted: 27 April 2010; published online: 14 July 2010.

*Citation: Valeeva G, Abdullin A, Tyzio R, Skorinkin A, Nikolski E, Ben-Ari Y and Khazipov R (2010) Temporal coding at the immature depolarizing GABAergic synapse. Front. Cell. Neurosci. **4**:17. doi: 10.3389/fncel.2010.00017*

frontiers in
CELLULAR NEUROSCIENCE

REVIEW ARTICLE
published: 30 July 2010
doi: 10.3389/fncel.2010.00026

The many tunes of perisomatic targeting interneurons in the hippocampal network

Tommas J. Ellender[1,2] and Ole Paulsen[1,3]*

[1] *OXION Initiative, Department of Physiology, Anatomy and Genetics, University of Oxford, Oxford, UK*
[2] *Medical Research Council Anatomical Neuropharmacology Unit, University of Oxford, Oxford, UK*
[3] *Physiological Laboratory, Department of Physiology, Development and Neuroscience, University of Cambridge, Cambridge, UK*

Edited by:
Yehezkel Ben-Ari, Institut National de la Santé et de la Recherche Médicale, France

Reviewed by:
Alain Destexhe, Unité de Neurosciences, Information and Complexité Centre National de la Recherche Scientifique, France
Barry W. Connors, Brown University, USA
Rustem Khazipov, Institut National de la Santé et de la Recherche Médicale, France
Krecho Krnkevic, McGill University, Canada

Correspondence:
Ole Paulsen, Physiological Laboratory, Department of Physiology, Development and Neuroscience, University of Cambridge, Downing Street, Cambridge CB2 3EG, UK.
e-mail: op210@cam.ac.uk

The axonal targets of perisomatic targeting interneurons make them ideally suited to synchronize excitatory neurons. As such they have been implicated in rhythm generation of network activity in many brain regions including the hippocampus. However, several recent publications indicate that their roles extend beyond that of rhythm generation. Firstly, it has been shown that, in addition to rhythm generation, GABAergic perisomatic inhibition also serves as a current generator contributing significantly to hippocampal oscillatory EEG signals. Furthermore, GABAergic interneurons have a previously unrecognized role in the initiation of hippocampal population bursts, both in the developing and adult hippocampus. In this review, we describe these new observations in detail and discuss the implications they have for our understanding of the mechanisms underlying physiological and pathological hippocampal network activities. This review is part of the Frontiers in Cellular Neuroscience's special topic entitled "GABA signaling in health and disease" based on the meeting at the CNCR Amsterdam.

Keywords: inhibition, GABA, perisomatic targeting interneuron, hippocampus, network oscillation, gamma oscillation, sharp wave-ripple, population burst

INTRODUCTION

Like many cortical structures, the hippocampal CA3 region consists of a large network of rather uniform, recurrently connected, excitatory neurons together with a smaller but diverse population of inhibitory neurons (Freund and Buzsaki, 1996; Vizi and Kiss, 1998; Klausberger and Somogyi, 2008). This interconnected network of excitatory and inhibitory neurons enables the CA3 circuitry to generate a wide range of network activities depending on its inputs and the state of the network. These network states have been ascribed important roles in hippocampal function, such as spatial navigation (O'Keefe and Dostrovsky, 1971; Huxter et al., 2003), memory encoding and retrieval (Lisman and Idiart, 1995; Jensen and Lisman, 1996), and memory consolidation (Buzsaki, 1986, 1989). Understanding the mechanisms by which these different network patterns are generated might shed light on the underlying computational principles by which they perform their functions. Many studies have indicated an important role of GABAergic inhibition in generating these patterns (Buzsaki et al., 1983; Ylinen et al., 1995; Csicsvari et al., 2003).

Several hippocampal slice preparations have been created which generate similar network activity to that seen *in vivo* (Ben-Ari et al., 1989; Fisahn et al., 1998; Kubota et al., 2003). These *in vitro* preparations enable investigation of network activity using extracellular field recording in combination with fast exchange of pharmacological agents, visually guided patch-clamp recordings and advanced imaging techniques (Hajos et al., 2009).

In this review, we discuss several recent papers that reveal two previously unrecognized roles of GABAergic transmission in hippocampal network activity, as seen in field recordings. Firstly, we discuss the finding that the local field potential (LFP) reflects more of inhibitory currents than previously thought. Secondly, we discuss the finding that some GABAergic neurons can initiate hippocampal population bursts, not only early in development, but, unexpectedly, also in the mature CA3 network. These findings emphasize the increasing number of roles ascribed to interneurons in the generation of physiological hippocampal network activity. We also briefly discuss the potential implications of these findings for our understanding of the mechanisms underlying pathological network activity (see **Table 1**).

HIPPOCAMPAL OSCILLATIONS

Many types of hippocampal network oscillations are driven by inhibitory neurons. Here we discuss the recent finding that inhibitory events not only generate the rhythm of these oscillations, but do in fact also contribute directly to the recorded oscillatory EEG signal. For the purpose of this review we focus mainly on perisomatic targeting interneurons, although dendritic targeting interneurons most likely also play an important role in oscillogenesis. For a recent review on the family of dendritic targeting interneurons and hippocampal network activity, see Klausberger (2009).

RHYTHM GENERATION

The involvement of interneurons in rhythm generation has been well documented. For theta oscillations (4–8 Hz), for example, it is thought that oscillations in individual cells (Alonso and Llinas, 1989; Strata, 1998; Buzsaki, 2002) are stabilized and synchronized by a set of inhibitory feedback circuits (Buzsaki et al., 1983; Leung and Yim, 1986; Soltesz and Deschenes, 1993; Cobb et al., 1995; Klausberger et al., 2003), as recently shown in an intact isolated hippocampus *in vitro* (Goutagny et al., 2009). In addition, external GABAergic inputs arriving from the medial septum and brainstem (Petsche and Stumpf, 1962; Stewart and Fox, 1990) could also contribute to rhythm generation, potentially serving as a pacemaker for the theta rhythm (Stewart and Fox, 1990).

Gamma oscillations (30–100 Hz) are commonly observed nested within theta oscillations in the hippocampus (Bragin et al., 1995; Buzsaki et al., 2003; Csicsvari et al., 2003). Studies into the mechanisms underlying carbachol-induced gamma oscillations in hippocampal slices have indicated an important role for perisomatic inhibition in rhythm generation (Fisahn et al., 1998; Mann et al., 2005; Oren et al., 2006). In particular, it was observed that prolongation of the $GABA_A$ receptor-mediated inhibitory postsynaptic currents (IPSCs) with barbiturate reduces the frequency of gamma oscillations (Fisahn et al., 1998). Modeling studies also implicate inhibitory interneurons in rhythm generation (Wang and Buzsaki, 1996; Traub et al., 1997; Brunel and Wang, 2003), as do *in vivo* recordings (Penttonen et al., 1998; Tukker et al., 2007). For a discussion of *in vitro* gamma oscillation models in relation to *in vivo* activity, see Hajos and Paulsen (2009).

Although the rhythm generation of many oscillations has been extensively studied, little is known about the currents underlying the observed field events. Field activity is generated by the sum of currents flowing into and out of cells. It has long been thought that excitatory currents contribute predominantly to the recorded field events (see **Figures 1A,B**). Several recent papers have now challenged this assumption and shown that inhibition, especially arising from perisomatic targeting interneurons, can contribute significantly to the current generation (see **Figures 1A,C**).

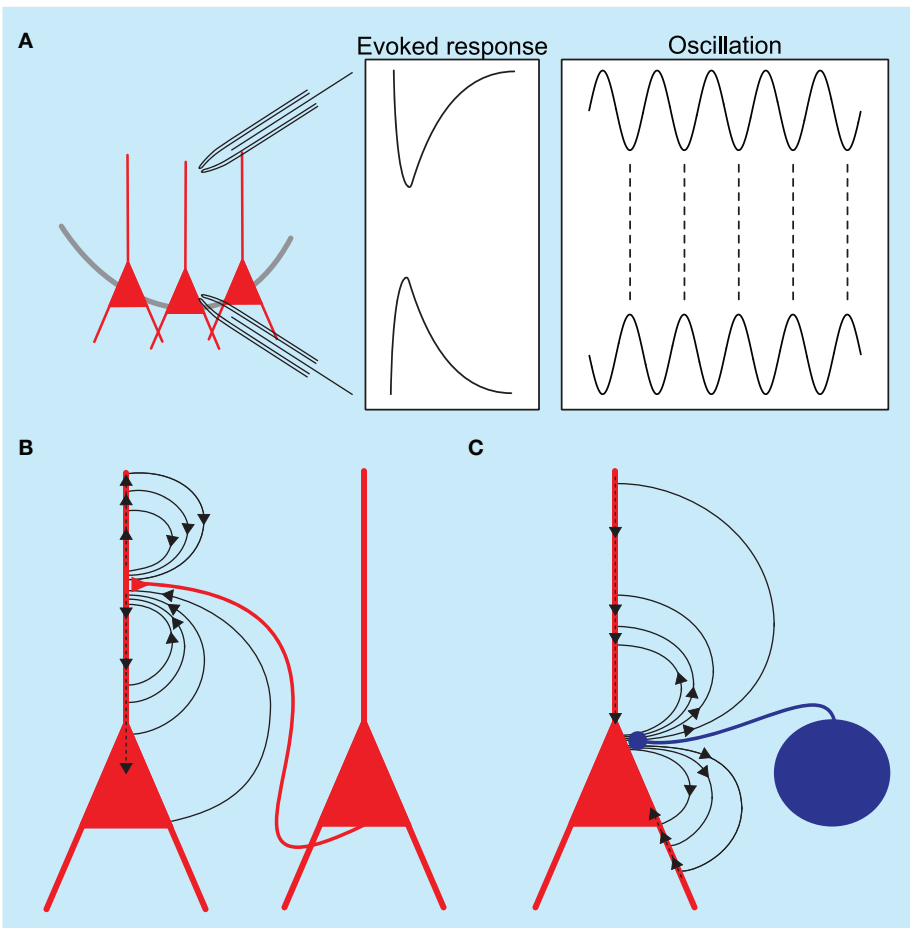

FIGURE 1 | Schematic diagram of hippocampal local field potentials and the underlying current sinks and sources. (A) Recording electrodes placed in the dendritic and somatic regions of the hippocampus show a phase reversal for both evoked responses and oscillatory activity. **(B)** Excitatory synaptic events at the apical dendrite of pyramidal neurons generate an active current sink as positive ions flow into neurons; a concurrent passive source is recorded from the somatic region. **(C)** Inhibitory synaptic events at the perisomatic regions of pyramidal neurons generate an active source accompanied by a passive current sink at the dendrites.

Table 1 | Involvement of perisomatic targeting interneurons in hippocampal network activity.

Network activity	Experimental observation	Reference
HIPPOCAMPAL FAST OSCILLATIONS		
Gamma frequency oscillations (30–100 Hz)	Importance of GABAergic inhibition *in vitro*	Whittington et al. (1995), Fisahn et al. (1998)
	Importance of GABAergic interneurons *in vivo*	Buzsaki et al. (1983), Penttonen et al. (1998), Csicsvari et al. (2003)
	Importance of perisomatic targeting interneurons *in vitro*	Hajos et al. (2004), Mann et al. (2005), Oren et al. (2010)
	Importance of perisomatic targeting interneurons *in vivo*	Klausberger et al. (2003)
Ripple oscillations (~200 Hz)	Importance of GABAergic inhibition *in vivo*	Csicsvari et al. (1999), Buhl et al. (2005)
	Importance of perisomatic targeting interneurons *in vivo*	Buzsaki et al. (1992), Ylinen et al. (1995), Klausberger et al. (2003)
Ultrafast oscillations (200–600 Hz)	Importance of perisomatic targeting interneurons *in vitro*	Trevelyan (2009)
HIPPOCAMPAL POPULATION BURSTS		
Spontaneous network synchronization during development	Importance of GABAergic excitation *in vitro*	Ben-ari et al. (1989), Bonifazi et al. (2009)
	Importance of GABAergic excitation *in vivo*	Leinekugel et al. (2002)
Sharp waves	Importance of perisomatic targeting interneurons *in vitro*	Ellender et al. (2010)
Epileptiform bursting	Reduced GABAergic inhibition	Ayala et al. (1973), Traub and Wong (1982), Miles and Wong (1983)
	Enhanced perisomatic GABAergic inhibition	Cossart et al. (2001), Wittner et al. (2001)

CURRENT GENERATION

A recent paper by Oren et al. (2010) analyzed the contribution of excitatory and inhibitory synaptic currents, as well as spiking activity of CA3 hippocampal neurons, to the LFP in carbachol-induced gamma oscillations. It was observed that gamma oscillation amplitude fluctuated over time. Changes in the oscillation amplitude were quantified by the amplitude of the wavelet transform. By correlating the amplitude of the oscillation as seen in the field and the activity in individual cells it was suggested that the largest contributor to the field was the inhibitory currents in excitatory neurons, with a smaller contribution from the spiking activity of pyramidal neurons. Three lines of evidence support this conclusion. Firstly, the mean cycle amplitude was significantly higher when perisomatic interneurons discharged. There was no such direct relationship between the discharge of a pyramidal neuron and the LFP amplitude, although a small contribution was found for the slow action currents, resulting from the activation of a repolarization conductance, to the early component of the LFP. Secondly, the amplitude of the LFP signal correlated significantly with the inhibitory synaptic currents, whereas no such correlation was seen with excitatory synaptic currents. Thirdly, the inhibitory events recorded from pyramidal neurons were highly synchronized with the LFP.

Direct evidence that inhibitory neurons can produce significant field events was provided in a recent study by Glickfeld et al. (2009), who investigated whether activity of single anatomically identified interneurons is inhibitory or excitatory for downstream targets, using a combination of single cell stimulation and LFP recording. Surprisingly, activity in a single interneuron generated a transmembrane current sufficiently large to be reflected in the LFP recorded with an extracellular electrode (Glickfeld et al., 2009). The largest field event was seen following stimulation of perisomatic targeting interneurons (basket and axo-axonic cells). This observation was recently confirmed in a study by Bazelot et al. (2010), who also showed that single interneurons can generate a measurable field response. They showed that stimulation of a single perisomatic targeting interneuron can generate a field response of ~30 μV. If field IPSPs add linearly, a field recording of hippocampal gamma oscillations in a hippocampal slice in the range of 100–500 μV (Fisahn et al., 1998) could be accounted for by the synchronous activity of approximately 10 perisomatic targeting interneurons.

RIPPLE AND ULTRAFAST OSCILLATIONS

The fact that perisomatic inhibition has a large contribution to gamma oscillations as measured in the field raises the possibility that they might also contribute to faster field oscillations, such as ripple oscillations as part of sharp wave-ripple complexes, or ultrafast oscillations, as seen in pathological states. The cellular basis of ripple oscillations is still a matter of debate, and several possible explanations have been proposed.

Firstly, it has been suggested that the synchronous depolarization of CA1 neurons by CA3 pyramidal neuron activity sets in motion a dynamic interaction between CA1 pyramidal cells and CA1 interneurons, resulting in an oscillatory field potential between 120 and 200 Hz as seen in the stratum pyramidale (Buzsaki et al., 1992). Occasionally, CA3 ripples were seen concurrent with those occurring in CA1, but the CA3 ripples were of a lower frequency (80–140 Hz) (Ylinen et al., 1995) and not correlated to unit activity in CA1. Combined, these results suggest that CA1 ripple oscillations emerge from the CA1 cell population rather than being a passive response to high frequency input from CA3 (Ylinen et al., 1995). The specific synaptic currents mediating ripple oscillations were suggested to be synchronized

somatic IPSCs in CA1 pyramidal neurons (Ylinen et al., 1995). Potentially, the interneurons could be synchronized by gap junctions (Katsumaru et al., 1988) as halothane anesthesia abolishes ripple activity (Ylinen et al., 1995). Interestingly, the emergence of ripple oscillations coincides with the transition from depolarizing to hyperpolarizing GABA action during development, suggesting that a dynamic interaction between excitation and inhibition is needed for ripple oscillations to occur (Buhl and Buzsaki, 2005).

A second proposed mechanism for CA1 ripple oscillations involves a network of pyramidal neurons interconnected by axonal gap junctions (Draguhn et al., 1998). It was shown that the CA1 region of hippocampal slices could produce ripple oscillations that were not affected by block of both excitatory and inhibitory synaptic currents, but disappeared when gap junction blockers were used, although these compounds are notoriously unspecific (Connors and Long, 2004). However, *in vivo*, CA1 pyramidal neurons tend to burst at higher frequencies than ripple oscillations, which would not support this hypothesis (Csicsvari et al., 1999).

Thirdly, it has been suggested that ripples observed in CA1 are the extracellular reflection of the synchronous firing of small groups of pyramidal neurons. These "population spikes" could be the result of intrinsically generated pyramidal neuron spiking, synchronized by recurrent connections (Dzhala and Staley, 2004). These three possibilities are not mutually exclusive and a combination of them is possible.

Similar explanations have been forwarded for ultrafast oscillations seen during epileptiform activity (Le Van Quyen et al., 2006), including the idea of synchronized "population spikes" (Bragin et al., 2000, 2002, 2007), although desynchronized spiking has also been proposed (Foffani et al., 2007). It has been suggested that ripple activity is crucial for the development of an epileptic focus in the developing (Khalilov et al., 2005), and adult brain (Traub et al., 2001b; Grenier et al., 2003), whereas others have proposed that ripples might rather be protective and restrict epileptiform spread (Trevelyan et al., 2006, 2007). A recent paper investigated the correlation between the fast oscillations seen in the field during interictal events in a 0 Mg^{2+} model of epileptiform activity and IPSCs recorded intracellularly from pyramidal neurons (Trevelyan, 2009). The author found that IPSCs recorded from closely located pyramidal neurons are highly synchronous, whereas IPSCs recorded from neurons located more than 200 μm apart were not synchronous. The author used dual whole-cell recordings with one pyramidal neuron held in voltage-clamp and another in current-clamp combined with an extracellular electrode to record the field potential. Using sophisticated analysis combined with modeling a close correlation was seen between the high frequency oscillation (HFO) in the field and the intracellular recordings from the pyramidal neurons. This correlation was strongest in the preictal period and fell as the event developed into a full ictal event. The author argued that it is the transmembrane currents generated by perisomatic inhibition that underlies these HFOs (Trevelyan, 2009).

In summary, for both gamma and ripple oscillations, recent evidence suggests that IPSCs of perisomatic origin contribute to the oscillatory field event.

HIPPOCAMPAL POPULATION BURSTS

In addition to regular oscillations, the hippocampal network spontaneously generates population bursts at irregular intervals both during development and in the adult animal. Here we discuss the involvement of GABAergic inhibition in initiating these events and compare the mechanisms of engagement in developing and mature tissue.

GIANT DEPOLARIZING POTENTIALS

Already at a very young age the hippocampal CA3 region generates intermittent synchronous bursts. First described by Ben-Ari et al. (1989), CA3 hippocampal neurons in slices taken from immature rats, postnatal day (P) 0 to P8, spontaneously display brief episodes of depolarization of 25–50 mV, so called giant depolarizing potentials (GDPs), lasting 300–500 ms with an incidence of about 0.1 per second, and often accompanied by action potentials (Ben-Ari et al., 1989; Ben-Ari, 2001). Later, elegant *in vivo* studies confirmed the presence of such bursts early in development which were shown to share common features with their *in vitro* counterparts (Leinekugel et al., 2002). The intracellular depolarization was synchronous with bursts observed in field recordings, suggesting that they are the result of synchronous firing of a large population of neurons. GDPs were shown to depend on GABAergic transmission, as they could be blocked by a variety of $GABA_A$ receptor antagonists (Ben-Ari et al., 1989). Further evidence corroborating a role for GABAergic transmission in generating these events was the observation that the incidence of GDPs decreased from P5 onwards, and finally disappeared by P12, coinciding with the developmental transition from GABA exerting a depolarizing effect to being hyperpolarizing on a postsynaptic neuron. It has been suggested that the depolarizing effect of GABA is the result of an active Na^+–K^+–Cl^--cotransporter (NKCC1) which sets up a Cl^- gradient responsible for the depolarizing effect (Russell, 2000; Delpire and Mount, 2002). The ontogenetic shift to hyperpolarizing GABA action is caused by a concomitant developmental down-regulation of NKCC1 and an up-regulation of a K^+–Cl^--cotransporter (KCC2) (Rivera et al., 1999).

Ben-Ari and colleagues suggest a mechanism by which activity of GABAergic neurons, spontaneous or induced by activation of their glutamatergic receptors, could depolarize populations of CA3 pyramidal neurons into generating such population bursts. Even though interneurons are more mature than pyramidal neurons at this stage (Soriano et al., 1986; Gozlan and Ben-Ari, 2003), the overall hippocampal circuitry and synaptic connections are still quite immature (Bahr and Wolff, 1985) with GABA being released mostly from axo-dendritic synapses or from non-synaptic free endings (Ben-Ari et al., 2004). It has been suggested that early network synchronization might have a role in controlling neuronal differentiation, synaptogenesis, and synaptic plasticity in the developing brain (Katz and Shatz, 1996; Khazipov and Luhmann, 2006; Blankenship and Feller, 2010).

HUB NEURONS

Far from being a homogeneous population of young immature interneurons, a recent study showed that not all inhibitory neurons are equal in the developing CA3 hippocampus. Already at such a

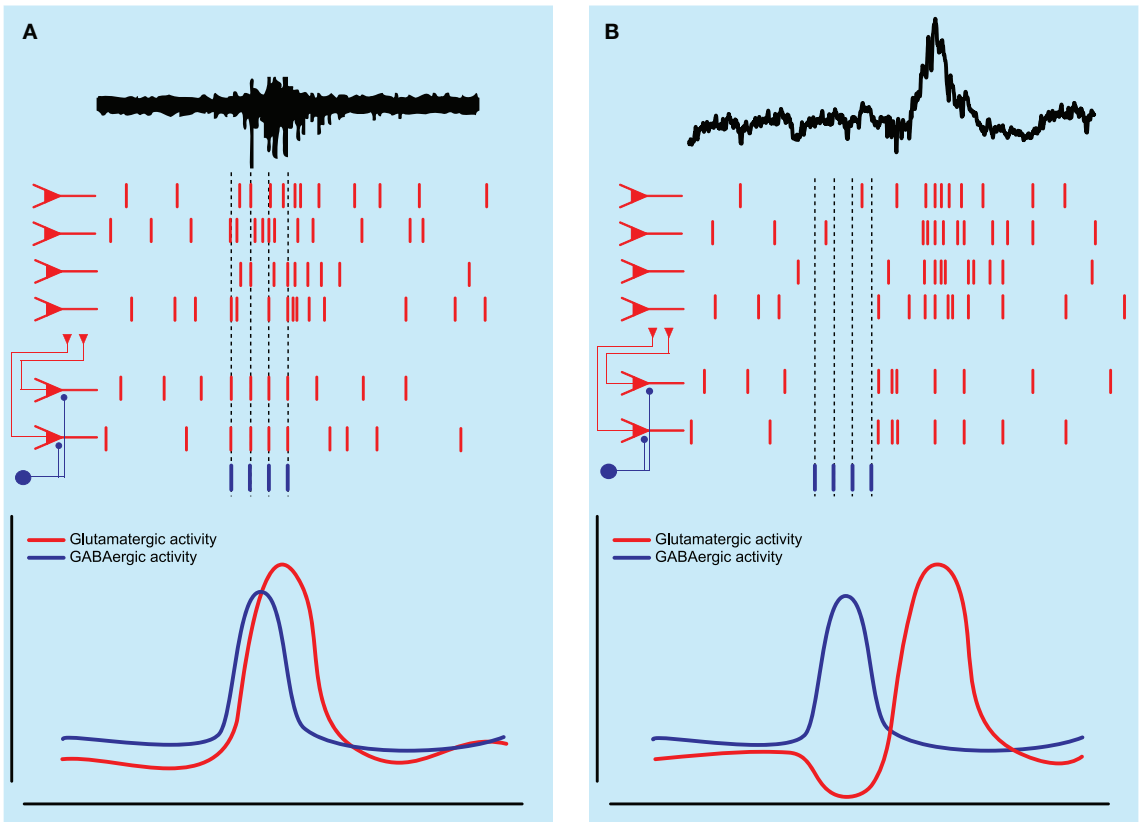

FIGURE 2 | Schematic diagram of network activity underlying hippocampal population bursts. (A) Spontaneous network synchronizations as seen in the immature hippocampus are thought to be generated by the excitatory action of GABAergic neurons, which depolarize and recruit a population of pyramidal neurons into a population burst. **(B)** Sharp wave-ripple population bursts as seen in the adult hippocampus may be initiated by the activity of an inhibitory interneuron temporarily silencing a subset of pyramidal neurons followed by rebound excitation, recruiting a larger population of pyramidal neurons into a population burst.

young age they exhibit a functional heterogeneity, differentially affecting spontaneous network synchronization (Bonifazi et al., 2009). The authors of this study combined multibeam two-photon calcium imaging of ongoing network synchronization events (the field equivalent of intracellularly recorded GDPs) with stimulation of individual anatomically identified neurons in slices taken from both rat and GAD67-GFP mice. Spontaneous network synchronization was observed as synchronous Ca^{2+} signals in a large population of neurons (Leinekugel et al., 1997). Using this technique the authors showed that some neurons in the developing hippocampus have a very high functional connectivity to other neurons in the slice, which was detected online by finding neurons which were consistently active before other neurons. If a neuron was consistently active prior to 40% of the total number of imaged neurons it was deemed a high connectivity (HC) neuron. The authors then repeatedly depolarized individual HC neurons to supra-threshold levels with 200-ms long current pulses and showed that eight out of 20 of these HC neurons could significantly alter ongoing spontaneous network activity (see **Figure 2A**). They were dubbed "hub neurons" and, as hub neurons found in GAD67-GFP mice were all GFP positive and all hub neurons were aspiny, they were suggested to be GABAergic. The network response to activation of individual hub neurons was heterogeneous as they could silence the network, delay the generation of spontaneous network synchronization or initiate network synchronization events. Part of the heterogeneity in responses was explained by the observation of two different groups of GABAergic neuron based on axon arborization. *Post hoc* anatomical investigation of these neurons revealed that those with an axonal arborization close to the pyramidal cell layer, reminiscent of perisomatic targeting interneurons found in the adult hippocampus, were responsible for the initiation of network synchronization events (Bonifazi et al., 2009). Conversely, hub neurons with long projecting axons and sparse collaterals were responsible for silencing or delaying the generation of these events. This study is one of the first demonstrations of a small-scale network architecture present in the developing brain (Bullmore and Sporns, 2009) and raises several interesting points.

Firstly, it has been reported that the first GABAergic synapses are preferentially made on the apical dendrites and not on the soma of pyramidal neurons (Tyzio et al., 1999) with axosomatic targeting neurons only appearing later (Ben-Ari et al., 2004). In particular, it has been shown that certain basket cells initially form dendritic synapses and only shift to their adult pattern of somatic innervation after P4 (Morozov and Freund, 2003). This would suggest that an individual hub neuron responsible for the initiation of network synchronization events, even though anatomically resembling future perisomatic targeting interneurons, might innervate the dendrites of pyramidal neurons, which seems sufficient for spike generation in pyramidal neurons at this age (Ben-Ari et al., 1989).

Secondly, a subset of HC neurons, shown to be pyramidal neurons, did not affect network activity suggesting that glutamatergic transmission is not sufficient to recruit large populations of neurons at this age.

Thirdly, the different responses found after activation of hub neurons might not only be the result of morphological differences between the two groups, possibly reflecting different developmental stages, but could also be influenced by the postsynaptic effect of GABA, since GABA might be both depolarizing and hyperpolarizing at this transitory phase of development.

In addition to the population of HC neurons there was a population of low connectivity (LC) neurons which had either a pyramidal neuron or interneuron morphology. These were classified according to the fact that their activity was not followed by any significant spontaneous population activity. Similarly, stimulating these neurons did not evoke any detectable changes in the network. The LC neurons were shown to have a shorter axonal length and this might explain their inability to synchronize a large population of neurons. As the immature hippocampus exhibits a high degree of heterogeneity, LC and HC neurons might actually represent the same types of neurons but at different stages in their development (de Lecea et al., 1995; Ben-Ari, 2001), or be differentially affected by the slicing procedure.

Lastly, it is unknown whether any further differences exist within the population of HC neurons or between the LC and HC neurons. Further investigation into the density, morphology, and location of synaptic contacts might be interesting.

It should be pointed out that both rat and mouse slices were used for these experiments (animals ranging in age from P5–P7) and it is at present unknown if there are developmental differences between the two rodent species in hub neuron function, reflecting differences in synapse development as well as differential transition between depolarizing and hyperpolarizing GABA action. It has recently been shown that there are both anatomical and electrophysiological differences between rat and mouse pyramidal neurons (Routh et al., 2009).

The paper by Bonifazi et al. raises the question whether neurons with similar properties exist in the adult hippocampus. A recent study by Ellender et al. (2010) would suggest that neurons with hub-like properties may exist also in the adult hippocampus.

SHARP WAVE – RIPPLES

At first it seems a daunting task to find hub neurons, bearing in mind the enormous diversity of interneurons in the adult hippocampus (Klausberger and Somogyi, 2008). Classifying the interneurons according to the location of their axonal targets already greatly facilitates the handling of such diversity (Freund and Buzsaki, 1996). Some of the hub neurons identified by Bonifazi et al., namely those that were able to initiate network synchronization events, had some morphological features similar to those described for the family of perisomatic targeting interneurons seen in the adult hippocampus, which can be subdivided into parvalbumin-positive basket cells (Kosaka et al., 1987), cholecystokinin-positive basket cells (Somogyi et al., 1984), and parvalbumin-positive axo-axonic cells (Somogyi, 1977; Somogyi et al., 1983). The different subtypes have been suggested to have different functions in the hippocampal network (Freund and Katona, 2007).

Similar to the very young hippocampus, the adult hippocampus (from P14 onwards) can also spontaneously generate bursts (Vanderwolf, 1969). These are called "ripples" (O'Keefe and Nadel, 1978) or sharp wave-ripple complexes (Buzsaki et al., 1983). Sharp wave-ripple complexes have two components. The sharp wave part is seen as a voltage deflection of around 1 mV and 50–100 ms duration (Buzsaki, 1986). The second component, the so called ripple, is a fast oscillation with a frequency between 120 and 200 Hz (Buzsaki et al., 1992; Ylinen et al., 1995; Chrobak and Buzsaki, 1996). Sharp wave-ripple activity is seen during rest (e.g. awake immobility or eating) and slow-wave sleep. Sharp wave-ripples have been implicated in the reactivation of spike sequences (Skaggs and McNaughton, 1996; Lee and Wilson, 2002; Foster and Wilson, 2006; Diba and Buzsaki, 2007) and could facilitate the strengthening of memories within the hippocampus during exploration (O'Neill et al., 2006) as well as mediate off-line memory transfer to extra-hippocampal regions for long-term storage (Buzsaki, 1989). They are thought to be the result of synchronous bursts of action potentials in a subset of hippocampal pyramidal neurons (Buzsaki, 1986; Csicsvari et al., 2000), initiated in the CA3 subfield by pyramidal neurons with strong synaptic interconnections (Buzsaki and Chrobak, 1995) or recent place-related firing (O'Neill et al., 2006; Diba and Buzsaki, 2007). The detailed mechanism of their initiation in hippocampal CA3 is unknown, but an involvement of interneurons in shaping this network pattern appears likely.

Ellender et al. used hippocampal slices taken from rats aged P14–P28, when neurons have axons and dendrites with adult-like features (Gaiarsa et al., 1992; Gomez-Di Cesare et al., 1997). Slices prepared at these ages can generate sharp wave-ripple activity spontaneously (Kubota et al., 2003). This model of sharp wave-ripples was adapted for submerged types of recording chamber (Hajos et al., 2009), which enabled visually guided patch-clamp recordings of neurons in CA3 with concomitant recording of ongoing sharp wave-ripple activity using planar multi-electrode arrays. The authors focused on the sharp waves and showed that they are associated with the synchronous firing of small changing populations of CA3 pyramidal neurons. Similar to the network synchronization events in developing hippocampus (Bonifazi et al. 2009), a high incidence of sharp waves was observed in region CA3c. The surrounding population of pyramidal neurons was inhibited; therefore, it was not surprising that blocking all $GABA_A$ receptor-mediated inhibition led to a transition from local sharp wave generation to large-scale epileptiform bursting (Miles and Wong, 1987). It was unexpected, however, that blocking only the phasic component of $GABA_A$ receptor-mediated inhibition completely and reversibly blocked all sharp wave generation (Ellender et al., 2010). This suggests that inhibition plays a previously unknown role in sharp wave initiation.

To investigate this further the authors performed whole-cell current-clamp recordings of anatomically identified neurons, which were repeatedly depolarized to supra-threshold levels with 500-ms long current pulses every 10 s, and observed the effect on network activity. Activation of either single pyramidal neurons or dendritic targeting interneurons did not affect network activity. In contrast, the activation of a subset of individual perisomatic targeting interneurons could both suppress (during activation), and subsequently enhance, the local generation of sharp waves. The authors investigated the mechanisms by which this subset

of perisomatic targeting interneurons could initiate sharp wave generation by combining stimulation of individual perisomatic targeting interneurons with whole-cell voltage-clamp recording of a neighboring neuron. Voltage-clamped neurons were used to record both the excitatory and inhibitory activity in the network before, during, and after activation of the perisomatic targeting interneuron. It was shown that activity in perisomatic targeting interneurons was followed by a transient increase in excitation over inhibition in the network which preceded the initiation of a sharp wave. The authors concluded that this increase in excitation over inhibition could facilitate population burst generation by bringing a population of pyramidal neurons closer to threshold (Ellender et al., 2010).

This study suggests that GABA released by interneurons in the adult hippocampus can initiate population bursts, albeit via a different mechanism to that seen in the immature hippocampus. Instead of a direct depolarizing effect of GABA on pyramidal neurons, it is suggested that activity of perisomatic targeting interneurons temporarily silences a population of pyramidal neurons after which rebound excitation can lead to the synchronization of this population of pyramidal neurons (see **Figure 2B**). As mature rats were used, in which pyramidal cells most likely exhibit a $GABA_A$ receptor reversal potential negative to resting membrane potential (Luhmann and Prince, 1991; Owens et al., 1996), it was suggested that GABA would be hyperpolarizing. Nevertheless, it might be that GABA was excitatory in a subset of pyramidal neurons, as can be seen in young animals, as well as in certain neuronal types and cortical states in adult brain (Cohen et al., 2002; Gulledge and Stuart, 2003; Wozny et al., 2003; Banke and McBain, 2006; Szabadics et al., 2006), or that GABA could be depolarizing in specific subregions of the pyramidal neuron (e.g., axon initial segment; Szabadics et al., 2006; but see Glickfeld et al., 2009).

A subset of anatomically identified perisomatic targeting interneurons was not able to initiate sharp wave population bursts. The authors did not find significant differences between the successful and unsuccessful perisomatic targeting interneurons in either their average firing frequency, location within hippocampal CA3 or axonal length (Ellender et al., 2010). As no immunocytochemistry or electron microscopy was performed to further subdivide the population of perisomatic targeting interneurons it was not possible to determine whether the failure of some perisomatic targeting interneurons to influence sharp wave initiation is due to the network state or because different subclasses of perisomatic targeting interneuron might have different effects on these network events. Studies in area CA1 of the hippocampus *in vivo* have shown that parvalbumin-positive basket cells fire preferentially during a sharp wave-ripple, whereas axo-axonic cells tend to fire immediately before, but remain silent during sharp wave-ripples (Klausberger et al., 2003). It has not been reported whether these types of neurons in area CA3 show similar behaviors. If axo-axonic cells in CA3 also fire preferentially prior to sharp wave-ripples, they may have a role in selecting the subpopulation of CA3 pyramidal neurons that initiate a sharp wave event. Their preference to make synaptic connections on the axon initial segment of pyramidal neurons would make them well suited to influence axonal output (Miles et al., 1996).

It is well established that some fast spiking interneurons innervate themselves (Tamas et al., 1997). Furthermore, fast spiking interneurons are vastly interconnected through chemical and electrical synapses (Fukuda and Kosaka, 2000), both of which contribute to the synchronization of interneuronal networks (Tamas et al., 2000; Traub et al., 2001a; Whittington and Traub, 2003). It is at present unknown whether chemical synapses or electrical synapses (gap junctions) are necessary for the ability of single hub neurons or perisomatic targeting interneurons to induce hippocampal population bursts. Gap junctions might contribute to the generation of some network patterns (Maier et al., 2002; Buhl et al., 2003), but studies into their involvement are notoriously difficult as the presently available pharmacological agents are non-specific (Connors and Long, 2004).

The finding that single interneurons can facilitate the generation of hippocampal population bursts in both young and adult hippocampus is novel. The question arises whether the neurons found by Ellender et al., are mature versions of the hub neurons found by Bonifazi et al., or whether they are different types of neurons with similar hub-like properties. It might be that the hub neurons described by Bonifazi et al. are a transient population that disappears and dies later in development (Super et al., 1998). Molecular markers (such as parvalbumin or cholecystokinin) are used to classify interneurons in the adult hippocampus (Klausberger et al., 2003, 2004, 2005; Klausberger and Somogyi, 2008), and it would be interesting to investigate the expression of these markers in both the hub neurons and the successful perisomatic targeting interneurons. Such analysis, in combination with studies of ion channel and transcription factor expression (Cobos et al., 2006), might provide a fingerprint of the type of neuron capable of initiating network events, facilitating possible detection in other brain regions.

EPILEPTIFORM BURSTS

Lastly, we will briefly discuss the potential implications of the studies by Bonifazi et al. and Ellender et al. on our understanding of the mechanisms underlying epileptiform bursting. These two studies suggest that inhibition not only keeps population bursts in check (Trevelyan et al., 2007), but could also be actively involved in the initiation of population bursts. Classically, the generation of pathological epileptiform bursts is suggested to depend on a reduction of $GABA_A$ receptor-mediated inhibition, which facilitates mutual synaptic excitation (Traub and Wong, 1982). In systems where glutamatergic transmission is immature (Bonifazi et al., 2009) or embedded in a mature inhibitory network (Ellender et al., 2010), activity of individual pyramidal neurons was not sufficient to initiate population bursts. In contrast, a single CA3 pyramidal neuron can initiate an epileptiform burst in disinhibited conditions (Miles and Wong, 1983) by recruiting sufficient pyramidal neurons to exceed a threshold for burst initiation (Menendez de la Prida et al., 2006).

It has been shown in surgically removed human epileptic tissue that perisomatic inhibition is retained in the CA1 region of the hippocampus (Wittner et al., 2005) and retained or enhanced in the dentate gyrus (Isokawa-Akesson et al., 1989; Wittner et al., 2001). Wittner et al. observed an increase in inhibitory contacts at the axon initial segments of granule cells of the dentate gyrus.

It was suggested that hyper-innervation of axon initial segments may lead to a more effective synchronization of granule cell firing and could in fact contribute to the generation or amplification of epileptic seizures (Wittner et al., 2001). More recently, it has been shown that nicotinic enhancement of GABA release can aggravate seizure generation in several models of autosomal dominant nocturnal frontal lobe epilepsy (Klaassen et al., 2006; Mann and Mody, 2008), further emphasizing the possibility that inhibition could facilitate pathological burst generation. It has also been shown that perisomatic targeting interneurons are massively recruited during epileptiform population bursts (Marchionni and Maccaferri, 2009).

Another possibility is that activity of perisomatic targeting interneurons is the last effort to keep a full burst at bay (Trevelyan et al., 2007; Trevelyan, 2009). In fact, it has been suggested that loss of dendritic inhibition could reduce seizure threshold, with preserved somatic inhibition keeping the network from a continuous occurrence of population bursts (Cossart et al., 2001). This would suggest that separate targeting of dendritic and perisomatic inhibition might be necessary for the effective treatment of epileptiform discharges (Magloczky and Freund, 2005). Lastly, it could also be that GABA swaps sides in pathology from being inhibitory to being excitatory due to a change in intracellular ion concentrations (Cohen et al., 2002).

In conclusion, both the studies by Bonifazi et al. (2009) and Ellender et al. (2010) imply that interneurons, rather than merely modulating pyramidal cell activity, can play an integral part in the local information processing that takes place in the hippocampal network. Furthermore, they suggest that neurons with hub-like properties exist in both the developing and mature hippocampus (Bullmore and Sporns, 2009) and corroborate the idea that single neurons can have a large effect on network activity (Brecht et al., 2004; Houweling and Brecht, 2008; Li et al., 2009). The finding that interneurons can initiate physiological hippocampal population bursts raises the possibility that they might also contribute to those seen in pathology.

FUTURE

The studies discussed here extend the roles of perisomatic inhibition beyond that of rhythm generation, showing that they can also contribute to the transmembrane currents underlying hippocampal field oscillations and are able to initiate hippocampal population bursts. It remains to be seen whether these observations hold for network activity *in vivo*. However, as these observations were made in slice preparations, in which axonal projections are markedly reduced, one might expect that their ability to generate transmembrane currents, as well as influence population burst activity, might be even greater *in vivo*.

With the development of *in vivo* recording techniques which enable monitoring extracellular activity early in development (Yang et al., 2009), as well as intracellularly in anatomically identified neurons in behaving animals (Epsztein et al., 2010) combined with optogenetics (Deisseroth et al., 2006) and modeling, *in vivo* investigation of these findings will be possible. By gaining a better understanding of the cellular mechanisms involved in network activity one may hope that their functions in cognitive processes will be uncovered, and such understanding might also help us in combating brain disorders (Uhlhaas and Singer, 2006, 2010; Hammond et al., 2007).

ACKNOWLEDGMENTS

We would like to thank Wiebke Nissen for careful reading of a draft of this review. The authors' research was supported by The Wellcome Trust.

REFERENCES

Alonso, A., and Llinas, R. R. (1989). Subthreshold Na+-dependent theta-like rhythmicity in stellate cells of entorhinal cortex layer II. *Nature* 342, 175–177.

Ayala, G. F., Dichter, M., Gumnit, R. J., Matsumoto, H., and Spencer, W. A. (1973). Genesis of epileptic interictal spikes. New knowledge of cortical feedback systems suggests a neurophysiological explanation of brief paroxysms. *Brain Res.* 52, 1–17.

Bahr, S., and Wolff, J. R. (1985). Postnatal development of axosomatic synapses in the rat visual cortex: morphogenesis and quantitative evaluation. *J. Comp. Neurol.* 233, 405–420.

Banke, T. G., and McBain, C. J. (2006). GABAergic input onto CA3 hippocampal interneurons remains shunting throughout development. *J. Neurosci.* 26, 11720–11725.

Bazelot, M., Dinocourt, C., Cohen, I., and Miles, R. (2010). Unitary inhibitory field potentials in the CA3 region of rat hippocampus. *J. Physiol.* 588, 2077–2090.

Ben-Ari, Y. (2001). Developing networks play a similar melody. *Trends Neurosci.* 24, 353–360.

Ben-Ari, Y., Cherubini, E., Corradetti, R., and Gaiarsa, J. L. (1989). Giant synaptic potentials in immature rat CA3 hippocampal neurones. *J. Physiol.* 416, 303–325.

Ben-Ari, Y., Khalilov, I., Represa, A., and Gozlan, H. (2004). Interneurons set the tune of developing networks. *Trends Neurosci.* 27, 422–427.

Blankenship, A. G., and Feller, M. B. (2010). Mechanisms underlying spontaneous patterned activity in developing neural circuits. *Nat. Rev. Neurosci.* 11, 18–29.

Bonifazi, P., Goldin, M., Picardo, M. A., Jorquera, I., Cattani, A., Bianconi, G., Represa, A., Ben-Ari, Y., and Cossart, R. (2009). GABAergic hub neurons orchestrate synchrony in developing hippocampal networks. *Science* 326, 1419–1424.

Bragin, A., Jando, G., Nadasdy, Z., Hetke, J., Wise, K., and Buzsaki, G. (1995). Gamma (40-100 Hz) oscillation in the hippocampus of the behaving rat. *J. Neurosci.* 15, 47–60.

Bragin, A., Mody, I., Wilson, C. L., and Engel, J. Jr. (2002). Local generation of fast ripples in epileptic brain. *J. Neurosci.* 22, 2012–2021.

Bragin, A., Wilson, C. L., and Engel, J. Jr. (2000). Chronic epileptogenesis requires development of a network of pathologically interconnected neuron clusters: a hypothesis. *Epilepsia* 41(Suppl. 6), S144–S152.

Bragin, A., Wilson, C. L., and Engel, J. Jr. (2007). Voltage depth profiles of high-frequency oscillations after kainic acid-induced status epilepticus. *Epilepsia* 48(Suppl. 5), 35–40.

Brecht, M., Schneider, M., Sakmann, B., and Margrie, T. W. (2004). Whisker movements evoked by stimulation of single pyramidal cells in rat motor cortex. *Nature* 427, 704–710.

Brunel, N., and Wang, X. J. (2003). What determines the frequency of fast network oscillations with irregular neural discharges? I. Synaptic dynamics and excitation-inhibition balance. *J. Neurophysiol.* 90, 415–430.

Buhl, D. L., and Buzsaki, G. (2005). Developmental emergence of hippocampal fast-field "ripple" oscillations in the behaving rat pups. *Neuroscience* 134, 1423–1430.

Buhl, D. L., Harris, K. D., Hormuzdi, S. G., Monyer, H., and Buzsaki, G. (2003). Selective impairment of hippocampal gamma oscillations in connexin-36 knock-out mouse in vivo. *J. Neurosci.* 23, 1013–1018.

Bullmore, E., and Sporns, O. (2009). Complex brain networks: graph theoretical analysis of structural and functional systems. *Nat. Rev. Neurosci.* 10, 186–198.

Buzsaki, G. (1986). Hippocampal sharp waves: their origin and significance. *Brain Res.* 398, 242–252.

Buzsaki, G. (1989). Two-stage model of memory trace formation: a role for "noisy" brain states. *Neuroscience* 31, 551–570.

Buzsaki, G. (2002). Theta oscillations in the hippocampus. *Neuron* 33, 325–340.

Buzsaki, G., Buhl, D. L., Harris, K. D., Csicsvari, J., Czeh, B., and Morozov, A. (2003). Hippocampal network patterns of activity in the mouse. *Neuroscience* 116, 201–211.

Buzsaki, G., and Chrobak, J. J. (1995). Temporal structure in spatially organized neuronal ensembles: a role for interneuronal networks. *Curr. Opin. Neurobiol.* 5, 504–510.

Buzsaki, G., Horvath, Z., Urioste, R., Hetke, J., and Wise, K. (1992). High-frequency network oscillation in the hippocampus. *Science* 256, 1025–1027.

Buzsaki, G., Leung, L. W., and Vanderwolf, C. H. (1983). Cellular bases of hippocampal EEG in the behaving rat. *Brain Res.* 287, 139–171.

Chrobak, J. J., and Buzsaki, G. (1996). High-frequency oscillations in the output networks of the hippocampal-entorhinal axis of the freely behaving rat. *J. Neurosci.* 16, 3056–3066.

Cobb, S. R., Buhl, E. H., Halasy, K., Paulsen, O., and Somogyi, P. (1995). Synchronization of neuronal activity in hippocampus by individual GABAergic interneurons. *Nature* 378, 75–78.

Cobos, I., Long, J. E., Thwin, M. T., and Rubenstein, J. L. (2006). Cellular patterns of transcription factor expression in developing cortical interneurons. *Cereb. Cortex* 16(Suppl. 1), i82–i88.

Cohen, I., Navarro, V., Clemenceau, S., Baulac, M., and Miles, R. (2002). On the origin of interictal activity in human temporal lobe epilepsy in vitro. *Science* 298, 1418–1421.

Connors, B. W., and Long, M. A. (2004). Electrical synapses in the mammalian brain. *Annu. Rev. Neurosci.* 27, 393–418.

Cossart, R., Dinocourt, C., Hirsch, J. C., Merchan-Perez, A., De Felipe, J., Ben-Ari, Y., Esclapez, M., and Bernard, C. (2001). Dendritic but not somatic GABAergic inhibition is decreased in experimental epilepsy. *Nat. Neurosci.* 4, 52–62.

Csicsvari, J., Hirase, H., Czurko, A., Mamiya, A., and Buzsaki, G. (1999). Fast network oscillations in the hippocampal CA1 region of the behaving rat. *J. Neurosci.* 19:RC20.

Csicsvari, J., Hirase, H., Mamiya, A., and Buzsaki, G. (2000). Ensemble patterns of hippocampal CA3-CA1 neurons during sharp wave-associated population events. *Neuron* 28, 585–594.

Csicsvari, J., Jamieson, B., Wise, K. D., and Buzsaki, G. (2003). Mechanisms of gamma oscillations in the hippocampus of the behaving rat. *Neuron* 37, 311–322.

Deisseroth, K., Feng, G., Majewska, A. K., Miesenbőck, G., Ting, A., and Schnitzer, M. J. (2006). Next generation optical technologies for illuminating genetically targeted brain circuits. *J. Neurosci.* 26, 10380–10386.

de Lecea, L., del Rio, J. A., and Soriano, E. (1995). Developmental expression of parvalbumin mRNA in the cerebral cortex and hippocampus of the rat. *Brain Res. Mol. Brain Res.* 32, 1–13.

Delpire, E., and Mount, D. B. (2002). Human and murine phenotypes associated with defects in cation-chloride cotransport. *Annu. Rev. Physiol.* 64, 803–843.

Diba, K., and Buzsaki, G. (2007). Forward and reverse hippocampal place-cell sequences during ripples. *Nat. Neurosci.* 10, 1241–1242.

Draguhn, A., Traub, R. D., Schmitz, D., and Jefferys, J. G. (1998). Electrical coupling underlies high-frequency oscillations in the hippocampus in vitro. *Nature* 394, 189–192.

Dzhala, V. I., and Staley, K. J. (2004). Mechanisms of fast ripples in the hippocampus. *J. Neurosci.* 24, 8896–8906.

Ellender, T. J., Nissen, W., Colgin, L. L., Mann, E. O., and Paulsen, O. (2010). Priming of hippocampal population bursts by individual perisomatic-targeting interneurons. *J. Neurosci.* 30, 5979–5991.

Epsztein, J., Lee, A. K., Chorev, E., and Brecht, M. (2010). Impact of spikelets on hippocampal CA1 pyramidal cell activity during spatial exploration. *Science* 327, 474–477.

Fisahn, A., Pike, F. G., Buhl, E. H., and Paulsen, O. (1998). Cholinergic induction of network oscillations at 40 Hz in the hippocampus in vitro. *Nature* 394, 186–189.

Foffani, G., Uzcategui, Y. G., Gal, B., and Menendez de la Prida, L. (2007). Reduced spike-timing reliability correlates with the emergence of fast ripples in the rat epileptic hippocampus. *Neuron* 55, 930–941.

Foster, D. J., and Wilson, M. A. (2006). Reverse replay of behavioural sequences in hippocampal place cells during the awake state. *Nature* 440, 680–683.

Freund, T. F., and Buzsaki, G. (1996). Interneurons of the hippocampus. *Hippocampus* 6, 347–470.

Freund, T. F., and Katona, I. (2007). Perisomatic inhibition. *Neuron* 56, 33–42.

Fukuda, T., and Kosaka, T. (2000). Gap junctions linking the dendritic network of GABAergic interneurons in the hippocampus. *J. Neurosci.* 20, 1519–1528.

Gaiarsa, J. L., Beaudoin, M., and Ben-Ari, Y. (1992). Effect of neonatal degranulation on the morphological development of rat CA3 pyramidal neurons: inductive role of mossy fibers on the formation of thorny excrescences. *J. Comp. Neurol.* 321, 612–625.

Glickfeld, L. L., Roberts, J. D., Somogyi, P., and Scanziani, M. (2009). Interneurons hyperpolarize pyramidal cells along their entire somatodendritic axis. *Nat. Neurosci.* 12, 21–23.

Gomez-Di Cesare, C. M., Smith, K. L., Rice, F. L., and Swann, J. W. (1997). Axonal remodeling during postnatal maturation of CA3 hippocampal pyramidal neurons. *J. Comp. Neurol.* 384, 165–180.

Goutagny, R., Jackson, J., and Williams, S. (2009). Self-generated theta oscillations in the hippocampus. *Nat. Neurosci.* 12, 1491–1493.

Gozlan, H., and Ben-Ari, Y. (2003). Interneurons are the source and the targets of the first synapses formed in the rat developing hippocampal circuit. *Cereb. Cortex* 13, 684–692.

Grenier, F., Timofeev, I., and Steriade, M. (2003). Neocortical very fast oscillations (ripples, 80-200 Hz) during seizures: intracellular correlates. *J. Neurophysiol.* 89, 841–852.

Gulledge, A. T., and Stuart, G. J. (2003). Excitatory actions of GABA in the cortex. *Neuron* 37, 299–309.

Hajos, N., Ellender, T. J., Zemankovics, R., Mann, E. O., Exley, R., Cragg, S. J., Freund, T. F., and Paulsen, O. (2009). Maintaining network activity in submerged hippocampal slices: importance of oxygen supply. *Eur. J. Neurosci.* 29, 319–327.

Hajos, N., Palhalmi, J., Mann, E. O., Nemeth, B., Paulsen, O., and Freund, T. F. (2004). Spike timing of distinct types of GABAergic interneuron during hippocampal gamma oscillations in vitro. *J. Neurosci.* 24, 9127–9137.

Hajos, N., and Paulsen, O. (2009). Network mechanisms of gamma oscillations in the CA3 region of the hippocampus. *Neural. Netw.* 22, 1113–1119.

Hammond, C., Bergman, H., and Brown, P. (2007). Pathological synchronization in Parkinson's disease: networks, models and treatments. *Trends Neurosci.* 30, 357–364.

Houweling, A. R., and Brecht, M. (2008). Behavioural report of single neuron stimulation in somatosensory cortex. *Nature* 451, 65–68.

Huxter, J., Burgess, N., and O'Keefe, J. (2003). Independent rate and temporal coding in hippocampal pyramidal cells. *Nature* 425, 828–832.

Isokawa-Akesson, M., Wilson, C. L., and Babb, T. L. (1989). Inhibition in synchronously firing human hippocampal neurons. *Epilepsy Res.* 3, 236–247.

Jensen, O., and Lisman, J. E. (1996). Theta/gamma networks with slow NMDA channels learn sequences and encode episodic memory: role of NMDA channels in recall. *Learn. Mem.* 3, 264–278.

Katsumaru, H., Kosaka, T., Heizmann, C. W., and Hama, K. (1988). Gap junctions on GABAergic neurons containing the calcium-binding protein parvalbumin in the rat hippocampus (CA1 region). *Exp. Brain Res.* 72, 363–370.

Katz, L. C., and Shatz, C. J. (1996). Synaptic activity and the construction of cortical circuits. *Science* 274, 1133–1138.

Khalilov, I., Le Van Quyen, M., Gozlan, H., and Ben-Ari, Y. (2005). Epileptogenic actions of GABA and fast oscillations in the developing hippocampus. *Neuron* 48, 787–796.

Khazipov, R., and Luhmann, H. J. (2006). Early patterns of electrical activity in the developing cerebral cortex of humans and rodents. *Trends Neurosci.* 29, 414–418.

Klaassen, A., Glykys, J., Maguire, J., Labarca, C., Mody, I., and Boulter, J. (2006). Seizures and enhanced cortical GABAergic inhibition in two mouse models of human autosomal dominant nocturnal frontal lobe epilepsy. *Proc. Natl. Acad. Sci. U.S.A.* 103, 19152–19157.

Klausberger, T. (2009). GABAergic interneurons targeting dendrites of pyramidal cells in the CA1 area of the hippocampus. *Eur. J. Neurosci.* 30, 947–957.

Klausberger, T., Magill, P. J., Marton, L. F., Roberts, J. D., Cobden, P. M., Buzsaki, G., and Somogyi, P. (2003). Brain-state- and cell-type-specific firing of hippocampal interneurons in vivo. *Nature* 421, 844–848.

Klausberger, T., Marton, L. F., Baude, A., Roberts, J. D., Magill, P. J., and Somogyi, P. (2004). Spike timing of dendrite-targeting bistratified cells during hippocampal network oscillations in vivo. *Nat. Neurosci.* 7, 41–47.

Klausberger, T., Marton, L. F., O'Neill, J., Huck, J. H., Dalezios, Y., Fuentealba, P., Suen, W. Y., Papp, E., Kaneko, T., Watanabe, M., Csicsvari, J., and Somogyi, P. (2005). Complementary roles of cholecystokinin- and parvalbumin-expressing GABAergic neurons in hippocampal network oscillations. *J. Neurosci.* 25, 9782–9793.

Klausberger, T., and Somogyi, P. (2008). Neuronal diversity and temporal dynamics: the unity of hippocampal circuit operations. *Science* 321, 53–57.

Kosaka, T., Katsumaru, H., Hama, K., Wu, J. Y., and Heizmann, C. W. (1987). GABAergic neurons containing the Ca^{2+}-binding protein parvalbumin in the rat hippocampus and dentate gyrus. *Brain Res.* 419, 119–130.

Kubota, D., Colgin, L. L., Casale, M., Brucher, F. A., and Lynch, G. (2003). Endogenous waves in hippocampal slices. *J. Neurophysiol.* 89, 81–89.

Lee, A. K., and Wilson, M. A. (2002). Memory of sequential experience in the hippocampus during slow wave sleep. *Neuron* 36, 1183–1194.

Leinekugel, X., Khazipov, R., Cannon, R., Hirase, H., Ben-Ari, Y., and Buzsaki, G. (2002). Correlated bursts of activity in the neonatal hippocampus in vivo. *Science* 296, 2049–2052.

Leinekugel, X., Medina, I., Khalilov, I., Ben-Ari, Y., and Khazipov, R. (1997). Ca^{2+} oscillations mediated by the synergistic excitatory actions of GABA(A) and NMDA receptors in the neonatal hippocampus. *Neuron* 18, 243–255.

Le Van Quyen, M., Khalilov, I., and Ben-Ari, Y. (2006). The dark side of high-frequency oscillations in the developing brain. *Trends Neurosci.* 29, 419–427.

Leung, L. S., and Yim, C. Y. (1986). Intracellular records of theta rhythm in hippocampal CA1 cells of the rat. *Brain Res.* 367, 323–327.

Li, C. Y., Poo, M. M., and Dan, Y. (2009). Burst spiking of a single cortical neuron modifies global brain state. *Science* 324, 643–646.

Lisman, J. E., and Idiart, M. A. (1995). Storage of 7±2 short-term memories in oscillatory subcycles. *Science* 267, 1512–1515.

Luhmann, H. J., and Prince, D. A. (1991). Postnatal maturation of the GABAergic system in rat neocortex. *J. Neurophysiol.* 65, 247–263.

Magloczky, Z., and Freund, T. F. (2005). Impaired and repaired inhibitory circuits in the epileptic human hippocampus. *Trends Neurosci.* 28, 334–340.

Maier, N., Guldenagel, M., Sohl, G., Siegmund, H., Willecke, K., and Draguhn, A. (2002). Reduction of high-frequency network oscillations (ripples) and pathological network discharges in hippocampal slices from connexin 36-deficient mice. *J. Physiol. (Lond.)* 541, 521–528.

Mann, E. O., and Mody, I. (2008). The multifaceted role of inhibition in epilepsy: seizure-genesis through excessive GABAergic inhibition in autosomal dominant nocturnal frontal lobe epilepsy. *Curr. Opin. Neurol.* 21, 155–160.

Mann, E. O., Suckling, J. M., Hajos, N., Greenfield, S. A., and Paulsen, O. (2005). Perisomatic feedback inhibition underlies cholinergically induced fast network oscillations in the rat hippocampus in vitro. *Neuron* 45, 105–117.

Marchionni, I., and Maccaferri, G. (2009). Quantitative dynamics and spatial profile of perisomatic GABAergic input during epileptiform synchronization in the CA1 hippocampus. *J. Physiol. (Lond.)* 587, 5691–5708.

Menendez de la Prida, L., Huberfeld, G., Cohen, I., and Miles, R. (2006). Threshold behavior in the initiation of hippocampal population bursts. *Neuron* 49, 131–142.

Miles, R., Toth, K., Gulyas, A. I., Hajos, N., and Freund, T. F. (1996). Differences between somatic and dendritic inhibition in the hippocampus. *Neuron* 16, 815–823.

Miles, R., and Wong, R. K. (1983). Single neurones can initiate synchronized population discharge in the hippocampus. *Nature* 306, 371–373.

Miles, R., and Wong, R. K. (1987). Inhibitory control of local excitatory circuits in the guinea-pig hippocampus. *J. Physiol. (Lond.)* 388, 611–629.

Morozov, Y. M., and Freund, T. F. (2003). Postnatal development and migration of cholecystokinin-immunoreactive interneurons in rat hippocampus. *Neuroscience* 120, 923–939.

O'Keefe, J., and Dostrovsky, J. (1971). The hippocampus as a spatial map. Preliminary evidence from unit activity in the freely-moving rat. *Brain Res.* 34, 171–175.

O'Keefe, J., and Nadel, L. (1978). *The Hippocampus as a Cognitive Map.* Oxford: Oxford University Press.

O'Neill, J., Senior, T., and Csicsvari, J. (2006). Place-selective firing of CA1 pyramidal cells during sharp wave/ripple network patterns in exploratory behavior. *Neuron* 49, 143–155.

Oren, I., Hajos, N., and Paulsen, O. (2010). Identification of the current generator underlying cholinergically induced gamma frequency field potential oscillations in the hippocampal CA3 region. *J. Physiol. (Lond.)* 588, 785–797.

Oren, I., Mann, E. O., Paulsen, O., and Hajos, N. (2006). Synaptic currents in anatomically identified CA3 neurons during hippocampal gamma oscillations in vitro. *J. Neurosci.* 26, 9923–9934.

Owens, D. F., Boyce, L. H., Davis, M. B., and Kriegstein, A. R. (1996). Excitatory GABA responses in embryonic and neonatal cortical slices demonstrated by gramicidin perforated-patch recordings and calcium imaging. *J. Neurosci.* 16, 6414–6423.

Penttonen, M., Kamondi, A., Acsady, L., and Buzsaki, G. (1998). Gamma frequency oscillation in the hippocampus of the rat: intracellular analysis in vivo. *Eur. J. Neurosci.* 10, 718–728.

Petsche, H., and Stumpf, C. (1962). [The origin of theta-rhytm in the rabbit hippocampus.]. *Wien Klin Wochenschr* 74, 696–700.

Rivera, C., Voipio, J., Payne, J. A., Ruusuvuori, E., Lahtinen, H., Lamsa, K., Pirvola, U., Saarma, M., and Kaila, K. (1999). The K^+/Cl- co-transporter KCC2 renders GABA hyperpolarizing during neuronal maturation. *Nature* 397, 251–255.

Routh, B. N., Johnston, D., Harris, K., and Chitwood, R. A. (2009). Anatomical and electrophysiological comparison of CA1 pyramidal neurons of the rat and mouse. *J. Neurophysiol.* 102, 2288–2302.

Russell, J. M. (2000). Sodium-potassium-chloride cotransport. *Physiol. Rev.* 80, 211–276.

Skaggs, W. E., and McNaughton, B. L. (1996). Replay of neuronal firing sequences in rat hippocampus during sleep following spatial experience. *Science* 271, 1870–1873.

Soltesz, I., and Deschenes, M. (1993). Low- and high-frequency membrane potential oscillations during theta activity in CA1 and CA3 pyramidal neurons of the rat hippocampus under ketamine-xylazine anesthesia. *J. Neurophysiol.* 70, 97–116.

Somogyi, P. (1977). A specific "axo-axonal" interneuron in the visual cortex of the rat. *Brain Res.* 136, 345–350.

Somogyi, P., Hodgson, A. J., Smith, A. D., Nunzi, M. G., Gorio, A., and Wu, J. Y. (1984). Different populations of GABAergic neurons in the visual cortex and hippocampus of cat contain somatostatin- or cholecystokinin-immunoreactive material. *J. Neurosci.* 4, 2590–2603.

Somogyi, P., Nunzi, M. G., Gorio, A., and Smith, A. D. (1983). A new type of specific interneuron in the monkey hippocampus forming synapses exclusively with the axon initial segments of pyramidal cells. *Brain Res.* 259, 137–142.

Soriano, E., Cobas, A., and Fairen, A. (1986). Asynchronism in the neurogenesis of GABAergic and non-GABAergic neurons in the mouse hippocampus. *Brain Res.* 395, 88–92.

Stewart, M., and Fox, S. E. (1990). Do septal neurons pace the hippocampal theta rhythm? *Trends Neurosci.* 13, 163–168.

Strata, F. (1998). Intrinsic oscillations in CA3 hippocampal pyramids: physiological relevance to theta rhythm generation. *Hippocampus* 8, 666–679.

Super, H., Martinez, A., Del Rio, J. A., and Soriano, E. (1998). Involvement of distinct pioneer neurons in the formation of layer-specific connections in the hippocampus. *J. Neurosci.* 18, 4616–4626.

Szabadics, J., Varga, C., Molnar, G., Olah, S., Barzo, P., and Tamas, G. (2006). Excitatory effect of GABAergic axo-axonic cells in cortical microcircuits. *Science* 311, 233–235.

Tamas, G., Buhl, E. H., Lorincz, A., and Somogyi, P. (2000). Proximally targeted GABAergic synapses and gap junctions synchronize cortical interneurons. *Nat. Neurosci.* 3, 366–371.

Tamas, G., Buhl, E. H., and Somogyi, P. (1997). Massive autaptic self-innervation of GABAergic neurons in cat visual cortex. *J. Neurosci.* 17, 6352–6364.

Traub, R. D., Jefferys, J. G., and Whittington, M. A. (1997). Simulation of gamma rhythms in networks of interneurons and pyramidal cells. *J. Comput. Neurosci.* 4, 141–150.

Traub, R. D., Kopell, N., Bibbig, A., Buhl, E. H., LeBeau, F. E., and Whittington, M. A. (2001a). Gap junctions between interneuron dendrites can enhance synchrony of gamma oscillations in distributed networks. *J. Neurosci.* 21, 9478–9486.

Traub, R. D., Whittington, M. A., Buhl, E. H., LeBeau, F. E., Bibbig, A., Boyd, S., Cross, H., and Baldeweg, T. (2001b). A possible role for gap junctions in generation of very fast EEG oscillations preceding the onset of, and perhaps initiating, seizures. *Epilepsia* 42, 153–170.

Traub, R. D., and Wong, R. K. (1982). Cellular mechanism of neuronal synchronization in epilepsy. *Science* 216, 745–747.

Trevelyan, A. J. (2009). The direct relationship between inhibitory currents and local field potentials. *J. Neurosci.* 29, 15299–15307.

Trevelyan, A. J., Sussillo, D., Watson, B. O., and Yuste, R. (2006). Modular propagation of epileptiform activity: evidence for an inhibitory veto in neocortex. *J. Neurosci.* 26, 12447–12455.

Trevelyan, A. J., Sussillo, D., and Yuste, R. (2007). Feedforward inhibition contributes to the control of epileptiform propagation speed. *J. Neurosci.* 27, 3383–3387.

Tukker, J. J., Fuentealba, P., Hartwich, K., Somogyi, P., and Klausberger, T. (2007). Cell type-specific tuning of hippocampal interneuron firing during gamma oscillations in vivo. *J. Neurosci.* 27, 8184–8189.

Tyzio, R., Represa, A., Jorquera, I., Ben-Ari, Y., Gozlan, H., and Aniksztejn, L. (1999). The establishment of GABAergic and glutamatergic synapses on CA1 pyramidal neurons is sequential and correlates with the development of the apical dendrite. *J. Neurosci.* 19, 10372–10382.

Uhlhaas, P. J., and Singer, W. (2006). Neural synchrony in brain disorders: relevance for cognitive dysfunctions and pathophysiology. *Neuron* 52, 155–168.

Uhlhaas, P. J., and Singer, W. (2010). Abnormal neural oscillations and synchrony in schizophrenia. *Nat. Rev. Neurosci.* 11, 100–113.

Vanderwolf, C. H. (1969). Hippocampal electrical activity and voluntary movement in the rat. *Electroencephalog.r Clin. Neurophysiol.* 26, 407–418.

Vizi, E. S., and Kiss, J. P. (1998). Neurochemistry and pharmacology of the major hippocampal transmitter systems: synaptic and nonsynaptic interactions. *Hippocampus* 8, 566–607.

Wang, X.-J., and Buzsaki, G. (1996). Gamma oscillation by synaptic inhibition in a hippocampal interneuronal network model. *J. Neurosci.* 16, 6402–6413.

Whittington, M. A., and Traub, R. D. (2003). Interneuron diversity series: inhibitory interneurons and network oscillations in vitro. *Trends Neurosci.* 26, 676–682.

Whittington, M. A., Traub, R. D., and Jefferys, J. G. (1995). Synchronized oscillations in interneuron networks driven by metabotropic glutamate receptor activation. *Nature* 373, 612–615.

Wittner, L., Eross, L., Czirjak, S., Halasz, P., Freund, T. F., and Magloczky, Z. (2005). Surviving CA1 pyramidal cells receive intact perisomatic inhibitory input in the human epileptic hippocampus. *Brain* 128, 138–152.

Wittner, L., Magloczky, Z., Borhegyi, Z., Halasz, P., Toth, S., Eross, L., Szabo, Z., and Freund, T. F. (2001). Preservation of perisomatic inhibitory input of granule cells in the epileptic human dentate gyrus. *Neuroscience* 108, 587–600.

Wozny, C., Kivi, A., Lehmann, T. N., Dehnicke, C., Heinemann, U., and Behr, J. (2003). Comment on "On the origin of interictal activity in human temporal lobe epilepsy in vitro". *Science* 301:463; author reply 463.

Yang, J. W., Hanganu-Opatz, I. L., Sun, J. J., and Luhmann, H. J. (2009). Three patterns of oscillatory activity differentially synchronize developing neocortical networks in vivo. *J. Neurosci.* 29, 9011–9025.

Ylinen, A., Bragin, A., Nadasdy, Z., Jando, G., Szabo, I., Sik, A., and Buzsaki, G. (1995). Sharp wave-associated high-frequency oscillation (200 Hz) in the intact hippocampus: network and intracellular mechanisms. *J. Neurosci.* 15, 30–46.

Conflict of Interest Statement: The authors declare that the research was conducted in the absence of any commercial or financial relationships that could be construed as a potential conflict of interest.

Received: 18 March 2010; paper pending published: 26 April 2010; accepted: 28 June 2010; published online: 30 July 2010.

*Citation: Ellender TJ and Paulsen O (2010) The many tunes of perisomatic targeting interneurons in the hippocampal network. Front. Cell. Neurosci. **4**:26. doi: 10.3389/fncel.2010.00026*

frontiers in
CELLULAR NEUROSCIENCE

ORIGINAL RESEARCH ARTICLE
published: 28 July 2011
doi: 10.3389/fncel.2011.00016

Phenobarbital but not diazepam reduces AMPA/kainate receptor mediated currents and exerts opposite actions on initial seizures in the neonatal rat hippocampus

Romain Nardou[1,2,3†], Sumii Yamamoto[1,2,3†], Asma Bhar[1,2,3†], Nail Burnashev[1,2,3], Yehezkel Ben-Ari[1,2,3]* and Ilgam Khalilov[1,2,3]

[1] *INSERM U-901, Marseille, France*
[2] *UMR S901 Aix-Marseille 2, Université de la Méditerranée, Marseille, France*
[3] *Institute for International Medicine, Marseille, France*

Edited by:
Enrico Cherubini, International School for Advanced Studies, Italy

Reviewed by:
Gianmaria Maccaferri, Northwestern University, USA
Shaoyu Ge, SUNY Stony Brook, USA

****Correspondence:***
Yehezkel Ben-Ari, Campus Scientifique de Luminy, 163 route de Luminy, 13009 Marseille, France.
e-mail: ben-ari@inmed.univ-mrs.fr

[†]Romain Nardou, Sumii Yamamoto and Asma Bhar have contributed equally to this work.

Diazepam (DZP) and phenobarbital (PB) are extensively used as first and second line drugs to treat acute seizures in neonates and their actions are thought to be mediated by increasing the actions of GABAergic signals. Yet, their efficacy is variable with occasional failure or even aggravation of recurrent seizures questioning whether other mechanisms are not involved in their actions. We have now compared the effects of DZP and PB on ictal-like events (ILEs) in an *in vitro* model of mirror focus (MF). Using the three-compartment chamber with the two immature hippocampi and their commissural fibers placed in three different compartments, kainate was applied to one hippocampus and PB or DZP to the contralateral one, either after one ILE, or after many recurrent ILEs that produce an epileptogenic MF. We report that in contrast to PB, DZP aggravated propagating ILEs from the start, and did not prevent the formation of MF. PB reduced and DZP increased the network driven giant depolarizing potentials suggesting that PB may exert additional actions that are not mediated by GABA signaling. In keeping with this, PB but not DZP reduced field potentials recorded in the presence of GABA and NMDA receptor antagonists. These effects are mediated by a direct action on AMPA/kainate receptors since PB: (i) reduced AMPA/kainate receptor mediated currents induced by focal applications of glutamate; (ii) reduced the amplitude and the frequency of AMPA but not NMDA receptor mediated miniature excitatory postsynaptic currents (EPSCs); (iii) augmented the number of AMPA receptor mediated EPSCs failures evoked by minimal stimulation. These effects persisted in MF. Therefore, PB exerts its anticonvulsive actions partly by reducing AMPA/kainate receptors mediated EPSCs in addition to the pro-GABA effects. We suggest that PB may have advantage over DZP in the treatment of initial neonatal seizures since the additional reduction of glutamate receptors mediated signals may reduce the severity of neonatal seizures.

Keywords: phenobarbital, diazepam, AMPA, immature hippocampus, seizures

INTRODUCTION

Neonatal seizures are inherently different from adult seizures and can be refractory to anti epileptic drugs (AEDs). Benzodiazepines – notably diazepam (DZP) – and phenobarbital (PB) are the AEDs of first choice to treat neonatal seizures (Wheless et al., 2007; Bassan et al., 2008). In general, PB is first used in neonatal seizures whereas diazepam or lorazepam are preferred in febrile seizures. They are thought to reduce seizures by reinforcing the efficacy of GABAergic inhibition through a direct action on GABA(A) receptors mediated currents. However, there are several complicating factors with their use. In many conditions they fail to block seizures, produce an electro-clinical disconnection of EEG and clinical signs (Connell et al., 1989; Painter et al., 1999; Boylan et al., 2002; Yanay et al., 2004; Guillet and Kwon, 2007; Kaindl et al., 2008) and even aggravate them (Loscher and Honack, 1989; Guerrini et al., 1998; Perucca et al., 1998; Painter et al., 1999; Goodkin et al., 2008; Goodkin and Kapur, 2009). These aggravating actions are at least partly mediated by a persistent increase of $[Cl^-]_i$ leading to more seizures by enhancing the excitatory actions of GABA that heavily depend on this parameter (also see Cohen et al., 2002; Khalilov et al., 2003, 2005; Rivera et al., 2004; Glykys et al., 2009; Dzhala et al., 2010; Nardou et al., 2011). Experimental observations indicate that PB efficiently blocks early seizures but aggravates

Abbreviations: AED, anti epileptic drug; APV, D-2-amino-5-phosphopentanoate; CNQX, 6-cyano-7-nitroquinoxaline-2,3 dione; DZP, diazepam; GABA, γ-aminobutyric acid; GDP, giant depolarizing potential; ILE, ictal-like event; IILE, interictal-like event; KCC2, potassium–chloride co-transporter 2; NKCC1, sodium–potassium–chloride co-transporter 1; PB, phenobarbital; PTX, picrotoxin; TTX, tetrodotoxin.

established ones when first applied after many recurrent seizures. This is due to a persistent accumulation of chloride and excitatory actions of GABA that will be further enhanced by PB (Glykys et al., 2009; Dzhala et al., 2010; Nardou et al., 2011). These effects are mediated by a persistent activation of the chloride importer NKCC1 and a down regulation and internalization of the chloride exporter KCC2 (Dzhala et al., 2010; Lee et al., 2010; Nardou et al., 2011). Clearly, the regulation of $[Cl^-]_i$ constitutes a major source of problem to the use of these AEDs and stresses the importance of the history of seizures prior to treatment in determining the efficacy of the treatment.

Collectively however, these observations are based on the assumption that the actions of PB, DZP, and other members of this family are solely mediated by GABA signaling. Yet, there are several indications that this may not be the case. Barbiturate anesthetics have been reported to antagonize glutamate evoked currents in spinal neurons (MacDonald and Barker, 1978a,b, 1982; Macdonald and Kelly, 1994) and to reduce recombinant AMPA-type glutamate receptor channels expressed in cell lines (Jin et al., 2010). Also, barbiturates are more efficacious than benzodiazepines to treat various brain disorders including neonatal seizures (Cheng et al., 2002; Soderpalm, 2002; Carmo and Barr, 2005; Bartha et al., 2007) raising the possibility that additional non-GABA mediated signaling may underlie a better efficacy to treat various neonatal seizures. These observations stress the importance of both determining the possible non-GABA mediated actions of these AEDs and taking into account the differences between acute and recurrent more chronic seizures in order to determine possible aggravating deleterious actions.

Here, we compared the actions of PB and DZP on glutamate receptor mediated currents in naïve and "epileptic" immature hippocampal neurons. In that purpose, we used the triple chamber preparation that enables to apply to one chamber a convulsive agent (kainate) and an AED to the other and interrupt the connections after one or more propagated seizures (Khalilov et al., 1997, 1999, 2003). In this preparation, the contralateral hippocampus becomes epileptic as it generates spontaneous seizures when disconnected from the kainate treated side. This enables to compare the actions of AEDs on naïve and epileptic mirror foci. Using this preparation, we showed recently (Nardou et al., 2011) that PB efficiently blocks paroxysmal activity when applied with the initial seizures but aggravates them when applied late on a newly formed mirror focus (MF). This is due to an excessive increase of $[Cl^-]_i$ leading to excitatory GABA that PB will further exacerbates (Nardou et al., 2011). We now report that in contrast to PB, DZP aggravates inaugurating, and established seizures. These differences are due to the selective actions of PB that reduces AMPA/kainate receptor mediated signals in addition to its pro-GABA actions. This dual action of PB on GABA and glutamate excitatory postsynaptic currents (EPSCs) provides an obvious important advantage of PB over DZP and may have as such important clinical implications.

MATERIALS AND METHODS

Experiments were performed on neonatal Wistar rats (postnatal days P6–P8). All experiments have been carried out in accordance with the European Communities Council Directive of the 24 November 1986 (86/609/EEC).

TISSUE PREPARATION

Intact hippocampal preparation

The interconnected intact hippocampi were prepared according to the procedures described previously (Khalilov et al., 1997). In brief, neonatal rats and mice (P6–P8) were decapitated after hypothermic anesthesia, the brain rapidly removed to oxygenated (95% O_2/5% CO_2) ice-cold artificial cerebrospinal fluid (ACSF) containing (in mM): NaCl 126, KCl 3.5, $CaCl_2$ 2.0, $MgCl_2$ 1.3, $NaHCO_3$ 25, NaH_2PO_4 1.2, and glucose 11 (pH 7.4). The two interconnected intact hippocampi were isolated and transferred into a beaker containing oxygenated ACSF and incubated at least 1 h before use. The hippocampi were placed into a fully submerged three-compartment chamber and superfused with oxygenated ACSF (30–32°C, 10–15 ml/min).

Slice preparation

Slices (thickness 450 μm) were cut using a Leica VT-1000E vibratome (Leica Microsystems GmbH, Nussloch, Germany) or a McIIwain tissue chopper (slices 600 μm thick) and kept in oxygenated ACSF at room temperature for at least 1 h before use (Khalilov et al., 2005). Slices from epileptic hippocampi were prepared as described earlier (Nardou et al., 2009). Individual slices were then transferred to the recording chamber where they were fully submerged and superfused with oxygenated ACSF (30–32°C, 2–3 ml/min).

ELECTROPHYSIOLOGICAL RECORDINGS AND DATA ANALYSIS

Hippocampal CA3 pyramidal neurons in the slices were visualized with infrared differential interference contrast microscopy (Nikon Eclipse FN).

Whole cell recordings were collected using an Axopatch 200B and MultiClamp 700B amplifiers (Axon Instruments, USA). Patch electrodes were made from borosilicate glass capillaries (G150F-15; Warner Instrument Corporation, Hamden, CT, USA) using the model PP-830 two-stage micropipette puller (Narishige, Tokyo, Japan). Patch pipette solution contained (in mM): CsCl 140, $CaCl_2$ 1, EGTA 10, HEPES 10, MgATP 2, and GTP 0.4 (pH 7.25), and an osmolarity of 280 mOsm. Patch pipettes had a resistance of 8–10 MΩ.

To evoke synaptic responses in pyramidal CA3 neurons, a concentric bipolar tungsten electrode (FHC, Bowdoinham, ME, USA) was placed in stratum lucidum. Single pulses were delivered using a Master-8 pulse generator (A.M.P.I., Jerusalem, Israel) controlled by a PC, and stimulus intensity was controlled by a constant current stimulus isolator. AMPA/kainate receptor mediated EPSCs. EPSCs were evoked in the presence of NMDA and GABA receptor antagonists (40 μM D-APV, 10 μM bicuculline, and 2 μM CGP55845) and minimal afferent stimulation was used to activate one or few fibers. The minimal EPSCs were associated with occasional response failures. Their number was usually estimated by visual discrimination. The means of evoked EPSCs was determined by excluding the failures and making only means of the successful evoked responses. To confirm that responses were AMPA/kainate receptor mediated, an AMPA/kainate receptor antagonist (10 or 20 μM CNQX) was used to block responses.

Cells were identified by adding biocytin (0.4%) to the pipette solution for *post hoc* morphological analysis.

Nucleated patch clamp recordings were performed from CA3 pyramidal neurons in hippocampal slices using fast agonist application techniques in the standard external solution. After the whole cell configuration was made, nucleated (Sather et al., 1992) patches were pulled from the cell and placed in front of a piezo-controlled (P 245.70, Physik Instrumente, Waldbronn, Germany) fast application system with a double-barreled application pipette (Colquhoun et al., 1992). Glutamate (1 mM) pulses of 2 ms duration were applied every 10 s. Recordings were made using an EPC-9 amplifier (HEKA Electronics, Lambrecht, Germany) under visualization with a Leica microscope. The resistance of the pipettes was 4–5 MΩ. PB (100 μM) and diazepam (2 μM) were added to the extracellular solution. Experiments were performed at a holding potential of –60 mV. Current traces shown are averages of four to eight sweeps. Stimulus delivery and data acquisition was performed using Pulse software (Heka Elektronik, Lambrecht, Germany). Analyses were performed using IgorPro software (WaveMetrics, Lake Oswego, OR, USA).

Extracellular field potentials and multi-unit activities (MUAs) were recorded in the hippocampal slices and in the intact hippocampal preparations *in vitro* using tungsten wire electrodes (diameter: 50 μm, California Fine Wire, Grover Beach, CA, USA) and a low-noise multichannel DAM-8A amplifiers (WPI, GB; low filter: 0.1 Hz; high filter: 3 KHz; ×1000). Electrical stimulations were performed with a bipolar electrode (10–20 V, 40 μs).

The signals were digitized using an analog-to-digital converter (Digidata 1440A, Axon Instruments, USA). pCLAMP 10.1, Clampfit 10.1 (Axon Instruments, USA), MiniAnalysis 6.03 (Synaptosoft, Decatur, CA, USA), and Origin 7.5 (Microcal Software, USA) programs were used for the acquisition and analysis of the synaptic activities. Sampling interval per signal was 100 μs (10 kHz). Spikes (single unit activity) in extracellular recordings were detected by amplitude thresholding using MiniAnalysis 6.03 program. Power spectrum analysis was performed after applying a Hamming window function. Power was calculated by integrating the root mean square value of the signal in frequency bands from 1 to 1000 Hz. Time–frequency representations of ictal-like events were obtained using continuous Morlet wavelet transforms using AutoSignal v1.7 software (SeaSolve Software Inc.).

FOCAL PUFF APPLICATIONS OF GLUTAMATE AND γ-AMINOBUTYRIC ACID

A picospritzer (General Valve Corporation, Fairfield, NJ, USA) was used to puff-apply (5–10 psi for 50–100 ms) of glutamate or GABA from a glass pipette at a distance of about 100–150 μm from the soma, adjusted such that postsynaptic current amplitudes did not exceed 300 pA.

STATISTICAL ANALYSIS

Group measures are expressed as mean ± SEM; error bars also indicate SEM. The statistical significance of differences was assessed with the Student's *t*-test. The level of significance was set at $p < 0.05$.

PHARMACOLOGICAL AGENTS

Antagonists bicuculline (10 μM), 6-cyano-7-nitroquinoxaline-2,3 dione (CNQX, 10 μM), D-2-Amino-5-phosphopentanoate (APV, 40 μM), tetrodotoxin (TTX, 1 μM), picrotoxin (PTX, 100 μM), CGP55845 (CGP, 2 μM); AEDs Diazepam (DZP, 2 μM) and (PB, 100 μM); and kainate (KA, 400 nM) were directly added to the perfusion solutions. The drugs used were purchased from Sigma (DZP, PB, TTX, PTX, CGP, glutamate, and kainic acid), Tocris (bicuculline, CNQX, APV), and Molecular Probes (biocytin).

RESULTS

DIAZEPAM AGGRAVATES THE PROPAGATING ICTAL-LIKE EVENTS AND DOES NOT PREVENT THE FORMATION OF A MIRROR FOCUS BY REPEATED ILES

We used the triple chamber preparation with the two intact hippocampi and the commissural connections in three different compartments (Khalilov et al., 1997, 1999). This enables to apply different agents on each compartment without diffusion and interference with the others (Khalilov et al., 2003). In a first series of experiments, we applied kainate (KA, 400 nM) to one hippocampus (referred to as the ipsilateral hippocampus, *ipsi*-) and recorded the activity from both the *ipsi*- and the contralateral (*contra*-) hippocampus that did not receive the convulsive agent (**Figure 1A**). In keeping with our earlier studies (Khalilov et al., 2003, 2005), KA generated an ictal-like event (ILE) with large amplitude (1–2 mV) and duration (1–2 min) ictal discharges (**Figure 1A**; see also Khalilov et al., 2003). These ILEs propagated to the contralateral hippocampus where they generated similar activities including high frequency (40–120 Hz) gamma oscillations (GOs; **Figures 1A,B**). In earlier experiments we have demonstrated that after circa 15 repeated unilateral KA applications, the contralateral hippocampus generated spontaneous ILEs when disconnected from the treated ipsilateral hippocampus (Khalilov et al., 2003, 2005). We referred to this as a newly formed secondary epileptogenic focus – or MF.

We have shown recently that early applications of (PB, 100 μM) to the contralateral hippocampus reduced dramatically the severity of propagating seizures and prevented the formation of a MF (Nardou et al., 2011). In contrast, in similar experiments, DZP (2 μM) augmented the severity of the propagating ILEs (**Figures 1C,C_1,D,D_1**).

The frequency of oscillations is an important component of the pathogenic actions of seizures. Indeed, in both human and experimental animals, high frequency oscillations (HFOs; >60 Hz) constitute a signature of the severity of recurrent seizures (Bragin et al., 1999; Khalilov et al., 2005; Le Van Quyen et al., 2006; Jacobs et al., 2008). In keeping with this, in the same preparation, the occurrence of GOs in propagating seizures is essential to induce the transformation of a naïve network to one that generates ILEs spontaneously (Khalilov et al., 2005). Whereas PB reduced the frequency of GOs and severity (power) of ILEs (Nardou et al., 2011), DZP augmented the range of GOs frequencies (**Figures 1C_1**) and the power of ILEs (by 19.2 ± 3.9%, $n = 7$, $p < 0.05$) in the contralateral hippocampus already with the first application (**Figures 1D_1**). DZP in contrast to PB did not prevent the formation of an epileptogenic MF (**Figure 1E**).

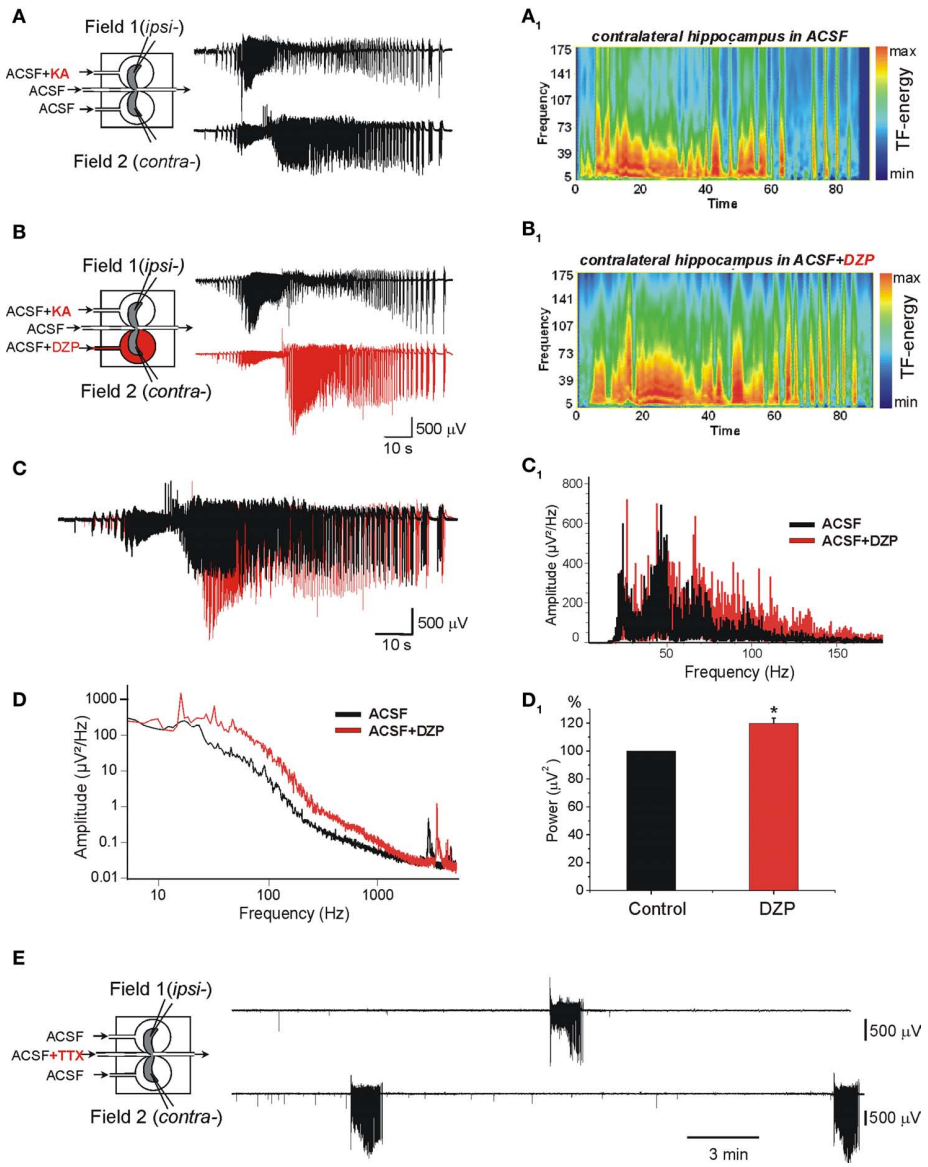

FIGURE 1 | Diazepam (DZP) aggravates the propagating ictal-like events (ILEs) and does not prevent the formation of a mirror focus by repeated ILEs. (A,B) The scheme of the triple chamber preparation with the two intact hippocampi and their connecting inter-hemispheric commissure in independent chambers (*left*). Field recordings were made in the two hippocampi. **(A)** Kainate (KA) applied to one hippocampus (ipsilateral: *ipsi-*) generated seizure activity referred to as ILE that propagated to the contralateral hippocampus (*contra-*). The ILEs included high frequency gamma oscillations (GOs, 40–120 Hz) as shown in the time–frequency (TF) analysis **(A_1)**. **(B)** Application of DZP to contralateral hippocampus (2 µM, 15 min) before a second application of KA increased the ILE and GOs. TF analysis of ILE recorded in *contra-* is shown in **(B_1)**. **(C)** Superimposed ILEs [from **(A,B)**] recorded in *contra-* before (black) and after DZP application (red). DZP increased the amplitude and duration of ILE. **(C_1)** Power spectra representation of ILEs recorded before (black) and after (red) DZP treatment [from **(C)**] after band-pass (40–150 Hz) filtering. **(D)** Example of power spectra of ILEs before and after DZP treatment [from **(A,B)**] used for calculation of power of ILEs. **(D_1)** Normalized average power histogram of contralateral ILEs before and after DZP. Note that DZP application significantly increased average power of ILEs (by 19.2 ± 3.9%, $n = 7$ experiments, $p < 0.05$). **(E)** After 15 transient applications of KA in *ipsi-* with continuous application of DZP in *contra-*, disconnection of the two hippocampi by applications of TTX to the commissural chamber revealed that contralateral hippocampus generated spontaneous ILEs.

Therefore, PB and DZP exert opposite actions on severity of early ILEs in the intact hippocampus: PB reduces and DZP aggravates the propagating ILEs from the onset of their applications.

DIAZEPAM AGGRAVATES THE SEVERITY OF EPILEPTIFORM ACTIVITIES IN THE ISOLATED MIRROR FOCUS

In earlier studies, we showed that once formed the MF generates spontaneous ILEs up to 1–2 days in an isolated hippocampus

in vitro, and slices prepared from this hippocampus generate spontaneous and evoked interictal-like events (IILEs; Khalilov et al., 2003, 2005; Nardou et al., 2009, 2011). In whole hippocampus after the formation of MF, application of DZP significantly increased the severity of ILEs. The average power of spontaneous ILEs in MF hippocampus after bath application of DZP increased by $80 \pm 19.8\%$ ($n = 4$, $p < 0.001$; **Figure 2A**). In slices prepared from the hippocampus after MF formation, DZP increased both the frequency of IILEs and extracellular recorded spikes generated by the MF neurons (**Figure 2B**). In similar experiments, PB also aggravated the epileptiform activity generated by the MF by enhancing the strong excitatory actions of GABA (Nardou et al., 2011). Therefore, the difference between DZP and PB is valid for initial propagating seizures but not for spontaneous seizures generated by an epileptogenic MF suggesting that the persistent accumulation of $[Cl^-]_i$ prevails in MF neurons rendering difficult the actions of GABA acting AEDs. Therefore, we next compared the actions of DZP and PB on ongoing network activity in slices obtained from control hippocampus.

DZP AUGMENTS ONGOING NEURONAL ACTIVITY AND FREQUENCY OF GDPs

In control conditions, the physiological pattern of the immature hippocampal network activity is characterized by spontaneous network driven giant depolarizing potentials (GDPs; Ben-Ari et al., 1989) that occur spontaneously and can be evoked by electrical stimulation. GDPs are generated by the converging actions of GABA and glutamatergic synapses (Ben Ari et al., 2007). We tested the effects of DZP on the frequency of occurrence of extracellular recorded GDPs and MUAs. As shown in **Figure 3** DZP, applied at a concentration of 2 μM, increased the frequency of GDPs by $215.1 \pm 13.6\%$ ($p < 0.001$, $n = 14$) and the frequency of spikes by $170 \pm 14.8\%$ ($p < 0.001$, $n = 14$). In similar experiments, bath application of PB substantially reduced the amplitude of GDPs. PB reduced also the frequency of spontaneous spikes generated in CA3 pyramidal neurons by ∼50% (see Nardou et al., 2011). An additional non-exclusive mechanism is that GDP frequency being increased, there may also be a short-term depression of GABAergic inputs that would be superimposed on the effect of DZP.

To determine the actions of DZP on GABA signaling, we tested the effects of DZP on responses generated by focal applications of GABA. As shown in **Figure 4A**, GABA was focally applied (100 μM, 100 ms) in the CA3c region while simultaneous CA3c field and whole cell recordings (from pyramidal neurons in CA3a region) were performed. Focal GABA application generated GDPs (**Figure 4B**). Application of DZP significantly increased the amplitude and duration of whole cell recorded responses (**Figures 4B–E**) accompanied by a $17.2 \pm 2.7\%$ ($p < 0.05$) as well as the area and decay time constant of the currents (**Figures 4C–E**) increase in the amplitude of extracellular recorded GDPs (not shown) and with a strong increase in the number of GDPs-associated spikes ($98.1 \pm 6.7\%$, $p < 0.001$, $n = 5$; **Figure 4F**). Similar focal application of GABA generated 2–3 action potentials (spikes) in cell attached recordings (see Nardou et al., 2011). In contrast to DZP, bath applications of PB (100 μM) significantly reduced the number of spikes (action potentials) from 2.7 ± 0.2 to 1.9 ± 0.2 (Nardou et al., 2011). Therefore, under control conditions PB reduces ongoing neuronal activity whereas DZP augments it. The observation that GABA acting PB reduces and DZP augments ongoing activity raises the possibility of non-GABA mediated actions of these AEDs. We therefore compared their effects on glutamatergic signals that are instrumental in the generation of early network activity.

PB BUT NOT DZP REDUCES AMPA/KAINATE RECEPTOR MEDIATED FIELD POTENTIALS

To determine the effects of DZP and PB on glutamatergic activity, we first studied their effects on field potentials recorded in control slices in the presence of bicuculline (10 μM), CGP (2 μM) and APV (40 μM), respectively, to block GABA(A), GABA(B), and NMDA receptors. In these conditions, all or none IILEs are generated spontaneously and by local electrical stimuli (**Figure 5**). IILEs are mediated by AMPA/kainate receptors as they were fully blocked by the selective antagonist CNQX (10 μM, $n = 13$; **Figure 5C**). PB fully blocked the evoked and spontaneous IILEs (**Figure 5A**; $n = 7$). The frequency histograms (**Figure 5Ad**) reflect the powerful blockade of spikes and IILEs by PB. As 10 μm bicuculline do not always fully block GABAergic signaling (Strata and Cherubini, 1994) we also repeated these experiments with 100 μM picrotoxin instead of bicuculline and observed similar actions of PB (not shown, $n = 3$). In contrast, DZP ($n = 6$) failed to block or reduce these field potentials (**Figure 5B**). Thus, DZP did not reduce the evoked or the spontaneous IILEs. Therefore, PB but not DZP exerts a non-GABA mediated action on hippocampal neurons.

PHENOBARBITAL BUT NOT DIAZEPAM REDUCES AMPA/KAINATE RECEPTOR MEDIATED CURRENTS

To examine the possible effects of PB and DZP on AMPA/kainate receptors, we next tested their effects on the currents evoked in whole cell recordings by focal pressure applications of glutamate. In the presence of NMDA and GABA receptor antagonists, focal applications of glutamate (100 μM, 100 ms) from patch pipettes generated large currents mediated by AMPA/kainate receptors as they are blocked by CNQX ($n = 9$; **Figure 6C**). PB reduced significantly the amplitude of these currents (to $67.2 \pm 8.1\%$, $p < 0.001$, $n = 4$; **Figure 6A**). These effects fully recovered after wash out of PB (**Figure 6Ad**). In contrast, DZP had no effects on these currents (mean amplitude in DZP was $100.3 \pm 4.9\%$ of the control values, $p > 0.05$, $n = 5$; **Figure 6B**). Next, in similar experimental conditions using fast agonist application techniques (Colquhoun et al., 1992) glutamate (1 mM, 2 ms) was applied to the nucleated patch clamp recorded CA3 pyramidal neurons. As shown in **Figure 7**, PB significantly reduced the amplitude of glutamate induced currents (by $25.5 \pm 0.5\%$, $p < 0.001$, $n = 8$). The decay time constant of these currents was not changed in the presence of PB (3.6 ± 0.5 ms in control and 3.4 ± 0.4 ms in the presence of PB, respectively, $p > 0.5$). In similar experiments DZP had no statistically significant effects on glutamate induced currents (mean current amplitude in DZP was $97.9 \pm 3\%$ of the control, $p > 0.3$, $n = 4$, not shown). In addition, we tested the effect of PB and DZP on NMDA receptor mediated currents. In the presence of AMPA/kainate and GABAreceptor antagonists focal puff

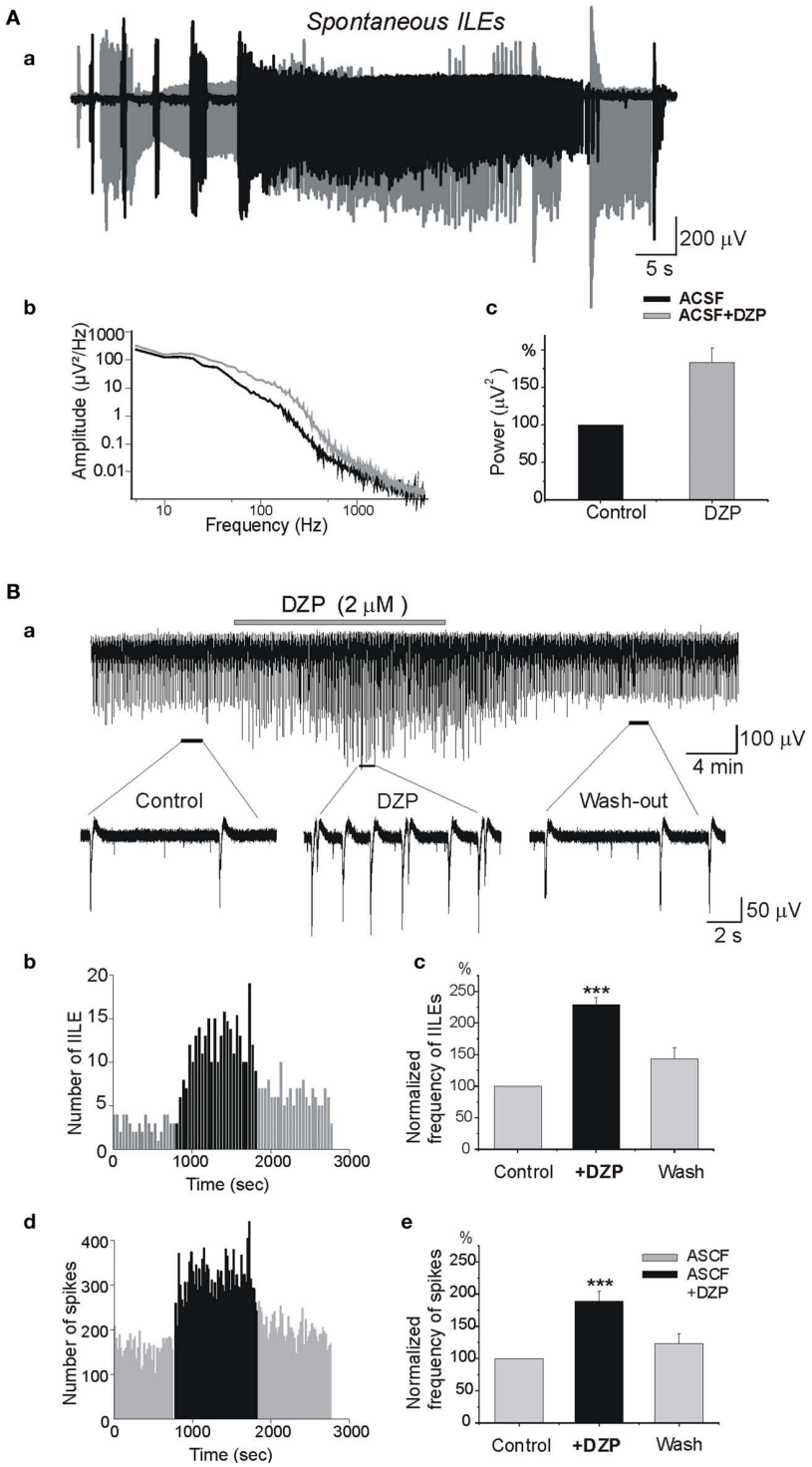

FIGURE 2 | Diazepam aggravates the severity of epileptiform activities in the isolated mirror focus. (Aa) Superimposed ILEs generated spontaneously in the contralateral hippocampus after formation of a MF before (black) and after (gray) DZP application. **(Ab)** Power spectra of spontaneous ILEs before and after DZP treatment [from **(Aa)**]. **(Ac)** Average power histogram of spontaneous ILEs before and after DZP. DZP application significantly increased power of ILEs (by $80 \pm 19.8\%$, $n = 4$, $p < 0.001$). **(Ba)** Extracellular recording in slices obtained from contralateral hippocampus after the formation of a MF. Slices generated spontaneous IILEs and multi-unit activities (MUAs) continuously that were reversibly aggravated by DZP (2 μM). **(Bb)** Quantification of IILEs from a single experiment [from **(Ba)**]. **(Bc)** Average quantification histogram of IILEs. **(Bd)** Quantification of spikes from single experiment [from **(Ba)**] and **(Be)** the average quantification histogram. Note that DZP increased the frequency of IILEs (by $128.7 \pm 12.2\%$, $n = 6$, $p < 0.001$) and spikes (by $88.6 \pm 16.2\%$, $n = 6$, $p < 0.001$).

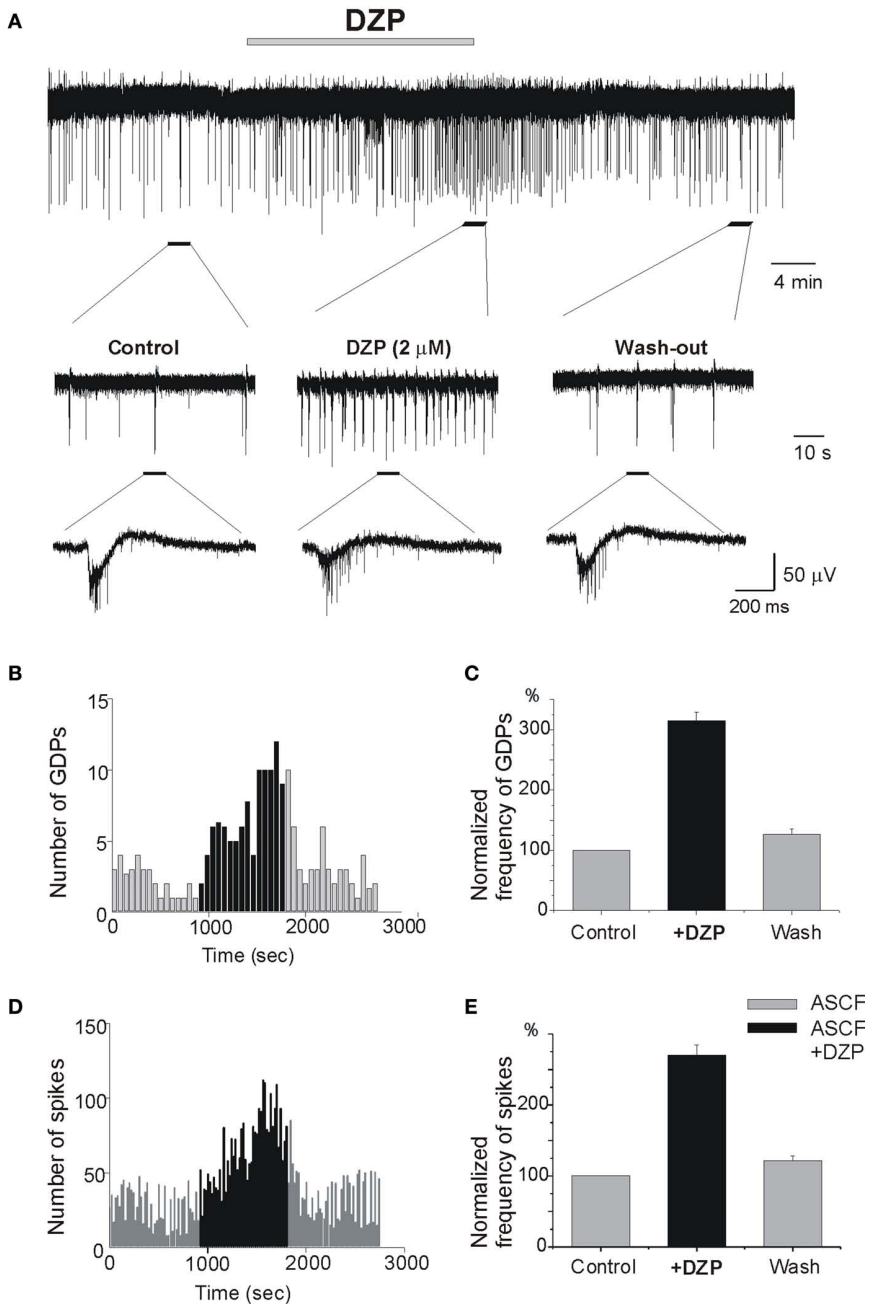

FIGURE 3 | Diazepam increases ongoing neuronal activity and network driven GDPs. (A) Extracellular recording of the Giant Depolarizing Potentials (GDPs) and multi-unit activities (MUAs) in control slices to record network driven events and individual neuronal spikes, respectively. Non-filtered faster display traces are depicted below to show spikes. Note the increase of frequency of GDPs **(B)** and spikes **(D)** by DZP: **(B–D)** quantification of recorded GDPs and spikes from **(A)**, Bin = 20 s. **(C–E)** Quantification of mean frequency of GDPs and spikes. DZP enhanced the frequency of GDPs **(C)** by 215.1 ± 13.6 ($p < 0.001$, $n = 14$) and spikes **(E)** by 170 ± 14.8% ($p < 0.001$, $n = 14$).

applications of glutamate (100 μM, 100 ms) generated (at +40 mV holding potential) large amplitude outward currents. These currents are mediated by NMDA receptors as they were blocked by the NMDA receptor antagonist APV (40 μM, $n = 11$, not shown). As shown in **Figure 8**, neither PB nor DZP altered these currents. Therefore, PB selectively reduces AMPA/kainate receptor mediated currents.

PRE- AND POSTSYNAPTIC ACTIONS OF PB ON AMPA RECEPTOR MEDIATED EXCITATORY POSTSYNAPTIC SYNAPTIC CURRENTS

To examine the pre- and postsynaptic mechanisms underlying the actions of PB, we used whole cell recordings to determined the effects of PB on the monosynaptic AMPA receptor-dependent EPSCs evoked by local electrical stimulations. We applied minimal electrical stimuli to generate all-or-none monosynaptic EPSCs

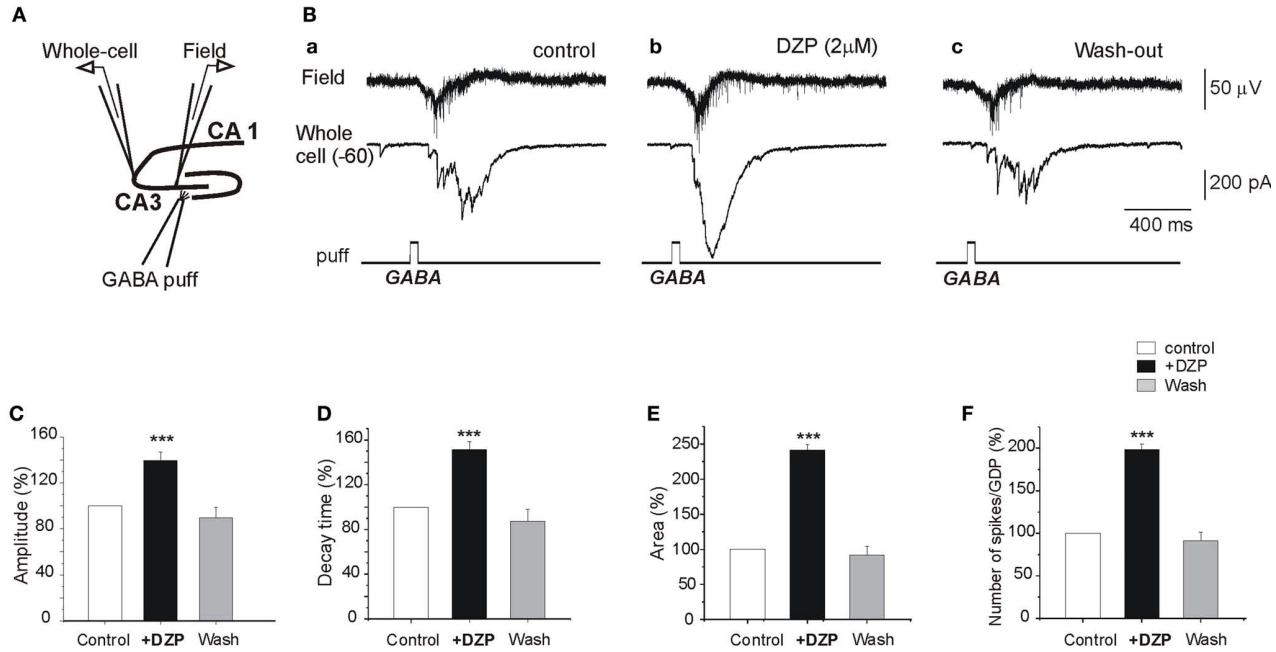

FIGURE 4 | DZP enhances GABA excitation in naive neurons. (A) Experimental design. Simultaneous whole cell patch clamp recordings of a CA3a pyramidal neuron and field recordings in the CA3c pyramidal layer were made in control slices and GABA (100 μM) was focally applied (100 ms) by puff in the CA3c part of the pyramidal layer. **(B)** GABA puff generated a field and whole cell recorded GDPs **(Ba)** that was strongly augmented by DZP **(Bb)**. The responses returned to control values after wash out of DZP **(Bc)**. **(C–E)** Quantification of the effects of DZP on whole cell recorded postsynaptic currents: the amplitudes of the currents, the decay time and the area of whole cell recorded responses were significantly augmented by DZP. **(F)** Quantification histogram of mean number of spikes associated with puff GABA generated GDPs (a time window of 1 s from the GDP onset from GABA puff was analyzed).

(see Kullmann, 1994; Stevens and Wang, 1994). In the presence of NMDA and GABA receptor antagonists, an electrical stimulation evoked an all-or-none evoked AMPA receptor mediated EPSC (**Figure 9**). PB increased the number of failures of evoked AMPA receptor-dependent EPSCs (by $92.1 \pm 30.1\%$, $p < 0.001$, $n = 8$; **Figure 9Ae**). In parallel experiments, miniature AMPA EPSCs (mEPSCs) were recorded in the presence of TTX to block ongoing network activity. PB reduced (**Figure 9B**) the amplitude (by 28.9%, from 25.9 ± 1.4 to 20.1 ± 0.9 pA, $p < 0.01$, $n = 8$ slices), and frequency of the mEPSCs (by $38.6 \pm 8.0\%$, $p < 0.01$, $n = 8$ slices, not shown, 5 min recordings analyzed before, during and after wash out of PB). Therefore, PB exerts a selective action on ongoing and evoked glutamatergic exogenous and synaptic currents that is mediated by AMPA/kainate but not NMDA receptors.

PRESERVATION OF THE AMPA/KAINATE RECEPTOR INHIBITORY ACTIONS OF PB IN MIRROR FOCUS NEURONS

To examine whether PB reduces the AMPA/kainate receptor mediated currents in "epileptic" tissue we used slices obtained from contralateral hippocampus after the formation of MF. As shown in **Figure 10Aa,b**, in control conditions these MF slices generate spontaneous IILEs (see also Khalilov et al., 2003, 2005; Nardou et al., 2009, 2011). After blockade of GABA and NMDA receptors, the IILEs transformed into AMPA/kainate receptor mediated ILEs (**Figure 10Ac**) as they were reversibly blocked by CNQX (10 μM, not shown). Addition of PB (100 μM) in these conditions significantly reduced the amplitude (by $22.7 \pm 4.2\%$ to controls, $n = 5$, $p < 0.001$, not shown) and frequency of ILEs: PB increased the mean interval between ictal-like events by $318.1 \pm 66.5\%$ ($p < 0.001$, $n = 5$ slices; **Figure 10C**). PB significantly decreased also the power of AMPA/kainate receptor-dependent ictal-like events **Figure 10B,C** (by $26.9 \pm 7.2\%$, $n = 5$, $p < 0.001$). Therefore, the inhibitory actions of PB on AMPA/kainate receptors are preserved in MF "epileptic" neurons.

DISCUSSION

Our results first suggest that PB has a higher efficacy than DZP to reduce early seizures thanks to its dual action on GABA and AMPA/kainate receptor mediated currents. DZP aggravates inaugurating propagated seizures most likely because at that developmental stage many naïve neurons have elevated $[Cl^-]_i$. (Nardou et al., 2009). However, in ongoing epileptogenic mirror foci, where GABA strongly excites neurons, PB like DZP aggravates seizures in spite of the reduction of glutamatergic currents that it produces. Therefore, the efficacy of DZP like PB in reducing seizures is conditioned by the actions of GABA. When these are strongly excitatory due to a strong increase of $[Cl^-]_i$, the reduction of the excitation by glutamate will not suffice to block seizures. Our observations of direct actions of PB on AMPA/kainate but not NMDA currents suggest a specific not yet identified recognition site. In spite of the inherent limitations of *in vitro* experimental models, the present results suggest that for the treatment of early

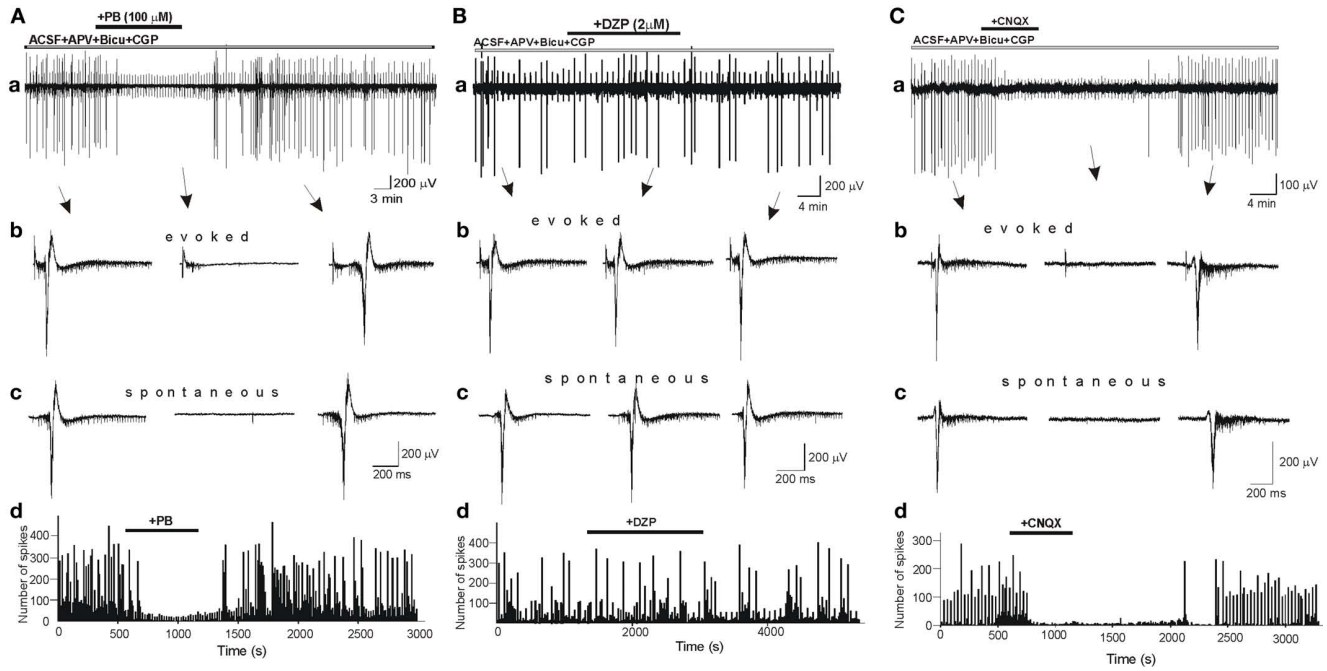

FIGURE 5 | Phenobarbital but not diazepam blocks AMPA/kainate mediated inter ictal-like events (IILEs). (Aa,Ba) Extracellular recordings of spontaneous and evoked (electrical stimulation every 30 s) IILEs generated in control slices in the presence of GABA receptors antagonists – bicuculline (10 μM), CGP (2 μM), – and NMDA receptors antagonist – APV (40 μM). Non-filtered faster display traces of evoked **(Ab,Bb,Cb)** and spontaneous **(Ac,Bc,Cc)** IILEs. Generation of IILEs in these conditions is mediated by AMPA/kainate receptors as they were reversibly blocked by CNQX **(C)**. Note that PB but not DZP completely blocked IILEs and reduced the frequency of spikes **(Ad,Bd)**.

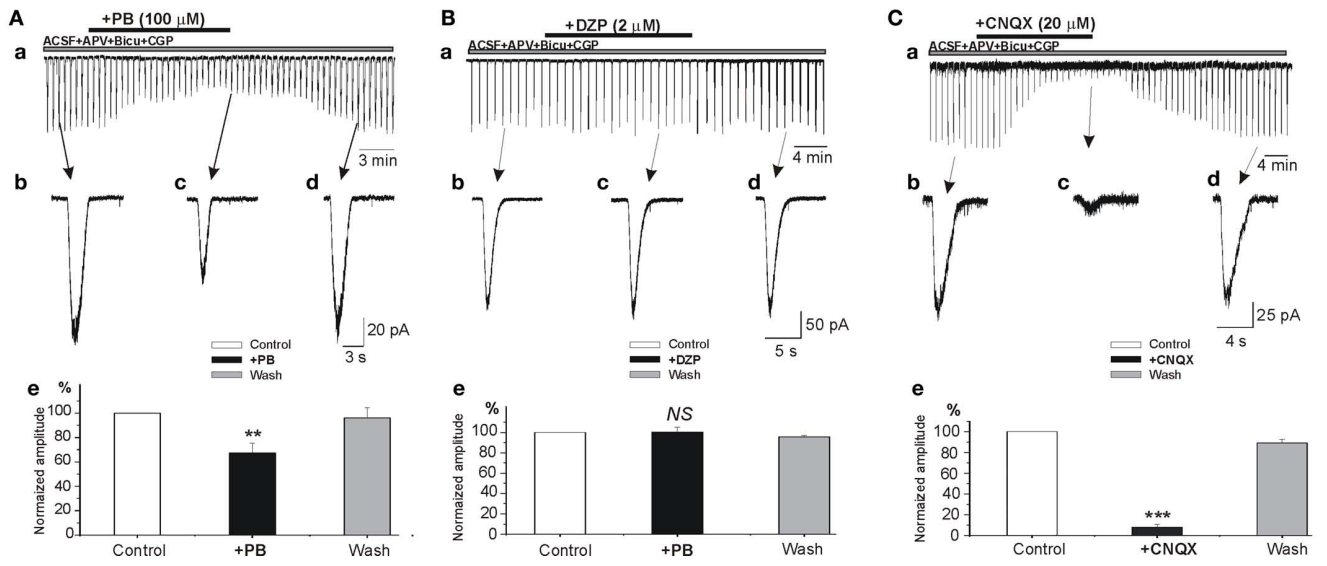

FIGURE 6 | Phenobarbital but not diazepam reduces AMPA/kainate mediated currents. (A–C) Whole cell patch clamp recordings of currents induced by focal application of glutamate (100 μM, 100 ms) in the presence APV (40 μM). **(Ae–Ce)** Histograms of normalized averaged amplitudes of glutamate induced currents showing the effects of PB **(Ae)**, DZP **(Be)**, and CNQX **(Ce)**. Note that phenobarbital but not diazepam significantly reduced the amplitude AMPA/kainate receptor mediated postsynaptic currents ($67.2 \pm 8.1\%$, $p < 0.001$, $n = 4$). NS, not statistically significant.

neonatal seizures PB may be more efficient than DZP. Furthermore, agents that exert a dual action on GABA and AMPA/kainate receptors may offer an interesting novel therapeutic perspective to treat neonatal seizures, provided that they are used at the earliest stages as the GABA polarity shift remains a fundamental point.

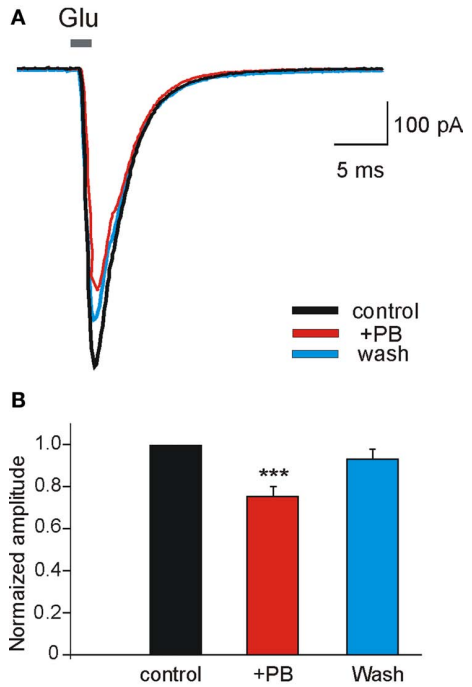

FIGURE 7 | Phenobarbital reduces AMPA receptor mediated currents in nucleated patches. (A) Currents evoked in nucleated patches from CA3 pyramidal neurons from control slices. L-Glutamate (***Glu***, 1 mM) was applied in 2 ms pulses at a holding potential of −60 mV. Each trace is the average of 4–8 sweeps. Note that PB [**(A)** red trace] reduced the amplitude of AMPA/kainate mediated currents. **(B)** PB significantly reduced (by $25.5 \pm 0.5\%$, $p < 0.001$, $n = 8$) the averaged amplitude of AMPA/kainate receptor mediated currents recorded in nucleated patches.

DZP AUGMENTS AND PB REDUCES ONGOING NEURONAL ACTIVITY AND EARLY SEIZURES

The effects of PB and DZP on GABAergic signals have been extensively investigated and will not be reviewed here (Barker and Gainer, 1973; Barker and Ransom, 1978; Barker and McBurney, 1979; Macdonald and Barker, 1979; Macdonald and McLean, 1982; Macdonald et al., 1986; Cheng et al., 2002; Soderpalm, 2002; Rogawski and Loscher, 2004; Czapinski et al., 2005; Macdonald and Rogawski, 2007; Stefan and Feuerstein, 2007). In short, both act directly on postsynaptic GABA receptors leading to a more powerful inhibition of target neurons. Classically, DZP potentiates GABA(A) receptor function by increasing channel opening frequency, whereas barbiturates increase channel open duration (Feng et al., 2004; Hanson and Czajkowski, 2008; Reid et al., 2009) by acting on different target sites on the GABA receptor channel complex (Feng et al., 2004; Hanson and Czajkowski, 2008; Mercado and Czajkowski, 2008). There are however several complicating factors. Benzodiazepine actions are highly dependent on the levels of GABA present (Mercik et al., 2007; Mozrzymas et al., 2007), the binding/unbinding of DZP from GABAA is highly complex (Jones-Davis et al., 2005; Bianchi et al., 2007a,b) and GABA receptor subunits and diazepam binding sites are internalized after seizures (Goodkin et al., 2008; Goodkin and Kapur, 2009). Systematic experimental comparisons of the actions of various GABA acting AEDs on neonatal network driven events have been seldom investigated. In the immature rat hippocampus, diazepam increases frequency yet slows down propagation of GDPs (Khalilov et al., 1999; Valeeva et al., 2010) whereas PB does not affect GDPs frequency (Dzhala et al., 2008) and reduces GDPs amplitude (Nardou et al., 2011). These observations are not readily compatible with an additional presynaptic action of PB on the release of GABA although this cannot be excluded at present. Collectively these observations are important considering the profound impact of ongoing network activity on transmitter release and the operation of developing cell assemblies. Thus, Cherubini and colleagues have elegantly shown that GDPs modulate GABA release via BDNF and other messengers (Sivakumaran et al., 2009). Since PB reduced and DZP augmented GDPs and early seizures we investigated the possibility that target sites other than GABA signaling could underline these differences.

PB REDUCED AMPA/KAINATE RECEPTOR MEDIATED CURRENTS

Several studies have shown earlier that PB (and pentobarbital) reduced glutamatergic AMPA/kainate receptor mediated currents including: (i) a subunit selective action on kainate-induced currents in Xenopus oocytes expressing different GluR subunits (DildyMayfield et al., 1996; Minami et al., 1998); (ii) a reduction of glutamate currents in spinal cord neurons (Barker and Gainer, 1973; MacDonald and Barker, 1978b; Taverna et al., 1994; Joo et al., 1999). PB – like DZP (Rovira and Ben-Ari, 1994) – also reduced calcium currents (Werz and Macdonald, 1985). In contrast, zolpidem had no effects in young animals but decreased calcium and barium spikes in adults whereas midazolam increased barium spikes in both young and adult animals (Rovira and Ben-Ari, 1994). The contributions of these non-GABA mediated signaling remained however controversial (Kamiya et al., 1999; also see Barker and Gainer, 1973; Barker and Ransom, 1978).

Present results provide direct evidence that PB but not DZP tested in the same preparation exerts a strong modulation of glutamatergic receptors and synaptic glutamatergic currents. Thus, PB strongly reduced the amplitude and frequency of miniature AMPA/kainate receptor mediated EPSCs generated in the presence of TTX, indicating a direct pre- and postsynaptic action of PB. This was confirmed directly by showing that PB increased the frequency of failures evoked in an all-or-none manner by minimal electrical stimuli, and reduced the amplitude of the responses evoked by focal applications of glutamate in the presence of the same cocktail of receptor antagonists and directly the amplitude but not the kinetic of AMPA/kainate currents in nucleated patches. The molecular targets of these actions have not been determined and are outside the scope of the present study. Interestingly, presynaptic activation of kainate receptors in CA3 neurons alters GABA release raising the possibility of an indirect modulation of GABAergic signals by PB (Caiati et al., 2010).

The increase of the number of failures by PB as well as the reduction of the frequency of miniature EPSCs suggests also presynaptic effects in addition to the postsynaptic ones. Such effects have long been observed in a variety of preparations. Thus, PB decrease mono- and polysynaptic reflexes in the spinal cord (Nicholson et al., 1988) and the anesthetic actions of barbiturates have been ascribed in part by a reduction of presynaptic calcium entry and

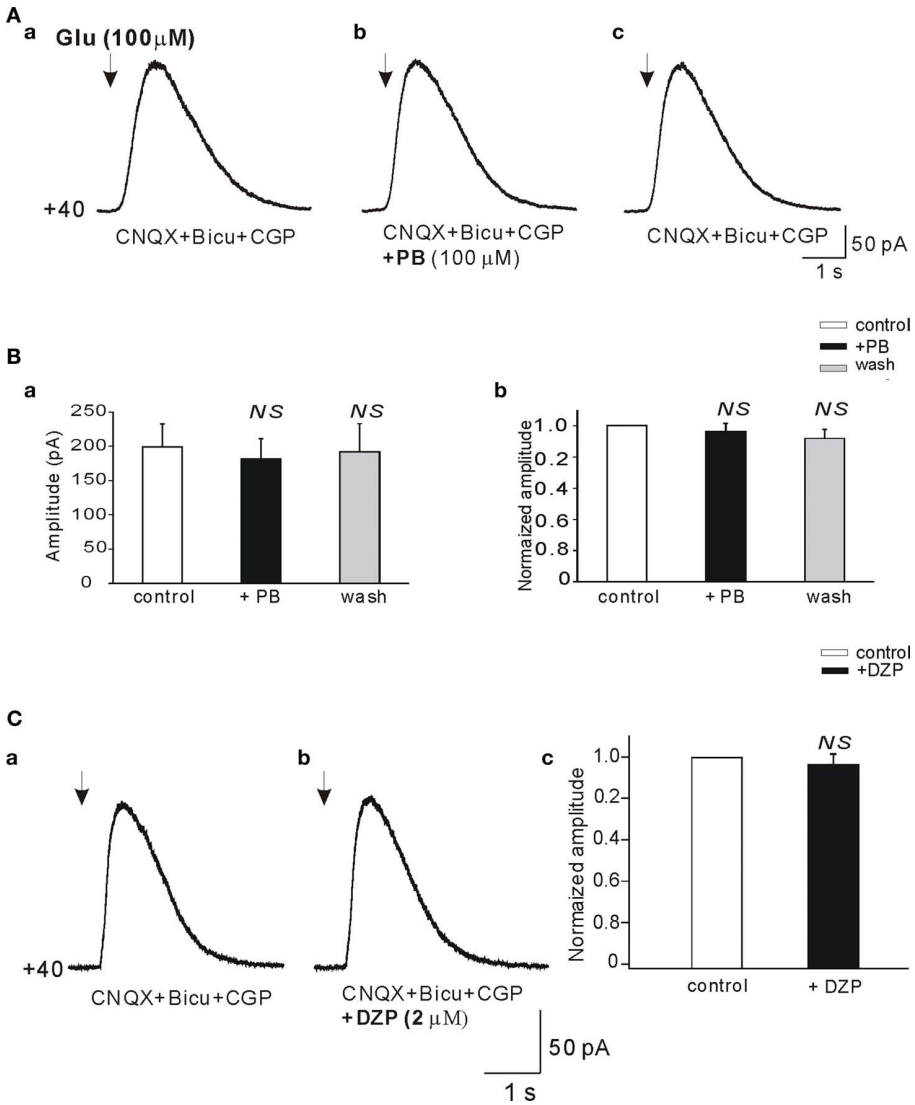

FIGURE 8 | Phenobarbital does not reduce the NMDA receptor mediated currents. (A,Da,b) Whole cell patch clamp recordings ($V_{clamp} = +40$ mV) of currents induced by focal application of glutamate (100 μM, 100 ms, arrows) in the presence of bicuculline (10 μM), CGP (2 μM), and CNQX (20 μM; antagonist of AMPA/kainate receptors). Averaged NMDA receptor mediated currents before **(Aa)**, in the presence **(Ab)**, and after wash out of PB **(Ac)** recorded from the same pyramidal cell. **(Ba)** Histogram of averaged ($n = 11$) amplitudes of NMDA receptor mediated currents. **(Bb)** Histogram of averaged amplitudes normalized to control. Averaged NMDA receptor mediated currents before (**Ca**) and in the presence of DZP **(Cb)**. **(Cc)** Histogram of averaged ($n = 5$) current amplitudes normalized to control. NS, not statistically significant.

consequent reduction of neurotransmitter release in mouse spinal cord neurons (Heyer and Macdonald, 1982). Different concentration dependent actions of the pre- and postsynaptic actions of PB and barbiturates have also been reported in the frog neuromuscular junction (Proctor and Weakly, 1976). Clearly, these effects may also contribute to the anticonvulsive actions of PB but the importance of their contribution remains to be determined.

DZP ENHANCES ONGOING ACTIVITY AND AGGRAVATES SEIZURES

The effects of DZP on GDPs are quite striking and to some extent unexpected. They suggest that by enhancing the excitatory actions of GABA on immature neurons, agents that exert solely this action will produce unwarranted effects. The underlying mechanisms are not clear at present; they may include specific effects on interneurons that orchestrate GDPs (Bonifazi et al., 2009) and/or enhance possible depolarizing tonic GABA currents in pyramidal cells that is important at that early stage and provides a large current (Ge et al., 2006; Sebe et al., 2010). Benzodiazepines are extensively used to block status epilepticus. In adult animal models diazepam is systematically injected after administrations of kainate or pilocarpine to prevent animal death consequently to the recurrent seizures (Ben-Ari et al., 1978; Ben-Ari, 1985; Cavalheiro et al., 1996). In contrast, DZP – like PB – is not efficient to block seizures after recurrent seizures have taken place (see below). Here, we show that

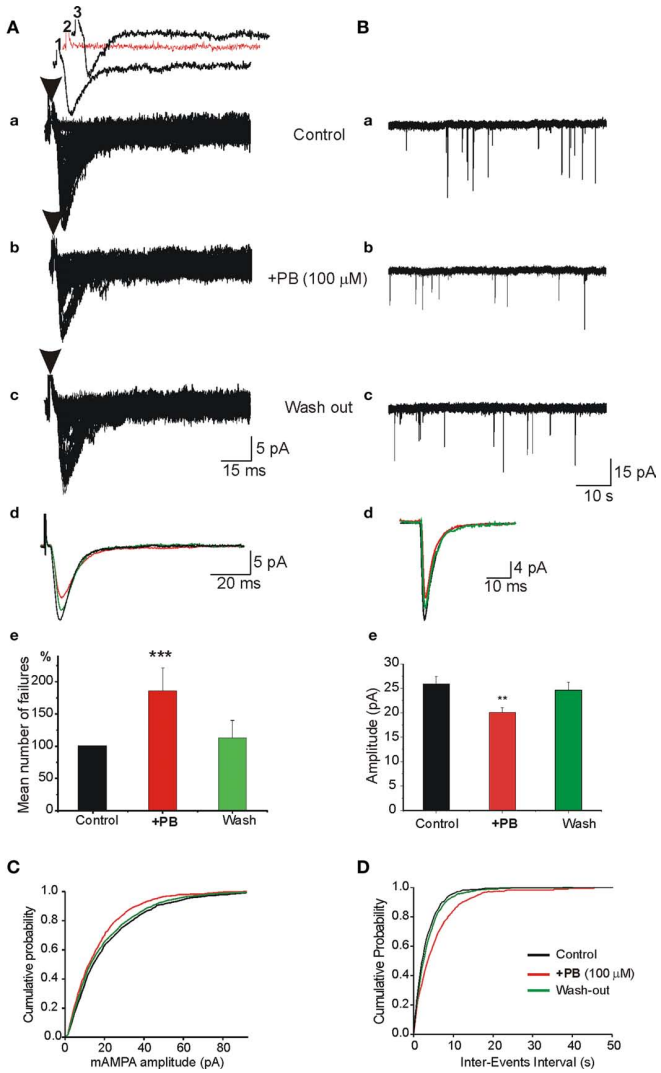

FIGURE 9 | Pre- and postsynaptic actions of PB on AMPA/kainate receptor mediated excitatory postsynaptic currents (EPSCc). (A) In the presence of APV (40 μM) and bicuculline (10 μM), single fibers were electrically stimulated to evoke a mono synaptic AMPA receptor mediated EPSCs. The stimulation was adjusted to induce ∼20–50% failures [shown as red trace in **(Aa2)**]. **(Aa–c)** Single experiment obtained with repeated stimuli (30 stimuli every 10 s). **(Aa)** Control, **(Ab)** PB strongly enhanced the number of failures and reduced the average amplitude of EPSCs [see also **(Ae)**], **(Ac)** wash out of PB. **(Ad)** Superimposed averaged responses (the failures were discarded) from **(Aa–c)** to illustrate the effects of PB. Note the reduction of the averaged amplitude of EPSCs in the presence of PB (red trace). **(Ae)** Quantification of the mean number of normalized failures. Failure rate presented as "percentage of failure" (number of failure/total number of stimulation). Note the highly significant increase of the number of failures in the presence of PB ($p < 0.001$, $n = 4$ experiments). **(B)** PB reduces the amplitude of miniature AMPA receptor mediated EPSCs (mEPSCs). APV (40 μM) and bicuculline (10 μM) were applied throughout the recordings as well as TTX (1 μM) to generate mEPSCs. **(Ba–c)** Single traces to illustrate the actions of PB on AMPA receptor mediated mEPSCs. Note that PB (middle trace) reduced the amplitude of the minis. **(Bd)** Superimposed averaged traces of single mEPSCs to illustrate the effects of PB [from **(Ba–c)**]. Note the reduction of the mEPSCs amplitude (red trace). **(Be)** Quantification of the effects of PB. Note that PB reduced significantly (by 28.9%; from 25.9 ± 1.4 to 20.1 ± 0.9 pA, $p < 0.01$, $n = 5$ cells from different slices) the averaged amplitude of mEPSCs. PB also reduced the frequency of mini EPSCs (see text). **(C)** Cumulative probability distributions of mEPSCs amplitude in the presence of PB (red curve) demonstrate a leftward shift as compared with control and wash out. **(D)** Cumulative probability distribution of mEPSCs inter-event intervals in the presence of PB demonstrates a rightward shift as compared with control and wash out.

DZP aggravates seizures from their onset in neonatal hippocampi. The effects of DZP were highly reproducible, associated with a significant increase of the HFOs and consequently with the formation by seizures of an epileptogenic MF. Indeed, as shown earlier, there is a direct link between HFOs and the formation by seizures of an independent MF capable of generating seizures (Khalilov et al., 2005). These actions are also in keeping with our earlier report showing that functional GABAergic receptors are essential for the formation by seizures of a MF, since applications of a GABA receptor antagonist generated epileptiform events that however were neither associated with HFOs nor with the formation of an epileptogenic MF (Khalilov et al., 2005).

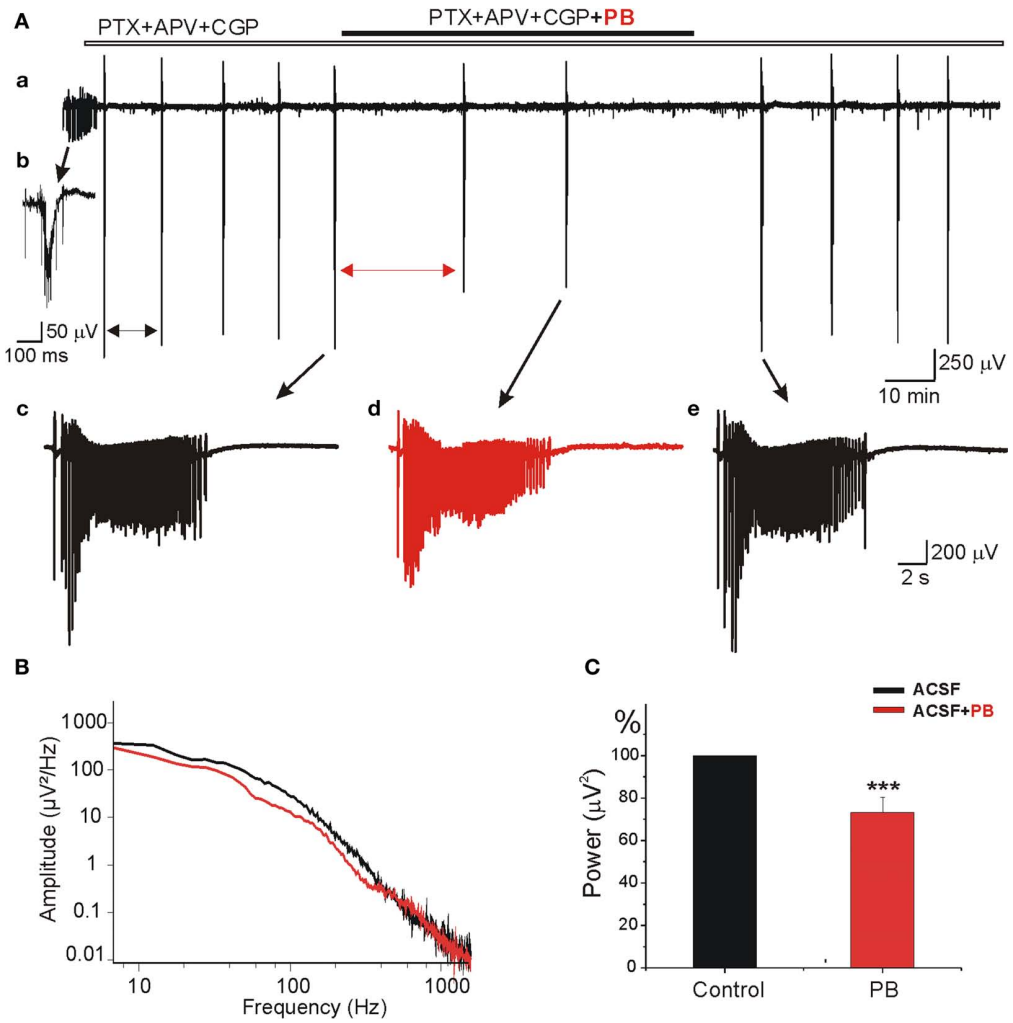

FIGURE 10 | Phenobarbital reduces AMPA/kainate receptors field potentials in mirror focus neurons. (A) Extracellular field recording of spontaneous epileptiform activities in slices obtained from contralateral hippocampus after mirror focus formation. Recordings were performed in the presence of GABA(A) and GABA(C) receptors antagonist PTX (100 µM), GABA(B) receptor antagonist CGP (2 µM), and NMDA receptor antagonist APV (40 µM). **(Ab)** Example of epileptiform activities recorded in an "epileptic" slice from mirror focus before application of antagonists. **(Ac–e)** Examples of ILEs in the presence of GABA and NMDA receptors antagonists: before application **(Ac)**, in the presence **(Ad)**, and after PB wash out **(Ae)**. Note the significant decrease of amplitude and frequency of ictal-like events. Mean interval between ictal-like events (double arrows) significantly increased (by 318.1 ± 66.5%, not shown). **(B)** Power spectrum [from **(Ac–d)**] showing the decrease of amplitude and frequency by PB. **(C)** Average power histogram of spontaneous ictal-like events before and after application of PB. PB significantly decreased the power of epileptiform events (by 26.9 ± 7.2%, $n = 5$, $p < 0.001$).

RECURRENT SEIZURES ABOLISH THE ADVANTAGES OF PB OVER DZP: CRUCIAL ROLE OF INTRACELLULAR CHLORIDE LEVELS

There is now direct evidence from humans and experimental animals that recurrent seizures produce an accumulation of $[Cl^-]_i$ associated with a shift of the actions of GABA from inhibitory to excitatory (Cohen et al., 2002; Khalilov et al., 2003, 2005; Payne et al., 2003; Blaesse et al., 2009; Nardou et al., 2011). The underlying mechanisms are now better understood. It has been recently shown that GABA excites epileptic neurons because of high intracellular chloride mediated by a combined action of the NKCC1 chloride importer (Dzhala et al., 2010) and a down regulation of the chloride exporter KCC2 (Lee et al., 2010; Nardou et al., 2011), leading to strong excitatory actions of GABA that are exacerbated by PB. Therefore, although PB is more efficient than DZP to block early neonatal seizures, by shifting the actions of GABA to strongly excitatory, recurrent seizures abolish this advantage stressing the importance of an early aggressive treatment of seizures to avoid the loss of KCC2 activity and preserve the efficient actions of PB.

CLINICAL IMPLICATIONS

There are many obvious limitations to the *in vitro* preparations that restrict the relevance of these observations to a clinical

situation including the lack of major cerebral connections, systemic events (vascular, hormonal, etc.) and the different species. Yet, the *in vitro* MF model used here has several advantages over conventional slices in that it enables to determine the activity of neuronal ensembles in relatively preserved conditions and to compare the actions of AEDs on acute and more chronic propagating seizures in neurons that have never been in contact with a convulsive agent. Our results suggest important advantages of PB over DZP since the former exerts a dual action and is not exclusively restricted to GABA signal. Although the magnitude of these effects is relatively small, they are stable and observed in naïve and "epileptic" neurons suggesting that AEDs with a dual action may be advantageous over agents that exert solely a pro-GABA action. This is particularly important in view of the vulnerability of intracellular chloride shifts with recurrent seizures that strongly limit the efficacy of GABA acting AEDs. There is now little doubt that in humans, like in experimental animals, GABA may excite epileptic neurons and this will seriously aggravate the situation. The history of seizures prior to AEDs is clearly an important element to take in consideration in order to preserve as much as possible the capacity of neurons to control their $[Cl^-]_i$.

ACKNOWLEDGMENTS

We thank Drs. Rustem Khazipov, Roman Tyzio and Diana Ferrari for their suggestions and criticism. Funding: This work was supported by the French Medical Research council (INSERM), the Université de la Méditerranée, the French agency of research ANR (L'Agence Nationale de la Recherche – to Ilgam Khalilov), Fondation pour la Recherche Médicale (FRM – to Romain Nardou), and the FP7 NEMO program: http://www.nemo-europe.com/(to Yehezkel Ben-Ari). Financial supported from University of Paris/INSERM "interface" programs to Yehezkel Ben-Ari.

REFERENCES

Barker, J. L., and Gainer, H. (1973). Pentobarbital: selective depression of excitatory postsynaptic potentials. *Science* 182, 720–722.

Barker, J. L., and McBurney, R. N. (1979). Phenobarbitone modulation of postsynaptic GABA receptor function on cultured mammalian neurons. *Proc. R. Soc. Lond. B Biol. Sci.* 206, 319–327.

Barker, J. L., and Ransom, B. R. (1978). Pentobarbitone pharmacology of mammalian central neurones grown in tissue culture. *J. Physiol.* 280, 355–372.

Bartha, A. I., Shen, J., Katz, K. H., Mischel, R. E., Yap, K. R., Ivacko, J. A., Andrews, E. M., Ferriero, D. M., Ment, L. R., and Silverstein, F. S. (2007). Neonatal seizures: multicenter variability in current treatment practices. *Pediatr. Neurol.* 37, 85–90.

Bassan, H., Bental, Y., Shany, E., Berger, I., Froom, P., Levi, L., and Shiff, Y. (2008). Neonatal seizures: dilemmas in workup and management. *Pediatr. Neurol.* 38, 415–421.

Ben Ari, Y., Gaiarsa, J. L., Tyzio, R., and Khazipov, R. (2007). GABA: a pioneer transmitter that excites immature neurons and generates primitive oscillations. *Physiol. Rev.* 87, 1215–1284.

Ben-Ari, Y. (1985). Limbic seizure and brain damage produced by kainic acid: mechanisms and relevance to human temporal lobe epilepsy. *Neuroscience* 14, 375–403.

Ben-Ari, Y., Cherubini, E., Corradetti, R., and Gaïarsa, J.-L. (1989). Giant synaptic potentials in immature rat CA3 hippocampal neurones. *J. Physiol. (Lond.)* 416, 303–325.

Ben-Ari, Y., Lagowska, Y., Le Gal La, S. G., Tremblay, E., Ottersen, O. P., and Naquet, R. (1978). Diazepam pretreatment reduces distant hippocampal damage induced by intra-amygdaloid injections of kainic acid. *Eur. J. Pharmacol.* 52, 419–420.

Bianchi, M. T., Botzolakis, E., and Macdonald, R. (2007a). Re-evaluating the benzodiazepine mechanism of action: from bench to bedside and back. *Neurology* 68, A269.

Bianchi, M. T., Botzolakis, E. J., Haas, K. F., Fisher, J. L., and Macdonald, R. L. (2007b). Microscopic kinetic determinants of macroscopic currents: insights from coupling and uncoupling of GABA(A) receptor desensitization and deactivation. *J. Physiol. (Lond.)* 584, 769–787.

Blaesse, P., Airaksinen, M. S., Rivera, C., and Kaila, K. (2009). Cation-chloride cotransporters and neuronal function. *Neuron* 61, 820–838.

Bonifazi, P., Goldin, M., Picardo, M. A., Jorquera, I., Cattani, A., Bianconi, G., Represa, A., Ben-Ari, Y., and Cossart, R. (2009). GABAergic hub neurons orchestrate synchrony in developing hippocampal networks. *Science* 326, 1419–1424.

Boylan, G. B., Rennie, J. M., Pressler, R. M., Wilson, G., Morton, M., and Binnie, C. D. (2002). Phenobarbitone, neonatal seizures, and video-EEG. *Arch. Dis. Child. Fetal Neonatal Ed.* 86, 165–170.

Bragin, A., Engel, J. Jr., Wilson, C. L., Vizentin, E., and Mathern, G. W. (1999). Electrophysiologic analysis of a chronic seizure model after unilateral hippocampal KA injection. *Epilepsia* 40, 1210–1221.

Caiati, M. D., Sivakumaran, S., and Cherubini, E. (2010). In the developing rat hippocampus, endogenous activation of presynaptic kainate receptors reduces GABA release from mossy fiber terminals. *J. Neurosci.* 30, 1750–1759.

Carmo, K. B., and Barr, P. (2005). Drug treatment of neonatal seizures by neonatologists and paediatric neurologists. *J. Paediatr. Child Health* 41, 313–316.

Cavalheiro, E. A., Santos, N. F., and Priel, M. R. (1996). The pilocarpine model of epilepsy in mice. *Epilepsia* 37, 1015–1019.

Cheng, C., Roemer-Becuwe, C., and Pereira, J. (2002). When midazolam fails. *J. Pain Symptom Manage.* 23, 256–265.

Cohen, I., Navarro, V., Clemenceau, S., Baulac, M., and Miles, R. (2002). On the origin of interictal activity in human temporal lobe epilepsy in vitro. *Science* 298, 1418–1421.

Colquhoun, D., Jonas, P., and Sakmann, B. (1992). Action of brief pulses of glutamate on AMPA/kainate receptors in patches from different neurones of rat hippocampal slices. *J. Physiol. (Lond.)* 458, 261–287.

Connell, J., Oozeer, R., de, V. L., Dubowitz, L. M., and Dubowitz, V. (1989). Clinical and EEG response to anticonvulsants in neonatal seizures. *Arch. Dis. Child.* 64, 459–464.

Czapinski, P., Blaszczyk, B., and Czuczwar, S. J. (2005). Mechanisms of action of antiepileptic drugs. *Curr. Top. Med. Chem.* 5, 3–14.

DildyMayfield, J. E., Eger, E. I., and Harris, R. A. (1996). Anesthetics produce subunit-selective actions on glutamate receptors. *J. Pharmacol. Exp. Ther.* 276, 1058–1065.

Dzhala, V. I., Brumback, A. C., and Staley, K. J. (2008). Bumetanide enhances phenobarbital efficacy in a neonatal seizure model. *Ann. Neurol.* 63, 222–235.

Dzhala, V. I., Kuchibhotla, K. V., Glykys, J. C., Kahle, K. T., Swiercz, W. B., Feng, G., Kuner, T., Augustine, G. J., Bacskai, B. J., and Staley, K. J. (2010). Progressive NKCC1-dependent neuronal chloride accumulation during neonatal seizures. *J. Neurosci.* 30, 11745–11761.

Feng, H. J., Bianchi, M. T., and Macdonald, R. L. (2004). Pentobarbital differentially modulates alpha 1 beta 3 delta and alpha 1 beta 3 gamma 2L GABA(A) receptor currents. *Mol. Pharmacol.* 66, 988–1003.

Ge, S., Goh, E. L., Sailor, K. A., Kitabatake, Y., Ming, G. L., and Song, H. (2006). GABA regulates synaptic integration of newly generated neurons in the adult brain. *Nature* 2, 589–593.

Glykys, J., Dzhala, V. I., Kuchibhotla, K. V., Feng, G., Kuner, T., Augustine, G., Bacskai, B. J., and Staley, K. J. (2009). Differences in cortical vs. subcortical GABAergic signaling: a candidate mechanism of electroclinical dissociation of neonatal seizures. *Neuron* 10, 657–672.

Goodkin, H. P., Joshi, S., Mtchedlishvili, Z., Brar, J., and Kapur, J. (2008). Subunit-specific trafficking of GABA(A) receptors during status epilepticus. *J. Neurosci.* 28, 2527–2538.

Goodkin, H. P., and Kapur, J. (2009). The impact of diazepam's discovery on the treatment and understanding of status epilepticus. *Epilepsia* 50, 2011–2018.

Guerrini, R., Belmonte, A., and Genton, P. (1998). Antiepileptic drug-induced worsening of seizures in children. *Epilepsia* 39(Suppl. 3), S2–S10.

Guillet, R., and Kwon, J. (2007). Seizure recurrence and developmental disabilities after neonatal seizures: outcomes are unrelated to use of phenobarbital prophylaxis. *J. Child Neurol.* 22, 389–395.

Hanson, S. M., and Czajkowski, C. (2008). Structural mechanisms underlying benzodiazepine modulation of the GABA(A) receptor. *J. Neurosci.* 28, 3490–3499.

Heyer, E. J., and Macdonald, R. L. (1982). Barbiturate reduction of calcium-dependent action-potentials – correlation with anesthetic action. *Brain Res.* 236, 157–171.

Jacobs, J., LeVan, P., Chander, R., Hall, J., Dubeau, F., and Gotman, J. (2008). Interictal high-frequency oscillations (80-500 Hz) are an indicator of seizure onset areas independent of spikes in the human epileptic brain. *Epilepsia* 49, 1893–1907.

Jin, L. J., Schlesinger, F., Song, Y. P., Dengler, R., and Krampfl, K. (2010). The interaction of the neuroprotective compounds riluzole and phenobarbital with AMPA-type glutamate receptors: a patch-clamp study. *Pharmacology* 85, 54–62.

Jones-Davis, D. M., Song, L. Y., Gallagher, M. J., and Macdonald, R. L. (2005). Structural determinants of benzodiazepine allosteric regulation of GABA(A) receptor currents. *J. Neurosci.* 25, 8056–8065.

Joo, D. T., Xiong, Z. G., MacDonald, J. F., Jia, Z., Roder, J., Sonner, J., and Orser, B. A. (1999). Blockade of glutamate receptors and barbiturate anesthesia – increased sensitivity to pentobarbital-induced anesthesia despite reduced inhibition of AMPA receptors in GluR2 null mutant mice. *Anesthesiology* 91, 1329–1341.

Kaindl, A. M., Koppelstaetter, A., Nebrich, G., Stuwe, J., Sifringer, M., Zabel, C., Klose, J., and Ikonomidou, C. (2008). Brief alteration of NMDA or GABAA receptor-mediated neurotransmission has long term effects on the developing cerebral cortex. *Mol. Cell. Proteomics* 7, 2293–2310.

Kamiya, Y., Andoh, T., Furuya, R., Hattori, S., Watanabe, I., Sasaki, T., Ito, H., and Okumura, F. (1999). Comparison of the effects of convulsant and depressant barbiturate stereoisomers on AMPA-type glutamate receptors. *Anesthesiology* 90, 1704–1713.

Khalilov, I., Dzhala, V., Medina, I., Leinekugel, X., Melyan, Z., Lamsa, K., Khazipov, R., and Ben-Ari, Y. (1999). Maturation of kainate-induced epileptiform activities in interconnected intact neonatal limbic structures in vitro. *Eur. J. Neurosci.* 11, 3468–3480.

Khalilov, I., Esclapez, M., Medina, I., Aggoun, D., Lamsa, K., Leinekugel, X., Khazipov, R., and Ben-Ari, Y. (1997). A novel in vitro preparation: the intact hippocampal formation. *Neuron* 19, 743–749.

Khalilov, I., Holmes, G. L., and Ben Ari, Y. (2003). In vitro formation of a secondary epileptogenic mirror focus by interhippocampal propagation of seizures. *Nat. Neurosci.* 6, 1079–1085.

Khalilov, I., Le Van, Q. M., Gozlan, H., and Ben Ari, Y. (2005). Epileptogenic actions of GABA and fast oscillations in the developing hippocampus. *Neuron* 48, 787–796.

Kullmann, D. M. (1994). Amplitude fluctuations of dual-component EPSCs in hippocampal pyramidal cells: implications for long-term potentiation. *Neuron* 12, 1111–1120.

Le Van Quyen, M., Khalilov, I., and Ben-Ari, Y. (2006). The dark side of high-frequency oscillations in the developing brain. *Trends Neurosci.* 29, 419–427.

Lee, H. H., Jurd, R., and Moss, S. J. (2010). Tyrosine phosphorylation regulates the membrane trafficking of the potassium chloride co-transporter KCC2. *Mol. Cell. Neurosci.* 45, 173–179.

Loscher, W., and Honack, D. (1989). Comparison of the anticonvulsant efficacy of primidone and phenobarbital during chronic treatment of amygdala-kindled rats. *Eur. J. Pharmacol.* 162, 309–322.

MacDonald, J. F., and Barker, J. L. (1982). Multiple actions of picomolar concentrations of flurazepam on the excitability of cultured mouse spinal neurons. *Brain Res.* 246, 257–264.

MacDonald, R., and Barker, J. L. (1978a). Benzodiazepines specifically modulate GABA-mediated postsynaptic inhibition in cultured mammalian neurones. *Nature* 271, 563–564.

MacDonald, R. L., and Barker, J. L. (1978b). Different actions of anticonvulsant and anesthetic barbiturates demonstrated using mammalian neurons in cell-culture. *Neurology* 28, 367.

Macdonald, R. L., and Barker, J. L. (1979). Enhancement of GABA-mediated postsynaptic inhibition in cultured mammalian spinal-cord neurons – common-mode of anticonvulsant action. *Brain Res.* 167, 323–336.

Macdonald, R. L., and Kelly, K. M. (1994). Mechanisms of action of currently prescribed and newly developed antiepileptic drugs. *Epilepsia* 35(Suppl. 4), S41–S50.

Macdonald, R. L., and McLean, M. J. (1982). Cellular bases of barbiturate and phenytoin anticonvulsant drug action. *Epilepsia* 23(Suppl. 1), S7–S18.

Macdonald, R. L., and Rogawski, M. A. (2007). "Cellular effects of antiepileptic drugs," in *Epilepsy: A Comprehensive Textbook*, 2nd Edn, eds J. Engel and T. A. Pedley (Philadelphia: Lippincott Williams and Wilkins), 1433–1445.

Macdonald, R. L., Weddle, M. G., and Gross, R. A. (1986). Benzodiazepine, beta-carboline, and barbiturate actions on GABA responses. *Adv. Biochem. Psychopharmacol.* 41, 67–78.

Mercado, J., and Czajkowski, C. (2008). Gamma-aminobutyric acid (GABA) and pentobarbital induce different conformational rearrangements in the GABA(A) receptor alpha 1 and beta(2) pre-M1 regions. *J. Biol. Chem.* 283, 15250–15257.

Mercik, K., Piast, M., and Mozrzymas, J. W. (2007). Benzodiazepine receptor agonists affect both binding and gating of recombinant alpha I beta 2 gamma 2 gamma-aminobutyric acid-A receptors. *Neuroreport* 18, 781–785.

Minami, K., Wick, M. J., Stern-Bach, Y., Dildy-Mayfield, J. E., Brozowski, S. J., Gonzales, E. L., Trudell, J. R., and Harris, R. A. (1998). Sites of volatile anesthetic action on kainate (glutamate receptor 6) receptors. *J. Biol. Chem.* 273, 8248–8255.

Mozrzymas, J. W., Wojtowicz, T., Piast, M., Lebida, K., Wyrembek, P., and Mercik, K. (2007). GABA transient sets the susceptibility of mIPSCs to modulation by benzodiazepine receptor agonists in rat hippocampal neurons. *J. Physiol. (Lond.)* 585, 29–46.

Nardou, R., Ben-Ari, Y., and Khalilov, I. (2009). Bumetanide, an NKCC1 antagonist, does not prevent formation of epileptogenic focus but blocks epileptic focus seizures in immature rat hippocampus. *J. Neurophysiol.* 101, 2878–2888.

Nardou, R., Yamamoto, S., Chazal, G., Bhar, A., Ferrand, N., Dulac, O., Ben-Ari, Y., and Khalilov, I. (2011). Neuronal chloride accumulation and excitatory GABA underlie aggravation of neonatal epileptiform activities by phenobarbital. *Brain* 134, 987–1002.

Nicholson, G. M., Spence, I., and Johnston, G. A. R. (1988). Differing actions of convulsant and nonconvulsant barbiturates – an electrophysiological study in the isolated spinal-cord of the rat. *Neuropharmacology* 27, 459–465.

Painter, M. J., Scher, M. S., Stein, A. D., Armatti, S., Wang, Z., Gardiner, J. C., Paneth, N., Minnigh, B., and Alvin, J. (1999). Phenobarbital compared with phenytoin for the treatment of neonatal seizures. *N. Engl. J. Med.* 341, 485–489.

Payne, J. A., Rivera, C., Voipio, J., and Kaila, K. (2003). Cation-chloride co-transporters in neuronal communication, development and trauma. *Trends Neurosci.* 26, 199–206.

Perucca, E., Gram, L., Avanzini, G., and Dulac, O. (1998). Antiepileptic drugs as a cause of worsening seizures. *Epilepsia* 39, 5–17.

Proctor, W. R., and Weakly, J. N. (1976). Comparison of presynaptic and post-synaptic actions of pentobarbital and phenobarbitone in neuromuscular-junction of frog. *J. Physiol. (Lond.)* 258, 257–268.

Reid, C. A., Taylor, N., Berkovic, S. F., and Petrou, S. (2009). Benzodiazepine efficacy in a mouse model of absence epilepsy based on a human mutation in the gamma2 GABA-A subunit. *Epilepsia* 50, 254–255.

Rivera, C., Voipio, J., Thomas-Crusells, J., Li, H., Emri, Z., Sipilä, S., Payne, J. A., Minichiello, L., Saarma, M., and Kaila, K. (2004). Mechanism of activity-dependent downregulation of the neuron-specific K-Cl cotransporter KCC2. *J. Neurosci.* 24, 4683–4691.

Rogawski, M. A., and Loscher, W. (2004). The neurobiology of antiepileptic drugs. *Nat. Rev. Neurosci.* 5, 553–564.

Rovira, C., and Ben-Ari, Y. (1994). Benzodiazepines modulate calcium spikes in young and adult hippocampal cells. *Neuroreport* 5, 2125–2129.

Sather, W., Dieudonné, S., MacDonald, J. F., and Ascher, P. (1992). Activation and desensitization of N-methyl-D-aspartate receptors in nucleated outside-out patches from mouse neurones. *J. Physiol.* 450, 643–672.

Sebe, J. Y., Looke-Stewart, E. C., Estrada, R. C., and Baraban, S. C. (2010). Robust tonic GABA currents can inhibit cell firing in mouse newborn neocortical pyramidal cells. *Eur. J. Neurosci.* 32, 1310–1318.

Sivakumaran, S., Mohajerani, M. H., and Cherubini, E. (2009). At immature mossy-fiber-CA3 synapses, correlated presynaptic and postsynaptic activity persistently enhances GABA release and network excitability via BDNF and cAMP-dependent PKA. *J. Neurosci.* 29, 2637–2647.

Soderpalm, B. (2002). Anticonvulsants: aspects of their mechanisms of action. *Eur. J. Pain (Lond.)* 6, 3–9.

Stefan, H., and Feuerstein, T. J. (2007). Novel anticonvulsant drugs. *Pharmacol. Ther.* 113, 165–183.

Stevens, C. F., and Wang, Y. (1994). Changes in reliability of synaptic function as a mechanism for plasticity. *Nature* 371, 704–707.

Strata, F., and Cherubini, E. (1994). Transient expression of a novel type of GABA response in rat CA3 hippocampal neurones during development. *J. Physiol. (Lond.)* 480, 493–503.

Taverna, F. A., Cameron, B. R., Hampson,D. L., Wang, L. Y., and MacDonald, J. F. (1994). Sensitivity of ampa receptors to pentobarbital. *Eur. J. Pharmacol. Mol. Pharmacol. Sec.* 267, R3–R5.

Valeeva, G., Abdullin, A., Tyzio, R., Skorinkin, A., Nikolski, E., Ben-Ari, Y., and Khazipov, R. (2010). Temporal coding at the immature depolarizing GABAergic synapse. *Front. Cell. Neurosci.* 4:17. doi: 10.3389/fncel.2010.00017

Werz, M. A., and Macdonald, R. L. (1985). Barbiturates decrease voltage-dependent calcium conductance of mouse neurons in dissociated cell-culture. *Mol. Pharmacol.* 28, 269–277.

Wheless, J. W., Clarke, D. F., Arzimanoglou, A., and Carpenter, D. (2007). Treatment of pediatric epilepsy: european expert opinion, 2007. *Epileptic Disord.* 9, 353–412.

Yanay, O., Brogan, T. V., and Martin, L. D. (2004). Continuous pentobarbital infusion in children is associated with high rates of complications. *J. Crit. Care* 19, 174–178.

Conflict of Interest Statement: The authors declare that the research was conducted in the absence of any commercial or financial relationships that could be construed as a potential conflict of interest.

Received: 01 June 2011; accepted: 19 July 2011; published online: 28 July 2011.

Citation: Nardou R, Yamamoto S, Bhar A, Burnashev N, Ben-Ari Y and Khalilov I (2011) Phenobarbital but not diazepam reduces AMPA/kainate receptor mediated currents and exerts opposite actions on initial seizures in the neonatal rat hippocampus. Front. Cell. Neurosci. ***5****:16. doi: 10.3389/fncel.2011.00016*

frontiers in
CELLULAR NEUROSCIENCE

ORIGINAL RESEARCH ARTICLE
published: 19 September 2011
doi: 10.3389/fncel.2011.00017

Disinhibition-mediated LTP in the hippocampus is synapse specific

Jake Ormond*† *and Melanie A. Woodin*

Department of Cell and Systems Biology, University of Toronto, Toronto, ON, Canada

Edited by:
Yehezkel Ben-Ari, Institut National de la Santé et de la Recherche Médicale, France

Reviewed by:
Gianmaria Maccaferri, Northwestern University, USA
Rustem Khazipov, Institut National de la Santé et de la Recherche Médicale, France
Shaoyu Ge, SUNY Stony Brook, USA

***Correspondence:**
Melanie A. Woodin, Department of Cell and Systems Biology, University of Toronto, 25 Harbord Street, Toronto, ON, Canada M5S 3G5.
e-mail: m.woodin@utoronto.ca

†***Present address:***
Jake Ormond, Canadian Centre for Behavioural Neuroscience, University of Lethbridge, Lethbridge, AB, Canada.

Paired pre- and postsynaptic activity in area CA1 of the hippocampus induces long-term inhibitory synaptic plasticity at GABAergic synapses. This pairing-induced GABAergic plasticity weakens synaptic inhibition due to a depolarization of the reversal potential for $GABA_A$ receptor-mediated currents (E_{GABA}) through a decrease in the function of the neuron-specific K^+–Cl^- cotransporter KCC2. When pairing-induced GABAergic plasticity is induced at feed-forward inhibitory synapses in the CA1, the decrease in inhibition produces an increase in the amplitude of Schaffer collateral-mediated postsynaptic potentials in pyramidal neurons. This form of inhibitory synaptic plasticity is termed disinhibition-mediated long-term potentiation (LTP). In the present study, we investigated whether disinhibition-mediated LTP is synapse specific. We performed these experiments in hippocampal slices prepared from adult Sprague Dawley rats. We found that the underlying depolarization of E_{GABA} is not restricted to the paired pathway, but rather is expressed to the same extent at unpaired control pathways. However, the overall strength of GABAergic transmission is maintained at the unpaired pathway by a heterosynaptic increase in GABAergic conductance. The pairing-induced depolarization of E_{GABA} at the paired and unpaired pathways required Ca^{2+}-influx through both the L-type voltage-gated Ca^{2+} channels and *N*-methyl-D-aspartic acid receptors. However, only Ca^{2+}-influx through L-type channels was required for the increased conductance at the unpaired pathway. As a result of this increased GABAergic conductance, disinhibition-mediated LTP remains confined to the paired pathway and thus is synapse specific, suggesting it may be a novel mechanism for hippocampal-dependent learning and memory.

Keywords: GABA, synaptic plasticity, spike-timing dependent plasticity, KCC2, chloride (Cl^-), LTP

INTRODUCTION

Inhibitory synaptic transmission plays a central role in regulating the output of neurons and neuronal circuits throughout the nervous system (Pouille and Scanziani, 2001; Markram et al., 2004; Akerman and Cline, 2006). Inhibitory synaptic plasticity can be induced by repetitively pairing pre- and postsynaptic activity at mature GABAergic synapses in the hippocampus (Woodin et al., 2003; Fiumelli and Woodin, 2007; Balena and Woodin, 2008; Lamsa et al., 2010), which results in a decrease in the strength of inhibition. The mechanism underlying this form of inhibitory spike-timing dependent plasticity (STDP) is a Ca^{2+}-dependent decrease in the function of KCC2 (Woodin et al., 2003; Balena et al., 2010), which is primarily responsible for maintaining neuronal Cl^- gradients in the mature CNS (Rivera et al., 1999; Blaesse et al., 2009).

In hippocampal area CA1, the firing of the presynaptic Schaffer collaterals produces a mixed postsynaptic potential (PSP) composed of an excitatory PSP (EPSP) and an overlapping inhibitory PSP (IPSP). The IPSP is generated disynaptically by Schaffer collateral-driven firing of GABAergic basket cells (Glickfeld and Scanziani, 2006), and normally arrives prior to the preceding EPSP reaching its maximal amplitude (Pouille and Scanziani, 2001). The effect of this overlapping IPSP is to profoundly attenuate the firing of the postsynaptic CA1 pyramidals (Pouille and Scanziani, 2001), an effect which can be at least partly explained by the ability of feed-forward inhibition to limit the degree to which dendritic EPSPs are able to depolarize the soma of the pyramidal neuron (Ormond and Woodin, 2009). We recently demonstrated that a form of inhibitory synaptic plasticity, termed disinhibition-mediated long-term potentiation (LTP), regulates the activity of pyramidal neurons in the hippocampus (Saraga et al., 2008; Ormond and Woodin, 2009). Disinhibition-mediated LTP occurs when repetitive pairing of pre- and postsynaptic activity weakens inhibition at feed-forward inhibitory synapses (Woodin et al., 2003), thereby potentiating Schaffer collateral-mediated PSPs (Ormond and Woodin, 2009) and increasing pyramidal neuron spiking (Saraga et al., 2008). Thus, plasticity at feed-forward inhibitory synapses has the potential to regulate the efficacy of synaptic transmission between areas CA3 and CA1, much like classic LTP expressed at glutamatergic synapses.

An important requirement for cellular mechanisms of learning and memory is that they demonstrate synapse specificity (Hebb, 1949; Marr, 1969; Albus, 1971). For example, the expression of glutamatergic LTP, thought to play a central role in hippocampal-dependent memory formation (Tsien et al., 1996; Morris and Frey, 1997), is input specific, meaning that LTP is largely restricted to the

pathway at which it was induced (Andersen et al., 1977; Engert and Bonhoeffer, 1997). Because the inhibitory plasticity underlying disinhibition-mediated LTP depends on a postsynaptic increase in intracellular chloride at feed-forward inhibitory synapses (Woodin et al., 2003; Ormond and Woodin, 2009), most of which are located on the soma (Glickfeld and Scanziani, 2006), we were doubtful that its expression would be confined to the set of synapses active during the induction. However, because the inhibitory effect of GABAergic transmission depends not just on the driving force for GABAergic currents, set primarily by chloride levels, but also on the size of the synaptic conductance, we investigated whether pairing might induce parallel changes in inhibitory synaptic conductance capable of confining disinhibition-mediated LTP to the pathway at which it was induced.

MATERIALS AND METHODS

BRAIN SLICE PREPARATION

Hippocampal brain slices were prepared from 50- to 75-day-old male Sprague Dawley rats as previously described (Ormond and Woodin, 2009). The Animal Care Ethics committee at the University of Toronto approved all experimental protocols. Briefly, rats were anesthetized with a mixture of xylazine and ketamine injected intraperitoneally (25 mg/kg), and the brain was perfused with chilled modified artificial cerebrospinal fluid (ACSF; saturated with 95% O_2/5% CO_2; pH 7.4, osmolarity ∼305 MΩ). Hippocampi were partially isolated by removing the midbrain and all cortex except that directly overlying the hippocampus, and 400 μm slices were cut with a Vibratome 1000 plus. Slices recovered for 1 h in 35–37°C ACSF saturated with 95% O_2/5% CO_2 (pH 7.4, osmolarity ∼305 mOsm).

ELECTROPHYSIOLOGY

Whole-cell recordings were made in oxygenated ACSF at 35–37°C from CA1 pyramidal cells. Pyramidal neurons were identified by the presence of an after-depolarization following action potential firing, as well as action potential accommodation during prolonged action potential trains. Recording pipettes were pulled from thin-walled borosilicate (TW-150F; World Precision Industries, Sarasota, FL, USA) to resistances of 5–8 MΩ with a Sutter Instruments P-87 (Novato, CA, USA). Pipettes were filled with: 130 mM potassium gluconate, 10 mM KCl, 10 mM HEPES, 0.2 mM EGTA, 4 mM ATP, 0.3 mM GTP, 10 mM phosphocreatine (pH 7.25, osmolarity 275–285 mOsm). Signals were amplified using an Axon Instruments MultiClamp 700b and digitized using an Axon Instruments Digidata 1322a (Molecular Devices, Sunnyvale, CA, USA). The bridge was balanced upon going whole-cell, and then monitored and adjusted as necessary throughout the recording (to a maximum of 10 MΩ/experiment). Extracellular stimulation was applied through a whole-cell recording pipette containing a silver chloride wire and filled with ACSF at a baseline recording frequency of 0.03 Hz. CNQX was used to block glutamatergic transmission for recordings of isolated IPSPs. APV, BAPTA, nimodipine, and CNQX were purchased from Sigma-Aldrich (ON, Canada).

Plasticity induction

Plasticity was induced by pairing extracellular stimulation with postsynaptic current injection (1 nA for 10 ms); synaptic stimulation occurred 1 ms after the beginning of the 10-ms pulse. During induction the postsynaptic cell typically fired two action potentials per pairing, with the first action potential occurring 2–4 ms after extracellular stimulation, and the second occurring about 5 ms after the first. Three-hundred pairings were made at a frequency of 5 Hz. During recordings of pharmacologically isolated inhibition, plasticity was only induced at synapses where the initial E_{GABA} value was between −70 and −80 mV.

Characterization of feed-forward inhibition, pathway independence, and stimulating electrode position

In experiments where E_{GABA} and GABAergic conductance were recorded (**Figures 1**, **2**, and **5**), interneurons were stimulated directly by placing the stimulating electrodes in *S. pyramidale*, on either side of the recorded neuron to stimulate the paired and unpaired pathways (**Figure 1A**). The independence of pathways was demonstrated by the confinement of short-term plasticity within pathways (**Figure A1** in Appendix). Four pulses at 20 Hz were applied to one pathway, followed by a pulse to other pathway; the protocol was then repeated with four pulses to the second pathway followed by one to the first. For each pathway, the ratio of the fourth to the first pulse was taken as the measure of short-term plasticity within the pathway, while the ratio of the single fifth pulse to the first pulse in the other recording gave the short-term plasticity between pathways.

In experiments where disinhibition-mediated LTP was recorded (**Figures 3**, **4**, and **6**), interneurons were not stimulated directly. In these experiments the stimulating electrodes were placed in the CA3 (**Figure 3Ai**). To verify that the recorded inhibition was feed-forward (activated by Schaeffer collateral-mediated excitation of interneurons), and not due to direct stimulation of inhibitory fibers, CNQX was perfused at the end of all mixed PSP recordings (**Figure 3Aii**) and its effect on the slope of the PSP vs. membrane potential (V_m) relationship was assessed; because glutamatergic EPSP amplitude does not show voltage dependence at the membrane potentials examined (Ormond and Woodin, 2009), the reduction in slope after CNQX can be attributed to reduced feed-forward inhibition. Application of 10 μM CNQX reduced the mean slope of the PSP vs. membrane potential (V_m) relationship for all recordings by 89%.

Measurement of E_{GABA}

E_{GABA} was determined in current clamp mode by evoking IPSPs from progressively more depolarized membrane potentials. The protocol for each E_{GABA} measurement consisted of 10 sweeps beginning with a negative current step (between −100 and −150 pA), with each subsequent step incremented by 25 pA; during each of these ten current steps an IPSP was evoked. These IPSPs were used to generate an IPSP–V_m curve (e.g., **Figure 1B**). IPSPs were stimulated with extracellular stimulating electrodes (described in Characterization of Feed-Forward Inhibition, Pathway Independence, and Stimulating Electrode Position) in the presence of 10 μM CNQX to block AMPA-mediated synaptic transmission. A linear regression of the IPSP amplitudes was then used to calculate the membrane potential dependence of IPSPs. The intercept of this line with the abscissa was taken as E_{GABA}. The slope of the same line was taken as a measure of relative

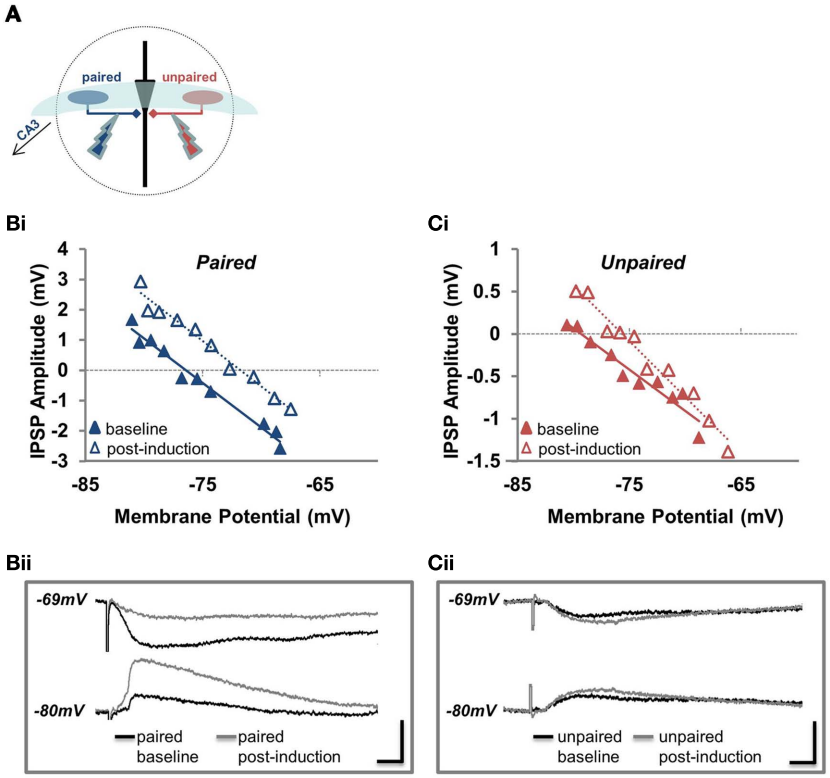

FIGURE 1 | E_{GABA} depolarizes and conductance increases at unpaired inhibitory synapses. (A) Position of the paired and unpaired stimulating electrodes for all experiments examining E_{GABA} depolarization and GABA conductance. **(Bi)** Example of a recording used to determine E_{GABA} at the paired pathway. IPSP amplitude plotted against V_m for the paired pathway before (baseline; solid blue triangles) and after pairing (post-induction; open blue triangles). **(Bii)** Sample traces from the experiment plotted in **(Bi)**. Current waveforms are overlaid from the baseline period (black) and from the last post-induction time point (gray), for relatively hyperpolarized and depolarized potentials. Scale bars: 2 mV, 10 ms. **(Ci)** Example of a recording used to determine E_{GABA} at the unpaired pathway. IPSP amplitude plotted against V_m for the unpaired pathway before (baseline; solid red triangles) and after pairing (post-induction; open red triangles). **(Cii)** Sample traces from the experiment plotted in **(Ci)**. Current waveforms are overlaid from the baseline period (black) and from the last post-induction time point (gray), for relatively hyperpolarized and depolarized potentials. Scale bars: 2 mV, 10 ms.

IPSP conductance, meaning slopes at different time points could be compared to determine whether conductance had changed. In some instances, when V_m was stepped to relatively depolarized potentials, the action potential threshold was reached and a spike was fired, which obscured the PSP. In these instances (such as **Figure 3Ci**), these data points were removed.

DATA ANALYSIS AND STATISTICS

Data was acquired using Axon Instruments Clampex 9 software, and analyzed using Axon Instruments Clampfit (Molecular Devices, Sunnyvale, CA, USA) as previously described (Ormond and Woodin, 2009). Results are expressed as mean ± SEM. All statistical tests were performed in SigmaStat (Systat Software, San Jose, CA, USA). Significance ($p < 0.05$) was determined using a two-way repeated measures ANOVA with *post hoc* Tukey test.

RESULTS

To investigate the synapse specificity of disinhibition-mediated LTP we first determined whether pairing-induced GABAergic plasticity was restricted to the stimulated pathway. To do this we made whole-cell patch-clamp recordings at 35–37°C from pyramidal neurons in hippocampal slices prepared from 50- to 75-day-old Sprague Dawley rats; GABAergic STDP is known to be expressed under whole-cell recording conditions (Woodin et al., 2003; Ormond and Woodin, 2009). We paired extracellular stimulation in *S. pyramidale* (see Characterization of Feed-Forward Inhibition, Pathway Independence, and Stimulating Electrode Position), the site of most interneurons providing feed-forward inhibition onto CA1 pyramidal neurons (**Figure 1A**; Pouille and Scanziani, 2001), with postsynaptic pyramidal neuron spiking evoked with intracellular current injection. We repeated this paired pre- and postsynaptic activity 300× at 5 Hz (see Plasticity Induction); from here forward we refer to this plasticity induction as "paired activity" (Woodin et al., 2003; Ormond and Woodin, 2009). We monitored E_{GABA} and GABAergic conductance at 5 min intervals before and after plasticity induction, at both the paired pathway where we stimulated plasticity, and at an unpaired (control) pathway. The extracellular stimulating electrode for the unpaired pathway was also placed in the *S. pyramidale*, but on the opposite sides of the recorded neuron (**Figure 1A**). The independence of these pathways was demonstrated by the confinement of short-term plasticity within pathways (see Characterization of Feed-Forward

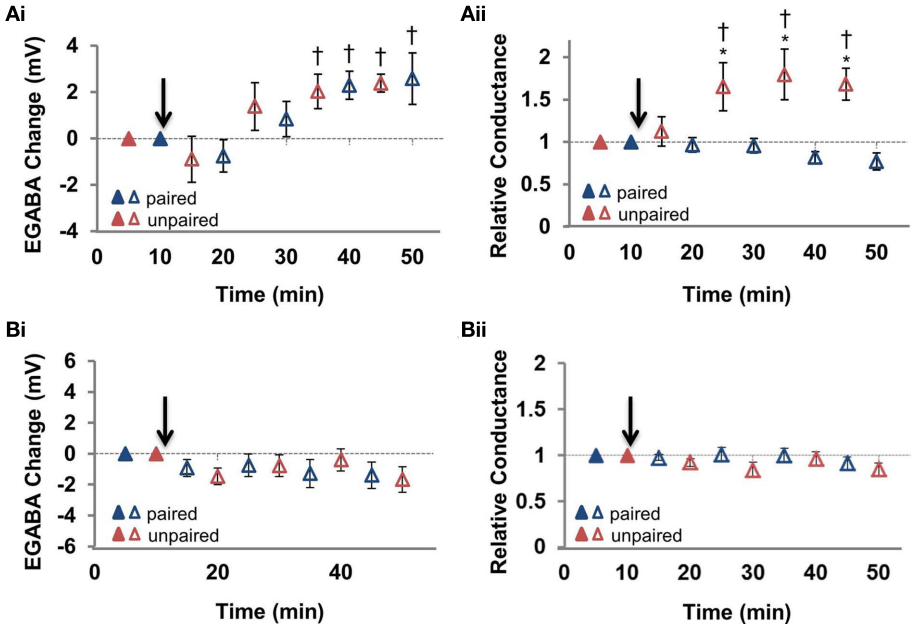

FIGURE 2 | Summary of the changes in E_{GABA} and conductance at the paired and unpaired pathways. (Ai) Summary of the change in E_{GABA} at the paired and unpaired pathways ($n = 6$). **(Aii)** Summary of the change in relative GABAergic conductance at the paired and unpaired pathways [for the same cells in **(Ai)**]. Blue triangles denote paired pathways, red triangles denote unpaired pathways; filled triangles represent baseline recordings, open triangles represent recordings following plasticity induction. **(Bi)** Summary of the change in E_{GABA} at the paired and unpaired pathways following stimulation of the postsynaptic neuron alone ($n = 7$). **(Bii)** Summary of the change in relative GABAergic conductance at the paired and unpaired pathways [for the same cells in **(Ai)**]. Blue triangles denote paired pathways, red triangles denote unpaired pathways; filled triangles represent baseline recordings, open triangles represent recordings following plasticity induction. IPSP–V_m curves were constructed at five time points, alternating between unpaired and paired pathways. Each of the five time points at the paired pathway were compared to the corresponding time point from the unpaired pathway.* Denotes statistical significance from unpaired pathway ($p < 0.05$). † Denotes statistical significance from baseline ($p < 0.05$). Paired activity denoted by arrow.

Inhibition, Pathway Independence, and Stimulating Electrode Position for detailed explanation; **Figure A1** in Appendix).

We found that paired activity induced a depolarization of E_{GABA} at the paired pathway (**Figures 1B** and **2Ai**; $p < 0.05$, $n = 6$): the magnitude of this depolarization is similar to that previously reported (Woodin et al., 2003; Ormond and Woodin, 2009). Likewise, E_{GABA} depolarized to a similar magnitude and with a similar time course at the unpaired control pathway (**Figures 1C** and **2Ai**; $p < 0.05$, $n = 6$), indicating that this form of synaptic plasticity is not pathway specific. However, synaptic conductance was significantly increased at the unpaired pathway (**Figures 1C** and **2Aii**; $p > 0.05$, $n = 6$). The absolute values of E_{GABA}, IPSP slope, and resting membrane potential (RMP) are listed in **Table 1**. Stimulation of only the postsynaptic neurons during the plasticity induction protocol failed to significantly alter E_{GABA} or conductance at the paired or unpaired pathways (**Figure 2B**; $p > 0.05$, $n = 7$). We have previously demonstrated, under the same recording conditions and in the same preparation, that E_{GABA} and GABAergic conductance does not significantly change during baseline recordings of the same duration as the recordings presented here (Ormond and Woodin, 2009).

We had initially hypothesized that if pairing-induced GABAergic plasticity was not synapse specific, then disinhibition-mediated LTP would also not be synapse specific. However our results demonstrating an increase in conductance accompanying the depolarization of E_{GABA} at unpaired pathways suggested our hypothesis might be false. To determine whether disinhibition-mediated LTP was in fact synapse specific we paired extracellular stimulation of the Schaffer collaterals in CA3 with postsynaptic pyramidal spiking (we were careful to place the stimulating electrode in the CA3 to avoid eliciting inhibition directly; **Figure 3Ai**; see Characterization of Feed-Forward Inhibition, Pathway Independence, and Stimulating Electrode Position for details). The absence of monosynaptic inhibition was confirmed at the end of recordings with CNQX, demonstrating that the majority of inhibition in these recordings was disynaptic and feed-forward (**Figure 3Aii**; see Characterization of Feed-Forward Inhibition, Pathway Independence, and Stimulating Electrode Position). This configuration allowed us to record mixed glutamatergic and GABAergic PSPs from pyramidal neurons; we refer to this recording configuration as "mixed recording." Following paired activity, we observed how the PSP amplitude changed relative to the membrane potential. In the example shown in **Figure 3B**, there was an increase in PSP amplitude at the paired pathway; this increase in PSP amplitude occurred at all membrane potentials from which PSPs were elicited (from −58 to −78 mV). However, the situation was different at the unpaired pathway; in the example shown in **Figure 3C**, there is an increase in PSP amplitude at −70 mV, but a decrease in amplitude at −60 mV. This suggests that the effect of inhibitory synaptic plasticity at the unpaired pathway,

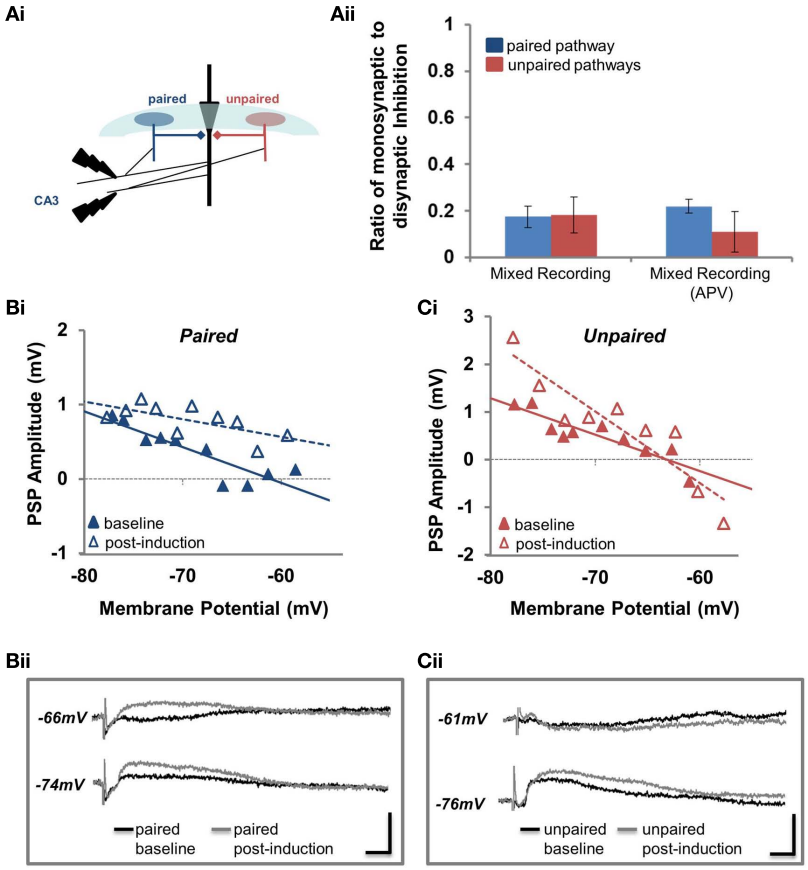

FIGURE 3 | Disinhibition-mediated LTP is pathway specific. (Ai) Position of the paired and unpaired stimulating electrodes for all experiments where inhibition was stimulated disynaptically. **(Aii)** The ratio of monosynaptic to disynaptic inhibition (see Materials and Methods for details) at the paired (blue) and unpaired (red) pathways for disinhibition-mediated LTP (mixed recording) experiments performed in the absence and presence of APV. **(Bi)** PSP amplitude is plotted against V_m for the paired pathway before (baseline; solid blue triangles) and after pairing (post-induction; open blue triangles). **(Bii)** Sample traces from the experiment plotted in **(Bi)**. Current waveforms are overlaid from the baseline period (black) and from the last post-induction time point (gray), for relatively hyperpolarized and depolarized potentials. Scale bars: 2 mV, 10 ms. **(Ci)** PSP amplitude is plotted against V_m for the unpaired pathway before (baseline; solid red triangles) and after pairing (post-induction; open red triangles). **(Cii)** Sample traces from the experiment plotted in **(Ci)**. Current waveforms are overlaid from the baseline period (black) and from the last post-induction time point (gray), for relatively hyperpolarized and depolarized potentials. Scale bars: 2 mV, 10 ms.

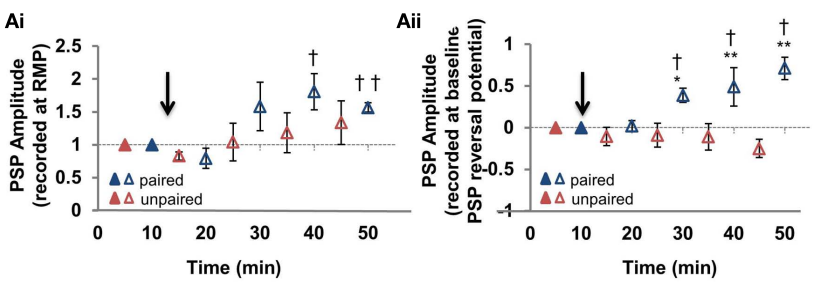

FIGURE 4 | Summary of disinhibition-mediated LTP pathway specificity. (Ai) Summary of the change in mixed PSP amplitude measured from the resting membrane potential, at the paired and unpaired pathways ($n = 6$). **(Aii)** Summary of the change in mixed PSP amplitude measured from the initial PSP reversal potential [for the same cells as in **(Ai)**]. Blue triangles denote paired pathways, red triangles denote unpaired pathways; filled triangles represent baseline recordings, open triangles represent recordings following plasticity induction. PSP–V_m curves were constructed at five time points, alternating between unpaired and paired pathways. Each of the five time points at the paired pathway were compared to the corresponding time point from the unpaired pathway. * Denotes statistical significance from unpaired pathway ($p < 0.05$). † Denotes statistical significance from baseline ($p < 0.05$). Paired activity denoted by arrow.

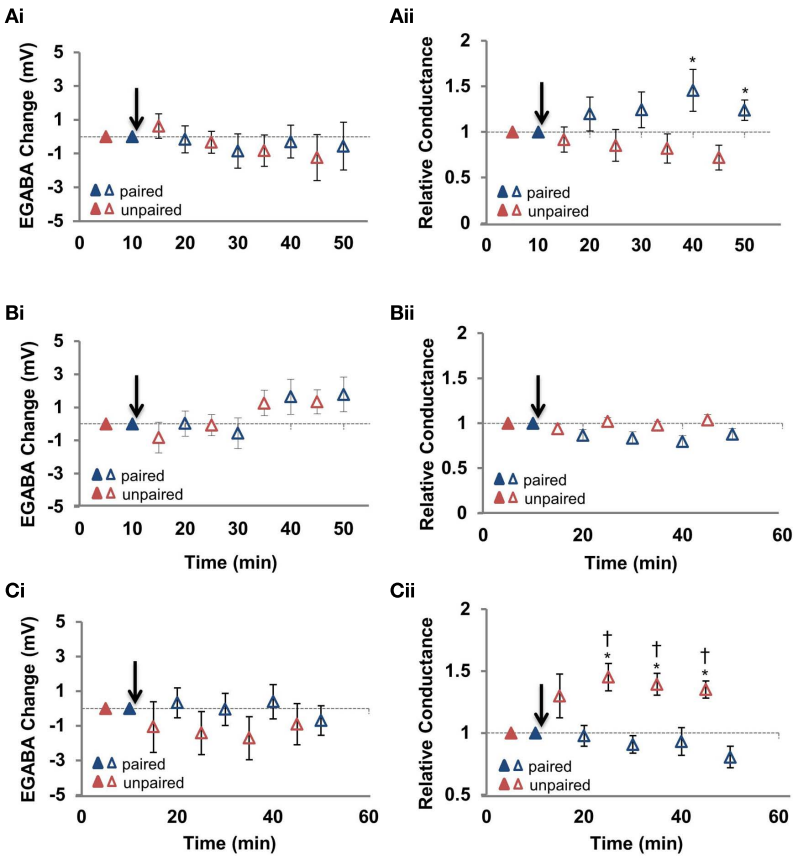

FIGURE 5 | *N*-methyl-D-aspartic acid receptor blockade with APV spares the increased GABAergic conductance at the unpaired pathway. (Ai) Summary of the change in E_{GABA} at the paired and unpaired pathways induced in the presence of cell-loaded BAPTA to chelate Ca^{2+} ($n = 5$). **(Aii)** Summary of the change in relative GABAergic conductance at the paired and unpaired pathways for all cells in **(Ai)**. **(Bi)** Summary of the change in E_{GABA} at the paired and unpaired pathways induced in the presence of bath applied nimodipine to block L-type Ca^{2+} channels (15 μM applied for the duration of the recording; $n = 5$). **(Bii)** Summary of the change in relative GABAergic conductance at the paired and unpaired pathways for all cells in **(Bi)**. **(Ci)** Summary of the change in E_{GABA} at the paired and unpaired pathways in the presence of bath applied APV to block NMDARs (25 μM applied for the duration of the recording; $n = 6$). **(Cii)** Summary of the change in relative GABAergic conductance at the paired and unpaired pathways for all cells in **(Ci)**. Blue triangles denote paired pathways, red triangles denote unpaired pathways; filled triangles represent baseline recordings, open triangles represent recordings following plasticity induction. IPSP–V_m curves were constructed at five time points, alternating between unpaired and paired pathways. Each of the five time points at the paired pathway were compared to the corresponding time point from the unpaired pathway. * Denotes statistical significance from unpaired pathway ($p < 0.05$). † Denotes statistical significance from baseline ($p < 0.05$). Paired activity denoted by arrow.

which is comprised of both E_{GABA} depolarization and increased conductance, depends on the membrane potential.

To examine this relationship more fully we used our PSP–V_m curves for each recording to calculate PSP amplitude at two membrane potentials: (1) the RMP (**Figure 4Ai**); and (2) the reversal potential of mixed PSPs recorded during the pre-induction baseline period (which was more depolarized than RMP; **Figure 4Aii**). Regardless of which PSP values we used (PSP amplitude at RMP or at initial PSP reversal potential), the paired pathway always demonstrated disinhibition-mediated LTP (**Figure 4**; $n = 6$; $p < 0.001$). However, at the unpaired pathway we did not observe disinhibition-mediated LTP. When RMP values were used (**Figure 4Ai**), there was neither a significant change from baseline ($p = 0.173$) nor from the potentiated pathway ($p = 0.345$). However, when measured from the baseline PSP reversal, our analysis showed that PSPs became slightly hyperpolarizing after pairing, making the paired and unpaired pathways significantly different (**Figure 4Aii**; $p < 0.001$). Because there is very little voltage dependence of EPSP amplitude in the range of membrane potentials we recorded (Ormond and Woodin, 2009), the voltage dependence of the change in PSP amplitude at the unpaired pathway strongly suggested the involvement of the GABAergic plasticity described above (**Figures 1** and **2**). Taken together, our recordings revealed that at the paired pathway the depolarization of E_{GABA} produced disinhibition-mediated LTP, while at the unpaired pathway the depolarization of E_{GABA} was counteracted by the increase in GABAergic conductance to prevent disinhibition-mediated LTP (**Figure 2Cii**). This counteracting effect increases when the membrane potential is depolarized.

To confirm that the increased GABAergic conductance at the unpaired pathway was in fact responsible for the synapse specificity

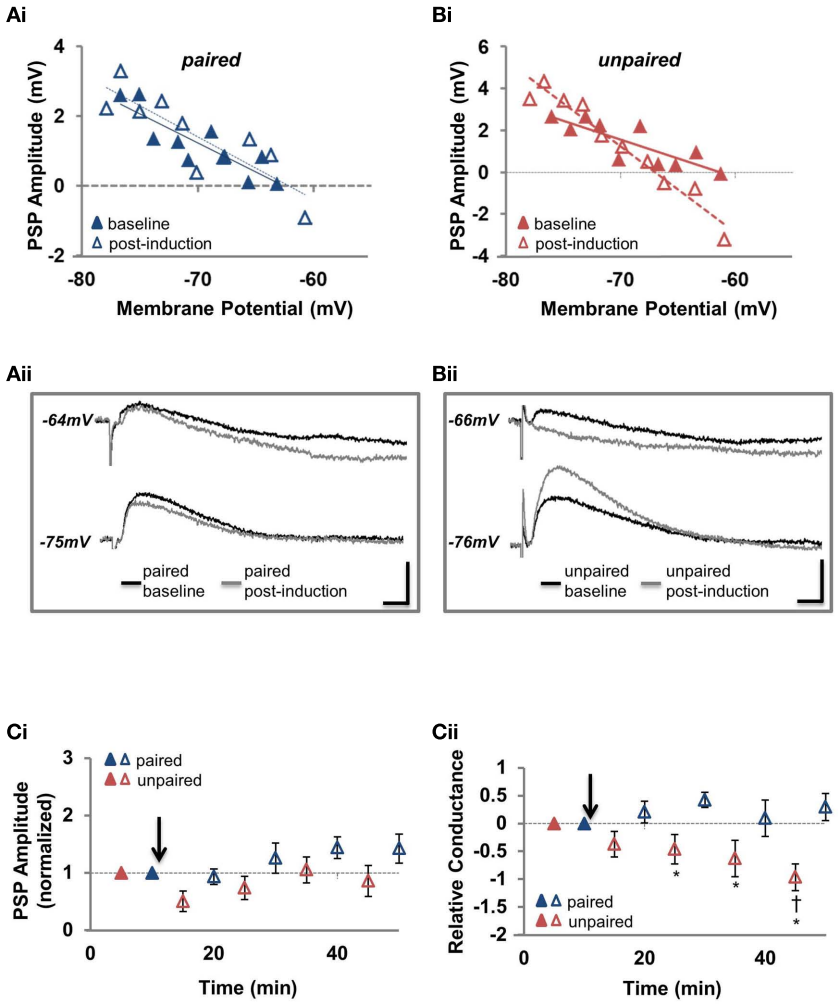

FIGURE 6 | *N*-methyl-D-aspartic acid receptor blockade reveals that increased GABAergic conductance at the unpaired pathway underlies the pathway specificity of disinhibition-mediated LTP. (Ai) Example recording of the PSP amplitude plotted against V_m for the paired pathway before and after pairing. **(Aii)** Sample traces before and after pairing for the same cell as in **(Ai)**. **(Bi)** Example recording of the PSP amplitude plotted against V_m for the unpaired pathway before and after pairing. **(Bii)** Sample traces before and after pairing for the same cell as in **(Bi)**. **(Ci)** Summary of the change in mixed PSP amplitude, measured from the resting membrane potential, at the paired and unpaired pathways with NMDARs antagonized ($n = 6$). **(Cii)** Summary of the change in mixed PSP amplitude, measured from the initial PSP reversal potential, at the paired and unpaired pathways with NMDARs antagonized [for the same cells as in **(Cii)**]. Blue triangles denote paired pathways, red triangles denote unpaired pathways; filled triangles represent baseline recordings, open triangles represent recordings following plasticity induction. PSP–V_m curves were constructed at five time points, alternating between unpaired and paired pathways. Each of the five time points at the paired pathway were compared to the corresponding time point from the unpaired pathway. * Denotes statistical significance from unpaired pathway ($p < 0.05$). † Denotes statistical significance from baseline ($p < 0.05$). Paired activity denoted by arrow.

of disinhibition-mediated LTP, we wanted to further examine the effect in pharmacological isolation from glutamatergic LTP and E_{GABA} depolarization. Because both glutamatergic LTP and pairing-induced E_{GABA} depolarization require an elevation in intracellular Ca^{2+} concentration, blocking this elevation seemed a logical approach for the first of these experiments. When postsynaptic Ca^{2+} was chelated by including 30 mM BAPTA in the pipette, both E_{GABA} and the increased conductance at the unpaired pathway were blocked (**Figures 5Ai,ii**); at the paired pathway, conductance increased slightly, and was significantly different from the unpaired pathway ($n = 6$; $p = 0.02$) but not baseline. Having failed to spare the increased conductance at the unpaired pathway, we next tried to block E_{GABA} depolarization using the L-type Ca^{2+} channel blocker nimodipine, as it has previously been reported to block the depolarization of E_{GABA} induced by pairing in hippocampal cell culture (Woodin et al., 2003). With nimodipine (15 μM) in the bath, pairing failed to produce a significant E_{GABA} depolarization at either pathway (**Figure 5Bi**; **Table 1**; $n = 6$; paired pathway $p = 0.162$, unpaired pathway $p = 0.137$). This suggests that E_{GABA} depolarization in hippocampal slices from adults also depends on Ca^{2+} entry through L-type Ca^{2+} channels. However, nimodipine also completely blocked the increase in GABAergic

Table 1 | Electrophysiological properties of CA1 pyramidal neurons. Reversal potential, PSP slope, and RMP are reported for baseline and post-induction recordings made during plasticity recordings at both paired and unpaired inputs.

	Reversal potential (mV)				Slope				RMP			
	Baseline		Post-induction		Baseline		Post-induction		Baseline		Post-induction	
	Mean	SEM	Mean	SEM	Mean	SEM	Mean	SEM	Mean	SEM	Mean	SEM
IPSP (CNQX) Figure 2												
Paired	−75.60	1.35	−73.02	2.11	−0.15	0.02	−0.12	0.03	−72.34	1.87	−71.60	1.59
Unpaired	−75.45	1.64	−73.07	1.44	−0.14	0.02	−0.22	0.02				
PSP (NO ANTAGONISTS) Figure 4												
Paired	−65.19	1.60	−51.87	4.63	−0.11	0.02	−0.09	0.02	−73.31	1.33	−73.16	1.21
Unpaired	−66.25	4.01	−67.13	4.15	−0.17	0.03	−0.20	0.02				
IPSP (CNQX AND NIMODIPINE) Figure 5A												
Paired	−74.14	0.67	−72.49	0.32	−0.26	0.02	−0.23	0.02	−73.38	0.95	−72.87	0.81
Unpaired	−74.62	0.64	−73.29	0.44	−0.34	0.03	−0.34	0.02				
IPSP (CNQX AND APV) Figure 5B												
Paired	−71.68	1.76	−72.67	2.20	−0.23	0.04	−0.19	0.04	−75.73	1.47	−75.35	1.34
Unpaired	−71.82	1.28	−72.56	2.25	−0.18	0.03	−0.24	0.03				
PSP (APV) Figure 6												
Paired	−62.10	1.04	−52.42	4.36	−0.12	0.02	−0.13	0.03	−72.77	1.24	−73.30	1.39
Unpaired	−62.63	1.90	−68.54	1.44	−0.10	0.02	−0.16	0.04				

conductance at the unpaired pathway (**Figure 5Bii**; **Table 1**; $n = 6$; $p = 0.551$), so it was of no use as a tool to isolate the increase in GABAergic conductance.

We next attempted to isolate the pairing-induced increase in conductance at the unpaired pathway with the *N*-methyl-D-aspartic acid receptor (NMDAR) antagonist APV. Previously, we found that pairing-induced depolarization of E_{GABA} is dependent on NMDARs (Ormond and Woodin, 2009), confirming the importance of postsynaptic Ca^{2+} influx for GABAergic plasticity demonstrated in hippocampal cell cultures and slices from juvenile animals (Woodin et al., 2003; Balena et al., 2010). NMDAR inhibition (with 25 μM APV) prevented E_{GABA} depolarization at both pathways (**Figure 5Ci**; **Table 1**; $n = 8$; paired pathway $p = 0.434$, unpaired pathway $p = 0.525$), but did not prevent the increase in conductance at the unpaired pathway (**Figure 5Cii**; **Table 1**; $n = 8$; $p < 0.05$), allowing us to test the ability of increased GABAergic conductance at the unpaired pathway to differentiate the gain of Schaffer collateral inputs relative to the paired pathway.

Our prediction was that this increase in conductance at unpaired synapses would depress PSP amplitude at depolarized membrane potentials in the absence of E_{GABA} depolarization. We returned to recording mixed PSPs (combined EPSPs and IPSPs; with the recording configuration in **Figure 3A**) and found that our prediction was correct. When PSPs were recorded at the RMP, there was no significant change seen at either pathway compared to baseline (**Figures 6A,B,Ci**; **Table 1**; $n = 6$; paired pathway $p = 0.147$, unpaired pathway $p = 0.617$) or between the two pathways ($p = 0.092$), but as the membrane was depolarized toward action potential threshold, the effect at the unpaired pathway became apparent. Specifically, when we calculated PSP amplitude at initial PSP reversal potential from our PSP–V_m plots (as in **Figure 4Aii**), we found PSPs became hyperpolarizing, indicating that the strength of inhibition was considerably increased relative to excitation (**Figures 6B,Cii**; **Table 1**; $p < 0.001$). These recordings confirm that increased synaptic conductance at the GABAergic synapses of the unpaired pathway underlies the synapse specificity of disinhibition-mediated LTP.

DISCUSSION

To our knowledge, this is the first report of a synapse specific enhancement of excitatory transmission by inhibitory plasticity. In our LTP recordings, we took great care to ensure we elicited inhibition physiologically in order to avoid overestimating its impact on disinhibition-mediated LTP. First, we confirmed inhibition was activated disynaptically to maintain the appropriate EPSP/IPSP delay, and to prevent the recruitment of additional non-feed-forward interneurons. Second, the chloride concentration (10 mM) used in our intracellular pipette maintains the driving force at the level measured when recording in the gramicidin perforated-patch configuration, which leaves intracellular chloride unperturbed (Ormond and Woodin, 2009); this is particularly important, as the effect of feed-forward inhibition on excitatory transmission can be enhanced artificially by increasing the driving force for Cl^- by lowering its concentration in the intracellular solution to levels below the physiological norm. Last, we used slices from adult rats in all experiments, as ongoing neural development, particularly as it relates to chloride regulation (Rivera et al., 1999), complicates the interpretation of data from younger animals. Highlighting this fact, we have previously shown using gramicidin perforated-patch recording that E_{GABA} hyperpolarizes a further 15 mV between 3 and 7 weeks of age (Ormond and Woodin, 2009), indicating that the developmental

changes involved in strengthening inhibition last much longer than the time it takes KCC2 expression to peak (Rivera et al., 1999).

While our data suggests that the pairing-induced depolarization of E_{GABA} is not synapse specific, it is entirely possible that the depolarization of E_{GABA} was confined to the soma if we were primarily stimulating somatic inhibitory synapses. Such a compartmentalized Cl^- regulation has been demonstrated in pyramidal cells of the cerebral cortex. In these cells, GABAergic inhibition is strongly depolarizing at the axon-initial segment, but not in the soma or dendrites, due to the absence of KCC2 expression (Szabadics et al., 2006) and the presence of the Na^+–K^+–$2Cl^-$ cotransporter NKCC1 in the axon (Khirug et al., 2008). In contrast, E_{GABA} is hyperpolarizing at the soma, and becomes progressively more negative with distance into the dendrites (Khirug et al., 2008). It will be interesting to examine in further studies whether the same phenomenon exists at inhibitory synapses made onto the distal dendrites of CA1 pyramidals, such as those made by the O-LM interneurons.

It is interesting to note that despite our results showing that the pairing-induced depolarization of E_{GABA} is not confined to the synapses at which it is induced, they also suggest a certain amount of synapse specific E_{GABA} regulation. This is because the value of E_{GABA} was never exactly the same at the paired and unpaired pathways (e.g., **Figures 1Bi,Ci**; unpublished observations). A recent study has shown that E_{GABA} can in fact be regulated locally at individual basket-cell synapses on the soma of CA1 pyramidals (Földy et al., 2010), so our observation is perhaps not so surprising. Nevertheless, current data suggests both global and local regulation of E_{GABA} at feed-forward inhibitory synapses in CA1. Thus, it should not be assumed that the pairing-induced E_{GABA} depolarization reported in the present study is expressed uniformly throughout the soma.

While many of the mechanisms underlying disinhibition-mediated LTP are likely quite different from those underlying classic LTP, there is one striking similarity. Classic LTP expression is accompanied by heterosynaptic plasticity expressed as a depression of glutamatergic transmission at control pathways which further differentiates the gain of test and control pathways (Lynch et al., 1977; Abraham and Goddard, 1983; Scanziani et al., 1996). This is not unlike the situation presented here, where the heterosynaptic GABAergic plasticity not only maintains inhibitory strength but actually strengthens it as the membrane potential is depolarized toward action potential threshold, enhancing the contrast between pathways.

Our results demonstrate that disinhibition-mediated LTP in the adult rodent hippocampus is synapse specific. The specificity arises from an increase in GABAergic conductance at the unpaired pathway that counteracts the non-specific increase in internal Cl^- concentration. We propose that disinhibition-mediated LTP may be a novel form of plasticity underlying learning and memory.

ACKNOWLEDGMENTS

This research was supported by a Natural Sciences and Engineering Research Council (NSERC) of Canada Graduate Scholarship to Jake Ormond and an NSERC Discovery Grant to Melanie A. Woodin.

REFERENCES

Abraham, W. C., and Goddard, G. V. (1983). Asymmetric relationships between homosynaptic long-term potentiation and heterosynaptic long-term depression. *Nature* 305, 717–719.

Akerman, C. J., and Cline, H. T. (2006). Depolarizing GABAergic conductances regulate the balance of excitation to inhibition in the developing retinotectal circuit in vivo. *J. Neurosci.* 26, 5117–5130.

Albus, J. (1971). A theory of cerebellar function. *Math. Biosci.* 28, 167–171.

Andersen, P., Sundberg, S. H., Sveen, O., and Wigstrom, H. (1977). Specific long-lasting potentiation of synaptic transmission in hippocampal slices. *Nature* 266, 736–737.

Balena, T., Acton, B. A., and Woodin, M. A. (2010). GABAergic synaptic transmission regulates calcium influx during spike-timing dependent plasticity. *Front. Synaptic Neurosci.* 2:16. doi: 10.3389/fnsyn.2010.00016

Balena, T., and Woodin, M. A. (2008). Coincident pre- and postsynaptic activity downregulates NKCC1 to hyperpolarize E(Cl) during development. *Eur. J. Neurosci.* 27, 2402–2412.

Blaesse, P., Airaksinen, M. S., Rivera, C., and Kaila, K. (2009). Cation-chloride cotransporters and neuronal function. *Neuron* 61, 820–838.

Engert, F., and Bonhoeffer, T. (1997). Synapse specificity of long-term potentiation breaks down at short distances. *Nature* 388, 279–284.

Fiumelli, H., and Woodin, M. A. (2007). Role of activity-dependent regulation of neuronal chloride homeostasis in development. *Curr. Opin. Neurobiol.* 17, 81–86.

Földy, C., Lee, S. H., Morgan, R. J., and Soltesz, I. (2010) Regulation of fast-spiking basket cell synapses by the chloride channel ClC-2. *Nat. Neurosci.* 13, 1047–1049.

Glickfeld, L. L., and Scanziani, M. (2006). Distinct timing in the activity of cannabinoid-sensitive and cannabinoid-insensitive basket cells. *Nat. Neurosci.* 9, 807–815.

Hebb, D. O. (1949). *The Organization of Behavior: A Neuropsychological Theory*. New York: Wiley.

Khirug, S., Yamada, J., Afzalov, R., Voipio, J., Khiroug, L., and Kaila, K. (2008). GABAergic depolarization of the axon initial segment in cortical principal neurons is caused by the Na-K-2Cl cotransporter NKCC1. *J. Neurosci.* 28, 4635–4639.

Lamsa, K., Kullmann, D. M., and Woodin, M. A. (2010). Inhibitory circuit plasticity. *Front. Synaptic Neurosci.* 2:8. doi: 10.3389/fnsyn.2010.00008

Lynch, G. S., Dunwiddie, T., and Gribkoff, V. (1977). Heterosynaptic depression: a postsynaptic correlate of long-term potentiation. *Nature* 266, 737–739.

Markram, H., Toledo-Rodriguez, M., Wang, Y., Gupta, A., Silberberg, G., and Wu, C. (2004). Interneurons of the neocortical inhibitory system. *Nat. Rev. Neurosci.* 5, 793–807.

Marr, D. (1969). A theory of cerebellar cortex. *J. Physiol. (Lond.)* 202, 437–470.

Morris, R. G., and Frey, U. (1997). Hippocampal synaptic plasticity: role in spatial learning or the automatic recording of attended experience? *Philos. Trans. R. Soc. Lond. B Biol. Sci.* 352, 1489–1503.

Ormond, J., and Woodin, M. A. (2009). Disinhibition mediates a form of hippocampal long-term potentiation in area CA1. *PLoS ONE* 4, e7224. doi: 10.1371/journal.pone.0007224

Pouille, F., and Scanziani, M. (2001). Enforcement of temporal fidelity in pyramidal cells by somatic feed-forward inhibition. *Science* 293, 1159–1163.

Rivera, C., Voipio, J., Payne, J. A., Ruusuvuori, E., Lahtinen, H., Lamsa, K., Pirvola, U., Saarma, M., and Kaila, K. (1999). The K+/Cl− co-transporter KCC2 renders GABA hyperpolarizing during neuronal maturation. *Nature* 397, 251–255.

Saraga, F., Balena, T., Wolansky, T., Dickson, C. T., and Woodin, M. A. (2008). Inhibitory synaptic plasticity regulates pyramidal neuron spiking in the rodent hippocampus. *Neuroscience* 155, 64–75.

Scanziani, M., Nicoll, R. A., and Malenka, R. C. (1996). Heterosynaptic long-term depression in the hippocampus. *J. Physiol. Paris* 90, 165–166.

Szabadics, J., Varga, C., Molnar, G., Olah, S., Barzo, P., and Tamas, G. (2006). Excitatory effect of GABAergic axo-axonic cells in cortical microcircuits. *Science* 311, 233–235.

Tsien, J. Z., Huerta, P. T., and Tonegawa, S. (1996). The essential role of hippocampal CA1 NMDA receptor-dependent synaptic plasticity in spatial memory. *Cell* 87, 1327–1338.

Woodin, M. A., Ganguly, K., and Poo, M. M. (2003). Coincident pre- and postsynaptic activity modifies GABAergic synapses by postsynaptic changes in Cl− transporter activity. *Neuron* 39, 807–820.

Conflict of Interest Statement: The authors declare that the research was conducted in the absence of any commercial or financial relationships that could be construed as a potential conflict of interest.

Received: 15 June 2011; accepted: 27 August 2011; published online: 19 September 2011.

Citation: Ormond J and Woodin MA (2011) Disinhibition-mediated LTP in the hippocampus is synapse specific. Front. Cell. Neurosci. ***5****:17. doi: 10.3389/fncel.2011.00017*

APPENDIX

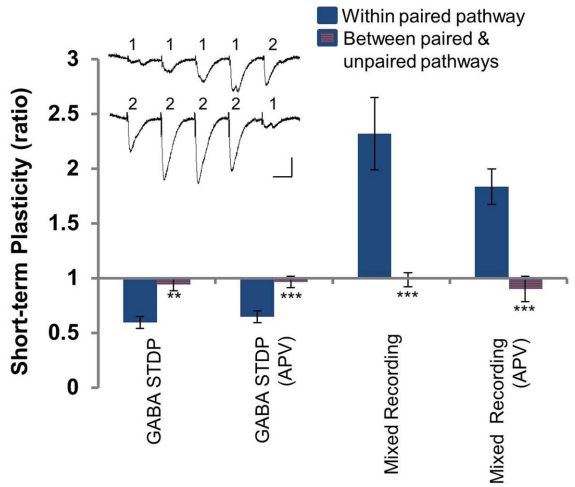

FIGURE A1 | Paired and unpaired pathways are independent. Short-term plasticity within the paired pathway (solid blue) and between the paired and unpaired pathways (blue and red hatched) for experimental conditions [GABA STDP, **Figures 1** and **2**; GABA STDP (APV), **Figure 5C**; Mixed LTP, **Figures 3** and **4**; Mixed LTP (APV), **Figure 6**]. Inset: sample recording demonstrating the protocol used. Scale bars: 50 pA, 25 ms. $*p < 0.05$; $**p < 0.005$; $***p < 0.001$.

frontiers in
CELLULAR NEUROSCIENCE

ORIGINAL RESEARCH ARTICLE
published: 01 November 2011
doi: 10.3389/fncel.2011.00023

Enhanced synaptic activity and epileptiform events in the embryonic KCC2 deficient hippocampus

Ilgam Khalilov[1,2,3‡], Geneviève Chazal[1,2,3‡], Ilona Chudotvorova[1,2,3†], Christophe Pellegrino[1,2,3], Séverine Corby[1,2,3], Nadine Ferrand[1,2,3], Olena Gubkina[1,2,3], Romain Nardou[1,2,3], Roman Tyzio[1,2,3], Sumii Yamamoto[1,2,3], Thomas J. Jentsch[4], Christian A. Hübner[5], Jean-Luc Gaiarsa[1,2,3], Yehezkel Ben-Ari[1,2,3] and Igor Medina[1,2,3]*

[1] *INSERM Unité 901, Marseille, France*
[2] *Université de la Méditerranée, UMR S901 Aix-Marseille 2, Marseille, France*
[3] *Institut de Neurobiologie de la Méditerranée, Marseille, France*
[4] *Leibniz-Institut für Molekulare Pharmakologie (FMP) and Max-Delbrück-Centrum für Molekulare Medizin (MDC), Berlin, Germany*
[5] *Institut für Humangenetik, University Hospital Jena, Friedrich Schiller University Jena, Jena, Germany*

Edited by:
Enrico Cherubini, International School for Advanced Studies, Italy

Reviewed by:
Kai Kaila, University of Helsinki, Finland
Raúl Eduardo Russo, Instituto de Investigaciones Biológicas Clemente Estable, Uruguay

***Correspondence:**
Igor Medina, Institut de Neurobiologie de la Méditerranée/INSERM Unité 901, 163 Route de Luminy, 13273 Marseille, France.
e-mail: medina@inmed.univ-mrs.fr

†Present address:
Ilona Chudotvorova, Brandeis University, 415 South Street, Waltham, MA 02453, USA.

‡Ilgam Khalilov and Geneviève Chazal have contributed equally to this work.

The neuronal potassium-chloride co-transporter 2 [indicated thereafter as KCC2 (for protein) and *Kcc2* (for gene)] is thought to play an important role in the post natal excitatory to inhibitory switch of GABA actions in the rodent hippocampus. Here, by studying hippocampi of wild-type ($Kcc2^{+/+}$) and *Kcc2* deficient ($Kcc2^{-/-}$) mouse embryos, we unexpectedly found increased spontaneous neuronal network activity at E18.5, a developmental stage when KCC2 is thought not to be functional in the hippocampus. Embryonic $Kcc2^{-/-}$ hippocampi have also an augmented synapse density and a higher frequency of spontaneous glutamatergic and GABA-ergic postsynaptic currents than naïve age matched neurons. However, intracellular chloride concentration ($[Cl^-]_i$) and the reversal potential of GABA-mediated currents (E_{GABA}) were similar in embryonic $Kcc2^{+/+}$ and $Kcc2^{-/-}$ CA3 neurons. In addition, KCC2 immunolabeling was cytoplasmic in the majority of neurons suggesting that the molecule is not functional as a plasma membrane chloride co-transporter. Collectively, our results show that already at an embryonic stage, KCC2 controls the formation of synapses and, when deleted, the hippocampus has a higher density of GABA-ergic and glutamatergic synapses and generates spontaneous and evoked epileptiform activities. These results may be explained either by a small population of orchestrating neurons in which KCC2 operates early as a chloride exporter or by transporter independent actions of KCC2 that are instrumental in synapse formation and networks construction.

Keywords: GABA, KCC2, neuron, development, synapse, network

INTRODUCTION

Kcc2 is a potassium-chloride co-transporter that is exclusively expressed in neurons of central nervous system (CNS; Payne et al., 1996; Williams et al., 1999). It plays an important role in regulating intracellular chloride concentrations ($[Cl^-]_i$), thereby heavily impacting the magnitude of the inhibitory action of GABA in physiological processes (Rivera et al., 1999). In a wide range of animal species and brain structures, $[Cl^-]_i$ is elevated in immature neurons leading to depolarizing and often excitatory actions of GABA (Ben-Ari et al., 1989, 2007; Leinekugel et al., 1997, 1999; Owens and Kriegstein, 2002; Caiati et al., 2010). GABA acquires progressively its hyperpolarizing actions in a time and brain structure dependent manner. In hippocampus of rat and mice, it is roughly completed by the second postnatal week. Extensive investigations suggest that this developmental sequence is determined by a progressive reduction of the NKCC1 chloride importer and a parallel progressive enhanced operation of the KCC2 chloride exporter (Rivera et al., 1999; Gulyas et al., 2001; Stein et al., 2004). The expression of KCC2 is thought to lead to a reduction of $[Cl^-]_i$ and a shift of the actions of GABA from excitation to inhibition, although other chloride regulators – channels and transporters – take part in this sequence (Medina and Chudotvorova, 2006; Blaesse et al., 2009).

Several observations suggest that KCC2 is less operational in immature than adult neurons. Thus, in the hippocampus of mice and rats KCC2 labeling is first detected at the end of embryonic development, peaking during the second postnatal week (Stein et al., 2004; Blaesse et al., 2006). KCC2 starts reducing $[Cl^-]_i$ in hippocampal pyramidal neurons 5 days after birth in rats (Khirug et al., 2005; Nardou et al., 2011). In addition, at P0–P1, KCC2 is in an inactive phosphorylated form (Rinehart et al., 2009) and forms monomers (Blaesse et al., 2006), whereas in mature structures (>P20), KCC2 is dephosphorylated (Rinehart et al., 2009) and is expressed as multimers (Blaesse et al., 2006). Collectively these studies suggest that in cortical structures of mice and rats the KCC2 is not functional as a transporter during embryonic development, starting to contribute to the neuronal ion homeostasis during the first postnatal week and becoming fully operational at P10–P15.

If KCC2 is not operative in embryos, its inactivation is expected to bear little effects on the embryonic maturation of brain networks. We now report that already at E18.5, *Kcc2*$^{-/-}$ mice hippocampal networks generate spontaneous epileptiform events and neurons have more GABA-ergic and glutamatergic synapses and currents than wild-type embryos (*Kcc2*$^{+/+}$) suggesting a requirement for the co-transporter in embryos. Yet, perforated patch-clamp recordings revealed no significant difference of $[Cl^-]_i$ between embryonic *Kcc2*$^{-/-}$ and *Kcc2*$^{+/+}$ hippocampal neurons and KCC2 was primarily cytoplasmic in *Kcc2*$^{+/+}$ suggesting that the co-transporter does not control $[Cl^-]_i$ in most embryonic pyramidal neurons of the hippocampus. These results are compatible with either a transport-unrelated function of embryonic KCC2 acting to control synapse formation and the emergence of networks and/or a cell autonomous action of KCC2 regulating $[Cl^-]_i$ in a small population of instructive neurons that play major roles in neuronal growth, synapse formation and network activity.

MATERIALS AND METHODS

ANIMALS AND GENOTYPING

The study was performed on E18.5 embryos of *Kcc2*$^{+/+}$ and *Kcc2*$^{-/-}$ mice as characterized previously (Hubner et al., 2001). The animal care and handling was performed in accordance with the guidelines of the European Union Council and the INSERM regulations on the use of laboratory animals.

HIPPOCAMPAL PREPARATION

Intact hippocampi were prepared as described previously (Khalilov et al., 1997). After cervical dislocation, the brain was removed quickly and submerged in ice-cold oxygenated (95% O_2/5% CO_2), choline-containing artificial CSF (ACSF) cutting solution, (in mM): 110 choline chloride, 2.5 KCl, 1.25 NaH_2PO_4, 0.5 $CaCl_2$, 7 $MgCl_2$, 25 $NaHCO_3$, 7 D-glucose, pH 7.4. The hemispheres were separated, and after removing the cerebellum, the frontal part of the neocortex, and surrounding structures, intact hippocampi were dissected from the septohippocampal complex and transferred into a beaker containing oxygenated ACSF containing (in mM):126 NaCl, 3.5 KCl, 2.0 $CaCl_2$, 1.3 $MgCl_2$, 25 $NaHCO_3$, 1.2 NaH_2PO_4, and 11 D-glucose (pH 7.4) and incubated at least 1 h before use. The intact hippocampi were placed into the conventional fully submerged chamber and superfused with oxygenated ACSF (30–32°C, 5–6 ml/min). The hippocampi were fixed by entomological needles to the sylgard-covered bottom.

Extracellular field potentials and multi unit activities (MUA) were recorded in the intact *in vitro* hippocampal preparations using tungsten wire electrodes (diameter: 50 μm, California Fine Wire, Grover Beach, CA, USA) and a low-noise multichannel DAM-8A amplifiers (WPI, GB; low filter: 0.1 Hz; high filter: 3 kHz; ×1000). Electrical stimulations were performed with a bipolar electrode (10–20 V, 40 μs). The signals were digitized using an analog-to-digital converter (Digidata 1440A, Axon Instruments, USA). pCLAMP 10.0.1.10 and Clampfit 10.1 (Axon Instruments, USA), MiniAnalysis 6.03 (Synaptosoft, Decatur, CA, USA) and Origin 7.5 (Microcal Software, USA) programs were used for the acquisition and analysis of Extracellular field potentials and MUA.

ACUTE HIPPOCAMPAL SLICES

Hippocampal transverse slices (300 μm) from the middle portion of each hippocampus were cut with a vibrating microtome (Leica VT 1000S, Germany) in ice-cold oxygenated (95% O_2/5% CO_2), choline-replaced ACSF and were incubated at room temperature in ACSF. Slices were allowed to recover for at least 90 min before recording.

Whole-cell recordings were performed from CA3 area in voltage clamp mode at different holding potential using Axopatch 200B (Axon Instruments, USA). The whole-cell patch pipettes had a resistance of 6–8 MΩ when filled with solution containing (in mM): 110 cesium methanesulfonate, 20 CsCl, 10 HEPES, 2 $MgCl_2$, 1 EGTA, 10 Na-phosphocreatine, 4 ATP–Mg, and 0.4 GTP–Na. The pH of the intracellular solutions was adjusted to 7.2 and the osmolarity to 280–290 mOsmol l^{-1}. The access resistance (15–30 MΩ) and input resistance (1–2 GΩ) were continuously monitored throughout the experiment. Occasional recordings with higher access resistance, lower input resistance, or those that displayed more than 20% changes in access and input resistances were discarded from analysis. External stimuli were applied using bipolar electrodes placed in the stratum radiatum (CA3 region). Stimulation intensity was adjusted during the first min of whole-cell recording to evoke 10–20 pA responses.

Gramicidin-perforated patch-clamp recordings were performed as described previously (Tyzio et al., 2003).

Drugs used were purchased from Sigma, (4-aminopyridine, 4-AP) or Tocris (bicuculline, CNQX, D-APV).

IMMUNOHISTOCHEMISTRY

The expression of KCC2 was studied by immunohistochemistry. Brains from E18.5 mice were fixed in paraformaldehyde 4% for 24 h, then embedded in optical cutting temperature (OCT) compound (Tissue-Tek, Sakura Finetek Inc., NL, USA) before serially cut, in 15 μm sections, with a cryostat. Selected sections were processed for immunocytochemistry. They were first incubated for 2 h, at room temperature, with a mixture of 5% normal goat serum (NGS) in PBS with 0.3% Triton X100. They were then, incubated overnight at 4°C with the primary antibody diluted in PBS with 1% NGS and 0.1% Triton X100. After rinsing in PBS, sections were incubated with the fluorescent-labeled secondary antibody (1/1000, Chemicon, France) for 1 h at room temperature. The primary antibodies were an anti-KCC2 antibody (rabbit; dilution 1/1000; US Biological, Euromedex, France) or an anti-synaptophysin antibody (mouse, dilution 1/150, Chemicon, France).

Images were taken using a Zeiss confocal microscope (Wetzlar, Germany). The quantitative analysis of the fluorescence was performed in blind using Metamorphe software (Roper Scientific, USA). For analysis, on each image we manually drew regions comprising stained tissue and excluding nuclei and casual irregularities (empty spaces). The threshold of the detection of fluorescence clusters was set as Mean + 3 SD of the fluorescence level in *Kcc2*$^{-/-}$ sections. The classification of the KCC2-positive neurons to groups "cytoplasm" or "membrane region" was done manually relying on the detectable fluorescence band on the periphery or center of the cell. All acquisitions and analysis were done blind.

RESULTS

EPILEPTIFORM EVENTS IN EMBRYONIC *Kcc2*$^{-/-}$ HIPPOCAMPUS

Field recordings of ongoing neuronal activity in intact hippocampi isolated from E18.5 *Kcc2*$^{+/+}$ and *Kcc2*$^{-/-}$ embryos revealed major differences between genotypes. In accordance with earlier studies, wild-type hippocampi generated the characteristic network recurrent population events that were reminiscent of giant depolarizing potentials (GDPs; Ben-Ari et al., 1989, 2007; Khalilov et al., 1999). In striking contrast, in *Kcc2*$^{-/-}$ hippocampi, the spontaneous network events were significantly more frequent, longer-lasting, had higher amplitudes, and contained more spikes (**Figures 1A,B**). Another difference was that while in wild-type hippocampi 98.3% of spontaneous events had characteristic bi-phasic form (examples in **Figures 1A** and **2A**, six experiments, 10 analyzed events per experiment), in *Kcc2*$^{-/-}$ hippocampi the majority of spontaneous events (72.7%, $n = 5$, 30 events per experiment) had sharp tri-phasic form (see example in **Figure 2B**). These electrical activities were similar to epileptiform events observed in epileptic tissue (Cohen et al., 2002; Khalilov et al., 2003; Nardou et al., 2009, 2011; Wittner et al., 2009). Consistent with different spontaneous activities, evoked field potentials in *Kcc2*$^{-/-}$ hippocampi differed clearly from those evoked in *Kcc2*$^{+/+}$ structures (**Figures 1A,B**).

To characterize the contribution of GABA-ergic and glutamatergic neurotransmission into generation of the spontaneous network activities we first exposed acute hippocampi to a CNQX, a blocker of AMPA receptors, and found that it fully abolished spontaneous events in both *Kcc2*$^{+/+}$ and *Kcc2*$^{-/-}$ hippocampi (not shown, $n = 5$ per condition). By contrast, the application of Bicuculline, a $GABA_A$ receptor antagonist, exerted different effects on *Kcc2*$^{+/+}$ and *Kcc2*$^{-/-}$ hippocampi. In wild-type structure it produced a transient (4–5 min) inhibition of the spontaneous GDPs (**Figure 2A**). During first 4 min of the exposure to bicuculline the frequency decreased more than fourfold from $(3.5 \pm 0.5) \times 10^{-3}$ Hz to $(0.6 \pm 0.1) \times 10^{-3}$ Hz, $n = 6$. This is in keeping with the important contribution of depolarizing GABA in their generation (see Ben-Ari et al., 1989; Khalilov et al., 1999; Ben-Ari et al., 2007; Cherubini et al., 2011). However, within longer time, the bicuculline led to the generation of interictal-like events (IILE) [$(6.8 \pm 0.7) \times 10^{-3}$ Hz, $n = 6$] reflecting the dual action of GABA, a depolarization, and a shunting action that, when blocked, enhances neuronal excitability (Khalilov et al., 1999). In contrast to naïve hippocampi, the ongoing spontaneous network activities recorded in *Kcc2*$^{-/-}$ hippocampi were fully blocked by bicuculline even during long-lasting applications. As shown in **Figure 2B**, ongoing activity did not re-appear even after >20 min of application ($n = 5$). To unravel synchronized activities, we applied the K^+ channel blocker 4-aminopyridine (4-AP, 100 μM, $n = 6$) that triggered IILEs similar to those observed spontaneously prior to the application of bicuculline (**Figure 2B**). Thus, embryonic *Kcc2*$^{-/-}$ hippocampi generate spontaneous events that require depolarizing/excitatory actions of GABA as they are fully blocked by GABA receptor antagonists. Yet, the properties of these events are reminiscent of events recorded in epileptic tissues (Cohen et al., 2002; Khalilov et al., 2003). Understanding of the cellular and molecular perturbations leading to

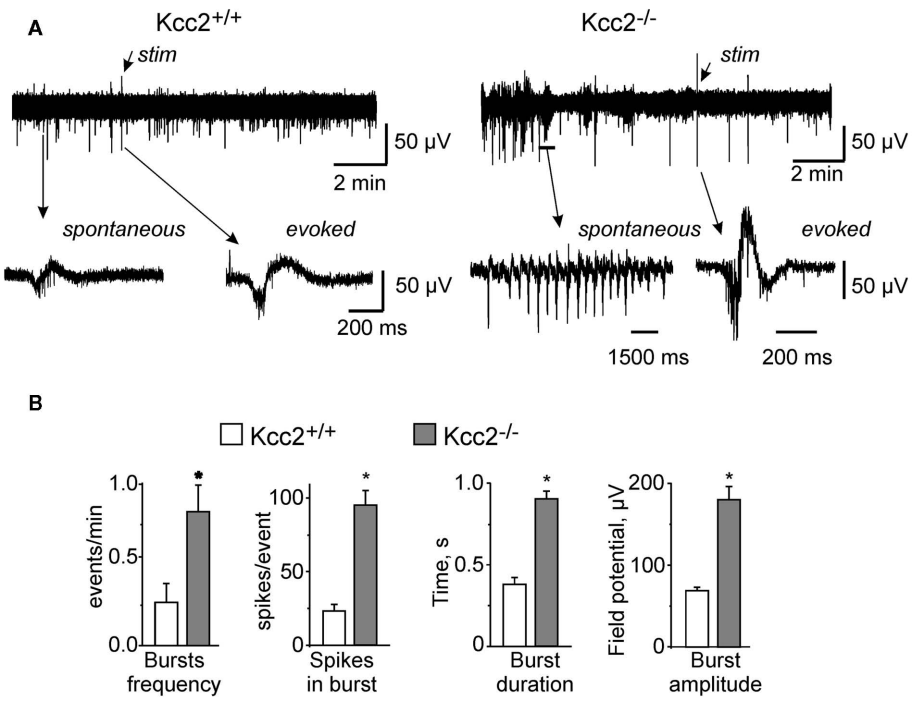

FIGURE 1 | Ongoing neuronal network activities in hippocampi (E18.5) from wild-type (*Kcc2*$^{+/+}$) and *Kcc2 knock-out* (*Kcc2*$^{-/-}$) mice. (A) Examples of field potential recordings from intact hippocampi of *Kcc2*$^{+/+}$ (left) and *Kcc2*$^{-/-}$ (right) mice. **(B)** Mean ± SEM data characterizing spontaneous events in experiments similar to those illustrated in **(A)**, $n = 9$. * = $P < 0.01$, *t*-test.

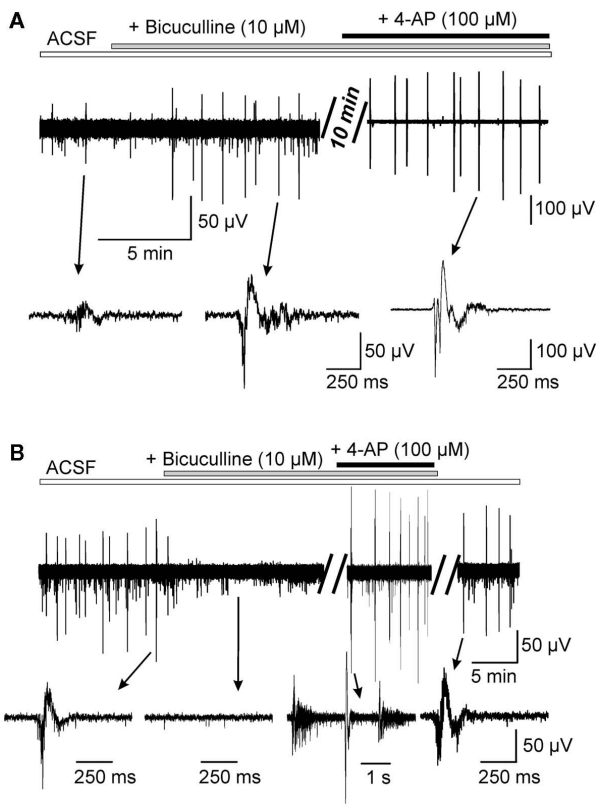

FIGURE 2 | Differential effects of the bicuculline on the spontaneous network activity in *Kcc2*$^{+/+}$ (A) and *Kcc2*$^{-/-}$ (B) acute hippocampi. Field potential recordings from the CA3 region of E18.5 hippocampi. Notice that in *Kcc2*$^{+/+}$ hippocampi the application of the bicuculline produced transient inhibition of spontaneous GDPs, whereas in *Kcc2*$^{-/-}$ hippocampi it produced long-lasting inhibition of spontaneous epileptiform activity.

change of the network properties in embryonic *Kcc2*$^{-/-}$ hippocampi and in epileptic tissue is an important subject for separate study.

PREMATURE FUNCTIONAL EXPRESSION OF GLUTAMATERGIC PSCs IN *Kcc2*$^{-/-}$ NEURONS

To determine the alterations of GABA and glutamatergic postsynaptic currents (PSCs) in *Kcc2*$^{-/-}$ in comparison to naïve neurons, we used whole-cell recordings from CA3 pyramidal neurons. We showed previously that in immature rat hippocampus most of CA1 pyramidal neurons are silent (Tyzio et al., 1999). In agreement with this, 14 out of 19 neurons recorded in E18.5 *Kcc2*$^{+/+}$ mice hippocampi were fully silent, generating neither spontaneous nor evoked PSCs (**Figure 3A**$_1$), four neurons showed GABA PSCs (**Figure 3A**$_{3,4}$), one neuron generated both GABA and glutamate PSCs but none had only glutamate PSCs as summarized in **Figure 3D**. In striking contrast, in *Kcc2*$^{-/-}$ slices most neurons were already active at the same age; only 5 out of 22 recorded neurons were silent, 17 neurons showed spontaneous GABA-ergic and/or glutamatergic PSCs (**Figures 3B,D**). Also, electrical stimuli generated long-lasting multisynaptic responses in *Kcc2*$^{-/-}$ slices that were never observed in *Kcc2*$^{+/+}$ slices ($n = 19$; **Figure 3C**).

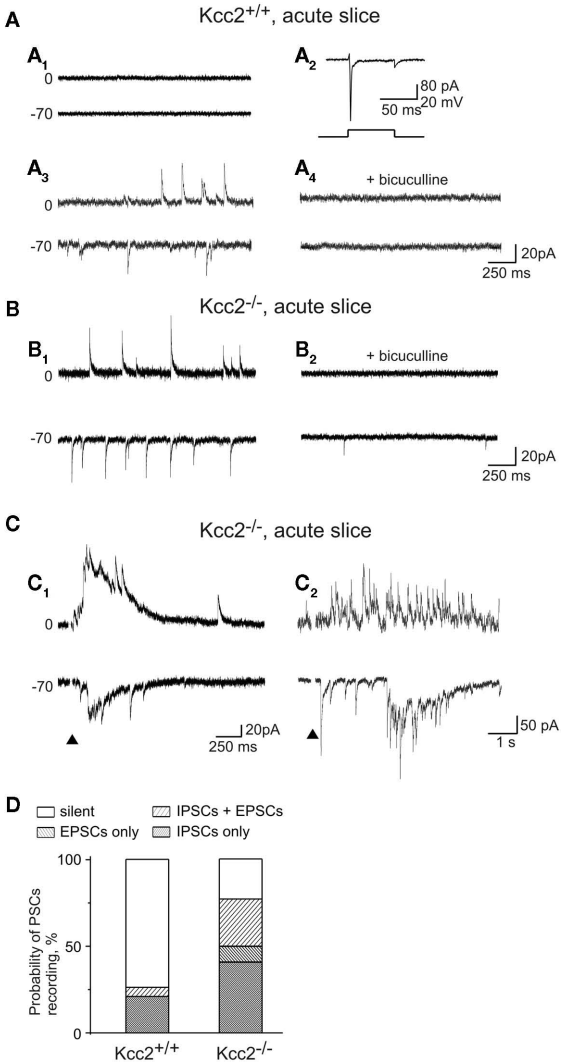

FIGURE 3 | Increased synaptic activity of CA3 pyramidal neurons in *Kcc2*$^{-/-}$ *hippocampus.* **(A)** Representative recordings of spontaneous synaptic activity in slices from *Kcc2*$^{+/+}$ mouse hippocampus. Most neurons were synaptically silent **(A$_1$)** although spikes could be induced by the application of positive voltage step **(A$_2$)**. Only few neurons showed spontaneous synaptic activity **(A$_3$)**. In the illustrated neuron all postsynaptic currents were GABA-mediated (GABA PSCs) as they had long-lasting kinetic, reversed at −30 mV and were inhibited by bicuculline **(A$_4$)**. **(B)** Spontaneous postsynaptic currents in *Kcc2*$^{-/-}$ neurons **(B$_1$).** Application of bicuculline revealed the presence of spontaneous glutamatergic postsynaptic currents (glutamate PSCs) at $V_h = -70$ mV **(B$_2$)**. The amplitude and kinetic of electrically isolated spontaneous GABA PSCs ($V_h = 0$ mV) did not differ in *Kcc2*$^{+/+}$ and *Kcc2*$^{-/-}$ neurons (statistics not shown). **(C)** Evoked postsynaptic responses in *Kcc2*$^{-/-}$ neurons lasting from hundreds of milliseconds **(C$_1$)** to few seconds **(C$_2$)**. **(D)** Relative proportion of silent neurons and neurons generating spontaneous GABA PSCs and/or glutamate PSCs in CA3 region of *Kcc2*$^{+/+}$ (19 neurons, six experiments) and *Kcc2*$^{-/-}$ (22 neurons, six experiments) hippocampal slices.

Consistent with the electrophysiology data, immunolabeling with anti-synaptophysin antibody revealed significant differences between *Kcc2*$^{-/-}$ and *Kcc2*$^{+/+}$ hippocampal sections (**Figure 4**).

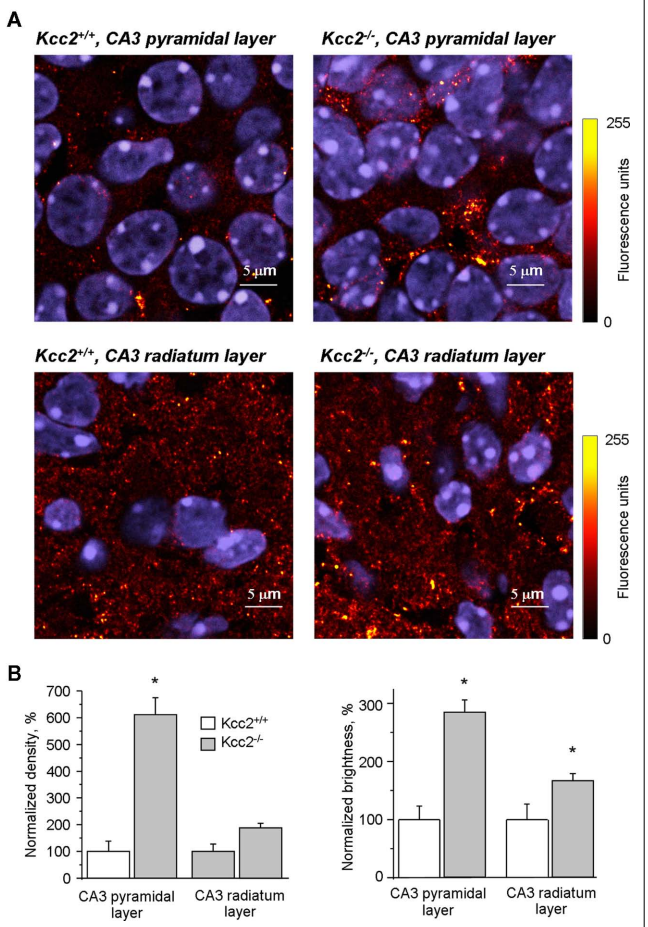

FIGURE 4 | Immunofluorescence of synaptophysin in CA3 hippocampal neurons. (A) Synaptophysin and DAPI fluorescence in CA3 pyramidal and radiatum cell layers of $Kcc2^{+/+}$ and $Kcc2^{-/-}$ hippocampi as indicated. Immunofluorescence of synaptophysin was pseudocolored (see scale on the right) for better cluster visualization. Immunofluorescence of DAPI is shown in blue. **(B)** Normalized density and brightness of synaptophysin positive clusters in CA3 pyramidal layer and CA3 radiatum layer of $Kcc2^{+/+}$ and $Kcc2^{-/-}$ hippocampi. Mean ± SEM, $n = 3$; * = $P < 0.05$, *t*-test.

Blind analysis revealed that *Kcc2* silencing induced a sixfold increase in the density of synaptophysin-positive clusters in CA3 pyramidal layer and twofold increase in CA3 stratum radiatum layer (**Figure 4B**, left panel). Moreover, in addition to increase of cluster density, there was also a significant increase of cluster brightness in $Kcc2^{-/-}$ sections (2.8-fold in pyramidal layer and 1.6-fold in radiatum layer; **Figure 4B**, right panel) indicating an enhanced synapse formation in $Kcc2^{-/-}$ versus $Kcc2^{+/+}$ mice. Thus, KCC2 controls the development of synaptic connections in the embryonic mice hippocampi.

EMBRYONIC KCC2 IMMUNOLABELING IS CYTOPLASMIC IN MOST NEURONS

As shown in **Figure 5A**, KCC2 was clearly detectable in CA3 pyramidal region of $Kcc2^{+/+}$ already 1 day before birth (E18.5), but not in $Kcc2^{-/-}$ hippocampi. In E18.5 sections the average intensity of KCC2 immunofluorescence in both CA3 pyramidal and radiatum layers was at least twofold higher than the background fluorescence measured in $Kcc2^{-/-}$ sections and constituted approximately 50% of the KCC2 immunofluorescence measured in sections obtained from older (P7) $Kcc2^{+/+}$ animals (**Figure 5B**). At E18.5 the KCC2-positive immunofluorescence was detected in 13.1 ± 1.9% ($n = 3$) of CA3 pyramidal neurons (**Figure 5C**). In the remaining 86.9 ± 1.9%, the level of KCC2 immunofluorescence was within the range of background variability (<mean + 3 SD; **Figure 5C**). Among KCC2-positive neurons, in the majority of cells the labeling was localized in the cytoplasm (**Figure 5A**, insert *i1*). Only 17.8% of KCC2-positive neurons (corresponding to 2.3 ± 0.5% of all analyzed neurons) included KCC2 in membrane region (**Figure 5A**, insert *i2*). Consistent with previous reports (Rivera et al., 1999; Stein et al., 2004), the expression of the KCC2 increased during development: at P7 82.7 ± 0.9% neurons were KCC2-positive and 79.3% of these neurons expressed KCC2 in their membrane region (**Figure 5A**, insert *i4* and **Figure 5C**).

Thus, already during embryonic hippocampal development, there is an expression of the KCC2 in individual neurons of CA3 pyramidal layer that is mainly localized in the cytoplasm. Some neurons at this stage of development start to express KCC2 in membrane region.

E_{GABA} IS DEPOLARIZING IN $Kcc2^{+/+}$ AND $Kcc2^{-/-}$ MICE

Earlier studies using perforated patch-clamp recordings [at P1–P3 (Stein et al., 2004)] or single channel analysis (Tyzio et al., 2007) have shown that E_{GABA} was strongly depolarizing in embryonic CA3 and CA1 pyramidal neurons, respectively. Using gramicidine-perforated patch-clamp recordings, we did not find a significant difference between E_{GABA} recorded from CA3 neurons of $Kcc2^{+/+}$ and $Kcc2^{-/-}$ embryonic hippocampi ($P = 0.87$, **Figure 5D**) confirming that $[Cl^-]_i$ is not regulated at this early developmental stage by KCC2. It is however possible that in naïve neurons KCC2 plays an important role in a small subpopulation of neurons (see Discussion).

DISCUSSION

The most conspicuous result of our study is that the ongoing neuronal activity is dramatically increased in hippocampi isolated from $Kcc2^{-/-}$ embryos when compared to age matched naïve structures. $Kcc2^{-/-}$ embryonic CA3 neurons express more GABA-ergic and glutamatergic PSCs, possess higher density of synaptic connections and show generation of epileptiform activities. Clearly, abolishing KCC2 accelerates synapse formation and enhances neuronal and network activity, suggesting that KCC2 modulates neuronal maturation, synapse formation and network operation at embryonic stage. The generation of epileptiform activities by networks deprived of KCC2 may impact the construction of functional networks illustrating the importance of this co-transporter for proper murine hippocampus development already *in utero*. This finding is not readily compatible with the suggested lack of embryonic function of the co-transporter (see Medina and Chudotvorova, 2006; Blaesse et al., 2009 for review). We show that although KCC2 does not appear to regulate

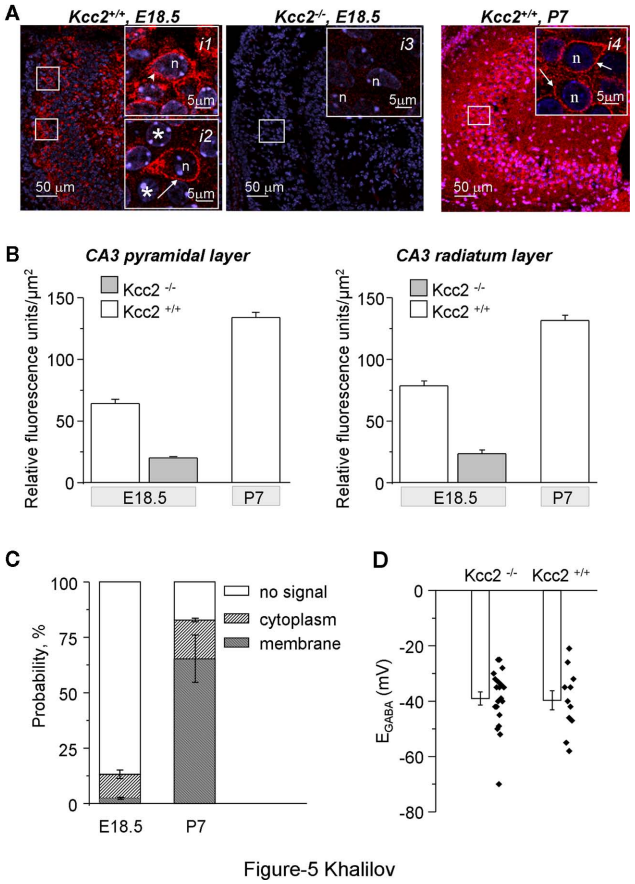

Figure-5 Khalilov

FIGURE 5 | Expression of the KCC2 in CA3 hippocampal neurons. (A) Immunoreactivity of KCC2 (red) in CA3 pyramidal neurons of *Kcc2*$^{+/+}$ and *Kcc2*$^{-/-}$ mouse as indicated. Notice the absence of the KCC2-positive immunoreactivity in *Kcc2*$^{-/-}$ samples characterizing high specificity of the antibody. The arrowhead in insert *i1* illustrates typical KCC2-positive CA3 neuron in E18.5 *Kcc2*$^{+/+}$ hippocampi with immunoreactivity localized in cytoplasm. Asterisks in insert *i2* indicate KCC2-negative neurons, whereas arrow indicates a rare neuron with KCC2 immunoreactivity localized in membrane region. For comparison, insert *i4* illustrates a typical KCC2 immunoreactivity distribution in CA3 neurons of P7 *Kcc2*$^{+/+}$ mouse that is localized in most of neurons in membrane region (shown by arrows). n = nucleus. **(B)** Quantification of the KCC2 immunoreactivity in CA3 pyramidal and radiatum layers of *Kcc2*$^{-/-}$ (E18.5) and *Kcc2*$^{+/+}$ (E18.5 and P7) hippocampi. Mean ± SEM, $n = 3$. The difference between any two values in both plots is highly significant ($P < 0.01$, *t*-test). **(C)** Age-dependent distribution of neurons' populations expressing KCC2 in membrane region ("membrane"), in the cytoplasm only ("cytoplasm"), and without detectable KCC2 immunoreactivity ("no signal"). Normalized values obtained after analysis of 50–100 neurons per animal, $n = 3$ *Kcc2*$^{+/+}$ mice per age. The background (no signal) level of fluorescence was determined after analysis of the immunofluorescence of sections prepared from E18.5 *Kcc2*$^{-/-}$ mice ($n = 3$; see Materials and Methods for details on fluorescence analysis). **(D)** Reversal potential of isoguvacine-induced responses in CA3 hippocampal neurons measured using gramicidin-perforated patch-clamp recording. Mean ± SEM, $n = 6$ mice per condition, two to four neurons per mouse. Dots show values in individual measurements. There was no difference in mean values of E_{GABA}.

intracellular chloride levels (but see below), its inactivation leads to change of neuronal network and, thus, raises important issues concerning its embryonic roles. Interestingly, genetic ablation of the NKcc1 chloride importer delays brain development with less functional synapses (Pfeffer et al., 2009; Marissal, Ben-Ari, unpublished data), but also see Sipila et al. (2006) suggesting that the two co-transporters act in opposite directions on these parameters as well.

CHLORIDE INDEPENDENT ACTIONS OF KCC2 ON EMBRYOS

There is a general consensus that the expression of the KCC2 starts during postnatal stages of the development of hippocampi in rat and mice (Stein et al., 2004; Blaesse et al., 2006; Zhu et al., 2008). This also implies a progressive externalization of the co-transporter possibly mediated by a developmental sequence of the phosphorylation mechanisms recently reported (Rinehart et al., 2009; Lee et al., 2010). Our observations of a similar E_{GABA} in *Kcc2*$^{-/-}$ and *Kcc2*$^{+/+}$ is in keeping with this suggestion and with the largely depolarizing action of GABA at early stages (Ben-Ari et al., 2007). A recent study elegantly showed that a regulatory action of KCC2 in immature neurons might indeed develop through an ion transport-independent mechanism, as the overexpression of inactive N-terminus KCC2 deleted construct produced similar to wild-type KCC2 effects (Horn et al., 2010). Similar results, but different conclusions concerning the mechanisms of KCC2 action, were obtained by Cancedda et al. (2007) who showed that viral overexpression of the KCC2 in immature cortical neurons slows-down neuronal maturation. Our work is the first study showing that endogenous KCC2 and not only artificially expressed KCC2, regulate maturation in immature neurons.

ALTERNATIVE POSSIBILITIES OF REGULATORY ACTIONS OF KCC2 IN EMBRYONIC HIPPOCAMPUS

Can we completely exclude the contribution of chloride shifts in the effects of KCC2 ablation? The finding that a GABA receptor antagonist generates epileptiform activities in naïve neurons – after long-lasting applications – but block fully ongoing activities generated by *Kcc2*$^{-/-}$ embryos is intriguing as it suggests that excitatory actions of GABA are enhanced in the *Kcc2* deficient in comparison to control mice. This stands in apparent contradiction with the similar E_{GABA} in *Kcc2*$^{-/-}$ and *Kcc2*$^{+/+}$. However, there are many observations showing that chloride levels play important roles at embryonic stages in selective cell populations. Thus, in developing neocortex, while the majority of pyramidal cells and interneurons are KCC2-negative, some interneurons express high amount of KCC2 and the activity of this transporter orchestrates interneuron migration (Bortone and Polleux, 2009). In keeping with this, bicuculline alters neuronal migration *in vitro* (Manent et al., 2005). In the present work we report an existence of small population of neurons with KCC2 expressed in membrane region (**Figure 5**). Thus, one chloride-based alternative possibility is that the loss of the co-transporter affects a subpopulation of neurons impacting the entire network. One more possibility could be that naïve KCC2-positive neurons exhibit difference in $[Cl^-]_i$ homeostasis on the level of dendrites, but not soma. Studies show the existence of KCC2-dependent somato-dendritic gradient of chloride in mature hippocampal neurons (Khirug et al., 2008; Pellegrino et al., 2011). Testing these hypotheses would require the development of appropriate models allowing $[Cl^-]_i$ measurement

in different neuronal compartments as well as suppression of the KCC2 in different neuron subpopulations during embryonic development.

AGE RESTRICTED REGULATORY ACTIONS OF KCC2

Our results show clearly that ablation of KCC2 enhances synaptogenesis in the immature hippocampus, i.e., endogenous KCC2 inhibits formation of the synaptic connections and neuronal network activity. This finding is in a good agreement with previous reports by Cancedda et al. (2007) and Horn et al. (2010) illustrating that *in vivo* overexpression of KCC2 in immature neurons slows-down neuronal development. Interestingly, all these results are in apparent contradiction with previous reports performed on primary neuronal cultures and showing that KCC2 is required for formation of GABA and glutamate synaptic connections. Particularly, we found that overexpression of KCC2 in immature neurons potentiated formation of GABA-ergic synapses (Chudotvorova et al., 2005) whereas knocking-out or knocking-down of KCC2 from cultured hippocampal neurons produced opposite effects (Medina et al., 2011). Another set of data show that the knocking-out (Li et al., 2007) or knocking-down (Gauvain et al., 2011) of the KCC2 in mature primary neuronal hippocampal cultures lead to structural modification in spines formation and decrease glutamatergic synaptic transmission. The overexpression of the KCC2 in these cultures rescued (i.e., potentiated) formation of glutamate synapses. An important task for future studies would be to determine the reason of this differential KCC2-dependent control of synaptogenesis in immature hippocampal neurons *in vivo* and mature hippocampal neurons *in vitro*.

In conclusion, we show that there is a prominent difference in neuronal network activity and formation of the functional GABA and glutamate synapses in immature CA3 hippocampal neurons of wild-type and *Kcc2* deficient mice embryos. This finding provides a novel point of view on the functional importance of KCC2 during early stages of neuronal network development when GABA is still depolarizing and opens new attractive directions in study of the mechanisms of KCC2 functioning.

AUTHORS CONTRIBUTION

Ilgam Khalilov, Romain Nardou, and Jean-Luc Gaiarsa performed recordings from entire hippocampi and acute hippocampal slices. Geneviève Chazal and Nadine Ferrand performed quantitative immunofluorescence analyses. Ilona Chudotvorova, Séverine Corby, Olena Gubkina, Christophe Pellegrino took care of the *Kcc2* deficient mice at the INMED at different stages of the work, made genotyping and part of the immunocytochemistry study. Sumii Yamamoto, Roman Tyzio, and Christophe Pellegrino performed analysis of $[Cl^-]_i$ using different approaches. Thomas J Jentsch, Christian A Hübner, created *Kcc2* deficient mouse, developed anti-KCC2 antibody, performed part of the immunocytochemistry study. Yehezkel Ben-Ari contributed to writing the manuscript and management of the experiments involving recording and analysis of $[Cl^-]_i$ from acute slices and spontaneous activity from entire hippocampi. Igor Medina was in charge of management of the project, writing manuscript, and performed part of the whole-cell recordings from acute slices.

ACKNOWLEDGMENTS

We are grateful to Diabé Diabira for excellent technical assistance. This study was supported by grants from the French Agence Nationale pour la Recherche (to Ilgam Khalilov, Igor Medina, and Jean-Luc Gaiarsa), the French Fondation pour la Recherche Médicale (to Ilona Chudotvorova and Romain Nardou), and NEMO EU FP7 grant (Yehezkel Ben-Ari).

REFERENCES

Ben-Ari, Y., Cherubini, E., Corradetti, R., and Gaiarsa, J. L. (1989). Giant synaptic potentials in immature rat CA3 hippocampal neurones. *J. Physiol. (Lond.)* 416, 303–325.

Ben-Ari, Y., Gaiarsa, J. L., Tyzio, R., and Khazipov, R. (2007). GABA: a pioneer transmitter that excites immature neurons and generates primitive oscillations. *Physiol. Rev.* 87, 1215–1284.

Blaesse, P., Airaksinen, M. S., Rivera, C., and Kaila, K. (2009). Cation-chloride cotransporters and neuronal function. *Neuron* 61, 820–838.

Blaesse, P., Guillemin, I., Schindler, J., Schweizer, M., Delpire, E., Khiroug, L., Friauf, E., and Nothwang, H. G. (2006). Oligomerization of KCC2 correlates with development of inhibitory neurotransmission. *J. Neurosci.* 26, 10407–10419.

Bortone, D., and Polleux, F. (2009). KCC2 expression promotes the termination of cortical interneuron migration in a voltage-sensitive calcium-dependent manner. *Neuron* 62, 53–71.

Caiati, M. D., Sivakumaran, S., and Cherubini, E. (2010). In the developing rat hippocampus, endogenous activation of presynaptic kainate receptors reduces GABA release from mossy fiber terminals. *J. Neurosci.* 30, 1750–1759.

Cancedda, L., Fiumelli, H., Chen, K., and Poo, M. M. (2007). Excitatory GABA action is essential for morphological maturation of cortical neurons in vivo. *J. Neurosci.* 27, 5224–5235.

Cherubini, E., Griguoli, M., Safiulina, V., and Lagostena, L. (2011). The depolarizing action of GABA controls early network activity in the developing hippocampus. *Mol. Neurobiol.* 43, 97–106.

Chudotvorova, I., Ivanov, A., Rama, S., Hubner, C. A., Pellegrino, C., Ben Ari, Y., and Medina, I. (2005). Early expression of KCC2 in rat hippocampal cultures augments expression of functional GABA synapses. *J. Physiol. (Lond.)* 566, 671–679.

Cohen, I., Navarro, V., Clemenceau, S., Baulac, M., and Miles, R. (2002). On the origin of interictal activity in human temporal lobe epilepsy in vitro. *Science* 298, 1418–1421.

Gauvain, G., Chamma, I., Chevy, Q., Cabezas, C., Irinopoulou, T., Bodrug, N., Carnaud, M., Levi, S., and Poncer, J. C. (2011). The neuronal K-Cl cotransporter KCC2 influences postsynaptic AMPA receptor content and lateral diffusion in dendritic spines. *Proc. Natl. Acad. Sci. U.S.A.* 108, 15474–15479.

Gulyas, A. I., Sik, A., Payne, J. A., Kaila, K., and Freund, T. F. (2001). The KCl cotransporter, KCC2, is highly expressed in the vicinity of excitatory synapses in the rat hippocampus. *Eur. J. Neurosci.* 13, 2205–2217.

Horn, Z., Ringstedt, T., Blaesse, P., Kaila, K., and Herlenius, E. (2010). Premature expression of KCC2 in embryonic mice perturbs neural development by an ion transport-independent mechanism. *Eur. J. Neurosci.* 31, 2142–2155.

Hubner, C. A., Stein, V., Hermans-Borgmeyer, I., Meyer, T., Ballanyi, K., and Jentsch, T. J. (2001). Disruption of KCC2 reveals an essential role of K-Cl cotransport already in early synaptic inhibition. *Neuron* 30, 515–524.

Khalilov, I., Dzhala, V., Ben-Ari, Y., and Khazipov, R. (1999). Dual role of GABA in the neonatal rat hippocampus. *Dev. Neurosci.* 21, 310–319.

Khalilov, I., Esclapez, M., Medina, I., Aggoun, D., Lamsa, K., Leinekugel, X., Khazipov, R., and Ben Ari, Y. (1997). A novel in vitro preparation: the intact hippocampal formation. *Neuron* 19, 743–749.

Khalilov, I., Holmes, G. L., and Ben Ari, Y. (2003) In vitro formation of a secondary epileptogenic mirror focus by interhippocampal propagation of seizures. *Nat. Neurosci.* 6, 1079–1085.

Khirug, S., Huttu, K., Ludwig, A., Smirnov, S., Voipio, J., Rivera, C., Kaila, K., and Khiroug, L. (2005). Distinct properties of functional KCC2 expression in immature mouse hippocampal neurons in culture and in acute slices. *Eur. J. Neurosci.* 21, 899–904.

Khirug, S., Yamada, J., Afzalov, R., Voipio, J., Khiroug, L., and Kaila, K. (2008). GABAergic depolarization of the axon initial segment in cortical principal neurons is caused by the Na-K-2Cl cotransporter NKCC1. *J. Neurosci.* 28, 4635–4639.

Lee, H. H., Jurd, R., and Moss, S. J. (2010). Tyrosine phosphorylation regulates the membrane trafficking of the potassium chloride co-transporter KCC2. *Mol. Cell. Neurosci.* 45, 173–179.

Leinekugel, X., Khalilov, I., McLean, H., Caillard, O., Gaiarsa, J. L., Ben-Ari, Y., and Khazipov, R. (1999). GABA is the principal fast-acting excitatory transmitter in the neonatal brain. *Adv. Neurol.* 79, 189–201.

Leinekugel, X., Medina, I., Khalilov, I., Ben Ari, Y., and Khazipov, R. (1997). Ca2+ oscillations mediated by the synergistic excitatory actions of GABA(A) and NMDA receptors in the neonatal hippocampus. *Neuron* 18, 243–255.

Li, H., Khirug, S., Cai, C., Ludwig, A., Blaesse, P., Kolikova, J., Afzalov, R., Coleman, S. K., Lauri, S., Airaksinen, M. S., Keinanen, K., Khiroug, L., Saarma, M., Kaila, K., and Rivera, C. (2007). KCC2 interacts with the dendritic cytoskeleton to promote spine development. *Neuron* 56, 1019–1033.

Manent, J. B., Demarque, M., Jorquera, I., Pellegrino, C., Ben-Ari, Y., Aniksztejn, L., and Represa, A. (2005). A noncanonical release of GABA and glutamate modulates neuronal migration. *J. Neurosci.* 25, 4755–4765.

Medina, I., and Chudotvorova, I. (2006). GABA neurotransmission and neural cation-chloride co-transporters: actions beyond ion transport. *Crit. Rev. Neurobiol.* 18, 105–112.

Medina, I., Friedel, P., Chudotvorova, I., Pellegrino, C., Schaefer, M., and Porcher, C. (2011). A critical role of potassium/chloride co-transport in formation of functional GABA synapses. *Soc. Neurosci.* [Washington (Abstr.)], 545.08.

Nardou, R., Ben-Ari, Y., and Khalilov, I. (2009). Bumetanide, an NKCC1 antagonist, does not prevent formation of epileptogenic focus but blocks epileptic focus seizures in immature rat hippocampus. *J. Neurophysiol.* 101, 2878–2888.

Nardou, R., Yamamoto, S., Chazal, G., Bhar, A., Ferrand, N., Dulac, O., Ben-Ari, Y., and Khalilov, I. (2011). Neuronal chloride accumulation and excitatory GABA underlie aggravation of neonatal epileptiform activities by phenobarbital. *Brain* 134, 987–1002.

Owens, D. F., and Kriegstein, A. R. (2002). Developmental neurotransmitters? *Neuron* 36, 989–991.

Payne, J. A., Stevenson, T. J., and Donaldson, L. F. (1996). Molecular characterization of a putative K-Cl cotransporter in rat brain. A neuronal-specific isoform. *J. Biol. Chem.* 271, 16245–16252.

Pellegrino, C., Gubkina, O., Schaefer, M., Becq, H., Ludwig, A., Mukhtarov, M., Chudotvorova, I., Corby, S., Salyha, Y., Salozhin, S., Bregestovski, P., and Medina, I. (2011). Knocking down of the KCC2 in rat hippocampal neurons increases intracellular chloride concentration and compromises neuronal survival. *J. Physiol. (Lond.)* 589, 2475–2496.

Pfeffer, C. K., Stein, V., Keating, D. J., Maier, H., Rinke, I., Rudhard, Y., Hentschke, M., Rune, G. M., Jentsch, T. J., and Hubner, C. A. (2009). NKCC1-dependent GABAergic excitation drives synaptic network maturation during early hippocampal development. *J. Neurosci.* 29, 3419–3430.

Rinehart, J., Maksimova, Y. D., Tanis, J. E., Stone, K. L., Hodson, C. A., Zhang, J., Risinger, M., Pan, W., Wu, D., Colangelo, C. M., Forbush, B., Joiner, C. H., Gulcicek, E. E., Gallagher, P. G., and Lifton, R. P. (2009). Sites of regulated phosphorylation that control K-Cl cotransporter activity. *Cell* 138, 525–536.

Rivera, C., Voipio, J., Payne, J. A., Ruusuvuori, E., Lahtinen, H., Lamsa, K., Pirvola, U., Saarma, M., and Kaila, K. (1999). The K+/Cl- co-transporter KCC2 renders GABA hyperpolarizing during neuronal maturation. *Nature* 397, 251–255.

Sipila, S. T., Schuchmann, S., Voipio, J., Yamada, J., and Kaila, K. (2006). The cation-chloride cotransporter NKCC1 promotes sharp waves in the neonatal rat hippocampus. *J. Physiol. (Lond.)* 573, 765–773.

Stein, V., Hermans-Borgmeyer, I., Jentsch, T. J., and Hubner, C. A. (2004). Expression of the KCl cotransporter KCC2 parallels neuronal maturation and the emergence of low intracellular chloride. *J. Comp. Neurol.* 468, 57–64.

Tyzio, R., Holmes, G. L., Ben-Ari, Y., and Khazipov, R. (2007). Timing of the developmental switch in GABA(A) mediated signaling from excitation to inhibition in CA3 rat hippocampus using gramicidin perforated patch and extracellular recordings. *Epilepsia* 48(Suppl. 5), 96–105.

Tyzio, R., Ivanov, A., Bernard, C., Holmes, G. L., Ben Ari, Y., and Khazipov, R. (2003). Membrane potential of CA3 hippocampal pyramidal cells during postnatal development. *J. Neurophysiol.* 90, 2964–2972.

Tyzio, R., Represa, A., Jorquera, I., Ben-Ari, Y., Gozlan, H., and Aniksztejn, L. (1999). The establishment of GABAergic and glutamatergic synapses on CA1 pyramidal neurons is sequential and correlates with the development of the apical dendrite. *J. Neurosci.* 19, 10372–10382.

Williams, J. R., Sharp, J. W., Kumari, V. G., Wilson, M., and Payne, J. A. (1999). The neuron-specific K-Cl cotransporter, KCC2. Antibody development and initial characterization of the protein. *J. Biol. Chem.* 274, 12656–12664.

Wittner, L., Huberfeld, G., Clemenceau, S., Eross, L., Dezamis, E., Entz, L., Ulbert, I., Baulac, M., Freund, T. F., Magloczky, Z., and Miles, R. (2009). The epileptic human hippocampal cornu ammonis 2 region generates spontaneous interictal-like activity in vitro. *Brain* 132, 3032–3046.

Zhu, L., Polley, N., Mathews, G. C., and Delpire, E. (2008). NKCC1 and KCC2 prevent hyperexcitability in the mouse hippocampus. *Epilepsy Res.* 79, 201–212.

Conflict of Interest Statement: The authors declare that the research was conducted in the absence of any commercial or financial relationships that could be construed as a potential conflict of interest.

Received: 24 August 2011; paper pending published: 09 September 2011; accepted: 13 October 2011; published online: 01 November 2011.

Citation: Khalilov I, Chazal G, Chudotvorova I, Pellegrino C, Corby S, Ferrand N, Gubkina O, Nardou R, Tyzio R, Yamamoto S, Jentsch TJ, Hübner CA, Gaiarsa J-L, Ben-Ari Y and Medina I (2011) Enhanced synaptic activity and epileptiform events in the embryonic KCC2 deficient hippocampus. Front. Cell. Neurosci. ***5****:23. doi: 10.3389/fncel.2011.00023*

frontiers in
CELLULAR NEUROSCIENCE

ORIGINAL RESEARCH ARTICLE
published: 21 November 2011
doi: 10.3389/fncel.2011.00024

Onset of pup locomotion coincides with loss of NR2C/D-mediated cortico-striatal EPSCs and dampening of striatal network immature activity

Nathalie Dehorter[1,2,3], François J. Michel[1,2,3], Thomas Marissal[1,2,3], Yann Rotrou[4,5], Boris Matrot[4,5], Catherine Lopez[1,2,3], Mark D. Humphries[6] and Constance Hammond[1,2,3]*

[1] INSERM Unité 901, Marseille, France
[2] UMR S901 Aix-Marseille 2, Université de la Méditerranée, Marseille, France
[3] INMD, Marseille, France
[4] INSERM Unité 676, Hôpital Robert Debré, Paris, France
[5] Université Paris Diderot, Paris, France
[6] Laboratoire de Neurosciences Cognitives, INSERM Unité 960, Ecole Normale Supérieure, Paris, France

Edited by:
Enrico Cherubini, International School for Advanced Studies, Italy

Reviewed by:
Enrico Bracci, University of Manchester, UK
Paolo Calabresi, Santa Maria Della Misericordia Hospital, Italy

***Correspondence:**
Constance Hammond, Institut de Neurobiologie de la Méditerranée, INSERM UMR 901, 163 route de Luminy, BP13, 13273 Marseille Cédex 9, France.
e-mail: hammond@inmed.univ-mrs.fr

Adult motor coordination requires strong coincident cortical excitatory input to hyperpolarized medium spiny neurons (MSNs), the dominant neuronal population of the striatum. However, cortical and subcortical neurons generate during development large ongoing patterns required for activity-dependent construction of networks. This raises the question of whether immature MSNs have adult features from early stages or whether they generate immature patterns that are timely silenced to enable locomotion. Using a wide range of techniques including dynamic two-photon imaging, whole cell or single-channel patch clamp recording in slices from Nkx2.1-GFP mice, we now report a silencing of MSNs that timely coincides with locomotion. At embryonic stage (as early as E16) and during early postnatal days, genetically identified MSNs have a depolarized resting membrane potential, a high input resistance and lack both inward rectifying (IK_{IR}) and early slowly inactivating (I_D) potassium currents. They generate intrinsic voltage-gated clustered calcium activity without synaptic components. From postnatal days 5–7, the striatal network transiently generates synapse-driven giant depolarizing potentials when activation of cortical inputs evokes long lasting EPSCs in MSNs. Both are mediated by NR2C/D-receptors. These immature features are abruptly replaced by adult ones before P10: MSNs express IK_{IR} and I_D and generate short lasting, time-locked cortico-striatal AMPA/NMDA EPSCs with no NR2C/D component. This shift parallels the onset of quadruped motion by the pup. Therefore, MSNs generate immature patterns that are timely shut off to enable the coordination of motor programs.

Keywords: development, basal ganglia, striatum, immature activity, locomotion, patch clamp, two-photons imaging, mouse pup

INTRODUCTION

Adult medium spiny neurons (MSNs), the GABAergic principal neurons of the striatum, have unique features required for the appropriate selection of motor programs (Grillner et al., 2005). They are highly hyperpolarized at rest and require strong coincident excitatory glutamatergic inputs for the execution of appropriate movements (Wilson and Kawaguchi, 1996). These unique features are due to strong inward rectifying (IK_{IR}) and slow inactivating (I_D) potassium currents and feedforward and feedback afferent inhibition that confer a low input resistance, hyperpolarized resting potential, and a long delay to initial spiking (Tepper et al., 2004). In a large range of animal species and brain structures, immature neurons are highly excitable and developing networks generate network-driven patterns that are instrumental in neuronal growth, synapse formation, and the formation of functional circuits (for review Ben-Ari, 2002; Spitzer, 2006; Huberman et al., 2008; Blankenship and Feller, 2010). These observations raise the question whether MSNs differ from other neuronal types and are silent from early developmental stages and if not when and how are the early patterns switched off to enable correct motor coordination and quadruped motion.

Medium spiny neurons originate in the lateral ganglionic eminence (Deacon et al., 1994; Olsson et al., 1998) and migrate radially into the developing striatum compartments (Van Der Kooy and Fishell, 1987). To understand MSN functional maturation, we targeted embryonic and early postnatal MSNs with the use of Nk2 homeobox 1 (Nkx2.1)-GFP Mice. Nkx2.1, also known as thyroid transcription factor-1 (TTF-1), is a protein that regulates transcription of genes and is specifically expressed by interneurons but not by MSNs in the striatum (Nobrega-Pereira et al., 2008). We determined MSNs' cellular properties using whole cell and single-channel recordings. In parallel we performed two-photon dynamic imaging that enables to determine the activity of large neuronal samples in slice preparation (Crepel et al., 2007). We

then used behavioral analysis to describe posture and onset of locomotion in newborn pups. We report an abrupt switch of cellular and synaptic properties in MSNs in parallel with the initiation of locomotion.

MATERIALS AND METHODS

EMBRYONIC AND POSTNATAL SLICE PREPARATIONS

We performed experiments in embryonic (E14, E16, E18) or postnatal (P0–P45) wild type C57BL/6 mice (Janvier, France) or Nkx2.1-GFP mice of either sex obtained by crossing Nkx2.1-CRE C57BL/6 mice (Jackson lab) and the RCE:LoxP reporter strain (Sousa et al., 2009). We anesthetized pregnant mice with xylazine (Rompun 2%; used at 0.05%) and ketamine (Imalgene 1000; used at 50 g/l; Volume injected: 0.2 ml/g) and postnatal mice with isoflurane. We kept brains in ice-cold oxygenated solution containing (in mM): 110 choline, 2.5 KCl, 1.25 NaH_2PO_4, 7 $MgCl_2$, 0.5 $CaCl_2$, 25 $NaHCO_3$, 7 glucose, and performed coronal, parasagittal, or horizontal slices (400 μm thick) using a vibratome (VT1200 Leica Microsystems Germany). During the recovery period, slices were placed at room temperature (RT) with standard artificial cerebrospinal fluid (ACSF) saturated with 95% O_2/5% CO_2 and containing (in mM): 126 NaCl, 3.5 KCl, 1.2 NaH_2PO_4, 1.3 $MgCl_2$, 2 $CaCl_2$, 25 $NaHCO_3$, 11 glucose.

CALCIUM IMAGING

Slices were incubated for 30 min in 2.5 ml of oxygenated ACSF (35–37°C) with 25 μl fura 2AM (1 mM, in DMSO + 0.8% pluronic acid; Molecular Probes). Imaging was performed with a multibeam two-photon laser scanning system (Trimscope-LaVision Biotec) coupled to an Olympus microscope with a high numerical aperture objective (20×, NA 0.95, Olympus). Images of the scan field (444 μm × 336 μm) were acquired via a CCD camera (4 × 4 binning; La Vision Imager 3QE) with a time resolution of 115–147 ms (non-ratiometric 1000–3000 images, laser at 780 nm) as previously described (Crepel et al., 2007). In slices from Nkx2.1-GFP mice, we first took images of the GFP-expressing neurons (laser at 910 nm) before acquiring spontaneous fura 2 fluorescence changes (laser at 780 nm). To patch clamp record particular neurons Fura pentapotassium salt (30 μM; Invitrogen) was added to the pipette solution to keep cells fluorescent.

PATCH CLAMP RECORDINGS

Cells were visualized with infrared-differential interference optics (Axioskop2; Zeiss). We performed recordings at 35–37°C. For current clamp recordings, the pipette contained (in mM): 15 KCl, 5 NaCl, 125 $KMeSO_4$, 10 HEPES, 2.5 Mg-ATP, 0.3 Na-GTP. For whole cell voltage-clamp recordings of postsynaptic $GABA_A$ (sIPSCs) and glutamatergic (sEPSCs) currents, the pipette (6–10 MΩ) contained (in mM): 120 Cs-gluconate, 13 CsCl, 1 $CaCl_2$, 10 HEPES, 10 EGTA, pH 7.2–7.4 (275–285 mOsm). We recorded sIPSCs at the reversal potential of sEPSCs (+10 mV). To record sEPSCs we continuously applied a $GABA_A$ receptor antagonist (bicuculline 20 μM or Gabazine 5 μM), and maintained the membrane potential at −80 or +40 mV to separately detect AMPA/kainate (KA) and NMDA sEPSCs, respectively (Groc et al., 2002). We recorded AMPA/KA sEPSCs in the continuous presence of APV (40 μM), the selective NMDA receptor antagonist, and separated AMPA from KA sEPSCs by applying NBQX at a dose (1 μM) that preferentially blocks AMPA receptors. We identified NMDA sEPSCs at +40 mV by their kinetics (the NMDA decay time is longer than the AMPA one) or insensitivity to the AMPA/KA receptor antagonist, NBQX (10 μM).

To record unitary $GABA_A$ currents the pipette (4–5 MΩ) contained (in mM): 120 NaCl, 20 TEA-Cl (tetraethylammonium chloride), 5 KCl, 5 4-aminopyridine, 0.1 $CaCl_2$, 10 $MgCl_2$, 10 glucose, 5 GABA, 5 isoguvacine, 3 CsCl, 10 HEPES-NaOH buffered to pH 7.2–7.3; osmolality of 300–320 mOsm. When Gabazine 10 μM was added to the above pipette solution no unitary currents were recorded. To record unitary NMDA currents, the pipette (4–5 MΩ) contained (in mM): 140 NaCl, 3.5 KCl, 1.8 $CaCl_2$, 10 HEPES, 10 NMDA, 10 glycine, 1 strychnine, buffered to pH 7.43; osmolality of 300–320 mOsm. When APV (40 μM) was added to the pipette solution, no unitary currents were recorded. To identify the morphology of neurons recorded in cell-attached configuration, we re-patched them with a conventional whole cell electrode containing neurobiotin (Abcys).

IDENTIFICATION OF IMMATURE MSNs VS. INTERNEURONS OR VS. ASTROCYTES

Since embryonic and early postnatal MSNs lack their characteristic adult K^+ currents, they could not be identified from their electrophysiological properties. We therefore identified them as GFP-negative neurons (Sousa et al., 2009) in striatal slices from Nkx2.1-GFP mice. To quantify the proportion of Nkx2.1-positive striatal interneurons that faintly expressed GFP and were therefore considered as MSNs, we performed immunocytochemistry of Nkx2.1 (see below; **Figure 1A**). From a total of 2767 Nkx2.1-expressing striatal neurons labeled with TTF-1 (red), 75% were also GFP positive (yellow, $n = 2077$), showing that in perinatal slices from Nkx2.1-GFP mice, 25% of the Nkx2.1-positive neurons, though GFP-negative, were not MSNs. In our two-photon recordings, GFP positive/fura 2-loaded neurons represented 10–20% of all fura 2-loaded cells. Therefore instead of 10–20% interneurons, we had around 13–27% interneurons in the field. We thus overestimated the proportion of MSNs by 3–7%.

To quantify the proportion of fura 2-loaded cells that were astrocytes and not neurons in slices from P10 to P12 mice, and could be erroneously considered as silent neurons, we performed double loading of slices with sulforhodamine 101 (SR101, 1 μM), a specific marker of astroglia (Nimmerjahn et al., 2004) during 20 min at 35–37°C and then with fura 2AM (**Figure 1B**). At P12, astrocytes represented around 25% of all the imaged cells ($n = 201/815$ from five slices). Among these astrocytes, around 40% were also positive for fura 2 ($n = 86/201$). Therefore around 10% of fura 2-loaded cells were astrocytes ($n = 86/815$). All these fura 2-loaded astrocytes were silent and could be erroneously counted as silent neurons.

IMMUNOCYTOCHEMISTRY AND DiI EXPERIMENTS

To reveal the neurobiotin injected during whole cell recordings, the sections were left 12 h in paraformaldehyde (3%) at 4°C, rinsed in PBS, left 12 h in PB-sucrose 20%, and then at −80°C for at least 2 h. They were thawed at RT, rinsed in PB and incubated

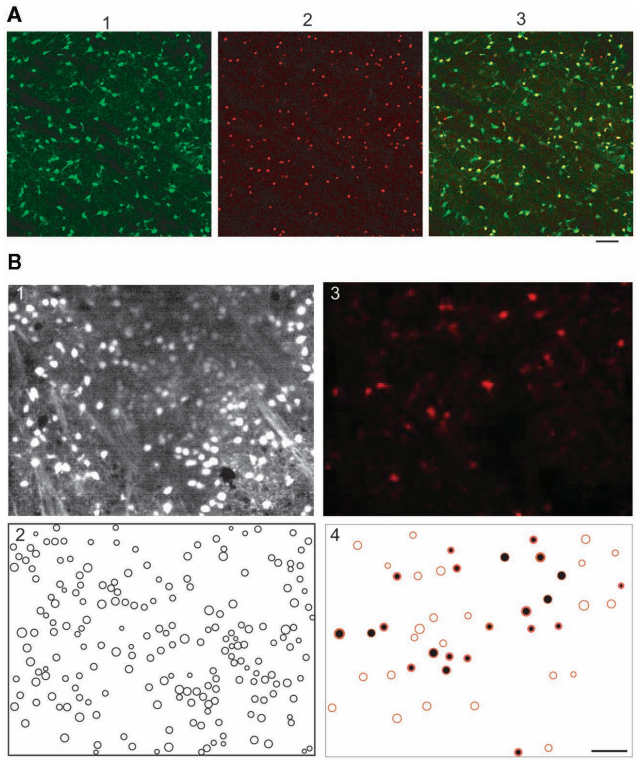

FIGURE 1 | Quantification of percent of GFP-negative/Nkx2.1-positive neuron in perinatal striatal slices and of percent of fura 2-loaded astrocytes in the P10–P12 striatal slices. (A1) Confocal image of the GFP-expressing neurons in the dorso-lateral region of the striatum (slice from a P2 Nkx2.1-GFP mouse). **(A2)** Nkx2.1-expressing neurons in the same field revealed with the TTF-1/111–121 antibody (in red, see Materials and Methods). **(A3)** The superimposition of the two images shows that of the 161 Nkx2.1-expressing neurons 13 were GFP-negative meaning that in this field 13 striatal interneurons out of 161 could be erroneously considered as MSNs. **(B)** Two-photon images of a striatal slice first loaded with sulforhodamine 101 (SR101, 1 μM) and then with fura 2AM. **(B1)** Fura 2 fluorescent cells ($n = 196$) imaged with excitation wavelength and emission filter parameters specific for fura 2 (laser at 780 nm and emission filter 535 ± 25 nm, parameters that give no images of cells loaded with SR101 only). **(B2)** Manually detected contours of the cells from the fluorescence images ($n = 196$ fura 2-loaded cells). **(B3)** SR101 fluorescent astrocytes ($n = 46$) imaged with excitation wavelength and emission filter parameters adjusted for SR101 (laser at 880 nm and emission filter 610 ± 37 nm, parameters that give faint images of few cells loaded with fura 2 only); same field as in **(A)**. **(B4)** Of these 46 SR101 loaded astrocytes half ($n = 22$) were also fura 2-loaded (black-filled red circles obtained by superimposition of 1 and 3) meaning that 22 cells out of the 196 fura 2-loaded cells were astrocytes. Scale bars 50 μm.

30 min in 1% H_2O_2 in PB. Slices were washed with PB and KPBS and incubated for 12 h in ABC complex at a dilution of 1:100 in KPBS + 0.3% triton (Abcys). They were rinsed in KPBS and incubated for approximately 10 min in 3,3′ diaminobenzidine (DAB 0.7 mg/ml) with peroxide (0.2 mg/ml; Sigma Fast), rinsed, mounted in Crystal/Mount (Electron Microscopy Sciences), coverslipped, and examined. Dendritic and axonal fields were reconstructed using the Neurolucida system (MicroBrightField Inc., Colchester, VT, USA).

To reveal the Nkx2.1-positive neurons we used the antibody TTF-1/111–121. Slices were cryoprotected in PB with 20% sucrose, freeze-thawed in isopentane, and rinsed in PB. Slices were then incubated in PBS Triton 0.3% normal goat serum (NGS, 2%) for 1 h and then in Nkx2.1 antibody (1:2500; TTF-1/111–121; Biopat, Italy) for 4 days at RT. After thorough rinsing, slices were incubated for 90 min at RT in alexa-488 goat anti-mouse (1:300; Molecular Probes, Leiden, the Netherlands) in PBS and NGS 2% overnight. After thorough rinsing, slices were mounted in fluoromount, coverslipped, and examined with a confocal microscope (Zeiss LSM 510). For double immunocytochemistry Neurobiotin-Nkx2.1, slices were treated as above for the revelation of Nkx2.1. Then after thorough rinsing, slices were again incubated in PBS and Cy3 streptavidin (1:300; Jackson, USA) to label the neurobiotin-loaded neuron(s) and then rinsed. After thorough rinsing, slices were mounted in fluoromount, coverslipped, and examined with a confocal microscope (Zeiss LSM 510).

To visualize cortico-striatal axons, we injected small amounts of DiI crystals diluted in ethanol in the neocortex of 400 μm thick slices from E16 to P2 brains postfixed by immersion for 2–4 weeks in 4% paraformaldehyde. Slices were then incubated in the fixative solution at 32°C for 2–3 weeks, coverslipped, and examined with a confocal microscope (Zeiss LSM 510).

ANALYSIS OF IMAGING DATA

We performed analysis of the calcium activity with custom-made software written in Matlab (MathWorks; Bonifazi et al., 2009). The contour of each loaded cell was semi-automatically detected and its fluorescence measured as a function of time. Active cells are neurons exhibiting any Ca^{2+} event of at least 5% DF/F deflection within the period of recording. Ca^{2+} spikes or Ca^{2+} plateaus cells were neurons exhibiting at least one Ca^{2+} spike or one Ca^{2+} plateau within the period of recording. Ca^{2+} plateaus were intrinsic correlated Ca^{2+} events of long duration (see Results). Giant depolarizing potentials (GDP) cells were cells generating synchronized synapse-driven Ca^{2+} spikes (GDPs). To compute the activity correlation of two cells, the onset of each event was represented by a Gaussian ($s = 1$ frame, to allow some jitter). The inner product of the resulting values was then calculated. The significance of each correlation value was estimated by direct comparison with a distribution computed from surrogate data sets, in which the events were randomly reshuffled in time.

To compare both network-wide and single-neuron activity between putative intrinsically driven activity at P2 (P2–P3 recordings) and synaptically driven activity at P6 (P5–P7 recordings), we used standard k-means clustering to determine how well event durations and frequencies distinguished P2 and P6 time-points. The k-means algorithm used minimization of city-block distance, with 30 replications from random starting positions, from which we retained the replicate with the minimum mean distance. We also sought evidence for differences in spontaneous neural ensembles in network-wide activity. Each recording's matrix of pair-wise correlations, computed by Gaussian convolution as above was partitioned into groups using a modified community detection algorithm, detailed in Humphries (2011), which finds the number and size of groups within the matrix that maximize benefit function $Q_{data} =$ (similarity within groups) − (expected similarity within

groups). The resulting partition thus corresponded to groups of neurons that were more similar in activity patterns than was expected given the total similarity of each neuron's activity to the whole data-set. We then ran a further stringent control for potentially spurious groupings, by first shuffling the inter-event intervals of each neuron in a recording, correlating the shuffled event onsets, and then running the algorithm on the shuffled data-set. This was repeated 100 times to get a distribution of Q for control data. The 95th percentile of these values was taken as the 95% confidence interval Q_{ctrl}. Any network with $Q_{data} > Q_{ctrl}$ thus contained significant ensemble structure, compared to that expected from just the firing statistics of the network.

ANALYSIS OF ELECTROPHYSIOLOGICAL DATA

We determined series resistance (R_s), membrane capacitance (C_m), and input resistance (R_{input}) by on-line fitting analysis of the transient currents in response to a 5-mV pulse at −70 mV. Criteria for considering a recording included $R_{input} > 100\,M\Omega$, $R_s < 25\,M\Omega$, with $R_s < 30\%$ change. We analyzed spontaneous postsynaptic currents (sPSCs) in 180 s recordings at a given membrane potential with the Mini-Analysis program (version 5.1.4; Synaptosoft, Decatur, GA, USA). Events were characterized by the following parameters: rise time (10–90%), amplitude, and decay time (τ). We discriminated mixed AMPA/KA events in the absence of specific receptor antagonists from the SD given by the fit of each event to determine whether one or two exponentials best fitted the decays (Epsztein et al., 2005). E16–P5 MSNs generating sEPSCs (61 out of 131) or sIPSCs (33 out of 79) with a frequency lower than 0.05 Hz were not included.

We filtered the single-channel currents at 1 kHz ($GABA_A$ channels) or 3 kHz (NMDA channels) and digitized them at 10 kHz. We discarded multilevel and short (2 ms) openings during the analysis. To obtain unitary current–voltage (*I–V)* relationships, we measured the amplitude of unitary GABA and NMDA currents evoked by steps from −120 to +40 mV. Histograms of cursor-measured amplitudes allowed determination of the mean unitary current amplitude at each voltage tested.

Measurements of V_{rest} and $E_{GABA(A)}$: to determine the action of GABA in a given neuron (depolarizing or hyperpolarizing), one must measure the reversal potential of the $GABA_A$-mediated current [$E_{GABA(A)}$] and the resting membrane potential (V_{rest}). However, conventional whole cell recordings introduce a number of errors in these measures in particular in developing neurons. We therefore estimated the value of V_{rest} from cell-attached recordings of the single-channel NMDA current (*i*NMDA), which is known to reverse at a membrane potential (V_m) close to 0 mV. We plotted the relationship between *i*NMDA and the extracellular potential applied to the patch of membrane (V_p) from experimental data (see **Figure 9B**). This curve [$i\text{NMDA} = f(V_p)$] gives the value of V_p when $i\text{NMDA} = 0$ pA. At this value of V_p, single-channel NMDA current is null because $V_m = V_p - V_{rest} = 0$ mV. This allows estimation of V_{rest} ($V_{rest} = V_p$). To estimate [$E_{GABA(A)}$], we plotted the relationship between the single-channel $GABA_A$ current ($i\text{GABA}_A$) and V_p. This curve [$i\text{GABA}_A = f(V_p)$] gives the value of V_p when $i\text{GABA}_A = 0$ pA (see **Figure 9A**), because by definition when $i\text{GABA}_A$ is null, $V_m = E_{GABA(A)}$. Therefore, when $i\text{GABA}_A = 0$ pA, $V_m = V_p - V_{rest} = E_{GABA(A)}$ (i.e., $E_{GABA(A)} - V_{rest} = -V_p$). By definition, $E_{GABA(A)} - V_{rest} = DF_{GABA}$, the driving force (DF) of chloride ions through the $GABA_A$ channel (Tyzio et al., 2003). Therefore, when $i\text{GABA}_A = 0$ pA, $DF_{GABA} = -V_p$. Knowing V_{rest} and DF_{GABA}, it is easy to calculate $E_{GABA(A)} = DF_{GABA} + V_{rest}$.

To obtain whole cell current–voltage (I–V) relationships, we measured voltages at the end of each hyperpolarizing current step (950 ms). The inward rectification was detected when the I–V relationship was not linear between −90 and −120 mV. To compare immature and adult MSNs delay of firing in response to depolarizing steps, we measured the first interspike interval (ISI) of the response. We then pooled the slope values of the linear regression lines and compared their distribution as a function of time (Belleau and Warren, 2000). We estimated the threshold potential for Na^+ spikes in whole cell current clamp recordings at V_{rest} (−70 mV for E16–P7 slices and −80 mV for the adult slices) by applying successive intracellular depolarizing steps (duration 950 ms) or in response to cortical stimulation.

DRUGS

Drugs were prepared as concentrated stock solutions and diluted in ACSF for bath application: bicuculline 20 μM, Gabazine 5 μM, $GABA_A$ receptor antagonists; (2*R*)-amino-5-phosphonovaleric acid (APV) 40 μM, a NMDA receptor antagonist and (2*S**, 3*R**)-1-(Phenanthren-2-carbonyl)piperazine-2, 3-dicarboxylic acid (PPDA) 100 nM, a NR2C/D subunits antagonist; 6-cyano-7-nitroquinoxaline 2,3-dione (CNQX) 10 μM, and (2,3-dihydroxy-6-nitro-7-sulfamoyl-benzo[f]quinoxaline-2, 3-dione)(NBQX) 1–10 μM, AMPA/kainate receptor antagonists. Nifedipine, an L-type Ca^{2+} channel antagonist; Ω-Conotoxin GVIA, an N-type Ca^{2+} channel antagonist; Ω-Agatoxin IVA a P/Q type Ca^{2+} channel antagonist; Isoguvacine 100 μM, a $GABA_A$ receptor agonist, was locally pressure-applied. All drugs were purchased from Sigma (St. Louis, MO, USA) except PPDA from Tocris and N or P/Q type antagonists from Alomone Labs.

MOTOR BEHAVIOR

Motion development was assessed in Swiss newborn mice ($n = 16$) from two different litters (Janvier SAS, Le Genest Saint Isle, France) between postnatal day 2 (P2, day of birth: P0) and P12. C57BL/6 pups could not be tested because of their low weight. We used an open field test to assess overall activity. We tested each pup twice a day, with a 20-min delay between the two tests. We placed the pup on a translucid acrylic plate (24 cm × 16 cm) covered with a silicone gel. Two cameras were placed below the plate. One acquired the pup's contact points with the floor which appeared as highly contrasted areas, based on the frustrated total internal reflection (FTIR) principle (Han, 2005). We identified the mouse abdominal contact points using custom-made software. The second camera acquired the trajectory of the pup. We calculated from this trajectory the total distance traveled, and the total distance traveled along straight line segments.

STATISTICS

Average values are presented as means ± SEM and we performed statistical comparisons with Student's t-test (SigmaStat 3.1, Origin 5.0), Mann–Whitney rank sum test (SigmaStat 3.1) or one way

ANOVA (Tukey's Test as *post hoc* test; SigmaStat 3.1, Origin 5.0). The appropriate descriptive statistic was chosen on this basis, as denoted in the text. We set the level of significance as $p \leq 0.05$. We grouped sets of data without statistical differences as follow: P2 (P0–P2), P6 (P3–P6), P8 (P7–P8), P10 (P9–P10), and P12 (P11–P12) except for **Figures 2**, **6**, and **8** where the ages indicated correspond to the exact age (−5 = E14; −3 = E16; −1 = E18; 0 = P0; 2–30 = P2–P30).

RESULTS

Fura 2-loaded striatal neurons were already active at E14, the youngest age tested. The percent of active cells was 16.8 ± 1.5% between E14 and P0, and did not change significantly over the first postnatal week (P0–P2: 17.5 ± 1.0% of imaged cells, P3–P6:14.4 ± 1.1%; $p = 0.07$). There were significantly fewer active cells at P7–P8 (8.3 ± 1.2%) and P9–P10 (4.2 ± 0.8%; $p = 0.0004$ between the two groups P3–P6 and P7–P8, one way ANOVA, n = a total of 177 movies covering 47062 neurons). We then focused specifically on the activity of striatal MSNs. They generated three distinct patterns of activity: Intrinsic voltage-gated Ca^{2+} spikes (E14–P10), correlated Ca^{2+} Plateaus (E14–P10) and correlated Ca^{2+} spikes associated with (GDPs, P5–P7; Crepel et al., 2007; Allene et al., 2008). Of these three, only the latter was sensitive to blockers of glutamate and GABA synaptic transmission.

EMBRYONIC AND EARLY POSTNATAL MSNS SPONTANEOUSLY GENERATE INTRINSICALLY DRIVEN CA^{2+} EVENTS IN THE ABSENCE OF SUBTHRESHOLD K^+ CURRENTS

Intrinsic voltage-gated Ca^{2+} spikes predominated between E14 (11.5 ± 4.3% of imaged cells, n = 2268 neurons in four fields, referred to as 2268/4), and P6 (10.2 ± 2.1%, 3143/12), and were significantly decreased at P10 (3.1 ± 0.9%, 2357/15; $p = 0.0008$, one way ANOVA; **Figure 2A** left, **Figure 2C**). Ca^{2+} spikes were not necessarily associated with Na^+ spikes (**Figure 2B** left), had a low frequency (0.028 ± 0.004 Hz, 777/18), and a longer time to peak at E14–E18 (1.31 ± 0.08 s, 777/18) than at P0–P5 (0.053 ± 0.006 Hz; 0.92 ± 0.07 s, 207/7; $p = 0.004$ and $p = 0.001$ respectively, Student's t-test) suggesting different Ca^{2+} channels and/or Ca^{2+} clearance properties. There were no cell pairs showing correlated Ca^{2+} spikes at any age (0.2% at E14, 0.6% at P6, and 0% at P10).

Synchronized Ca^{2+} Plateaus were rare at E14 (1.5 ± 0.4% of imaged cells, 2268/4), peaked at P4 (6.7 ± 1.5%, 1166/5), and absent at P11–P12 (0%, 1350/11; **Figure 2A** right, C). Ca^{2+} Plateaus were long lasting Ca^{2+} events (6.45 ± 2.01 s, 234/22, at E14–E18) that significantly differed from Ca^{2+} spikes (1.31 ± 0.08 s, 777/19, at E14–E18) in terms of duration ($p = 2.2 \times 10^{-7}$, Student's t-test). The percentage of cell pairs with correlated Ca^{2+} plateaus was around 5% (6% at E14, 5% at P4). Ca^{2+} plateaus had a similar mean frequency at E18 and P4 (0.014 ± 0.003 vs. 0.017 ± 0.002 Hz; $p = 0.8$, Student's t-test) and a similar mean duration (14.4 ± 1.9 vs. 14.5 ± 0.8 s; $p = 0.1$, Student's t-test; 107/10 and 89/5). Patch clamp recordings revealed underlying recurrent depolarizations (22 ± 2 mV, 2.3 ± 0.6 s, at a frequency around 0.4 Hz, $n = 9$) or a single long lasting depolarization (23 ± 6 mV, 10.0 ± 3.7 s, $n = 4$) that generated Na^+ spikes (**Figure 2B** right).

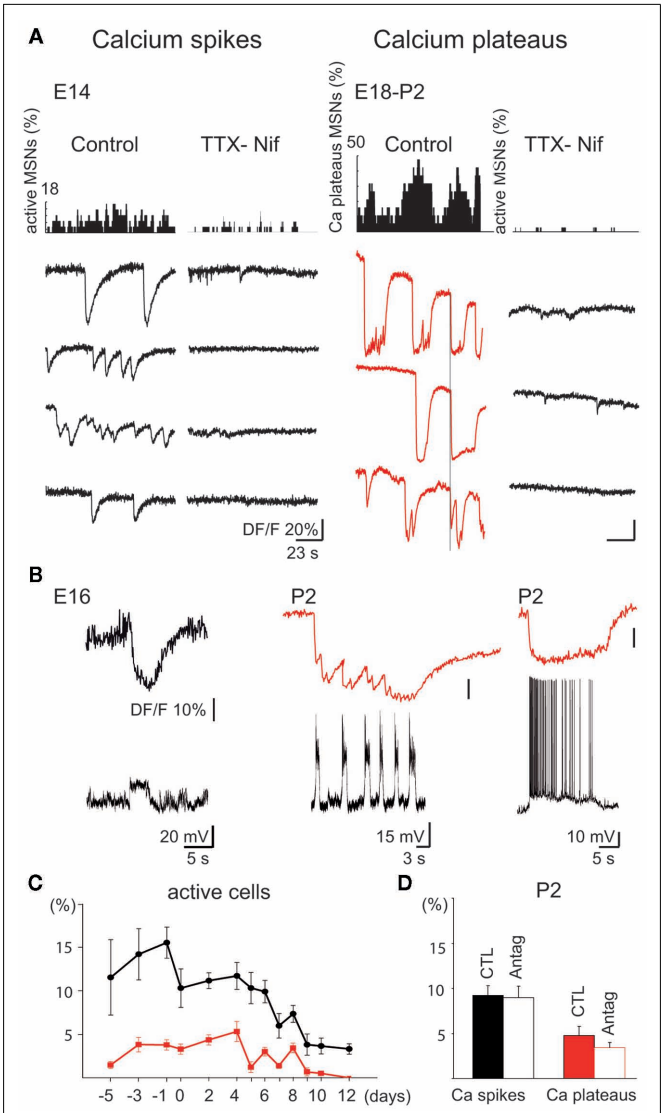

FIGURE 2 | Intrinsically driven Ca^{2+} events in immature MSNs (E14–P2). (A) Representative histograms (top) indicating the fraction of MSNs evoking Ca^{2+} spikes (left) or Ca^{2+} plateaus (right) and corresponding representative calcium fluorescence traces from single MSNs (bottom; Ca^{2+} spikes in black, Ca^{2+} plateaus in red) in control ACSF or in the presence of blockers of voltage-gated channels [TTX (1 μM)-Nifedipine (Nif) 10 μM]. In control ACSF, some Ca^{2+} plateaus were temporally correlated (vertical line). **(B)** Simultaneous optical (top) and current clamp (bottom) recordings of Ca^{2+} spikes ($V_m = -70$ mV, left) and Ca^{2+} plateaus ($V_m = -50$ mV, right). **(C)** Mean percentage (±SEM) of fura 2-loaded cells evoking at least one Ca^{2+} spike (black) or one Ca^{2+} plateau (red) as a function of age. **(D)** Mean percentage (±SEM) of active cells generating at least one Ca^{2+} spike (black) or one Ca^{2+} plateau (red) at P2 in control ACSF (CTL) and in the presence of antagonists of ionotropic glutamate and $GABA_A$ receptors (APV 40 μM-CNQX 10 μM-bicuculline 10 μM; Antag).

The blockers of Na^+ and Ca^{2+} voltage-gated channels, TTX (1 μM)–nifedipine (10 μM) decreased threefold the percent of active cells (from 12.4 ± 2.9 to 4.6 ± 2.2% of imaged cells at P2 (**Figure 2A**). Nifedipine alone at a concentration specific for L-type Ca^{2+} channels (3 μM) decreased the percent of active cells

by 40% (from 13.9 ± 3.6 to 8.4 ± 3.1%; $p = 0.04$, paired Student's t-test, 897/4) and ω-Conotoxin GVIA (1 μM), the N-type Ca^{2+} channel blocker, halved the percent of active cells (from 13.5 ± 1.4%, 9682/33 to 6.4 ± 0.8%, 1321/6; $p = 0.0001$, Student's t-test; not shown). In contrast, Ω-Agatoxin IVA (100 nM), the specific blocker of P/Q type channels had no significant effect. Ionotropic glutamate and GABA antagonists did not affect the percentage of Ca^{2+} spike cells (9.2 ± 1.1 vs. 9.0 ± 1.3% at P2, $p = 0.79$, paired Student's t-test) or Ca^{2+} plateaus cells (**Figure 2D**). These antagonists also did not significantly affect the coherence between calcium plateaus (4.5% pairs of plateaus cells correlated in the presence of antagonists vs. 5% pairs in control at P2).

The time coherence between some Ca^{2+} plateaus could be explained by the presence of gap junctions between immature neurons (Crepel et al., 2007). Single MSN recordings with neurobiotin-containing pipettes revealed clusters of 6 ± 1 neurobiotin-labeled neurons at E14–E18 ($n = 13/17$ patches), but of only two MSNs at P30–P40 ($n = 3/38$ patches). The majority of clusters were exclusively composed of MSNs (E14–P2, $n = 36/37$ clusters) and were abundant until P0–P2 (**Figure 3**). This suggested the presence of gap junctions permeable to neurobiotin at perinatal stages as described in juvenile rodent MSNs (Tepper et al., 1998; Venance et al., 2004) and required for the formation of synaptically connected networks (Todd et al., 2010). But carbenoxolone (100 μM), like mefloquine (25 μM) applied during 10–20 min, similarly reduced the probability of occurrence of all types of immature Ca^{2+} activities (data not shown, E14–P4, 5653/17). This non-specific effect precluded their use for demonstrating the role of gap junctions in Ca^{2+} plateaus' occurrence. These results suggested that Ca^{2+} spikes and Ca^{2+} plateaus are non-synaptic, intrinsic, voltage-gated events generated by Na^+ and L and N-types Ca^{2+} channels. To understand how MSNs spontaneously generate intrinsically driven calcium events, we next investigated the development of their intrinsic membrane properties.

The membrane potential trajectory attributable to the activation of the *inwardly rectifying K^+ current* (IK_{IR}) was not detected in any MSNs at E14, was present in 17% of MSNs at P7 ($n = 3/44$) and in all MSNs at P10 and P30 ($n = 8/8$ and 6/6, respectively). It greatly increased from P10 to P30 (**Figures 4A,B**). Accordingly, bath application of cesium (3 mM), a blocker of IK_{IR}, increased the proportion of active cells by 240% at P6–P10 (from 4.3 ± 1.1 to 10.4 ± 1.7%, 1349/6; $p = 0.04$ paired Student's t-test; data not shown). The mean *input resistance* (R_m) of MSNs was high until P6 and significantly decreased by approximately 75% between P6 and P10 (from 982 ± 129 MΩ at P6, $n = 21$ to 263 ± 19 MΩ at P10, $n = 11$; $p = 0.004$, one way ANOVA; **Figure 4C**). *Spiking threshold* ($V_{threshold}$) did not change from P2 to P30 (P2: −32.2 ± 1.7 mV, $n = 14$ and P30: −30.8 ± 0.8 mV, $n = 10$; $p = 0.51$ one way ANOVA) but the instantaneous firing frequency did. The first ISI of a firing train as a function of injected current was stable until P6 and was then significantly reduced between P6 and P10 (1.44 ± 0.14 Hz/pA, $n = 11$ at P6 vs. 0.91 ± 0.08 Hz/pA, $n = 7$ at P10; $p = 0.03$, one way ANOVA) showing an increased delay to spiking at P10 (**Figures 4D,E**). The depolarization needed to generate spikes calculated as ($V_{threshold} - V_{rest}$) from whole cell recordings (**Figures 4F,G**) was significantly lower until P6

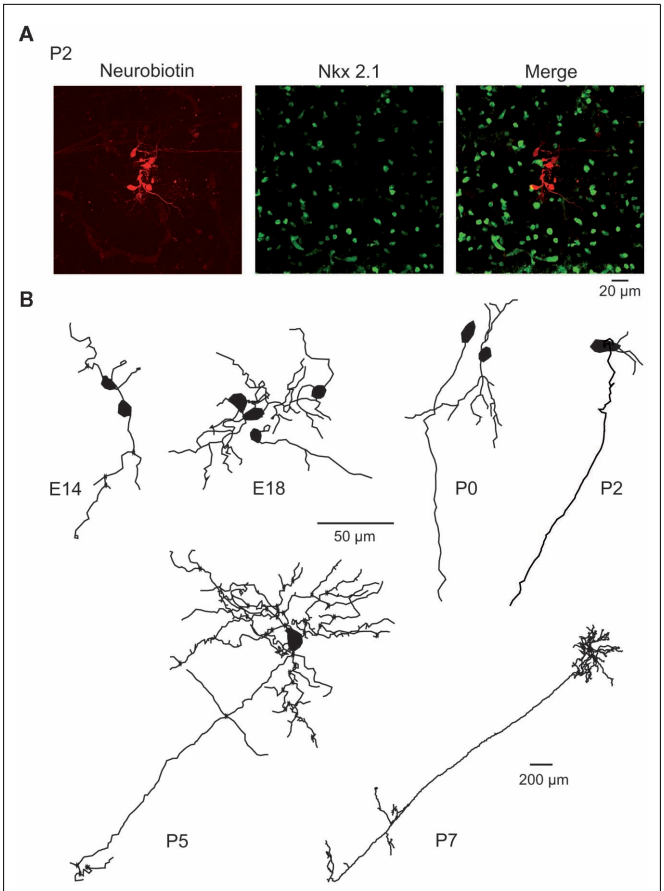

FIGURE 3 | Morphology of embryonic and early postnatal MSNs. (A) Cluster of seven neurobiotin-filled (left) and Nkx2.1-negative (middle) MSNs (merge) revealed by double immunocytochemistry performed after whole cell recording of a single MSN in a P2 striatal slice. **(B)** Neurolucida reconstruction of neurobiotin-filled Nkx-negative neurons (MSNs) at the indicated ages. Dendrites and axons were MSNs had 2.8 ± 0.3 primary dendrites at E16–E18 ($n = 23$), 3.9 ± 0.4 at P0 ($n = 19$), 5.1 ± 1.1 at P2 ($n = 9$), and 5.8 ± 0.3 at P7 ($n = 11$). They gave rise to 6–25 dendritic ends (6 at E16–18, 13 at P0, 17 at P2, 18 at P5, and 25 at P7). The total dendritic length was multiplied by 5 between E16–18 and P7 (339 ± 64 μm at E16–18, 646 ± 148 μm at P0, 574 ± 123 μm at P2, 818 ± 161 μm at P5, and 1751 ± 219 μm at P7). Dendritic spines were virtually absent at all ages. Average cell capacitance progressively increased from E16 to P7 (14.3 ± 0.9 pF at P2, $n = 47$, compared to 51.7 ± 5.3 pF, $n = 74$ at P30; $p < 0.001$). Axons coursing down to the globus pallidus were identified in few E18 MSNs but were consistently observed for P5–P7 MSNs. Same scale bar (50 μm) from E14 to P5.

than after (23 ± 3 mV at P6, $n = 15$ and 37 ± 2 mV at P10, $n = 6$; $p = 0.023$, one way ANOVA). V_{rest} measured from unitary NMDA currents was also significantly hyperpolarized between P2 and P10. Using single-channel recordings of NMDARs to provide an accurate measure of V_{rest} in young neurons (Tyzio et al., 2003; see Results of **Figure 9**), we found a significant decrease in V_{rest} between P2 and P10 (−70.0 ± 1.7 mV at P2, −77.0 ± 1.3 mV at P10; $n = 11$ and 11, respectively; $p = 0.009$, one way ANOVA test; see Dehorter et al., 2009 for extensive discussion of the method; **Figure 4G**). These results suggest that until P6, MSNs lack K^+ currents like K_{iR}, K_D, and probably leak K^+ currents as well, including

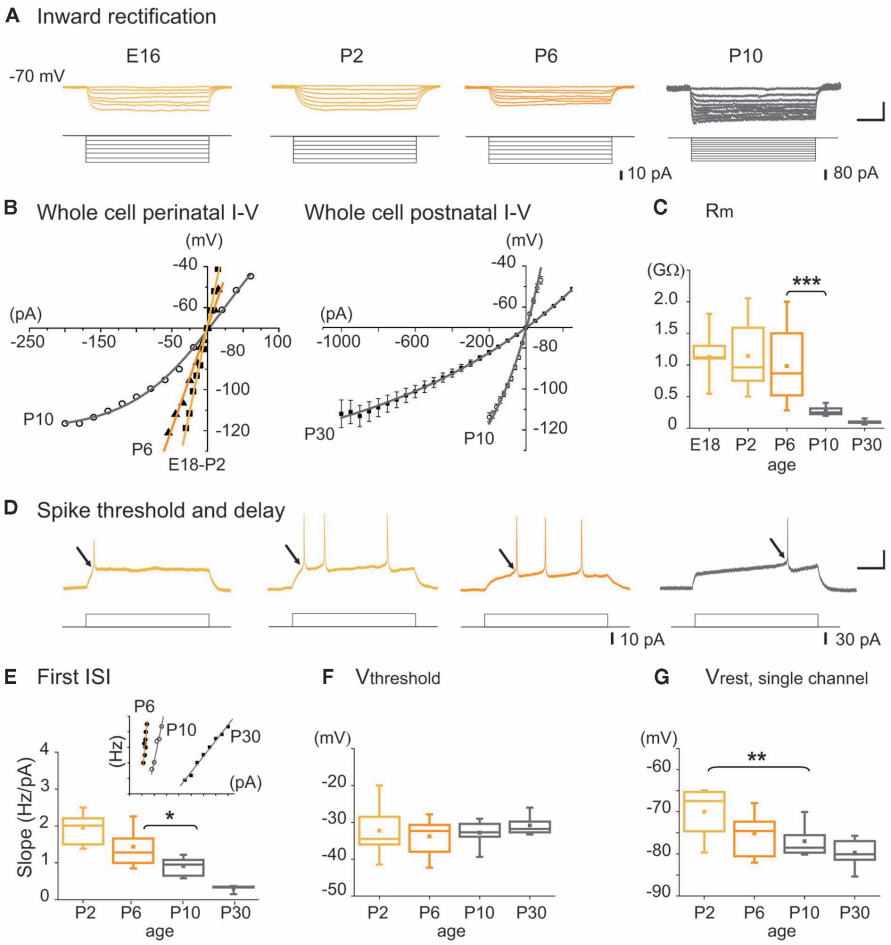

FIGURE 4 | Intrinsic membrane properties of MSNs as a function of age. (A) Representative whole cell current clamp responses of embryonic and postnatal MSNs to intracellular hyperpolarizing steps ($V_m = -70$ mV). Note the absence of inward rectification before P10. Scale bars: 25 mV; 200 ms. **(B)** Whole cell *I–V* relationships at the indicated ages, obtained from experiments in **(A)**. **(C)** Input membrane resistance (R_m) as a function of age obtained from experiments in a. **(D)** Representative whole cell current clamp responses to intracellular depolarizing steps ($V_m = -70$ mV). At E16–E18 few MSNs generated suprathreshold Na^+ spikes (14%, $n = 1/8$), 50% at P0 ($n = 3/6$), 64% at P2 ($n = 16/25$), 87% at P5 ($n = 21/24$), and 100% at P7 ($n = 12/12$). Scale bars: 25 mV; 200 ms. **(E)** Instantaneous firing frequency to the first interspike interval (ISI) of a firing train as a function of injected current (insert, scale: 20 Hz, 100 pA). Slope values given by each linear regression lines fitted to frequency curves (correlation coefficient were all >0.9) as a function of postnatal age. **(F)** Threshold potential ($V_{threshold}$) as a function of age calculated from experiments in d. **(G)** Resting membrane potential (V_{rest}) determined from the reversal potential of unitary NMDA currents in MSNs.

members of the KCNK class expressed in adult MSNs (Shen et al., 2007). Consequently, R_m is high (900 MΩ), V_{rest} is only 20 mV more hyperpolarized than $V_{threshold}$ and there is no spiking delay. Because of this, spontaneous Ca^{2+} channel openings may occur and give rise to spontaneous Ca^{2+} events.

EARLY POSTNATAL MSNs GENERATE CORRELATED Ca^{2+} SPIKES WHEN THEY EXPRESS THE NR2C/D NMDA SYNAPTIC CURRENT AND MEMBRANE PROPERTIES ARE STILL IMMATURE

The first synapse-driven pattern observed in postnatal MSNs was correlated Ca^{2+} spikes (GDPs), that appeared at P5–P7 (10% of the recordings, 969/5; mean frequency: 0.10 ± 0.05 Hz and mean duration: 0.70 ± 0.10 s, 102/5), and subsequently disappeared. The vast majority of active striatal neurons (84.0 ± 9.7%) were engaged in this activity with a large number of correlated cell pairs (24%), attesting to the large neuronal ensemble that fired together during these events (**Figure 5A** left). Electrophysiological activity underlying each GDP consisted of bursts of 2–3 Na^+ spikes (**Figure 5B**). Ionotropic glutamate and GABA receptor antagonists abolished GDPs, but left other Ca^{2+} events (uncorrelated Ca^{2+} spikes or Ca^{2+} plateaus) intact ($p = 0.02$ and 0.52 respectively, paired Student's *t*-test; **Figures 5A–D**). Since GDPs were also suppressed by APV (40 μM) alone, suggesting that NMDA receptors were heavily involved, we tested their sensitivity to PPDA (Feng et al., 2004), the preferential antagonist of NR2C/D NMDA receptors. At 100 nM PPDA removed most of the correlations between neurons (from 45 to 11%). Most of the GDP cells stopped their activity and the few who did not, evoked Ca^{2+} spikes at a much lower frequency (from 0.17 ± 0.01 to 0.07 ± 0.01 Hz; $p = 0.0003$, Mann–Whitney test; **Figures 5C,D**).

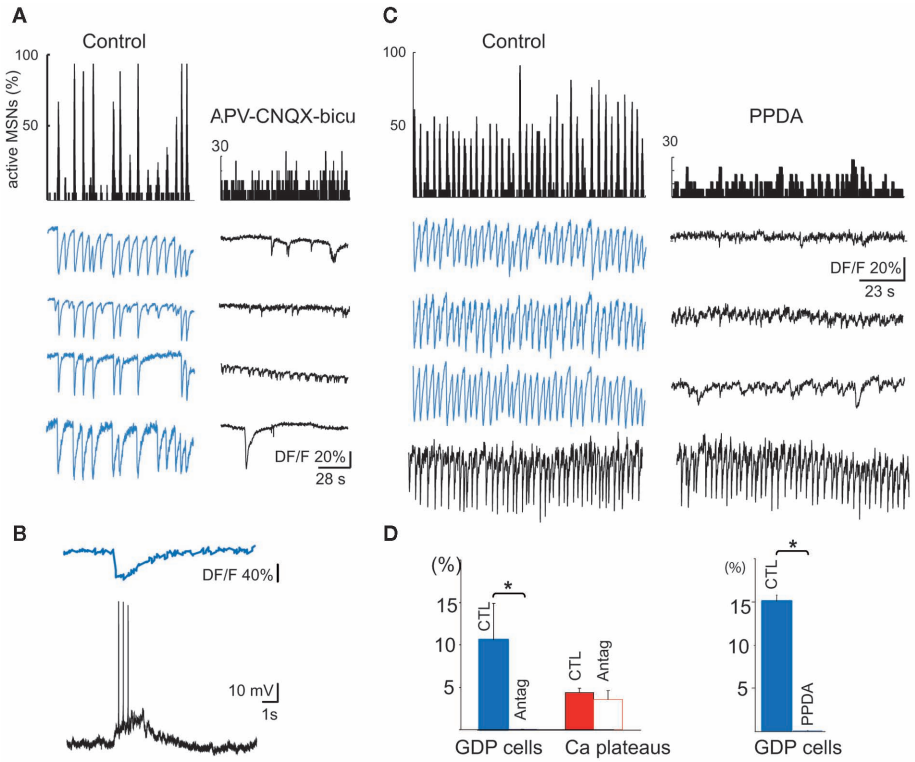

FIGURE 5 | Synapse-driven, correlated Ca^{2+} events in immature MSNs. (A) Representative histograms (top) indicating the fraction of active MSNs in the field and representative calcium fluorescence traces from MSNs (GDPs, in blue; bottom) in control ACSF (left) or in the presence of antagonists of ionotropic glutamate and $GABA_A$ receptors. **(B)** Simultaneous optical (top) and current clamp (bottom) recordings of GDPs ($V_m = -60$ mV). **(C)** Same as in **(A)** but in the presence of PPDA 100 nM. Note the specific disappearance of correlated GDPs (blue traces) during PPDA application, but not of Ca^{2+} spikes generated at a different frequency (black trace). **(D)** Left: mean percentage (±SEM) of active cells generating GDPs (blue) or Ca^{2+} plateaus (red) in control ACSF (CTL) and in the presence of antagonists of ionotropic glutamate and $GABA_A$ receptors (Antag). Right: mean percentage of cells participating in GDPs in control (CTL) or in the presence of PPDA.

To understand the time course of development of the spontaneous synaptic activities afferent to MSNs and that could play a role in the transiently expressed GDPs, we performed separate recordings of glutamatergic and GABAergic synaptic events. *Glutamatergic events*: the fraction of MSNs exhibiting AMPA- or KA-mediated sEPSCs steadily increased from E16 to E18 (38 and 50%) to a maximum at P5–P7 (100%). The mean frequency of AMPA or KA receptor-mediated EPSCs gradually increased from E16 to E18 (0.11 ± 0.04 and 0.3 ± 0.1 Hz; $n = 5$ and 5 MSNs) to P30 (1.3 ± 0.7 and 0.9 ± 0.2 Hz; $n = 5$ and 6 MSNs; $p = 0.03$ and $p = 0.004$ respectively, one way ANOVA) but their amplitude ($p = 0.3$ for AMPA, $p = 0.07$ for KA, one way ANOVA), rise times and decay times remained constant (**Figures 6A–E** left and middle). In contrast, the fraction of MSNs showing spontaneous NMDA receptor-mediated EPSCs shifted from 40% at P0 (5/12 cells) to more than 90% at P5–7 (16/18), and decreased thereafter to 30% at P30 (4/12; **Figures 6A,B** right). Their frequency stayed constant and low (around 0.1 Hz, $p = 0.9$; one way ANOVA) and also their amplitude ($p = 0.9$) and rise times but their decay time significantly decreased in the same period (**Figures 6C–E** right).

Since the cortex provides a major source of glutamatergic inputs to MSNs, we studied the development of these inputs. DiI labeling of the neocortex ($n = 5$) revealed fiber staining in the striatum as early as E16 (**Figure 7A**). These inputs are functional, because cortical stimulation evoked glutamatergic EPSPs in 10% of MSNs at E16 ($n = 2/18$), 64% at P0–P2 ($n = 20/31$), 75% at P5–P7 ($n = 9/12$), 80% at P10 ($n = 9/11$), and 86% at P30 ($n = 12/14$). This was associated with a dramatic decrease in EPSP duration between P6 and P30 (−82%) and of the number of spikes they generated. At P2, EPSPs (311 ± 32 ms; $n = 6$) generated 1 spike or spikelet, at P6 (420 ± 41 ms; $n = 8$) 2–5 spikes, while by P10 EPSPs had shortened to 276 ± 36 ms ($n = 7$; $p = 0.03$, between P6 and P10, one way ANOVA) and only gave rise to one spike as at P30 (74 ± 7 ms, $n = 7$; **Figure 7B**). At P6, the large EPSPs (and GDPs) were mostly blocked by the NMDA receptor antagonist APV, suggesting that NMDA receptors were heavily involved in early cortico-striatal activity. The long decay of P6 EPSPs suggested a preferential contribution of NR2C/D subunits of NMDA receptors with their long kinetics and reduced voltage-dependent magnesium block (Monyer et al., 1994). The NR2C/D subunit inhibitor PPDA (100 nM; Feng et al., 2004) significantly reduced evoked EPSPs at P6 (−54%; $p = 0.01$, $n = 6$; paired Student's t-test) but not at P2 (−13%; $p = 0.18$, $n = 5$; paired Student's t-test) or P10 (−9%; $p = 0.15$, $n = 5$; paired Student's t-test; **Figure 7C**),

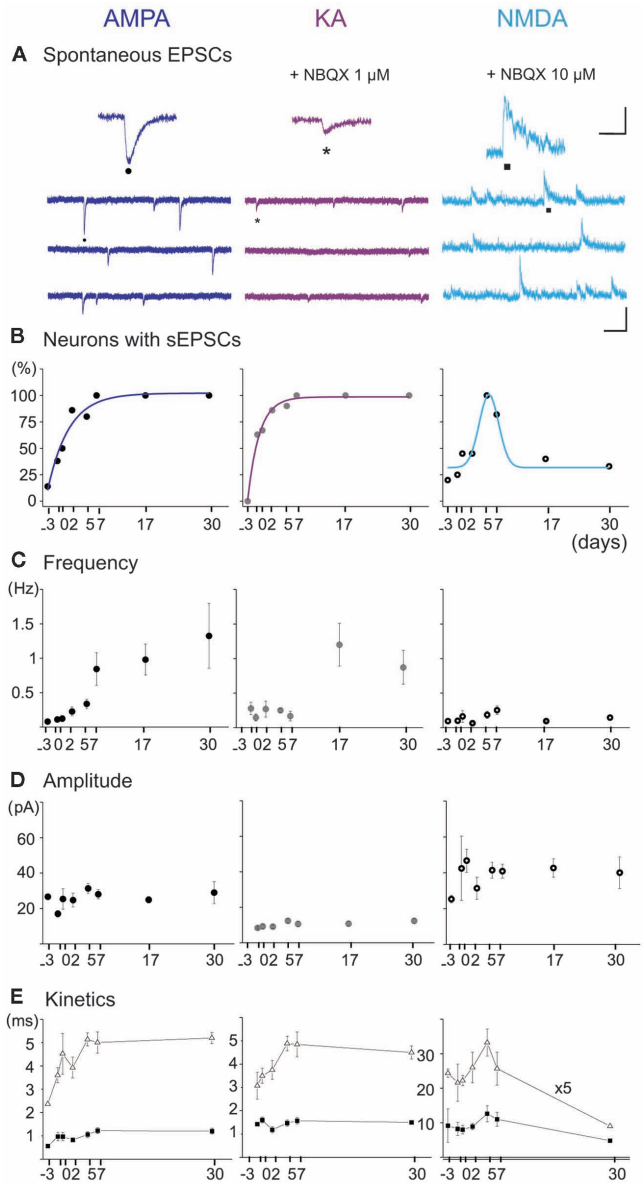

FIGURE 6 | Spontaneous AMPA, KA, and NMDA receptor-mediated postsynaptic currents (EPSCs) from E16 to P30 MSNs. (A) Representative voltage-clamp recordings of spontaneous AMPA ($V_H = -80$ mV), KA ($V_H = -80$ mV under NBQX 1 μM), and NMDA ($V_H = +40$ mV under NBQX 10 μM) receptor-mediated EPSCs (CsGlu intrapipette solution) at P6. Scale: 100 pA, 200 ms (AMPA and KA), and 2 s (NMDA). (Top) Close up of each spontaneous current (Insets: 50 pA, 125 ms). **(B)** Fraction of the recorded MSNs which displayed AMPA, KA, and NMDA sEPSCs, as a function of age ($n = 43$, 54, and 36 MSNs). **(C)** Frequency and **(D)** amplitude of AMPA, KA, and NMDA receptor-mediated sEPSCs as a function of age. **(E)** Kinetics of the three types of sEPSCs. The rise times remained stable from E18 to P30 for AMPA (0.7 ± 0.1 vs. 0.8 ± 0.2 ms; $p = 0.83$), KA (1.0 ± 0.3 vs. 1.1 ± 0.2 ms; $p = 0.84$), and NMDA (7.1 ± 0.8 vs. 5.2 ± 1.1 ms; $p = 0.33$) currents. The decay times (τ) stayed constant for AMPA (1.8 ± 0.3 ms at E18 vs. 2.9 ± 0.5 ms at P30, $p = 0.16$) and KA (2.1 ± 0.3 ms at E18 vs. 2.9 ± 0.3 at P30, $p = 0.08$) currents whereas it significantly decreased for NMDA currents (203 ± 16 ms at P7, $n = 9/11$ vs. 87 ± 9 ms at P30, $n = 4/12$; $p = 0.009$).

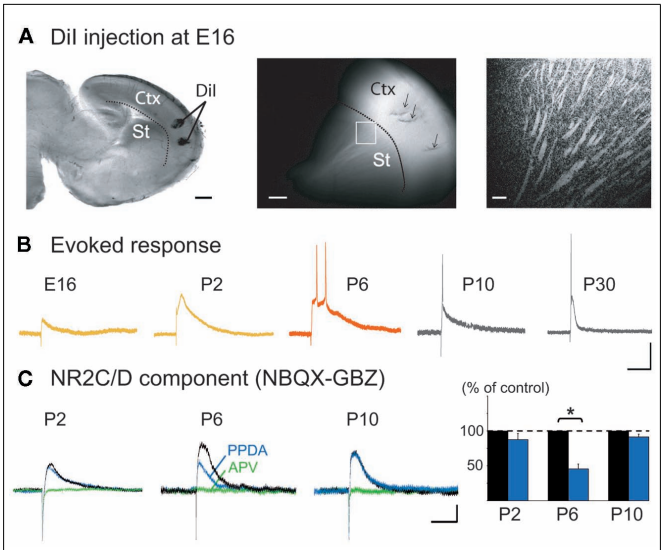

FIGURE 7 | Embryonic presence of cortico-striatal EPSPs and postnatal transient expression of the NR2C/D-mediated NMDA component. (A) DiI injections in neocortex in an E16 sagittal slice (left). DiI-labeled cortical fibers observed in the striatum after 15 days of incubation, as shown in the confocal image (right) of the region indicated by a square (middle). Scale bars: 500, 200, and 50 μm. **(B)** Whole cell current clamp responses of embryonic and postnatal MSNs to intra-cortical stimulation in the absence of synaptic blockers ($V_m = -70$ mV), scale bars: 25 mV, 100 ms. **(C)** Effect of PPDA (100 nM, 15 min, blue) and APV (40 μM, green) on the NBQX (10 μM)/gabazine (GBZ, 10 μM) insensitive whole cell EPSP (black) at P2 ($n = 5$), P6 ($n = 6$), and P10 ($n = 5$), scale bars 10 mV, 250 ms.

showing a restricted participation of NR2C/D before and after P6. The presence of a large NR2C/D-mediated NMDA component enables cortico-striatal synapses to generate large EPSCs associated with bursts of spikes at P5–P7, but not at P10.

GABAergic events

The fraction of MSNs exhibiting spontaneous $GABA_A$R-mediated currents steadily increased from E16 to a maximum at P5–P7 and the mean frequency of these currents ($GABA_A$ PSCs) progressively increased from E16 up to P30 (519 MSNs; **Figures 8A–C**). The DF of GABA (DF_{GABA}), determined from single-channel recordings of $GABA_A$Rs (see Materials and Methods; Tyzio et al., 2003), was similarly depolarizing by 15 mV at P2 ($+15.3 \pm 3.4$ mV; $n = 8$ MSNs, **Figures 9A,B**) and P30 (Dehorter et al., 2009; $+16.1 \pm 1.9$ mV, $n = 11$; $p = 0.8$, Student's t-test). To estimate (E_{GABA_A}), we plotted the relationship between the single-channel $GABA_A$ current ($iGABA_A$) and the pipette potential (V_p). This curve [$iGABA_A = f(V_p)$] gives the value of V_p when $iGABA_A = 0$ pA (**Figures 9A,B** right), because when $iGABA_A$ is null, $V_m = E_{GABA_A}$. Therefore, when $iGABA_A = 0$ pA, $V_m = V_p - V_{rest} = E_{GABA_A}$ (i.e., $E_{GABA_A} - V_{rest} = -V_p$). By definition, $E_{GABA_A} - V_{rest} = DF_{GABA_A}$, the DF of chloride ions through the $GABA_A$ channel (Tyzio et al., 2003). Therefore, when $I_{GABA_A} = 0$ pA, $DF_{GABA_A} = -V_p$. Knowing V_{rest} and DF_{GABA_A}, we can calculate the reversal potential for $GABA_A$, $E_{GABA_A} = DF_{GABA_A} + V_{rest}$. The reversal potential of $GABA_A$ currents was

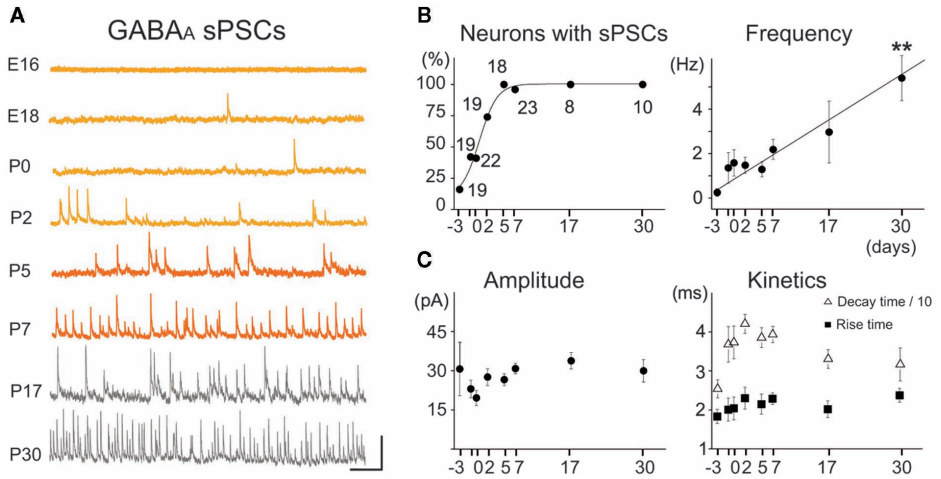

FIGURE 8 | Spontaneous $GABA_A$ postsynaptic currents ($GABA_A$-sPSCs) from E16 to P30 MSNs. (A) Voltage-clamp recordings of $GABA_A$-sPSCs at the indicated ages with CsGlu intrapipette solution ($V_H = +10$ mV). Scale: 50 pA, 500 ms. **(B)** Fraction of recorded MSNs which displayed $GABA_A$-sPSCs and frequency of $GABA_A$-sPSCs ($R > 0.9$) from E16 to P30 (for comparison, 2.1 ± 0.4 Hz at P7 vs. 5.4 ± 1.0 Hz at P30, $n = 22$ and $n = 10$, respectively; $p < 0.01$, one way ANOVA). **(C)** Amplitude and kinetics of $GABA_A$-sPSCs did not significantly change from E16 to P30 ($p > 0.05$ for both, one way ANOVA; 30.3 ± 2.0 pA at E16 vs. 30.0 ± 4.3 pA at P30, $n = 19$ and $n = 10$, respectively; one way ANOVA). Neither the rise or decay time constants of GABAergic PSCs differed significantly during development: rise time (ν) around 2 ms (2.3 ± 0.1 ms at P7 vs. 2.4 ± 0.2 ms at P30), and decay time (Δ) around 35 ms (39.3 ± 2.1 ms at P7 vs. 32.0 ± 4.2 ms at P30; $n = 22$ at P7 and $n = 10$ at P30).

10 mV more depolarized at P2 than at P30 (**Figure 9C**). These values are based on the assumption that the NMDA current reverses at 0 mV in MSNs. Although an error of 5 mV may exist (Tyzio et al., 2003), the comparison of V_{rest} and E_{GABA} obtained with the same methods at P2 and P30 confirms the validity of our conclusions. Therefore, GABAergic synapses depolarize MSNs from V_{rest} to a value closer to the action potential threshold than in the adult (Misgeld et al., 1982; Koos and Tepper, 1999). However, GABA does not excite immature MSNs. Focal applications of the $GABA_A$ receptor agonist isoguvacine failed to generate action potentials in cell-attached recordings from P2 ($n = 6$, **Figure 9D**) or P5 ($n = 7$, data not shown) MSNs. Similarly, stimulation of the striatal neuropil failed to evoke action potentials in cell-attached recordings of MSNs in the continuous presence of ionotropic glutamate receptors antagonists (data not shown).

The above data show that striatal neurons generate GDPs during a transient period when all MSNs are connected to glutamatergic and GABAergic neurons and still exhibit immature membrane properties (see **Figure 4**). There is a more efficient GABAergic depolarizing drive than at P30 that may participate in the GDPs of P5–P7 MSNs (together with glutamatergic EPSPs; Bracci and Panzeri, 2006) but these events are mainly driven by cortico-striatal synapses at a time where cortical neurons also generate GDPs (Allene et al., 2008).

INTRINSIC AND SYNAPSE-DRIVEN IMMATURE ACTIVITY DERIVE FROM DISTINCT NEURAL ENSEMBLES

Because approximately 90% of the P5–P7 striatal networks did not generate GDPs at the time of recording, we wanted to understand whether synapse formation in some way altered the dynamics of the network. We compared network-wide activity at P2–P3 (when synapse density is low) to that at P5–P7 (when all MSNs are innervated by glutamatergic and GABAergic inputs). We found that both frequency and duration of events changed from P2–P3 to P5–P7 (**Figures 10A,B**). The distributions of mean event frequency significantly differed between P2–P3 and P5–P7 (Mann–Whitney U-test; $n_{P2} = 18$, $n_{P6} = 33$; $U = 320$; $p = 0.02$). Similarly, the distributions of median event duration significantly differed between P2–P3 and P5–P7 ($U = 569.5$, $p = 0.0046$). To gage the size of these differences between P2–P3 and P5–P7, we used k-means clustering to assign each recording to either P2–P3 or P5–P7 on the basis of its event statistics. We found that both duration (70% correct assignments) and frequency (64% correct) reliably indicated a recording's developmental stage. Thus, the switch from intrinsically to synaptically driven activity reliably decreased duration and increased the frequency of calcium events in the immature striatal network.

Both P2–P3 and P5–P7 networks were capable of showing spontaneous formation of neural ensembles (**Figures 10C,D**). We found markedly more P5–P7 (43%, 9/21) than P2–P3 (29%, 4/18) recordings with significant ensemble structure. Conversely, these P2–P3 recordings contained more ensembles (range 5–9) than the P5–P7 recordings (range 2–6). We also found that the P5–P7 recordings with GDP-driven, network-wide synchronization could be sub-divided into ensembles that indicated the delay in a neuron's participation of the network-wide synchronization (**Figure 10E**). These results suggest that the transition from intrinsic to synaptically driven activity promoted the appearance of putative cell assemblies.

ABRUPT LOSS OF GDPs AND SWITCH TO ADULT-LIKE INTRINSIC PROPERTIES OCCURS BEFORE COORDINATED LOCOMOTION

As shown in **Figures 11A–E**, many MSN characteristics changed abruptly between P6 and P10. MSNs become mostly silent

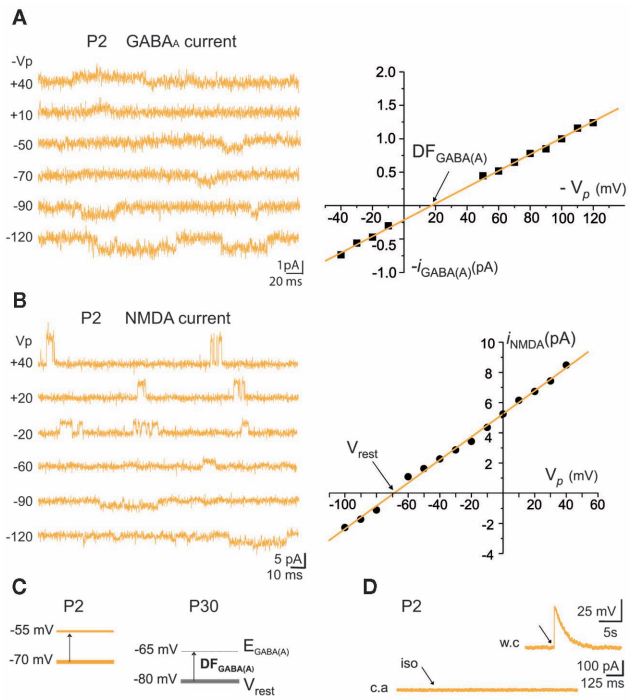

FIGURE 9 | Resting membrane potential (V_{rest}) and reversal potential for $GABA_A$-mediated currents [$E_{GABA(A)}$] of immature MSNs. (A) Representative cell-attached recordings of unitary $GABA_A$ currents at the indicated pipette potential (V_p in mV) and corresponding *I–V* relationship of the recorded $GABA_A$ currents to determine the driving force (DF) for GABA ($DF_{GABA} = +17$ mV). **(B)** Representative cell-attached recordings of unitary NMDA currents at the indicated V_p (in mV) and corresponding *I–V* relationship of the recorded currents to determine V_{rest} (−67 mV). **(C)** DF_{GABA} was around 15 mV at P2 and P30 (Dehorter et al., 2009), which gives $E_{GABA(A)} = -55$ mV at P2 and −65 mV at P30. **(D)** Pressure application of isoguvacine (iso, 100 μM) during cell-attached recordings. Inset shows the depolarization evoked by the same pressure application of isoguvacine during whole cell recording of the same MSN, to test the pressure application of isoguvacine. For DF_{GABA} calculation Section "Materials and Methods," analysis of electrophysiological data.

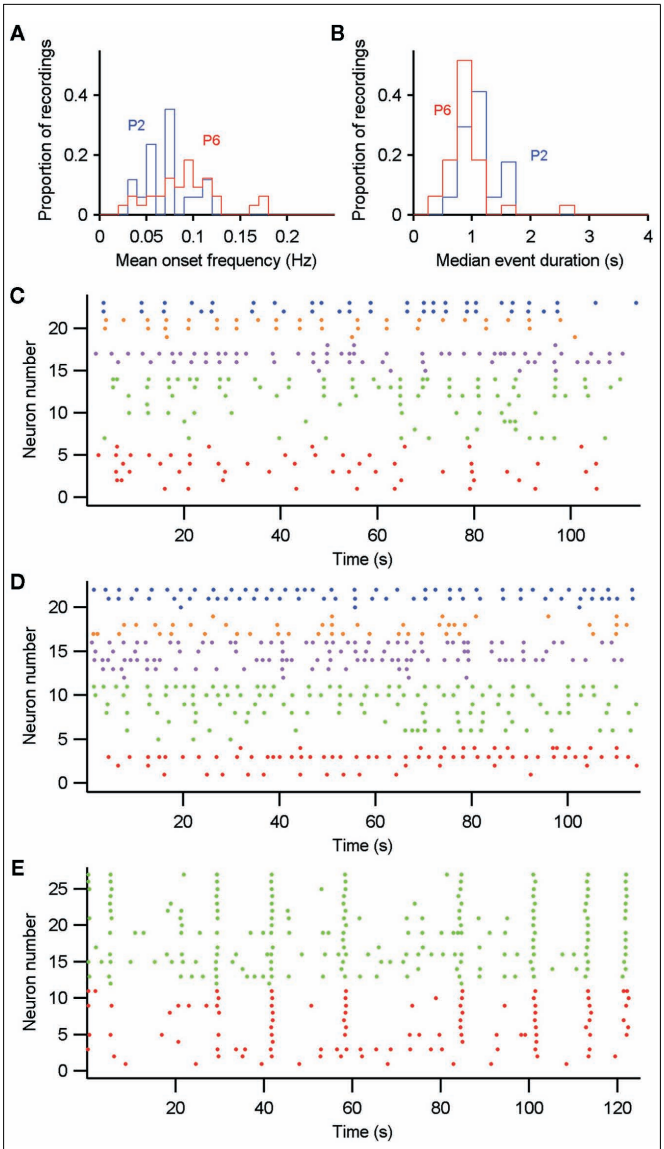

FIGURE 10 | Comparison of intrinsically (P2–P3) and synaptically (P5–P7) driven immature spontaneous Ca^{2+} activity. (A,B) Distributions of each recording's mean event frequency and median event duration for P2–P3 (P2) and P5–P7 (P6). **(C,D)** Example recordings at P2 **(C)** and P6 **(D)** with significant neural ensemble structure; both contain five groups. **(E)** Neural ensembles within GDP-driven network-wide synchronization at P6. In **(C–E)**, neuron activity is color-coded by ensemble membership, as determined by the algorithm of Humphries (2011) – Section "Materials and Methods."

at P10, entering an adult-like phase. AMPA or KA receptor-mediated signals are probably not involved in the extinction of early spontaneous activity in MSNs because their frequency continuously increases with age. In contrast, the switch in other properties such as the abrupt loss of NR2C/D, expression of IK_{IR}, decrease in R_m, hyperpolarization of V_{rest}, and hyperpolarization of E_{GABA_A} all coincided with the silencing of MSNs.

In order to identify when the transition of MSNs from immature to adult-like state occurs in relation to a motor behavioral output, we quantified the maturation of pup body contacts and motion. At P2, prior to the onset of quadruped ambulation, the duration of abdominal contact with the cage surface was high ($35.3 \pm 4.9\%$ of total time), then progressively decreased at P3–P6 ($17.8 \pm 1.6\%$) and P7–P8 ($2.9 \pm 0.7\%$), disappearing by P9–P10 ($n = 16$; $p = 1 \times 10^{-8}$ between P3–P6 and P7–P8; one way ANOVA; **Figures 11F,G**, top). Body motion was practically absent at P2, with pivoting and crawling predominating in P3–P7 pups. The total distance pups traveled along straight line segments underwent a marked increase from P3 to P6 (0.2 ± 0.1 cm, $n = 56$) to P9–P10 (7.9 ± 1.6 cm, $n = 28$; $p = 0.0002$, one way ANOVA test). By P12 pups traversed relatively large distances (28.9 ± 3.5 cm, $n = 14$; $p = 1 \times 10^{-12}$ compared to P9–P10; one way ANOVA test; **Figures 11F,G**, bottom). Thus, spontaneous displacement with the ventral surface of the body held above the floor was first observed in P9–P10 mouse pups, in parallel with the chronology of MSN silencing.

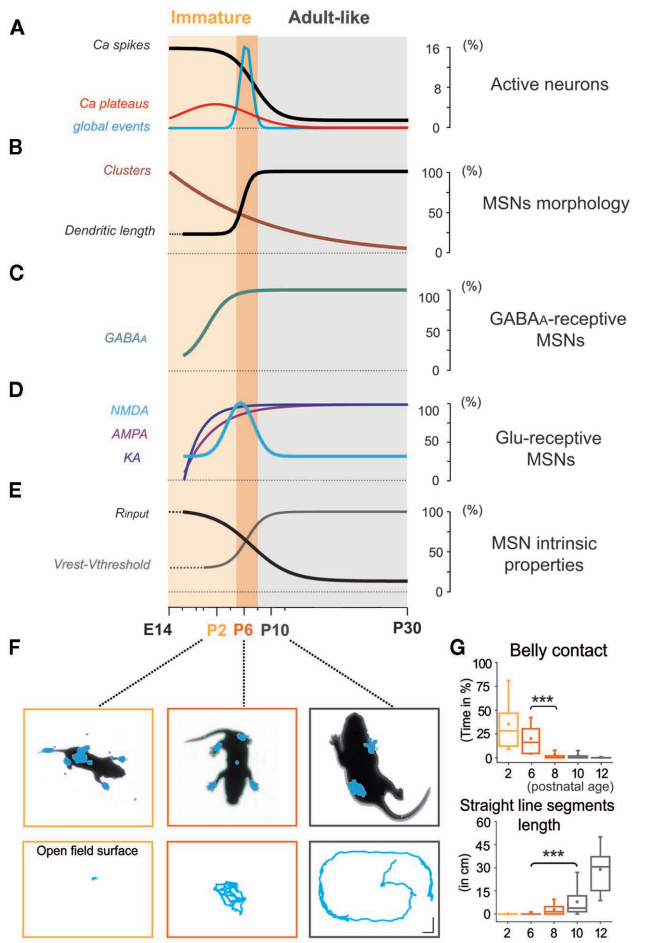

FIGURE 11 | Medium spiny neurons have entered the adult-like phase before pups start quadruped locomotion. (A–E) Immature (light orange) and adult-like (gray) phases are separated by a transitory immature period (orange). Development of MSN intrinsic and synaptic properties from experiments of **Figures 1–7**. **(F)** Photos of representative postnatal mice showing the number and extent of pressure points (in blue) at P2, P6, and P10 (top). Body motion of the same pups in the open field (calibration bars 3 cm) during a 1-min test (bottom). **(G)** Mean percentage (±SEM) of belly contact time ($n = 16$, top) and total distance traveled along straight line segments ($n = 14$, bottom) as a function of postnatal age (see Movies S1–S3 in Supplementary Material).

DISCUSSION

Our results show that MSNs, the dominant neuronal population of the striatum, generate immature patterns of activity at embryonic and early postnatal stages that are reminiscent of the patterns observed in developing cortical structures (Garaschuk et al., 2000; Corlew et al., 2004; Allene et al., 2008). This confirms the similarity between developmental activities of networks independently of their neuronal structure and final function (Ben-Ari, 2001). In the middle of the second postnatal week, MSNs shift to an adult-like pattern characterized by little activity *in vitro* (Carrillo-Reid et al., 2008), just before pups lift their body and begin to walk. Underlying this transition is a change in the fundamental characteristics of MSNs (**Figure 11**). This suggests that the development of MSNs and striatal network activity parallels the development of locomotor structures and pathways (Grillner et al., 2005).

Two features of immature MSNs emerge as central players in this progression. (i) Intrinsic voltage-gated Ca^{2+} currents: we propose that the reduced K^+ currents and the consequent depolarized resting membrane potential allow spontaneous opening of N and L-type voltage-gated Ca^{2+} channels, then quieted near P10 by resting membrane potential hyperpolarization and/or developmental changes of Ca^{2+} channel properties; (ii) The transient NR2C/D-mediated cationic current: the expression of long lasting NMDA EPSCs mediated by the NR2C/D receptor subunit is a general feature of different developing brain structures (Monyer et al., 1994; Nansen et al., 2000; Logan et al., 2007; Dravid et al., 2008). NMDA receptor-mediated EPSCs are conspicuous in cortico-striatal neurons as early as P2 (see Hurst et al., 2001) for contradictory results). Using a dose of PPDA (100 nM) that preferentially antagonizes NR2C/D subunits ($K_D = 0.096$ and 0.130 μM, respectively; Traynelis et al., 2010), we demonstrate that the window of operation of NR2C/D-mediated events is highly restricted to P5–P8 (Dunah et al., 1996). Therefore, as in other brain structures, immature neurons first generate long lasting synapse-driven patterns of activity that include large NMDA receptor driven currents. These currents, together with voltage-gated Ca^{2+} currents, trigger the large calcium fluxes needed for a wide range of essential developmental functions including neuronal growth, synapse formation, and the formation of neuronal ensembles (Spitzer, 2006). Indeed, we demonstrated that during this P5–P8 window, network-wide changes in calcium event statistics correlated with the reliable formation of neural ensembles.

Our observations also provide interesting insights concerning the generation of GDPs that have been observed in a wide range of brain networks but investigated primarily in cortical structures (Ben-Ari et al., 2007). GDPs are generated both by depolarizing GABAergic and glutamatergic notably NMDA receptors-mediated currents. The striatum is an interesting site to investigate the debated role of glutamate in GDPs generation because it has in contrast with other investigated structures no internal glutamatergic neurons. Clearly, the maturation of the glutamatergic cortico-striatal inputs is instrumental in the emergence of GDPs and particularly the long lasting NR2C/D component.

Adesnik et al. (2008) suggested that modest activity through NMDA receptors prevents the constitutive trafficking of AMPA receptors to the postsynaptic density via an LTD type mechanism. This ensures that synapses become functional only after strong or correlated activity, when enough calcium entry through these NMDA receptors overrides the inhibitory pathway and drives AMPA receptor insertion. This surge is provided by bursts of action potentials during GDPs and NMDA-mediated cortico-striatal EPSPs as shown here. From this perspective the elimination of the long lasting NR2C/D component in cortico-striatal EPSPs would constitute a gating device to induce the expression of AMPAergic currents in MSNs.

Therefore, our results suggest an intrinsic program that switches MSN activity from an immature low threshold activation state to a high threshold state in the adult with a low activity profile during resting conditions, coincident with the emergence of locomotion. In a more conceptual frame, in addition to ubiquitous

developmental patterns of activity, there would be a superimposed sequence, unique to each brain structure, which takes over at an appropriate time to enable the generation of patterns required for specific functions. The adult-like state described here is accompanied by several additional factors including the development of the dendritic arbor and spines of MSNs and the increased density of asymmetric glutamatergic synapses (Tepper et al., 1998; Belleau and Warren, 2000), a second wave of nigro-striatal dopaminergic innervation (Moon and Herkenham, 1984), the development of thalamo-cortical loops, and sensori-motor cortex (Gianino et al., 1999; Vinay et al., 2002; Allene et al., 2008; Evrard and Ropert, 2009). It is also accompanied functionally by a dopamine- and D2 receptor-dependent decrease in the efficacy of glutamatergic transmission that takes place *in vivo* during weeks 2–3 of postnatal development and is a consequence of a number of physiological changes in the maturing striatum (Choi and Lovinger, 1997; Tang et al., 2001). Also, comparison of the present data with that obtained in rodents lacking dopaminergic substantia nigra neurons (pitx3$^{-/-}$ mice for example, Smidt et al., 2004), will allow understanding of the early role of endogenous dopamine on the development of the striatal network (Ohtani et al., 2003; Goffin et al., 2010).

Finally, present observations may be of clinical relevance because adult MSNs from the R6/2 rodent model of Huntington's disease resemble immature MSNs described here in several respects, including an increased input resistance, depolarized resting membrane potential, low level of inwardly and outwardly rectifying K^+ currents (Ariano et al., 2005), increased sensitivity to NMDA receptor activation (Cepeda et al., 2001) and decreased sensitivity of NMDA receptors to Mg^{2+} block (Starling et al., 2005).

ACKNOWLEDGMENTS

The RCE:LoxP reporter strain was a gift of the Fishell laboratory. We thank R. Cossart, D. Aronov, and P. Bonifazi who developed the analysis method of the imaging data, J. Gallego for the use of the motricity platform facility and Y. Ben Ari for helpful discussions. This work was supported by grants from Institut National de La Santé et de la Recherche Médicale (INSERM), Fédération pour la Rechercher sur le Cerveau (FRC), Association Française contre les Myophaties (AFM), and Fondation Motrice. Nathalie Dehorter held a studentship from Région Provence Alpes Côte d'Azur, Neuroservice (Dir B. Buisson), and Association France Parkinson.

SUPPLEMENTARY MATERIAL

The Supplementary Material for this article can be found online at http://www.frontiersin.org/cellular_neuroscience/10.3389/fncel.2011.00024/abstract

REFERENCES

Adesnik, H., Li, G., During, M. J., Pleasure, S. J., and Nicoll, R. A. (2008). NMDA receptors inhibit synapse unsilencing during brain development. *Proc. Natl. Acad. Sci. U.S.A.* 105, 5597–5602.

Allene, C., Cattani, A., Ackman, J. B., Bonifazi, P., Aniksztejn, L., Ben-Ari, Y., and Cossart, R. (2008). Sequential generation of two distinct synapse-driven network patterns in developing neocortex. *J. Neurosci.* 28, 12851–12863.

Ariano, M. A., Cepeda, C., Calvert, C. R., Flores-Hernandez, J., Hernandez-Echeagaray, E., Klapstein, G. J., Chandler, S. H., Aronin, N., DiFiglia, M., and Levine, M. S. (2005). Striatal potassium channel dysfunction in Huntington's disease transgenic mice. *J. Neurophysiol.* 93, 2565–2574.

Belleau, M. L., and Warren, R. A. (2000). Postnatal development of electrophysiological properties of nucleus accumbens neurons. *J. Neurophysiol.* 84, 2204–2216.

Ben-Ari, Y. (2001). Developing networks play a similar melody. *Trends Neurosci.* 24, 353–360.

Ben-Ari, Y. (2002). Excitatory actions of gaba during development: the nature of the nurture. *Nat. Rev. Neurosci.* 3, 728–739.

Ben-Ari, Y., Gaiarsa, J. L., Tyzio, R., and Khazipov, R. (2007). GABA: a pioneer transmitter that excites immature neurons and generates primitive oscillations. *Physiol. Rev.* 87, 1215–1284.

Blankenship, A. G., and Feller, M. B. (2010). Mechanisms underlying spontaneous patterned activity in developing neural circuits. *Nat. Rev. Neurosci.* 11, 18–29.

Bonifazi, P., Goldin, M., Picardo, M. A., Jorquera, I., Cattani, A., Bianconi, G., Represa, A., Ben-Ari, Y., and Cossart, R. (2009). GABAergic hub neurons orchestrate synchrony in developing hippocampal networks. *Science* 326, 1419–1424.

Bracci, E., and Panzeri, S. (2006). Excitatory GABAergic effects in striatal projection neurons. *J. Neurophysiol.* 95, 1285–1290.

Carrillo-Reid, L., Tecuapetla, F., Tapia, D., Hernandez-Cruz, A., Galarraga, E., Drucker-Colin, R., and Bargas, J. (2008). Encoding network states by striatal cell assemblies. *J. Neurophysiol.* 99, 1435–1450.

Cepeda, C., Ariano, M. A., Calvert, C. R., Flores-Hernandez, J., Chandler, S. H., Leavitt, B. R., Hayden, M. R., and Levine, M. S. (2001). NMDA receptor function in mouse models of Huntington disease. *J. Neurosci. Res.* 66, 525–539.

Choi, S., and Lovinger, D. M. (1997). Decreased probability of neurotransmitter release underlies striatal long-term depression and postnatal development of corticostriatal synapses. *Proc. Natl. Acad. Sci. U.S.A.* 94, 2665–2670.

Corlew, R., Bosma, M. M., and Moody, W. J. (2004). Spontaneous, synchronous electrical activity in neonatal mouse cortical neurones. *J. Physiol.* 560, 377–390.

Crepel, V., Aronov, D., Jorquera, I., Represa, A., Ben-Ari, Y., and Cossart, R. (2007). A parturition-associated nonsynaptic coherent activity pattern in the developing hippocampus. *Neuron* 54, 105–120.

Deacon, T. W., Pakzaban, P., and Isacson, O. (1994). The lateral ganglionic eminence is the origin of cells committed to striatal phenotypes: neural transplantation and developmental evidence. *Brain Res.* 668, 211–219.

Dehorter, N., Guigoni, C., Lopez, C., Hirsch, J., Eusebio, A., Ben-Ari, Y., and Hammond, C. (2009). Dopamine-deprived striatal GABAergic interneurons burst and generate repetitive gigantic IPSCs in medium spiny neurons. *J. Neurosci.* 29, 7776–7787.

Dravid, S. M., Prakash, A., and Traynelis, S. F. (2008). Activation of recombinant NR1/NR2C NMDA receptors. *J. Physiol.* 586, 4425–4439.

Dunah, A. W., Yasuda, R. P., Wang, Y. H., Luo, J., vila-Garcia, M., Gbadegesin, M., Vicini, S., and Wolfe, B. B. (1996). Regional and ontogenic expression of the NMDA receptor subunit NR2D protein in rat brain using a subunit-specific antibody. *J. Neurochem.* 67, 2335–2345.

Epsztein, J., Represa, A., Jorquera, I., Ben-Ari, Y., and Crepel, V. (2005). Recurrent mossy fibers establish aberrant kainate receptor-operated synapses on granule cells from epileptic rats. *J. Neurosci.* 25, 8229–8239.

Evrard, A., and Ropert, N. (2009). Early development of the thalamic inhibitory feedback loop in the primary somatosensory system of the newborn mice. *J. Neurosci.* 29, 9930–9940.

Feng, B., Tse, H. W., Skifter, D. A., Morley, R., Jane, D. E., and Monaghan, D. T. (2004). Structure-activity analysis of a novel NR2C/NR2D-preferring NMDA receptor antagonist: 1-(phenanthrene-2-carbonyl) piperazine-2,3-dicarboxylic acid. *Br. J. Pharmacol.* 141, 508–516.

Garaschuk, O., Linn, J., Eilers, J., and Konnerth, A. (2000). Large-scale oscillatory calcium waves in the immature cortex. *Nat. Neurosci.* 3, 452–459.

Gianino, S., Stein, S. A., Li, H., Lu, X., Biesiada, E., Ulas, J., and Xu, X. M. (1999). Postnatal growth of corticospinal axons in the spinal cord of developing mice. *Brain Res. Dev. Brain Res.* 112, 189–204.

Goffin, D., Ali, A. B., Rampersaud, N., Harkavyi, A., Fuchs, C., Whitton, P. S., Nairn, A. C., and Jovanovic, J. N. (2010). Dopamine-dependent tuning of striatal inhibitory synaptogenesis. *J. Neurosci.* 30, 2935–2950.

Grillner, S., Hellgren, J., Menard, A., Saitoh, K., and Wikstrom, M. A. (2005). Mechanisms for selection of basic motor programs–roles for the striatum and pallidum. *Trends Neurosci.* 28, 364–370.

Groc, L., Gustafsson, B., and Hanse, E. (2002). Spontaneous unitary synaptic activity in CA1 pyramidal neurons during early postnatal development: constant contribution of AMPA and NMDA receptors. *J. Neurosci.* 22, 5552–5562.

Han, J. Y. (2005). "Low-cost multi-touch sensing through frustrated total internal reflection," in *Proceedings of the 18th Annual ACM Symposium on User Interface Software and Technology – UIST* (New York, NY: ACM Press), 115–118.

Huberman, A. D., Feller, M. B., and Chapman, B. (2008). Mechanisms underlying development of visual maps and receptive fields. *Annu. Rev. Neurosci.* 31, 479–509.

Humphries, M. D. (2011). Spike-train communities: finding groups of similar spike trains. *J. Neurosci.* 31, 2321–2336.

Hurst, R. S., Cepeda, C., Shumate, L. W., and Levine, M. S. (2001). Delayed postnatal development of NMDA receptor function in medium-sized neurons of the rat striatum. *Dev. Neurosci.* 23, 122–134.

Koos, T., and Tepper, J. M. (1999). Inhibitory control of neostriatal projection neurons by GABAergic interneurons. *Nat. Neurosci.* 2, 467–472.

Logan, S. M., Partridge, J. G., Matta, J. A., Buonanno, A., and Vicini, S. (2007). Long-lasting NMDA receptor-mediated EPSCs in mouse striatal medium spiny neurons. *J. Neurophysiol.* 98, 2693–2704.

Misgeld, U., Wagner, A., and Ohno, T. (1982). Depolarizing IPSPs and Depolarization by GABA of rat neostriatum cells in vitro. *Exp. Brain Res.* 45, 108–114.

Monyer, H., Burnashev, N., Laurie, D. J., Sakmann, B., and Seeburg, P. H. (1994). Developmental and regional expression in the rat brain and functional properties of four NMDA receptors. *Neuron* 12, 529–540.

Moon, E. S., and Herkenham, M. (1984). Comparative development of striatal opiate receptors and dopamine revealed by autoradiography and histofluorescence. *Brain Res.* 305, 27–42.

Nansen, E. A., Jokel, E. S., Lobo, M. K., Micevych, P. E., Ariano, M. A., and Levine, M. S. (2000). Striatal ionotropic glutamate receptor ontogeny in the rat. *Dev. Neurosci.* 22, 329–340.

Nimmerjahn, A., Kirchhoff, F., Kerr, J. N., and Helmchen, F. (2004). Sulforhodamine 101 as a specific marker of astroglia in the neocortex in vivo. *Nat. Methods* 1, 31–37.

Nobrega-Pereira, S., Kessaris, N., Du, T., Kimura, S., Anderson, S. A., and Marin, O. (2008). Postmitotic Nkx2-1 controls the migration of telencephalic interneurons by direct repression of guidance receptors. *Neuron* 59, 733–745.

Ohtani, N., Goto, T., Waeber, C., and Bhide, P. G. (2003). Dopamine modulates cell cycle in the lateral ganglionic eminence. *J. Neurosci.* 23, 2840–2850.

Olsson, M., Bjorklund, A., and Campbell, K. (1998). Early specification of striatal projection neurons and interneuronal subtypes in the lateral and medial ganglionic eminence. *Neuroscience* 84, 867–876.

Shen, W., Tian, X., Day, M., Ulrich, S., Tkatch, T., Nathanson, N. M., and Surmeier, D. J. (2007). Cholinergic modulation of Kir2 channels selectively elevates dendritic excitability in striatopallidal neurons. *Nat. Neurosci.* 10, 1458–1466.

Smidt, M. P., Smits, S. M., Bouwmeester, H., Hamers, F. P., van der Linden, A. J., Hellemons, A. J., Graw, J., and Burbach, J. P. (2004). Early developmental failure of substantia nigra dopamine neurons in mice lacking the homeodomain gene Pitx3. *Development* 131, 1145–1155.

Sousa, V. H., Miyoshi, G., Hjerling-Leffler, J., Karayannis, T., and Fishell, G. (2009). Characterization of Nkx6-2-derived neocortical interneuron lineages. *Cereb. Cortex* 19(Suppl. 1), i1–i10.

Spitzer, N. C. (2006). Electrical activity in early neuronal development. *Nature* 444, 707–712.

Starling, A. J., Andre, V. M., Cepeda, C., de, L. M., Chandler, S. H., and Levine, M. S. (2005). Alterations in N-methyl-D-aspartate receptor sensitivity and magnesium blockade occur early in development in the R6/2 mouse model of Huntington's disease. *J. Neurosci. Res.* 82, 377–386.

Tang, K., Low, M. J., Grandy, D. K., and Lovinger, D. M. (2001). Dopamine-dependent synaptic plasticity in striatum during in vivo development. *Proc. Natl. Acad. Sci. U.S.A.* 98, 1255–1260.

Tepper, J. M., Koos, T., and Wilson, C. J. (2004). GABAergic microcircuits in the neostriatum. *Trends Neurosci.* 27, 662–669.

Tepper, J. M., Sharpe, N. A., Koos, T. Z., and Trent, F. (1998). Postnatal development of the rat neostriatum: electrophysiological, light- and electron-microscopic studies. *Dev. Neurosci.* 20, 125–145.

Todd, K. L., Kristan, W. B. Jr., and French, K. A. (2010). Gap junction expression is required for normal chemical synapse formation. *J. Neurosci.* 30, 15277–15285.

Traynelis, S. F., Wollmuth, L. P., McBain, C. J., Menniti, F. S., Vance, K. M., Ogden, K. K., Hansen, K. B., Yuan, H., Myers, S. J., Dingledine, R., and Sibley, D. (2010). Glutamate receptor ion channels: structure, regulation, and function. *Pharmacol. Rev.* 62, 405–496.

Tyzio, R., Ivanov, A., Bernard, C., Holmes, G. L., Ben-Ari, Y., and Khazipov, R. (2003). Membrane potential of CA3 hippocampal pyramidal cells during postnatal development. *J. Neurophysiol.* 90, 2964–2972.

Van Der Kooy, D., and Fishell, G. (1987). Neuronal birthdate underlies the development of striatal compartments. *Brain Res.* 401, 155–161.

Venance, L., Glowinski, J., and Giaume, C. (2004). Electrical and chemical transmission between striatal GABAergic output neurones in rat brain slices. *J. Physiol.* 559, 215–230.

Vinay, L., Brocard, F., Clarac, F., Norreel, J. C., Pearlstein, E., and Pflieger, J. F. (2002). Development of posture and locomotion: an interplay of endogenously generated activities and neurotrophic actions by descending pathways. *Brain Res. Brain Res. Rev.* 40, 118–129.

Wilson, C. J., and Kawaguchi, Y. (1996). The origins of two-state spontaneous membrane potential fluctuations of neostriatal spiny neurons. *J. Neurosci.* 16, 2397–2410.

Conflict of Interest Statement: The authors declare that the research was conducted in the absence of any commercial or financial relationships that could be construed as a potential conflict of interest.

Received: 14 September 2011; paper pending published: 06 October 2011; accepted: 21 October 2011; published online: 21 November 2011.

Citation: Dehorter N, Michel FJ, Marissal T, Rotrou Y, Matrot B, Lopez C, Humphries MD and Hammond C (2011) Onset of pup locomotion coincides with loss of NR2C/D-mediated cortico-striatal EPSCs and dampening of striatal network immature activity. Front. Cell. Neurosci. ***5****:24. doi: 10.3389/fncel.2011.00024*

frontiers in
CELLULAR NEUROSCIENCE

REVIEW ARTICLE
published: 24 November 2011
doi: 10.3389/fncel.2011.00025

New perspectives in amblyopia therapy on adults: a critical role for the excitatory/inhibitory balance

***Laura Baroncelli*[1], *Lamberto Maffei*[1,2] *and Alessandro Sale*[1]*

[1] *Institute of Neuroscience, National Research Council, Pisa, Italy*
[2] *Laboratory of Neurobiology, Scuola Normale Superiore, Pisa, Italy*

Edited by:
Yehezkel Ben-Ari, Institut National de la Santé et de la Recherche Médicale, France

Reviewed by:
Enrico Cherubini, International School for Advanced Studies, Italy
Corette Wierenga, Max Planck Institute of Neurobiology, Germany

***Correspondence:**
Alessandro Sale, Institute of Neuroscience, National Research Council, Via Moruzzi 1, I-56124 Pisa, Italy.
e-mail: sale@in.cnr.it

Amblyopia is the most common form of impairment of visual function affecting one eye, with a prevalence of about 1–5% of the total world population. This pathology is caused by early abnormal visual experience with a functional imbalance between the two eyes owing to anisometropia, strabismus, or congenital cataract, resulting in a dramatic loss of visual acuity in an apparently healthy eye and various other perceptual abnormalities, including deficits in contrast sensitivity and in stereopsis. It is currently accepted that, due to a lack of sufficient plasticity within the brain, amblyopia is untreatable in adulthood. However, recent results obtained both in clinical trials and in animal models have challenged this traditional view, unmasking a previously unsuspected potential for promoting recovery after the end of the critical period for visual cortex plasticity. These studies point toward the intracortical inhibitory transmission as a crucial brake for therapeutic rehabilitation and recovery from amblyopia in the adult brain.

Keywords: amblyopia, neural plasticity, environmental enrichment, fluoxetine, perceptual learning, GABAergic inhibition

The development of brain circuitry is the result of a complex interaction between genetic programs defining the gross cerebral architecture and activity-driven processes of synaptic fine tuning. In the visual system of primates, a significant portion of neuronal pathways' maturation is accomplished during prenatal development, allowing vision to start at birth. Initially, however, visual function abilities are still highly immature and they undertake strong improvements during the successive months of life, when sensory experience exerts a dramatic influence in driving the subtle wiring of neural circuitries (Weliky, 2000; Lewis and Maurer, 2009).

The essential role of experience is particularly evident within restricted time windows in early postnatal life, the so-called critical periods (CPs; Berardi et al., 2000), during which brain circuits display a high sensitivity to acquire instructive and adaptive signals from the external environment. Accordingly, early disruption of proper environmental inputs caused by conditions of visual deprivation or ocular abnormalities can result in long-term or even permanent brain diseases (Brémond-Gignac et al., 2011). Among them, amblyopia (lazy eye) is a severe disorder that, aside from refractive error, is the most common cause of vision loss during infancy, with an estimated prevalence of 1–5% in the population (Holmes and Clarke, 2006). Amblyopia emerges from untreated conditions of early abnormal visual experience in which a functional imbalance between the two eyes is predominant owing to anisometropia (unequal refractive power in the two eyes), strabismus (abnormal alignment of ocular axes with each other), or congenital cataract (clouding in the crystalline lens obstructing light transmission; Mittelman, 2003).

Much of our current understanding of the neural mechanisms underlying this disorder derives from studies on animal models, revealing that the major pathological changes in amblyopia occur at the cortical level. The seminal work performed by Hubel and Wiesel in kittens showed that reducing input from one eye by lid suture, a treatment usually referred to as monocular deprivation (MD), severely affects the physiology and anatomy of the visual cortex, with a delayed development of visual acuity and contrast sensitivity for the deprived-eye accompanied by disruption of cortical binocularity properties (Wiesel and Hubel, 1963). Similarly, amblyopia in humans is characterized by a dysfunction of sensory information neural processing, leading to a dramatic degradation of visual acuity in absence of structural abnormalities at the ocular examination and despite appropriate optical correction (Holmes and Clarke, 2006). In addition, the clinical picture of amblyopia is frequently complicated by the presence of a broad range of other perceptual deficits, including contrast sensitivity and stereopsis defects (Kiorpes, 2006; Levi, 2006).

The prevailing consensus is that amblyopia reversal is only possible early in life, before the closure of CP. Accordingly, precocious diagnosis and correction of any visual deprivation source is crucial for preventing visual impairments to become permanent (Holmes and Clarke, 2006). The traditional amblyopia therapy consists in patching or penalizing the fellow preferred eye, thus forcing the brain to use the visual input carried by the amblyopic eye (Wu and Hunter, 2006). The success rate of this treatment is dependent on several factors, including seriousness of visual ability disruption, type of amblyopia, occlusion dose, patient compliance, and age of onset (Stewart et al., 2005).

Despite the dogma that amblyopia is an untreatable pathology in adults, recent studies on animal models and clinical trials have challenged this picture, providing exciting evidence that intervention strategies boosting brain plasticity in adulthood may allow

the reinstatement of visual functions in amblyopic subjects well after the end of the CP.

RECOVERY FROM LONG-TERM VISUAL DEPRIVATION: LESSONS FROM ANIMAL MODELS

Significant effort is being made in multiple laboratories to elaborate new intervention procedures aimed at inducing juvenile-like neural plasticity in the adult brain. In addition to the theoretical relevance of these studies in a basis research perspective, they may have a great impact also on clinical practice: promoting plasticity in the adult nervous system, indeed, could pave the way for the development of innovative therapies for brain disorders for which a suitable treatment is still not available in adulthood (Bavelier et al., 2010).

In animal models, the amblyopic condition can be induced by long-term MD starting during the CP and protracted until adulthood. New experimental protocols successfully employed as strategies for enhancing adult brain plasticity can be classified in two categories on the basis of the general approach followed (**Figure 1**).

On the one hand, pharmacological manipulations of functional and structural brakes limiting plasticity to the CP have been shown to restore normal visual functions in adult amblyopic animals. Several studies pointed to intracortical inhibition as a key factor for defining the boundaries of plasticity, suggesting that a reduction of transmission in interneurons that release GABA (γ-aminobutyric acid) could be a crucial step for the restoration of plasticity processes in adulthood (for review, see Hensch, 2005 and Baroncelli et al., 2011).

The most direct demonstration that inhibitory transmission limits plasticity in the adult brain derives from a recent study reporting that pharmacological reduction of intracortical inhibition is sufficient to reopen a window of plasticity in the visual cortex well after the closure of the CP (Harauzov et al., 2010). First studies in animal models of amblyopia reported that the administration of anti-inhibitory compounds leads to a substantial restoration of the input from the deprived eye to the visual cortex (Duffy et al., 1976). Despite its theoretical appealing, reducing inhibition levels with direct pharmacological treatments can raise concerns about the effective clinical value, since some GABAergic transmission antagonists are of very limited utility for their pro-convulsive action, while others have not been approved by the FDA.

Brainstem neuromodulatory systems, such as those containing noradrenalin, serotonin, and acetylcholine, project to the cortex targeting GABAergic interneuron and specifically affecting the output of these cells (Bacci et al., 2005). Thus, an alternative way for adjusting the balance between excitatory and inhibitory transmission to levels favorable for plasticity may be an artificial regulation of the endogenous release of these transmitters. About 30 years ago, it has been reported that an increase in the local availability of noradrenalin enhances neuronal plasticity, accelerating cortical recovery from the effects of prior MD (Kasamatsu, 1982). In agreement with this previous finding, we recently demonstrated that chronic administration of fluoxetine, a selective serotonin reuptake inhibitor enhancing extracellular serotonin and noradrenalin levels, reactivates cortical plasticity in adulthood promoting a full recovery of visual functions in amblyopic animals through a reduction of inhibitory transmission (Maya Vetencourt et al., 2008). Treating amblyopia with fluoxetine is a promising approach if one considers that this substance is a FDA-approved drug widely prescribed in the treatment of depression and for which a very good knowledge of both beneficial and side effects is available. Interestingly, the permissive action of neuromodulatory transmitters on brain plasticity is developmentally regulated by increased levels of molecules that limit cerebral circuit reorganization in adulthood. It has been shown, indeed, that the expression of Lynx1, an endogenous prototoxin which directly binds to nicotinic receptors reducing their sensitivity to acetylcholine, increases after the closure of the CP and that the genetic removal of the molecular brake provided by this protein restores visual cortex plasticity in adult animals (Morishita et al., 2010).

Another molecular factor recently linked to the control of cortical plasticity levels is histone acetylation. Acetylation of histones H3 and H4 is developmentally down-regulated by an experience-dependent process related to the closure of the CP for visual cortex plasticity (Putignano et al., 2007). A pharmacological epigenetic treatment increasing histone acetylation (i.p. injection of valproic acid, VPA) emerged to be effective in adult rats in reversing visual acuity deficits induced by long-term MD (Silingardi et al., 2010). To date, no effects on the inhibitory transmission have been documented following manipulations of the epigenetic machinery. However, since prenatal exposure to inhibitors of histone deacetylases decreases the number of parvalbumin-positive inhibitory neurons in the neocortex of adult mice, it has been proposed that one mechanism of action for drugs targeting histone acetylation may be an adjustment of the excitatory–inhibitory ratio in cerebral circuitries (Gogolla et al., 2009).

Moving from the intracellular to the extracellular milieu, it has been shown that infusion in the mature cortex of amblyopic rats of an enzyme (chondroitinase ABC) that degrades chondroitin sulfate proteoglycans (CSPGs), an essential component of the brain extracellular matrix (ECM), produces a marked reinstatement of both visual acuity and binocularity. Since most CSPG-containing nets are localized around the soma of inhibitory interneurons, the permissive action of ECM degradation on cortical plasticity could occur through a direct structural and functional remodeling of inhibitory synapses (Pizzorusso et al., 2006).

On the other hand, pronounced improvements in visual functions have been obtained by experimental paradigms based on the manipulation of environmental stimulation levels. A recent study reported that exposing adult animals to complete darkness can induce vision recovery in amblyopic rats, providing evidence that the enhanced cortical plasticity is related to a shift in the balance between excitation and inhibition toward juvenile-like levels (He et al., 2007). Clinical translation of this treatment, however, remains uncertain, since a long dark exposure is likely to be disruptive for most people.

A more promising approach is environmental enrichment (EE). The goal of EE is to improve the animals' quality of life by providing them with a combination of multi-sensory/cognitive stimulation, increased physical activity and enhanced social interactions. EE is a gain-of-function paradigm allowing the study of the influence elicited by increased levels of environmental stimulation on brain

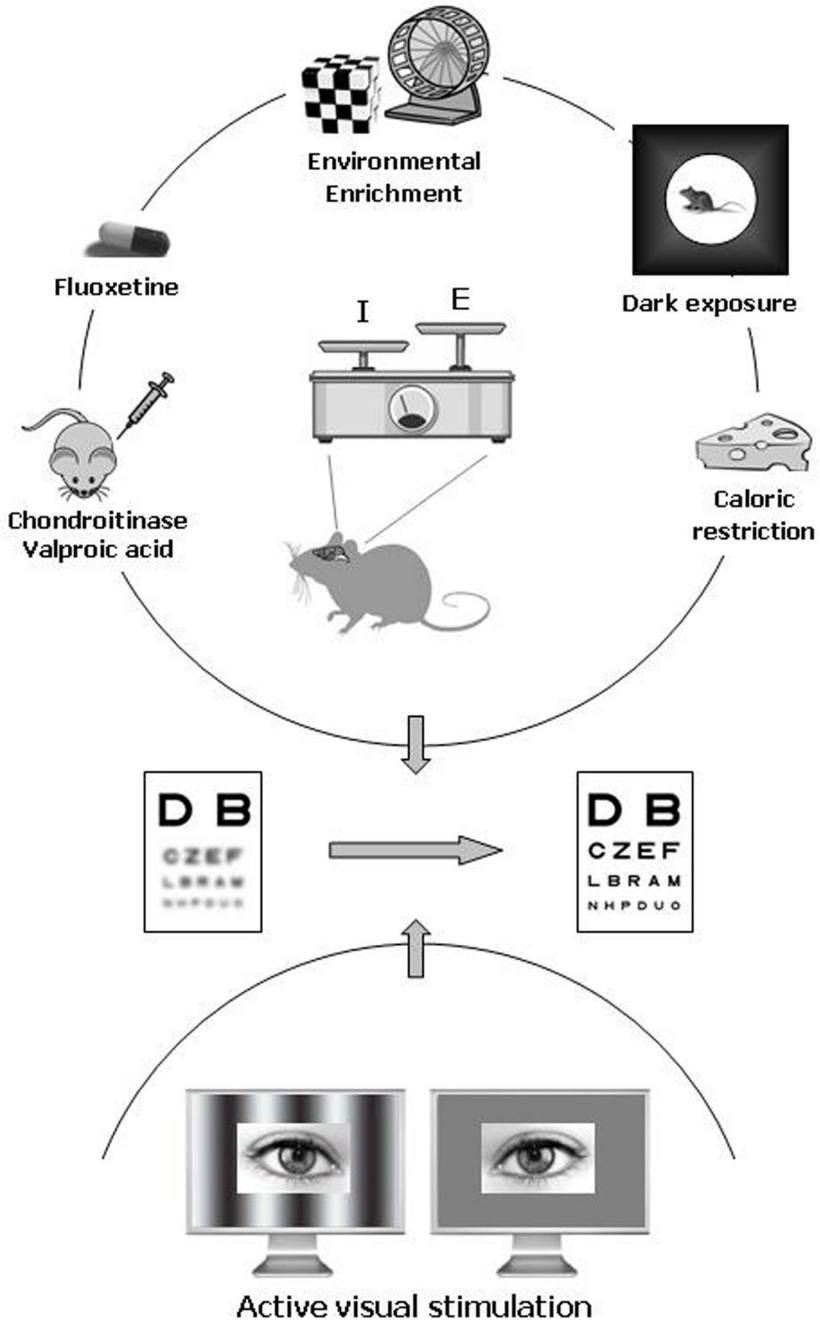

FIGURE 1 | Pharmacological and environmental therapeutic strategies for amblyopia in adulthood. Recent data have documented a previously unsuspected high potential of neuronal plasticity in the adult visual cortex. In animal models, plasticity can be elicited either by pharmacological treatment with chronic administration of antidepressants (fluoxetine), valproic acid (an inhibitor of histone deacetylases), or chondroitinase ABC (which degrades the extracellular matrix chondroitin sulfate proteoglycans), and by exposure to environmental enrichment, housing in complete darkness, or caloric restriction. In humans, emerging clinical studies point to active visual stimulation obtained with perceptual learning or playing video games as a promising strategy for treating amblyopia in adulthood. An increased ratio between excitation and inhibition owing to a reduced intracortical inhibitory tone is thought to be a central hub triggering plasticity in the adult visual cortex.

plasticity (van Praag et al., 2000; Sale et al., 2009; Baroncelli et al., 2010). We showed that EE is highly effective for treating amblyopia in adulthood: a brief exposure of adult amblyopic rats to EE promotes a complete recovery of both visual acuity and ocular dominance. Recovery of plasticity in enriched animals is paralleled by a marked reduction of the visual cortex inhibitory tone, for which we demonstrated a causal role in the enhancement of plasticity induced by EE (Sale et al., 2007).

An alternative approach for modulating physiological brain function has been shown to be the regulation of caloric intake. Nutrition is a fundamental component of the environment playing a key role in prenatal and postnatal visual development (Brémond-Gignac et al., 2011). It has been recently reported that a short-term protocol of food restriction starting in adulthood is able to restore neural plasticity in the visual system, renewing the capability of recovery from amblyopia in long-term deprived animals. Also in this case the effects on cortical plasticity were associated with a marked reduction of GABAergic inhibition (Spolidoro et al., 2011).

The picture emerging from this brief survey of the most recent literature in animal models is that the ratio between excitation and inhibition is a critical factor controlling the possibility to induce recovery from amblyopia in the adult. Given the morphological and functional complexity of inhibitory circuitries in the vertebrate brain, the precise role of GABAergic inhibition in limiting plasticity in the adult cortex is still under debate. Neural circuits, indeed, rely on inhibition mediated by diverse classes of interneurons with distinct morphologies, physiological properties, and subcellular innervation patterns. Moreover, GABAergic transmission fulfills multiple functions going from regulation of synaptic integration and timing of action potential generation to control of network oscillations (Huang et al., 2007). Parvalbumin-positive basket cells innervating the soma of target neurons with synapses containing the α1 subunit of $GABA_A$ receptors are currently considered critical for visual cortex plasticity regulation (Hensch, 2005).

It has been suggested that reducing inhibition promotes adult visual cortical plasticity by increasing the capability of the cortex to relay incoming patterns of activity to the supragranular layers (Kirkwood and Bear, 1994; Rozas et al., 2001). In agreement with this hypothesis, infusion of MPA or picrotoxin in the adult visual cortex enhances the possibility to induce activity-dependent long-term potentiation (LTP) of synaptic efficacy, but not long-term depression, both in layers II–III and IV (Harauzov et al., 2010). Thus, a reduction of GABAergic activity would favor recovery from amblyopia by facilitating a potentiation of the excitatory inputs from the undeprived eye.

Even if the prevailing consensus is that the major functional effects of vision deprivation in one eye result from plasticity at excitatory connections in the visual cortex, recent research has brought attention to the alternative possibility that intracortical inhibition of deprived-eye inputs could also increase, leading to a suppression of the visual responses evoked by the deprived eye (for review, see Smith and Bear, 2010). However, dissecting the role of plasticity at both excitatory and inhibitory synapses in the amblyopic condition deserves further investigation. It is also worth stressing that, to our knowledge, amblyopia has been never associated with a depolarizing and excitatory action of GABA, which has been instead reported for other pathological conditions, including epilepsy (Cohen et al., 2002; Huberfeld et al., 2007), neuropathic pain (Coull et al., 2005), inflammatory hyperalgesia and allodynia (Funk et al., 2008), and Alzheimer's disease (Lagostena et al., 2010).

IMPACT OF ACTIVE VISUAL STIMULATION IN ADULT AMBLYOPIC HUMAN SUBJECTS

At the clinical level, biological manipulations effective in restoring neural plasticity in the mature brain should be translated into feasible and safe interventions in order to represent a significant advance in the field of amblyopia treatment. A growing number of recent clinical studies pointed to perceptual learning (PL) as a very promising strategy for treating amblyopia in adulthood (**Figure 1**). PL refers to any change in perceptual ability as a result of practice and can be observed in all sensory modalities. In the visual system, practice with procedures of specific sensory enrichment improves performance in a variety of tasks, such as grating, texture, hyperacuity, or stereoscopic discrimination (for review, see Fine and Jacobs, 2002; Fahle, 2004, 2005). This form of neural plasticity does not seem to be an exclusive prerogative of a physiologically normal visual system, since it has been repeatedly observed also in adult people with amblyopia.

As early as 1970s, Campbell et al. (1978) reported that passive stimulation of the amblyopic eye with high-contrast square-wave rotating gratings of different spatial frequencies induced a substantial improvement in high-frequency contrast sensitivity and grating acuity in children. The method used in this seminal work, usually referred to as the Cambridge stimulator or CAM treatment, can be considered as a first example of a very simple PL procedure applied to the treatment of amblyopia. After a successive period of criticism in which the validity of this concept has been challenged by a number of negative results, in the last 15 years numerous papers have started to document various and robust beneficial effects on visual functions elicited by PL in adult amblyopes whose age was always higher than the 7-years cut-off classically considered the limit for a successful intervention. Importantly, no correlation between population age and functional outcome of the treatment has been ever reported in these studies (e.g., Polat et al., 2004; Chen et al., 2008). Moreover, a comparative inspection of the obtained results has allowed noticing that the age of the subjects enrolled in the various tested experimental procedures is not the main factor accounting for the variance across studies (see Levi and Li, 2009a).

While it is undisputed that PL involves changes on high cognitive levels of visual information processing, it also relies at least partly on modifications on earlier levels (Fahle, 2004). It has been reported, indeed, that PL has the ability to elicit plastic changes in the visual cortex, as shown by Yotsumoto et al. (2008) who observed a change in blood-oxygen-level dependence (BOLD) signal in human primary visual cortex (V1) following visual PL. In the same line, we recently observed that visual PL is accompanied by LTP of thalamo-cortical and cortico–cortical synaptic responses in the rat V1 (Sale et al., 2011), a direct demonstration that PL results in V1 neural plasticity. Accordingly, Cooke and Bear (2010) reported that repeated presentation of a sinusoidal grating stimulus over days induces LTP in the V1 of awake mice. Since it is currently believed that alterations in neural responses in the early visual cortex are the primary cause of vision dysfunction in amblyopia (Kiorpes, 2006; Levi, 2006), the possibility to promote V1 plasticity in a totally non-invasive manner with PL is very promising in the context of amblyopia treatment.

On the other side, since PL also occurs at early stages of visual processing, it may show a striking selectivity for the stimulus parameters. This raises one caveat to its therapeutic value in the treatment of amblyopia, because the achievable improvements might be limited to the selected trained stimulus, condition, or task (Levi and Li, 2009b). However, differently from what found in healthy subjects, the available results reported until nowadays do not show such a narrow specificity for the trained task in amblyopic patients. Indeed, even if the published studies adopted training tasks as various as practicing Vernier acuity (Levi and Polat, 1996; Levi et al., 1997), position discrimination (Li and Levi, 2004; Li et al., 2005, 2007, 2008), contrast detection (Polat et al., 2004; Zhou et al., 2006), and letter identification (Levi, 2005; Chung et al., 2008), a certain degree of transfer to improvements in Snellen acuity globally emerges. This property is essential for amblyopia treatment, because the main deficit in amblyopia is reduced visual acuity and a substantial improvement in this basic visual function is required for a real advance of the patient quality of life.

It has been suggested that one reason why PL is so effective in reversing amblyopia in adult people might be that it requires subjects to make fine visual discriminations using their amblyopic eye under conditions of "active" visual system stimulation (Levi, 2005). Thus, visual attention may be a fundamental component of the therapeutic potential of PL. A recent study in non-amblyopic subjects provided indirect support to the important role of visual attention in driving visual cortex plasticity, showing that normal-sighted people trained with action-based video games have robust improvements in basic visual functions (Li et al., 2009). The same effect was not observed after playing non-action video games that were equally engaging and visually complex, but operated at a slower pace and did not require precise visually guided actions. The effectiveness of this approach has promoted further research aimed at testing the value of active visual stimulation in amblyopic subjects. A substantial improvement in a wide range of visual functions including visual acuity, positional acuity, and stereopsis were also found in adults with amblyopia after a period of playing an action video game (Li et al., 2011; **Figure 1**). In this case, vision recovery was also triggered by playing a non-action version of the games, leading to the interpretation that the threshold to elicit plasticity in a defective amblyopic visual eye might be lower than that required to achieve further improvement under conditions of normal vision (Bavelier et al., 2010).

As reviewed in the previous section, experiments made on rodent models of amblyopia have underscored a pivotal role of cortical GABAergic inhibition in limiting plasticity and amblyopia recovery in adulthood. Interestingly, the balance between excitation and inhibition has been suggested to be impaired during development also in amblyopic human subjects and cortical over-inhibition could underlie the degradation of spatial vision abilities (Polat, 1999; Levi et al., 2002; Wong et al., 2005). In agreement with this hypothesis, repetitive transcranial magnetic stimulation (rTMS), which increases cortical excitability, transiently improves contrast sensitivity in adult amblyopes, likely acting on the excitation/inhibition balance (Thompson et al., 2008). A reduction of intracortical inhibition after rTMS has been also demonstrated in the motor cortex for both 1 and 10 Hz stimulations (Pascual-Leone et al., 1994; Modugno et al., 2003).

At the moment, it remains unknown whether the beneficial effects elicited by PL on amblyopia recovery are linked to changes in levels of brain inhibition. Preliminary experiments in our laboratory suggest a decrease of GABAergic inhibition in adult amblyopic rats that recover their visual functions in an active visual PL task. It is possible that the attention level required to perform PL tasks or to play video games might finally engage neuromodulatory systems of the brainstem, which may favor plasticity by increasing the excitatory/inhibitory ratio (Kasamatsu, 1991; Maya Vetencourt et al., 2008; Bavelier et al., 2010). Future studies should help further elucidate whether the molecular and cellular factors triggering brain plasticity in animal models are also crucial for a successful recovery of visual functions in human amblyopic subjects.

REFERENCES

Bacci, A., Huguenard, J. R., and Prince, D. A. (2005). Modulation of neocortical interneurons: extrinsic influences and exercises in self-control. *Trends Neurosci.* 28, 602–610.

Baroncelli, L., Braschi, C., Spolidoro, M., Begenisic, T., Maffei, L., and Sale, A. (2011). Brain plasticity and disease: a matter of inhibition. *Neural Plast.* 2011, 286073–286083.

Baroncelli, L., Braschi, C., Spolidoro, M., Begenisic, T., Sale, A., and Maffei, L. (2010). Nurturing brain plasticity: impact of environmental enrichment. *Cell Death Differ.* 17, 1092–1103.

Bavelier, D., Levi, D. M., Li, R. W., Dan, Y., and Hensch, T. K. (2010). Removing brakes on adult brain plasticity: from molecular to behavioral interventions. *J. Neurosci.* 30, 14964–14971.

Berardi, N., Pizzorusso, T., and Maffei, L. (2000). Critical periods during sensory development. *Curr. Opin. Neurobiol.* 10, 138–145.

Brémond-Gignac, D., Copin, H., Lapillonne, A., and Milazzo, S. (2011). Visual development in infants: physiological and pathological mechanisms. *Curr. Opin. Ophthalmol.* 22, S1–S8.

Campbell, F. W., Hess, R. F., Watson, P. G., and Banks, R. (1978). Preliminary results of a physiologically based treatment of amblyopia. *Br. J. Ophthalmol.* 62, 748–755.

Chen, P. L., Chen, J. T., Fu, J. J., Chien, K. H., and Lu, D. W. (2008). A pilot study of anisometropic amblyopia improved in adults and children by perceptual learning: an alternative treatment to patching. *Ophthalmic Physiol. Opt.* 28, 422–428.

Chung, S. T. L., Li, R. W., and Levi, D. M. (2008). Learning to identify near-threshold luminance-defined and contrast-defined letters in observers with amblyopia. *Vision Res.* 48, 2739–2750.

Cohen, I., Navarro, V., Clemenceau, S., Baulac, M., and Miles, R. (2002). On the origin of interictal activity in human temporal lobe epilepsy in vitro. *Science* 298, 1418–1421.

Cooke, S. F., and Bear, M. F. (2010). Visual experience induces long-term potentiation in the primary visual cortex. *J. Neurosci.* 30, 16304–16313.

Coull, J. A., Beggs, S., Boudreau, D., Boivin, D., Tsuda, M., Inoue, K., Gravel, C., Salter, M. W., and De Koninck, Y. (2005). BDNF from microglia causes the shift in neuronal anion gradient underlying neuropathic pain. *Nature* 438, 1017–1021.

Duffy, F. H., Burchfiel, J. L., and Conway, J. L. (1976). Bicuculline reversal of deprivation amblyopia in the cat. *Nature* 260, 256–257.

Fahle, M. (2004). Perceptual learning: a case for early selection. *J. Vis.* 4, 879–890.

Fahle, M. (2005). Learning to tell apples from oranges. *Trends Cogn. Sci. (Regul. Ed.)* 9, 455–457.

Fine, I., and Jacobs, R. A. (2002). Comparing perceptual learning tasks: a review. *J. Vis.* 2, 190–203.

Funk, K., Woitecki, A., Franjic-Würtz, C., Gensch, T., Möhrlen, F., and Frings, S. (2008). Modulation of chloride homeostasis by inflammatory mediators in dorsal root ganglion neurons. *Mol. Pain* 4, 32–44.

Gogolla, N., Leblanc, J. J., Quast, K. B., Südhof, T., Fagiolini, M., and Hensch, T. K. (2009). Common circuit defect of excitatory-inhibitory balance in mouse models of autism. *J. Neurodev. Disord.* 1, 172–181.

Harauzov, A., Spolidoro, M., DiCristo, G., De Pasquale, R., Cancedda, L., Pizzorusso, T., Viegi, A., Berardi, N., and Maffei, L. (2010). Reducing intracortical inhibition in the adult visual cortex promotes ocular dominance plasticity. *J. Neurosci.* 30, 361–371.

He, H. Y., Ray, B., Dennis, K., and Quinlan, E. M. (2007). Experience-dependent recovery of vision following chronic deprivation amblyopia. *Nat. Neurosci.* 10, 1134–1136.

Hensch, T. K. (2005). Critical period plasticity in local cortical circuits. *Nat. Rev. Neurosci.* 6, 877–888.

Holmes, J. M., and Clarke, M. P. (2006). Amblyopia. *Lancet* 367, 1343–1351.

Huang, Z. J., Di Cristo, G., and Ango, F. (2007). Development of GABA innervation in the cerebral and cerebellar cortices. *Nat. Rev. Neurosci.* 8, 673–686.

Huberfeld, G., Wittner, L., Clemenceau, S., Baulac, M., Kaila, K., Miles, R., and Rivera, C. (2007). Perturbed chloride homeostasis and GABAergic signaling in human temporal lobe epilepsy. *J. Neurosci.* 27, 9866–9873.

Kasamatsu, T. (1982). Enhancement of neuronal plasticity by activating the norepinephrine system in the brain: a remedy for amblyopia. *Hum. Neurobiol.* 1, 49–54.

Kasamatsu, T. (1991). Adrenergic regulation of visuocortical plasticity: a role of the locus coeruleus system. *Prog. Brain Res.* 88, 599–616.

Kiorpes, L. (2006). Visual processing in amblyopia: animal studies. *Strabismus* 14, 3–10.

Kirkwood, A., and Bear, M. F. (1994). Hebbian synapses in visual cortex. *J. Neurosci.* 14, 1634–1645.

Lagostena, L., Rosato-Siri, M., D'Onofrio, M., Brandi, R., Arisi, I., Capsoni, S., Franzot, J., Cattaneo, A., and Cherubini, E. (2010). In the adult hippocampus, chronic nerve growth factor deprivation shifts GABAergic signaling from the hyperpolarizing to the depolarizing direction. *J. Neurosci.* 30, 885–893.

Levi, D. M. (2005). Perceptual learning in adults with amblyopia: a re-evaluation of critical periods in human vision. *Dev. Psychobiol.* 46, 222–232.

Levi, D. M. (2006). Visual processing in amblyopia: human studies. *Strabismus* 14, 11–19.

Levi, D. M., Hariharan, S., and Klein, S. A. (2002). Suppressive and facilitatory spatial interactions in amblyopic vision. *Vision Res.* 42, 1379–1394.

Levi, D. M., and Li, R. W. (2009a). Perceptual learning as a potential treatment for amblyopia: a mini-review. *Vision Res.* 49, 2535–2549.

Levi, D. M., and Li, R. W. (2009b). Improving the performance of the amblyopic visual system. *Philos. Trans. R. Soc. Lond. B Biol. Sci.* 364, 399–407.

Levi, D. M., and Polat, U. (1996). Neural plasticity in adults with amblyopia. *Proc. Natl. Acad. Sci. U.S.A.* 93, 6830–6834.

Levi, D. M., Polat, U., and Hu, Y. S. (1997). Improvement in Vernier acuity in adults with amblyopia. Practice makes better. *Invest. Ophthalmol. Vis. Sci.* 38, 1493–1510.

Lewis, T. L., and Maurer, D. (2009). Effects of early pattern deprivation on visual development. *Optom. Vis. Sci.* 86, 640–646.

Li, R., Polat, U., Makous, W., and Bavelier, D. (2009). Enhancing the contrast sensitivity function through action video game training. *Nat. Neurosci.* 12, 549–551.

Li, R. W., Klein, S. A., and Levi, D. M. (2008). Prolonged perceptual learning of positional acuity in adult amblyopia: perceptual template retuning dynamics. *J. Neurosci.* 28, 14223–14229.

Li, R. W., and Levi, D. M. (2004). Characterizing the mechanisms of improvement for position discrimination in adult amblyopia. *J. Vis.* 4, 476–487.

Li, R. W., Ngo, C., Nguyen, J., and Levi, D. M. (2011). Video-game play induces plasticity in the visual system of adults with amblyopia. *PLoS Biol.* 9, e1001135. doi:10.1371/journal.pbio.1001135

Li, R. W., Provost, A., and Levi, D. M. (2007). Extended perceptual learning results in substantial recovery of positional acuity and visual acuity in juvenile amblyopia. *Invest. Ophthalmol. Vis. Sci.* 48, 5046–5051.

Li, R. W., Young, K. G., Hoenig, P., and Levi, D. M. (2005). Perceptual learning improves visual perception in juvenile amblyopia. *Invest. Ophthalmol. Vis. Sci.* 46, 3161–3168.

Maya Vetencourt, J. F., Sale, A., Viegi, A., Baroncelli, L., De Pasquale, R., O'Leary, O. F., Castren, E., and Maffei, L. (2008). The antidepressant fluoxetine restores plasticity in the adult visual cortex. *Science* 320, 385–388.

Mittelman, D. (2003). Amblyopia. *Pediatr. Clin. North Am.* 50, 189–196.

Modugno, N., Currà, A., Conte, A., Inghilleri, M., Fofi, L., Agostino, R., Manfredi, M., and Berardelli, A. (2003). Depressed intracortical inhibition after long trains of subthreshold repetitive magnetic stimuli at low frequency. *Clin. Neurophysiol.* 114, 2416–2422.

Morishita, H., Miwa, J. M., Heintz, N., and Hensch, T. K. (2010). Lynx1, a cholinergic brake, limits plasticity in adult visual cortex. *Science* 330, 1238–1240.

Pascual-Leone, A., Valls-Sole, J., Wassermann, E. M., and Hallett, M. (1994). Responses to rapid-rate transcranial magnetic stimulation of the human motor cortex. *Brain* 117, 847–858.

Pizzorusso, T., Medini, P., Landi, S., Baldini, S., Berardi, N., and Maffei, L. (2006). Structural and functional recovery from early monocular deprivation in adult rats. *Proc. Natl. Acad. Sci. U.S.A.* 103, 8517–8522.

Polat, U. (1999). Functional architecture of long-range perceptual interactions. *Spat. Vis.* 12, 143–162.

Polat, U., Ma-Naim, T., Belkin, M., and Sagi, D. (2004). Improving vision in adult amblyopia by perceptual learning. *Proc. Natl. Acad. Sci. U.S. A.* 101, 6692–6697.

Putignano, E., Lonetti, G., Cancedda, L., Ratto, G., Costa, M., Maffei, L., and Pizzorusso, T. (2007). Developmental downregulation of histone post-translational modifications regulates visual cortical plasticity. *Neuron* 53, 747–759.

Rozas, C., Frank, H., Heynen, A. J., Morales, B., Bear, M. F., and Kirkwood, A. (2001). Developmental inhibitory gate controls the relay of activity to the superficial layers of the visual cortex. *J. Neurosci.* 21, 6791–6801.

Sale, A., Berardi, N., and Maffei, L. (2009). Enrich the environment to empower the brain. *Trends Neurosci.* 32, 233–239.

Sale, A., De Pasquale, R., Bonaccorsi, J., Pietra, G., Olivieri, D., Berardi, N., and Maffei, L. (2011). Visual perceptual learning induces long-term potentiation in the visual cortex. *Neuroscience* 172, 219–225.

Sale, A., Maya Vetencourt, J. F., Medini, P., Cenni, M. C., Baroncelli, L., De Pasquale, R., and Maffei, L. (2007). Environmental enrichment in adulthood promotes amblyopia recovery through a reduction of intracortical inhibition. *Nat. Neurosci.* 10, 679–681.

Silingardi, D., Scali, M., Belluomini, G., and Pizzorusso, T. (2010). Epigenetic treatments of adult rats promote recovery from visual acuity deficits induced by long-term monocular deprivation. *Eur. J. Neurosci.* 31, 2185–2192.

Smith, G. B., and Bear, M. F. (2010). Bidirectional ocular dominance plasticity of inhibitory networks: recent advances and unresolved questions. *Front Cell. Neurosci.* 4:21. doi:10.3389/fncel.2010.00021

Spolidoro, M., Baroncelli, L., Putignano, E., Maya Vetencourt, J. F., Viegi, A., and Maffei, L. (2011). Food restriction enhances visual cortex plasticity in adulthood. *Nat. Commun.* 2, 320–327.

Stewart, C. E., Fielder, A. R., Stephens, D. A., and Moseley, M. J. (2005). Treatment of unilateral amblyopia: factors influencing visual outcome. *Invest. Ophthalmol. Vis. Sci.* 46, 3152–3160.

Thompson, B., Mansouri, B., Koski, L., and Hess, R. F. (2008). Brain plasticity in the adult: modulation of function in amblyopia with rTMS. *Curr. Biol.* 18, 1067–1071.

van Praag, H., Kempermann, G., and Gage, F. H. (2000). Neural consequences of environmental enrichment. *Nat. Rev. Neurosci.* 1, 191–198.

Weliky, M. (2000). Correlated neuronal activity and visual cortical development. *Neuron* 27, 427–430.

Wiesel, T. N., and Hubel, D. H. (1963). Single-cell responses in striate cortex of kittens deprived of vision in one eye. *J. Neurophysiol.* 26, 1003–1017.

Wong, E. H., Levi, D. M., and McGraw, P. V. (2005). Spatial interactions reveal inhibitory cortical networks in human amblyopia. *Vision Res.* 45, 2810–2819.

Wu, C., and Hunter, D. G. (2006). Amblyopia: diagnostic and therapeutic options. *Am. J. Ophthalmol.* 141, 175–184.

Yotsumoto, Y., Watanabe, T., and Sasaki, Y. (2008). Different dynamics of performance and brain activation in the time course of perceptual learning. *Neuron* 57, 827–833.

Zhou, Y., Huang, C., Xu, P., Tao, L., Qiu, Z., Li, X., and Lu, Z. (2006). Perceptual learning improves contrast sensitivity and visual acuity in adults with anisometropic amblyopia. *Vision Res.* 46, 739–750.

Conflict of Interest Statement: The authors declare that the research was conducted in the absence of any commercial or financial relationships that could be construed as a potential conflict of interest.

Received: 26 September 2011; paper pending published: 11 October 2011; accepted: 07 November 2011; published online: 24 November 2011.

Citation: Baroncelli L, Maffei L and Sale A (2011) New perspectives in amblyopia therapy on adults: a critical role for the excitatory/inhibitory balance. Front. Cell. Neurosci. ***5****:25. doi: 10.3389/fncel.2011.00025*

frontiers in
CELLULAR NEUROSCIENCE

REVIEW ARTICLE
published: 30 January 2012
doi: 10.3389/fncel.2012.00003

GABA not only a neurotransmitter: osmotic regulation by $GABA_AR$ signaling

***Tiziana Cesetti*[1], *Francesca Ciccolini*[2]* *and Yuting Li*[2]**

[1] *Department of Physiology and Pathophysiology, Interdisciplinary Center for Neurosciences, University of Heidelberg, Heidelberg, Germany*
[2] *Department of Neurobiology, Interdisciplinary Center for Neurosciences, University of Heidelberg, Heidelberg, Germany*

Edited by:
Yehezkel Ben-Ari, Institut National de la Santé et de la Recherche Médicale, France

Reviewed by:
Valentin Nägerl, Université de Bordeaux, France
Melanie A. Woodin, University of Toronto, Canada

***Correspondence:**
Francesca Ciccolini, Department of Neurobiology, Interdisciplinary Center for Neurosciences, University of Heidelberg, INF 364 Heidelberg, Germany.
e-mail: ciccolini@nbio.uni-heidelberg.de

Mature macroglia and almost all neural progenitor types express γ-aminobutyric (GABA) A receptors ($GABA_ARs$), whose activation by ambient or synaptic GABA, leads to influx or efflux of chloride (Cl^-) depending on its electro-chemical gradient (E_{Cl}). Since the flux of Cl^- is indissolubly associated to that of osmotically obliged water, $GABA_ARs$ regulate water movements by modulating ion gradients. In addition, since water movements also occur through specialized water channels and transporters, $GABA_AR$ signaling could affect the movement of water by regulating the function of the channels and transporters involved, thereby affecting not only the direction of the water fluxes but also their dynamics. We will here review recent observations indicating that in neural cells $GABA_AR$-mediated osmotic regulation affects the cellular volume thereby activating multiple intracellular signaling mechanisms important for cell proliferation, maturation, and survival. In addition, we will discuss evidence that the osmotic regulation exerted by GABA may contribute to brain water homeostasis in physiological and in pathological conditions causing brain edema, in which the GABAergic transmission is often altered.

Keywords: GABA, $GABA_AR$, osmotic swelling, chloride, cell volume

INTRODUCTION

In the mammalian central nervous system (CNS) three classes of GABARs have been identified, two of which, $GABA_ARs$ and $GABA_CRs$, are ligand activated pentameric anion channels. Besides the differences in subunit composition, biophysical characteristics, and pharmacological properties (Chebib and Johnston, 1999), the two classes of ionotropic receptors also exhibit a different pattern of expression. Whereas $GABA_ARs$ are present throughout the CNS, including non-neuronal cells and precursors, GABAcRs are mainly found in neurons in a few brain structures (Frazao et al., 2007). As yet GABAcRs have not been detected in mature glial cells or in oligodendrocyte progenitors (OPCs; Williamson et al., 1998). Although the transcripts of ρ subunits are expressed in some populations of neural progenitors (Fukui et al., 2008; Cesetti et al., 2010), the information concerning the functional role of $GABA_CRs$ in these cells is still scarce. Therefore, we will here focus only on $GABA_ARs$. Moreover, since the presence $GABA_ARs$ in microglia cells *in vivo* is still controversial (Velez-Fort et al., 2011), we will not include this cell population in our discussion.

With a few exceptions, in mature neurons activation of $GABA_ARs$ leads to Cl^- influx and hyperpolarization, whereas in immature neuronal cells it generally causes a depolarizing efflux of Cl^-. This in turn triggers a voltage-dependent influx of Ca^{2+}, which is essential for the morphological and electrical maturation of young neurons (Ben-Ari et al., 1989).

The consequence of $GABA_AR$ activation in non-neuronal cells is far less predictable than in neurons. Moreover its functional significance is still tentative. In non-neuronal cells, Cl^- fluxes via $GABA_ARs$ occur in both directions according to the cellular electro-chemical Cl^- gradient (E_{Cl}), thereby contributing to the regulation of osmotic tension. Therefore, activation of $GABA_ARs$ in these cells may directly affect the cell volume and indirectly control neuronal excitability by regulating the extracellular space and the concentration of Cl^-. Whereas in neurons changes in cell size and osmotic tension are often associated to cell death and apoptosis (Pasantes-Morales and Tuz, 2006), in non-neuronal cells such changes may activate several intracellular signaling mechanisms important for cell survival, proliferation, and maturation.

We will here review evidence indicating that in the adult brain $GABA_AR$ activation regulates osmotic tension as, despite its potential importance both at the cellular and systemic level, this function of $GABA_ARs$ has been so far less investigated than its role in neurotransmission. After introducing the basic concepts of tissue and cell volume regulation in the brain (**Figure 1**), we will then describe the molecular machinery involved in water movements and the anionic fluxes activated by $GABA_AR$ with a special focus on non-neural cells, i.e. macroglia and different precursor types (**Figure 2**). In the second part of the review we will discuss the role of GABA in the context of cell volume regulation and water exchange in the brain, its physiological significance and potential clinical relevance.

BASIC PRINCIPLES OF BRAIN WATER HOMEOSTASIS

Normal brain function is inextricably coupled to water homeostasis, which is the result of central osmoreception, osmolarity compensation, and cell volume regulation. More than 75% of the adult mammalian brain weight is represented by water subdivided in four distinct compartments: the blood of the cerebral vasculature, the cerebrospinal fluid (CSF) in the ventricular system

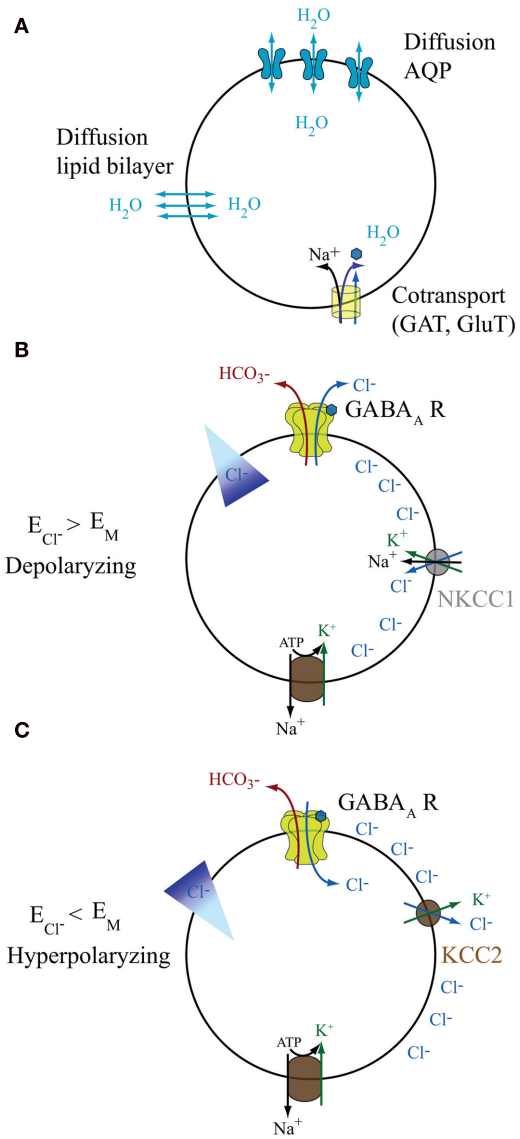

FIGURE 1 | Basic properties of water and anions fluxes. (A) Water can diffuse according to the osmotic pressure through the membrane lipid bilayer or via the dedicated channels AQP. Additionally it can be transported against its gradient by cotransporters, such as those for GABA and glutamate that use the driving force of Na^+ to move the neurotransmitters and eventually water against their gradient. **(B,C)** The activity of different transporters and exchangers determines the steady-state gradient for Cl^- and consequently regulates the E_{Cl}. Cl^- transport via cation–chloride cotransporters is fueled by the Na^+ and K^+ gradients generated by the Na–K ATPase. Two of the major players in neural cells are NKCC1 and KCC2, by which Cl^- is transported inside and outside the cells respectively. When E_{Cl} (see **Box 1**), is more positive that the E_M, opening of $GABA_AR$ would mediate an efflux of Cl^- (for convention called inward current) that depolarizes the cells **(B)**. Conversely when E_{Cl} is more negative that the E_M, GABAergic currents (outward) bring the membrane potential close to these values and are hyperpolarizing **(C)**. In this case to determine the E_{GABA} is important to consider also the flux of HCO_3^- since $GABA_ARs$ are permeable to this anion. Due to its higher level inside the cells, opening of $GABA_AR$ would drive a depolarizing efflux of HCO_3^- that, counteracting the influx of Cl^-, contributes to deviate E_{GABA} to value more positive than that of HCO_3^- (For Rev, see Andrew et al., 2007; Blaesse et al., 2009; Risher et al., 2009).

and subarachnoid space, the extracellular fluid (ECF) in the brain parenchyma, and the intracellular fluid (ICF). Three main barriers maintain a distinct fluidic composition among these compartments: the blood–brain barrier (BBB), the blood–CSF barrier (BCSFB) formed by the surface of the arachnoidea and choroid plexus epithelial cells, and the plasma membranes of the neural cells. Although the bulk of the ECF is generated from the metabolism of neural cells, around 30% is secreted from the endothelial cells of the brain capillary. The composition of the ECF depends on the interaction between the BBB, the BCSFB, and the activity of transporters on the membrane of neural cells, primarily astrocytes. The bulk of the CSF is largely the result of its secretion by the choroids plexus epithelium and its re-adsorption into the blood plasma at the dural sinuses in the subarachnoid space. In addition, according to recent evidence there is a flow of fluid from the ECF to the CSF. Although its composition displays regional variation, compared to the plasma, the CSF is generally slightly hypertonic containing moderately higher Na^+ and HCO_3^- and lower K^+ and Cl^- concentration. The K^+ concentration, which is critical for the regulation of the neuronal resting potential, is even lower in the ECF but it is increased in the ICF, which also contains lower Ca^{2+} and Na^+ concentrations than the ECF. The volume and ionic composition of the ICF depend on cellular metabolic activity and active transport of ions, and therefore, the ICF compartment is particularly sensitive to traumatic or ischemic injury. In general, the maintenance of these compartments depends on the existence of ionic gradients and water transport that are tightly regulated. For a comprehensive discussion of this complex topic we refer the reader to recently published excellent reviews (Strange, 1993; Kahle et al., 2009; Oreskovic and Klarica, 2010; Redzic, 2011).

Water homeostasis in the brain is necessary to prevent changes in the brain volume that could critically affect intracerebral pressure. As in other tissues, also in the brain changes in the extracellular or intracellular content of osmolytes are coupled to movements of osmotically obliged water. In normal conditions a redistribution of water between the intra and extracellular space occurs, which modifies the volume of the neural cells but not of the total brain. These changes in cell volume are referred to as isosmotic or anisosmotic depending on whether they originate from a change in the intracellular solute content or of the extracellular osmotic pressure, respectively. For example, neural activity determines isosmotic volume changes as a consequence of the ionic fluxes across the cell membrane occurring during neuronal firing. Cells counteract a decrease or an increase in volume by activating accordingly the processes of regulatory volume increase (RVI) and decrease (RVD). These processes of volume regulation involve increase or decrease of intracellular ionic and organic osmolytes achieved by modifying the expression and activity of ion channels and transporters and by metabolic changes. Different pathologies lead to isosmotic cytotoxic swelling. For example, energetic failure and dissipation of Na^+ gradients during hypoxia/ischemia, increase in the extracellular K^+ concentration such as during ischemia, epilepsies, and cortical spreading depression or ammonium accumulation occurring during hepatic encephalopathy, they all lead to cytotoxic swelling. Swelling in isosmotic conditions alters neuronal activity since changes in the extracellular/intracellular ionic equilibrium, which determine the resting membrane potential and

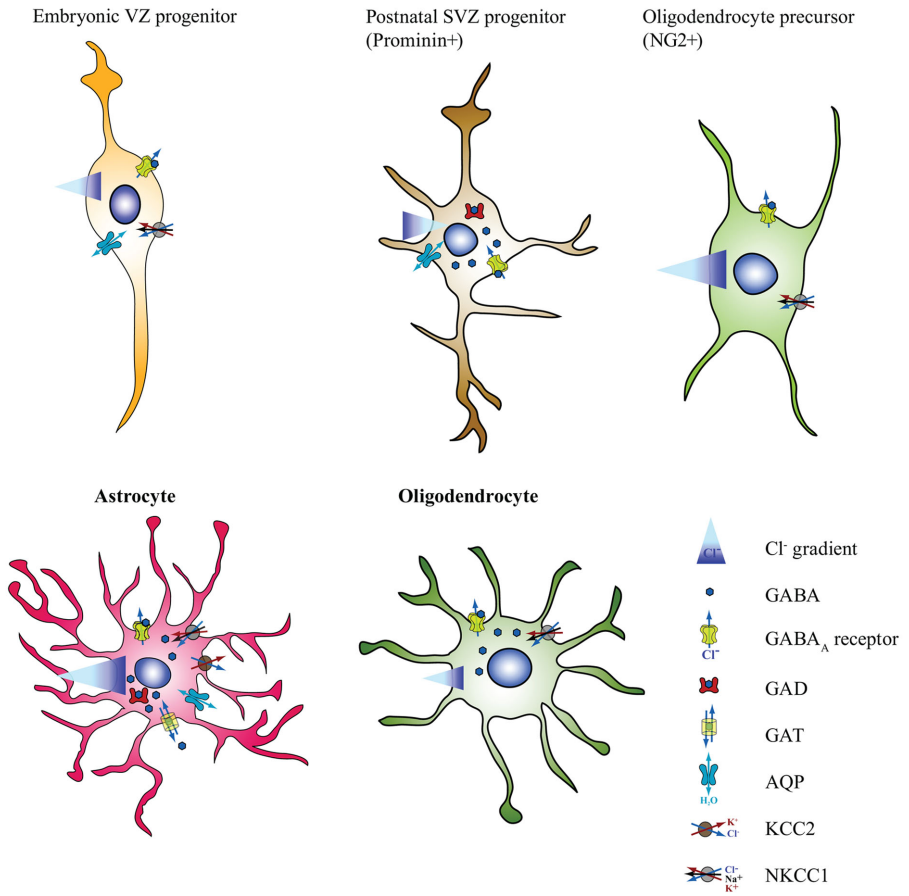

FIGURE 2 | GABA-mediated osmotic regulation in non-neuronal cells. Schematic representation summarizing the current knowledge concerning the expression of the neurotransmitter GABA, the synthesizing enzyme GAD, the membrane transporter GAT, which can work in both directions, and the ionic $GABA_AR$ in the indicated non-neuronal cell types of the mammalian CNS. Depicted is also the direction of water flux and of the Cl^- gradient, as estimated in resting physiological conditions. The scheme also illustrates the expression of the aquaporin (AQP) water channels and of the $Na^+/K^+/Cl^-$ (NKCC) and K^+/Cl^- (KCC) transporters in those cell types where their expression has been directly investigated. As in neurons, GABA promotes swelling in neural stem cells (NSC) but not in $NG2^+$ oligodendrocyte precursors (OPCs) and in mature macroglia, where $GABA_AR$ activation induces Cl^- exit and water efflux. Note that here the information concerning neural stem cells (NSCs) is gathered from the analysis of neural precursors isolated from the postnatal SVZ on the basis of Prominin expression. We did not include in this diagram the information concerning GFAP expressing cells in neurogenic regions of the adult brain because they mainly consist of niche astrocytes. Moreover, the properties illustrated in the diagram were not directly investigated in these populations. However, as discussed in the text, the available information indicates that these GFAP populations resemble mature astrocytes with respect to the direction of the GABA evoked Cl^- currents.

the driving force for the different ions (see **Box 1**), directly impact the discharge pattern of the neurons. Neurons are very sensitive to isosmotic swelling which is usually detrimental for these cells, since they cannot recover their original volume. Astrocytes instead should be better geared than neurons to counteract cytotoxic swelling, as they can undergo RVD. However, in intact tissue under physiologically relevant osmotic conditions, swelled astrocytes recover their volume only when the osmotic challenge is removed and control condition are re-established (Risher et al., 2009).

The blood plasma osmolality is strictly regulated and the solute content of the ECF and CSF is kept constant by the balanced influx/efflux across the plasma membrane and production/removal of osmotically active substances. Thus, under normal physiological conditions, neural cells are relatively protected against drastic anisosmotic volume changes. However, many pathological processes can cause drastic changes in the blood plasma osmolarity that in turn can affect brain volume. In particular, hypoosmolar states can lead to brain swelling whereas hyperosmotic changes cause brain dehydration. For example, hyponatremia associated with clinical conditions such as heart failure, nephritic syndromes, and hepatic cirrhosis may cause hyposmotic swelling of neural cells. Hyponatremia, even if drastic, rarely results in neuronal death, since neurons use compensatory mechanisms to retain their volume such as unconventional release of neurotransmitters (Tuz et al., 2004). On the contrary, hyposmolarity causes astrocytes swelling due to water fluxes across the membrane. Water can also diffuse to neighbor astrocytes via gap-junctions. Swelling of astrocytes may represent a protective mechanism for neurons since they clear from the extracellular space not only water but also the neurotransmitters in excess. This

Box 1 | Basic elements of electrophysiology

The direction of the current flow is conventionally defined as the movements of positive charges: an inward currents (depolarizing) means that cations enter the cells or/and anions exit. Respectively an outward current (hyperpolarizing) is determined by the efflux of cations or influx of anions. By convention, an inward current is displayed in voltage clamp as a downward deflection, while an outward current (positive charge moving out of the cell) is shown as an upward deflection.
The concentration gradient ($\Delta C = [X]_o/[X]_i$) depends on the concentration of the ion outside and inside of the cells and it determines the reversal potential (E_X) for a defined ion (X) according to the Nernst Equation:

$$E_X = RT/zF\,ln[X]_o/[X]_i.$$

At the reversal potential (E_X) the electrical force (membrane potential) counteracts the chemical force (concentration gradient ΔC) so that the ion influx is equal to the efflux. Changes in the extracellular and/or intracellular volume would impact ΔC and thus the E_X.
The resting membrane potential (E_M) in general depend on the driving force of Cl^-, Na^+, and K^+ and their relative permeability (P_X) according to the Goldmann-Hodgkin-Katz equation:

$$E_M = (P_K/P_{tot})E_K + (P_{Na}/P_{tot})E_{Na} + (P_{Cl}/P_{tot})E_{Cl}$$

In resting condition, having K^+ the higher permeability, the E_M is closer to the E_K that is about −80 mV.
The current (i) through a single ionic channel is dependent on the channel conductance (g) and the "driving force" of the permeant ion. The driving force is determined according to the E_X and the resting membrane potential (E_M). The single channel current is calculated as follow:

$$i = g(E_M - E_X).$$

The whole-cell current (I) through specific ion channels is proportional to the single channel current (i) and the number of opened channels at the membrane (n) according to the equation:

$$I = n \cdot i.$$

HOW CAN WE MEASURE. . .?

THE REAL RESTING MEMBRANE POTENTIAL (E_M)

In whole-cell patch-clamp measurements, due to dialysis of the cytoplasm, the intracellular ionic composition is altered therefore the measure of E_M in current-clamp does not correspond to the real value. The real E_M can be better estimated by measuring the amplitude of the current of a single K^+ channel versus the voltage in cell-attached configuration (Soltesz and Mody, 1994). Another approach takes advantage of voltage-sensitive dyes: changes in fluorescence visualized with live microscopic imaging or fluorescent activated cell sorting (FACS) correspond to changes in the membrane potential. Membrane potential can be calibrated by permeabilizing the cells with gramicidin and applying different Na^+ concentrations (Maric et al., 2000). Recently also voltage-sensitive genetically encoded sensors have been developed (Mutoh et al., 2011).

THE REVERSAL POTENTIAL FOR $GABA_AR$ (E_{GABA})

It can be experimentally determined in whole-cell perforated patch-clamp recording using gramicidin, which is not permeable to Cl^- and therefore does not alter the intracellular Cl^- concentration. Using a ramp or step protocol in the presence of a GABAergic agonist the current versus voltage relationship is measured: the E_{GABA} corresponds to the voltage at which the currents is zero (Ge et al., 2006). Another possibilty is to block Na^+, Ca^{2+}, and K^+ currents and, in perforated current-clamp recording, measure the maximum depolarization produced by the application of a saturating concentration of a GABAergic agonist (Owens et al., 1996). E_{GABA} can also be measured on the basis of the reversal potential of single GABA and NMDA receptor channels (Tyzio et al., 2006).

INTRACELLULAR Cl^- CONCENTRATION

It can be established with Cl^- sensitive intracellular microelectrodes (Kettenmann et al., 1987) and radioactive studies (Kimelberg, 1981). Additionally it can be estimated with Cl^- sensitive dye, such as MEQ, (Bevensee et al., 1997) or genetically encoded probes, such as Clomeleon (Kuner and Augustine, 2000): both allow the analysis, with cellular resolution, of real-time changes in $[Cl^-]_i$ by microscopic imaging.

CHANGES IN CELL VOLUME

Since in cells undergoing osmotic changes the intensity of light scattering varies inversely with the cell volume, changes in forward scattering measured by FACS analysis, can be related to changes in cell volume of a whole-cell population (McGann et al., 1988). To measure changes in the volume of single cells, optical measurement of calcein fluorescence quenching can be employed (Solenov et al., 2004). Also in slices intrinsic optic signals are a read out of volume changes: when cells swell light scattering decreases and the tissue shows increased light transmittance (MacVicar and Hochman, 1991; Andrew and MacVicar, 1994; Holthoff and Witte, 1996). However, with this technique it is not possible to distinguish which cell type changes its volume. On the contrary with the two-photon microscopic technique the time course of swelling in slice and in living brain can be monitored at cellular and subcellular levels (Andrew et al., 2007; Risher et al., 2009). Additionally with electrophysiology, the amplitude of evoked field potential is an indirect way to measure tissue swelling: since the extracellular resistance is inversely proportional to the osmolarity, a reduction of the latter induces an increase in the evoked field potential (Andrew et al., 2007).
In vivo changes in human brain volume can be revealed by monitoring intracranial pressure, by computed tomography and by MRI. These techniques provide a measure of the total water content at a given anatomical location.

function of the astroglia is crucial to synaptic transmission since it counteracts the effect that hyposmolarity may have on the extracellular concentration of neurotransmitters and the size of the extracellular space.

WATER MOVEMENT AND TRANSPORT IN BRAIN CELLS

Cell membranes are highly permeable to water and cannot resist hydrostatic pressure. Therefore, water movements occurring by diffusion across the cell membrane and through the aquaporin (AQP) water channels, are largely driven by the transmembrane difference in chemical potential. However, water can also be actively transported in the brain, and it is widely accepted that some cotransporters and uniporters contribute to this flux exchange (Agre, 2004).

WATER MOVEMENT VIA AQPs

AQPs are a family of tetrameric water channels assembled at the cell membrane or, as in the case of AQP6, inside the cell. Thirteen homologs of AQPs (AQP0–AQP12) have been identified so far in mammals (Verkman, 2005). AQPs display a variable tissue distribution, depending on their distinct physiological functions. They mediate movements of water and small solutes, such as glycerol, across membranes according to osmotic gradients and differences in hydrostatic pressures (Verkman, 2005). AQPs have recently been subdivided into three functional groups based on permeability characteristics (Verkman, 2000): the water selective aquaporins, including AQP0, AQP1, AQP2, AQP4, AQP5, AQP6; the aquaglyceroporins, including AQP3, AQP7, AQP8, permeable to water, glycerol, and urea; the neutral solute channels, including AQP9, allowing the passage of water, glycerol, urea, purines, pyrimidines, and monocarboxylates. AQP10, like AQP9, is permeable to water and neutral solutes, but not to urea and glycerol (Hatakeyama et al., 2001).

Three AQPs have been functionally involved in the regulation of water movements in the CNS: AQP1, AQP4, and AQP9. Among these, AQP4 is the most abundant. It is strongly expressed at the borders between the brain parenchyma and major fluid compartments, including the foot processes of astrocytes, the glia limitans, and the ependyma lining the lateral ventricle. AQP4 is also expressed in the astrocytes of the two major neurogenic regions in the postnatal CNS: the subventricular zone (SVZ; Rash et al., 1998) and the hippocampal dentate gyrus (DG; Venero et al., 2001). In the brain, AQP4 normally displays a polarized cellular distribution, being expressed in astroglial foot processes adjacent to the endothelial cells (Nielsen et al., 1997). In general, AQPs are not expressed in neurons and it is still unclear whether these cells possess a dedicated molecular machinery mediating water movements (Andrew et al., 2007).

The levels of AQP expression are not constant but functionally regulated. For example they are increased in brain regions where the BBB is disrupted following brain injury, ischemia, or tumor (Vizuete et al., 1999; Taniguchi et al., 2000; Saadoun et al., 2002). The amount of AQPs expressed at the cell surface is regulated both at the levels of RNA transcription (Wen et al., 1999) and of channel assembly. Multiple phosphorylation sites and different kinases have been involved in this complex regulation (Zelenina et al., 2002; Carmosino et al., 2007) and the precise regulatory mechanisms of AQP expression in different brain cell types remain unclear.

AQP4 has been involved in brain water homeostasis. Deficiency of AQP4 in mouse markedly reduces brain swelling in cytotoxic brain edema and tissue swelling mediated by physiological neuronal activity (Papadopoulos and Verkman, 2005), while it worsens the outcome in vasogenic brain edema (Zador et al., 2007), indicating that AQP4 facilitates the redistribution and absorption of excessive brain fluid. Several evidences point at functional and physical interaction between AQPs and ion channels in the regulation of water homeostasis. For example, in astrocytes AQP4 interacts with the inward rectifier K^+-channel (Kir 4.1; Nagelhus et al., 2004). Tetraethylammonium, a blocker of voltage-dependent K^+-channel, also inhibits water permeability of AQP1 (Brooks et al., 2000). Lack (Binder et al., 2006) or mislocation (Amiry-Moghaddam et al., 2003) of AQP4 causes impaired K^+ clearance following neuronal stimulation, suggesting that K^+ clearance is mediated by the AQP4–Kir4.1 complex. In astrocytes, the complex between AQP4 and the transient receptor potential vanilloid 4 (TRPV4) is essential to induce $[Ca^{2+}]_i$ increase and promote RVD upon hypotonic challenge (Benfenati and Ferroni, 2010).

Besides the systemic regulation of water exchange, AQP4 contributes to multiple steps of adult neurogenesis (i.e., proliferation, migration, and differentiation). Adult neural stem cells express AQP4 (Cavazzin et al., 2006) and its level of expression in neural precursors changes during brain development (Wen et al., 1999). Genetic ablation of AQP4 impairs proliferation, migration, and neuronal differentiation of adult neural stem cells (Kong et al., 2008). Using microarray and quantitative mRNA analysis in neural precursors prospectively isolated from the neonatal SVZ, we have also recently confirmed that neural stem cells, and particularly activated neural stem cells, express AQP4 at higher levels in comparison to later stages of differentiation (Li and Ciccolini, unpublished observations). Our observations also indicate a similar expression pattern for AQP4 and $GABA_AR$ in the neonatal SVZ. We showed that activation of $GABA_ARs$ induces Cl^- entry and osmotic swelling of neural stem cells (Cesetti et al., 2010), opening up to the possibility that $GABA_ARs$ and water channels interact to mediate cell volume changes in the neonatal SVZ niche.

Interestingly, $GABA_ARs$ and AQPs are involved in the regulation of similar processes. For example, they both enhance migration in response to a chemotactic stimulus *in vitro* in various neural cell types (Behar et al., 1998; Saadoun et al., 2005). They also modulate Ca^{2+} homeostasis and promote neuronal differentiation in neural precursors. Lack of AQP4 in adult neural stem cells significantly decreases their ability to generate neurons, alters spontaneous Ca^{2+} oscillations, and suppresses depolarization-induced Ca^{2+} influx (Kong et al., 2008). Similarly $GABA_AR$ signaling increases $[Ca^{2+}]_i$ and promotes neuronal differentiation of progenitors in the adult hippocampus (Tozuka et al., 2005). Moreover, we found that $GABA_AR$ activation modulates spontaneous Ca^{2+} oscillations in culture of neural stem cells isolated from the neonatal SVZ (**Figure 2**; Cesetti et al., 2010). The analysis of mice lacking the intracellular membrane protein dystrophin provides a further hint of a possible connection between $GABA_AR$ and AQPs. Dystrophin in the brain is important for clustering and stabilizing $GABA_AR$ in neurons (Brunig et al., 2002). It is also responsible

for anchoring AQP4 at the membrane of perivascular astrocytes (Nicchia et al., 2008). The expression of AQP4 in ependymal cells and in astrocytic endfeet of the lateral ventricle is reduced in a dystrophic mice model (*mdx*; Frigeri et al., 2001) and hippocampal neurogenesis is altered in these mice (Deng et al., 2009), suggesting that dystrophin may be important for stem cell function.

However, despite being coexpressed in non-neuronal cells and regulating similar mechanisms, a direct functional interaction between AQPs and $GABA_AR$ has not been yet demonstrated.

WATER TRANSPORT

It has been recently recognized that some cotransporters and uniporters also transport water (MacAulay et al., 2001). Extensive data show that water molecules move in association with the transport of ions and substrates.

Cotransporters are a group of membrane-spanning transport proteins which can couple ion and substrate transport. For example, it is well known that Na^+ is employed as the principal cotransported ion for its large inwardly directed electro-chemical gradient. In this process, Na^+ can force the uptake of a substrate against its chemical gradient. The ratio between the various fluxes is a fixed property of the transporter protein and the energy for the water transport can be derived from the transport of the non-aqueous substrates. Thus, cotransport may carry a fixed number of water molecules together with each transported solute against the osmotic gradients.

Various cotransporters are able to transport water against the osmotic gradient, such as for example the K^+/Cl^- cotransporter (KCC) in the choroid plexus (Zeuthen, 1994), the $Na^+/K^+/2Cl^-$ (NKCC; Hamann et al., 2005), the glial Na^+-coupled glutamate (EAAT1; MacAulay et al., 2001), and the Na^+/GABA (GAT-1) cotransporters (MacAulay et al., 2002). Similar phenomena are also associated to glucose uniporters (GLUT1 and GLUT2; Zeuthen and Zeuthen, 2007). For some ionic cotransporters, water transport is closely coupled to the transport of the other substrates. Other cotransporters, such as EAAT1 and GAT-1, not only cotransport water but also have water channel properties. Therefore, the total water transported is the sum of the cotransported and the osmotic components. In GAT-1 expressing oocytes, water can move passively through GAT-1 under external osmotic challenge. However, upon addition of GABA the influx of water increases and it is strictly coupled to the transport of GABA through GAT-1, independent of the external osmotic gradient (MacAulay et al., 2002). Thus, ambient GABA in the brain could also affect osmotic gradients by enhancing water transport via GATs activation.

$GABA_AR$ SIGNALING IN NON-NEURONAL CELLS OF THE CNS

Despite the difficulties in detecting GABAergic currents in astrocytes due to their electrical coupling, it has been proved that glial cells express $GABA_ARs$ in a functionally significant amount.

The astrocytic $GABA_ARs$ have many pharmacological similarities to the receptors on neuronal cells, such as barbiturate- and benzodiazepine-mediated potentiation. Differently from neurons, the inverse benzodiazepine agonist DMCM enhances the GABAergic currents of some subpopulations of astrocytes, suggesting that the subunit composition of $GABA_ARs$ among different populations of astrocytes is heterogeneous (Bormann and Kettenmann, 1988). Analyses *in vitro* and *in vivo* have shown that in the SVZ niche glial fibrillary acidic protein (GFAP)/nestin immunopositive cells, pre-neuroblasts, and especially neuroblasts also express functional $GABA_ARs$ (Stewart et al., 2002; Liu et al., 2005; Cesetti et al., 2010). $GABA_ARs$ are also expressed in mature oligodendrocytes (Von Blankenfeld et al., 1991) and the mRNAs for $GABA_AR$ α_{2-5}, γ_{2-3} and to a lesser extent γ_1 subunits have been found in $NG2^+$ OPCs. Different sources of GABA activate $GABA_ARs$ in non-neuronal cells. Some progenitor cells, such as the OPCs in the gray and cerebellar white matter, receive direct GABAergic synaptic input, which regulates their proliferation and differentiation (Lin and Bergles, 2004). Newly born granule cells in the adult DG of the hippocampus also display during their maturation first tonic and then phasic GABAergic currents. These currents are evoked by GABA released from mature interneurons, which modulates morphological development and connectivity of new born granule cells (Ge et al., 2006; Markwardt et al., 2009). Despite these examples of phasic currents, in non-neuronal cells $GABA_AR$ activation is mostly tonic, mediated by GABA derived from non-synaptic release or synaptic spillover. Neurons may release $GABA_AR$ modulators such as taurine and GABA upon osmotic stress, via a mechanism similar to Ca^{2+} mediated exocytosis that can be blocked by tetanus toxin (Tuz et al., 2004). Additionally, alternative mechanisms, such as reverse operation of the transporters have been reported (Koch and Magnusson, 2009). Glial cells are also a source of ambient GABA, although it is unclear whether this reflects uptake/release dynamics or synthesis and whether GABA acts as an autocrine factor on glial cells. The fact that glial cells can release GABA in culture has been long known. Already 40 years ago low activity of the glutamic acid decarboxylase (GAD), the rate-limiting enzyme in the synthesis of GABA, and modest production of GABA (Wu et al., 1979) were observed in astrocytes and GABA concentration in culture was estimated to be 3.5 mM (Bardakdjian et al., 1979). The finding that astrocytes *in situ* are immunopositive for GABA (Blomqvist and Broman, 1988) and for GAD (Martinez-Rodriguez et al., 1993) has been recently confirmed also in human astrocytes (Benagiano et al., 2000). Recent evidence suggests that GABA released by astrocytes can modulate the neuronal network by inducing either tonic or transient currents in neurons (Angulo et al., 2008). It was originally proposed that GABA may be released by cultured cerebellar astrocytes via the GABA transporter working in the reverse mode (Gallo et al., 1991). This mechanism has been later confirmed in Bergman glial cells in acute slices (Barakat and Bordey, 2002). Outwardly directed GABA currents occur when the cells are filled with GABA 10 mM and Na^+ 12.5 mM. However, it is still unclear whether in physiological conditions the intracellular concentration of GABA is enough to activate this mechanism (Barakat and Bordey, 2002). Astrocytes of the olfactory bulb can release not only glutamate but also GABA that leads to a long lasting synchronous inhibition of both mitral and granule cells (Kozlov et al., 2006). As the frequency of these inhibitory slow outward currents is sensitive to extracellular osmolarity, the mechanism proposed involved a release from volume activated anion channels. Such a mechanism has been confirmed only recently in the cerebellum Bergmann glial cells that have been shown to release GABA via the Bestrophin 1 anion channel, providing a tonic inhibition for cerebellar granule

cells (Lee et al., 2010). Bestrophins are enigmatic anion channels, permeable to HCO_3^-, large anions, and even to glutamate; they are activated by increases in the intracellular Ca^{2+} and cell swelling, but they are active also at resting Ca^{2+} levels and normal cell volume.

In the neonatal SVZ both neuroblasts and neural precursors are immunopositive for GABA, GAD65, and GAD67. However, mRNA levels are much higher in neuroblasts than in neural precursors (Cesetti et al., 2010). On the contrary, GABA has not been detected in SVZ astrocytes. It is believed that in this region GABA is manly synthesized and released by neuroblasts via an unknown non-synaptic mechanism which is SNARE-independent but mediated by depolarization, acting as "volume neurotransmitter" (Liu et al., 2005). Despite the presence of GAD65/67 in this region, GABA in neonatal tissue is mainly produced via monoacetylation of putrescine (Sequerra et al., 2007). Similarly, O2-A progenitor cells of the optic nerve synthesize GABA from putrescine (Barres et al., 1990).

EFFECT OF GABAergic SIGNALING ON ANIONIC DISTRIBUTION IN NEURAL CELLS

ASTROCYTES

The concept that astrocytes regulate K^+ homeostasis by clearing it from the extracellular space (K^+ siphoning) has been proposed a long time ago along with the idea that astrocytes have no resting Cl^- conductance (Ballanyi et al., 1987; Walz and Wuttke, 1999). Glial cells in resting condition are indeed permeable to K^+ therefore their resting potential (E_M) is more negative than −75 mV. However, it is quite intuitive that in order to maintain the E_M and the osmotic pressure constant, K^+ fluxes must be followed by Cl^- and water fluxes. During neuronal activity, astrocytes accumulate K^+, which causes an influx of Cl^- and osmotically obliged water, thereby increasing their cell volume. Astrocytes counteract this volume increase by releasing Cl^- and other anions. Thus, K^+ and Cl^- homeostasis are crucially linked. In astrocytes the regulation of Cl^- fluxes is quite complex involving a large number of exchangers, transporters as well as ion channels (Walz, 2002). Although reactive, neoplastic, and deformed astrocytes can express a significant resting Cl^- conductance (Walz and Wuttke, 1999), astrocytes have generally a low permeability to Cl^- and are able to accumulate it. When 30 years ago functional $GABA_A$Rs were firstly identified in astrocytes *in situ*, the depolarizing effect of GABA was thought to be indirect, due to the increase in $[K^+]_o$ upon its release from adjacent neurons (Hosli et al., 1978, 1981). Later evidence proved that $GABA_A$Rs in glial cells *in situ* mediate Cl^- outward currents (MacVicar et al., 1989; Steinhauser et al., 1992; Pastor et al., 1995), in agreement with previous data *in vitro* (Kettenmann et al., 1987). Confirming that astrocytes have a E_{Cl} much more depolarized than their E_M, the analysis of $GABA_A$R-mediated currents (see **Box 1**) showed that the E_{Cl} of astrocytes in cultures is around −40 mV that corresponds to a $[Cl^-]_i$ of 29 mM (Bekar and Walz, 2002). Using more direct experimental approaches, such as intracellular microelectrodes (Kettenmann et al., 1987), radioactive studies (Kimelberg, 1981), and Cl^--sensitive dyes (Bevensee et al., 1997), both in cell culture and *in vivo*, the intracellular Cl^- concentration has been calculated between 30 and 40 mM. In contrast to neurons, where GABAergic currents shift from depolarizing to hyperpolarizing during the second week after birth, the direction and the density of GABAergic currents in astrocytes do not change during development (Bekar et al., 1999). The absence of phasic $GABA_A$Rs activation in astrocytes suggests that they would mainly sense ambient GABA rather than transient high concentrations from synaptic release.

Analyses *in vitro* have implicated two major transport systems in the accumulation of Cl^- in astrocytes: NKCC1 (Jayakumar and Norenberg, 2010) and the Cl^-/HCO_3^- exchanger (Kimelberg, 1981). NKCC1 plays a major role in setting Cl^- gradients in resting condition as well as during astrocytes swelling which occurs in pathological conditions such as brain edema, ischemia, and trauma (Chen et al., 2005). As the activity of NKCC1 is strongly stimulated by cell swelling (Mongin et al., 1994), a positive feedforward mechanism further contributes to cell volume increase. The K^+/Cl^- (KCC) cotransporter is also responsible for the maintenance and regulation of the cell volume of cultured astrocytes, but it is mainly involved in RVD (Ringel and Plesnila, 2008). The expression of these carriers in astrocytes *in vivo* is still controversial: whereas previous works failed to detect them (Plotkin et al., 1997; Clayton et al., 1998), one recent study reported the expression of NKCC1 and KCC1 mRNAs also in glial and ependymal cells (Kanaka et al., 2001), which is consistent with functional evidence (Tas et al., 1987). Indeed, application of GABA after pharmacological blockade of NKCC1 no longer depolarizes the membrane of astrocytes, since the outwardly directed Cl^- gradient is dissipated (Kimelberg and Frangakis, 1985).

The role of $GABA_A$Rs in astrocytes is still an open question. Interestingly, GABA signaling regulates the differentiation of immature astrocytes (Matsutani and Yamamoto, 1997; Mong et al., 2002). In the brain there is a positive correlation between the numbers of GABAergic axonal terminals and the expression of GFAP, suggesting that GABA released by neurons may promote GFAP expression and stellation of astrocytes. This hypothesis has been strengthened by the observation that increasing GABAergic signaling *in vivo* induces a striking modification of the structural organization of $GFAP^+$ astrocytes, increasing the number of branches. The mechanism underlying these modifications is not known but it could be direct and mediated by the efflux of Cl^- (Runquist and Alonso, 2003). We also showed that a systemic administration of diazepam increased the number of GFAP expressing cells in the SVZ of the lateral ventricle, where GFAP expression identifies both niche astrocytes and stem cells (Cesetti et al., 2010).

OLIGODENDROCYTES

Similar to astrocytes, oligodendrocytes actively accumulate Cl^- via NKCC1 and their $[Cl^-]_i$, measured with microelectrodes, is 2–3 mM higher than the one expected for a passive distribution (Hoppe and Kettenmann, 1989). Cumulative evidence indicates that a higher resting permeability accounts for the lower $[Cl^-]_i$ observed in oligodendrocytes as compared to astrocytes. A resting Cl^- conductance was detected in most cultured oligodendrocytes and the E_{Cl} (−61 mV) is only slightly more positive than the E_M (−64 mV), in line with the observation that GABA depolarizes oligodendrocytes by 4 mV (Kettenmann et al., 1984). GABAergic currents were recorded in oligodendrocytes in brain slices in the

corpus callosum (Berger et al., 1992) and in the hippocampus (Von Blankenfeld et al., 1991). However, $GABA_AR$-mediated currents in oligodendrocytes are smaller than in astrocytes, probably depending on both a reduced expression of $GABA_ARs$ and a smaller outwardly directed driving force for Cl^-. It was first shown that oligodendrocytes in explant cultures of the spinal cord can be directly depolarized by the activation of $GABA_ARs$ (Kettenmann et al., 1984). Later on it was shown that the mechanism underlying the depolarization is an efflux of Cl^- via $GABA_ARs$ (Wang et al., 2003). However, only a subpopulation of the oligodendrocytes investigated was GABA-sensitive, indicating heterogeneity in the cell population in culture or in its differentiation stage. Indeed, $NG2^+$ OPCs have larger GABAergic currents compared to their differentiated counterpart: the density of $GABA_ARs$ decreases by a factor 100 when OPCs in culture maturate along the oligodendrocytic lineage, indicating a developmental down-regulation of $GABA_AR$ expression (Von Blankenfeld et al., 1991). A difference in Cl^- driving force could also contribute to the larger GABAergic currents in OPCs. In line with this, in OPCs of the adult neocortex $[Cl^-]_i$ was estimated to be 45 mM and the E_{Cl} to be −30 mV (Tanaka et al., 2009). Furthermore, a robust expression of NKCC1 was reported in satellite $NG2^+$ glial cells (Price et al., 2006). These developmental changes in the GABAergic signaling suggest that GABA may exert different physiological roles during oligodendrocytes lineage progression. Unlike astrocytes, $GABA_ARs$ in OPCs are transiently activated by synaptically released GABA, since it was shown that in the hippocampus OPCs form real functional synapses with neuronal axons thereby sensing the activity of the dense inhibitory network surrounding them. Despite the depolarizing E_{Cl}, GABA regulates OPCs membrane excitability with a shunting effect on AMPA currents due to an increase in membrane conductance and alteration of $[Cl]_i$ (Lin and Bergles, 2004). In cultured oligodendrocytes muscimol promoted cell survival upon growth factor withdrawal by reducing $[Cl^-]_i$, which in turn induced cell shrinkage and a subsequent Ca^{2+} signal. NKCC1 activity was required for both effects, confirming the importance of NKCC1 for maintaining $[Cl^-]_i$ above the electro-chemical gradient (Wang et al., 2003). Thus, in OPCs the signaling pathways downstream $GABA_AR$ involve alternative mechanisms such as shunting inhibition, modulation of transporter activity and control of ion homeostasis and cell volume.

NEURAL PROGENITORS

In progenitors of the embryonic (E16) ventricular zone $[Cl^-]_i$ has been estimated to be 37 mM, based on the measurement of an E_{GABA} of −30 mV (see **Box 1**). The E_{GABA} becomes progressively more negative during development reaching about −60 mV at P16. This gradient is dissipated upon pharmacological blockade of NKCC1 (Owens et al., 1996) or by the overexpression of exogenous KCC2 (Cancedda et al., 2007). The development of neuronal progenitors is ubiquitously characterized by changes in Cl^- transporters expression. This was also observed in the neurogenic niche of the adult DG. The measurement of the E_{GABA} in DG precursors at different stages of lineage progression revealed that at early stages of neuronal differentiation the E_{GABA} is more positive than the E_M. With the progressive maturation of granule neurons, E_{GABA} gradually decreases to finally switch to values more negative than the E_M. The estimated change in $[Cl^-]_i$ during this process, i.e., from about 30–10 mM, is likely due to the fact that the pattern of cotransporter expression changes from high NKCC1/low KCC2 to low NKCC1/high KCC2 between the beginning and the end of this maturation period. Indeed, down-regulation of NKCC1 expression resulted in a shift of E_{GABA} from depolarizing to hyperpolarizing at all time-points analyzed (Ge et al., 2006). However, even if depolarizing, in differentiating granule neurons GABAergic currents have a shunting effect (Overstreet Wadiche et al., 2005). Within the DG, GABA released by interneurons evokes currents not only in newborn neurons but also in progenitors, albeit there is still controversy over the developmental stage at which the switch from tonic to phasic currents occurs (Overstreet Wadiche et al., 2005; Tozuka et al., 2005; Wang et al., 2005; Ge et al., 2006).

In the postnatal SVZ, GABA elicits Cl^- currents in neuroblasts and pre-neuroblasts and in two cell populations defined as stem cells on the basis of the expression of either Prominin (Cesetti et al., 2010) or GFAP (Wang et al., 2003; Liu et al., 2005). The largest currents were observed in neuroblasts (Wang et al., 2003; Cesetti et al., 2010). In these cells E_{GABA}, estimated via gramicidin perforated whole-cell recording (see **Box 1**), is about −40 mV, which is more positive than their E_M and corresponds to a $[Cl^-]_i$ of 26.7 mM (Wang et al., 2003). Considering their very small size, the current density is also high (*in vitro* estimated about 190 pA/pF) and consistent with the very strong $GABA_AR$ immunoreactivity displayed by these cells (Cesetti et al., 2010). These huge GABAergic currents depolarize very efficiently neuroblasts (Wang et al., 2003), which have already a depolarized E_M (−55 mV) and a very high R_M (1–3 GΩ). Indeed, spontaneous depolarizations of 15–20 mV were previously observed in neuroblasts (Liu et al., 2005). It is very likely that GABA regulates the osmotic pressure in neuroblasts since $GABA_ARs$ are present at high density and are tonically activated. Thus, a persistent Cl^- efflux may affect the osmolarity of the intracellular milieu from such small cells.

In contrast to neuroblasts, the Cl^- gradient of SVZ stem cells is still unclear. Compared to neuroblasts, neonatal $Prominin^+$ precursors have a much smaller (30 times) density of GABAergic current (5 pA/pF), which likely reflects the differences in levels of receptor expression between the two populations (Cesetti et al., 2010). However, larger GABAergic currents were measured from precursor cells contacting each other *in vitro*, possibly due to electrical coupling. A similar phenomenon was previously observed in precursors of the embryonic ventricular zone, where GABA elicited small (around 5 pA) currents on isolated cells and almost 100 times larger currents in coupled cells (Owens et al., 1996). Although the exact $[Cl^-]_i$ and the absolute value of E_M are not known, using a voltage-sensitive dye (see **Box 1**) we showed that muscimol hyperpolarizes precursors, suggesting that $GABA_AR$ activation leads to Cl^- influx in this cell population (Cesetti et al., 2010). Instead, in $GFAP^+$ cells of the adult SVZ $GABA_AR$ activation elicited Ca^{2+} increases (Young et al., 2010). This indirectly suggests that, as in mature astrocytes, also in $GFAP^+$ cells of the SVZ GABA has a depolarizing effect.

PHYSIOLOGICAL ROLE OF $GABA_AR$-MEDIATED OSMOTIC REGULATION

Osmotic swelling may affect brain physiology by different mechanisms. For example, it may change the ionic gradients, which are key for setting the resting membrane potential and the driving force of the ionic currents. It may modulate the extracellular concentration of neurotransmitters, either inducing their release or regulating the size of the extracellular space. Osmotic swelling can also represent a signaling mechanism, by activating different intracellular pathways. While the first two scenarios are more relevant to the regulation of systemic processes, for example water balance and synaptic transmission, the last one can transduce signals regulating cell growth and proliferation as it can modulate the activity of membrane and intracellular signaling molecules.

Below, we will suggest ways in which $GABA_AR$ activation can modulate these different processes and discuss a few studies that have indicated a physiological role for $GABA_AR$-mediated osmotic regulation.

WATER BALANCE IN THE BRAIN

A few studies have indicated that $GABA_AR$ activation may affect brain water homeostasis. For example the anti-epileptic drug vigabatrin, which raises extracellular GABA levels by inhibiting the GABA degrading enzyme GABA transaminase, can cause swelling and loss of myelin (Sidhu et al., 1997), suggesting that excessive activation of $GABA_ARs$ in the myelinating processes of oligodendrocytes may damage them. In one patient it was also found that cerebral edema induced by valproate overdose can be aggravated by diazepam (Rupasinghe and Jasinarachchi, 2011). Since conditions such as energy deprivation and brain trauma lead to a temporary increase in the concentration of extracellular GABA (Hagberg et al., 1985; Shimada et al., 1993), $GABA_AR$-mediated osmotic regulation may also play a significant role in the regulation of water balance in pathological conditions. For neurons an excess of GABA may have contrasting consequences. On one hand, it will protect neurons by decreasing the membrane depolarization caused by glutamate. On the other hand, it will induce entry of Cl^- ions through $GABA_ARs$, leading to water influx and cell swelling (Chen et al., 1999; Allen et al., 2004). Indeed, diazepam elicits opposite responses depending on the concentration and time of application (Ricci et al., 2007). Benzodiazepines can also ameliorate the effect of ammonia-induced swelling *in vitro* (Bender and Norenberg, 1998). Additionally, in an *in vitro* model of ischemic insult, the inhibitory effect of taurine on water gain required active $GABA_AR$, indicating a potential involvement of $GABA_AR$ on osmotic regulation (Ricci et al., 2009). However these studies have neither investigated the direct target of the treatment nor elucidated the mechanisms underlying its effect and they cannot be used as evidence that $GABA_AR$ signaling plays a role in osmotic regulation. Also in astrocytes, the activation of $GABA_ARs$ generates physiologically important changes in ion distribution. For example, $GABA_AR$ function in astrocytes may be important for the maintenance of the extracellular Cl^- concentration in the vicinity of neuronal GABAergic synapses, to prevent the sink in $[Cl^-]_o$ during high inhibitory activity. In addition, GABA modulates voltage-dependent K^+ channels within astrocytes themselves, by depressing A-type outward K^+-currents (Bekar and Walz, 2002). Such modulation of K^+ conductance may have important consequences for the progression of spreading depression through the brain and for astrocytic swelling in pathological conditions. In contrast to neurons, activation of $GABA_ARs$ in conditions of cytotoxic swelling may be beneficial to astrocytes since their E_{Cl} is depolarizing. Therefore, the activation of $GABA_AR$ will decrease the intracellular osmolarity of these cells, thereby preventing cellular edema.

However, so far activation of $GABA_AR$ in astrocytes has not been directly associated to osmotic regulation. Moreover, although there is good evidence that following ischemic or traumatic brain injury the levels of ambient GABA increase, the rapid release of GABA is followed in various cases by a decrease in its synthesis (Green et al., 1992). Thus it remains still unclear whether GABAergic function is effectively increased in these conditions (Green et al., 2000). Therefore, the hypothesis that $GABA_AR$ contributes to the regulation of osmotic tension in the CNS needs experimental confirmation.

NEURAL ACTIVITY-MEDIATED OSMOTIC SWELLING

A functional connection between swelling and neural activity was indirectly suggested by the observation that the intake of water in healthy subjects leads to an increased synchronization of the spontaneous magnetoencephalogram during hyperventilation with an increase in the spectral power in all frequency bands (Muller et al., 2002). Moreover, hyposmolarity induces hyperexcitability and increases evoked epileptiform activity (Rosen and Andrew, 1990; Saly and Andrew, 1993). Neuron swelling occurs also in physiological conditions. For example, changes in tissue volume in the brain related to neuronal activity and cell swelling may occur *in vivo* in the human visual cortex (Darquie et al., 2001). In hippocampal slices, high frequency stimulation of the Schaffer collateral fibers increases the transmittance of the somatic and dendritic CA1 regions, in concomitance with the evoked postsynaptic field potential (fEPSP), indicating a relationship between tissue swelling and neuronal activity. GABA negatively modulates the generation of fEPSP and at the same time promotes swelling. Moreover, lowering the $[Cl^-]_o$ to create an outwardly directed driving force for Cl^- produces the opposite effect on transmittance, leading to the interpretation that neuronal swelling is mediated mainly by Cl^- synaptic influx via $GABA_AR$ (Takagi et al., 2002). However, so far the change in neuronal volume has not been directly analyzed at the cellular level and it is still unknown to which extent GABA modulates cell volume during normal network activity. A functional consequence of the osmotic pressure generated by GABA may include the modulation of neuronal plasticity and the generation of an alternative way of signal propagation in a network of neurons and glia.

Prolonged activation of $GABA_ARs$, such as during high frequency activity of inter-neuronal network, induces in postnatal cerebellar interneurons an increase in $[Ca^{2+}]_i$, which can be observed up to 3 weeks after birth (Chavas et al., 2004). Since the membrane potential measured in these cells in such conditions is more negative than the activation threshold of VDCCs, it has been suggested that the increase in $[Ca^{2+}]_i$, is triggered by a Ca^{2+} influx independent from VDCCs and/or by a release from intracellular stores in response to the rising osmotic tension

within the neuronal dendrites. According to this hypothesis, it was suggested that prolonged opening of $GABA_AR$ causes a persistent HCO_3^- efflux, which in turn exerts a continuous depolarizing force favoring a large Cl^- influx. As Cl^- carriers correct variations in the $[Cl^-]_i$ on a slow time scale, this large Cl^- influxes cannot be immediately compensated and they lead to water entry and swelling. Consistently with this hypothesis, the application of a $GABA_AR$ agonist increases the dimension of the dendrites (Chavas et al., 2004). However, the exact link between osmotic tension and Ca^{2+} elevations remains so far unknown.

NEUROGENESIS

Despite the intense scrutiny, many aspects of the regulation of GABA on neurogenesis are still unclear. This concerns especially the downstream mechanisms involved, the role of this regulation *in vivo* and the differences associated to age and regional factors. The concept that GABA regulates neural progenitor behavior mainly via $GABA_AR$-mediated depolarization and consequent activation of VDCCs has become widely accepted. However, considering the wide range of cell types within the stem cell niches and the relative differences in their GABAergic currents and in the source of GABA, it is likely that several downstream transduction mechanisms are involved. Moreover, often the conclusion that VDCCs are activated by $GABA_ARs$-mediated depolarization has been indirectly drawn from the observation that VDCC antagonists impact the physiological effect mediated by GABA. Although some studies have provided evidence that $GABA_ARs$ activation depolarizes neural precursors in the embryonic and adult neurogenic niche (Owens et al., 1996; Liu et al., 2005; Young et al., 2010), it is often unclear whether this effect can be obtained at physiological concentrations of GABA, whether functional VDCCs are present and are activated by the GABA-induced depolarization. This analysis is further complicated by the technical challenge posed by the simultaneous measurement of membrane potential and Ca^{2+} signals without interfering with Cl^- homeostasis, and by the identification of the different cell types within the adult neurogenic niche. By combining antigenic and functional characterization we have previously detected VDCCs in neuroblasts, but not in more immature precursor cells of the neonatal SVZ (Cesetti et al., 2009). Consistently, GABA evoked a rapid Ca^{2+} increase in neuroblasts but not in precursor cells (Cesetti et al., 2010). However, spontaneous Ca^{2+} signals occur *in vitro* both in embryonic (Ciccolini et al., 2003; Gakhar-Koppole et al., 2008) and in neonatal neural progenitors (Cesetti et al., 2009) and they can be modulated by GABA (**Figure 3**). GABAergic modulation of spontaneous Ca^{2+} signals was also observed *in situ* in GFAP expressing cells of the SVZ; these spontaneous Ca^{2+} signals depended on IP_3 mediated Ca^{2+} release from the stores. In about half of these cells the $GABA_AR$ antagonist bicuculline reduced the frequency of the Ca^{2+} transients while in the other half it produced an increase (Young et al., 2010). Likewise, GABA evoked Ca^{2+} signals mediated by VDCCs only in half of the $GFAP^+$ cells. Since all $GFAP^+$ cells respond to GABA (Liu et al., 2005), these results underscore the heterogeneity of the $GFAP^+$ cell population that, beside a small fraction of stem cells, mostly consists of niche astrocytes. They also suggest the involvement of different downstream signaling cascades in the GABAergic response.

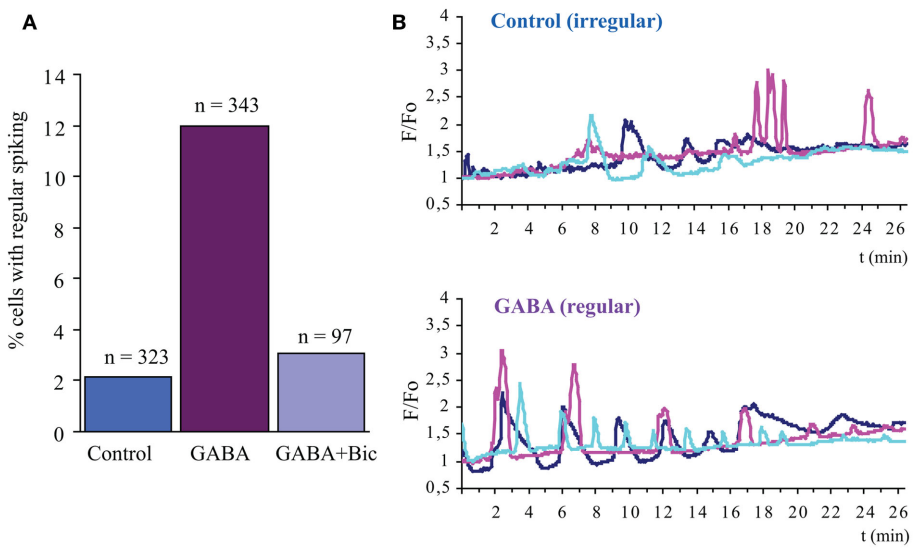

FIGURE 3 | $GABA_AR$ signaling promotes regular Ca^{2+} transients on proliferating neural precursors. Analysis of spontaneous Ca^{2+} transients in a population enriched in neural stem cells, purified by fluorescence activated cell sorting from the postnatal SVZ on the basis of the expression of high levels of EGFR ($EGFR^{high}$ cells; Ciccolini et al., 2005). After isolation the cells were plated on coverslips and maintained in medium containing EGF and FGF-2 for 2 days (Cesetti et al., 2009). Upon loading with the Ca^{2+} indicator fluo-3, in control conditions the $EGFR^{high}$ cells displayed a very low incidence of regular Ca^{2+} oscillation (regular oscillation defined as at least three spikes with similar amplitude and interspike interval within 15 min recording) **(A,B)**. However the addition of GABA (100 μM) to the medium before (15 min) and during the imaging led to a dramatic increase in the incidence of the cells displaying regular Ca^{2+} oscillation **(A,B)**, an effect that was blocked by the $GABA_AR$ bicuculline (50 μM) **(A)**. In **(B)** three representative traces of Ca^{2+} changes are shown, respectively in control condition and upon GABA treatment, after background subtraction, and normalization to baseline values.

Indeed we have shown that in stem cells of the neonatal SVZ, identified according Prominin and GFAP expression, activation of $GABA_AR$s produces a Cl^- influx which promotes osmotic swelling and insertion of epidermal growth factor receptor (EGFR) in the cell membrane. In the presence of EGF, this event leads to a change in the expression of the phosphatase and tensin homolog deleted on chromosome 10 (PTEN) tumor suppressor and Cyclin D1 and promotes cell cycle entry (Cesetti et al., 2010). Since osmotic swelling can spread through gap junction coupling, potentially this mechanism could synchronize the cell cycle of several progenitor cells (Cesetti et al., 2009). However, GABA evokes very small Cl^- currents in these progenitor cells, raising the question of whether $GABA_AR$ activation alone is enough to cause swelling and stem cell proliferation *in vivo*. Supporting this possibility we found that a single intraperitoneal injection of diazepam promotes massive stem cell proliferation and increased EGFR expression (Cesetti et al., 2010). It is possible that the amplitude of GABAergic currents measured *in vitro* does not reflect the degree of activation *in vivo*. This could be due to the modulation of $GABA_AR$ by endogenous ligands such as neurosteroids. Indeed, using gene array analysis we have recently found that precursors express the E18-kDa translocator protein (Tspo) and the 11-kDa diazepam binding inhibitor, a polypeptide that is a well-characterized ligand for Tspo (Obernier and Ciccolini, unpublished observation). Activation of Tspo results in an increased production of the neurosteroid precursor pregnenolone that in turn potentiates GABAergic currents (Mellon and Griffin, 2002).

In embryonic and peripheral neural crest stem cells, activation of $GABA_AR$ also induced swelling associated to hyperpolarization, but it had an opposite effect on cell proliferation, as it led to the generation of phosphorylated histone γH2AX, which in turn inhibited cell cycle progression (Andang et al., 2008). It has been proposed that GABA prevents proliferation in the adult SVZ by a similar mechanism (Fernando et al., 2011). However, we found that activation of $GABA_AR$ in the neonatal SVZ did not lead to the generation of γH2AX (Cesetti et al., 2010), suggesting that the responses of neonatal and adult SVZ precursors to GABA may differ. Thus, in more primitive neural precursors $GABA_AR$-mediated cell swelling plays an important role in proliferation control.

CONCLUDING REMARKS AND PERSPECTIVES

So far only a few studies have clearly indicated a role for $GABA_AR$ activation in the osmotic regulation of brain.

One possible reason of such limited number of observations is the difficulty to discriminate *in vivo* between the effect of GABA as neurotransmitter and as osmotic modulator due to the interdependency between neural activity and osmotic regulation in the brain. Another limiting factor may be the technical difficulties associated to the measurement of cell volume changes *in situ* or *in vivo*. The regulation of water and ion balance in the brain is crucial for normal functions and for recovery from pathological swelling. A constant redistribution of water occurs across the membrane of the different neural cell types, accompanying fluxes of ions and release and uptake of neurotransmitters. However the measurement of water diffusion/transport with cellular resolution is still technically challenging. Magnetic resonance imaging (MRI) permits the quantification of global or local increase in water content at specific anatomical location but without cell specificity. Only recently, with the development of two-photon laser scanning microscopy and of transgenic mice with intrinsic fluorescent neurons or glia, it has been possible to monitor real-time changes in cell volume in brain slice and *in vivo* with cellular and even subcellular resolution. However the molecular mechanism involved in cell volume changes and the downstream activated signaling have been mainly investigated in isolated cell systems which do not reflect the complexity of the situation *in vivo*. Although the picture is still fragmented and incomplete, new concepts start to emerge. GABA regulates not only inter-neuronal communication but also the communication between neurons and non-neuronal cells. GABAergic signaling between astrocytes and neurons can be bidirectional, with astrocytes sensing extrasynaptic GABA and releasing GABA and taurine upon osmotic challenge, providing a feedback mechanism of volume regulation. Oligodendrocytes instead receive a dedicated synaptic GABAergic input. Adult neural precursors in the DG and SVZ of the adult brain sense synaptic or ambient GABA, respectively.

Thus, although many questions are still open, recent evidence indicates that $GABA_AR$-mediated osmotic regulation may have consequences at the cellular and at the systemic level. Therefore, GABAergic osmotic regulation should be taken into account during the treatment of pathologies requiring the administration of $GABA_AR$ modulators and for the development of therapies for diseases causing water unbalance in the brain.

ACKNOWLEDGMENTS

We would like to thank Prof. A. Draguhn for critical reading of the manuscript.

REFERENCES

Agre, P. (2004). Nobel lecture. Aquaporin water channels. *Biosci. Rep.* 24, 127–163.

Allen, N. J., Rossi, D. J., and Attwell, D. (2004). Sequential release of GABA by exocytosis and reversed uptake leads to neuronal swelling in simulated ischemia of hippocampal slices. *J. Neurosci.* 24, 3837–3849.

Amiry-Moghaddam, M., Williamson, A., Palomba, M., Eid, T., de Lanerolle, N. C., Nagelhus, E. A., Adams, M. E., Froehner, S. C., Agre, P., and Ottersen, O. P. (2003). Delayed K+ clearance associated with aquaporin-4 mislocalization: phenotypic defects in brains of alpha-syntrophin-null mice. *Proc. Natl. Acad. Sci. U.S.A.* 100, 13615–13620.

Andang, M., Hjerling-Leffler, J., Moliner, A., Lundgren, T. K., Castelo-Branco, G., Nanou, E., Pozas, E., Bryja, V., Halliez, S., Nishimaru, H., Wilbertz, J., Arenas, E., Koltzenburg, M., Charnay, P., El Manira, A., Ibanez, C. F., and Ernfors, P. (2008). Histone H2AX-dependent GABA(A) receptor regulation of stem cell proliferation. *Nature* 451, 460–464.

Andrew, R. D., Labron, M. W., Boehnke, S. E., Carnduff, L., and Kirov, S. A. (2007). Physiological evidence that pyramidal neurons lack functional water channels. *Cereb. Cortex* 17, 787–802.

Andrew, R. D., and MacVicar, B. A. (1994). Imaging cell volume changes and neuronal excitation in the hippocampal slice. *Neuroscience* 62, 371–383.

Angulo, M. C., Le Meur, K., Kozlov, A. S., Charpak, S., and Audinat, E. (2008). GABA, a forgotten gliotransmitter. *Prog. Neurobiol.* 86, 297–303.

Ballanyi, K., Grafe, P., and ten Bruggencate, G. (1987). Ion activities and potassium uptake mechanisms of glial cells in guinea-pig olfactory

cortex slices. *J. Physiol. (Lond.)* 382, 159–174.

Barakat, L., and Bordey, A. (2002). GAT-1 and reversible GABA transport in Bergmann glia in slices. *J. Neurophysiol.* 88, 1407–1419.

Bardakdjian, J., Tardy, M., Pimoule, C., and Gonnard, P. (1979). GABA metabolism in cultured glial cells. *Neurochem. Res.* 4, 517–527.

Barres, B. A., Koroshetz, W. J., Swartz, K. J., Chun, L. L., and Corey, D. P. (1990). Ion channel expression by white matter glia: the O-2A glial progenitor cell. *Neuron* 4, 507–524.

Behar, T. N., Schaffner, A. E., Scott, C. A., O'Connell, C., and Barker, J. L. (1998). Differential response of cortical plate and ventricular zone cells to GABA as a migration stimulus. *J. Neurosci.* 18, 6378–6387.

Bekar, L. K., Jabs, R., and Walz, W. (1999). GABAA receptor agonists modulate K+ currents in adult hippocampal glial cells in situ. *Glia* 26, 129–138.

Bekar, L. K., and Walz, W. (2002). Intracellular chloride modulates A-type potassium currents in astrocytes. *Glia* 39, 207–216.

Benagiano, V., Flace, P., Virgintino, D., Rizzi, A., Roncali, L., and Ambrosi, G. (2000). Immunolocalization of glutamic acid decarboxylase in postmortem human cerebellar cortex. A light microscopy study. *Histochem. Cell Biol.* 114, 191–195.

Ben-Ari, Y., Cherubini, E., Corradetti, R., and Gaiarsa, J. L. (1989). Giant synaptic potentials in immature rat CA3 hippocampal neurones. *J. Physiol. (Lond.)* 416, 303–325.

Bender, A. S., and Norenberg, M. D. (1998). Effect of benzodiazepines and neurosteroids on ammonia-induced swelling in cultured astrocytes. *J. Neurosci. Res.* 54, 673–680.

Benfenati, V., and Ferroni, S. (2010). Water transport between CNS compartments: functional and molecular interactions between aquaporins and ion channels. *Neuroscience* 168, 926–940.

Berger, T., Walz, W., Schnitzer, J., and Kettenmann, H. (1992). GABA- and glutamate-activated currents in glial cells of the mouse corpus callosum slice. *J. Neurosci. Res.* 31, 21–27.

Bevensee, M. O., Apkon, M., and Boron, W. F. (1997). Intracellular pH regulation in cultured astrocytes from rat hippocampus. II. Electrogenic Na/HCO_3 cotransport. *J. Gen. Physiol.* 110, 467–483.

Binder, D. K., Yao, X., Zador, Z., Sick, T. J., Verkman, A. S., and Manley, G. T. (2006). Increased seizure duration and slowed potassium kinetics in mice lacking aquaporin-4 water channels. *Glia* 53, 631–636.

Blaesse, P., Airaksinen, M. S., Rivera, C., and Kaila, K. (2009). Cation-chloride cotransporters and neuronal function. *Neuron* 61, 820–838.

Blomqvist, A., and Broman, J. (1988). Light and electron microscopic immunohistochemical demonstration of GABA-immunoreactive astrocytes in the brain stem of the rat. *J. Neurocytol.* 17, 629–637.

Bormann, J., and Kettenmann, H. (1988). Patch-clamp study of gamma-aminobutyric acid receptor Cl- channels in cultured astrocytes. *Proc. Natl. Acad. Sci. U.S.A.* 85, 9336–9340.

Brooks, H. L., Regan, J. W., and Yool, A. J. (2000). Inhibition of aquaporin-1 water permeability by tetraethylammonium: involvement of the loop E pore region. *Mol. Pharmacol.* 57, 1021–1026.

Brunig, I., Suter, A., Knuesel, I., Luscher, B., and Fritschy, J. M. (2002). GABAergic terminals are required for postsynaptic clustering of dystrophin but not of GABA(A) receptors and gephyrin. *J. Neurosci.* 22, 4805–4813.

Cancedda, L., Fiumelli, H., Chen, K., and Poo, M. M. (2007). Excitatory GABA action is essential for morphological maturation of cortical neurons in vivo. *J. Neurosci.* 27, 5224–5235.

Carmosino, M., Procino, G., Tamma, G., Mannucci, R., Svelto, M., and Valenti, G. (2007). Trafficking and phosphorylation dynamics of AQP4 in histamine-treated human gastric cells. *Biol. Cell* 99, 25–36.

Cavazzin, C., Ferrari, D., Facchetti, F., Russignan, A., Vescovi, A. L., La Porta, C. A., and Gritti, A. (2006). Unique expression and localization of aquaporin-4 and aquaporin-9 in murine and human neural stem cells and in their glial progeny. *Glia* 53, 167–181.

Cesetti, T., Fila, T., Obernier, K., Bengtson, C. P., Li, Y., Mandl, C., Holzl-Wenig, G., and Ciccolini, F. (2010). GABA(A) receptor signalling induces osmotic swelling and cell cycle activation of neonatal prominin(+) precursors. *Stem Cells* 29, 307–319.

Cesetti, T., Obernier, K., Bengtson, C. P., Fila, T., Mandl, C., Holzl-Wenig, G., Worner, K., Eckstein, V., and Ciccolini, F. (2009). Analysis of stem cell lineage progression in the neonatal subventricular zone identifies EGFR+/NG2− cells as transit-amplifying precursors. *Stem Cells* 27, 1443–1454.

Chavas, J., Forero, M. E., Collin, T., Llano, I., and Marty, A. (2004). Osmotic tension as a possible link between GABA(A) receptor activation and intracellular calcium elevation. *Neuron* 44, 701–713.

Chebib, M., and Johnston, G. A. (1999). The 'ABC' of GABA receptors: a brief review. *Clin. Exp. Pharmacol. Physiol.* 26, 937–940.

Chen, H., Luo, J., Kintner, D. B., Shull, G. E., and Sun, D. (2005). Na(+)-dependent chloride transporter (NKCC1)-null mice exhibit less gray and white matter damage after focal cerebral ischemia. *J. Cereb. Blood Flow Metab.* 25, 54–66.

Chen, Q., Moulder, K., Tenkova, T., Hardy, K., Olney, J. W., and Romano, C. (1999). Excitotoxic cell death dependent on inhibitory receptor activation. *Exp. Neurol.* 160, 215–225.

Ciccolini, F., Collins, T. J., Sudhoelter, J., Lipp, P., Berridge, M. J., and Bootman, M. D. (2003). Local and global spontaneous calcium events regulate neurite outgrowth and onset of GABAergic phenotype during neural precursor differentiation. *J. Neurosci.* 23, 103–111.

Ciccolini, F., Mandl, C., Holzl-Wenig, G., Kehlenbach, A., and Hellwig, A. (2005). Prospective isolation of late development multipotent precursors whose migration is promoted by EGFR. *Dev. Biol.* 284, 112–125.

Clayton, G. H., Owens, G. C., Wolff, J. S., and Smith, R. L. (1998). Ontogeny of cation-Cl- cotransporter expression in rat neocortex. *Brain Res. Dev. Brain Res.* 109, 281–292.

Darquie, A., Poline, J. B., Poupon, C., Saint-Jalmes, H., and Le Bihan, D. (2001). Transient decrease in water diffusion observed in human occipital cortex during visual stimulation. *Proc. Natl. Acad. Sci. U.S.A.* 98, 9391–9395.

Deng, B., Glanzman, D., and Tidball, J. G. (2009). Nitric oxide generated by muscle corrects defects in hippocampal neurogenesis and neural differentiation caused by muscular dystrophy. *J. Physiol. (Lond.)* 587(Pt 8), 1769–1778.

Fernando, R. N., Eleuteri, B., Abdelhady, S., Nussenzweig, A., Andang, M., and Ernfors, P. (2011). Cell cycle restriction by histone H2AX limits proliferation of adult neural stem cells. *Proc. Natl. Acad. Sci. U.S.A.* 108, 5837–5842.

Frazao, R., Nogueira, M. I., and Wassle, H. (2007). Colocalization of synaptic GABA(C)-receptors with GABA (A)-receptors and glycine-receptors in the rodent central nervous system. *Cell Tissue Res.* 330, 1–15.

Frigeri, A., Nicchia, G. P., Nico, B., Quondamatteo, F., Herken, R., Roncali, L., and Svelto, M. (2001). Aquaporin-4 deficiency in skeletal muscle and brain of dystrophic mdx mice. *FASEB J.* 15, 90–98.

Fukui, M., Nakamichi, N., Yoneyama, M., Ozawa, S., Fujimori, S., Takahata, Y., Nakamura, N., Taniura, H., and Yoneda, Y. (2008). Modulation of cellular proliferation and differentiation through GABA(B) receptors expressed by undifferentiated neural progenitor cells isolated from fetal mouse brain. *J. Cell. Physiol.* 216, 507–519.

Gakhar-Koppole, N., Bengtson, C. P., Parlato, R., Horsch, K., Eckstein, V., and Ciccolini, F. (2008). Depolarization promotes GAD 65-mediated GABA synthesis by a post-translational mechanism in neural stem cell-derived neurons. *Eur. J. Neurosci.* 27, 269–283.

Gallo, V., Patrizio, M., and Levi, G. (1991). GABA release triggered by the activation of neuron-like non-NMDA receptors in cultured type 2 astrocytes is carrier-mediated. *Glia* 4, 245–255.

Ge, S., Goh, E. L., Sailor, K. A., Kitabatake, Y., Ming, G. L., and Song, H. (2006). GABA regulates synaptic integration of newly generated neurons in the adult brain. *Nature* 439, 589–593.

Green, A. R., Cross, A. J., Snape, M. F., and De Souza, R. J. (1992). The immediate consequences of middle cerebral artery occlusion on GABA synthesis in mouse cortex and cerebellum. *Neurosci. Lett.* 138, 141–144.

Green, A. R., Hainsworth, A. H., and Jackson, D. M. (2000). GABA potentiation: a logical pharmacological approach for the treatment of acute ischaemic stroke. *Neuropharmacology* 39, 1483–1494.

Hagberg, H., Lehmann, A., Sandberg, M., Nystrom, B., Jacobson, I., and Hamberger, A. (1985). Ischemia-induced shift of inhibitory and excitatory amino acids from intra- to extracellular compartments. *J. Cereb. Blood Flow Metab.* 5, 413–419.

Hamann, S., Herrera-Perez, J. J., Bundgaard, M., Alvarez-Leefmans, F. J., and Zeuthen, T. (2005). Water permeability of Na+-K+-2Cl− cotransporters in mammalian epithelial cells. *J. Physiol. (Lond.)* 568(Pt 1), 123–135.

Hatakeyama, S., Yoshida, Y., Tani, T., Koyama, Y., Nihei, K., Ohshiro, K., Kamiie, J. I., Yaoita, E., Suda, T., Hatakeyama, K., and Yamamoto, T.

(2001). Cloning of a new aquaporin (AQP10) abundantly expressed in duodenum and jejunum. *Biochem. Biophys. Res. Commun.* 287, 814–819.

Holthoff, K., and Witte, O. W. (1996). Intrinsic optical signals in rat neocortical slices measured with near-infrared dark-field microscopy reveal changes in extracellular space. *J. Neurosci.* 16, 2740–2749.

Hoppe, D., and Kettenmann, H. (1989). Carrier-mediated Cl- transport in cultured mouse oligodendrocytes. *J. Neurosci. Res.* 23, 467–475.

Hosli, L., Andres, P. F., and Hosli, E. (1978). Neuron-glia interactions: indirect effect of GABA on cultured glial cells. *Exp. Brain Res.* 33, 425–434.

Hosli, L., Hosli, E., Andres, P. F., and Landolt, H. (1981). Evidence that the depolarization of glial cells by inhibitory amino acids is caused by an efflux of K+ from neurones. *Exp. Brain Res.* 42, 43–48.

Jayakumar, A. R., and Norenberg, M. D. (2010). The Na-K-Cl co-transporter in astrocyte swelling. *Metab. Brain Dis.* 25, 31–38.

Kahle, K. T., Simard, J. M., Staley, K. J., Nahed, B. V., Jones, P. S., and Sun, D. (2009). Molecular mechanisms of ischemic cerebral edema: role of electroneutral ion transport. *Physiology (Bethesda)* 24, 257–265.

Kanaka, C., Ohno, K., Okabe, A., Kuriyama, K., Itoh, T., Fukuda, A., and Sato, K. (2001). The differential expression patterns of messenger RNAs encoding K-Cl cotransporters (KCC1,2) and Na-K-2Cl cotransporter (NKCC1) in the rat nervous system. *Neuroscience* 104, 933–946.

Kettenmann, H., Backus, K. H., and Schachner, M. (1987). Gamma-aminobutyric acid opens Cl-channels in cultured astrocytes. *Brain Res.* 404, 1–9.

Kettenmann, H., Gilbert, P., and Schachner, M. (1984). Depolarization of cultured oligodendrocytes by glutamate and GABA. *Neurosci. Lett.* 47, 271–276.

Kimelberg, H. K. (1981). Active accumulation and exchange transport of chloride in astroglial cells in culture. *Biochim. Biophys. Acta* 646, 179–184.

Kimelberg, H. K., and Frangakis, M. V. (1985). Furosemide- and bumetanide-sensitive ion transport and volume control in primary astrocyte cultures from rat brain. *Brain Res.* 361, 125–134.

Koch, U., and Magnusson, A. K. (2009). Unconventional GABA release: mechanisms and function. *Curr. Opin. Neurobiol.* 19, 305–310.

Kong, H., Fan, Y., Xie, J., Ding, J., Sha, L., Shi, X., Sun, X., and Hu, G. (2008). AQP4 knockout impairs proliferation, migration and neuronal differentiation of adult neural stem cells. *J. Cell. Sci.* 121(Pt 24), 4029–4036.

Kozlov, A. S., Angulo, M. C., Audinat, E., and Charpak, S. (2006). Target cell-specific modulation of neuronal activity by astrocytes. *Proc. Natl. Acad. Sci. U.S.A.* 103, 10058–10063.

Kuner, T., and Augustine, G. J. (2000). A genetically encoded ratiometric indicator for chloride: capturing chloride transients in cultured hippocampal neurons. *Neuron* 27, 447–459.

Lee, S., Yoon, B. E., Berglund, K., Oh, S. J., Park, H., Shin, H. S., Augustine, G. J., and Lee, C. J. (2010). Channel-mediated tonic GABA release from glia. *Science* 330, 790–796.

Lin, S. C., and Bergles, D. E. (2004). Synaptic signaling between GABAergic interneurons and oligodendrocyte precursor cells in the hippocampus. *Nat. Neurosci.* 7, 24–32.

Liu, X., Wang, Q., Haydar, T. F., and Bordey, A. (2005). Nonsynaptic GABA signaling in postnatal subventricular zone controls proliferation of GFAP-expressing progenitors. *Nat. Neurosci.* 8, 1179–1187.

MacAulay, N., Gether, U., Klaerke, D. A., and Zeuthen, T. (2001). Water transport by the human Na+-coupled glutamate cotransporter expressed in *Xenopus* oocytes. *J. Physiol. (Lond.)* 530(Pt 3), 367–378.

MacAulay, N., Zeuthen, T., and Gether, U. (2002). Conformational basis for the Li(+)-induced leak current in the rat gamma-aminobutyric acid (GABA) transporter-1. *J. Physiol. (Lond.)* 544(Pt 2), 447–458.

MacVicar, B. A., and Hochman, D. (1991). Imaging of synaptically evoked intrinsic optical signals in hippocampal slices. *J. Neurosci.* 11, 1458–1469.

MacVicar, B. A., Tse, F. W., Crichton, S. A., and Kettenmann, H. (1989). GABA-activated Cl- channels in astrocytes of hippocampal slices. *J. Neurosci.* 9, 3577–3583.

Maric, D., Maric, I., and Barker, J. L. (2000). Dual video microscopic imaging of membrane potential and cytosolic calcium of immunoidentified embryonic rat cortical cells. *Methods* 21, 335–347.

Markwardt, S. J., Wadiche, J. I., and Overstreet-Wadiche, L. S. (2009). Input-specific GABAergic signaling to newborn neurons in adult dentate gyrus. *J. Neurosci.* 29, 15063–15072.

Martinez-Rodriguez, R., Tonda, A., Gragera, R. R., Paz-Doel, R., Garcia-Cordovilla, R., Fernandez-Fernandez, E., Fernandez, A. M., Gonzalez-Romero, F., and Lopez-Bravo, A. (1993). Synaptic and non-synaptic immunolocalization of GABA and glutamate acid decarboxylase (GAD) in cerebellar cortex of rat. *Cell. Mol. Biol. (Noisy-le-grand)* 39, 115–123.

Matsutani, S., and Yamamoto, N. (1997). Neuronal regulation of astrocyte morphology in vitro is mediated by GABAergic signaling. *Glia* 20, 1–9.

McGann, L. E., Walterson, M. L., and Hogg, L. M. (1988). Light scattering and cell volumes in osmotically stressed and frozen-thawed cells. *Cytometry* 9, 33–38.

Mellon, S. H., and Griffin, L. D. (2002). Neurosteroids: biochemistry and clinical significance. *Trends Endocrinol. Metab.* 13, 35–43.

Mong, J. A., Nunez, J. L., and McCarthy, M. M. (2002). GABA mediates steroid-induced astrocyte differentiation in the neonatal rat hypothalamus. *J. Neuroendocrinol.* 14, 45–55.

Mongin, A. A., Aksentsev, S. L., Orlov, S. N., Slepko, N. G., Kozlova, M. V., Maximov, G. V., and Konev, S. V. (1994). Swelling-induced K+ influx in cultured primary astrocytes. *Brain Res.* 655, 110–114.

Muller, V., Birbaumer, N., Preissl, H., Braun, C., and Lang, F. (2002). Effects of water on cortical excitability in humans. *Eur. J. Neurosci.* 15, 528–538.

Mutoh, H., Perron, A., Akemann, W., Iwamoto, Y., and Knopfel, T. (2011). Optogenetic monitoring of membrane potentials. *Exp. Physiol.* 96, 13–18.

Nagelhus, E. A., Mathiisen, T. M., and Ottersen, O. P. (2004). Aquaporin-4 in the central nervous system: cellular and subcellular distribution and coexpression with KIR4.1. *Neuroscience* 129, 905–913.

Nicchia, G. P., Rossi, A., Nudel, U., Svelto, M., and Frigeri, A. (2008). Dystrophin-dependent and -independent AQP4 pools are expressed in the mouse brain. *Glia* 56, 869–876.

Nielsen, S., King, L. S., Christensen, B. M., and Agre, P. (1997). Aquaporins in complex tissues. II. Subcellular distribution in respiratory and glandular tissues of rat. *Am. J. Physiol.* 273(5 Pt 1), C1549–C1561.

Oreskovic, D., and Klarica, M. (2010). The formation of cerebrospinal fluid: nearly a hundred years of interpretations and misinterpretations. *Brain Res. Rev.* 64, 241–262.

Overstreet Wadiche, L., Bromberg, D. A., Bensen, A. L., and Westbrook, G. L. (2005). GABAergic signaling to newborn neurons in dentate gyrus. *J. Neurophysiol.* 94, 4528–4532.

Owens, D. F., Boyce, L. H., Davis, M. B., and Kriegstein, A. R. (1996). Excitatory GABA responses in embryonic and neonatal cortical slices demonstrated by gramicidin perforated-patch recordings and calcium imaging. *J. Neurosci.* 16, 6414–6423.

Papadopoulos, M. C., and Verkman, A. S. (2005). Aquaporin-4 gene disruption in mice reduces brain swelling and mortality in pneumococcal meningitis. *J. Biol. Chem.* 280, 13906–13912.

Pasantes-Morales, H., and Tuz, K. (2006). Volume changes in neurons: hyperexcitability and neuronal death. *Contrib. Nephrol.* 152, 221–240.

Pastor, A., Chvatal, A., Sykova, E., and Kettenmann, H. (1995). Glycine- and GABA-activated currents in identified glial cells of the developing rat spinal cord slice. *Eur. J. Neurosci.* 7, 1188–1198.

Plotkin, M. D., Kaplan, M. R., Peterson, L. N., Gullans, S. R., Hebert, S. C., and Delpire, E. (1997). Expression of the Na(+)-K(+)-2Cl- cotransporter BSC2 in the nervous system. *Am. J. Physiol.* 272(1 Pt 1), C173–C183.

Price, T. J., Hargreaves, K. M., and Cervero, F. (2006). Protein expression and mRNA cellular distribution of the NKCC1 cotransporter in the dorsal root and trigeminal ganglia of the rat. *Brain Res.* 1112, 146–158.

Rash, J. E., Yasumura, T., Hudson, C. S., Agre, P., and Nielsen, S. (1998). Direct immunogold labeling of aquaporin-4 in square arrays of astrocyte and ependymocyte plasma membranes in rat brain and spinal cord. *Proc. Natl. Acad. Sci. U.S.A.* 95, 11981–11986.

Redzic, Z. (2011). Molecular biology of the blood-brain and the blood-cerebrospinal fluid barriers: similarities and differences. *Fluids Barriers CNS* 8, 3.

Ricci, L., Valoti, M., Sgaragli, G., and Frosini, M. (2007). Neuroprotection afforded by diazepam against oxygen/glucose deprivation-induced injury in rat cortical brain slices. *Eur. J. Pharmacol.* 561, 80–84.

Ricci, L., Valoti, M., Sgaragli, G., and Frosini, M. (2009). Protection by taurine of rat brain cortical slices against oxygen glucose deprivation- and reoxygenation-induced damage. *Eur. J. Pharmacol.* 621, 26–32.

Ringel, F., and Plesnila, N. (2008). Expression and functional role of potassium-chloride cotransporters (KCC) in astrocytes and C6 glioma cells. *Neurosci. Lett.* 442, 219–223.

Risher, W. C., Andrew, R. D., and Kirov, S. A. (2009). Real-time passive volume responses of astrocytes to acute osmotic and ischemic stress in cortical slices and in vivo revealed by two-photon microscopy. *Glia* 57, 207–221.

Rosen, A. S., and Andrew, R. D. (1990). Osmotic effects upon excitability in rat neocortical slices. *Neuroscience* 38, 579–590.

Runquist, M., and Alonso, G. (2003). Gabaergic signaling mediates the morphological organization of astrocytes in the adult rat forebrain. *Glia* 41, 137–151.

Rupasinghe, J., and Jasinarachchi, M. (2011). Progressive encephalopathy with cerebral oedema and infarctions associated with valproate and diazepam overdose. *J. Clin. Neurosci.* 18, 710-711.

Saadoun, S., Papadopoulos, M. C., Davies, D. C., Bell, B. A., and Krishna, S. (2002). Increased aquaporin 1 water channel expression in human brain tumours. *Br. J. Cancer* 87, 621–623.

Saadoun, S., Papadopoulos, M. C., Watanabe, H., Yan, D., Manley, G. T., and Verkman, A. S. (2005). Involvement of aquaporin-4 in astroglial cell migration and glial scar formation. *J. Cell. Sci.* 118(Pt 24), 5691–5698.

Saly, V., and Andrew, R. D. (1993). CA3 neuron excitation and epileptiform discharge are sensitive to osmolality. *J. Neurophysiol.* 69, 2200–2208.

Sequerra, E. B., Gardino, P., Hedin-Pereira, C., and de Mello, F. G. (2007). Putrescine as an important source of GABA in the postnatal rat subventricular zone. *Neuroscience* 146, 489–493.

Shimada, N., Graf, R., Rosner, G., and Heiss, W. D. (1993). Ischemia-induced accumulation of extracellular amino acids in cerebral cortex, white matter, and cerebrospinal fluid. *J. Neurochem.* 60, 66–71.

Sidhu, R. S., Del Bigio, M. R., Tuor, U. I., and Seshia, S. S. (1997). Low-dose vigabatrin (gamma-vinyl GABA)-induced damage in the immature rat brain. *Exp. Neurol.* 144, 400–405.

Solenov, E., Watanabe, H., Manley, G. T., and Verkman, A. S. (2004). Sevenfold-reduced osmotic water permeability in primary astrocyte cultures from AQP-4-deficient mice, measured by a fluorescence quenching method. *Am. J. Physiol. Cell Physiol.* 286, C426–C432.

Soltesz, I., and Mody, I. (1994). Patch-clamp recordings reveal powerful GABAergic inhibition in dentate hilar neurons. *J. Neurosci.* 14, 2365–2376.

Steinhauser, C., Berger, T., Frotscher, M., and Kettenmann, H. (1992). Heterogeneity in the Membrane current pattern of identified glial cells in the hippocampal slice. *Eur. J. Neurosci.* 4, 472–484.

Stewart, R. R., Hoge, G. J., Zigova, T., and Luskin, M. B. (2002). Neural progenitor cells of the neonatal rat anterior subventricular zone express functional GABA(A) receptors. *J. Neurobiol.* 50, 305–322.

Strange, K. (1993). Maintenance of cell volume in the central nervous system. *Pediatr. Nephrol.* 7, 689–697.

Takagi, S., Obata, K., and Tsubokawa, H. (2002). GABAergic input contributes to activity-dependent change in cell volume in the hippocampal CA1 region. *Neurosci. Res.* 44, 315–324.

Tanaka, Y., Tozuka, Y., Takata, T., Shimazu, N., Matsumura, N., Ohta, A., and Hisatsune, T. (2009). Excitatory GABAergic activation of cortical dividing glial cells. *Cereb. Cortex* 19, 2181–2195.

Taniguchi, M., Yamashita, T., Kumura, E., Tamatani, M., Kobayashi, A., Yokawa, T., Maruno, M., Kato, A., Ohnishi, T., Kohmura, E., Tohyama, M., and Yoshimine, T. (2000). Induction of aquaporin-4 water channel mRNA after focal cerebral ischemia in rat. *Brain Res. Mol. Brain Res.* 78, 131–137.

Tas, P. W., Massa, P. T., Kress, H. G., and Koschel, K. (1987). Characterization of an Na+/K+/Cl- co-transport in primary cultures of rat astrocytes. *Biochim. Biophys. Acta* 903, 411–416.

Tozuka, Y., Fukuda, S., Namba, T., Seki, T., and Hisatsune, T. (2005). GABAergic excitation promotes neuronal differentiation in adult hippocampal progenitor cells. *Neuron* 47, 803–815.

Tuz, K., Pena-Segura, C., Franco, R., and Pasantes-Morales, H. (2004). Depolarization, exocytosis and amino acid release evoked by hyposmolarity from cortical synaptosomes. *Eur. J. Neurosci.* 19, 916–924.

Tyzio, R., Cossart, R., Khalilov, I., Minlebaev, M., Hubner, C. A., Represa, A., Ben-Ari, Y., and Khazipov, R. (2006). Maternal oxytocin triggers a transient inhibitory switch in GABA signaling in the fetal brain during delivery. *Science* 314, 1788–1792.

Velez-Fort, M., Audinat, E., and Angulo, M. C. (2011). Central role of GABA in neuron-glia interactions. *Neuroscientist.* doi: 10.1177/1073858411403317. [Epub ahead of print]

Venero, J. L., Vizuete, M. L., Machado, A., and Cano, J. (2001). Aquaporins in the central nervous system. *Prog. Neurobiol.* 63, 321–336.

Verkman, A. S. (2000). Physiological importance of aquaporins: lessons from knockout mice. *Curr. Opin. Nephrol. Hypertens.* 9, 517–522.

Verkman, A. S. (2005). More than just water channels: unexpected cellular roles of aquaporins. *J. Cell. Sci.* 118(Pt 15), 3225–3232.

Vizuete, M. L., Venero, J. L., Vargas, C., Ilundain, A. A., Echevarria, M., Machado, A., and Cano, J. (1999). Differential upregulation of aquaporin-4 mRNA expression in reactive astrocytes after brain injury: potential role in brain edema. *Neurobiol. Dis.* 6, 245–258.

Von Blankenfeld, G., Trotter, J., and Kettenmann, H. (1991). Expression and developmental regulation of a GABAA receptor in cultured murine cells of the oligodendrocyte lineage. *Eur. J. Neurosci.* 3, 310–316.

Walz, W. (2002). Chloride/anion channels in glial cell membranes. *Glia* 40, 1–10.

Walz, W., and Wuttke, W. A. (1999). Independent mechanisms of potassium clearance by astrocytes in gliotic tissue. *J. Neurosci. Res.* 56, 595–603.

Wang, H., Yan, Y., Kintner, D. B., Lytle, C., and Sun, D. (2003). GABA-mediated trophic effect on oligodendrocytes requires Na-K-2Cl cotransport activity. *J. Neurophysiol.* 90, 1257–1265.

Wang, L. P., Kempermann, G., and Kettenmann, H. (2005). A subpopulation of precursor cells in the mouse dentate gyrus receives synaptic GABAergic input. *Mol. Cell. Neurosci.* 29, 181–189.

Wen, H., Nagelhus, E. A., Amiry-Moghaddam, M., Agre, P., Ottersen, O. P., and Nielsen, S. (1999). Ontogeny of water transport in rat brain: postnatal expression of the aquaporin-4 water channel. *Eur. J. Neurosci.* 11, 935–945.

Williamson, A. V., Mellor, J. R., Grant, A. L., and Randall, A. D. (1998). Properties of GABA(A) receptors in cultured rat oligodendrocyte progenitor cells. *Neuropharmacology* 37, 859–873.

Wu, P. H., Durden, D. A., and Hertz, L. (1979). Net production of gamma-aminobutyric acid in astrocytes in primary cultures determined by a sensitive mass spectrometric method. *J. Neurochem.* 32, 379–390.

Young, S. Z., Platel, J. C., Nielsen, J. V., Jensen, N. A., and Bordey, A. (2010). GABA(A) Increases calcium in subventricular zone astrocyte-like cells through L- and T-type voltage-gated calcium channels. *Front. Cell. Neurosci.* 4:8. doi:10.3389/fncel.2010.00008

Zador, Z., Bloch, O., Yao, X., and Manley, G. T. (2007). Aquaporins: role in cerebral edema and brain water balance. *Prog. Brain Res.* 161, 185–194.

Zelenina, M., Zelenin, S., Bondar, A. A., Brismar, H., and Aperia, A. (2002). Water permeability of aquaporin-4 is decreased by protein kinase C and dopamine. *Am. J. Physiol. Renal Physiol.* 283, F309–F318.

Zeuthen, T. (1994). Cotransport of K+, Cl- and H_2O by membrane proteins from choroid plexus epithelium of *Necturus maculosus*. *J. Physiol. (Lond.)* 478(Pt 2), 203–219.

Zeuthen, T., and Zeuthen, E. (2007). The mechanism of water transport in Na+-coupled glucose transporters expressed in *Xenopus* oocytes. *Biophys. J.* 93, 1413–1416; discussion 1417–1419.

Conflict of Interest Statement: The authors declare that the research was conducted in the absence of any commercial or financial relationships that could be construed as a potential conflict of interest.

Received: 30 September 2011; accepted: 10 January 2012; published online: 30 January 2012.

Citation: Cesetti T, Ciccolini F and Li Y (2012) GABA not only a neurotransmitter: osmotic regulation by $GABA_AR$ signaling. Front. Cell. Neurosci. ***6****:3. doi: 10.3389/fncel.2012.00003*